Deliverable 6.4: Training materials of the 2nd GAS/HITEC Joint training course

Work Package GAS

The project leading to this application has received funding from the European Union's Horizon 2020 research and innovation programme under grant agreement No 847593.

Document information

Project Acronym	**EURAD**
Project Title	**European Joint Programme on Radioactive Waste Management**
Project Type	**European Joint Programme (EJP)**
EC grant agreement No.	**847593**
Project starting / end date	**1st June 2019 – 30 May 2024**
Work Package No.	**6**
Work Package Title	**Mechanistic understanding of gas transport in clay materials**
Work Package Acronym	**EURAD-GAS**
Deliverable No.	**D6.4**
Deliverable Title	**Training materials of the 2nd GAS/HITEC joint training course**
Lead Beneficiary	**32 – ONDRAF/NIRAS[ULiège]**
Contractual Delivery Date	**November 2023**
Actual Delivery Date	
Type	**Report**
Dissemination level	**PU**
Authors	**Frédéric COLLIN (ULIEGE)**

To be cited as:

Collin F. (2023): Training materials of the 2nd GAS/HITEC joint training course. Final version as of xx.xx.xxxx of deliverable D6.4 of the HORIZON 2020 project EURAD. EC Grant agreement no: 847593.

Disclaimer

Acknowledgement

This document is a deliverable of the European Joint Programme on Radioactive Waste Management (EURAD). EURAD has received funding from the European Union's Horizon 2020 research and innovation programme under grant agreement No 847593.

Status of deliverable		
	By	Date
Delivered (Lead Beneficiary)	ONDRAF/NIRAS[ULiège]	27/11/2023
Verified (WP Leader)	ONDRAF/NIRAS	27/11/2023
Reviewed (Reviewers)	ONDRAF/NIRAS	27/11/2023
Approved (PMO)	Bharti Reddy on behalf of the PMO	10/01/2024
Submitted to EC (Coordinator)	ANDRA	15/01/2024

Executive Summary

The second GAS/HITEC Joint training course has been organised jointly with the ALERT Geomaterials network. The Alliance of Laboratories in Europe for Education, Research and Technology (ALERT) "Geomaterials" has been created in 1989 by Roberto Nova, Manuel Pastor, Ian Smith, Peter Vermeer, Olek Zienkiewicz and Félix Darve as a pioneering (at that time!) effort to develop a European School of Thinking in the field of the Mechanics of Geomaterials. ALERT Geomaterials includes 38 Universities or Organisations, which are most active in the field of numerical and experimental modelling of geomaterials and geostructures.

The 2023 Doctoral School is entitled "Multiphysics and multiscale coupled processes in Geomaterials, a focus on thermal effect and gas transfer impact on the behaviour of geomaterials". The school was organized from 28th August to 1st September 2023 at Liège University, within the framework of EURAD, the European Joint programme on Radioactive waste management (grant agreement No 847593). Objectives of EURAD include the development of new knowledge and consolidation of existing knowledge for the safe start of operation of the first geological disposal facilities for spent fuel, HLW, and other long-lived radioactive waste, and supporting optimization linked with the step wise implementation of disposal.

This doctoral school is related to two of the WPs of the EURAD Joint Programme, namely the GAS and HITEC WPs. Geomechanics plays a significant role in the understanding of the multiphysics and multiscale processes taking place in a geological disposal facility for radioactive waste. The objective of the school is to introduce state-of-the-art understanding, concepts and methods related to thermo-hydro-mechanical coupled processes, the physical impacts of thermal loading and the mechanistic understanding of gas migration in geomaterials. Results arising in the past 4 years from the EURAD projects and the scientific community of ALERT have been integrated to the school. As requested by the participants after the first Doctoral training school in 2020, a visit to the HADES Underground Research Laboratory was organised on the last day of the school. A half day has been dedicated to presentations by early-career researchers (in order to further develop and broaden the interactions within the EURAD/ALERT community) and a visit of the Geotechnical Laboratory from ULiège. The second Doctoral Training course was therefore organised over five days!

The school was organized firstly for people coming from institutions active in EURAD or in ALERT, including staff members from agencies as well as young researchers, involved or interested in the geomechanics field. The school also offered a limited number of places to people from institutions not directly participating in EURAD and ALERT. About 15% of the attendees did not come from an Institution belonging to EURAD or ALERT. The attendance was limited to 80 people. The number of registered participants was about 70, among which, 45% were PhD students.

After the first Doctoral school, the final presentations of the lecturers and the related reference papers were made permanently available on Projectplace (for the members of the EURAD project):

https://service.projectplace.com/#project/1763332387/documents/813993294

During the second Doctoral School, all the lectures were recorded. The final presentations and the videos of all the lectures are available for all the scientific community on the ALERT webpage:

https://alertgeomaterials.eu/oz-course-2023-2/

Table of content

List of Tables

1. Introduction

The second EURAD (GAS & HITEC WPs) / ALERT Joint training course is a Doctoral School entitled "Multiphysics and multiscale coupled processes in Geomaterials, a focus on thermal effect and gas transfer impact on the behaviour of geomaterials".

This school is organized within the framework of EURAD, the European Joint programme on Radioactive waste management (grant agreement No 847593) and the ALERT Geomaterials network. The Alliance of Laboratories in Europe for Education, Research and Technology (ALERT) "Geomaterials" has been created in 1989 as a pioneering (at that time!) effort to develop a European School of Thinking in the field of the Mechanics of Geomaterials. Objectives of EURAD include the development of new knowledge and consolidation of existing knowledge for the safe start of operation of the first geological disposal facilities for spent fuel, HLW, and other long-lived radioactive waste, and supporting optimization linked with the step wise implementation of disposal.

This doctoral school is thus related on the one hand, to two of the Work Packages of the EURAD Joint Programme (namely the GAS and HITEC WPs), and the ALERT institutions on the other hand.

Geomechanics plays a significant role in the understanding of the multiphysics and multiscale processes taking place in a geological disposal facility for radioactive waste. The objective of the school is to introduce state-of-the-art understanding, concepts and methods related to thermo-hydro-mechanical coupled processes, the physical impacts of thermal loading and the mechanistic understanding of gas migration in geomaterials. Results arising in the past 4 years from the EURAD project and the scientific community of ALERT have been integrated to the school. A visit to the HADES Underground Research Laboratory was organised on the last day of the school. A half day has been dedicated to presentations by early-career researchers, in order to further develop and broaden the interactions within the EURAD/ALERT community.

1.1 Topics and target audience

The HITEC WP deals with thermal impact and the GAS WP concerns gas transfer, both in the context of geological disposal of radioactive waste. This school allows the attendees to improve their understanding of heat transfers, water and gas migration and stress and strain evolution in a repository. The school addresses both experimental and numerical investigations, at small (lab) and large (in situ) scale. These investigations involve geomaterials such as the host rock, either clayey or crystalline rock, but also bentonite which is typically used in engineered barriers for its sealing capacity.

During the first GAS/HITEC EURAD joint training course, a selection of key references in these fields (e.g. state-of-the-art scientific papers) was made available and is still a part of the teaching material of this second school (Deliverable 6.3: Training materials of the 1st GAS/HITEC Joint training course, F.Collin and R. Charlier, 2020). The aim of this second school is twofold: first to provide the basics of physical THM phenomena and experimental testing and secondly, to evidence the scientific results obtained recently on the physical understanding, the experimental (both laboratory and in situ) development and numerical achievement.

The school was organized firstly for people coming from institutions active in EURAD and in ALERT Geomaterials network, including staff members from agencies as well as young researchers, involved or interested in the geomechanics field. The school also offered a limited number of places to people from institutions not directly participating to EURAD and ALERT. The attendance was limited to 80 people. The number of registered participants was about 70. These are mainly (early-career) researchers involved in the WP GAS or WP HITEC of EURAD and/or affiliated to an ALERT Geomaterials member, as well as members of waste management organisations and technology support organisations.

1.2 Learning outcomes

At the end of the school, participants had a broad view of the state-of-the-art and of the challenges related to the GAS and HITEC WP research programmes. They met a number of key researchers on THM and gas transport in the context of geological disposal, fostering information exchange and cooperation within the geomechanics community.

In particular, the attendees were able to:

- Understand the basics of the thermo-hydro-mechanical (multi-physical) couplings in geomaterials;
- Perceive the experimental evidences and figure out the physical processes at the laboratory scale and from in situ tests;
- Capture the fundamentals on constitutive modelling of the relevant phenomena;
- Identify the challenges in numerical modelling of these physical processes;
- Appreciate/better appreciate the application of THM (multi-physical) couplings in geomaterials within geological disposal facility post-closure safety cases (e.g. claims arguments and evidence).

2. School program

The school was organized from 28th August to 1st September 2023 at the "Institut de Mathématique" of the Liège University. The 5-day school was divided into 7 lectures and 3 visits.

Here is the programme of the school:

Monday 28/08

8h30 Welcome, registration and coffee

9h00 Introduction

General aspects (school organizers)

9h15 **Basics of thermo-hydro-mechanical processes in geomaterials** (F. Collin – Appendix B)

12h30 Lunch

13h30 **Basics of experimental testing of geomaterials** (A. Ferrari – Appendix C)

17h00 Closure

Tuesday 29/08

9h00 **Constitutive modelling of thermo-hydro-mechanical processes in geomaterials** (J.M. Pereira – Appendix D)

12h Lunch

13h30 **Development, validation and maintenance of numerical codes** (O. Kolditz – Appendices E & F)

16h30 Closure

19h30 Banquet at Selys Vander Valk Restaurant

Wednesday 30/08

9h30 **PhD day: poster sessions and pitches** (All)

11h00 **Visit of the Laboratory of Geotechnologies from ULiège** (All)

12h30 Lunch

13h30 **Advanced multiphysics experimental testing and imaging of geomaterials** (L. Gonzalez-Blanco, J. Svoboda, A. Wiseall – Appendices G-H-I)

17h00 Closure

Thursday 31/08

9h00 **Advanced multiphysics modelling of geomaterials: multiscale approaches and heterogeneities** (P. Bésuelle, F. Collin, A.-C. Dieudonné – Appendices J-K-L-M)

12h30 Lunch

13h30 **In situ THM and gas experiments** (A. Dizier, E. Stopelli, C. Plua, M. V. Villar – Appendices N-O-P-Q)

17h00 Closure

Friday 1/09

9h30 Visit of HADES underground research laboratory at EURIDICE

12h15 Lunch

13h15 Visit of Tabloo expositions (visitor centre about radioactivity, the management of radioactive waste and research into nuclear applications managed by ONDRAF/NIRAS).

15h30 School closure

And the list of the lecturers:

Frédéric Collin, Université de Liège (Belgium)

Alessio Ferrari, Ecole Polytechnique Fédérale de Lausane (Switzerland)

Jean-Michel Pereira, Ecole des Ponts et Chaussées (France)

Olaf Kolditz, Helmholtz Centre for Environmental Research UFZ (Germany)

Laura Gonzalez-Blanco, CIMNE, Universitat Politècnica de Catalunya (Spain)

Jiri Svoboda, CTU (Check Republic)

Andrew Wiseall, British Geological Survey (United Kingdom)

Anne-Catherine Dieudonné, TU Delft (Nederland)

Pierre Bésuelle, CNRS, Université Grenoble-Alpes (France)

Arnaud Dizier, ESV Euridice (Belgium)

Carlos Plua, ANDRA (France)

Maria Victoria Villar, CIEMAT (Spain)

Emiliano Stopelli, NAGRA (Switzerland)

The list of participants is given in appendix A of this document.

3. Training materials

The school has been divided into lectures given by academic members and people from national agencies, e.g. WMOs, TSOs/Regulators, national RE representatives. For each lecture, the final presentations of the lecturers were made available on Projectplace (https://service.projectplace.com/#project/1763332387/documents/118871763/1085011482). A copy of each presentation is also given in appendix of this document. During the second Doctoral School, all the lectures were recorded. The final presentations and the videos of all the lectures are available for all the scientific community on the ALERT webpage: https://alertgeomaterials.eu/oz-course-2023-2/

4. Conclusions

During the EURAD joint programme, two doctoral schools were organised within WP HITEC and WP GAS. They were thought in a global perspective, meaning that the teaching material (reference papers, presentations) developed within the first school was considered for the second one (Deliverable 6.3: Training materials of the 1st GAS/HITEC Joint training course, F.Collin and R. Charlier, 2020). The first training course (3 days) in January 2020 focused on "Multiphysical Couplings in Geomechanics, a focus on thermal effect and gas transfer impact on the behaviour of geomaterials". The aim of this first doctoral school was to provide state-of-the-art understanding, concepts and methods related to thermo-hydro-mechanical coupled processes, the physical impacts of thermal loading and the mechanistic understanding of gas migration in geomaterials. The second doctoral school organised in August 2023 kept the same objectives but the focus was also made on the results arising in the past 4 years of the EURAD projects. This second doctoral school offered also the opportunity to disseminate the results of the two WPs in a broader audience. Indeed, the school was jointly organised with the ALERT Geomaterials network (https://alertgeomaterials.eu/). The Alliance of Laboratories in Europe for Education, Research and Technology (ALERT) "Geomaterials" has been created in 1989 by Roberto Nova, Manuel Pastor, Ian Smith, Peter Vermeer, Olek Zienkiewicz and Félix Darve as a pioneering (at that time!) effort to develop a European School of Thinking in the field of the Mechanics of Geomaterials. ALERT Geomaterials includes today 38 Universities or Organisations, which are most active in the field of numerical and experimental modelling of geomaterials and geostructures. The lecturers were therefore coming from both EURAD and ALERT institutions. During the second Doctoral School, all the lectures were recorded. The final presentations and the videos of all the lectures are available for all the scientific community on the ALERT webpage: https://alertgeomaterials.eu/oz-course-2023-2/

Based on the feedback from the first school, the programme was extended in order to include a visit to a laboratory in University of Liège and to the HADES Underground Research Laboratory managed by EURIDICE. This second course was therefore organised over 5 days! Moreover, the school provided also the opportunity for the early-stage researcher to present their research to the audience. A half-day session was therefore organised with a pitch presentation followed by a poster session. The school offered a limited number of places to people from institutions not directly participating in EURAD and ALERT. About 15% of the attendees did not come from an institution belonging to EURAD or ALERT. The attendance was limited to 80 people. The number of registered participants was about 70, among which, 45% were PhD students.

In conclusion, the second GAS/HITEC EURAD school entitled "Multiphysics and multiscale coupled processes in Geomaterials, a focus on thermal effect and gas transfer impact on the behaviour of geomaterials" offered a good opportunity to disseminate the results obtained within the WPs HITEC and GAS, not only within the EURAD community but also to a broader scientific community thanks to the joint organisation with ALERT Geomaterials. From the poster session and pitch presentations, fruitful discussions between the PhD students took place and made it possible to train a future generation of researchers.

Appendix A. List of participants

Last name	First name	Company
ABDELRAHMAN ABUSERRIYA	Abdelrahman	Sinnar University
AGHAJANLOO	Mahnaz	TUDelft
ANDRADE	Cristhian	TU Delft
BABIY	Svetlana	EPFL
BARROO	Cédric	AFCN/FANC
BÉSUELLE	Pierre	UGA/CNRS
BHINI RANI CHANDAN MALAGAR	Bhini	TU Delft
CAPOUET	Manuel	Ondraf/Niras
CHARLIER	Robert	University of Liege
COLLIN	Frédéric	ULiège
COOKE	Andy	Nuclear Waste Services
CORMAN	Gilles	ULiège
DE JONG	Ties	TU Delft
DE KOCK	Sophie	Université de Liège
DEPAUS	Christophe	ONDRAF/NIRAS
DIEUDONNÉ	Anne-Catherine	Delft University of Technology
DIZIER	Arnaud	ESV EURIDICE GIE
ELFAR	Abdelrazik	University of Manchester
FANARA	Arthur	University of Liège
FERRARI	Alessio	EPFL
FIAZ	Umer	TU Braunschweig
FLETCHER	Cameron	British Geological Survey (UKRI)
FRANCOIS	Bertrand	ULiège
FREWEYNI	Kassa	Ethiopia Institute of Technology(Mekelle University)
FUSELIER	Héloïse	EPFL - LMS

GAFOOR	Ajmal	BGE TECHNOLOGY GmbH, Peine
GANESHALINGAM	Kayani	IRSN
GEORGIEVA	Temenuga	SCK CEN
GINTAUTAS	Poskas	Lithuanian Energy Institute (LEI)
GONZALEZ-BLANCO	Laura	UPC
GOWRISHANKAR	Aadithya	SCK CEN/ KU Leuven
GRGIC	Dragan	Université de Lorraine-CNRS
HOEDEMAKER	Rik	TU Delft
HUANG	Zhaojiang	TU Delft
ILSHAT SAIFULLIN	Ilshat	TU Delft
KATERINA	Cernochova	Czech Technical University in Prague
KOLDITZ	Olaf	Helmholtz Centre for Environmental Research UFZ
LEVASSEUR	Séverine	ONDRAF/NIRAS
MARCO	Starvaggi	Università degli Studi di Palermo
MATTHEW KIRBY	Matthew	Nuclear Waste Services
MATTHIAS	Wojnarowicz	EPFL
MOHAMED	Alatar	University of manchester
MULAW TAFERE BAHTA	Mulaw	University of Gondar
MURATOVA	Kseniia	Chalmers University of Technology
NATALIA	Gimeno	CIEMAT
NICLAES	Jens	UCLouvain
PARRA GOMEZ	Luis Jose	Delft University of Technology
PARSONS	Sam	NWS
PEREIRA	Jean-Michel	ENPC
PLUA	Carlos	ANDRA
RAWAT	Abhishek	University of Liege
SAC-MORANE	Alexandre	Duke University
SHIHAO FU	Shihao	TU Delft

SONG	Hangbiao	ULiège
STOPELLI	Emiliano	Nagra
SVOBODA	Jiří	CTU in Prague
TENGBLAD GARCÍA	Erik	Castilla-La Mancha University (UCLM)
URRACA	Gema	University of Castilla La-Mancha
VAEZI	Iman	Universitat Politècnica de Catalunya · Barcelona Tech - UPC
VILLAR	María Victoria	CIEMAT
WEBBER	Holiness	SUBATECH -IMT Atlantique, Nantes.
WENQING CAI	Wenqing	École des Ponts ParisTech
WISEALL	Andrew	Nuclear Waste Services
XIAOYANG CHENG	Xiaoyang	Chalmers University of Technology
XU	Man	Technische Universiteit Delft (TU Delft)
XU	Yifan	Georessources, University of Lorraine
YI	Susan	Delft University of Technology
ZAIDI	Mohammed	Institut de radioprotection et de sûreté nucléaire (IRSN)
ZHANG	Aoxi	ULiège

Table 1 – List of participants

Appendix B. Basics of thermo-hydro-mechanical processes in geomaterials (F Collin)

Multiphysics and multiscale coupled processes in geomaterials.

Focus on thermal effects and gas transfer impact on the behaviour of geomaterials.

S. Levasseur, A-C Dieudonné, Frédéric Collin

This project has received funding from the European Union's Horizon 2020 research and innovation programme under grant agreement N°847593

WELCOME

What about ALERT Geomaterials ?

The Alliance of Laboratories in Europe for Education, Research and Technology (ALERT) "Geomaterials" has been **created in 1989** by ***Roberto Nova, Manuel Pastor, Ian Smith, Peter Vermeer, Olek Zienkiewicz and Félix Darve*** as a pioneering (at that time!) effort to develop a **European School of Thinking in the field of the Mechanics of Geomaterials**. The generic name "**Geomaterials**" is viewed as gathering together **materials, whose mechanical behaviour depends on the pressure level**, which can be dilatant under shearing and which are multiphase because of their porous structure. So, **the "geomaterials" label brings together mainly soils, rocks and concrete**. It has been obvious from the very beginning that there is a crucial need for a joint Graduate School in order to build firmly this European scientific group in the Mechanics of Geomaterials, in **close link with the doctoral students**.

WELCOME

Who are ALERT Geomaterials members? 38 Universities or organizations

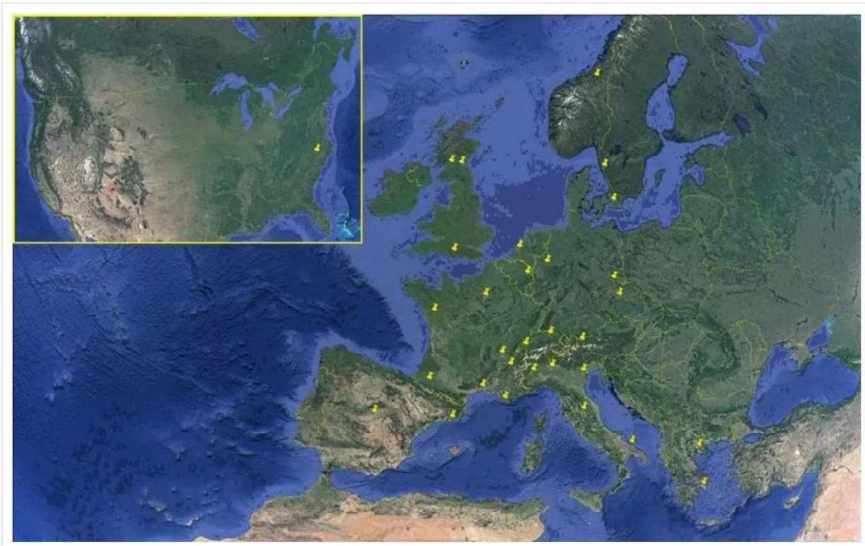

WELCOME

What are the activities of ALERT Geomaterials members?

ALERT Workshop

ALERT Doctoral school

Every year in end September in Aussois (France)

WELCOME

What are the activities of ALERT Geomaterials members?

ALERT Workshop

ALERT Doctoral school

Every y… …per i…

ALERT … …urs

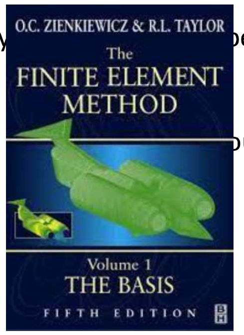

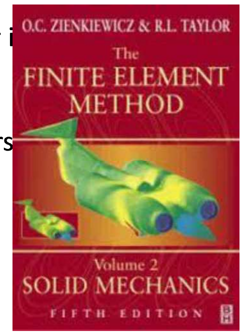

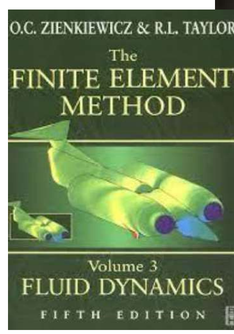

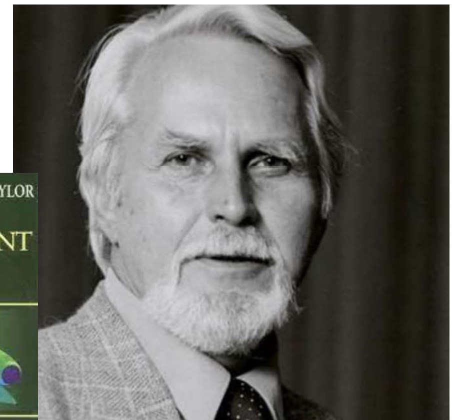

Olek Zienkiewick (1921-2009)

eurad

WELCOME

What about EURAD (Grant agreement ID: 847593) ?

The European Joint Programme on Radioactive Waste Management (EURAD/2019-2024) is a project that will **help the EU member states implement Directive 2011/70/Euratom (Waste Directive)** by working with their national programmes. It will also coordinate action on joint targets among all related organisations involved at European level, whether in research or technical support. Building on the EC JOPRAD project, the EURAD project will help member states obtain the know-how required to **implement safe and long-term management of radioactive waste**. EURAD will also provide management knowledge to operate disposal facilities, and help transfer that knowledge between countries and organisations.

eurad

WELCOME

Who are EURAD participants?

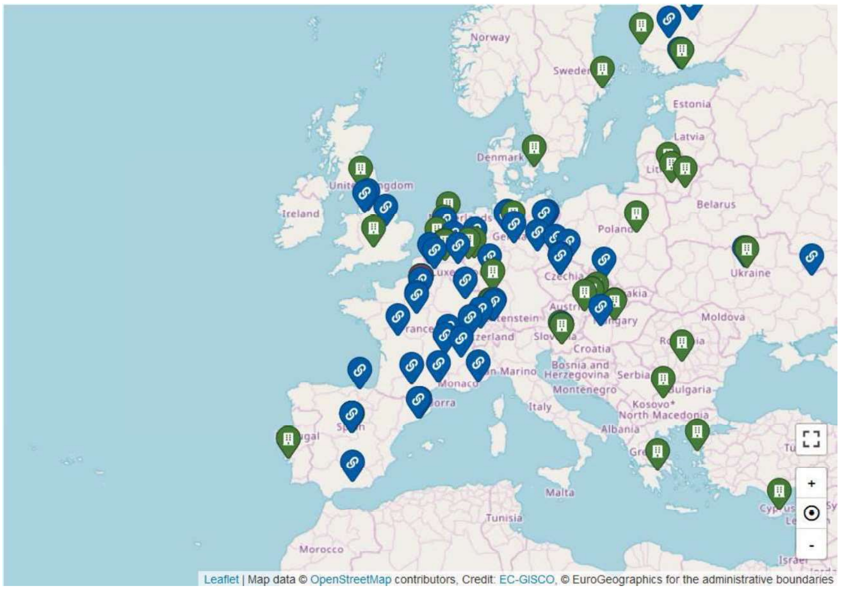

eurad

WELCOME

What are the activities of EURAD?

EURAD - GAS WP

Mechanistic understanding of gas transport in clay materials (GAS)

The main objectives of this WP are:

To improve the mechanistic understanding of gas transport processes in natural and engineered clay materials, their couplings with the mechanical behaviour and their impact on the properties of these materials;

To evaluate the gas transport regimes that can be active at the scale of a geological disposal system and their potential impact on barrier integrity and repository performance.

eurad

WELCOME

What are the activities of EURAD?

EURAD - HITEC WP

The overall objective is to evaluate whether an increase of temperature is feasible and safe by applying existing and within the work package produced novel knowledge about the behaviour of clay materials at elevated temperatures:

to improve understanding of the THM behaviour of clay rock and engineered clay material (buffer) under high temperature and provide suitable THM models both for clay rock and buffer,
to better assess effect of overpressures build up induced by the heat produced from the radioactive waste on the THM behaviour and properties of the clay host rock, and
to identify processes at high temperature and the impact of high temperature on the THM properties of the buffer material.

eurad

WELCOME

What will you do during this school?

Monday 28 August	
9.00 – 12.30	Basics of thermo-hydro-mechanical processes in geomaterials F. Collin, ULiège
13.30 – 17.00	Basics of experimental testing of geomaterials Alessio Ferrari, EPFL
Tuesday 29 August	
9.00 – 12.30	Constitutive modelling of thermo-hydro-mechanical processes in geomaterials Jean-Michel Pereira, ENPC
13.30 – 17.00	Development, validation and maintenance of numerical codes Olaf Kolditz, UFZ
19.30	Banquet at the city center

eurad

WELCOME

What will you do during this school?

Banquet at Selys Vander Valk Restaurant close to the city center

eurad

WELCOME

What will you do during this school?

Wednesday 30 August	
9.00 – 12.30	PhD day: poster sessions and pitches
13.30 – 17.00	Advanced multiphysics experimental testing and imaging of geomaterials Laura Gonzalez-Blanco (UPC), Dragan Grigc (U Lorraine), Jiri Svoboda (CTU), Andrew Wiseall (BGS)
Thursday 31 August	
9.00 – 12.30	Advanced multiphysics modelling of geomaterials: multiscale approaches and heterogeneities Pierre Bésuelle (UGA), Frédéric Collin (ULiège), Anne-Catherine Dieudonné (TU Delft), Sebastià Olivella (UPC)
13.30 – 17.00	*In situ* THM and gas experiments Arnaud Dizier (Euridice), Emiliano Stopelli (TBC), Carlos Plua (ANDRA), Maria Victoria Villar (CIEMAT)

eurad

WELCOME

What will you do during this school?

Friday 1 September	
Departure to Mol at 8.00	
9.30 – 12.00	Group 1 visits Tabloo expositions Group 2 visits EURIDICE_HADES underground research laboratory
12.15 – 13.15	Sandwich lunch
13.15 – 15.30	Group 2 visits Tabloo expositions Group 1 visits EURIDICE_HADES underground research laboratory
Return from Mol at 15.45	

ALERT Geomaterials

Alliance of Laboratories in Europe for Education, Research and Technology

http://alertgeomaterials.eu

European Joint Programme on Radioactive Waste Management

Multiphysics and multiscale coupled processes in geomaterials.

Focus on thermal effects and gas transfer impact on the behaviour of geomaterials.

Basics of thermo-hydro-mechanical processes in geomaterials

Frédéric **COLLIN**

University of Liège – UEE Research Unit

This project has received funding from the European Union's Horizon 2020 research and innovation programme under grant agreement N°847593

TABLE OF CONTENT

eurad

INTRODUCTION

Nuclear electricity production :

+ Low CO_2 emission

- Noxious ionizing radiations
- Radioactive waste production

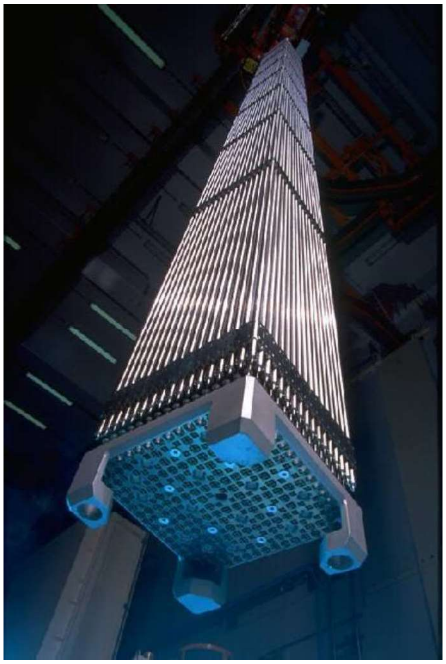

eurad

INTRODUCTION

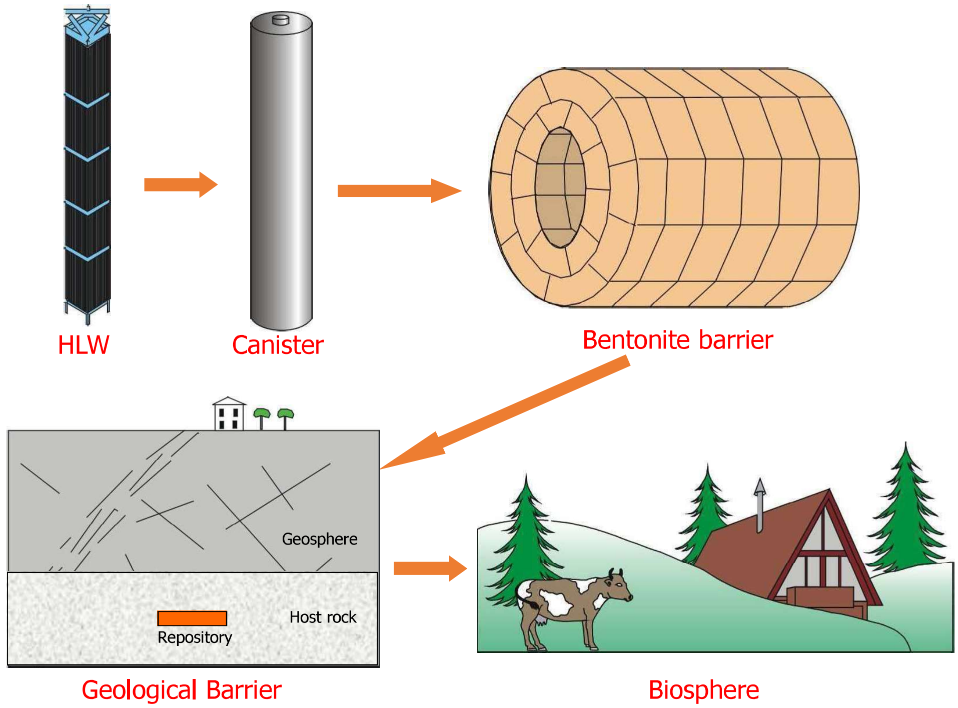

INTRODUCTION

Intermediate
(long-lived)
&
high activity
wastes

Deep geological disposal

Repository in deep geological media with good confining properties

(Low permeability $K<10^{-12}$ m/s)

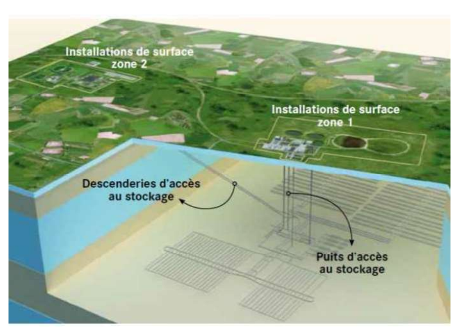

Disposal facility of Cigéo project in France
(Labalette et al., 2013)

INTRODUCTION

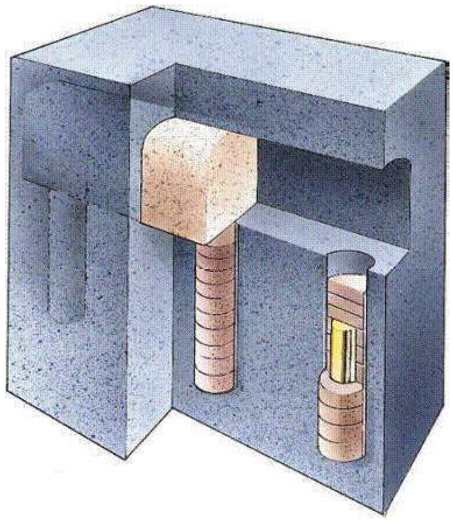

Disposal in vertical shaft

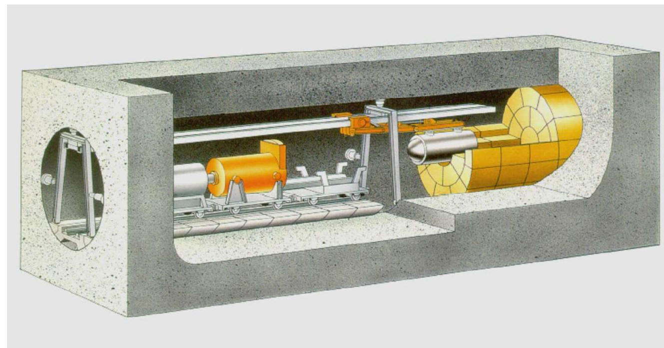

Disposal in horizontal gallery

INTRODUCTION

Repository phases

Time

Construction
↳ Excavation

Maintenance
↳ Ventilation

Repository
↳ Sealing

Long term
↳ Corrosion,
heat generation

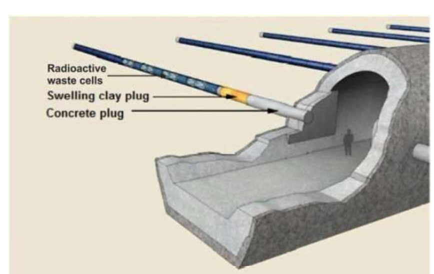

Type C wastes (Andra, 2005)

INTRODUCTION

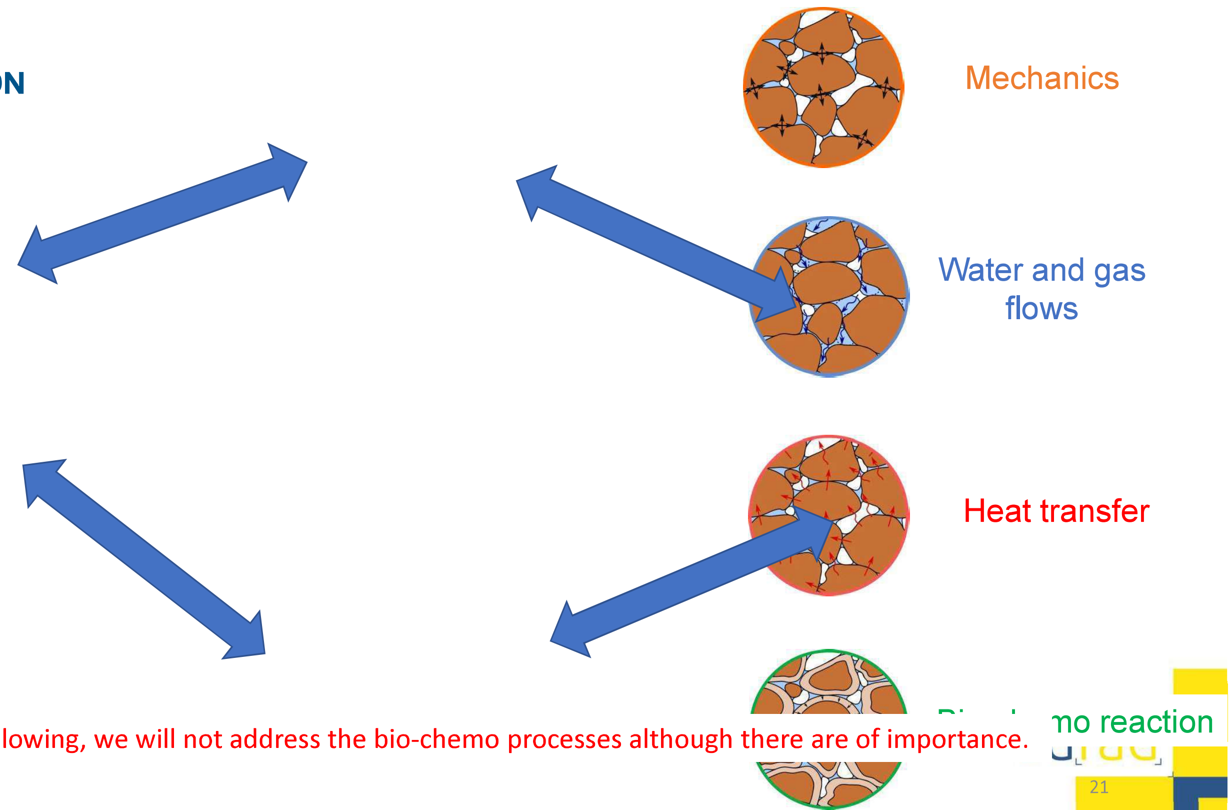

In the following, we will not address the bio-chemo processes although there are of importance.

INTRODUCTION

The material involved in the processes are Saturated/Unsaturated porous media

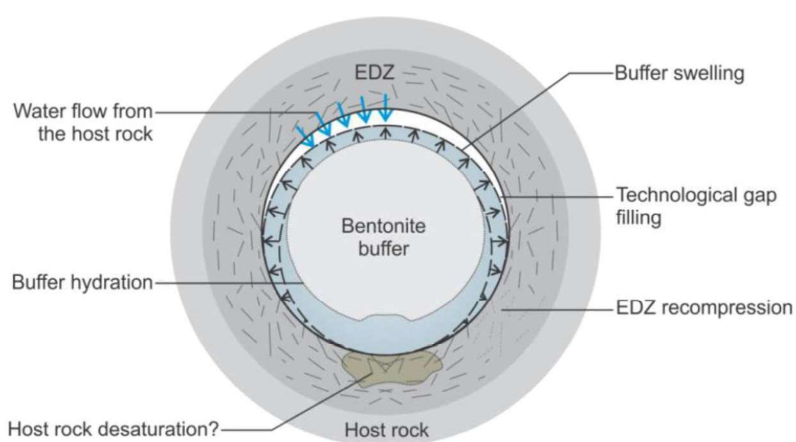

INTRODUCTION

The material involved in the processes are Saturated/Unsaturated porous media

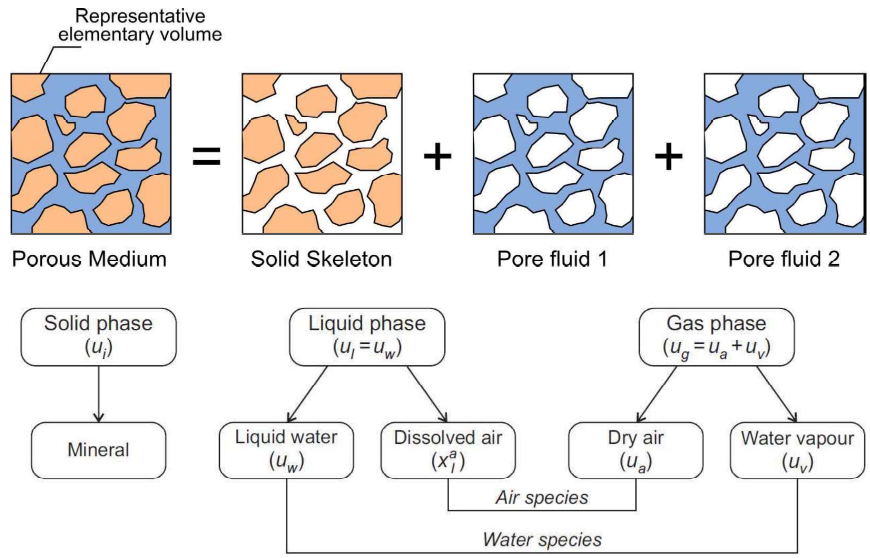

Phases:

Species:

INTRODUCTION

The material involved in the processes are Saturated/Unsaturated porous media

	Solid phase (u_i)	Liquid phase ($u_l = u_w$)	Gas phase ($u_g = u_a + u_v$)
Volume fraction:	$1 - \phi$	$S_r \cdot \phi$	$(1-S_r) \cdot \phi$

Porosity: $$\phi = \frac{\Omega_v}{\Omega} = \frac{\Omega_l + \Omega_g}{\Omega}$$

Saturation: $$S_r = \frac{\Omega_l}{\Omega_v}.$$

Ω_v Porous volume

Ω_l Liquid phase volume

Ω_g Gas phase volume

INTRODUCTION

Repository phases

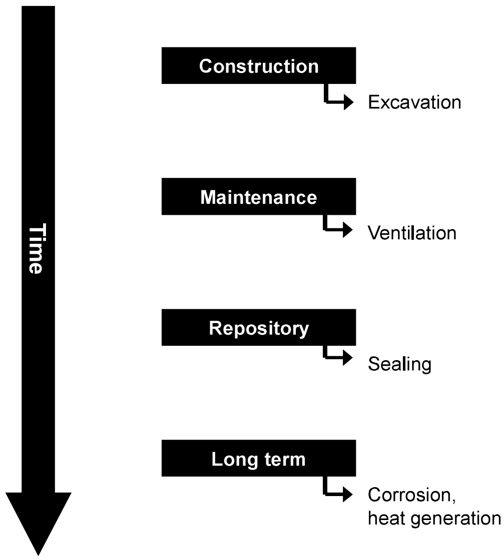

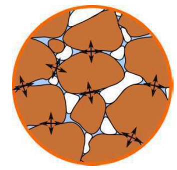

Mechanics

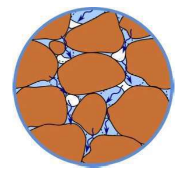

Water and gas flows

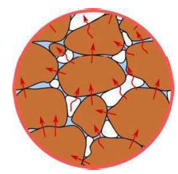

Heat transfer

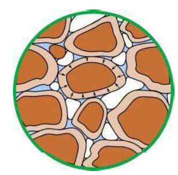

Bio-chemo reaction

TABLE OF CONTENT

THERMO-HYDRAULIC PROCESSES (SATURATED CONDITIONS)

In the sound host rock, the medium remains saturated (most of the time) and the three main processes are heat transfer, liquid transport and mechanical behaviour.

We will focus first on the coupled thermo-hydraulic processes:

- Physical phenomena
- Constitutive equations
- Balance equations

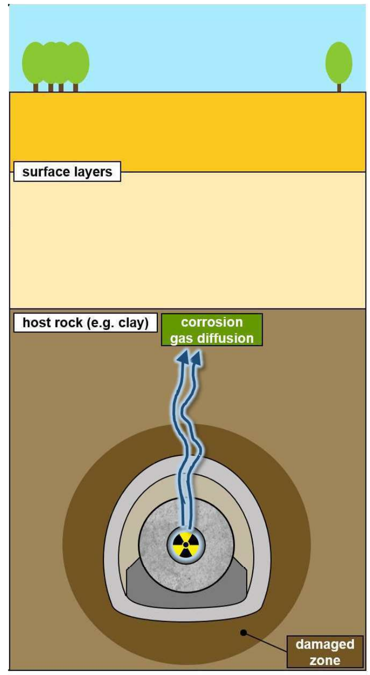

Supercontainer reference design, adapted from *Grunwald (2021).*

THERMO-HYDRAULIC PROCESSES (SATURATED CONDITIONS)

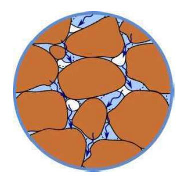

Advection flow of the liquid phase: Darcy's law

$$\underline{q_l} = -\frac{\underline{\underline{K}}_{int}^{sat}}{\mu_w}\left[\underline{\mathrm{grad}}(p_w) + g\,\rho_w\,\underline{\mathrm{grad}}\,(z)\right]$$

where

- $\underline{\underline{K}}_{int}^{sat}$ [m²] is the intrinsic permeability
- μ_w [Pa.s] is the water dynamic viscosity
- p_w [Pa] is the pore water pressure
- ρ_w [kg/m³] is the liquid water density

THERMO-HYDRAULIC PROCESSES (SATURATED CONDITIONS)

Water properties

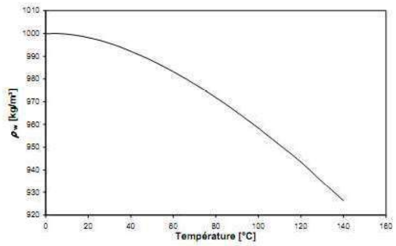

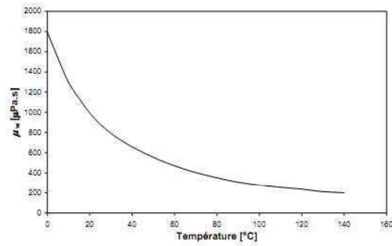

The water dynamic viscosity μ_w [Pa.s] and the liquid water density ρ_w [kg/m³] (related to the thermal dilation coefficient) are a function of the temperature.

$$\alpha_w = 1/\rho_w \frac{\partial \rho_w}{\partial T}$$

α_w [10^{-4} 1/°C] = 4E-06 T^3 - 0,001 T^2 + 0,1404T - 0,3795 [Kell,1975]

$\mu = e^{A+\frac{B}{C+T}}$ [Rumble, 2019]

THERMO-HYDRAULIC PROCESSES (SATURATED CONDITIONS)

Water properties

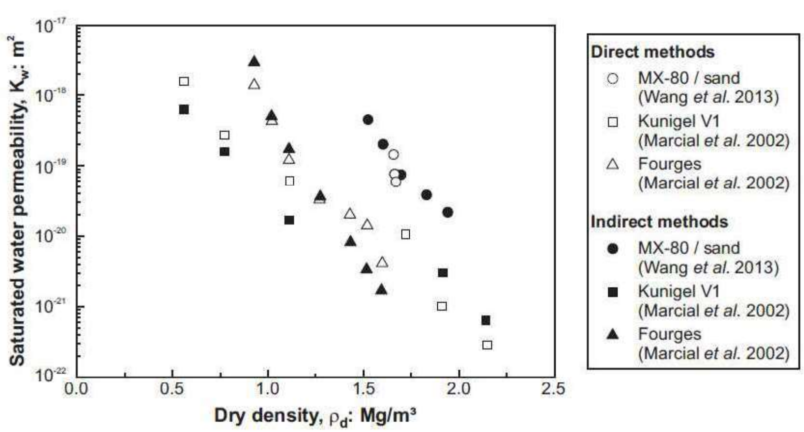

The intrinsic permeability [m²] depends on the density.

Kozeni-Carman law: $$K_w = K_{w0} \frac{\phi^N}{(1-\phi)^M} \frac{(1-\phi_0)^M}{\phi_0^N}$$

THERMO-HYDRAULIC PROCESSES (SATURATED CONDITIONS)

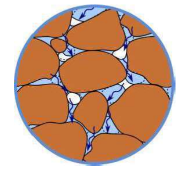

Storage of the liquid phase per unit volume:

$$S_w = \rho_w . n$$

The influence of the temperature on the density explains the thermal pressurization mechanism in undrained conditions:

$$dp = \Pi d\sigma + \Lambda dT$$ [Minh. 2020]

Isotropic case

$$\begin{cases} \Pi = \dfrac{-\frac{b}{K}}{\frac{b^2}{K} + \frac{b-\phi}{K_s} + \frac{\phi}{K_w}} \\ \Lambda = \dfrac{3\phi(\alpha_l - \alpha)}{\frac{b^2}{K} + \frac{b-\phi}{K_s} + \frac{\phi}{K_w}} \end{cases}$$

THERMO-HYDRAULIC PROCESSES (SATURATED CONDITIONS)

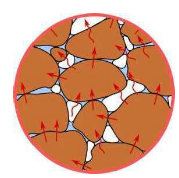

Modes of heat transfer

- *Conduction*

Heat transfer by direct contact of particles

- *Advection*

Heat transfer by mass movement

The term convection is used when the mass movement is driven by buoyancy (density differences) caused by the thermal field

- *Radiation*

Heat transfer by electromagnetic waves

THERMO-HYDRAULIC PROCESSES (SATURATED CONDITIONS)

Modes of heat transfer

- *Conduction : Fourier's law*

$$\underline{i}_{cond} = -\Gamma_m . \underline{grad}(T)$$

Γ_m is the thermal conductivity of the medium. It depends on the thermal conductivity of its constituents (solid and liquid phase).

Serial constituents (S + L): $1/\Gamma_m = 1/\Gamma_s(1-n) + 1/\Gamma_w\, n$

Constituents in parallel (S+L): $\Gamma_m = \Gamma_s(1-n) + \Gamma_w\, n$

Geometric mean (S+L): $\Gamma_m = \Gamma_s{}^{(1-n)} + \Gamma_w{}^{n}$

THERMO-HYDRAULIC PROCESSES (SATURATED CONDITIONS)

Modes of heat transfer

- *Internal energy per unit volume*

$$\rho_m c_{p,m}(T - T_0)$$

where ρ_m is the density of the medium, $c_{p,m}$ is the heat capacity of the medium (under constant pressure).

In order to evidence the influence of each constituent, an additive formulation is also used:

$$\rho_s c_{p,s}(1-n)(T - T_0) + \rho_w c_{p,w} n (T - T_0)$$

THERMO-HYDRAULIC PROCESSES (SATURATED CONDITIONS)

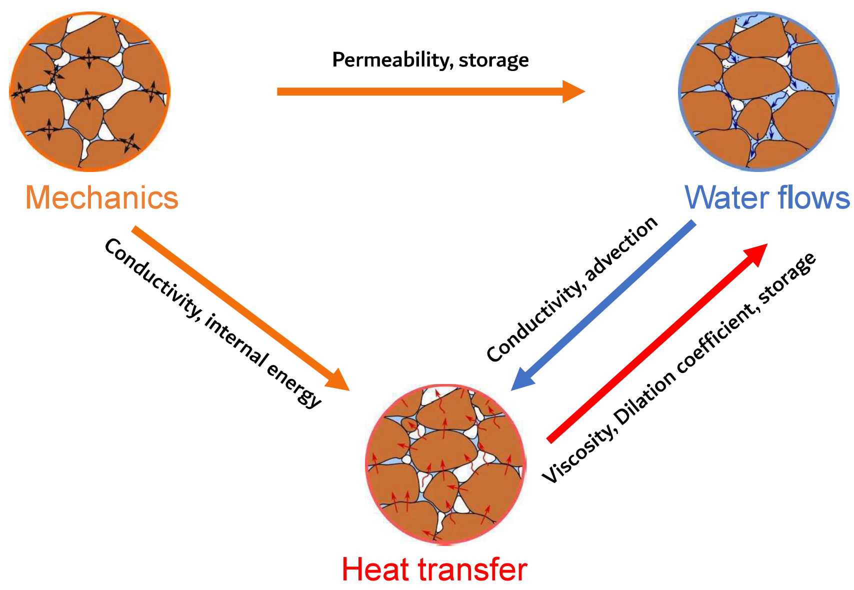

eurad

THERMO-HYDRAULIC PROCESSES (SATURATED CONDITIONS)

Balance equations

- **Water mass balance**

$$\frac{\partial}{\partial t}(\rho_w\, n) + \mathrm{div}\left(\underline{f_w}\right) - Q_w = 0 \qquad \underline{f_w} = \rho_w\, \underline{q_l}$$

- **Internal energy balance**

$$\frac{\partial S_T}{\partial t} + \mathrm{div}\left(\underline{V_T}\right) - Q_T = 0$$

$$S_T = n\, \rho_w\, c_{pw}\, (\mathrm{T} - \mathrm{T}_0) + (1-n)\, \rho_s\, c_{ps}\, (\mathrm{T} - \mathrm{T}_0)$$

$$V_T = -\Gamma\, \nabla \mathrm{T} + c_{pw}\, \rho_w\, \underline{q_l}\, (\mathrm{T} - \mathrm{T}_0)$$

eurad

THERMO-HYDRAULIC PROCESSES (SATURATED CONDITIONS)

Praclay heater test in Mol

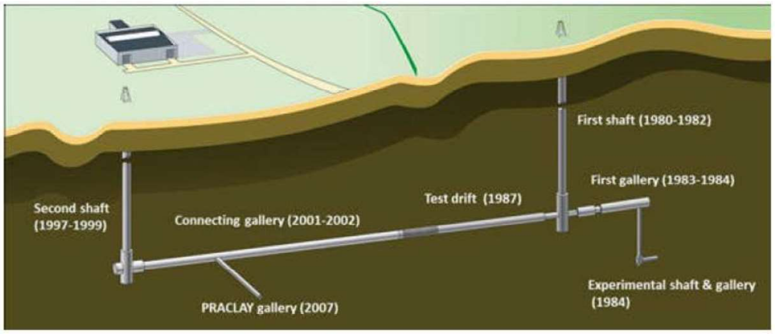

Layout of the underground laboratory at Mol, Belgium (EURIDICE website, 2018)

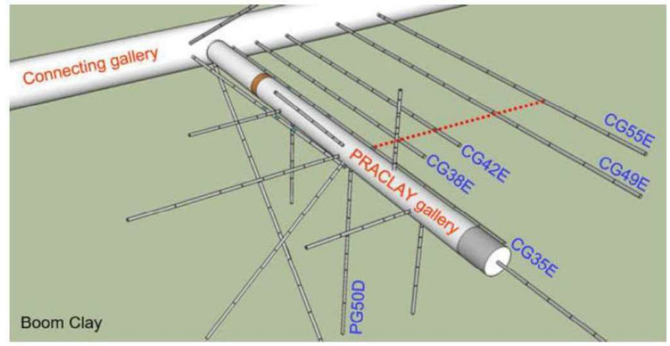

Layout of the monitoring boreholes around the PRACLAY gallery

THERMO-HYDRAULIC PROCESSES (SATURATED CONDITIONS)

Benchmark excercise (EURAD-HITEC WP – Task 2.3)

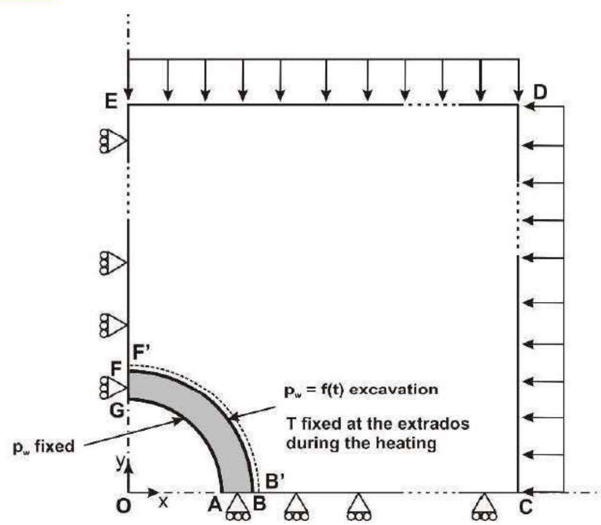

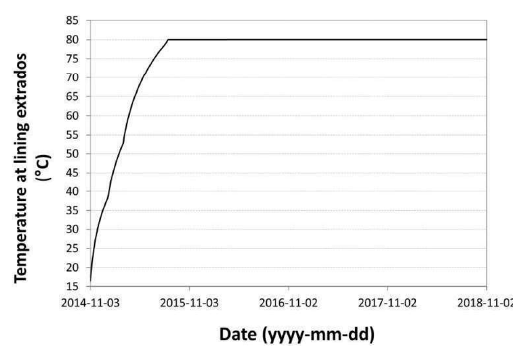

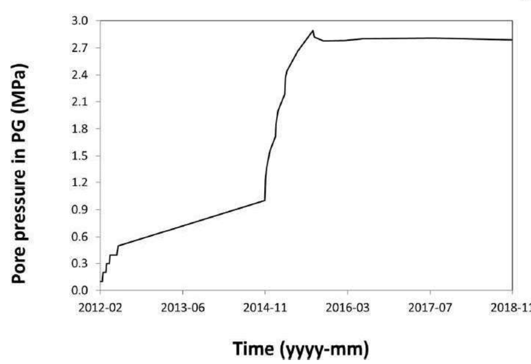

THERMO-HYDRAULIC PROCESSES (SATURATED CONDITIONS)

Monitoring boreholes around the PRACLAY gallery

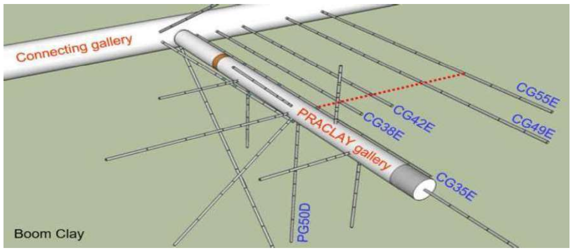

Main physical, thermo-hydraulic parameters for the Boom Clay

Material parameters		Boom Clay
Solid phase density [kg/m³]	ρ_s	2639
Porosity [-]	n	0.39
Vertical intrinsic permeability [m²]	k_v	$2E^{-19}$
Horizontal intrinsic permeability [m²]	k_h	$4E^{-19}$
Vertical thermal conductivity [W/mK]	λ_v	1.31
Horizontal thermal conductivity [W/mK]	λ_h	1.65
Linear thermal expansion coefficient [°C⁻¹]	α_s	$1E^{-5}$
Solid phase specific heat [J/(kg.K)]	C_p	769
Young's modulus parallel to bedding [MPa]	$E_{\parallel}$	400
Young's modulus normal to bedding [MPa]	$E_{\perp}$	200
Poisson's ratio parallel to bedding [-]	$\nu_{\parallel\parallel}$	0.25
Poisson's ratio normal to bedding [-]	$\nu_{\parallel\perp}$	0.25
Shear modulus normal to bedding [MPa]	$G_{\perp}$	80

Evolution of temperature

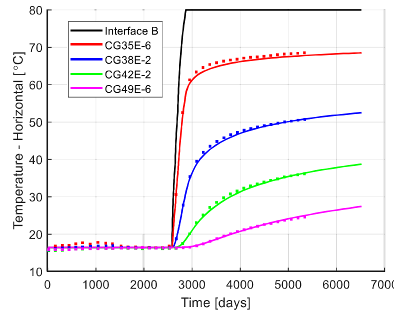

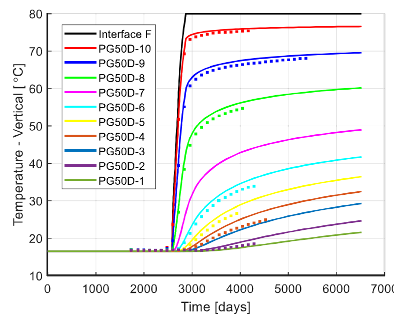

Conclusions:

- Anisotropy of the thermal conductivity
- Negligible influence of the water advection

THERMO-HYDRAULIC PROCESSES (SATURATED CONDITIONS)

Benchmark excercise: Near field case (EURAD-HITEC WP – Task 2.3)

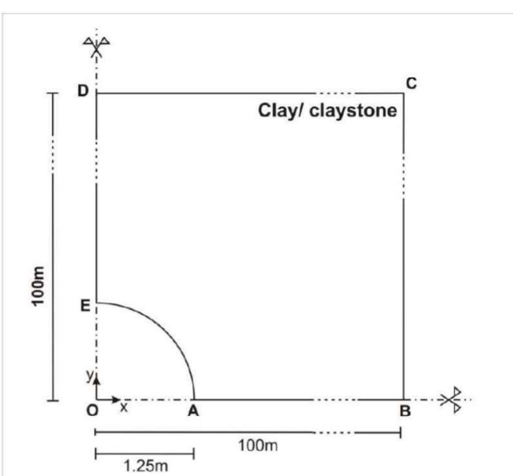

		Boom Clay	COx	OPA
Solid phase density [kg/m3]	ρ_s	2639	2690	2340
Bulk density [kg/m3]	ρ'	2000	2450	2030
Porosity	n	0.39	0.18	0.13
Isotropic intrinsic permeability [m²]	K	$2.83E^{-19}$	$2.3E^{-20}$	$3.0E^{-20}$
Isotropic Young's modulus [MPa]	E	300	7000	6000
Poisson's ratio [-]	ν	0.125	0.3	0.3
Isotropic thermal conductivity [W/m/K]	λ	1.47	1.67	1.85
Linear thermal expansion coefficient [°C⁻¹]	α_s	$1E^{-5}$	$1.25E^{-5}$	$1.7E^{-5}$
Solid phase specific heat [J/kg/K]	c_p	769	978	995

THERMO-HYDRAULIC PROCESSES (SATURATED CONDITIONS)

Benchmark excercise: Near field case (EURAD-HITEC WP – Task 2.3)

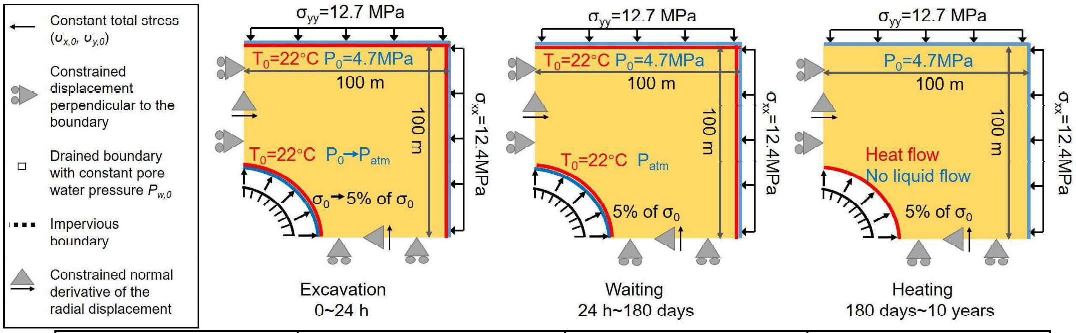

Period	Mechanical conditions	Hydraulic conditions	Thermal conditions
T_0 - T_0 + 24 hours : excavation	Stress reduction to 5% of the initial in-situ stress	Pore pressure reduced to P_{atm} (0.1 MPa)	No flow at the borehole wall
T_0 + 24 hours - T_0 + 6 months : waiting	As above	PP = P_{atm}	As above
T_0 + 6 months - T_0 + 10 years : heating	As above	No flow	Thermal flow outside the lining (200 W/m)

THERMO-HYDRAULIC PROCESSES (SATURATED CONDITIONS)

From experimental values of the density (Kell, 1975), the dilation coefficient is computed as:

$$\alpha_w = 1/\rho_w \frac{\partial \rho_w}{\partial T}$$

α_w [10^{-4} 1/°C] = 4E-06 T^3 - 0,001 T^2 + 0,1404T - 0,3795 [Kell,1975]

$\mu = e^{A+\frac{B}{C+T}}$ [Rumble, 2019]

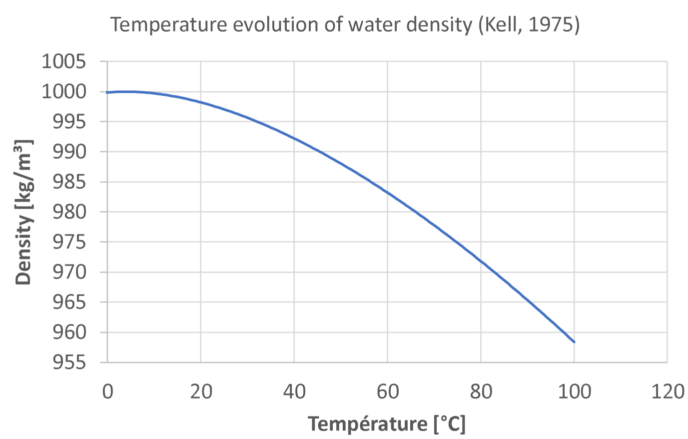

THERMO-HYDRAULIC PROCESSES (SATURATED CONDITIONS)

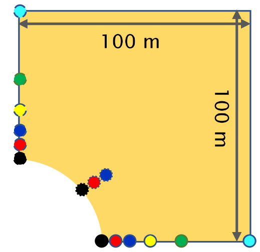

Figure: Schematic distribution of the output nodes

COx in isotropic elasticity

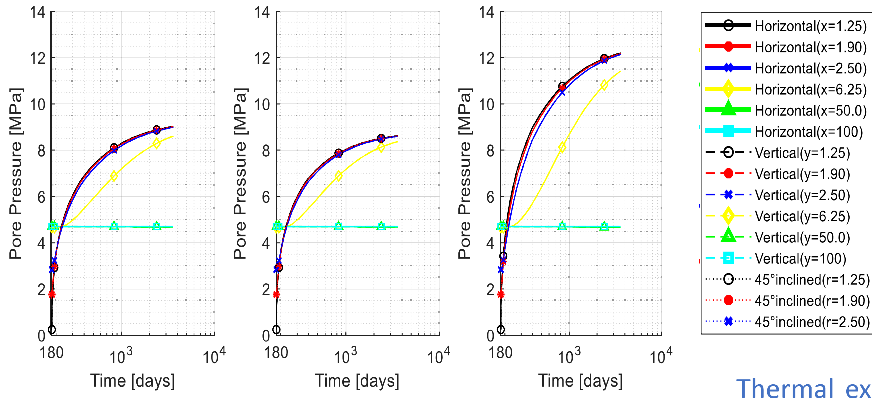

(a) constant value (b) Modified μ (c) modified μ and α_w

Figure: Pore pressure at heating

Thermal expansion coefficient of water has larger influence on the evolution of pore pressure, displacement, etc. than its viscosity.

eurad

THERMO-HYDRAULIC PROCESSES (SATURATED CONDITIONS)

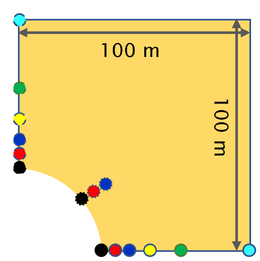

Figure: Schematic distribution of the output nodes

Boom clay in isotropic elasticity

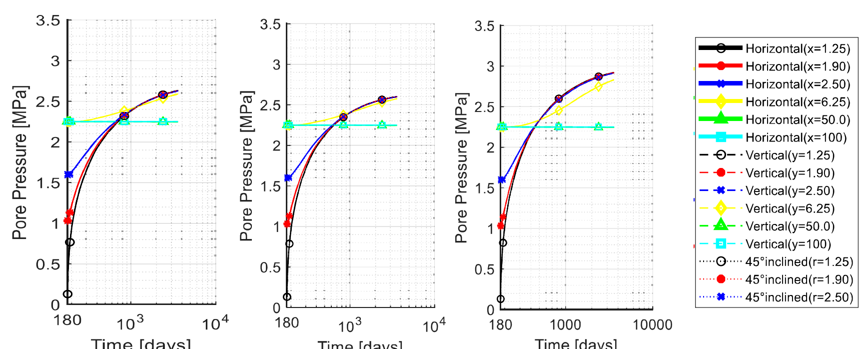

(a) constant value (b) Modified μ (c) modified μ and α_w

Figure: Pore pressure at heating

Thermal expansion coefficient of water has larger influence on the evolution of pore pressure, displacement, etc. than its viscosity.

eurad

THERMO-HYDRAULIC PROCESSES (SATURATED CONDITIONS)

Conclusion :

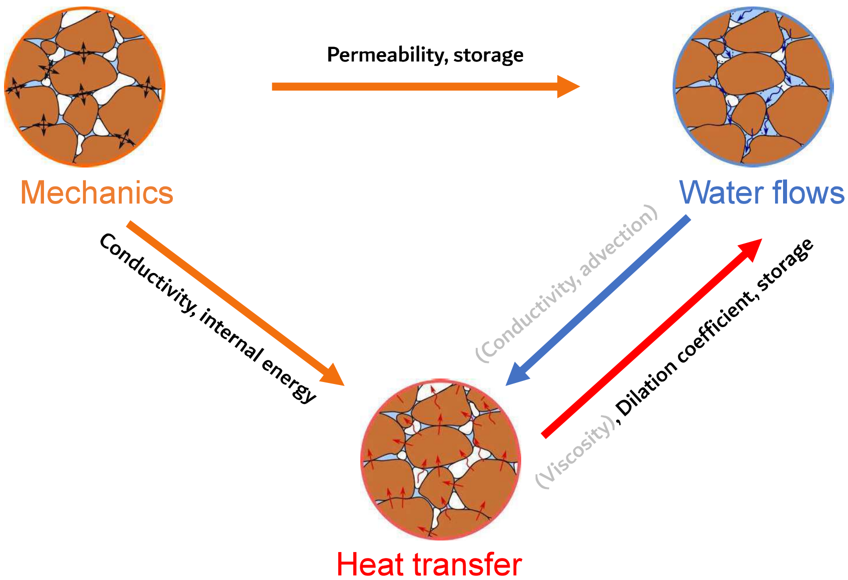

TABLE OF CONTENT

UNSATURATED FLOW PROCESSES

The material involved in the processes are Saturated/Unsaturated porous media

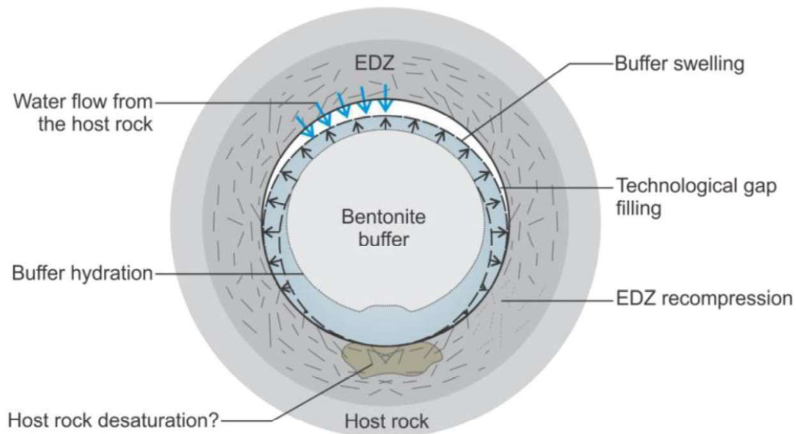

UNSATURATED FLOW PROCESSES

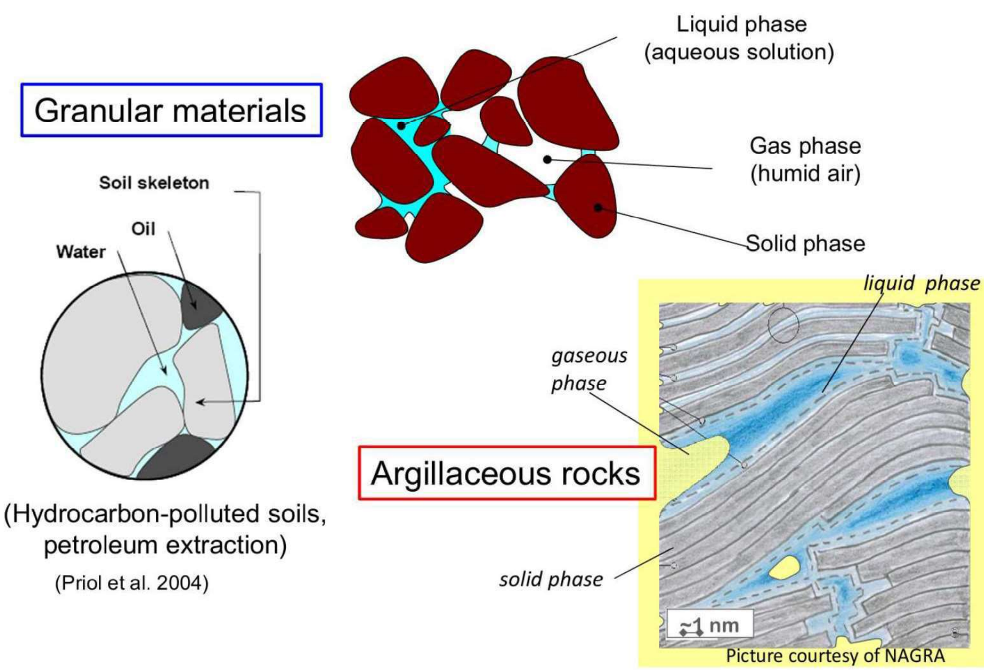

UNSATURATED FLOW PROCESSES

WATER POTENTIAL AND CONCEPT OF SUCTION

The total potential of water ψ is defined as the amount of work (per unit mass of pure Water) required to transport reversibly and isothermally an infinitesimal quantity of water from a reservoir of pure water at a specified elevation and atmospheric pressure to the point under consideration (Aitchison, 1965).

The total potential is often expressed as the sum of four contributions, such that:

$$\psi = \psi_g + \psi_p + \psi_m + \psi_o$$

where ψ_g is the gravitational potential, ψ_p the external pressure potential, ψ_m the matric potential and ψ_o the osmotic potential. The sum of the matric and osmotic potentials is referred to as the internal potential.

UNSATURATED FLOW PROCESSES

WATER POTENTIAL AND CONCEPT OF SUCTION

In soil mechanics, the concept of suction is often used as an alternative to the internal potential. The gravitational and external pressure potentials are indeed not relevant for constitutive modelling of the soil (Gens, 2010). The suction is an energy per unit volume (instead of per unit mass) and is expressed in terms of pressure. The total suction s_t is defined as:

$$s_t = s + \pi_{osm} \qquad s = -\rho_w \psi_m \qquad \pi_{osm} = -\rho_w \psi_o$$

where s is the matric suction and π_{osm} is the osmotic suction. The matric suction is associated to the interactions between liquid and solid, while the osmotic suction is related to differences in water chemistry.

The total suction is directly related to relative humidity.

UNSATURATED FLOW PROCESSES

WATER POTENTIAL AND CONCEPT OF SUCTION

The matric suction *s* contains two distinct contributions, namely the capillary suction and the adsorption suction (Baker & Frydman, 2009; Frydman, 2012; Blatz et al., 2009; Lu & Likos, 2004).

The capillary suction is associated to capillary phenomena, while the adsorption suction results from electrochemical interactions between the water and the clay minerals.

UNSATURATED FLOW PROCESSES

CAPILLARY SUCTION

The surface tension is able to maintain different pressure of liquid and gas in the interface.

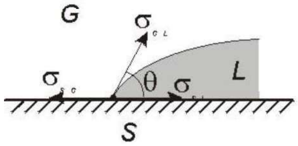

The height of capillary rise depends on the surface tension between the two phases

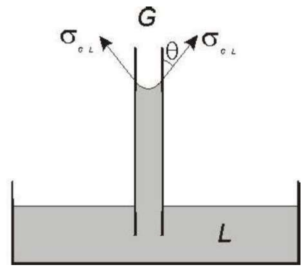

UNSATURATED FLOW PROCESSES

CAPILLARY SUCTION: Laplace's law

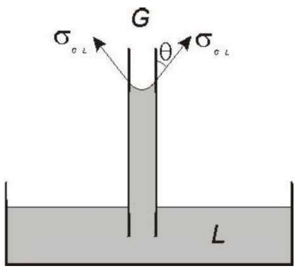

Force equilibrium

$$\pi . r_c^2 . h . \gamma_w = 2\pi . r_c . \sigma_{GL} \cos\theta$$

$$h = \frac{2.\sigma_{GL} \cos\theta}{r_c . \gamma_w}$$

θ : contact angle
σ_{GL} : Surface tension between phases G and L
r_C : capillary tube radius

$$s = p_g - p_w = \gamma_w . h = \frac{2.\sigma_{GL} \cos\theta}{r_c}$$

If $\theta < 90°$, the liquid enters the cavities in the solid surface and the liquid is said to wet the surface

If $\theta < 90°$, the air pressure is partly sustained by the meniscus. The water presure is lower than the air pressure.

UNSATURATED FLOW PROCESSES

CAPILLARY SUCTION: Laplace's law

θ = 0°
σ_{GL} = 0.073 N/m (20°C)
p_g = 100 kPa (absolute pressure)

r (mm)	1	0.01	0.001	10^{-4}
s (kPa)	0.146	14.6	146	1460
p_w (kPa)	99.854	85.4	-46	-1360

UNSATURATED FLOW PROCESSES

CAPILLARY SUCTION: Laplace’s law

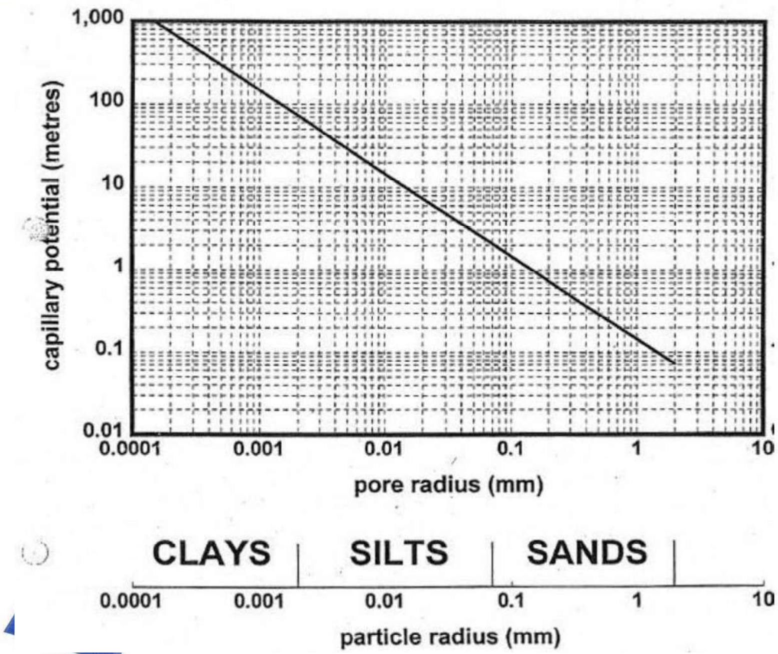

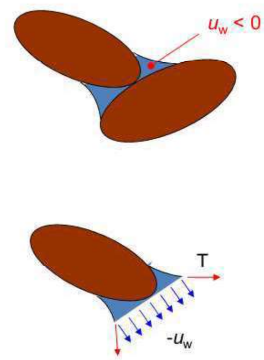

The contact angle of water with the particle surface is less than 90°

The meniscus is concave toward the air side and pore water presure is negative

Particles are stuck together by surface tension and negative pressure

(Ferrari, 2020)

UNSATURATED FLOW PROCESSES

CAPILLARY SUCTION: Laplace’s law

The capillary suction is defined as the gas pressure in excess of the water pressure

$$s = p_g - p_w$$

This definition corresponds to the capillary suction, and not to the matric suction (see Baker & Frydman, 2009, for a discussion). However, essentially for historical reasons, it is used to express quantitatively the degree of attachment of the liquid phase onto the solid phase, regardless the attraction mechanism.

Therefore, the suction as defined by this Equation reflects interactions between water and solid and should be differentiated from capillary phenomena (Gens, 2010).

Very large negative ‘water pressures’ are just an expression of the potential. They do not correspond to the usual bulk thermodynamic pressures.

“*suction must be considered merely as a convenient index of the affinity of soil for free water*” (Blight, 1965)

UNSATURATED FLOW PROCESSES

Retention properties

The water retention curve is defined as the relationship between the amount of water stored in a porous medium and suction. The amount of water stored may be expressed in terms of water content, water ratio or degree of saturation. Yet, the degree of saturation, which provides normalisation of the volume fractions of the liquid and gas phases, is directly involved in the mass balance equations

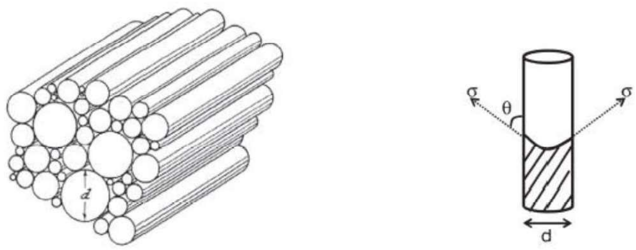

Bundle of capillary tubes model. After [Gates et al., 1950] and [Chen et al., 2013].

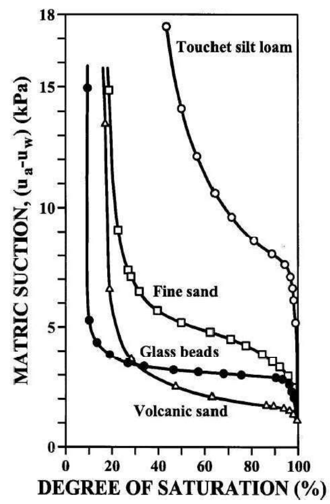

Retention curve [Brooks and Corey, 1964]

UNSATURATED FLOW PROCESSES

Retention properties

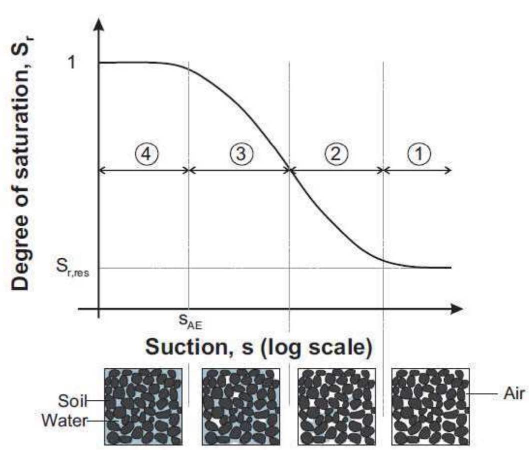

Water retention curve and schematic stages of saturation in porous media (modified after Nuth & Laloui, 2008a)

UNSATURATED FLOW PROCESSES

Retention properties: hysteresis

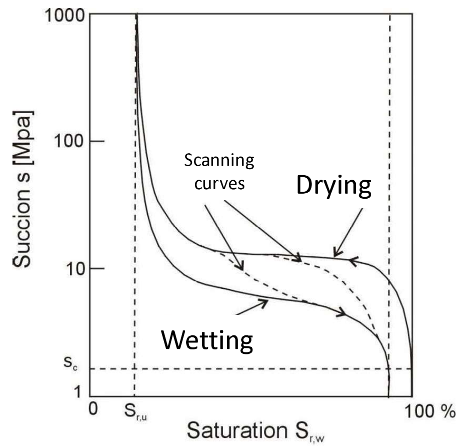

Retention curves

UNSATURATED FLOW PROCESSES

Retention properties: influence of the dry density

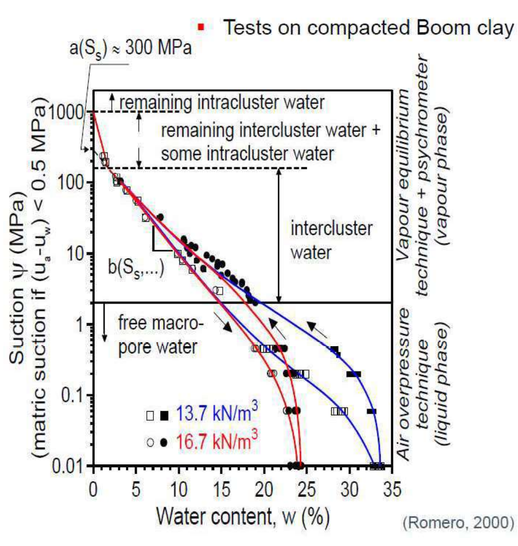

UNSATURATED FLOW PROCESSES

Transfer properties

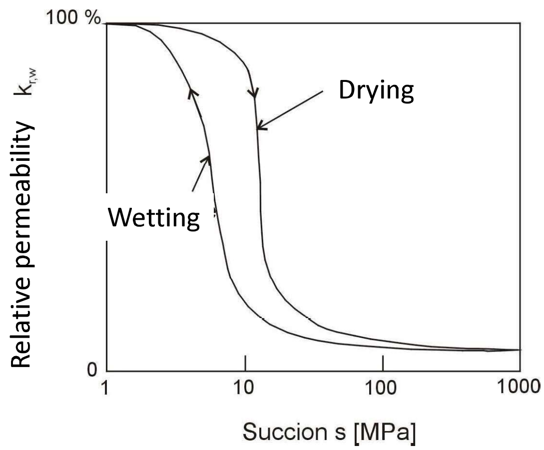

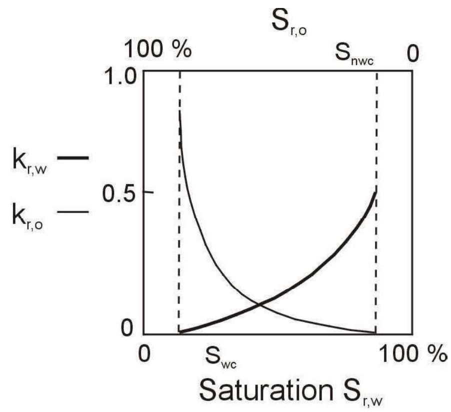

Permeability

UNSATURATED FLOW PROCESSES

Equilibrium restrictions

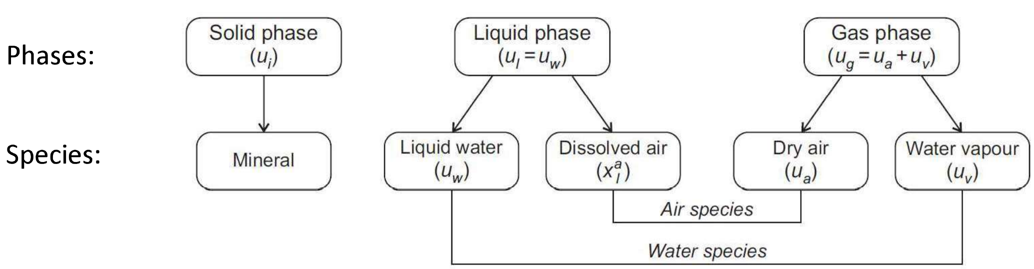

Equilibrium restrictions relate dependent variables with the kinematics variables. They are obtained assuming thermodynamic equilibrium between the different phases of the species. This hypothesis is justified by the fast kinetics of the dissolution processes compared to the transport phenomena.

UNSATURATED FLOW PROCESSES

Equilibrium restrictions: Kelvin's law

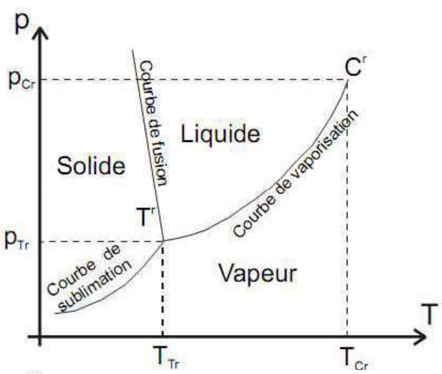

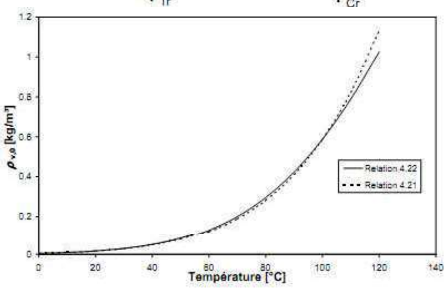

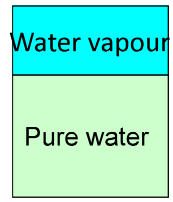

RH = 100%

$$\frac{1}{\rho^{g}_{H_2O,0}} = 194.4\ \exp\left(-0.06374\,(T-273) + 0.1634\,10^{-3}\,(T-273)^2\right)$$

$$p^{g}_{H_2O,0} = \frac{\rho^{g}_{H_2O,0}}{M_{H_2O}} RT$$

UNSATURATED FLOW PROCESSES

Equilibrium restrictions: Kelvin's law

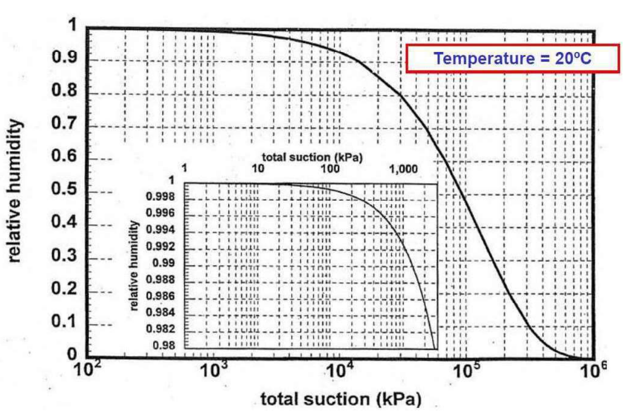

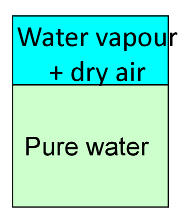

RH < 100%

Kelvin's law: $\rho^{g}_{H_2O} = \rho^{g}_{H_2O,0}.\exp\left(\frac{(p_w - p_g)M_{H_2O}}{\rho_w RT}\right)$

$$RH = \frac{p^{g}_{H_2O}}{p^{g}_{H_2O,0}} = \frac{\rho^{g}_{H_2O}}{\rho^{g}_{H_2O,0}}$$

UNSATURATED FLOW PROCESSES

Equilibrium restrictions: Henry's law

Henry's law expresses the equilibrium between dissolved air in the liquid phase and dry air in the gas phase. Under constant temperature, the amount of dissolved air is proportional to the air partial pressure

$p_a = K_{al}\, x_{al}$

where K_a is a constant. This law may be written in terms of densities, so that

$\rho_{da} = H_a\, \rho_a$

where H_a is called the Henry's constant and is equal to 0.0234 for air.

UNSATURATED FLOW PROCESSES

Balance equations

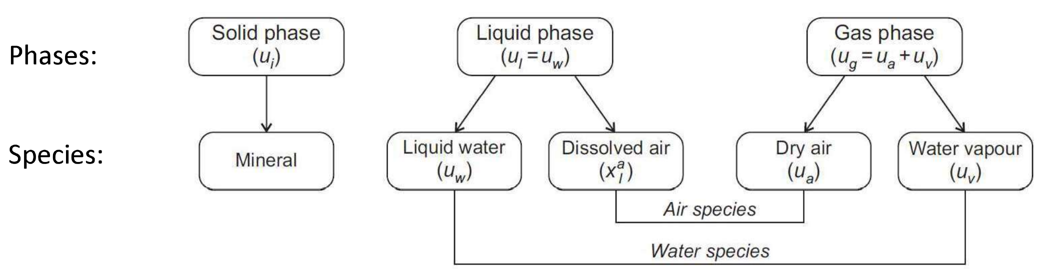

The compositional approach (Panday & Corapcioglu, 1989; Olivella et al., 1994; Collin, 2003) is adopted to establish the mass balance equations. It consists of balancing species rather than phases. This approach has the advantage that phase exchange terms cancel out, which is particularly useful when equilibrium is assumed.

UNSATURATED FLOW PROCESSES

Water Mass Balance

$$\frac{\partial}{\partial t}(\rho_w \, n \, S_{rw}) + \mathrm{div}\left(\underline{f_w}\right) + \frac{\partial}{\partial t}(\rho_v \, n \, S_{rg}) + \mathrm{div}\left(\underline{f_v}\right) - Q_w = 0$$

Liquid water, S_{rw} water saturation degree
Water vapour, $S_{rg} = 1 - S_{rw}$ gas saturation degree
Source term

Gas Mass Balance

$$\frac{\partial}{\partial t}(\rho_{d,a} \, n \, S_{rw}) + \mathrm{div}\left(\underline{f_{d,a}}\right) + \frac{\partial}{\partial t}(\rho_a \, n \, S_{rg}) + \mathrm{div}\left(\underline{f_a}\right) - Q_a = 0$$

Dissolved air, S_{rw} water saturation degree
Dry air, $S_{rg} = 1 - S_{rw}$ gas saturation degree
Source term

eurad

UNSATURATED FLOW PROCESSES

Fluid transfer equations

In both liquid and gas phases, water and air fluxes are a combination of advective and non-advective fluxes. Advective fluxes are associated to the phase movements, while non-advective fluxes are associated to the motion of species within phases. The mass fluxes of liquid water, water vapour, dry gas and dissolved gas are given respectively by

$$\underline{f}_{(H_2O)_l} = \rho_w . \underline{q}_l$$

$$\underline{f}_{(H_2O)_g} = \rho^g_{H_2O} . \underline{q}_g + \underline{i}_{(H_2O)_g}$$

$$\underline{f}_{(Air)_g} = \rho^g_{Air} . \underline{q}_g + \underline{i}_{(Air)_g}$$

$$\underline{f}_{(Air)_d} = \rho^g_{Air} . H_{Air} . \underline{q}_l + \underline{i}_{(Air)_d}$$

eurad

UNSATURATED FLOW PROCESSES

Fluid transfer equations: advective fluxes

Advective fluxes of both liquid and gas phases are described by the generalized Darcy's law for partially saturated porous media.

$$\underline{q_l} = -\frac{\underline{\underline{K_{int}^{sat}}} \cdot k_{rw}}{\mu_w} \left[\underline{\text{grad}}(p_w) + g\,\rho_w\,\underline{\text{grad}}\,(z)\right]$$

where

- $\underline{\underline{K_{int}^{sat}}}$ [m²] is the intrinsic permeability
- k_{rw} [-] is the water relative permeability function
- μ_w [Pa.s] is the water dynamic viscosity
- p_w [Pa] is the pore water pressure
- ρ_w [kg/m³] is the liquid water density

UNSATURATED FLOW PROCESSES

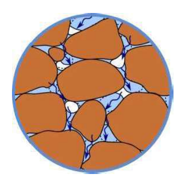

Transfer properties

The intrinsic permeability [m²] depends on the density.

Kozeni-Carman law: $$K_w = K_{w0} \frac{\phi^N}{(1-\phi)^M} \frac{(1-\phi_0)^M}{\phi_0^N}$$

The intrinsic permeability depends on the pore size (and the interconnectivity of the pores)

The pore size of expansive clays may change very significantly due to hydration (even during constant volume conditions)

UNSATURATED FLOW PROCESSES

Transfer properties

The intrinsic permeability [m²] to gas and liquid are not the same !

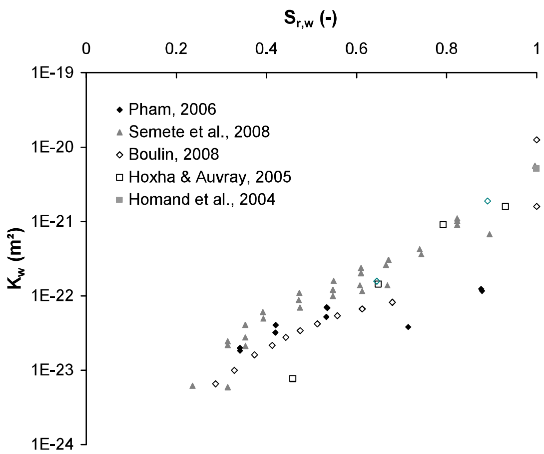

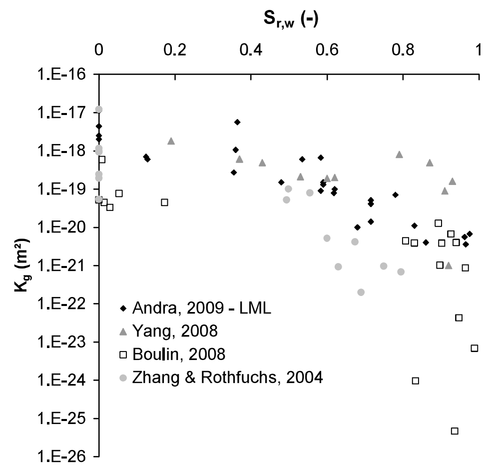

UNSATURATED FLOW PROCESSES

Fluid transfer equations: advective fluxes

Advective fluxes of both liquid and gas phases are described by the generalized Darcy’s law for partially saturated porous media.

$$\underline{q_g} = -\frac{\underline{\underline{K_{int}^{sat}}} \cdot k_{rg}}{\mu_g}\left[\underline{\mathrm{grad}}(p_g) + g\,\rho_g\,\underline{\mathrm{grad}}\,(z)\right]$$

where

- $\underline{\underline{K_{int}^{sat}}}$ [m²] is the intrinsic permeability
- k_{rg} [-] is the gas relative permeability function
- μ_g [Pa.s] is the gas dynamic viscosity
- p_g [Pa] is the pore gas pressure
- ρ_g [kg/m³] is the gas density

UNSATURATED FLOW PROCESSES

Fluid transfer equations: non-advective fluxes

The diffusive fluxes are governed by Fick's law. According to Fick's law, the diffusive flux is proportional to the gradient of mass fraction of species, the proportionality coefficient being the hydrodynamic dispersion coefficient. The diffusive fluxes of water vapour and dissolved air read

Diffusion within the gaseous phase

$$\underline{i}_v = -n\, S_{rg}\, \tau\, D_{v/a} \rho_g\, \underline{\mathrm{grad}}\, (\rho_v/\rho_g) = -\underline{i}_a$$

- $D_{v/a}$ [m²/s] is the diffusion coefficient of water vapour in dry air
- τ [-] is the tortuosity

$D_{v/a} = D_0 \frac{p_0}{p_g} \left(\frac{T}{T_0}\right)^{1,75}$ with p_0=101 kPa, D_0= 2.42 10^{-5} m²/s and T_0=303°K

eurad

UNSATURATED FLOW PROCESSES

Fluid transfer equations: non-advective fluxes

The diffusive fluxes are governed by Fick's law. According to Fick's law, the diffusive flux is proportional to the gradient of mass fraction of species, the proportionality coefficient being the hydrodynamic dispersion coefficient. The diffusive fluxes of water vapour and dissolved air read

Diffusion within the liquid phase

$$\underline{i}_{d,a} = -n\, S_{rw}\, \tau\, D_{d-a/w} \rho_w\, \underline{\mathrm{grad}}\, (\rho_{\boldsymbol{d},\boldsymbol{a}}/\rho_w)$$

- $D_{d-a/w}$ [m²/s] is the diffusion coefficient of dissolved air in water

eurad

UNSATURATED FLOW PROCESSES

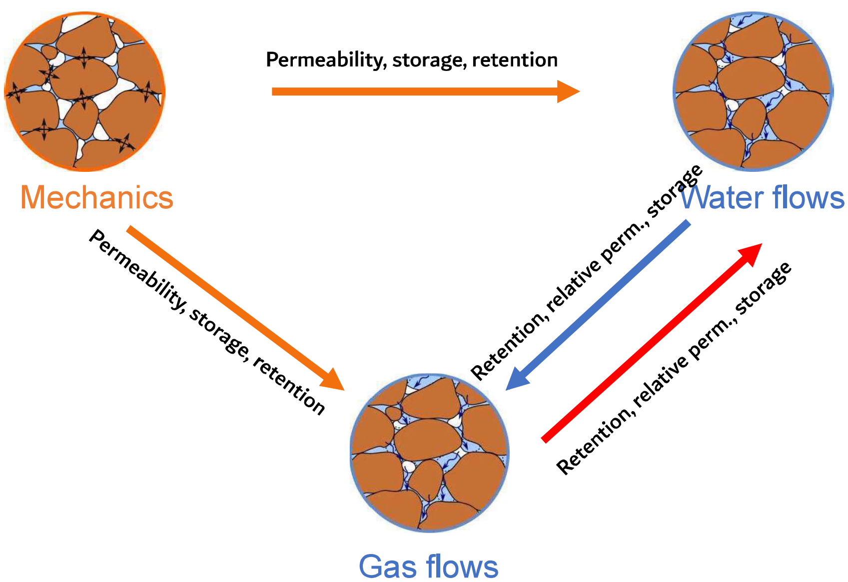

UNSATURATED FLOW PROCESSES

Balance equations

- Water mass balance

$$\frac{\partial}{\partial t}(\rho_w \, n \, S_{rw}) + \mathrm{div}\left(\underline{f_w}\right) + \frac{\partial}{\partial t}(\rho_v \, n \, S_{rg}) + \mathrm{div}\left(\rho_v \, \underline{q_g} + \underline{i_v}\right) - Q_w = 0$$

- **Gas mass balance**

$$\frac{\partial}{\partial t}(\rho_{d,a} \, n \, S_{rw}) + \mathrm{div}\left(\rho_{d,a} \, \underline{q_l} + \underline{i_{d,a}}\right) + \frac{\partial}{\partial t}(\rho_a \, n \, S_{rg}) + \mathrm{div}\left(\rho_a \, \underline{q_g} + \underline{i_a}\right) - Q_a = 0$$

UNSATURATED FLOW PROCESSES

Liakopoulos (1965) experiment on a column of del Monte sand

Benchmark exercise*

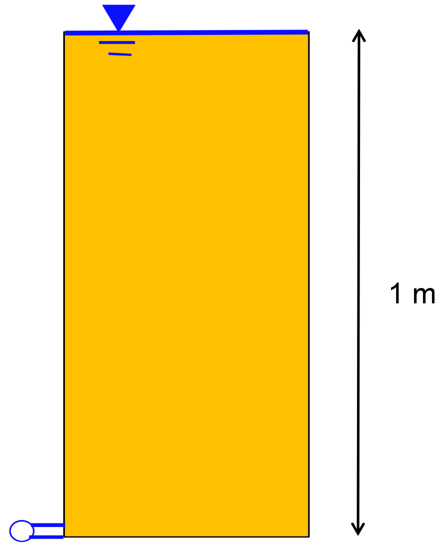

- JOMMI C., VAUNAT J., GENS A., GAWIN D. & SCHREFLER B. – Multiphase flow in porous media : a numerical benchmark – Proceedings NAFEMS World Congress Stuttgart, 1997.
- VAUNAT J., GENS A. & JOMMI C. – A Strategy for Numerical Analysis of the Transition between Saturated and Unsaturated Flow Conditions – Numerical Models in Geomechanics, pp. 297-302, 1997.

UNSATURATED FLOW PROCESSES

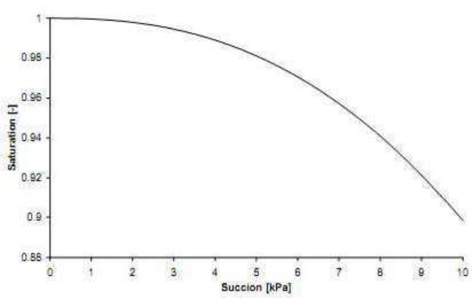

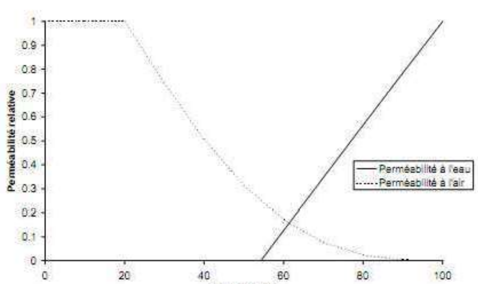

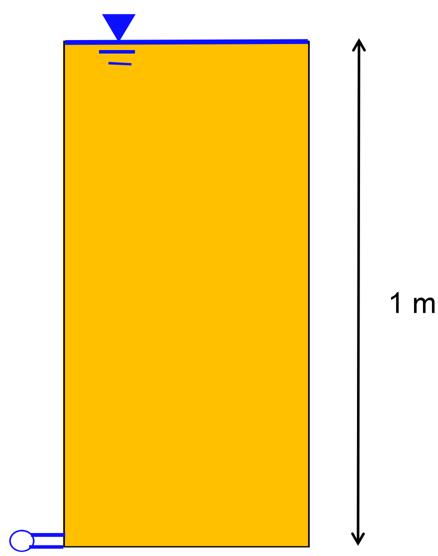

UNSATURATED FLOW PROCESSES

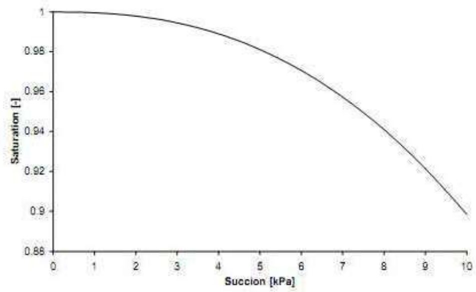

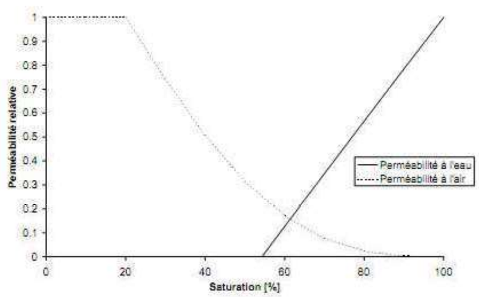

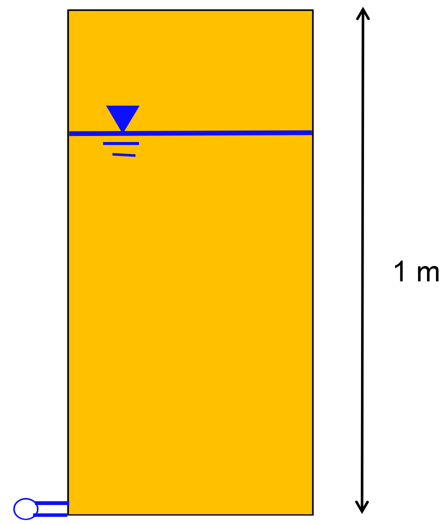

UNSATURATED FLOW PROCESSES

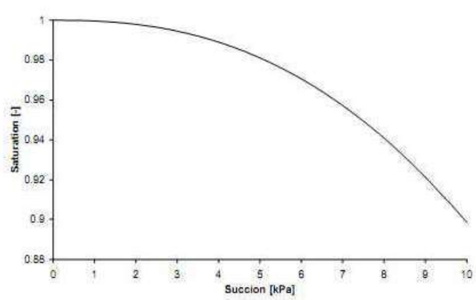

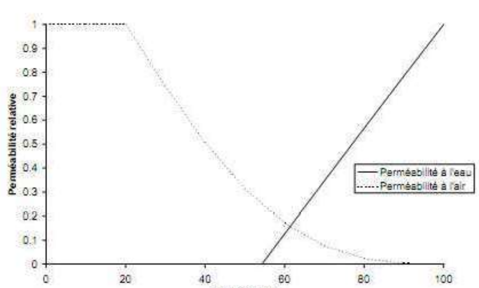

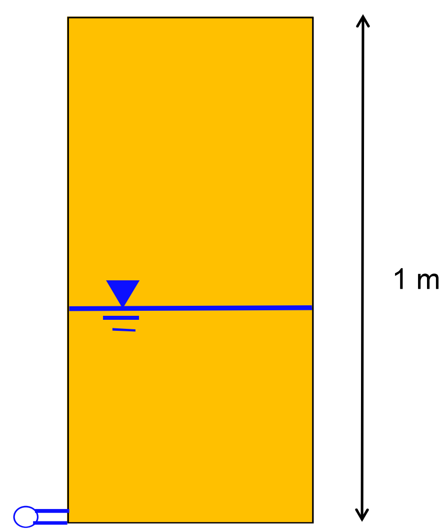

UNSATURATED FLOW PROCESSES

Modelling with fixed gas pressure

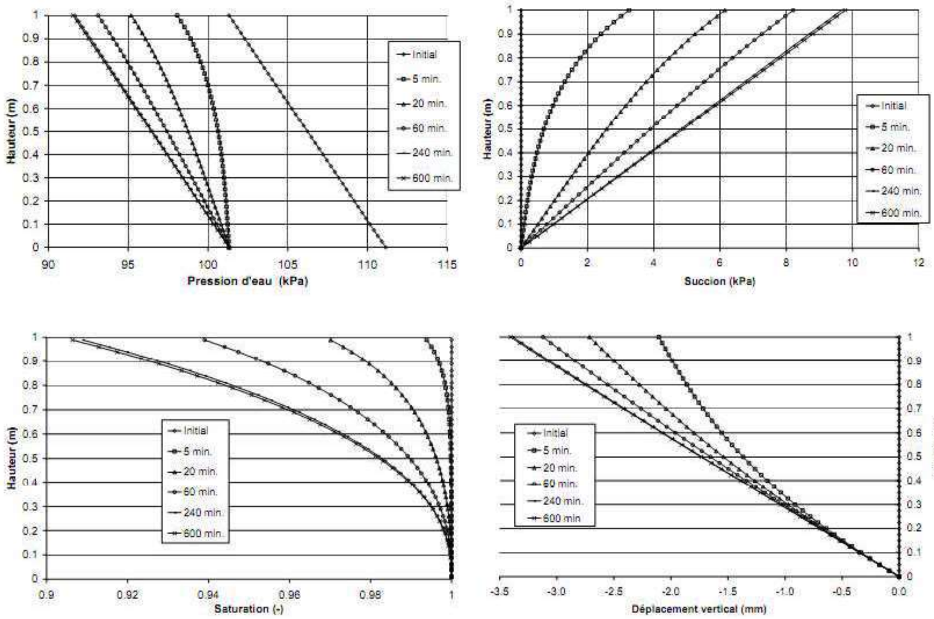

eurad

UNSATURATED FLOW PROCESSES

Modelling with variable gas pressure (+dissolved gas)

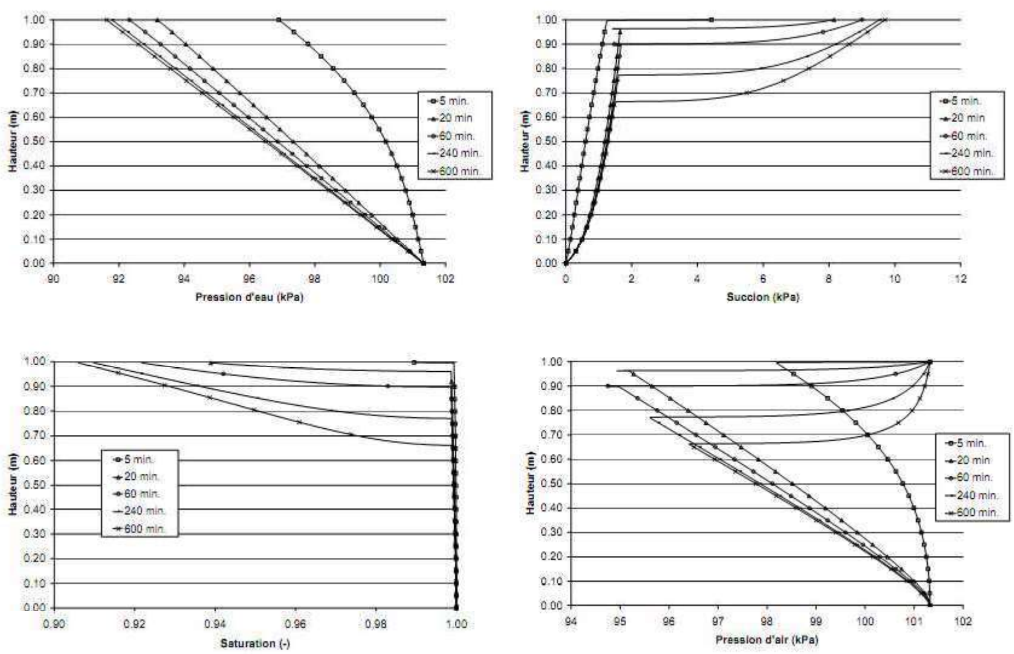

eurad

UNSATURATED FLOW PROCESSES

Benchmark exercise to study the gas migration around a drift

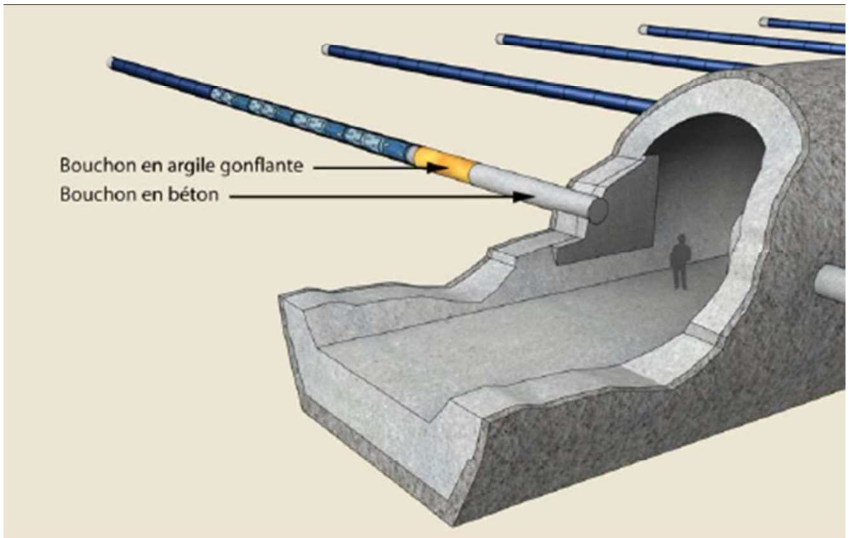

UNSATURATED FLOW PROCESSES

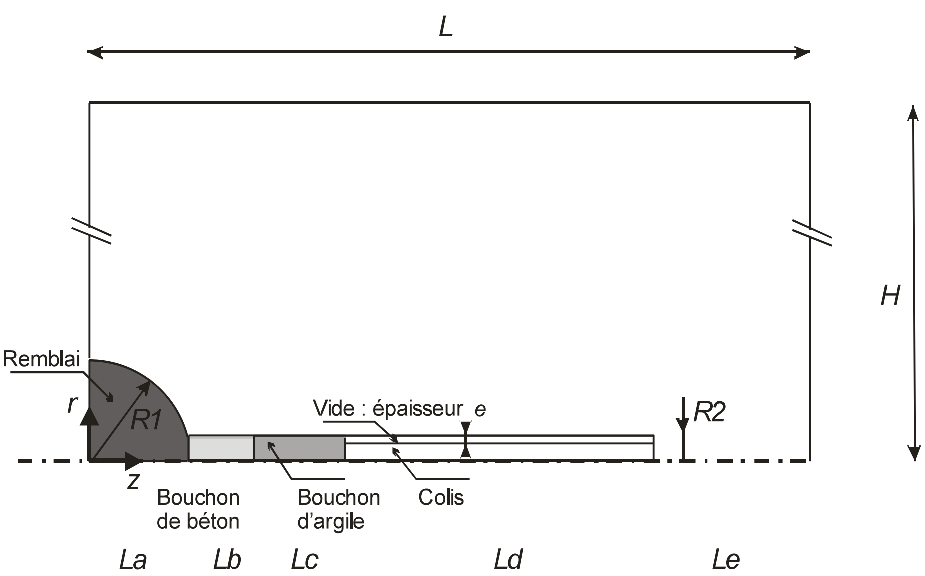

UNSATURATED FLOW PROCESSES

Geometry

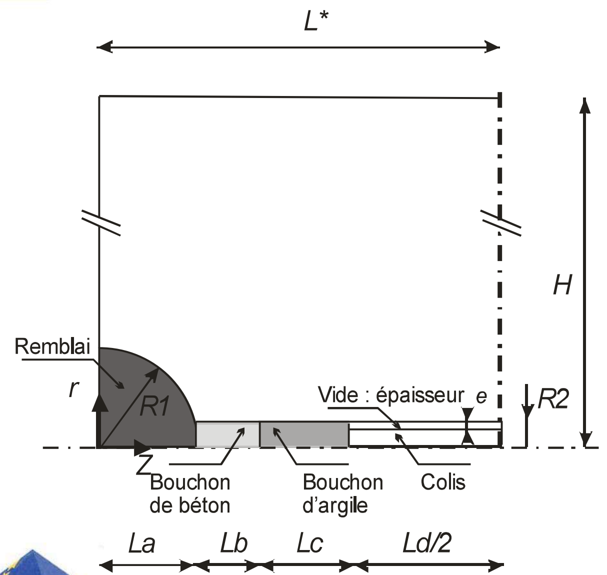

H = 82 m

L = 51 m

R1 = La = 4 m

Lb = 3.3 m

Lc = 3 m

Ld = 30.7 m

Le = 10 m

R2 = 0.35 m

E = 0.0125 m

UNSATURATED FLOW PROCESSES

Initial conditions

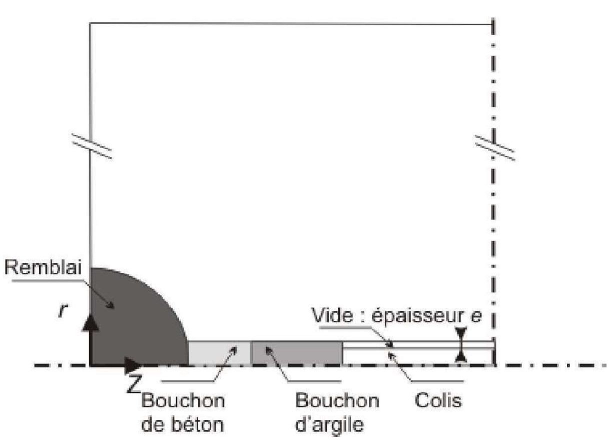

Clay rock:

σ_0 = 12.3 MPa
P_w = 5 MPa
P_g = 0.1 MPa
T = 303°K

Swelling clay:

σ_0 = 0.1 MPa
$S_{r,w}$ = 0.80
P_g = 0.1 MPa
T = 303°K

Concrete plug:

σ_0 = 0.1 MPa
P_w = 0.1 MPa
P_g = 0.1 MPa
T = 303°K

Backfill:

σ_0 = 0.1 MPa
Sr,w = 0.80
P_g = 0.1 MPa
T = 303°K

UNSATURATED FLOW PROCESSES

Modelling steps and boundary conditions

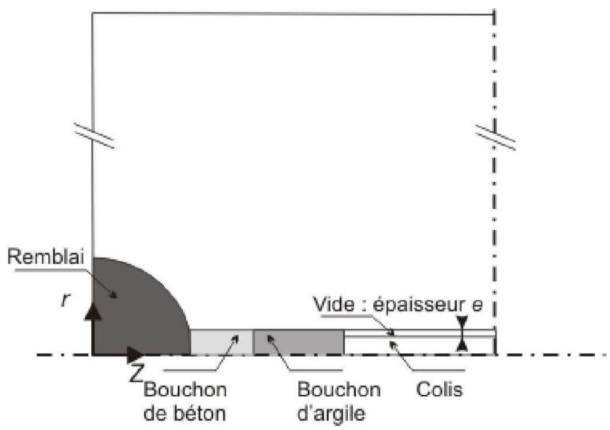

- **Step 1** : Excavation and waiting phase (→ 2 years)
- **Step 2** : Water resaturation of the void space and activation of the plugs (→ 3 years)
- **Step 3** : Hydrogene production and backfilling (→ 100 000 years)

UNSATURATED FLOW PROCESSES

Boundary conditions - Step 1 : Excavation + Waiting phase

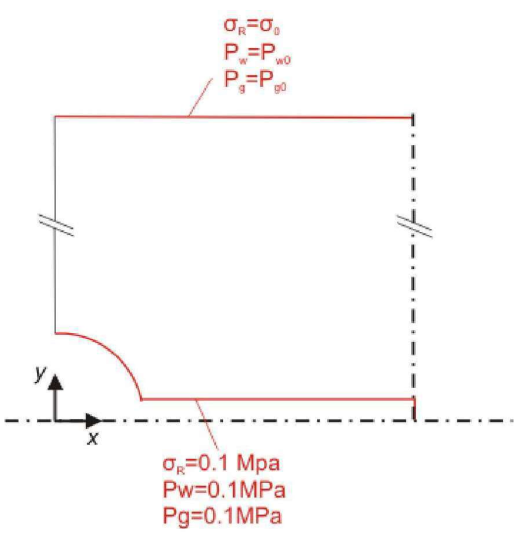

Simultaneous excavation of the main drift and the alveole (→ 3 days) :

Deconfinement ➔ σ_R decreased at the wall down to P_{atm}

Drained condition ➔ P_w decreased to P_{atm}

P_g fixed

UNSATURATED FLOW PROCESSES

Boundary conditions - Step 1 : Excavation + Waiting phase

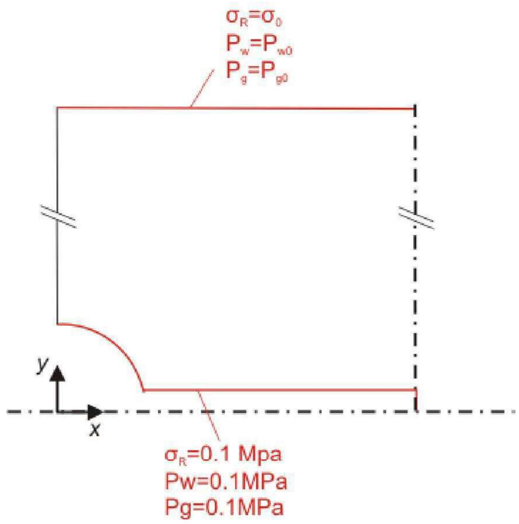

Waiting phase (→ 2 years) :

σ_R = 0.1 MPa

Drained condition

Pg fixed

UNSATURATED FLOW PROCESSES

Boundary conditions - Step 2 : Activation of the plugs and the cannisters + water Resaturation of the void space

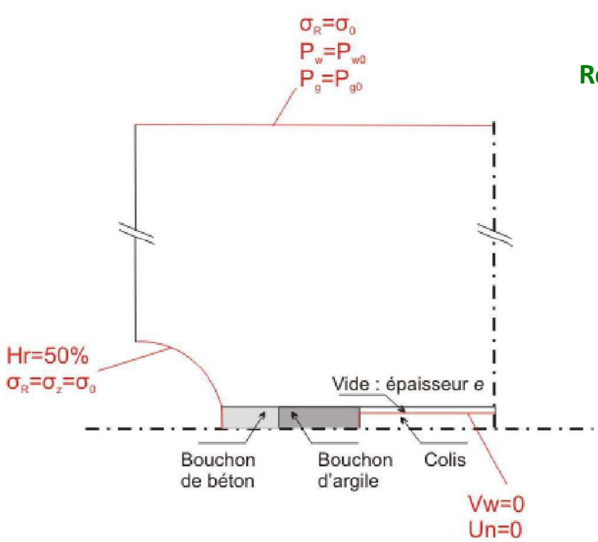

Resaturation of the void space (→ 3 years):

Pg fixed

<u>Main shaft</u>

Constant relative humidity

σ_R = σ_z = 0.1 MPa

<u>Alveole</u>

Cannister: impervious to fluids ➔ Resaturation of the void space

Fixed radial displacement

UNSATURATED FLOW PROCESSES

Boundary conditions - Step 3 : Hydrogene Injection + Backfilling

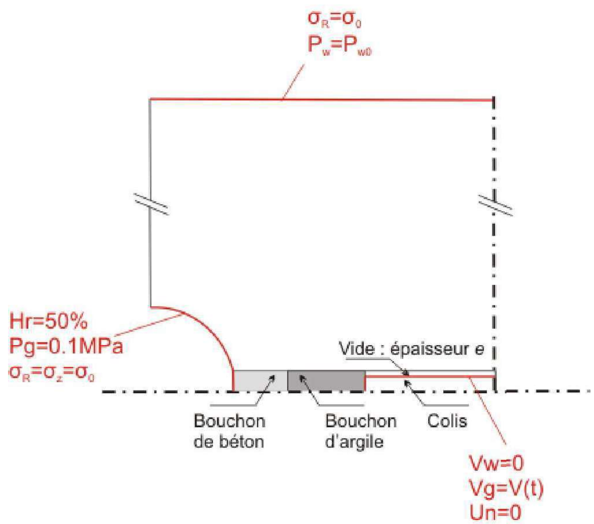

Hydrogene Injection without backfill
(3→ 100 years):

<u>Main drift</u>

Constant relative humidity

Pg = 0.1 MPa at the wall

$\sigma_R = \sigma_z = 0.1$ MPa

<u>Alveole</u>

Cannister impervious to fluid

Hydrogene flux imposed at the wall

Fixed radial displacement

UNSATURATED FLOW PROCESSES

Boundary conditions - Step 3 : Hydrogene Injection + Backfilling

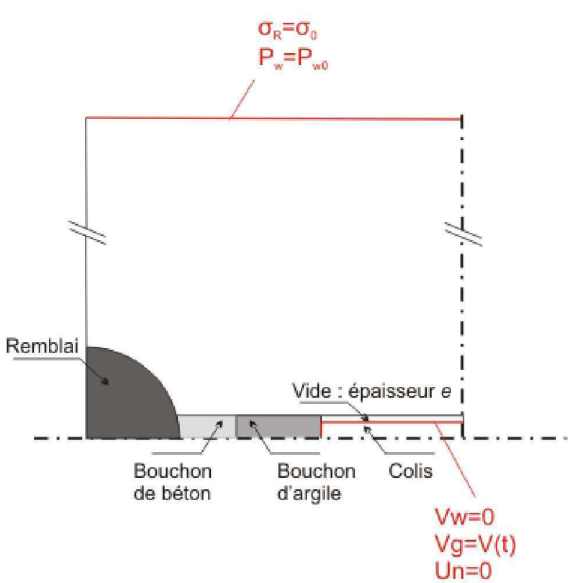

Hydrogene injection with the backfill
(100→ 100 000 years):

<u>Main drift</u>

-

<u>Alveole</u>

Cannister impervious to fluid

Hydrogene flux imposed at the wall

Fixed radial displacement

UNSATURATED FLOW PROCESSES

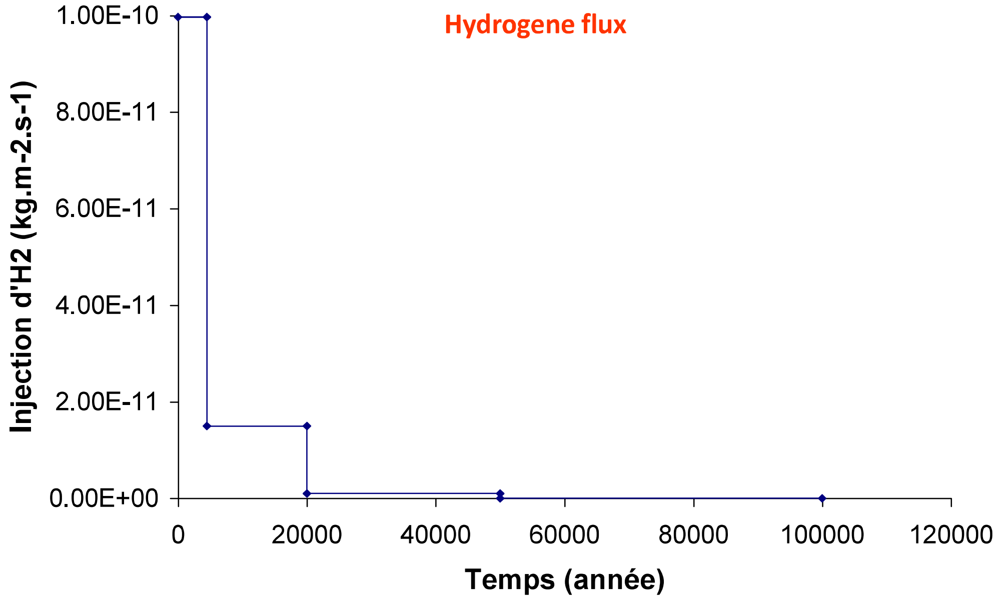

UNSATURATED FLOW PROCESSES

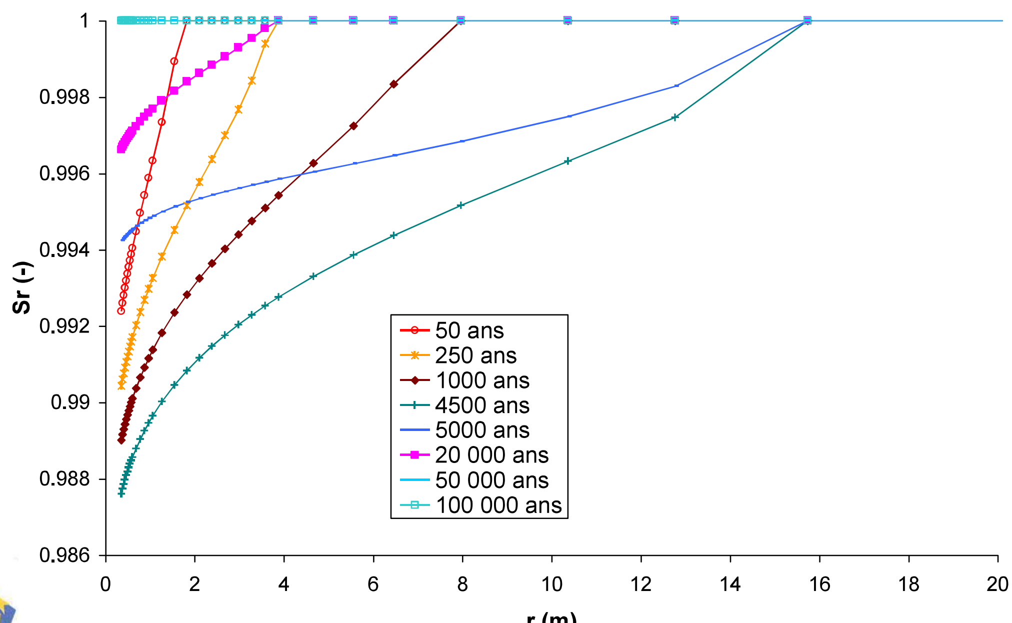

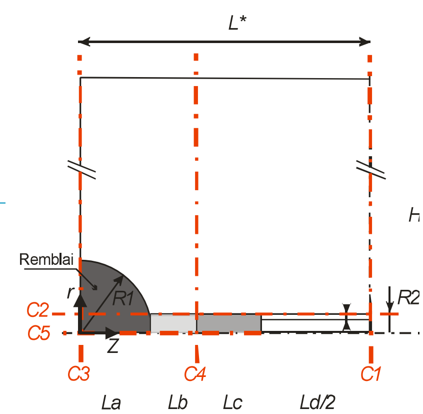

UNSATURATED FLOW PROCESSES

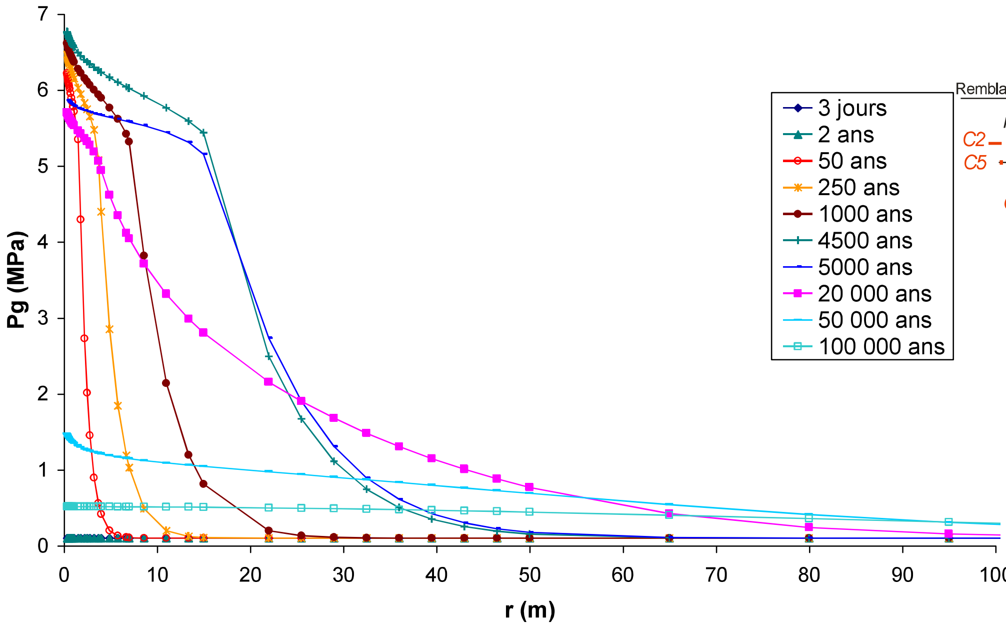

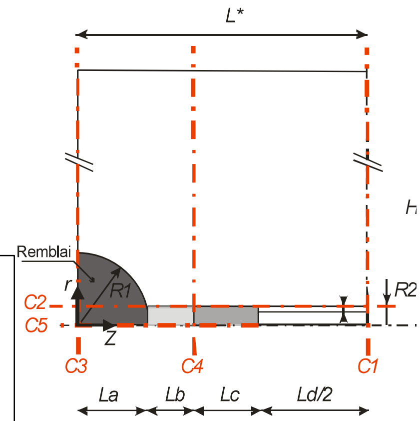

UNSATURATED FLOW PROCESSES

Total imposed flux = Gaseous Flux + dissolved Flux

- Unsaturated Zone → Gaseous Flux >>> Dissolved Flux
- Saturated Zone → Dissolved Flux > Gaseous Flux

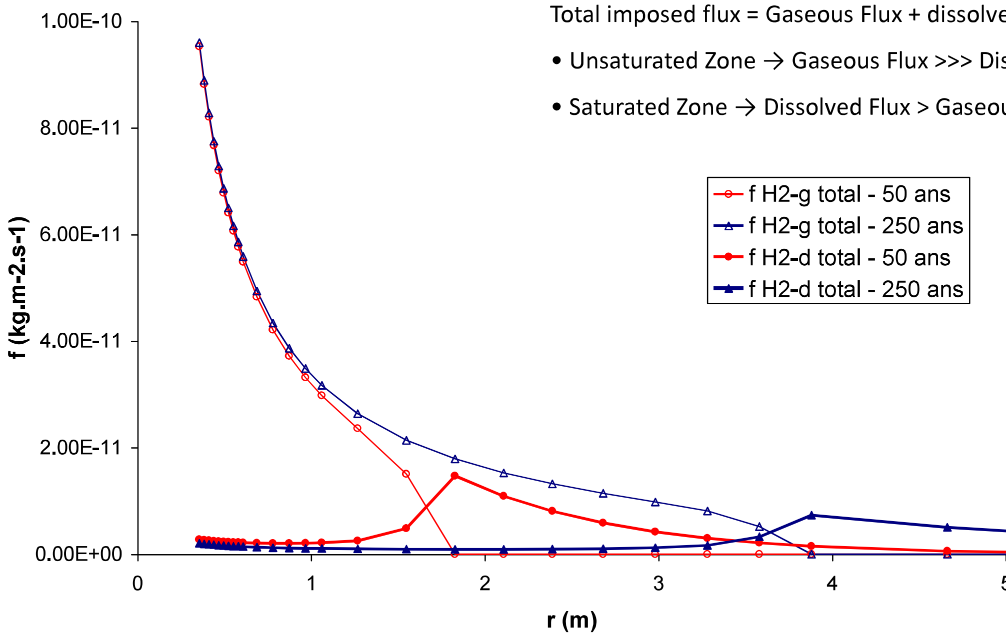

UNSATURATED FLOW PROCESSES

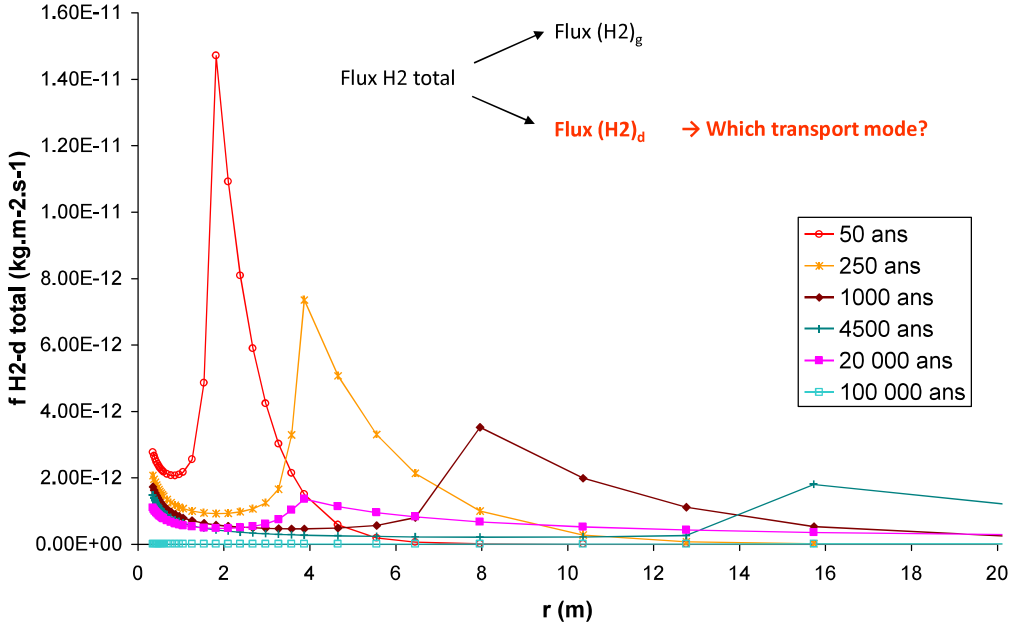

eurad

UNSATURATED FLOW PROCESSES

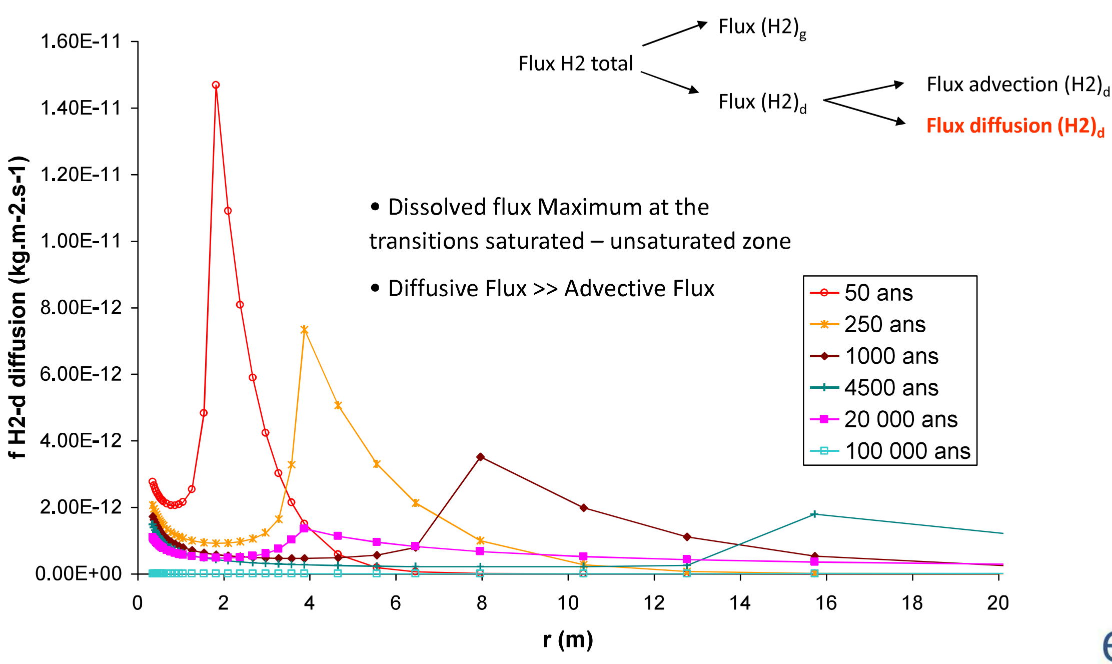

eurad

UNSATURATED FLOW PROCESSES

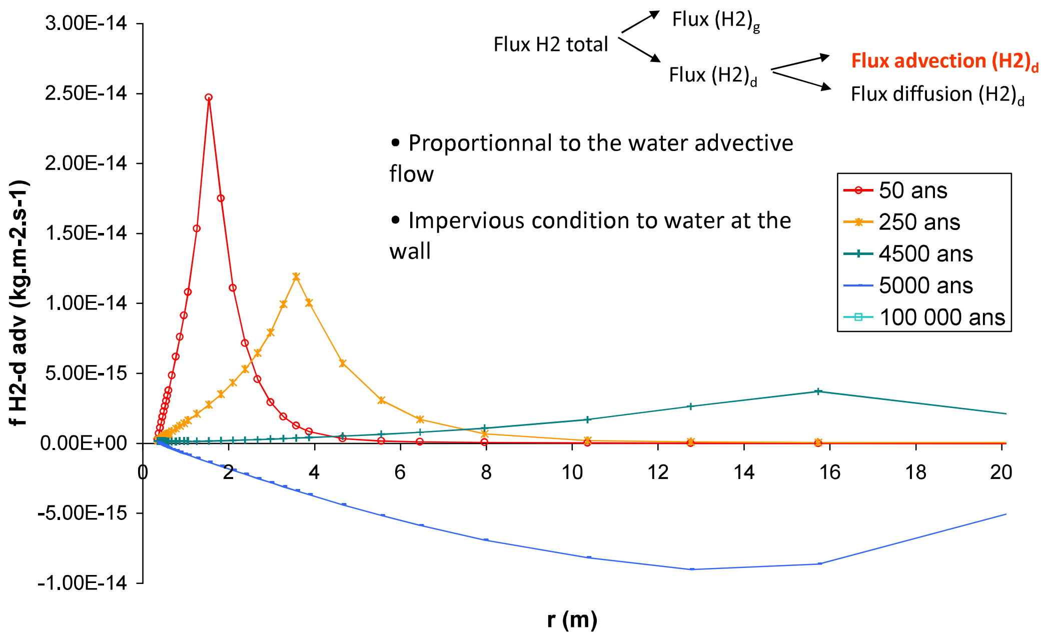

UNSATURATED FLOW PROCESSES

Retention curve

$$S_{r,w} = S_{res} + \frac{S_{\max} - S_{res}}{\left[1 + \left(\frac{p_c}{P_r}\right)^n\right]^m}$$

If $S_{max} < 1$ ➔ H_2 injection is easier

➔ Pg ↓

UNSATURATED FLOW PROCESSES

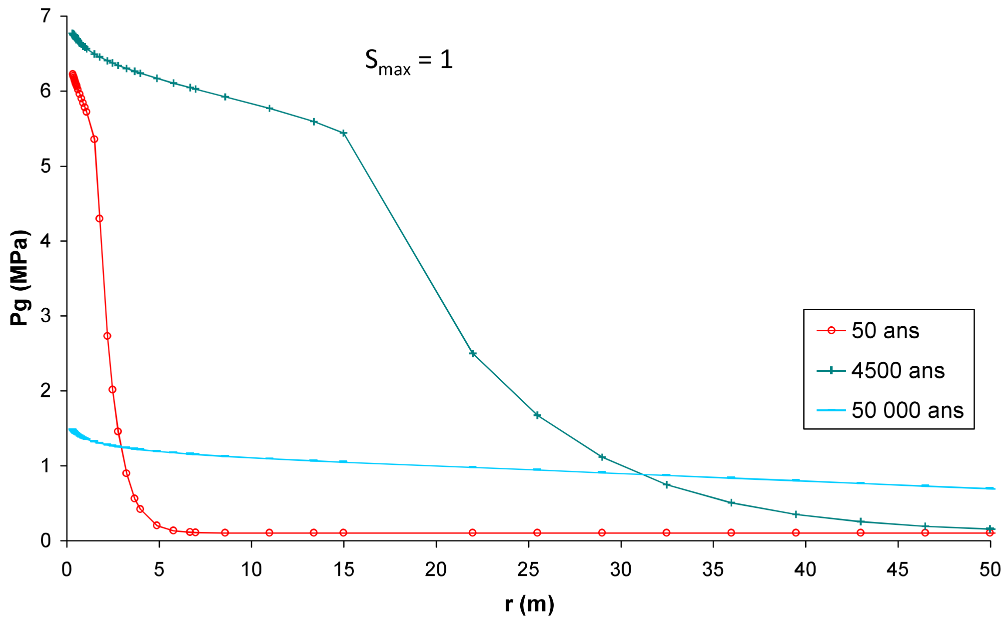

UNSATURATED FLOW PROCESSES

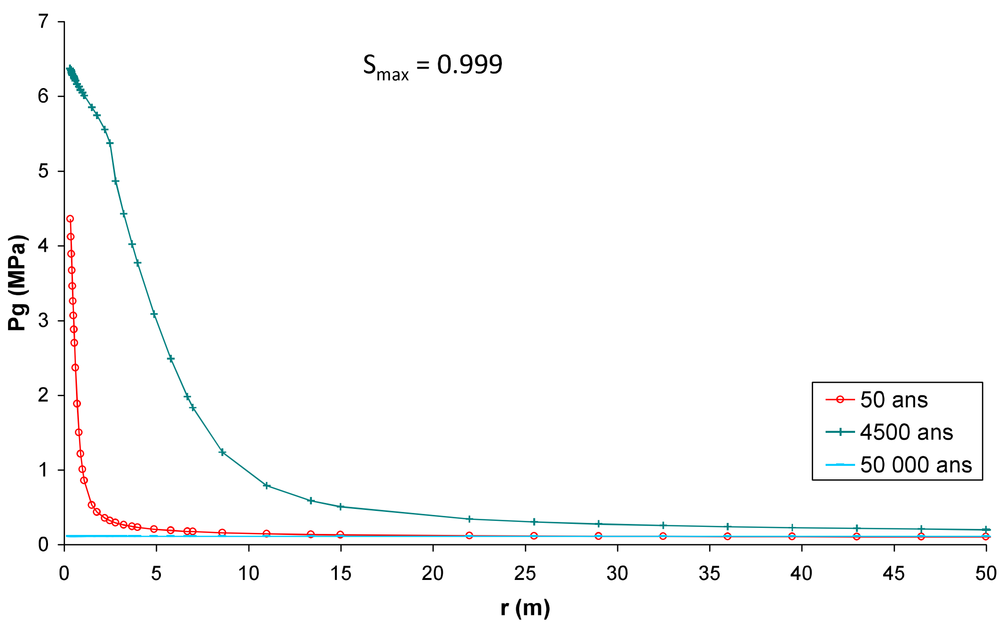

UNSATURATED FLOW PROCESSES

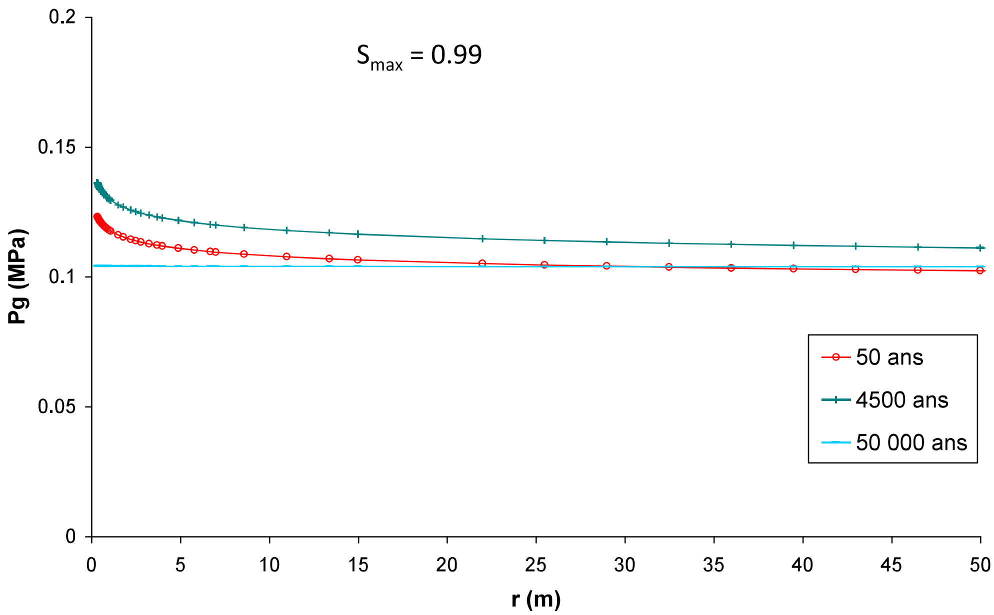

UNSATURATED FLOW PROCESSES

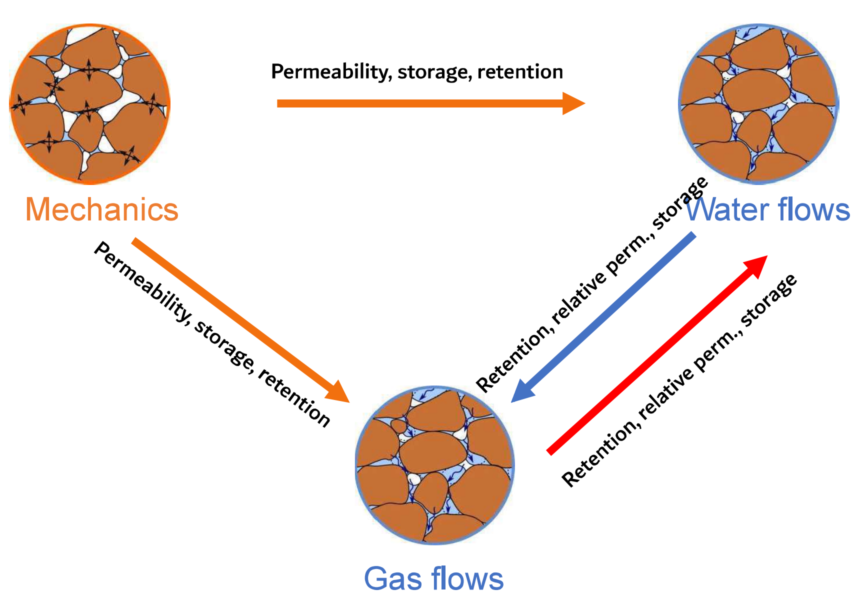

TABLE OF CONTENT

THMG PROCESSES

Mechanical behaviour

The mechanical behaviour of a gematerial is by essence highly complex:

- Non linear
- Reversible/Permanent deformation
- Time dependent behaviour
- Cyclic behaviour

In geomeachnics, the stress increment is generaly computed from the strain increment as:

$$d\sigma = D(\sigma, \epsilon, \dot{\varepsilon}, \kappa) d\epsilon$$

Where σ is the stress tensor, ε the strain tensor, κ the internal variables

THMG PROCESSES

Mechanical behaviour

Contrary to classic continuous media, the mechanical behaviour of porous media is not only controlled by the total stress, but it is also influenced by the fluids occupying the porous space. Therefore, alternative stress variable(s) should be defined. In the case of saturated porous media, the concept of effective stress was early introduced by Terzaghi (1936).

Terzaghi (1936) introduced the concept of effective stress to describe the mechanical behavior of fully saturated porous media. The effective stress transforms a real multiphase porous medium into a mechanically equivalent single-phase continuum. It is defined as:

$$\sigma'_{ij} = \sigma_{ij} - u_w \delta_{ij}$$

And the previous relationship is written as:

$$d\sigma' = D(\sigma', \epsilon, \dot{\varepsilon}, \kappa) d\epsilon$$

Where σ' is the effective stress tensor, ε the strain tensor, κ the internal variables

THMG PROCESSES

Mechanical behaviour in unsaturated medium

The choice of constitutive variables is an inevitable issue in modelling unsaturated soils. Over the years, the choice of appropriate stress variables to model the behaviour of unsaturated soils has indeed been an intensively debated issue. Two main approaches are generally distinguished:

- The extension of the effective stress definition for saturated porous media towards unsaturated states;
- The definition of two independent stress variables (while only one, the effective stress, is used for saturated media).

Each of these two approaches has advantages and drawbacks. They are briefly described in the newt two sections. Further discussion and historical review can be found in Khalili et al. (2004) and Nuth & Laloui (2008b).

THMG PROCESSES

Mechanical behaviour in unsaturated medium

Extension of the effective stress definition

In the effective stress approach, Terzaghi's definition of the effective stress is extended to the partial saturation domain. One of the most famous definition was proposed by Bishop (1959). It is given by:

$$\sigma'_{ij} = \sigma_{ij} - u_a\delta_{ij} + \chi(u_a - u_w)\delta_{ij}$$

where χ is a material parameter, called Bishop's parameter, which depends on the degree of saturation. It takes the value of 1 for fully saturated states and 0 for totally dry states. Experimental results on unsaturated soils evidence the relation between and the degree of saturation (Jennings & Burland, 1962; Fredlund & Rahardjo, 1993). Note that, since Bishop's stress depends on the material properties, it is not strictly speaking an effective stress (Sheng et al., 2008b).

THMG PROCESSES

Mechanical behaviour in unsaturated medium

Extension of the effective stress definition

When working with constitutive models for unsaturated soils, the main advantage of the effective stress approach is that the models previously developed for saturated soils are straightforwardly extended to the unsaturated domain. In addition, there is a continuous and smooth transition from saturated to unsaturated states. However, the determination of the different model parameters from laboratory tests is often complex.

The effective stress approach has shown limitations in representing the important swelling of compacted clays and bentonites. The approach is also incapable of reproducing the collapse phenomenon upon wetting paths under high stress levels. Indeed, upon hydration, the fluid pressure increases, producing a decrease in the effective stress. Accordingly, the material swells, while compaction is observed experimentally.

In order to overcome this issue, constitutive models written in terms of a generalized effective stress generally introduce suction as a variable and define a Loading-Collapse curve, similarly to the Barcelona Basic Model.

THMG PROCESSES

Mechanical behaviour in unsaturated medium

Independent variable approach

According to Fredlund & Rahardjo (1993), the number of independent variables is directly linked to the number of phases. For a saturated porous material, only one variable is required: the effective stress. For partially saturated soils, Coleman (1962), Bishop & Blight (1963), Fredlund & Morgenstern (1977) and Alonso et al. (1990), among others, showed that two independent variables enable to overcome the limitations of the single effective stress. In particular, Fredlund & Morgenstern (1977) demonstrated that any pair of net stress, effective stress and suction.

$$\overline{\sigma}_{ij} = \sigma_{ij} - u_a \delta_{ij}$$

The couple of variables net stress and suction is primarily justified by the fact that the variables are directly accessible during experimental tests. Once that the material is saturated, the effective stress is often used instead of the net stress.

THMG PROCESSES

Mechanical behaviour in unsaturated medium

Independent variable approach

The first and most famous complete constitutive model for unsaturated soils is the Barcelona Basic Model (BBM) developed by Alonso et al. (1990). The model uses suction and net stress as independent variables. As an extension of the Modified Cam-Clay model (Roscoe & Burland, 1968), the Barcelona Basic Model is formulated in the framework of elastoplasticity theory and critical state models. An important contribution of the BBM is the definition of the Loading-Collapse (LC) curve.

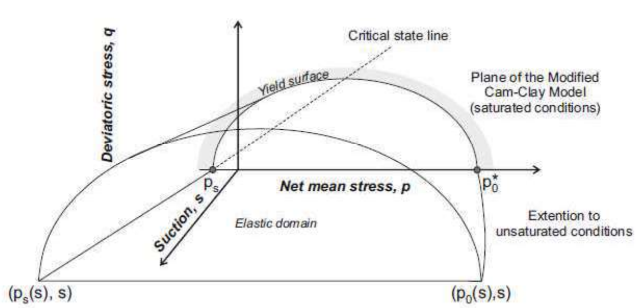

Three dimensional yield surface of Barcelona Basic Model (Alonso et al., 1990).

THMG PROCESSES

Mechanical behaviour in unsaturated medium and non-isothermal conditions

Following the same approach of independent variables:

$$d\overline{\sigma} = D(\overline{\sigma}, \epsilon, \dot{\varepsilon}, \kappa, s, T)d\epsilon + hds + \beta dT$$

Where h constitutive vector net stress-suction and β is the constitutive vector net stress temperature.

THMG PROCESSES

Mechanical behaviour in unsaturated medium and non-isothermal conditions

Mechanical problem

Soils and rocks have a non linear behaviour and may undergo very large deformations. Lagamine code has been developed in the context of large strain, large displacement problems.

In this case, the initial configuration is different from the actual one. One may write the balance equations in the initial configuration or in the current one.

This latter choice is made in Lagamine code: we use the actualised deformed configuration as reference one (Up-dated Lagrangian formulation).

The flow problem is also written in this actualised deformed configuration and the modification of water storage due to solid displacement is therefore implicitly taken into account.

THMG PROCESSES

Mechanical behaviour in unsaturated medium and non-isothermal conditions

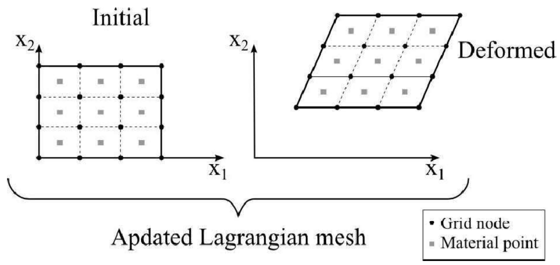

Among the different types of stress formulation (and the deformations associated with them), we will use the Cauchy stress tensor and the Cauchy strain rate defined as:

$$\sigma_{ij}$$

$$\dot{\varepsilon}_{ij} = \frac{1}{2}\left(\frac{\partial \dot{u}_i}{\partial x_j} + \frac{\partial \dot{u}_j}{\partial x_i}\right)$$

THMG PROCESSES

Solid Mass Balance

As far as the reference configuration follows the solid phase, the solid mass balance equation is automaticaly met.

It provides the porosity evolution equation:

$$d\varphi = (b - \varphi).(d\varepsilon_v + \frac{S_{r,w}.dp_w + S_{r,g}.dp_g + (p_g - p_g)dS_{r,w}}{K_s} - 3\alpha_s dT)$$

Linear momentum Balance

$$div(\sigma_{ij}) + \rho g_i = 0$$

Where σ_{ij} is the total stress tensor and ρ is the bulk density of the soil

Water Mass Balance

$$\frac{\partial}{\partial t}(\rho_w\, n\, S_{rw}) + \mathrm{div}\left(\underline{f_w}\right) + \frac{\partial}{\partial t}(\rho_v\, n\, S_{rg}) + \mathrm{div}\left(\underline{f_v}\right) - Q_w = 0$$

Liquid water, S_{rw} water saturation degree
Water vapour, $S_{rg} = 1 - S_{rw}$ gas saturation degree
Source term

Gas Mass Balance

$$\frac{\partial}{\partial t}(\rho_{d,a}\, n\, S_{rw}) + \mathrm{div}\left(\underline{f_{d,a}}\right) + \frac{\partial}{\partial t}(\rho_a\, n\, S_{rg}) + \mathrm{div}\left(\underline{f_a}\right) - Q_a = 0$$

Dissolved air, S_{rw} water saturation degree
Dry air, $S_{rg} = 1 - S_{rw}$ gas saturation degree
Source term

Retention properties: influence of the temperature

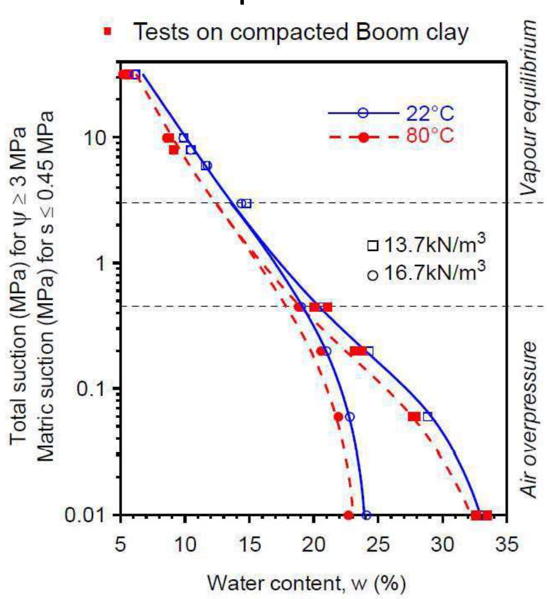

(Romero, Gens & Lloret, 2001)

THMG PROCESSES

Retention properties: influence of the temperature

In the Van Genuchten expression, P_r is a function of the air entry pressure depending on the max. pore radius and the surface tension:

$$P_r = \frac{2\sigma_{G-L}}{r}$$

And the surface tension depends on the temperature as:

$$\sigma_{G-L} = 0.0359 \exp\left(\frac{252.93}{T}\right)$$

The Pr parameter can thus be adapted as:

$$\frac{P_r(T)}{P_r(T0)} = \frac{\sigma_{G-L}(T)}{\sigma_{G-L}(T0)}$$

THMG PROCESSES

Relative water permeability: influence of the temperature

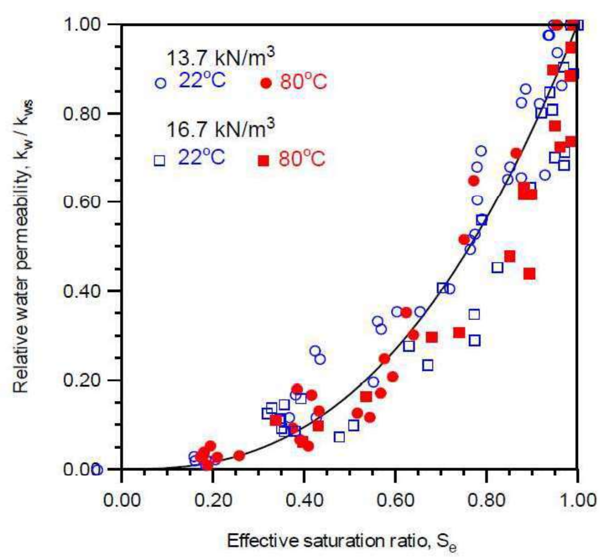

(Romero, Gens & Lloret, 2001)

THMG PROCESSES

Internal energy Balance

$$\frac{\partial S_T}{\partial t} + \mathrm{div}(\underline{V_T}) + \dot{E}_{H2O}^{w \to v} L - Q_T = 0$$

$$S_T = n\,\rho_w\,S_{rw} c_{pw}\,(\mathrm{T} - \mathrm{T}_0) + n\,\rho_v\,S_{rg} c_{pv}\,(\mathrm{T} - \mathrm{T}_0) + n\,\rho_a\,S_{rg} c_{pa}\,(\mathrm{T} - \mathrm{T}_0) + n\,\rho_{da}\,S_{rw} c_{pda}\,(\mathrm{T} - \mathrm{T}_0) + (1-n)\,\rho_s\,c_{ps}\,(\mathrm{T} - \mathrm{T}_0)$$

$$V_T = -\Gamma\,\nabla \mathrm{T} + c_{pw}\,\rho_w\,\underline{q_l}\,(\mathrm{T} - \mathrm{T}_0) + c_{pv}\left(\rho_v\,\underline{q_g} + \underline{i_v}\right)(\mathrm{T} - \mathrm{T}_0) + c_{pa}\left(\rho_a\,\underline{q_g} + \underline{i_a}\right)(\mathrm{T} - \mathrm{T}_0)$$

Water vapour mass balance equation : $\frac{\partial S_v}{\partial t} + \mathrm{div}\left(\underline{f_v}\right) - \dot{E}_{H2O}^{w \to v} = 0$

THMG PROCESSES

Internal energy Balance

$$\frac{\partial S_T}{\partial t} + \mathrm{div}(\underline{V_T}) + \left(\frac{\partial S_v}{\partial t} + \mathrm{div}\left(\underline{f_v}\right)\right) L - Q_T = 0$$

$$S_T^* = n\,\rho_w\,S_{rw} c_{pw}\,(\mathrm{T} - \mathrm{T}_0) + n\,\rho_v\,S_{rg} c_{pv}\,(\mathrm{T} - \mathrm{T}_0) + n\,\rho_a\,S_{rg} c_{pa}\,(\mathrm{T} - \mathrm{T}_0) + n\,\rho_{da}\,S_{rw} c_{pda}\,(\mathrm{T} - \mathrm{T}_0) + (1-n)\,\rho_s\,c_{ps}\,(\mathrm{T} - \mathrm{T}_0) + L\,n\,S_{rg}\,\rho_v$$

$$V_T^* = -\Gamma\,\nabla \mathrm{T} + c_{pw}\,\rho_w\,\underline{q_l}\,(\mathrm{T} - \mathrm{T}_0) + c_{pv}\left(\rho_v\,\underline{q_g} + \underline{i_v}\right)(\mathrm{T} - \mathrm{T}_0) + c_{pa}\left(\rho_a\,\underline{q_g} + \underline{i_a}\right)(\mathrm{T} - \mathrm{T}_0) + \left(\rho_v\,\underline{q_g} + \underline{i_v}\right) L$$

THMG PROCESSES

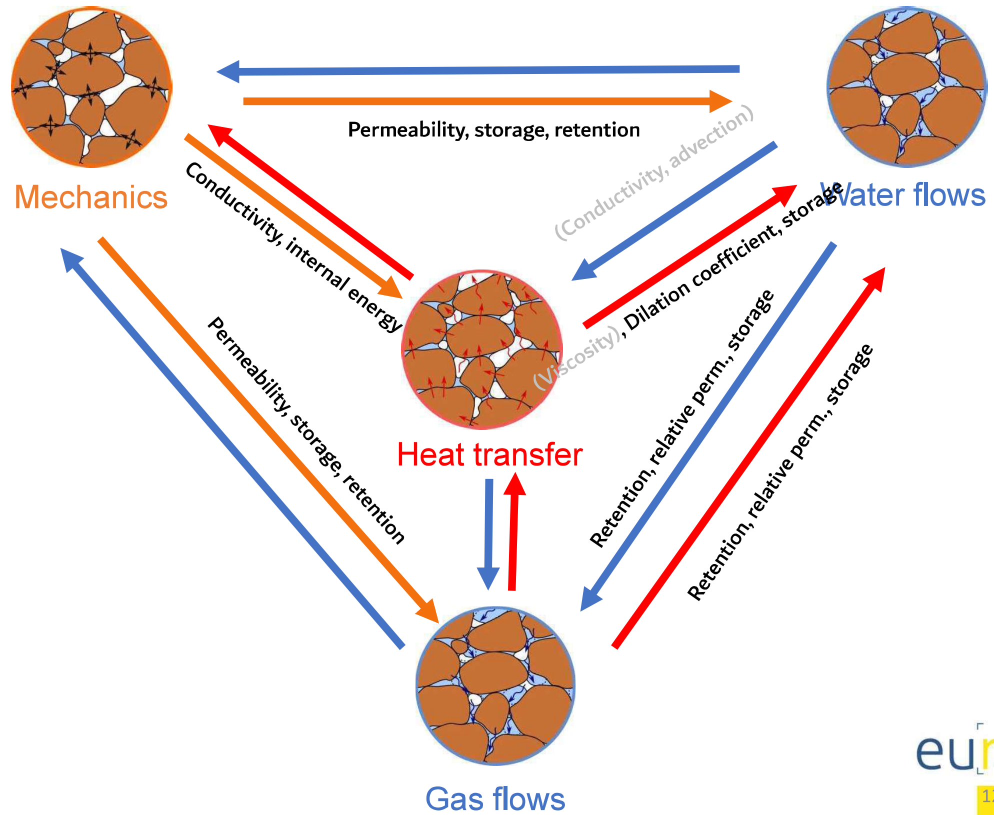

THMG PROCESSES

TASK 4.2: MECHANISTIC UNDERSTANDING OF GAS TRANSPORT AT THE SCALE OF A REPOSITORY

- **Preliminary Technical Information**
  - Generic repository configuration with material parameters for three cases:
    - Storage Zone A (ILW, NAGRA)
    - **Storage Zone B (HLW, ONDRAF)**
    - **Storage Zone C (HLW, ANDRA)**
  - Initial boundary conditions in terms of T, P_W and $\sigma_{v/h}$
  - Time varying conditions

Stage	Scenario	Time scale
I.	Initial stage (No repository)	T < 0
2.	Instantaneous excavation	T = 0
3.	Ventilation	T = 0 to 50 Years
4.	Waste emplacement	T = 50

  - Source terms for temperature and gas injection

Schematic horizontal slice at generic repository depth

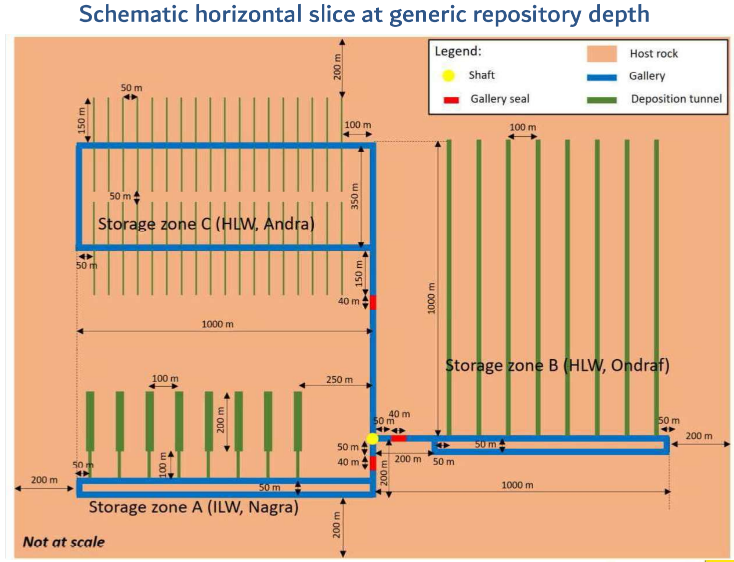

THMG PROCESSES

TASK 4.2: MECHANISTIC UNDERSTANDING OF GAS TRANSPORT AT THE SCALE OF A REPOSITORY

Zone B

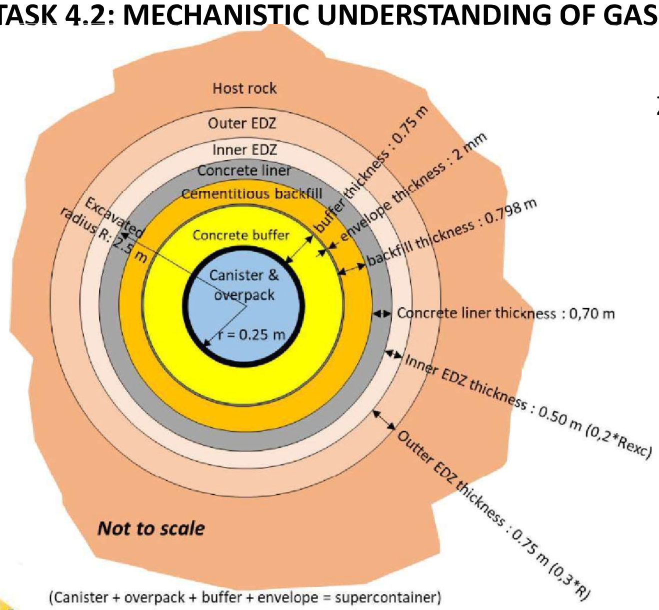

(Canister + overpack + buffer + envelope = supercontainer)

AA' vertical cross-section perpendicular to the axis of the tunnel

Zone C

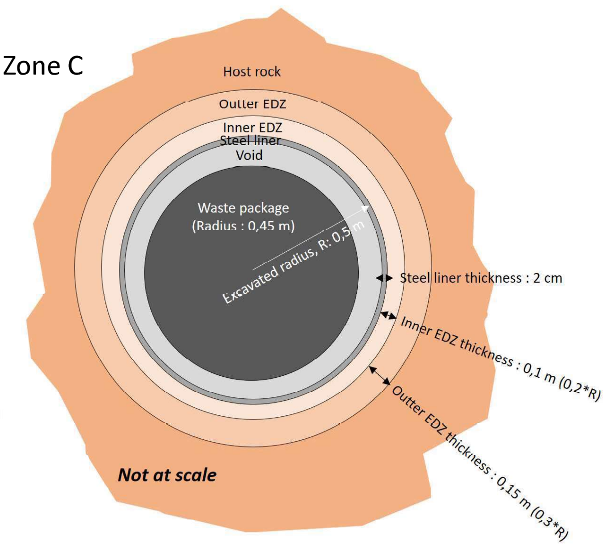

AA' vertical cut perpendicular to the axis of the tunnel

THMG PROCESSES

TASK 4.2: MECHANISTIC UNDERSTANDING OF GAS TRANSPORT AT THE SCALE OF A REPOSITORY

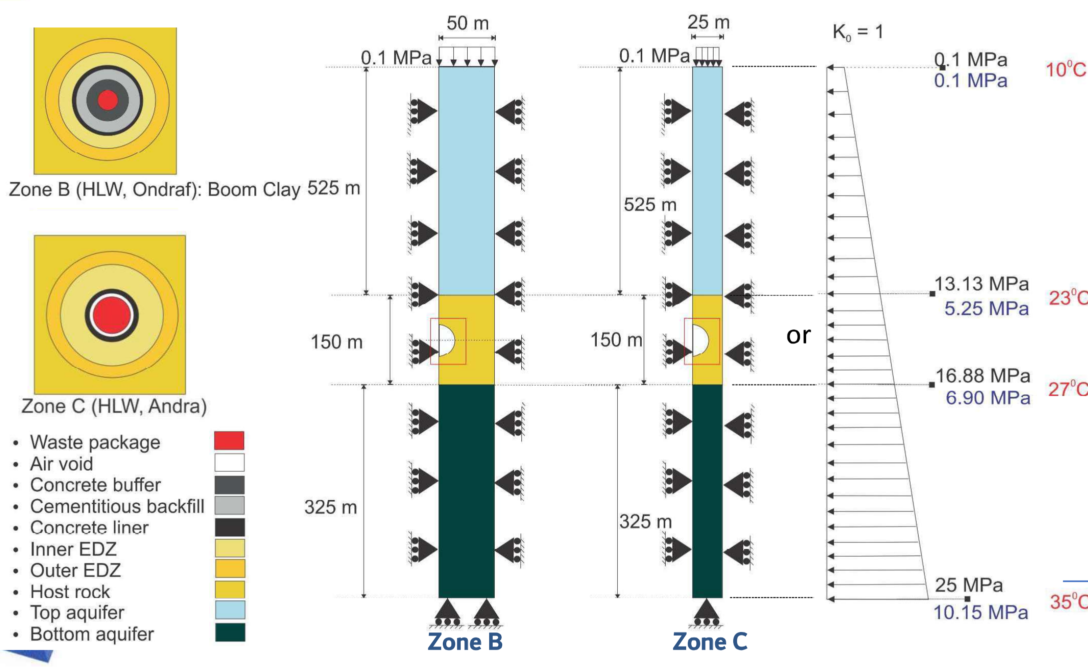

10^0C → FIXED p_w & T at top

Components	Biot's Coefficient
Inner EDZ	0.8
Outer EDZ	0.8
Undist. Rock	0.8
Top aq.	0.8
Bottom aq.	0.8
Others	1

23^0C

27^0C

35^0C → FIXED p_w & T at bottom

THMG PROCESSES

Phase	Time [Years]	Scenario	Features
Initial	T < 0	No Repository **(Instantaneous excavation)**	• In-situ stress regime (σ_v ; σ_h) • Hydrostatic pressure (p_w) • Natural geothermal field (T)
Phase-I	T = 0-50	**Ventilation (Zone B)** **Dewatering (Zone C)**	• Ventilation/Dewatering effect ○ Zone B ≈ 80% RH (s_t = 30.60 MPa) ○ Zone C (p_w ≈ 0.1 MPa)
Phase-II	T = 50-100,000	**Instantaneous waste emplacement**	• Thermal load and gas generation (Hydrogen)

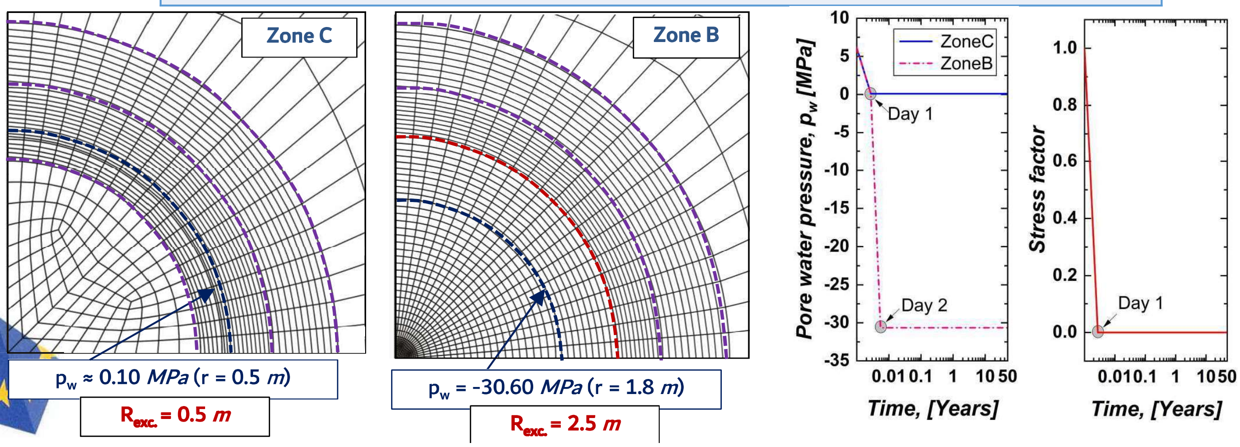

THMG PROCESSES

- **For Zone B (HLW, ONDRAF)**
  - Gas-H_2 source term [mol/y] = 0.25 (per m of cell) for 100,000 years
  - Gas flux-H_2 = 0.141E-11 [kg/s.m^2] @ at liner intrados (r= 1.80 m)
  - Max. heat flux = 123.00 [W/m^2] along the canister circumference (r=0.25m)

- **For Zone C (HLW, ANDRA)**
  - Gas-H_2 source term [mol/y] = 1.90 (per m of cell) for 40,000 years
  - Gas flux-H_2 = 4.295E-11 [kg/s.m^2] along the canister circumference (r=0.45m)
  - Max. heat flux = 88.42 [W/m^2] along the canister circumference (r=0.45m)

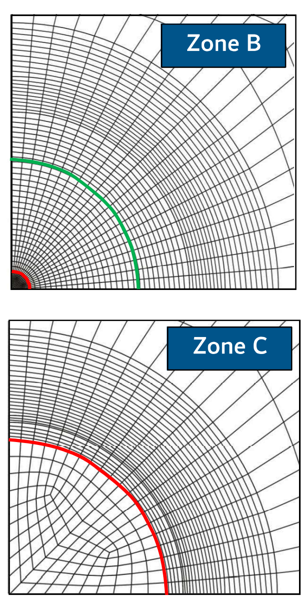

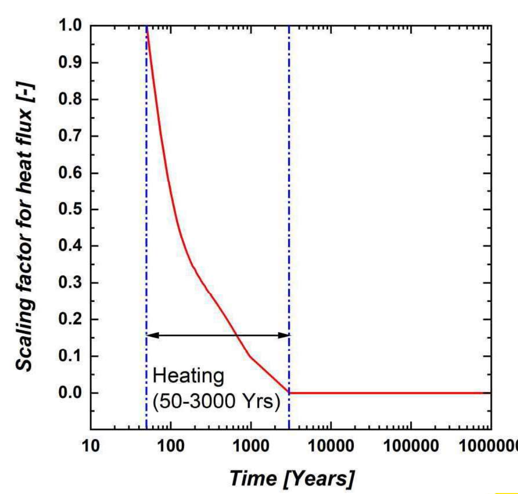

THMG PROCESSES

EFFECT OF THE GEOMETRY (TOP/BOTTOM AQUIFER)

Table: Different cases for evaluating the effect of overlaying and underlaying aquifers.

Cases	Specified SWRC	Spec. Rel. Per. Funs.	Remark
Case 4	✓	✓	*With Top/Bottom aquifers (THMG)*
Case 5	✓	✓	Without Top/Bottom aquifer (THMG)

In Case5:

Nodes in Top and bottom aquifers are fixed for p_w, p_g, and T

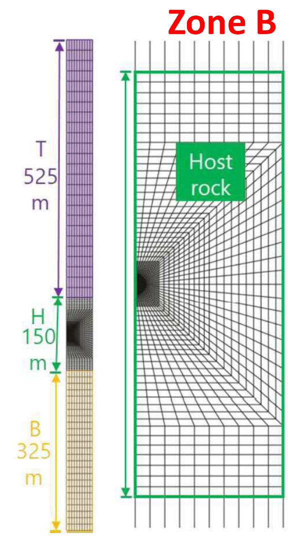

THMG PROCESSES

EFFECT OF THE GEOMETRY (TOP/BOTTOM AQUIFER)

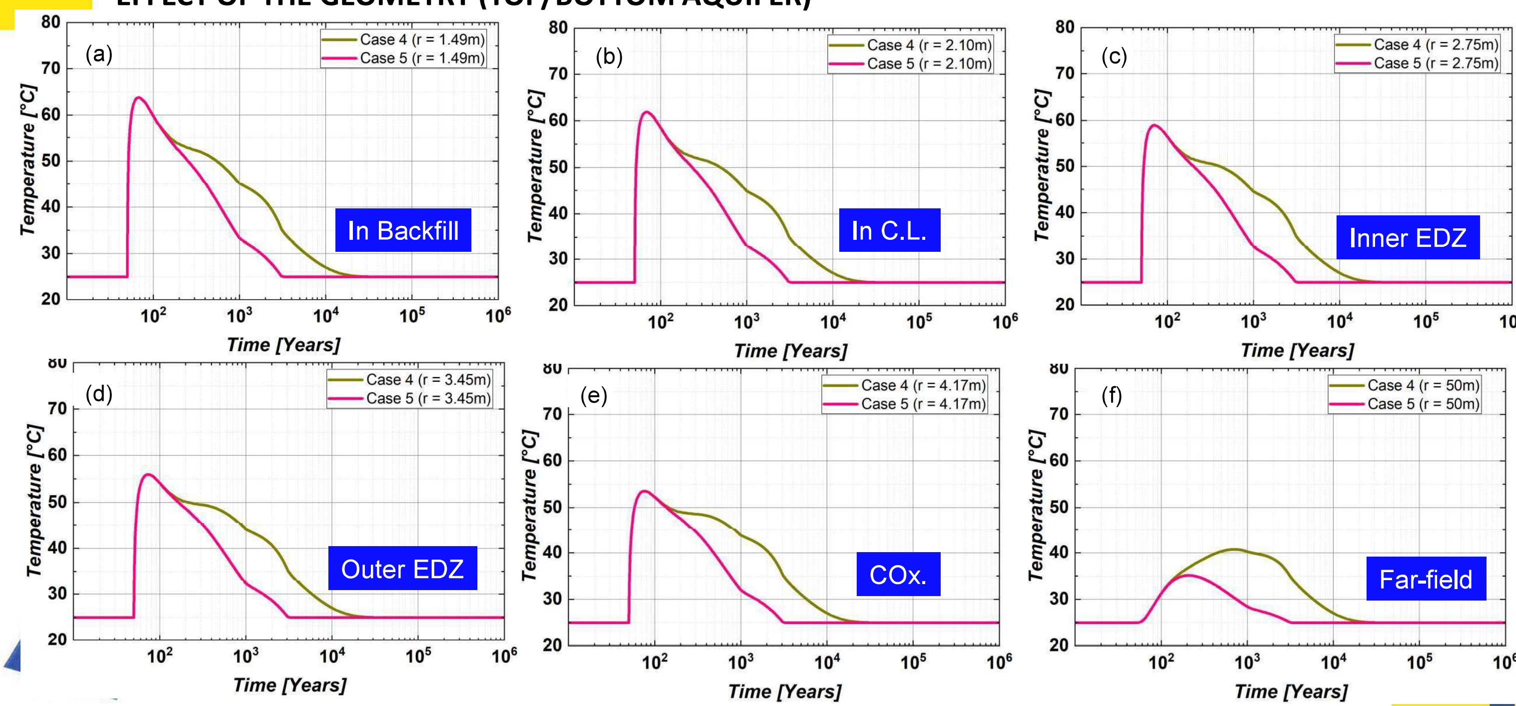

THMG PROCESSES
EFFECT OF THE GEOMETRY (TOP/BOTTOM AQUIFER)

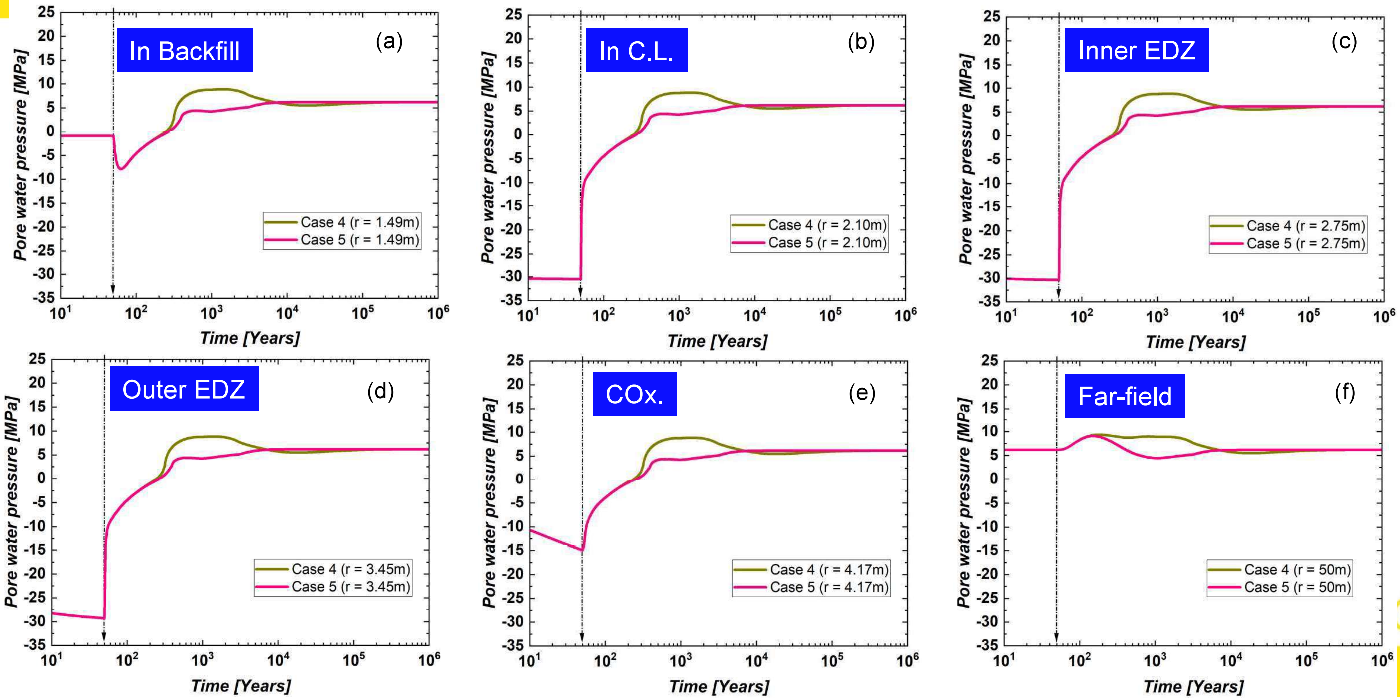

THMG PROCESSES
EFFECT OF THE GEOMETRY (TOP/BOTTOM AQUIFER)

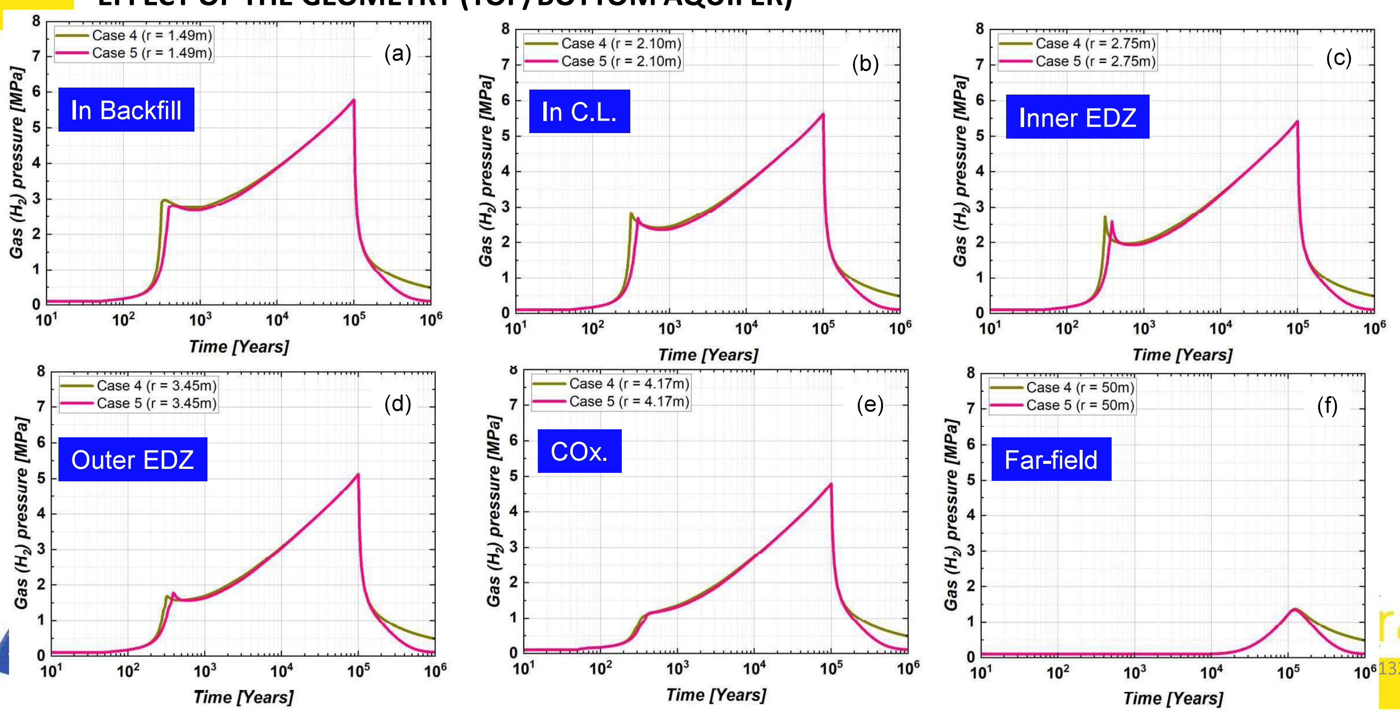

THMG PROCESSES
EFFECT OF TEMPERATURE ON GAS/POREWATER PRESSURE EVOLUTION (THMG VERSUS HMG)

Table: Different cases for evaluating the effect of overlaying and underlaying aquifers.

Cases	Specified SWRC	Spec. Rel. per. funs.	Remark	Coupling case
Case 5	✓	✓	Without Top/Bottom aquifer	THMG
Case 6	✓	✓	Without Top/Bottom aquifer	HMG- T is fixed at all the nodes

THMG PROCESSES
EFFECT OF TEMPERATURE ON GAS/POREWATER PRESSURE EVOLUTION (THMG VERSUS HMG)

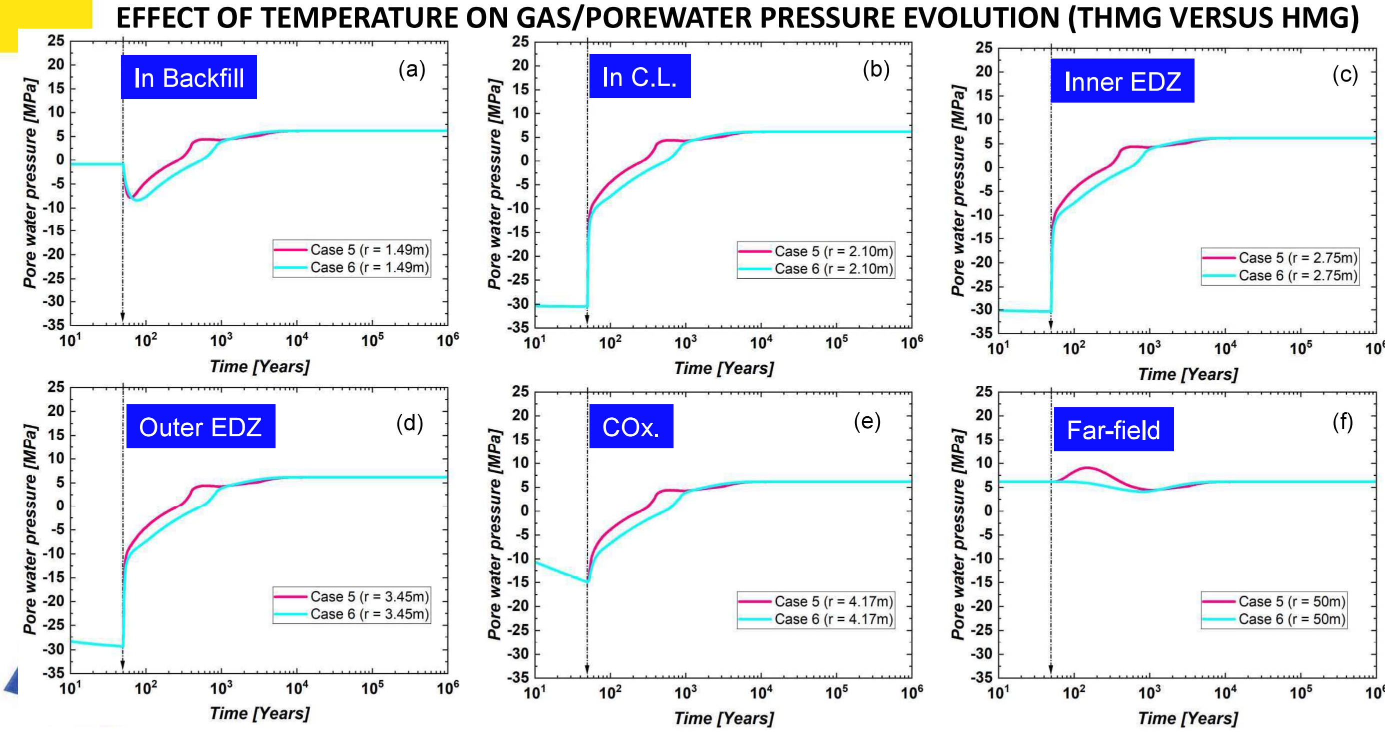

THMG PROCESSES

EFFECT OF TEMPERATURE ON GAS/POREWATER PRESSURE EVOLUTION (THMG VERSUS HMG)

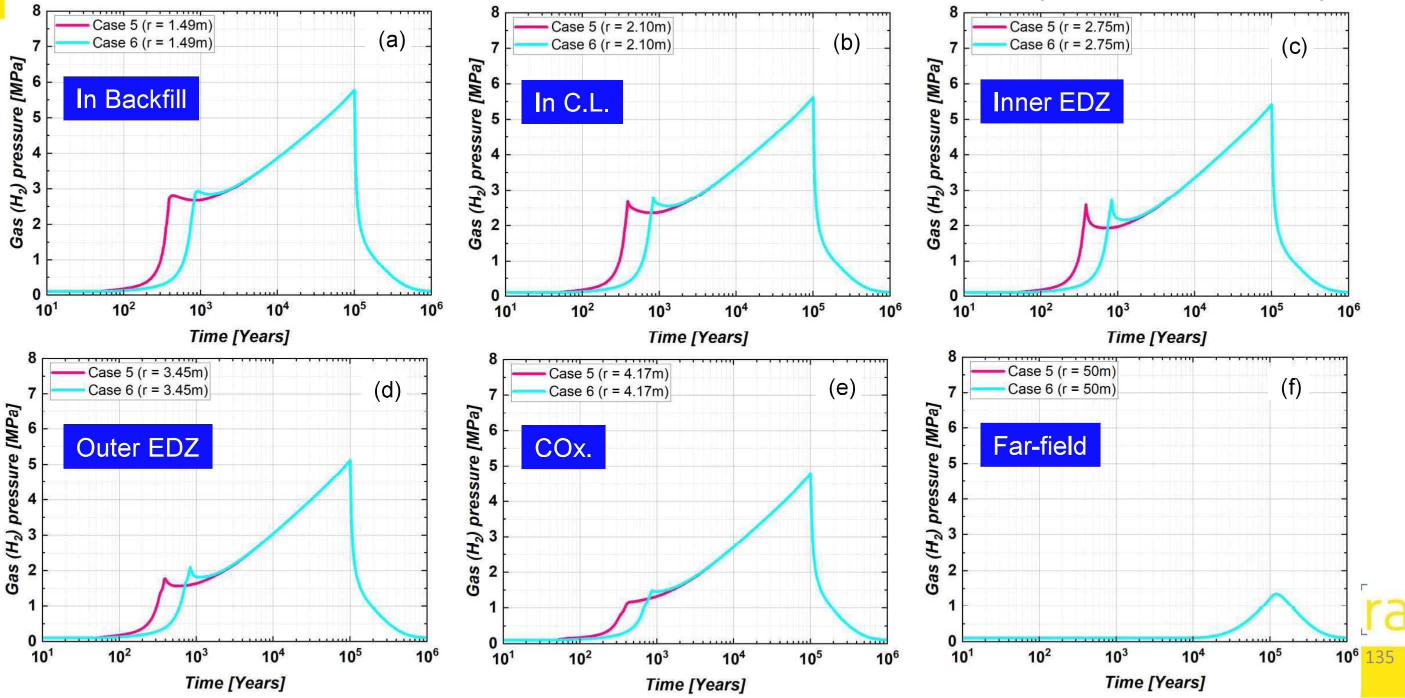

THMG PROCESSES

EFFECT OF GAS GENERATION (THMG VERSUS THM-COUPLING)

Table: Different cases for examining the effect of gas pressure on the porewater evolution.

Cases	Specified SWRC	Spec. Rel. per. funs.	Remark	Coupling case
Case 5	✓	✓	Without top/bottom aquifer	THMG
Case 7	✓	✓	Without top/bottom aquifer	THM (G is fixed at all the nodes)

THMG PROCESSES
EFFECT OF GAS GENERATION (THMG VERSUS THM-COUPLING)

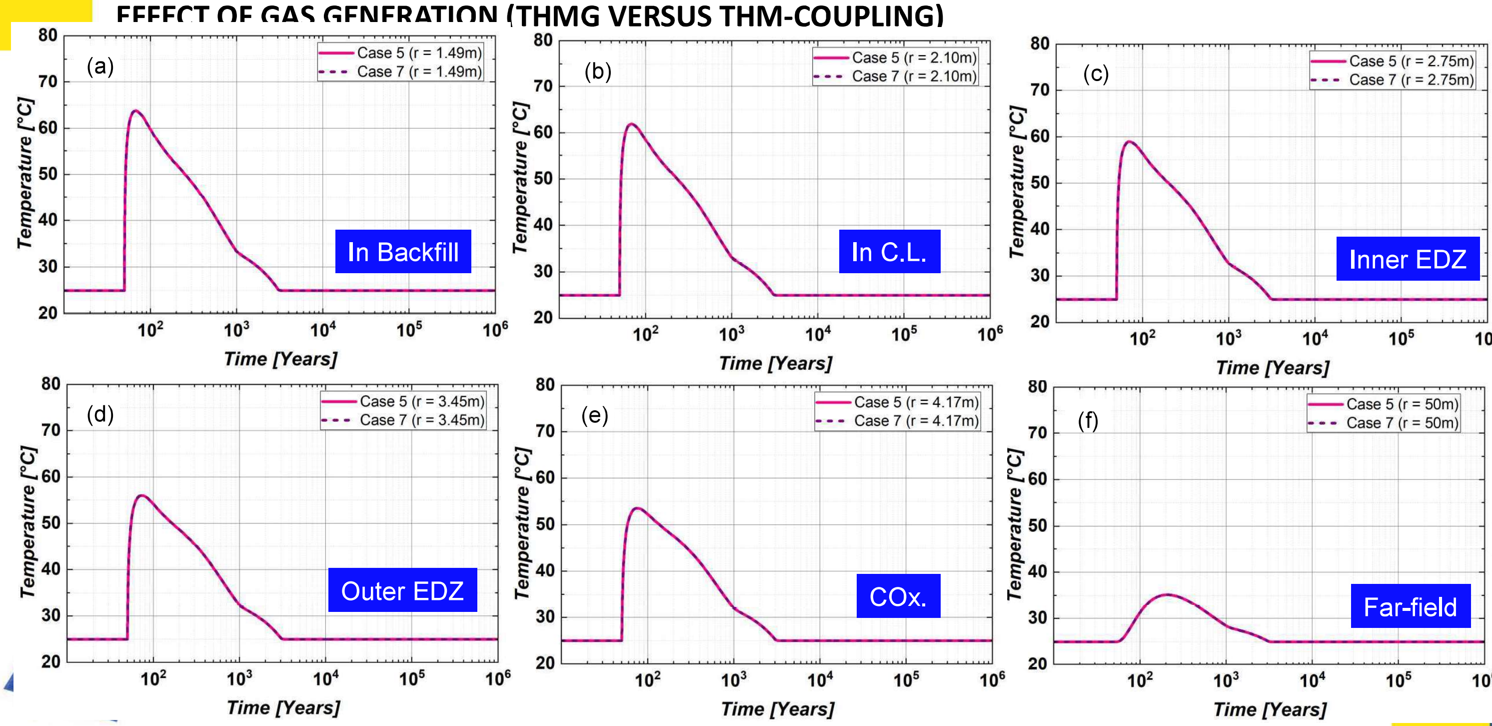

THMG PROCESSES
EFFECT OF GAS GENERATION (THMG VERSUS THM-COUPLING)

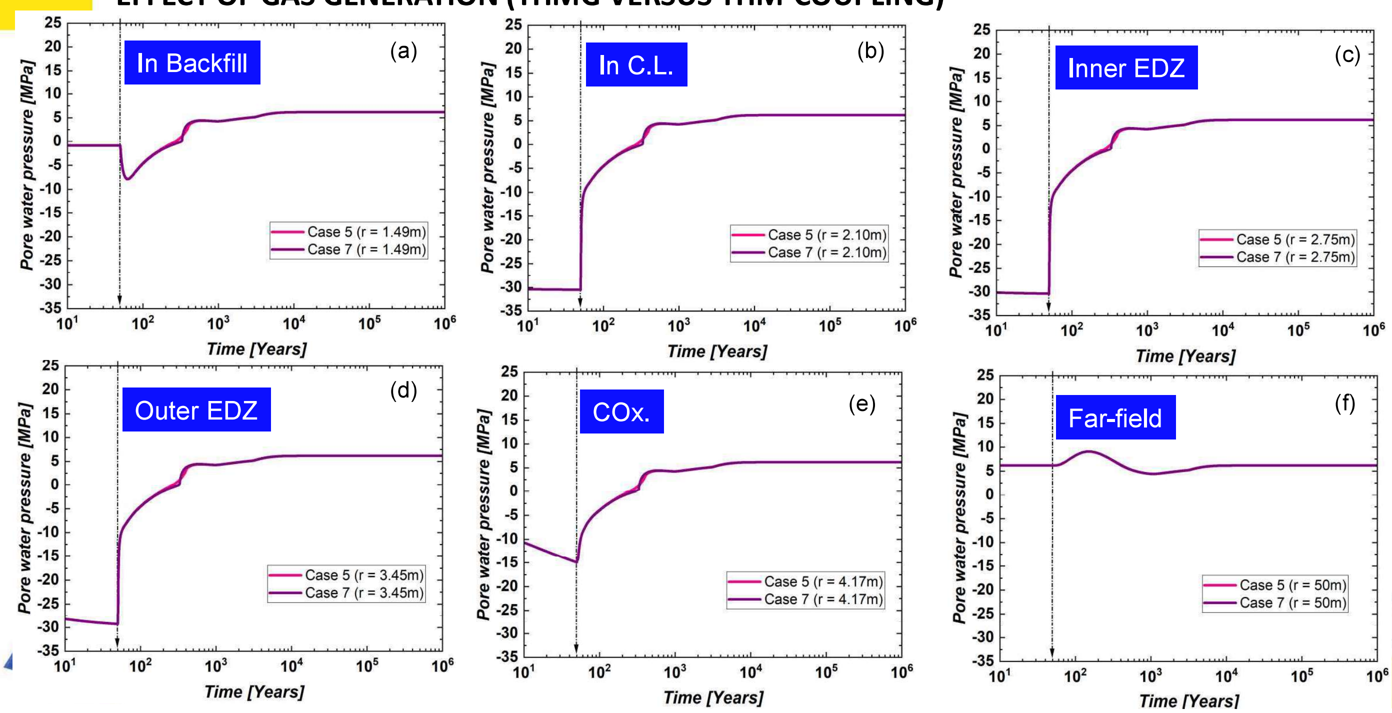

THMG PROCESSES

EFFECT OF THE GEOMETRY (TOP/BOTTOM AQUIFER)

Table: Different cases for evaluating the effect of overlaying and underlaying aquifers.

Cases	Specified SWRC	Spec. Rel. Per. Funs.	Remark
Case 4	✓	✓	*With Top/Bottom aquifers (THMG)*
Case 5	✓	✓	Without Top/Bottom aquifer (THMG)

In Case5:

Nodes in Top and bottom aquifers are fixed for p_w, p_g, and T

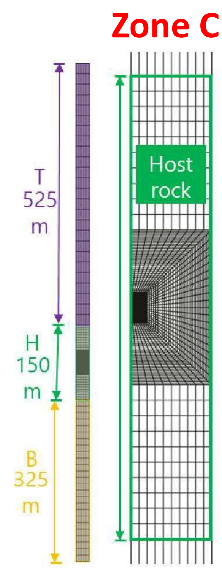

THMG PROCESSES

EFFECT OF THE GEOMETRY (TOP/BOTTOM AQUIFER)

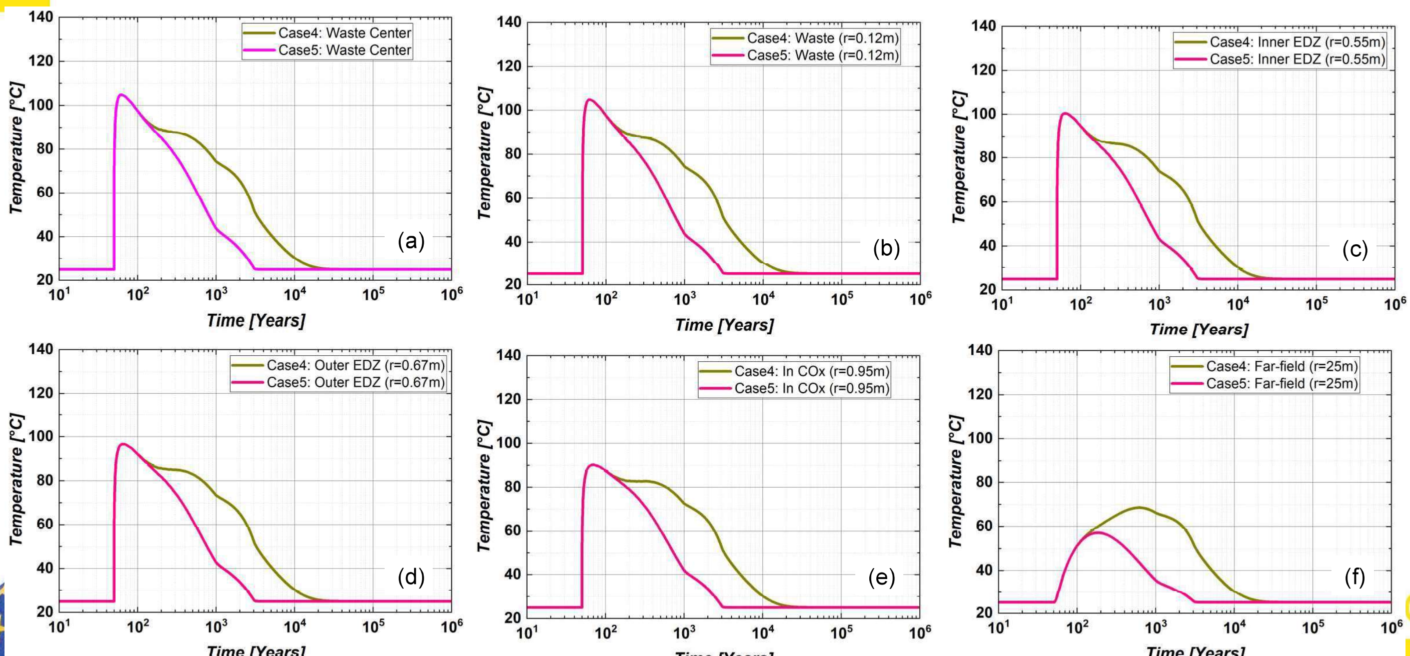

THMG PROCESSES
EFFECT OF THE GEOMETRY (TOP/BOTTOM AQUIFER)

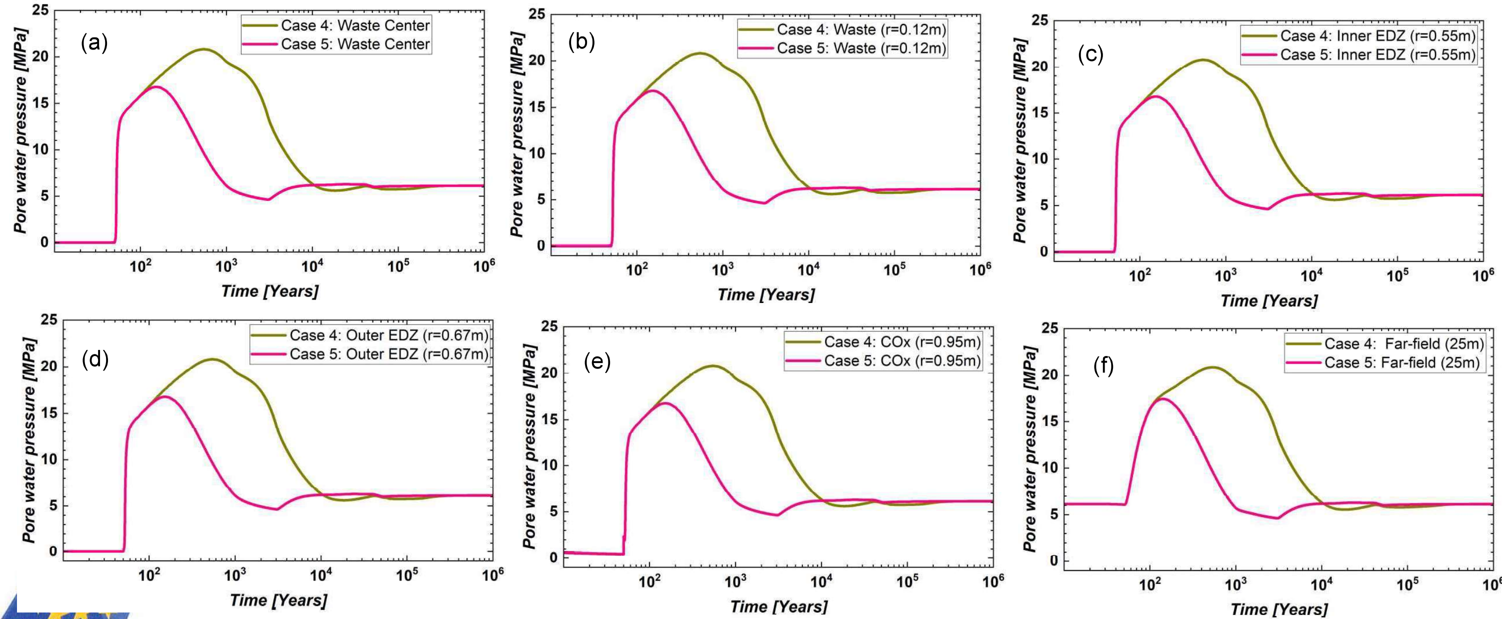

THMG PROCESSES
EFFECT OF THE GEOMETRY (TOP/BOTTOM AQUIFER)

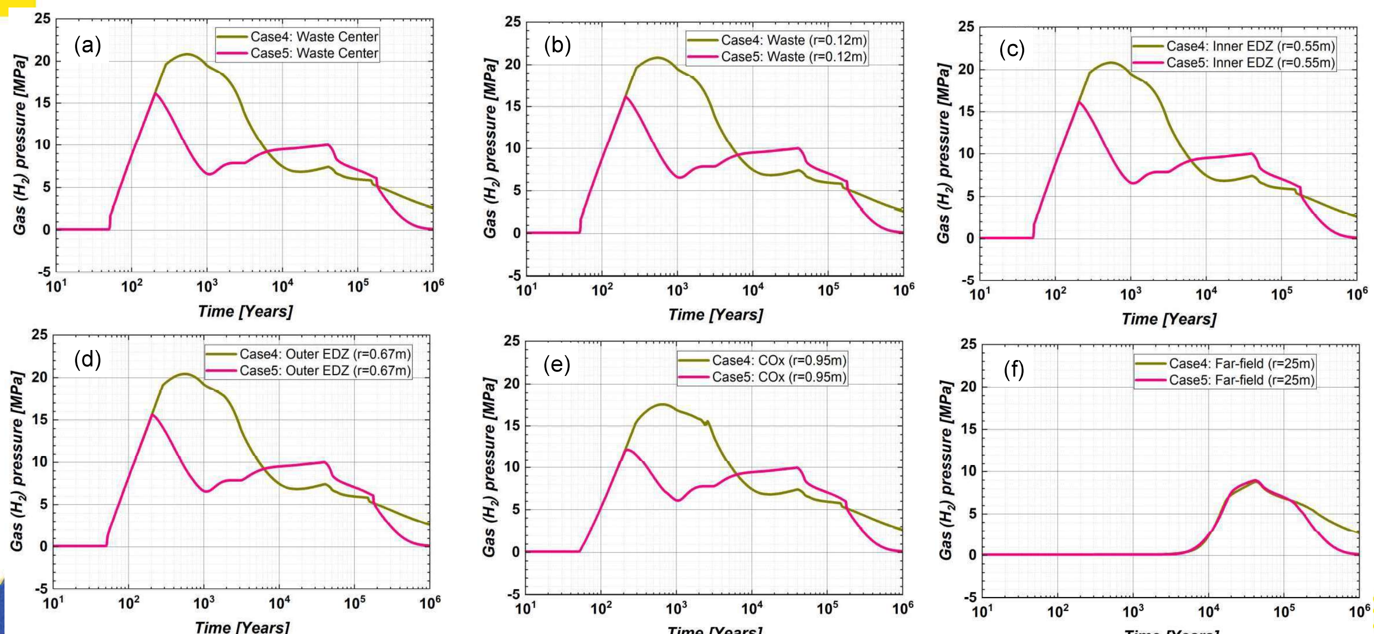

THMG PROCESSES
EFFECT OF TEMPERATURE ON GAS/POREWATER PRESSURE EVOLUTION (THMG VERSUS HMG)

Table: Different cases for evaluating the effect of overlaying and underlaying aquifers.

Cases	Specified SWRC	Spec. Rel. per. funs.	Remark	Coupling case
Case 5	✓	✓	Without Top/Bottom aquifer	THMG
Case 6	✓	✓	Without Top/Bottom aquifer	HMG- T is fixed at all the nodes

THMG PROCESSES
EFFECT OF TEMPERATURE ON GAS/POREWATER PRESSURE EVOLUTION (THMG VERSUS HMG)

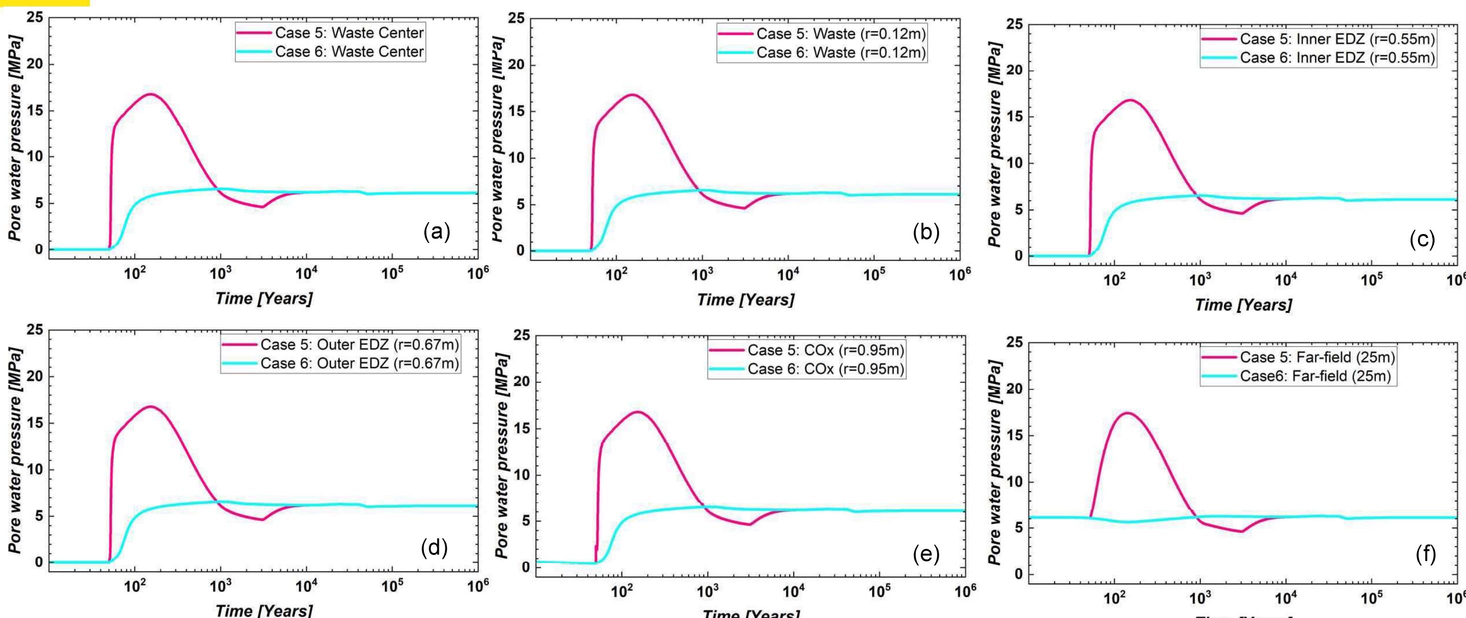

THMG PROCESSES

EFFECT OF TEMPERATURE ON GAS/POREWATER PRESSURE EVOLUTION (THMG VERSUS HMG)

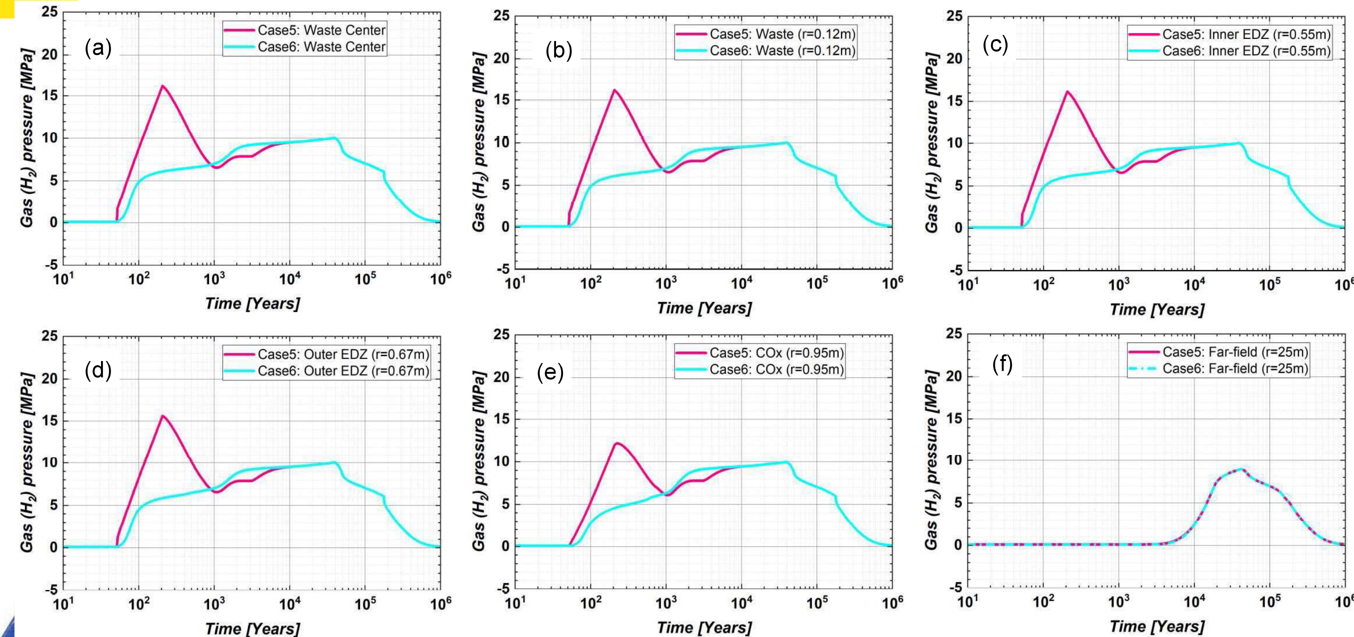

THMG PROCESSES

EFFECT OF GAS GENERATION (THMG VERSUS THM-COUPLING)

Table: Different cases for examining the effect of gas pressure on the porewater evolution.

Cases	Specified SWRC	Spec. Rel. per. funs.	Remark	Coupling case
Case 5	✓	✓	Without top/bottom aquifer	THMG
Case 7	✓	✓	Without top/bottom aquifer	THM (G is fixed at all the nodes)

THMG PROCESSES
EFFECT OF GAS GENERATION (THMG VERSUS THM-COUPLING)

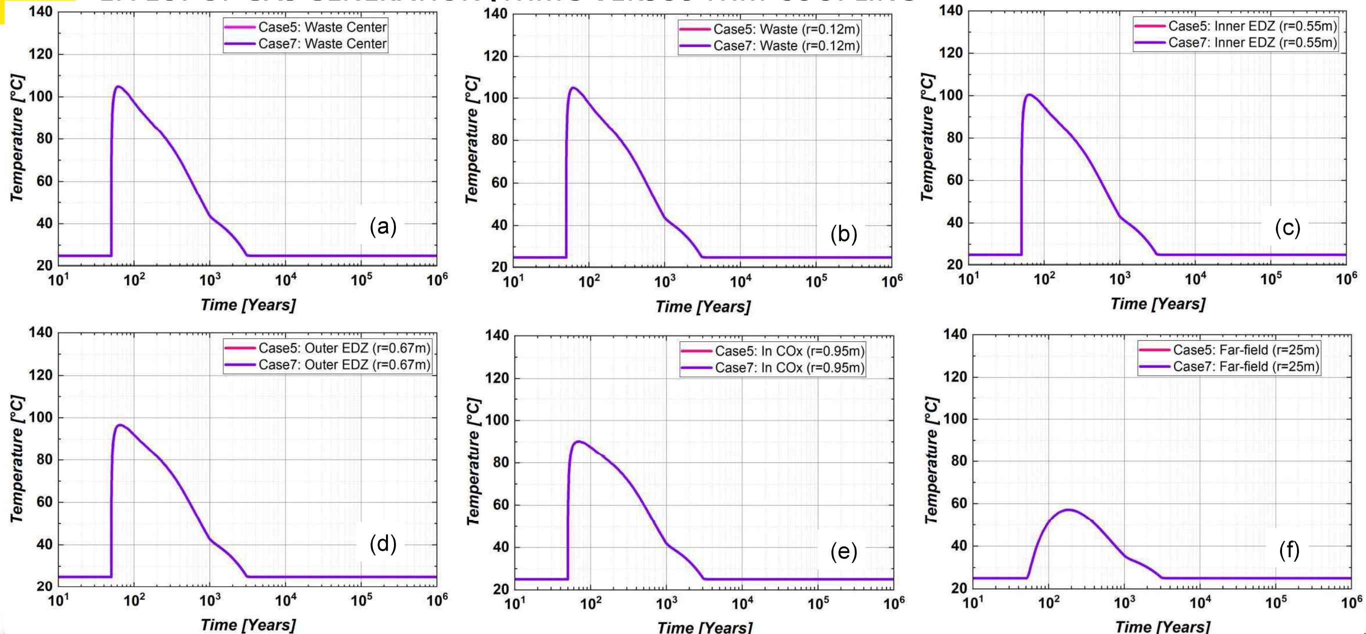

THMG PROCESSES
EFFECT OF GAS GENERATION (THMG VERSUS THM-COUPLING)

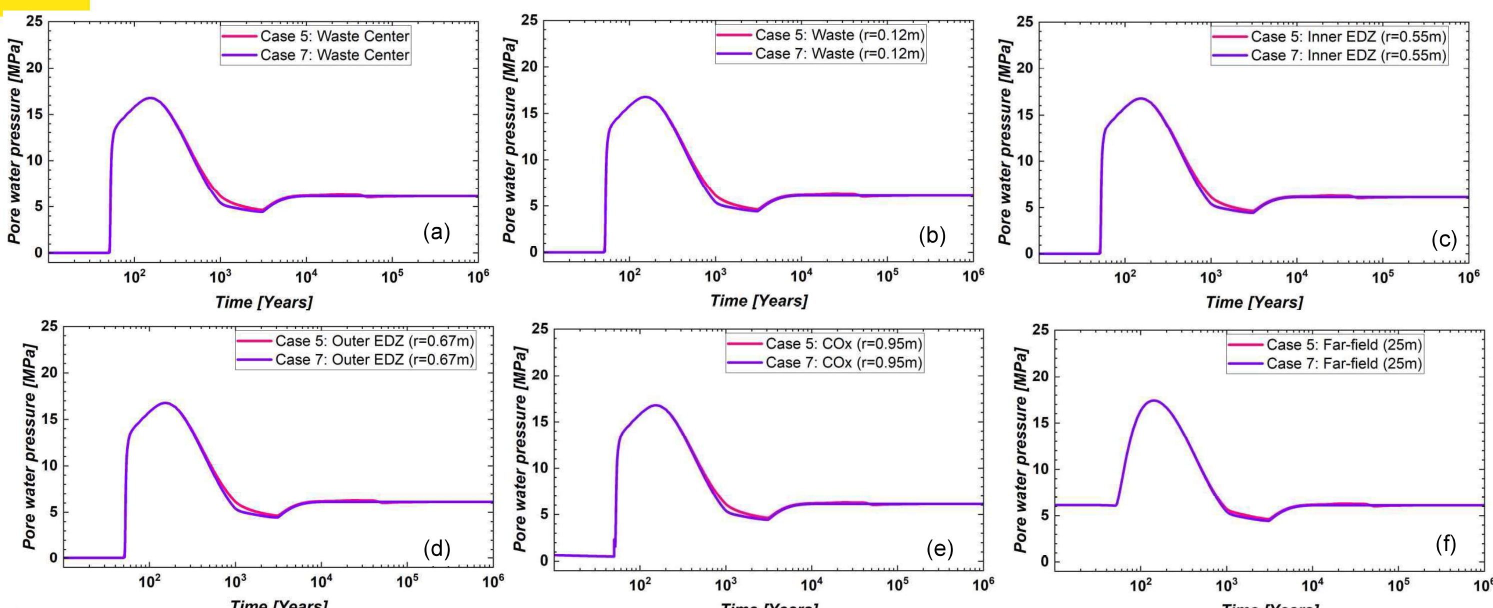

THMG PROCESSES

Effect of Geometry (Presence of Top/Bottom Aquifers):

- Primarily affect the thermal response (peak value, and post-peak distribution), as a result, a much shorter thermal period (3000 years) is observed without the top/bottom aquifers as compared to the opposite case (20,000 years).
- A change in the thermal response induces cascading effect on the PWP and Gas pressure evolution.

Effect of Temperature on Gas/PWP Evolution (THMG *versus* HMG-coupling):

- Rise in the temperature induces excess PWP, thus affects the gas pressure (H_2) evolution.
- As a result, higher PWP and Gas pressure are observed in THMG case as compared to HMG coupling scenario.

Effect of Gas Pressure on PWP Evolution:

- The gas pressure does not affect the temperature or PWP evolution.

CONCLUSIONS

- The different physical phenomena occurring in the geomaterials are by essence coupled.
- The effective existence of this coupling will depend on the nature, properties, environmental loads acting on the geomaterials
- Experimental (in the lab and in situ) are of paramount importance in order to assess the coupling between the processes. A process and a coupling both observed at lab scale and in situ is probably to be considered
- The next step to predict the long term behavior of the geomaterial is the development of constitutive models based on the lab observations.
- From a numerical perspective, the couplings are challenges that the numerical codes have to tackle. A step by step procedure in the modelling of THMG processes is often a reasonable approach.

Appendix C. Basics of experimental testing of geomaterials (A Ferrari)

EPFL

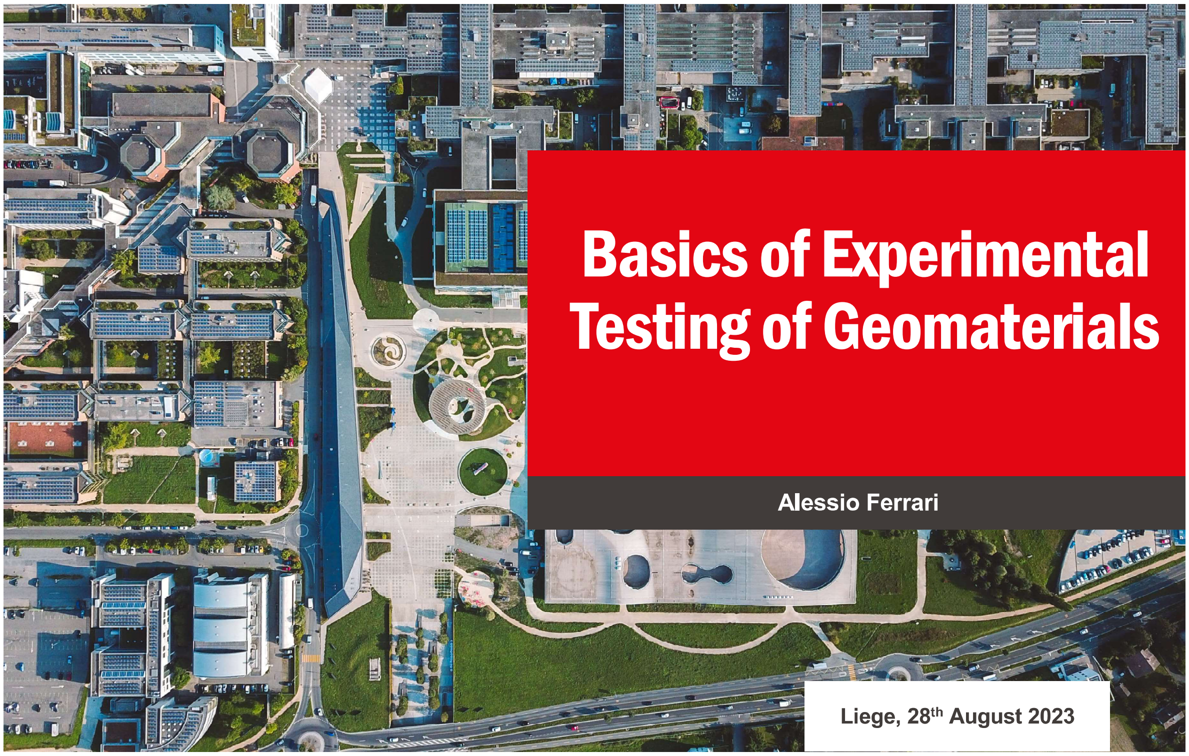

Basics of Experimental Testing of Geomaterials

Alessio Ferrari

Liege, 28th August 2023

École polytechnique fédérale de Lausanne

Representative Elementary Volume, REV

- REV allows to use Continuum Mechanics for geomaterials.
- Size of REV depends on the material and on the considered problem.

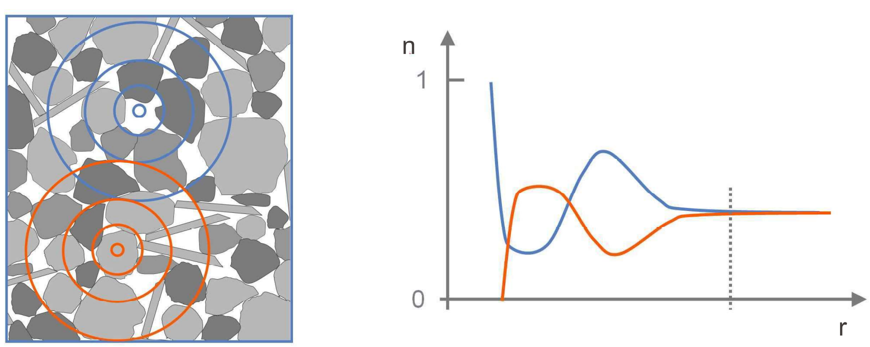

The constitutive approach

Constitutive laws

$$\boxed{\dot{\boldsymbol{\varepsilon}} = \mathbf{D} : \dot{\boldsymbol{\sigma}}'}$$

$$\boldsymbol{\varepsilon} = \begin{pmatrix} \varepsilon_x \\ \varepsilon_y \\ \varepsilon_z \\ \gamma_{xy} \\ \gamma_{xz} \\ \gamma_{yz} \end{pmatrix} \qquad \boldsymbol{\sigma}' = \begin{pmatrix} \sigma_x - u \\ \sigma_y - u \\ \sigma_z - u \\ \tau_{xy} \\ \tau_{xz} \\ \tau_{yz} \end{pmatrix}$$

Fundamental questions to address in any experimental set-up:

Which components to be controlled?
Which components to be measured?

Direct vs. indirect determination of **D** components

Unconfined Compression Strength (UCS) test

Method 1: constant stress rate

Controlled variables: $\dot{\sigma}_1$

$\sigma_2 = \sigma_3 = 0$

Measured variables: $\dot{\varepsilon}_1$

$\dot{\varepsilon}_2, \dot{\varepsilon}_3$ *optional*

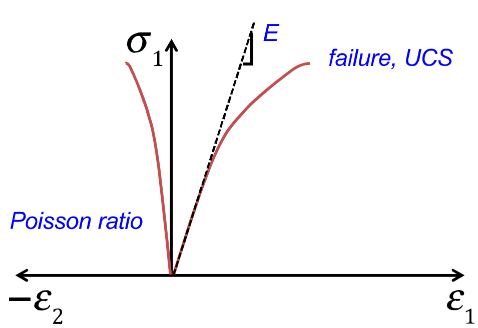

Unconfined Compression Strength (UCS) test

Method 2: constant strain rate

Controlled variables: $\dot{\varepsilon}_1$

$$\sigma_2 = \sigma_3 = 0$$

Measured variables: $\dot{\sigma}_1$

$\dot{\varepsilon}_2, \dot{\varepsilon}_3$ *optional*

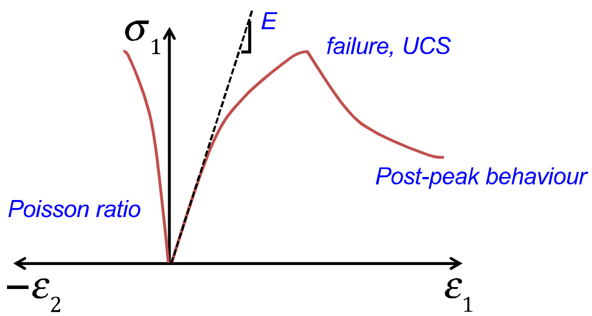

Control of stresses / strains / mixed control

From a geomechanical perspective every testing set-up must be conceived in terms of the mechanical variables to be measured and/or controlled

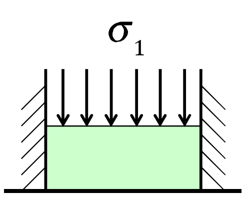

Oedometric (or 1D) compression test

Controlled variables: σ_1

$$\varepsilon_2 = \varepsilon_3 = 0$$

Mixed control

Measured variables: ε_1

σ_2, σ_3 ?

Incomplete definition of the mechanical response

Control of stresses / strains / mixed control

Control of stresses and pore water pressure
Control of the drainage conditions

Triaxial test, Consolidated Drained, CD

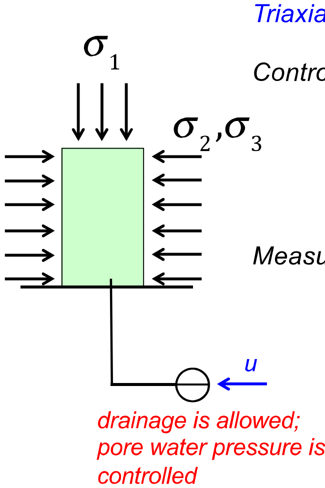

Controlled variables: σ_1

$\sigma_2 = \sigma_3$

u

All stress variables are controlled

Measured variables: ε_1

ε_{vol}

$$\varepsilon_2 = \varepsilon_3 = \left(\varepsilon_{vol} - \varepsilon_1\right)/2$$

Complete definition of the strain state

Radial strain is computed

General considerations

- Uniqueness of constitutive parameters?
  - Critical state parameters (e.g. constant volume shear strength angle)
  - A matter of interpretation

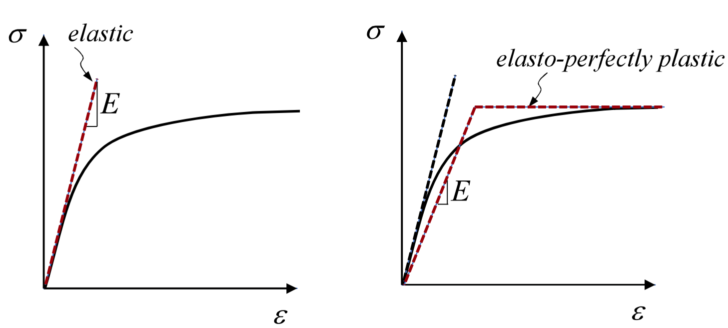

  - Stress dependency (e.g. dilatancy)
  - Stress history

Stress history and soil response

Overconsolidation ratio

- Need to gain awareness on the stress history.

$$OCR = \sigma'_{vp} / \sigma'_v \qquad \sigma'_{vp}\text{, maximum experienced vertical effective stress} \quad \sigma'_v\text{, current vertical effective stress}$$

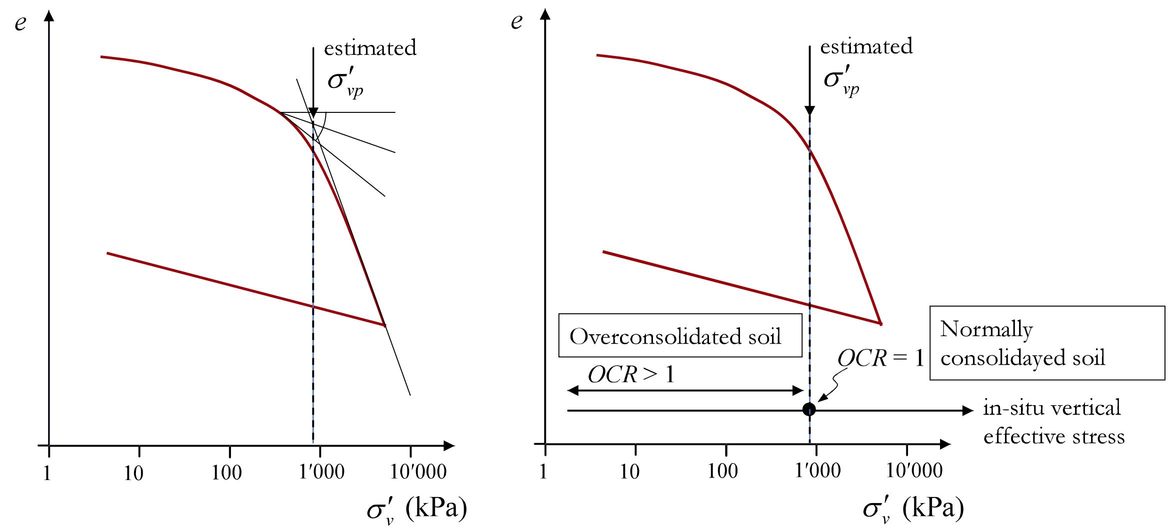

Stress history and soil response

Preserving soil history

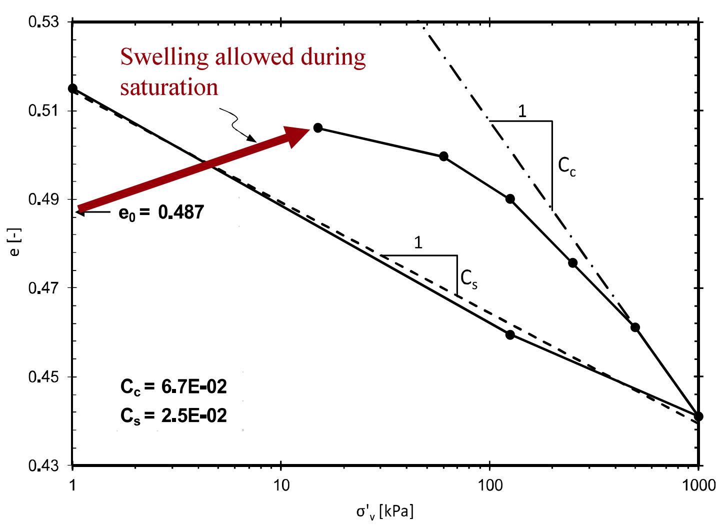

Computed in-situ vertical effective stress:

$\sigma'_v = 310$ kPa

Estimated max. vertical effective stress:

$\sigma'_{vp} = 180$ kPa

Computed OCR:

$OCR = 0.58$ <1 !!!

Stiffness

Isotropic Linear Elasticity

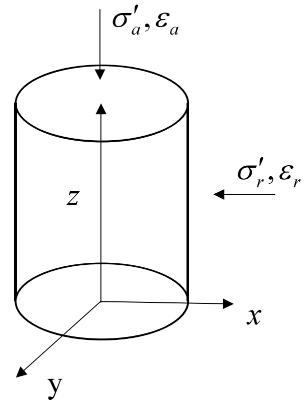

- Triaxial work-conjugated stress-strain variables

$$p' = (\sigma'_a + 2\sigma'_r)/3 \qquad q = \sigma_a - \sigma_r$$

$$\delta\varepsilon_{vol} = \delta\varepsilon_a + 2\delta\varepsilon_r \qquad \delta\varepsilon_q = \frac{2}{3}(\delta\varepsilon_a - \delta\varepsilon_r)$$

- Stiffness and compliance forms

$$\begin{bmatrix}\delta p' \\ \delta q\end{bmatrix} = \begin{bmatrix}K & 0 \\ 0 & 3G\end{bmatrix}\begin{bmatrix}\delta\varepsilon_{vol} \\ \delta\varepsilon_q\end{bmatrix}$$

$$\begin{bmatrix}\delta\varepsilon_{vol} \\ \delta\varepsilon_q\end{bmatrix} = \begin{bmatrix}1/K & 0 \\ 0 & 1/3G\end{bmatrix}\begin{bmatrix}\delta p' \\ \delta q\end{bmatrix}$$

- Two independent parameters
  - K, Bulk modulus
  - G, Shear modulus

$$K = \frac{E}{3(1-2\nu)} \qquad G = \frac{E}{2(1+\nu)}$$

$$E = \frac{9KG}{G+3K} \qquad \nu = \frac{3-2G/K}{2(G/K+3)}$$

Stiffness

Stiffness and strain ranges

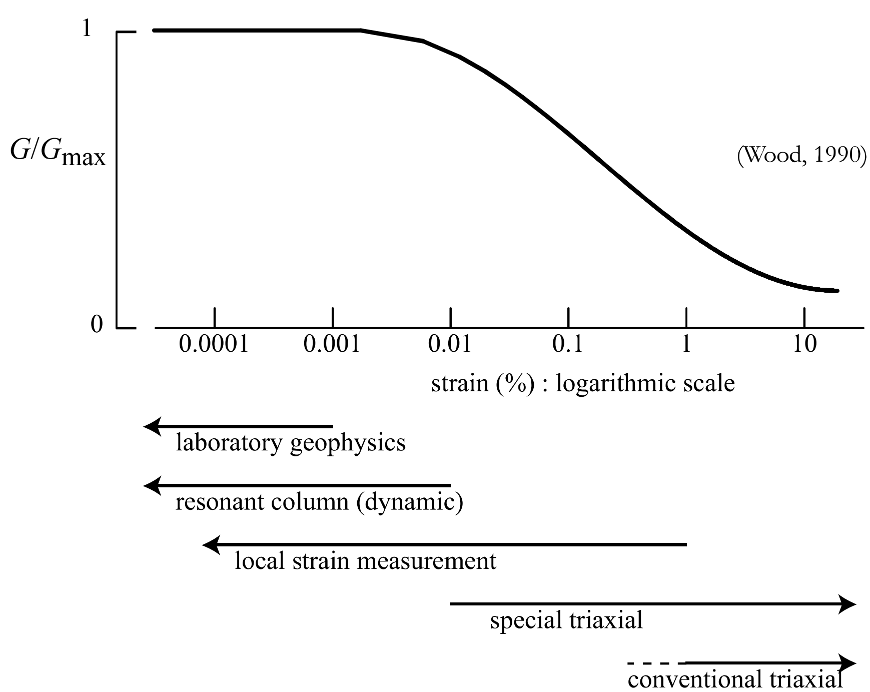

Stiffness

Isotropic Linear Elasticity

- Elastic parameters from the initial stages of CD tests

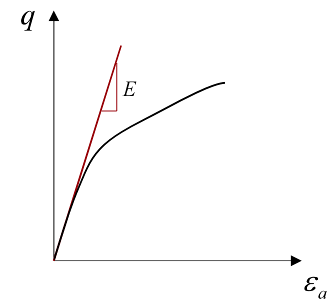

$$as\ \delta\sigma'_r = 0$$
$$\delta q = \delta\sigma'_a = \delta\varepsilon_a E$$
$$\rightarrow \frac{\delta q}{\delta\varepsilon_a} = E$$

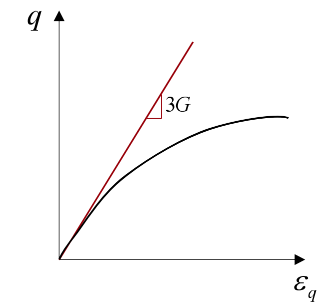

$$\delta\varepsilon_q = \frac{\delta q}{3G}$$
$$\rightarrow \frac{\delta q}{\delta\varepsilon_q} = 3G$$

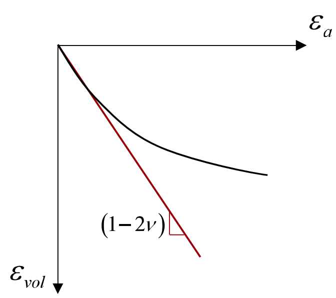

$$\delta\varepsilon_{vol} = \delta\varepsilon_a + 2\delta\varepsilon_v$$
$$\frac{\delta\varepsilon_{vol}}{\delta\varepsilon_a} = 1 + 2\frac{\delta\varepsilon_v}{\delta\varepsilon_a} =$$
$$\rightarrow \frac{\delta\varepsilon_{vol}}{\delta\varepsilon_a} = 1 - 2\nu$$

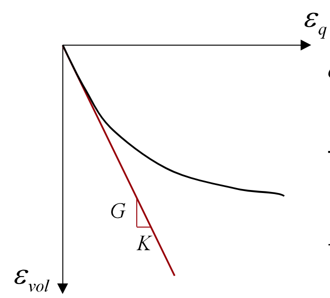

$$\delta\varepsilon_{vol} = \frac{\delta p'}{K};\ \delta\varepsilon_q = \frac{\delta q}{3G}$$
$$\frac{\delta\varepsilon_{vol}}{\delta\varepsilon_q} = \frac{3G}{K}\frac{\delta p'}{\delta q}$$
$$\rightarrow \frac{\delta\varepsilon_{vol}}{\delta\varepsilon_q} = \frac{G}{K}$$

Stiffness

Elastic parameters from CU triaxial tests

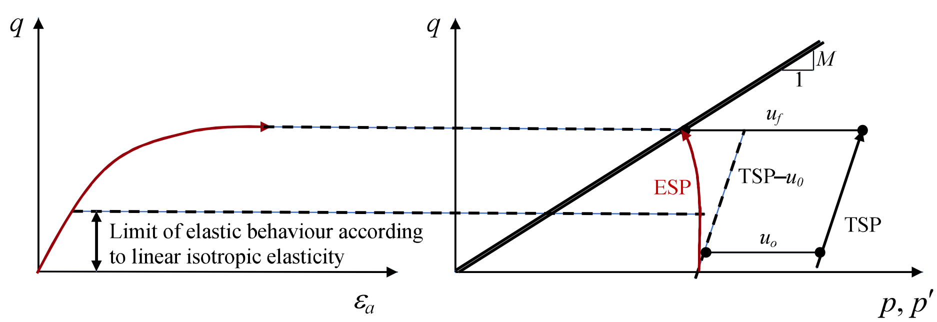

Stiffness

Elastic parameters from CU triaxial tests

- Interpretation in total stresses

$$\begin{bmatrix} \delta\varepsilon_{vol} \\ \delta\varepsilon_q \end{bmatrix} = \begin{bmatrix} 1/K_u & 0 \\ 0 & 1/3G_u \end{bmatrix} \begin{bmatrix} \delta p \\ \delta q \end{bmatrix}$$

1) Undrained bulk modulus $K_u = +\infty$ because $\delta\varepsilon_{vol} = 0$

It means $K_u = +\infty = \dfrac{E_u}{3(1-2\nu_u)} \Leftrightarrow \nu_u = 0.5$

2) $\delta\varepsilon_q = \dfrac{1}{3G_u}\delta q \Leftrightarrow G_u = G$ (same stiffness)

$$G_u = \frac{E_u}{2(1+\nu_u)} = \frac{E_u}{3} = G = \frac{E}{2(1+\nu)}$$

$$E_u = 3G_u = 3G = \frac{3E}{2(1+\nu)}$$

Undrainded and drained parameters are linked

Strength

Representation of strength in Mohr Coulomb type models

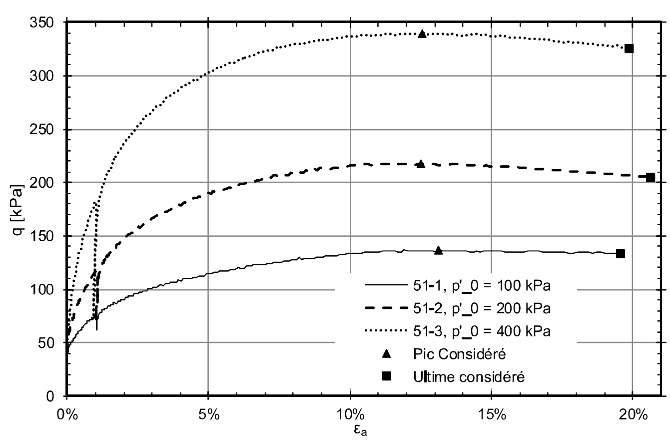

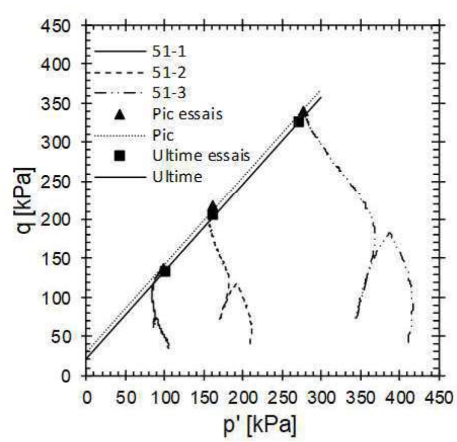

	φ' [°]	c' [kPa]	α' [°]	a' [kPa]
Pic	28.5	13.4	48.6	28.0
Ultime	28.2	9.9	48.3	20.7

Strength

Representation of strength in Mohr Coulomb type models

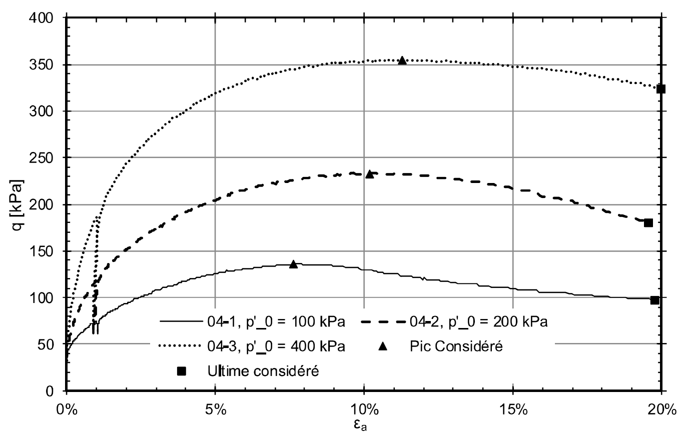

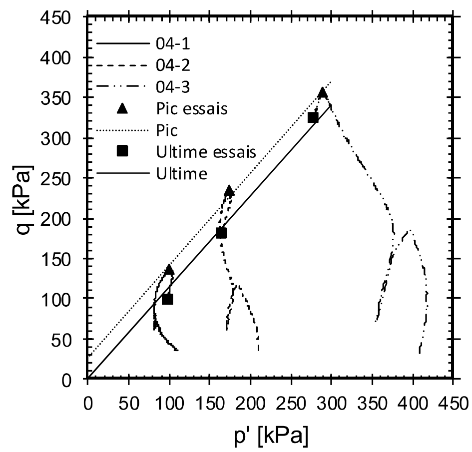

	φ' [°]	c' [kPa]	α' [°]	a' [kPa]
Pic	28.9	12.2	49.0	25.5
Ultime	28.5	0.0	48.6	0.0

Strength

Consolidation pressures in CD and CU triaxial tests

- CD tests allow a precise control of the stress paths
- CU tests: stress paths are not controllable

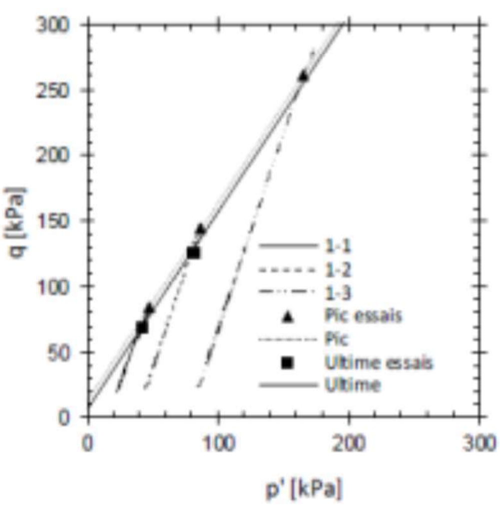

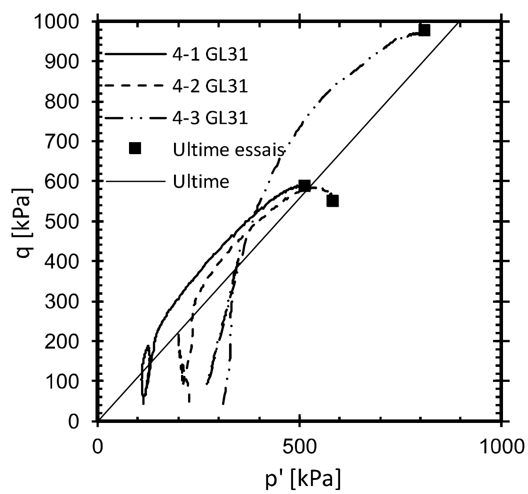

Energy Geotechnics, TC308 ISSMGE

- Geotechnical engineering is at the core of the energy challenge, from production and transportation, to waste management and carbon sequestration.
  - Energy Geo-Structure and Storage of Thermal Energy in the Ground
  - Carbon Dioxide Geological Storage
  - Energy Geo-storage
  - Unconventional Hydrocarbon. Hydraulic Fracturing
  - High Level Radioactive Waste Disposal
  - Low-carbon geotechnical engineering
  - …

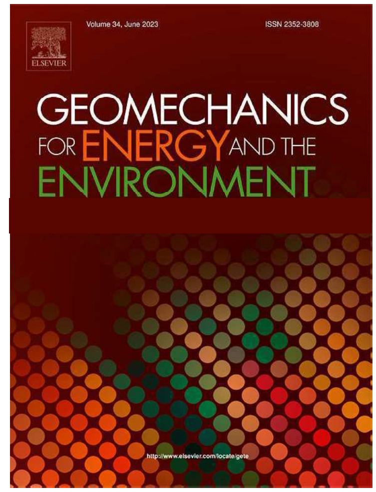

Water Retention Behaviour

Suction: a very brief introduction

- Suction imposition and measurement techniques depend on the component of the pore water potential to control/measure

Pore water potential = (- total suction)

Related to the relative humidity and temperature of pore air

$$\psi = \frac{\rho_w RT}{M_w} \ln(RH)$$

Capillary component (matric suction) +

Associated to presence of water menisci

$$s = u_a - u_w$$

Chemical component (osmotic suction)

Related to the composition of the pore water

$$\psi = s + \pi$$

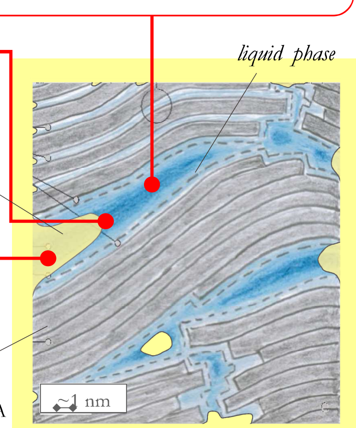

Picture courtesy of NAGRA

Suction control

Romero (2001). Controlled-suction techniques. Proc. 4º Simp. Brasileiro de Solos Nâo Saturados

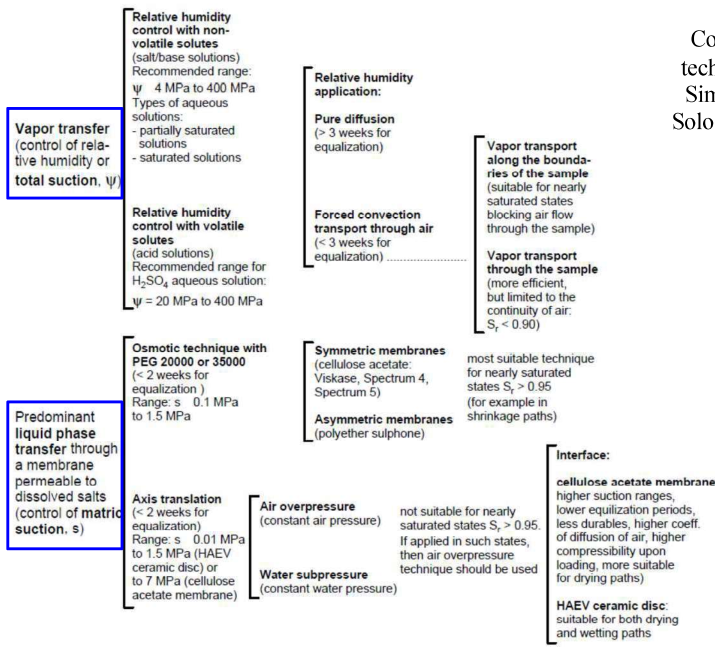

Suction control

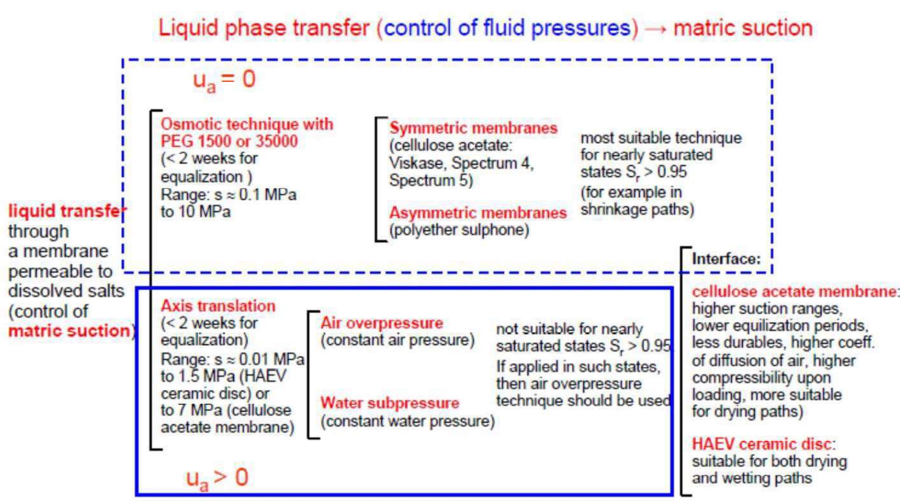

Axis translation technique

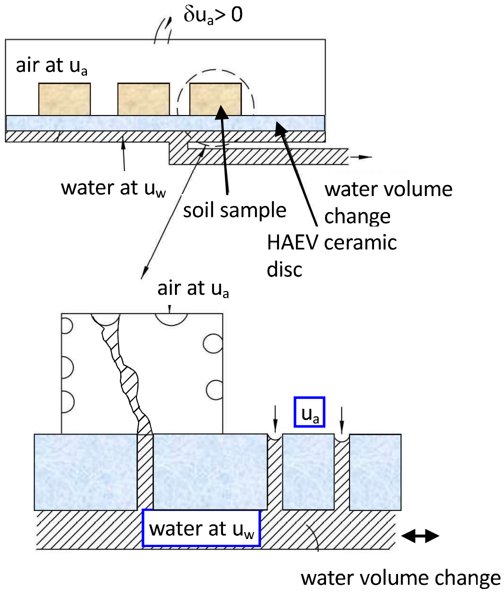

Axis translation (Hilf 1956)

$\delta u_a > 0$ (not representative of field conditions) brings water pressure in the positve range

HAEV ceramic disks

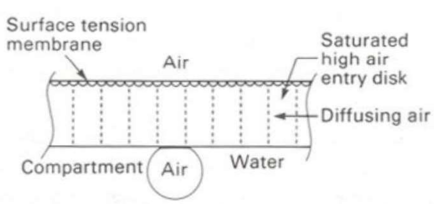

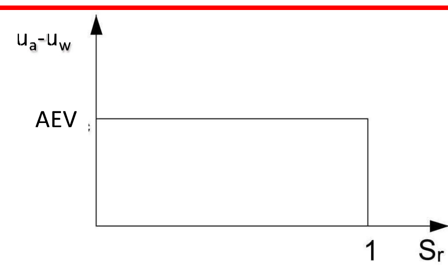

coarse porous metallic disc, air pressure at u_a

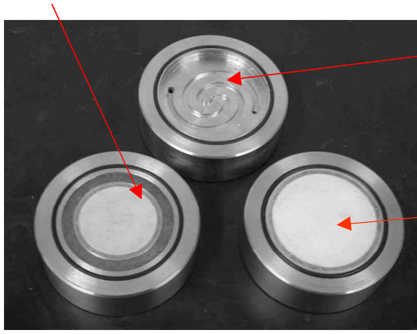

grooves to flush dissolved air

HAEV ceramic disc, water pressure at u_w

Pressure plate apparatus

Pressure plate apparatus

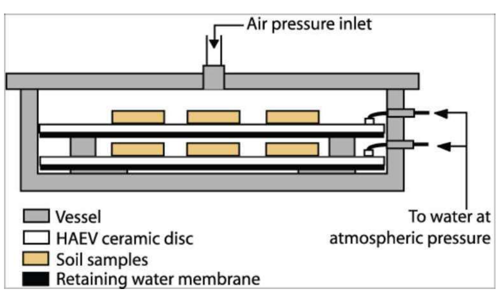

Bishop and Donald's traxial cell (1961)

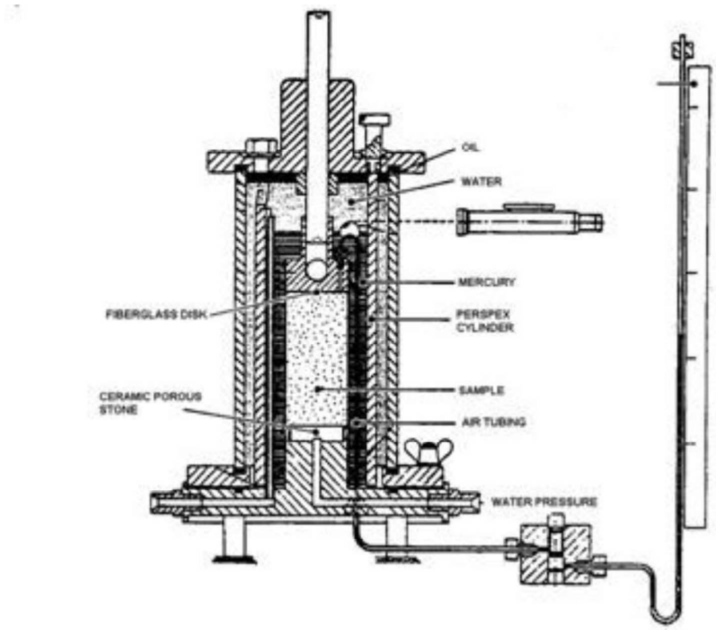

EPFL controlled suction oedometric cell

- Axis translation technique
- Suction control up to 500 kPa
- Continuous monitoring of vertical strain and water volume change

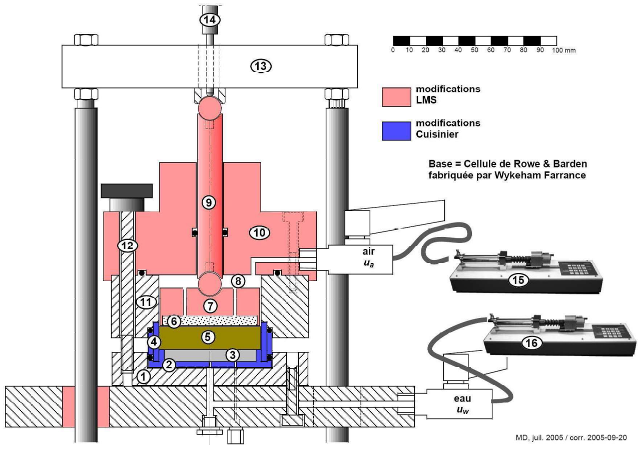

Axis Translation technique

- Advantages
  - Large experience available
  - Easily applicable to common geotechnical testing devices
  - Hydraulic paths (wetting/dryng) are clearly controlled

- Issues
  - Difficoult for very high and very low degrees of saturation
  - Lost of water-phase continuity the with ceramic disk
  - Air diffused beneath the HAEV ceramic disk
  - Evaporation or water from the sample

Evaporation from sample

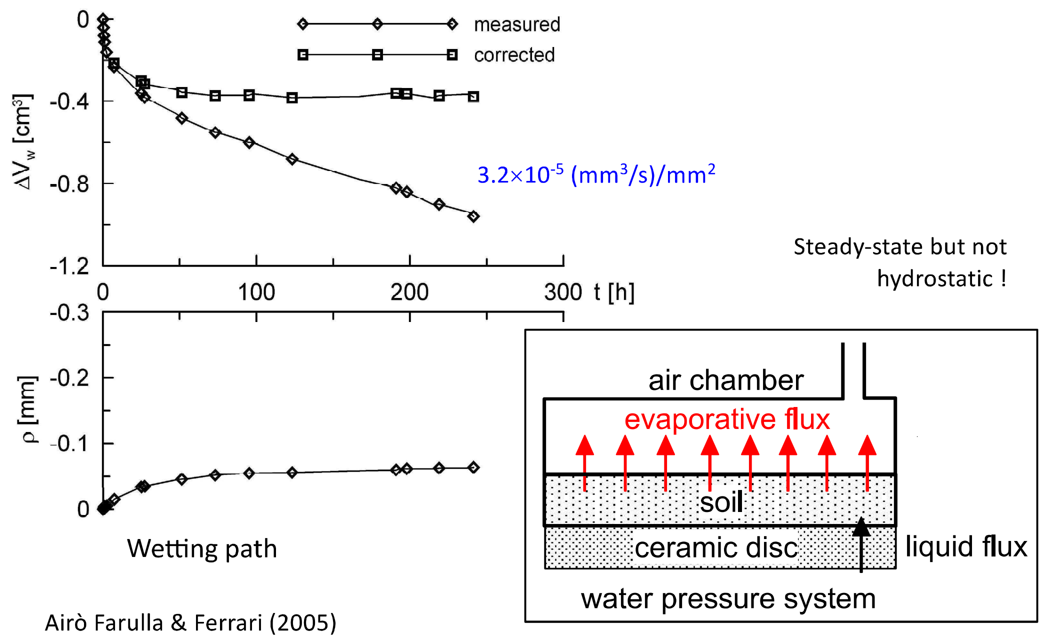

Airò Farulla & Ferrari (2005)

Effect of air diffusion

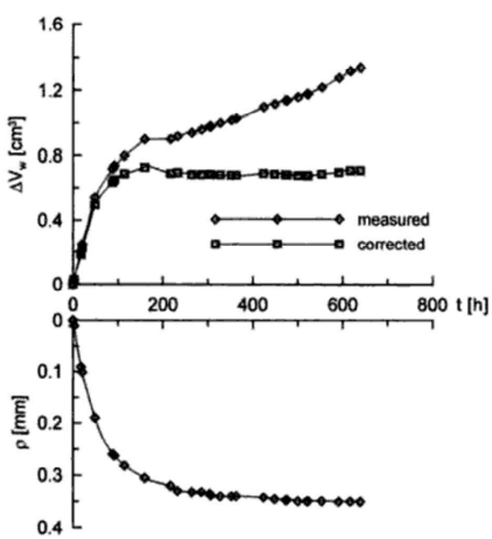

Airò Farulla & Ferrari (2005)

Coupled hydro-mechanical response

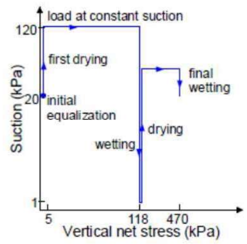

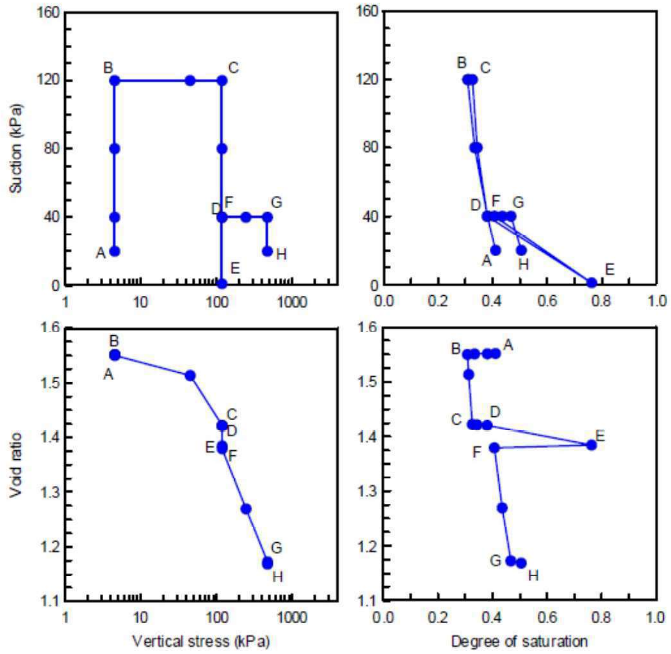

Controlled-suction oedometric tests on a volcanic soil - Ferrari et al. (2013)

Suction control

Vapour transfer (control of relative humidity) → total suction

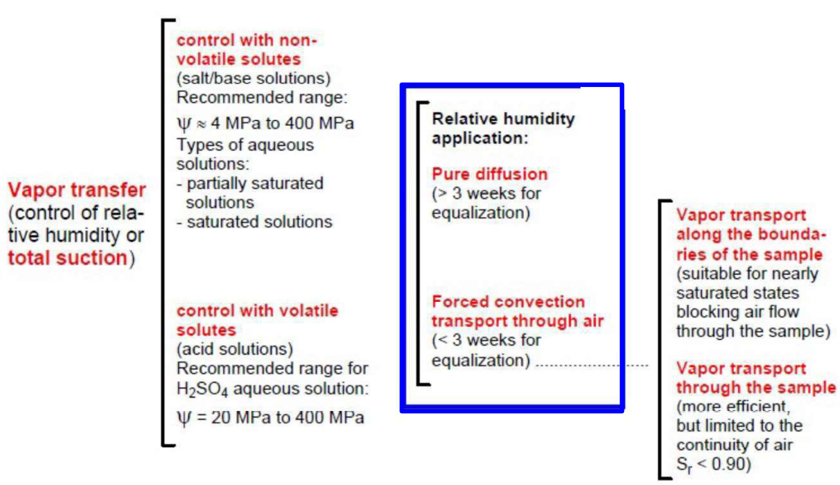

Volumetric behaviour (free stress)

- Water content and volume change assessment
- Specimen size: d=30mm, h=20mm
- Biaxial strain gauges (anisotropy)

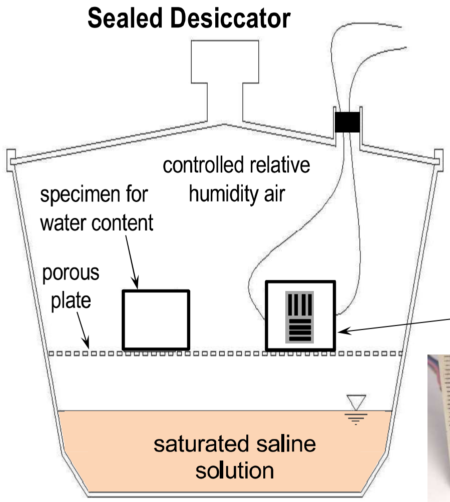

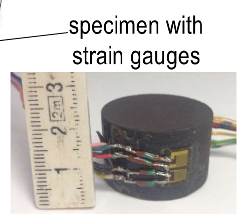

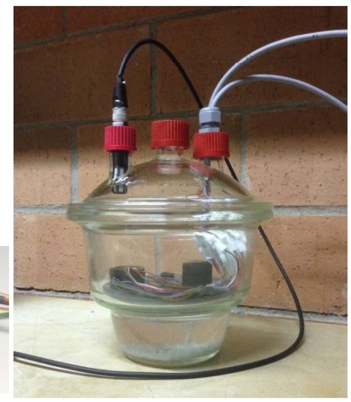

Vapour equilibrium technique and volume change assessment

Tests on Opalinus Clay shales

Minardi et al. 2016
Geotechnique Letters

- Two cylindrical specimens are used for each tested facies (d=25 mm, h=20 mm)
- Two biaxial strain gages with macrostrain accuracy (10^{-6} ε) for strain measurement perpendicular ($\varepsilon^{\perp}$) and parallel ($\varepsilon^{//}$) to bedding

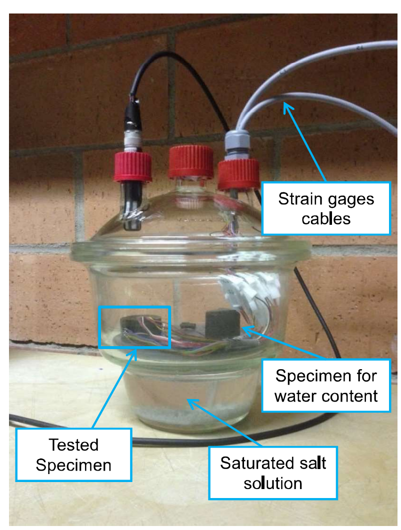

Results – Water Retention Curve

Minardi et al. 2016
Geotechnique Letters

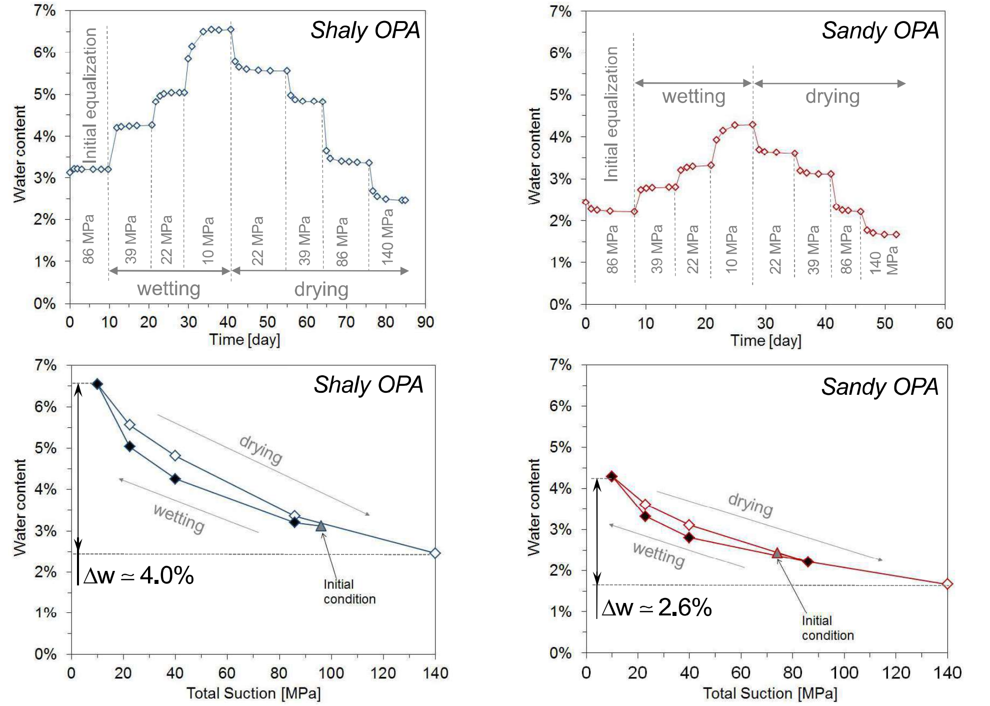

Results – Water Retention Curve

Minardi et al. 2016
Geotechnique Letters

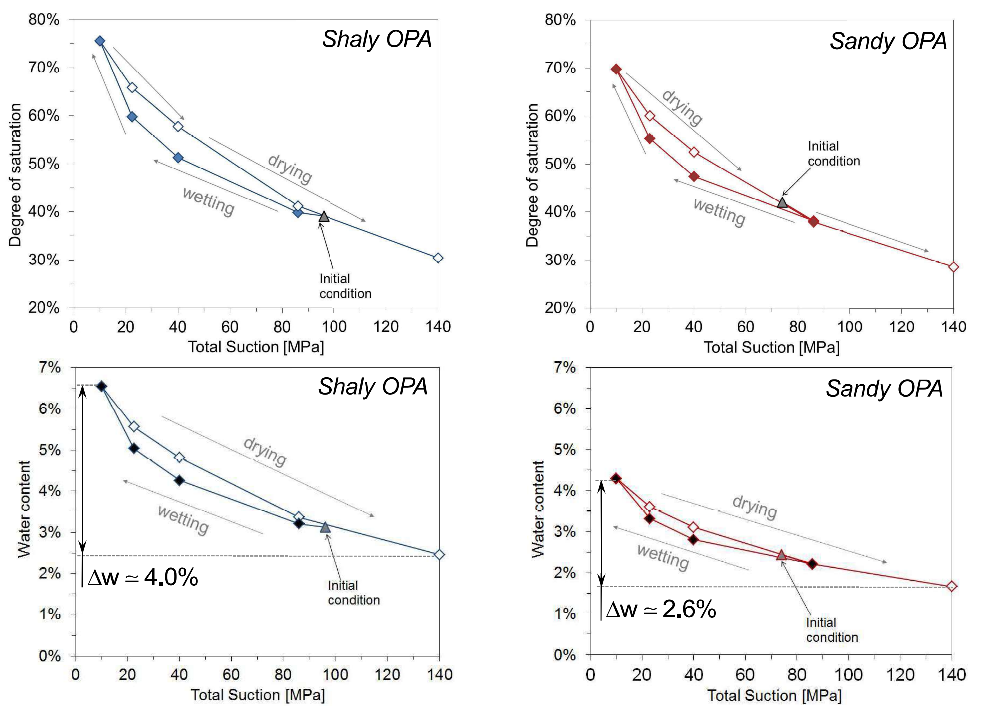

Vapour equilibrium technique implementation in an oedometric setup

Experimental setup for implementation of hydro-mechanical paths on shot-clay MX-80 bentonite (total suction application with partially saturated NaCl solutions)

Ferrari, Seiphoori & Laloui, 2014
Eng. Geology

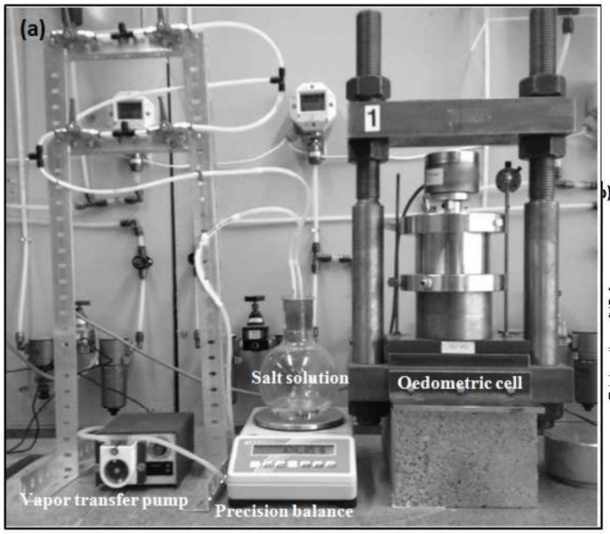

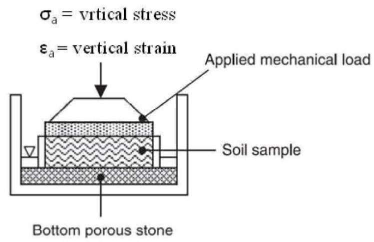

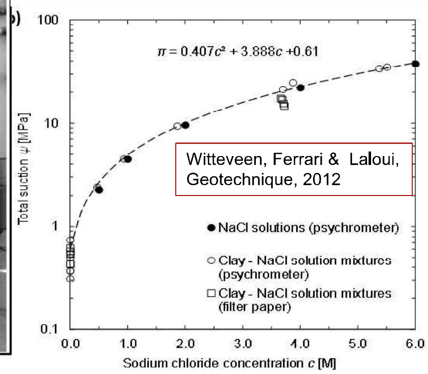

MX-80 Shot-clay: hydro-mechanical stress path

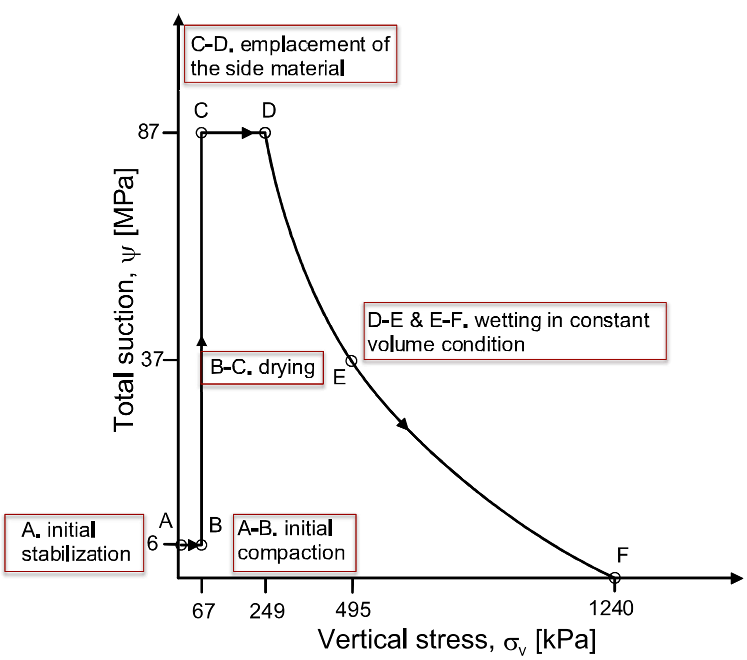

MX-80 Shot-clay: hydro-mechanical response

Ferrari, Seiphoori & Laloui, 2014

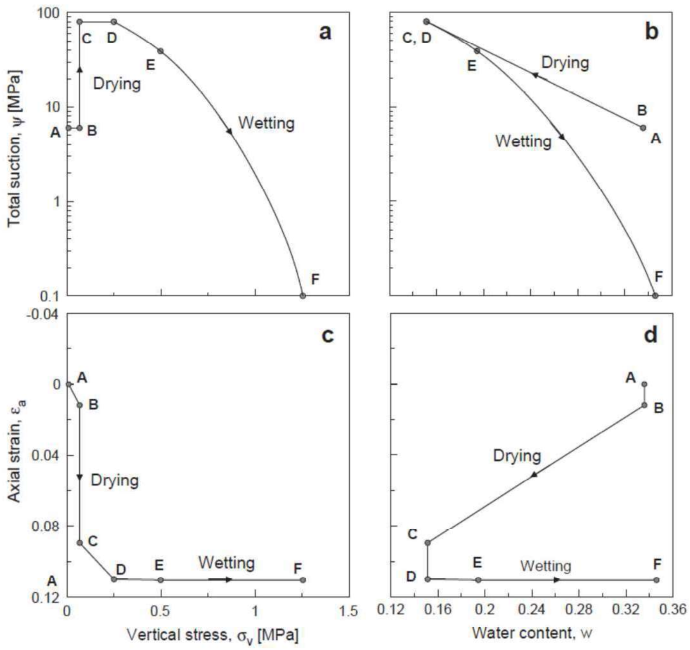

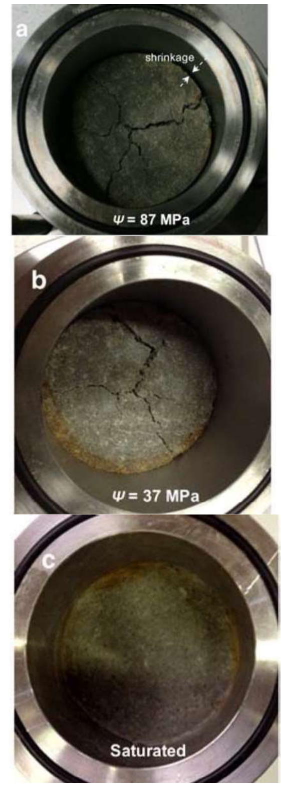

Vapour-controlled testing of gas shales

Testing set-up & Specimen preparation

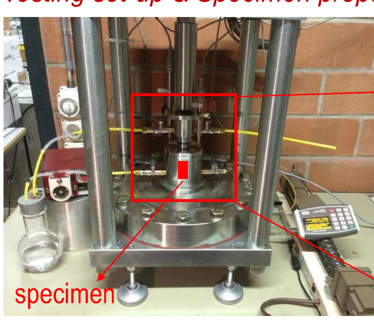

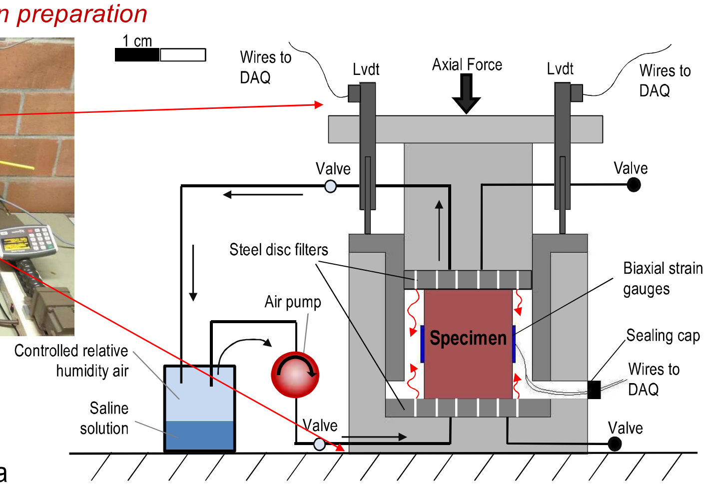

Main features

- Axial stress up to 100 MPa
- Specimen size d≃20 mm, h≃30-40 mm
- Vapor equilibrium technique to control total suction
- Apparatus deformation are considered for LVDTs readings
- Air pump to force vapor circulation towards the specimen

Specimens tested in uniaxial stress conditions

Minardi et al. 2017

Vapour-controlled testing of gas shales

Minardi et al. 2017

Overview of the results

- Negative strain → expansion
- Response in the axial and radial direction

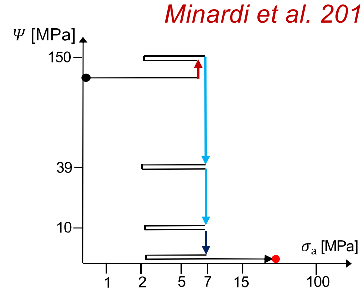

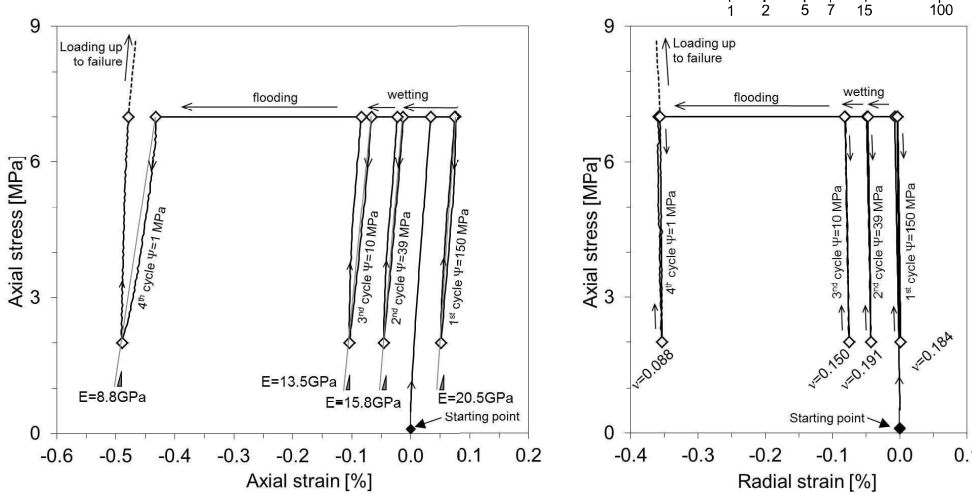

Suction measurement

Instrument	Suction component measured	Typical measurement range (kPa)	Equilibration time
		Suction measurement	
Pressure plate	Matric	0–1,500	Several hours to days
Tensiometers and suction probes	Matric	0–1,500	Several minutes
Thermal conductivity sensors	Matric	1–1,500	Several hours to days
Electrical conductivity sensors	Matric	50–1,500	Several hours to weeks
Filter paper contact	Matric	0–10,000 or greater	2–57 days
Thermocouple psychrometers	Total	100–8,000	Several minutes to several hours
Transistor psychrometers	Total	100–70,000	About 1 hour
Chilled mirror psychrometer	Total	1–60,000	3–10 minutes
Filter paper non-contact	Total	1,000–10,000 or greater	2–14 days
Electrical conductivity of pore water extracted using pore fluid squeezer	Osmotic	entire range	—

Murray and Sivakumar (2010)

The Chilled-mirror dew-point psychrometer

Suction measurement by the chilled mirror dew-point psychrometer

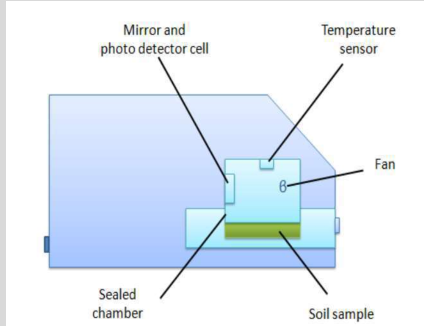

- Total suction measurement
- Suction measurements from 3 to 300 MPa
- Temperature range (15 - 40 °C)
- Fast suction measurement

Leong et al. 2005
Cardoso et al. 2007

Main Components

- Mirror
- Thermoelectric (Peltier) cooler
- Photoelectric cell → detects the point at which the condensation appears in the mirror
- Infrared thermometer → detects the specimen temperature
- Fan → speed up the equilibrium time

Water retention analysis through the use of the WP4

Results: Opalinus Clay Shale

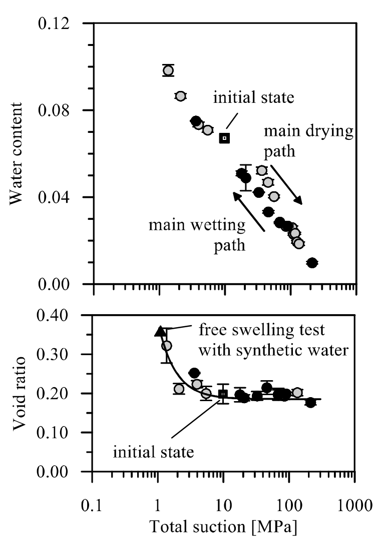

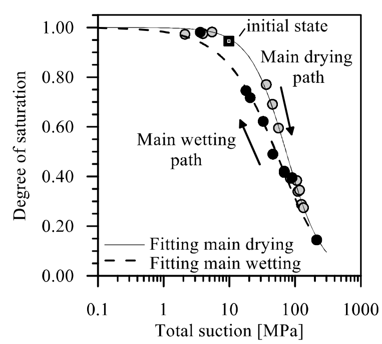

Air entry value ~ 13 MPa

Ferrari et al. 2014, IJRMMS

Water retention analysis through the use of the WP4

Results: Opalinus Clay shale

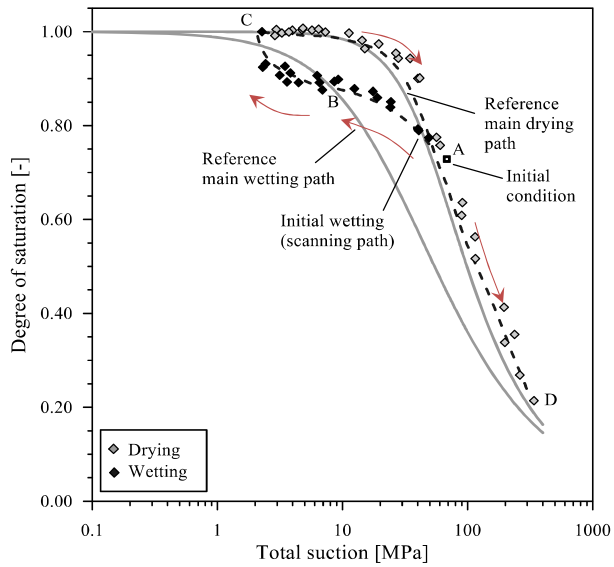

Ferrari et al. 2014, IJRMMS

Measurement of the osmotic component

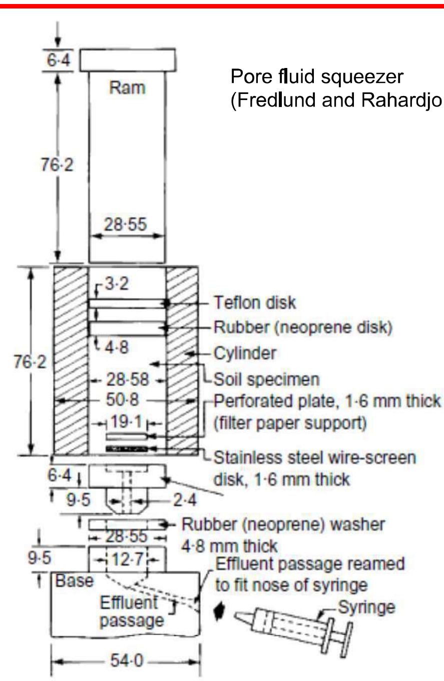

Pore fluid squeezer
(Fredlund and Rahardjo, 1993)

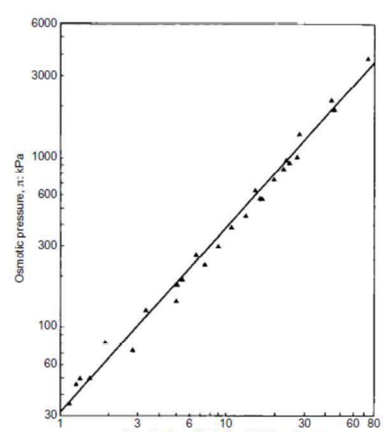

Thermo-mechanical testing

"Extended" stress-paths

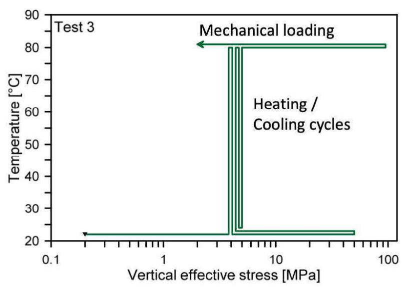

oedometer

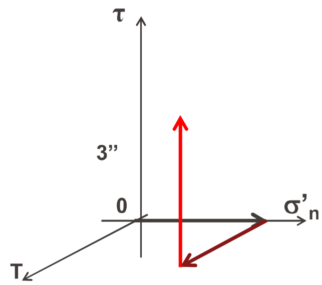

direct shear

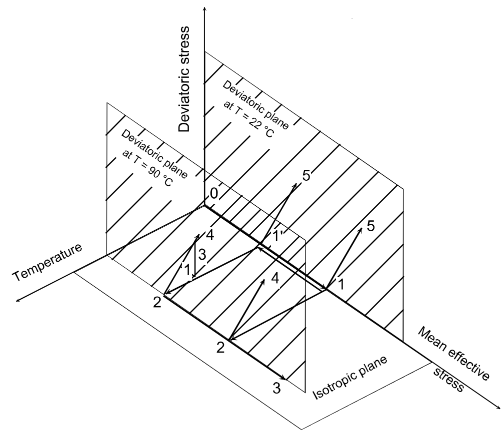

triax

Thermo-mechanical testing

Controlled-temperature oedometers

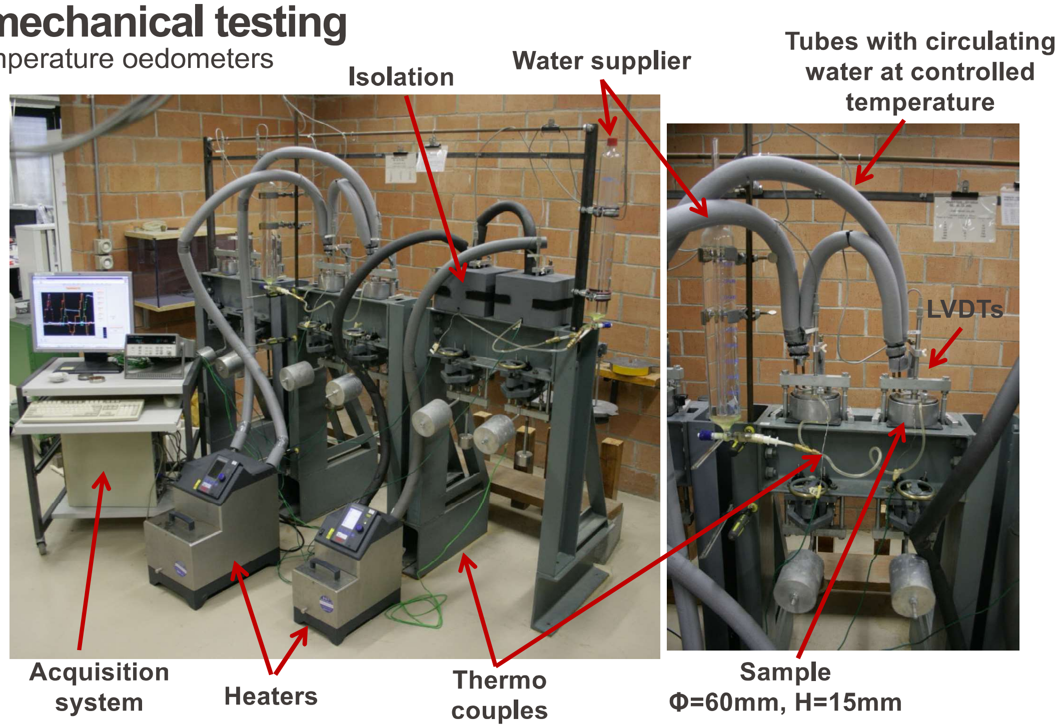

Thermo-mechanical testing

Controlled-temperature oedometers

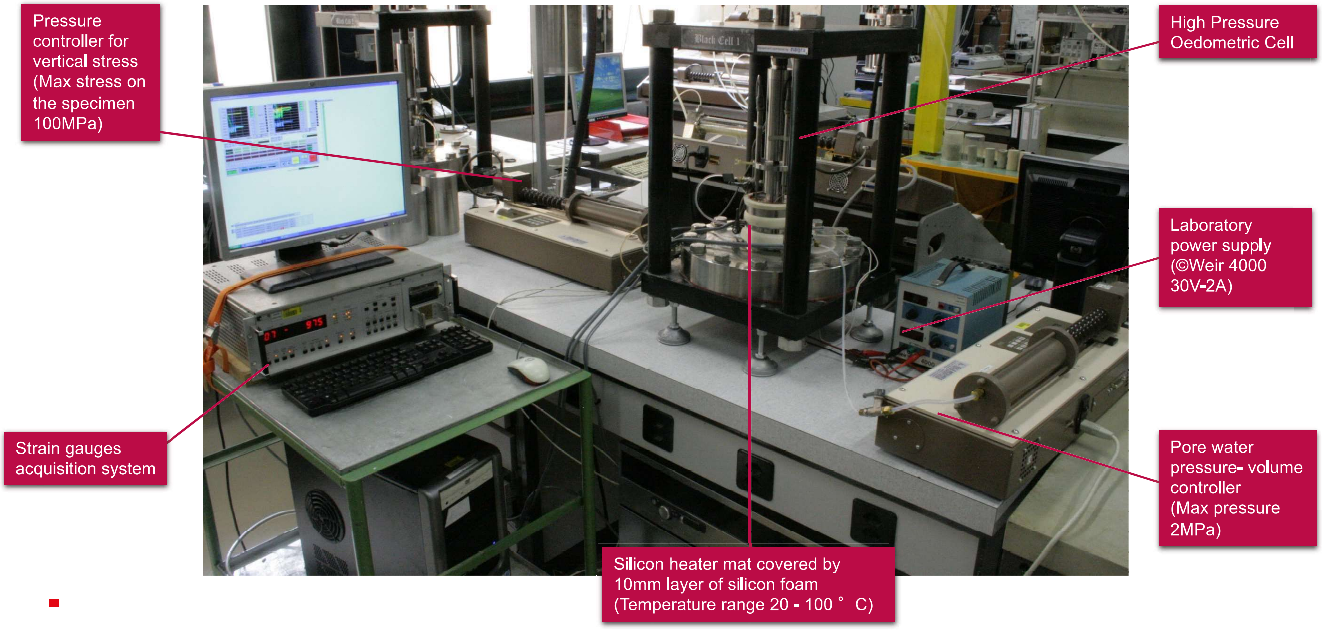

Thermo-mechanical testing

(Favero, Ferrari and Laloui, 2016)

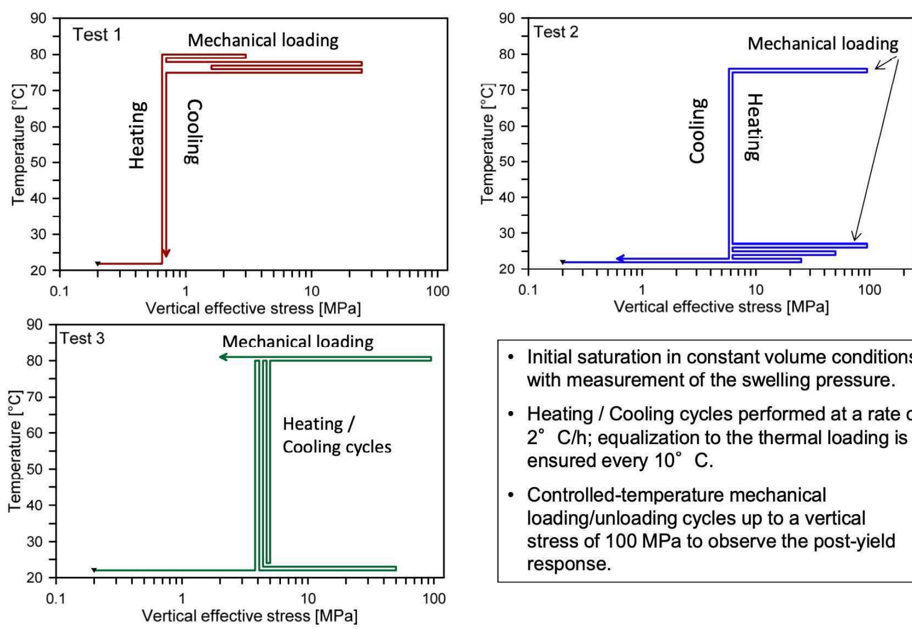

- Initial saturation in constant volume conditions with measurement of the swelling pressure.
- Heating / Cooling cycles performed at a rate of 2° C/h; equalization to the thermal loading is ensured every 10° C.
- Controlled-temperature mechanical loading/unloading cycles up to a vertical stress of 100 MPa to observe the post-yield response.

Thermo-mechanical testing

Test phases: - heating after saturation → thermal collapse

- oedometric compression at room temperature
- oedometric recompression at high temperature

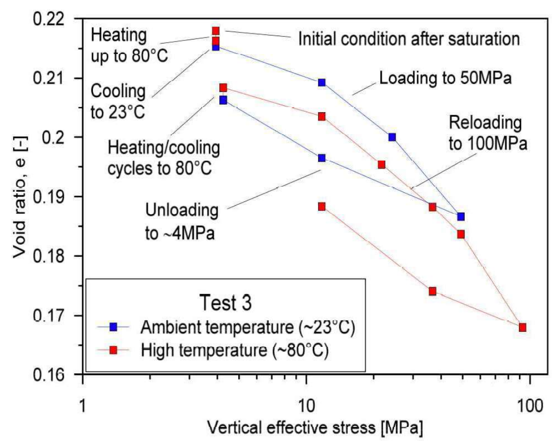

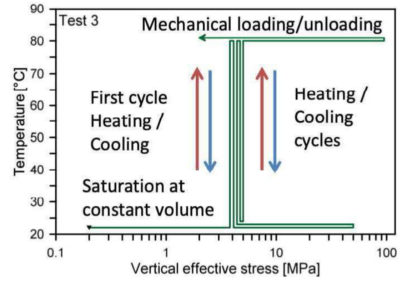

- Thermal compaction during first heating
- Thermal expansion during second heating
- Lower void ratio at the same vertical stress after reloading at high temperature

Thermo-mechanical testing

Impact of temperature on the hydro-mechanical behaviour

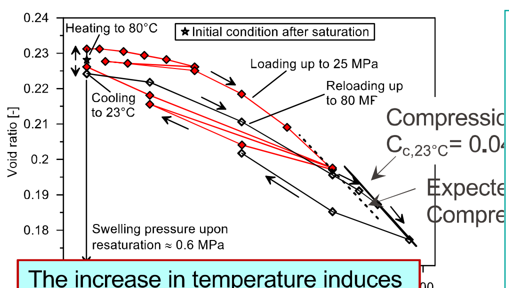

The increase in temperature induces a decrease in the yield stress

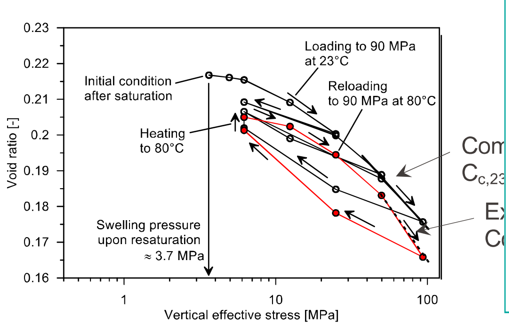

(Favero, Ferrari and Laloui, 2016)

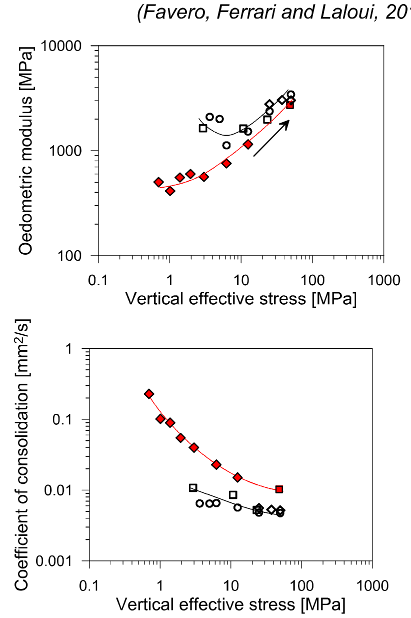

Thermo-mechanical testing

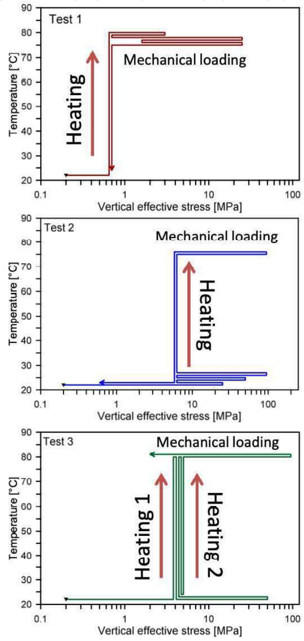

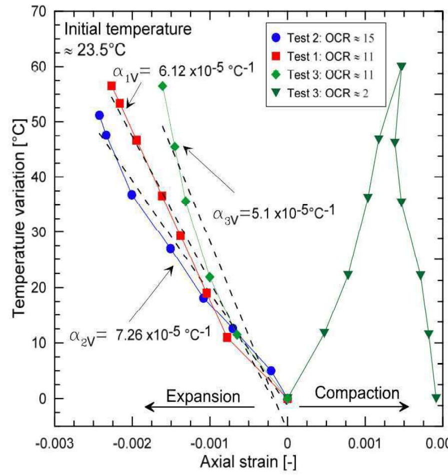

- Thermal expansion upon heating in overconsolidated conditions.
- Irreversible compaction upon heating in conditions close to normal consolidation.

Thermo-mechanical modelling

- Extension of (Critical State) Geomechanical models to incorporate thermal effects
  - Thermo-elasticity

$$d\varepsilon_V^e = \frac{dp'}{K} - \beta_s' dT$$

$$K = K_{ref}\left(\frac{p'}{p_{ref}}\right)^n$$

$$\beta_s' = (\beta_{s0}' - \frac{\beta_{s0}}{100}T)\,\frac{p'_{c0}}{p'}$$

  - Ultimate shear strength

$$M = M_0 + g\left(T - T_0\right)$$

  - T-dependent yield surface

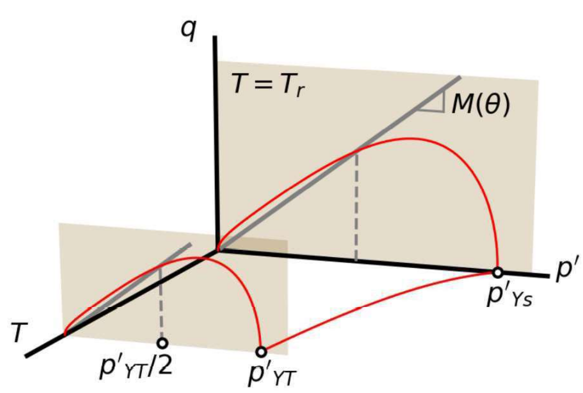

$$p'_{YT} = p'_{Ys(Tr)}\left[1 - \gamma_T \ln\left(\frac{T}{T_r}\right)\right]$$

(Bosch, Qiao, Ferrari, Laloui, 2023)

Thermo-mechanical testing

Direct shear

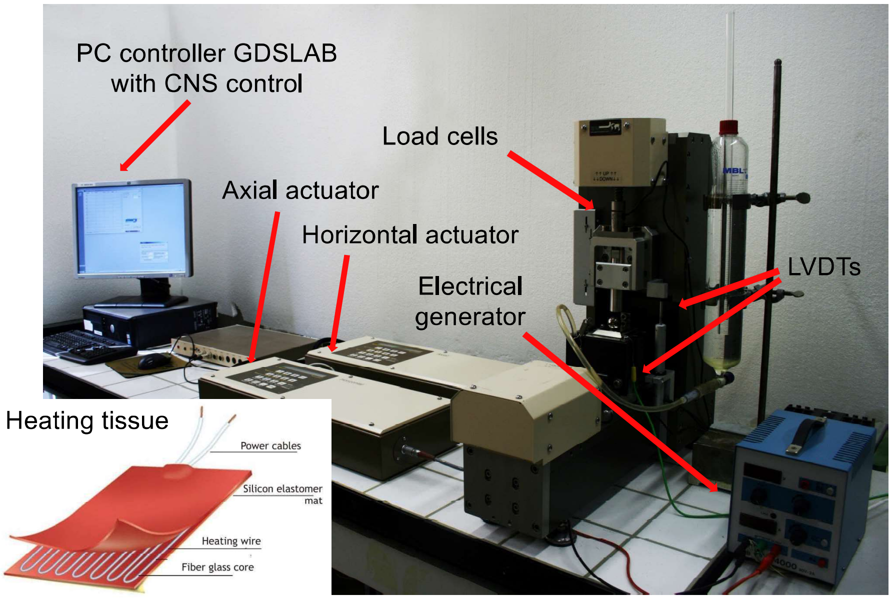

(Di Donna, Ferrari and Laloui, 2016)

Sand-concrete interface

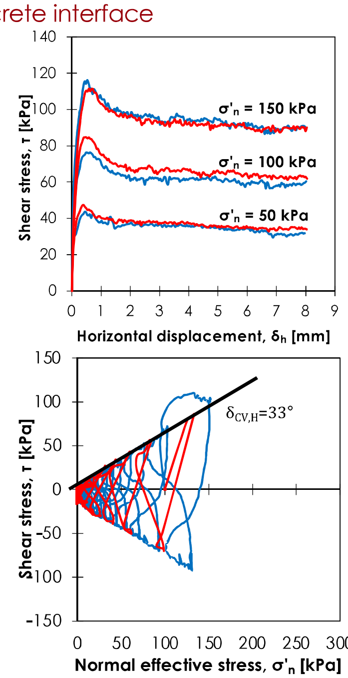

- Monotonic CNL medium roughness

20 °C
50 °C

- Cyclic CNS (**K= 500 kPa/mm**) high roughness

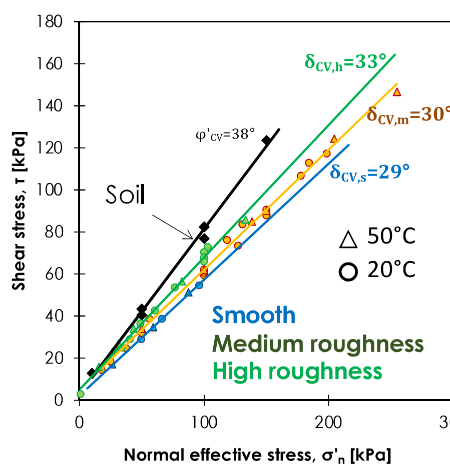

- There is **no effect of temperature** under **monotonic CNL** or **cyclic CNS** for every **roughness**

Clay-concrete interface

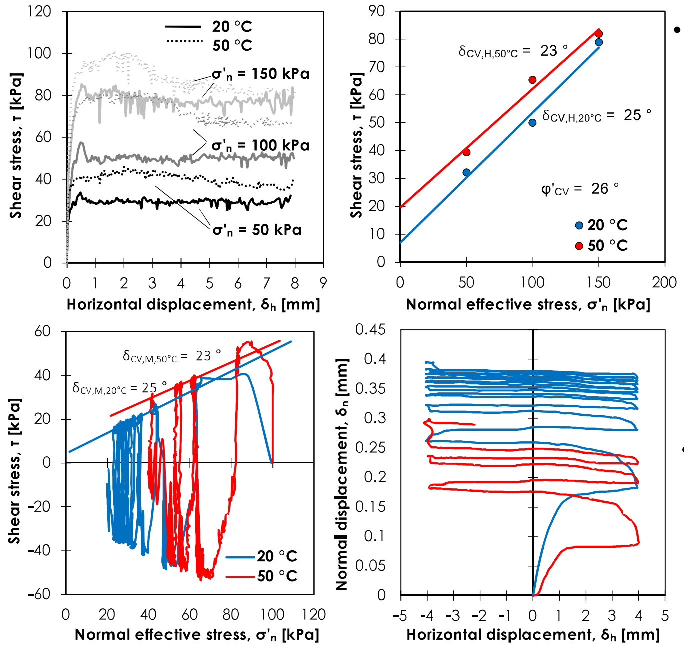

- Monotonic CNL high roughness
- The increase in **temperature** induces an **increase of strength** due to thermal consolidation of NC clay which increases the **adhesion**
- Cyclic CNS (K= 200 kPa/mm) medium roughness

Appendix D. Thermo-hydro-mechanical processes in geomaterials: constitutive modelling (J.M Pereira)

Thermo-hydro-mechanical processes in geomaterials: constitutive modelling

Jean-Michel Pereira

ALERT O.Z. & eurad PhD School, August 2023, Liège

Laboratoire Navier, École des Ponts ParisTech

Breaking eggs...

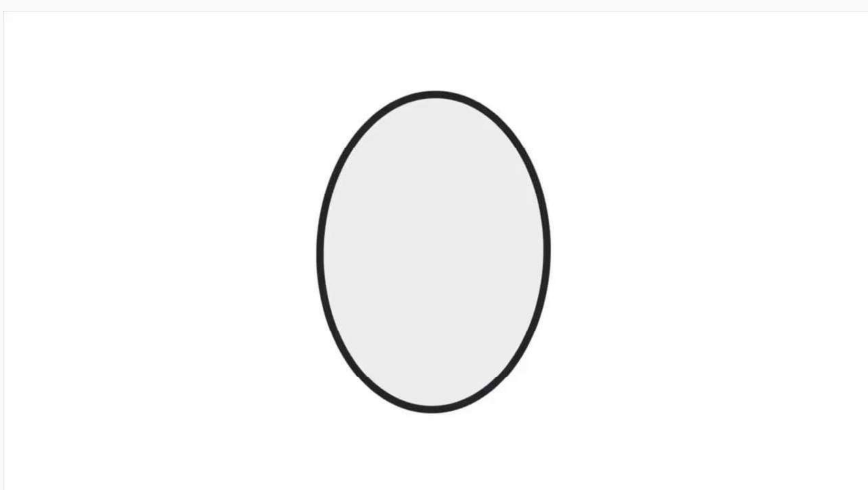

(https://www.youtube.com/@TheScienceClassroom)

THM processess in geomaterials

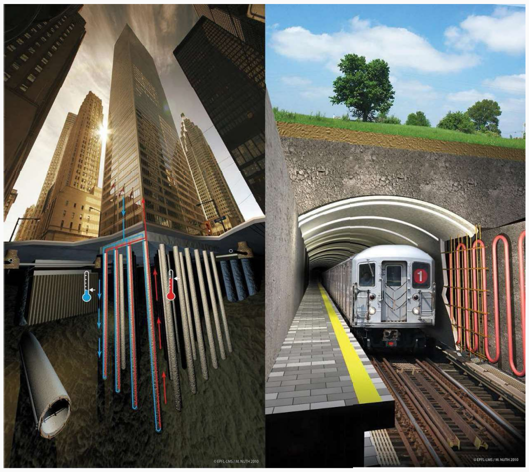

(EPFL – Mathieu Nuth)

Applications:

- shallow energy geostructures
- slope stability, incl. permafrost
- energy production and storage
- nuclear waste disposal
- CO_2 geological storage
- ...

THM processess in geomaterials

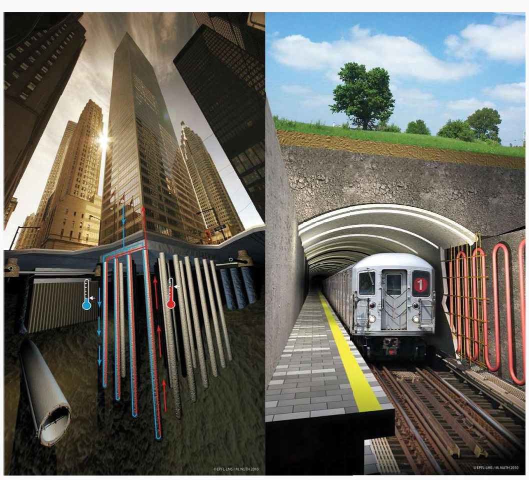

(EPFL – Mathieu Nuth)

Physical processes:

- humidity effects
- thermal stress/strains
- thermal pressurisation
- phase changes
- ...

Outline

Back to thermodynamics

Pioneers

Pioneers

Karl von Terzaghi
(1883-1963)

Maurice A. Biot
(1905-1985)

Prof. Olivier Coussy

(1953 – 2010)

A poromechanics legacy

- 5 books
- c.a. 100 papers in scientific journals
- Laboratoire Navier (ENPC/UGE/CNRS)

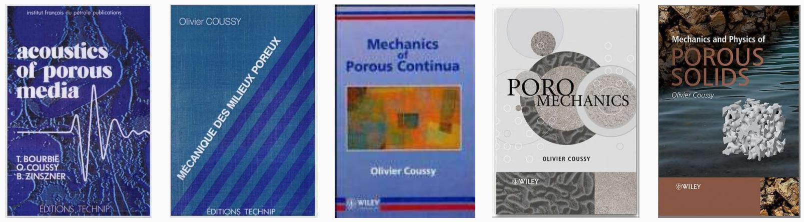

Porous media: a few definitions

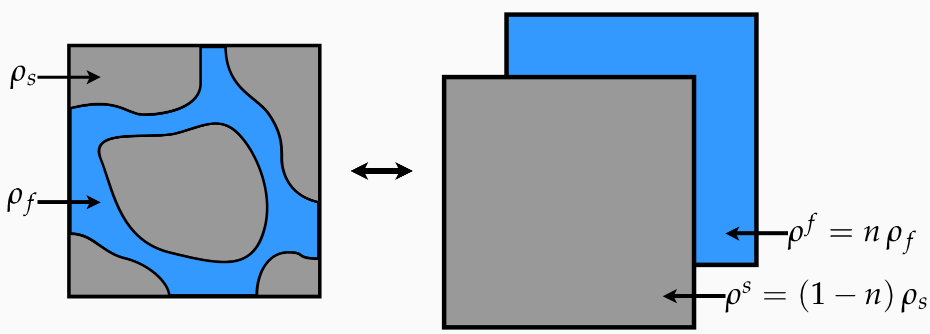

Porous media: a few definitions

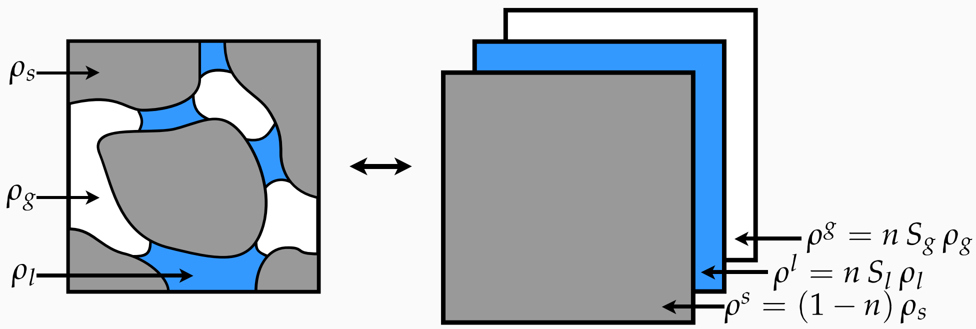

Porous media: a few definitions

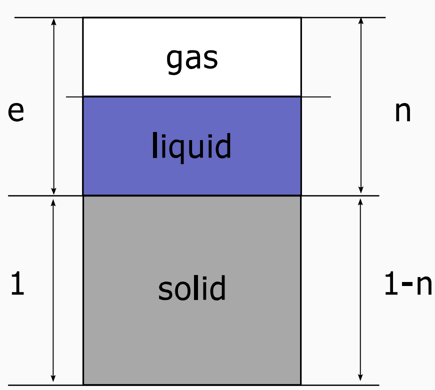

Porosity and degree of saturation:

$$n \text{ or } \phi = \frac{\text{pores vol.}}{\text{total vol.}}$$

$$S_l = \frac{\text{liquid vol.}}{\text{pores vol.}} = 1 - S_g$$

j.m. pereira – alert oz & eurad PhD school, 2023 6/87

Thermodynamic/energetic approach: overview i

- Define the system!
- Balance of energy at continuum scale[1] (Coussy 2004)
  - state equations (energy potential and state variables)
  - conjugate variables
- Identify an energy potential
  - deduce the constitutive relations
  - e.g. quadratic potential provides linear behaviour

[1]RVE, macroscale

Thermodynamic/energetic approach: overview ii

Up-scaling techniques based on microscructure (often idealized structures)

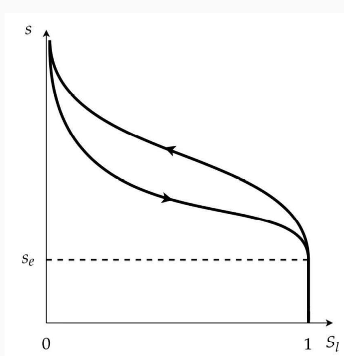

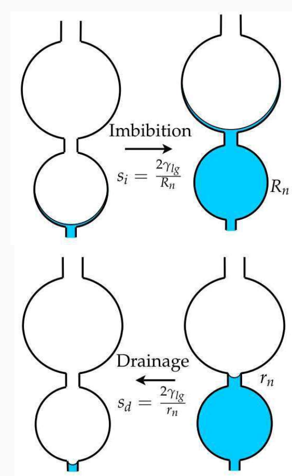

Energetic approach – illustration

Work input (reversible case)

Infinitesimal work to the initial volume

$$\text{for a 1D spring:} \qquad dW = F\,dx$$

Work input (reversible case)

Infinitesimal work to the initial volume

$$\begin{aligned} \text{for a 1D spring:} \quad dW &= F\,\mathrm{d}x \\ \text{for a non porous solid:} \quad dW &= -p\,\mathrm{d}V \end{aligned}$$

Work input (reversible case)

Infinitesimal work to the initial volume

$$\begin{aligned} \text{for a 1D spring:} \quad dW &= F\,\mathrm{d}x \\ \text{for a non porous solid:} \quad dW &= -p\,\mathrm{d}V \\ \text{for a porous solid:} \quad dW &= -p\,\mathrm{d}V + p_l\,\mathrm{d}(n\,V) \end{aligned}$$

Work input (reversible case)

Infinitesimal work to the initial volume

$$\begin{aligned} \text{for a 1D spring:} \quad dW &= F\,\mathrm{d}x \\ \text{for a non porous solid:} \quad dW &= -p\,\mathrm{d}V \\ \text{for a porous solid:} \quad dW &= -p\,\mathrm{d}V + p_l\,\mathrm{d}(n\,V) \end{aligned}$$

Infinitesimal strain work (solid skeleton) $\mathrm{d}W = \mathrm{d}w\,V_0$

$$\text{for a porous solid:} \quad dw = p\,\mathrm{d}\epsilon_v + p_l\,\mathrm{d}\phi$$

Conjugate variables

Work input (extended to triaxial space)

$$\mathrm{d}w = p\,\mathrm{d}\epsilon_v + q\,\mathrm{d}\epsilon_q + p_l\,\mathrm{d}\phi$$

Strain-work conjugate variables

$$\begin{aligned} p &\longleftrightarrow \epsilon_v \\ q &\longleftrightarrow \epsilon_q \\ p_l &\longleftrightarrow \phi \end{aligned}$$

Conjugate variables – Terzaghi stress

Incompressibility of the solid grains ($K_s \gg K$) (Coussy 2004)

$$\mathrm{d}\epsilon_v = -\mathrm{d}\phi$$

Strain work input (Schofield and Wroth 1968)

$$\begin{aligned} dw &= (p - p_l)\,\mathrm{d}\epsilon_v + q\,\mathrm{d}\epsilon_q \\ &= p'\,\mathrm{d}\epsilon_v + q\,\mathrm{d}\epsilon_q \end{aligned}$$

Conjugate variables

$$\begin{aligned} p' = \frac{1}{3}(\sigma_1' + 2\sigma_3') \quad &\longleftrightarrow \quad \epsilon_v = \epsilon_1 + 2\epsilon_3 \\ q = \sigma_1 - \sigma_3 \quad &\longleftrightarrow \quad \epsilon_q = \frac{2}{3}(\epsilon_1 - \epsilon_3) \end{aligned}$$

Conjugate variables – tensorial form

Work input

$$\mathrm{d}w = \boldsymbol{\sigma} : \mathrm{d}\boldsymbol{\epsilon} + p_l\,\mathrm{d}\phi = \sigma_{ij}\,\mathrm{d}\epsilon_{ij} + p_l\,\mathrm{d}\phi$$

Strain-work conjugate variables

$$\begin{aligned} \boldsymbol{\sigma} &\longleftrightarrow \boldsymbol{\epsilon} \\ p_l &\longleftrightarrow \phi \end{aligned}$$

Work input (imcompressibility)

$$\mathrm{d}w = \boldsymbol{\sigma}' : \mathrm{d}\boldsymbol{\epsilon} = \sigma_{ij}'\,\mathrm{d}\epsilon_{ij}$$

Strain-work conjugate variables

$$\boldsymbol{\sigma}' \longleftrightarrow \boldsymbol{\epsilon}$$

How to get the constitutive laws?

Work input and dissipation – Clausius-Duhem inequality

Beyond reversibility?

Application of first and second laws of thermodynamics

$$\mathrm{d}D = \mathrm{d}w - \mathrm{d}F \geq 0$$

D: dissipation
F: free energy of the solid skeleton

State equations in reversible case

Clausius-Duhem inequality

$$dD = \sigma_{ij}\, d\epsilon_{ij} + p_l\, d\phi - dF \geq 0$$

Elasticity $\Leftrightarrow$ reversibility i.e. no dissipation ($dD = 0$ and $\boldsymbol{\epsilon} = \boldsymbol{\epsilon}^e$ and $d\phi = d\phi^e$)

$$dF = \sigma_{ij}\, d\epsilon_{ij} + p_l\, d\phi$$

Hence $F = F(\boldsymbol{\epsilon}, \phi)$ and the following state equations hold

$$\begin{aligned} \boldsymbol{\sigma} &= \frac{\partial F}{\partial \boldsymbol{\epsilon}} \\ p_l &= \frac{\partial F}{\partial \phi} \end{aligned}$$

Linear poroelasticity

Energy potential F

Inspecting the state equations, it appears that a linear behaviour stems from a quadratic potential

$\rightarrow$ From a stress- and pressure-free reference state

$$\begin{aligned} \boldsymbol{\sigma} &= \mathbb{D}\,\boldsymbol{\epsilon} - b\, p_l\, \boldsymbol{\delta} \\ \phi - \phi_0 &= -b\, \epsilon_v + \frac{p_l}{N} \end{aligned}$$

Linear poroelasticity

Energy potential F

Inspecting the state equations, it appears that a linear behaviour stems from a quadratic potential

→ From a stress- and pressure-free reference state

$$
\begin{aligned}
\boldsymbol{\sigma} &= \mathbb{D}\,\boldsymbol{\epsilon} - b\,p_l\,\boldsymbol{\delta} \\
\phi - \phi_0 &= -b\,\epsilon_v + \frac{p_l}{N}
\end{aligned}
$$

$\mathbb{D}$: stiffness matrix
b: Biot coefficient, $b = 1 - \dfrac{K}{K_s}$
N: Biot modulus, $\dfrac{1}{N} = \dfrac{b - \phi_0}{K_s}$

Linear poroelasticity

Energy potential F

Inspecting the state equations, it appears that a linear behaviour stems from a quadratic potential

→ From a pre-stressed state

$$
\begin{aligned}
\boldsymbol{\sigma} - \boldsymbol{\sigma}_0 &= \mathbb{D}\,\boldsymbol{\epsilon} - b\,(p_l - p_{l,0})\,\boldsymbol{\delta} \\
\phi - \phi_0 &= -b\,\epsilon_v + \frac{p_l - p_{l,0}}{N}
\end{aligned}
$$

$\mathbb{D}$: stiffness matrix
b: Biot coefficient, $b = 1 - \dfrac{K}{K_s}$
N: Biot modulus, $\dfrac{1}{N} = \dfrac{b - \phi_0}{K_s}$

Nonlinear poroelasticity

Incremental form of the constitutive equations

$$\begin{aligned} \mathrm{d}\boldsymbol{\sigma} &= \mathbb{D}(\boldsymbol{\sigma}, p_l)\,\mathrm{d}\epsilon - b(\boldsymbol{\sigma}, p_l)\,\mathrm{d}p_l\,\boldsymbol{\delta} \\ \mathrm{d}\phi &= -b(\boldsymbol{\sigma}, p_l)\,\mathrm{d}\epsilon_v + \frac{\mathrm{d}p_l}{N(\boldsymbol{\sigma}, p_l)} \end{aligned}$$

Material parameters are tangent properties, and depend on material state

Stress variable(s) – Biot stress and Biot coefficient

From $\mathrm{d}\sigma = K\,\mathrm{d}\epsilon_v + b\,\mathrm{d}p_l$, introduce the Biot stress: $\mathrm{d}\sigma" = \mathrm{d}\sigma - b\,\mathrm{d}p_l$ so that $\mathrm{d}\sigma" = K\,\mathrm{d}\epsilon_v$

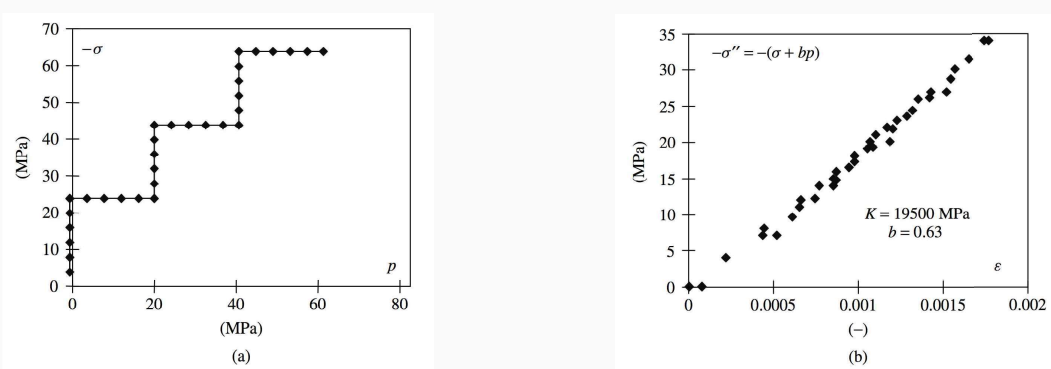

Unjacketed test on a limestone ($K_s = 52.7$ GPa) (Coussy 2004)

Stress variable(s) – poromechanical properties

Material	ϕ (%)	K (MPa $\times 10^3$)	b (–)	N (MPa $\times 10^3$)
Cement paste	40–63	15–2	0.07–0.37	1170–20
Mortar	27–40	15–3	0.04–0.35	2340–40
Bone	5	12	0.14	160
Granites	1–2	25–35	0.22–0.44	280–370
Marble	2	40	0.20	280
Sandstones	2–26	4.6–13	0.69–0.85	~17
Limestones	4–29	5–39	0.34–0.88	100–400

Order of magnitude of poroelastic properties for different materials (Coussy 2004)

For soils: $b = 1 - \dfrac{K}{K_s} \approx 1$ and $N \to \infty$.

Biot (effective?) stress – case of non-linearity

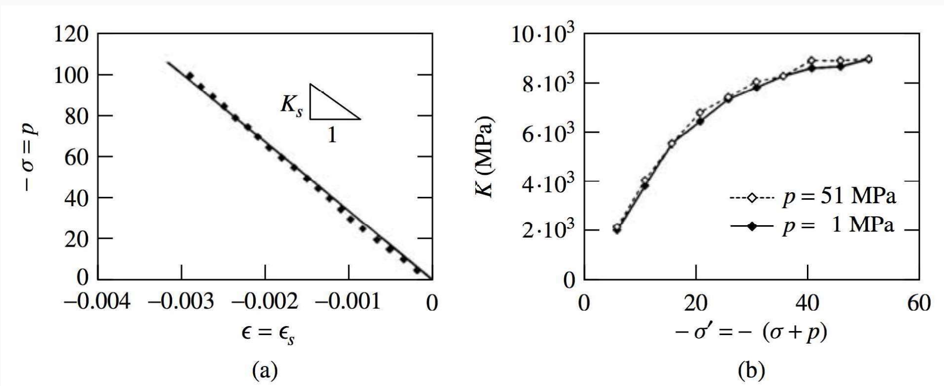

Experimental confirmation of non-linear constitutive equations for a sandstone (after Bemer et al., 2001), cited by (Coussy 2004)

Biot (effective?) stress – yield function

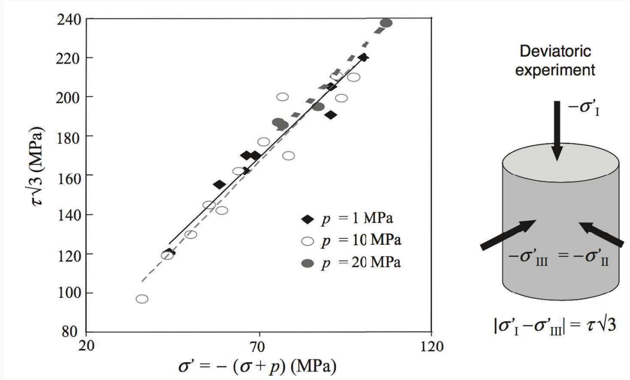

Experimental validation of yield function in terms of Terzaghi stress for a limestone with $b = 0.63$ (after Vincké et al., 1998), cited by (Coussy 2010)

Thermodynamics? What for?

Non-isothermal evolutions

$$\mathrm{d}F = \boldsymbol{\sigma} : \mathrm{d}\boldsymbol{\epsilon} + p_l \,\mathrm{d}\phi - \mathcal{S}_s \,\mathrm{d}T$$

→ identifying conjugate variables
→ derive proper constitutive equations

Starting from $\mathrm{d}F = p' \,\mathrm{d}\epsilon_v + q \,\mathrm{d}\epsilon_s$ for soils:

$$\begin{pmatrix} \mathrm{d}\epsilon_v \\ \mathrm{d}\epsilon_s \end{pmatrix} = \begin{pmatrix} \dfrac{1}{K(p',q)} & \dfrac{1}{C(p',q)} \\ \dfrac{1}{C(p',q)} & \dfrac{1}{3G(p',q)} \end{pmatrix} \begin{pmatrix} \mathrm{d}p' \\ \mathrm{d}q \end{pmatrix}$$

with

$$\frac{\partial}{\partial q}\left(\frac{1}{K}\right) = \frac{\partial}{\partial p'}\left(\frac{1}{C}\right) \quad ; \quad \frac{\partial}{\partial p'}\left(\frac{1}{3G}\right) = \frac{\partial}{\partial q}\left(\frac{1}{C}\right)$$

Back to Clausius-Duhem inequality, beyond reversibility?

$$\mathrm{d}D = \sigma_{ij}\,\mathrm{d}\epsilon_{ij} + p_l\,\mathrm{d}\phi - \mathrm{d}F \geq 0$$

Assuming that elasticity still gives

$$\mathrm{d}F = \sigma_{ij}\,\mathrm{d}\epsilon^e_{ij} + p_l\,\mathrm{d}\phi^e$$

But this time, $\mathrm{d}D \neq 0$ and $\boldsymbol{\epsilon} = \boldsymbol{\epsilon}^e + \boldsymbol{\epsilon}^p$ and $\mathrm{d}\phi = \mathrm{d}\phi^e + \mathrm{d}\phi^p$

Dissipation

$$\mathrm{d}D = \sigma_{ij}\,\mathrm{d}\epsilon^p_{ij} + p_l\,\mathrm{d}\phi^p \geq 0$$

See also hyperplasticity theory (Houlsby and Puzrin 2006) to go further

Basics of constitutive modelling

“A model is a lie that helps you see the truth.”

— Howard Skipper

Definitions

Constitutive relations

- Mathematical relation between conjugate variables
- Introduce material parameters
- Allow closing the problem

Example in mechanics

Unknowns	Equations
σ, 6	Equilibrium, 3
u, 3	Compatibility, 6
ϵ, 6	Constitutive law, 6

Illustration

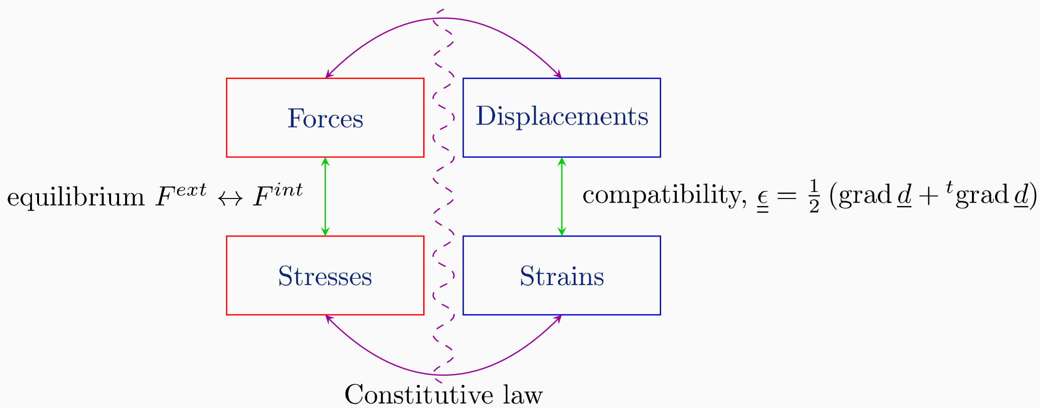

Examples of constitutive relations

Problem	Variables	Relation	Parameters
Thermal	$\boldsymbol{q}_t,\ T$	Fourier law	λ
Hydraulic	$\boldsymbol{q}_l,\ p_l$	Darcy law	κ
Mechanical	$\boldsymbol{\sigma},\ \boldsymbol{\epsilon}$	Hooke's law	$E,\ \nu$

Basics of constitutive modelling

Thermal problem

Heat transfer

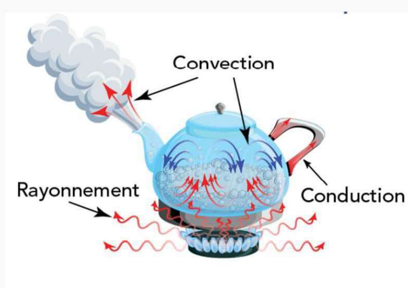

(parlonssciences.ca)

Definitions

Conduction	Heat transfer through diffusion within the material (no mass transfer)
Convection	Heat transfer through mass transfer
Radiation	Heat transfer through electomagnetic waves (no mass support required)

Heat transfer in porous media

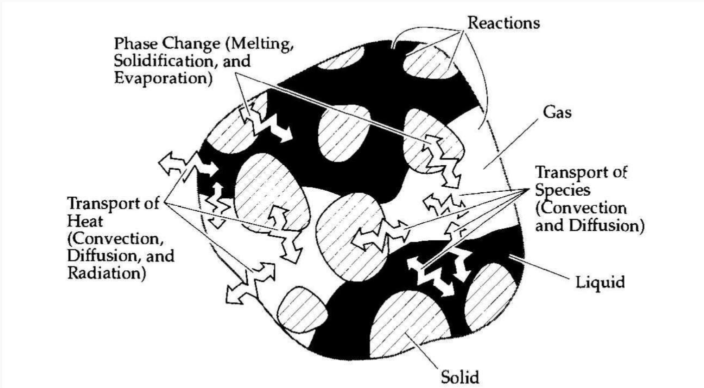

(Kaviany 1998)

Fourier law

Joseph Fourier
(1768–1830)

Isotropic material

$$q_{t,i} = -\lambda \frac{\partial T}{\partial x_i}$$

with λ: thermal conductivity (scalar) [W / K m]

Anisotropic material

$$q_{t,i} = -\lambda_{ij} \frac{\partial T}{\partial x_j}$$

with $\boldsymbol{\lambda}$: thermal conductivity tensor [W / K m]

Thermal diffusivity

Heat equation (energy balance equation & Fourier law)

$$\frac{\partial T}{\partial t} = \frac{\lambda}{\rho\, c} \Delta T + R$$

$D = \dfrac{\lambda}{\rho\, c}$: thermal diffusivity [$m^2/s$]
R: volumetric heat source

Phase change (e.g. water solidification)

Heat equation (energy balance equation & Fourier law)

$$\rho\, c \frac{\partial T}{\partial t} = \lambda\, \Delta T + L_f \frac{\rho_{ice}}{\rho_w} \frac{\partial \theta_{ice}}{\partial t} + R'$$

R': heat source

Need for a freezing curve $\theta_{ice} = \mathcal{F}(T)$

$$\left(\rho\, c + L_f'\right) \frac{\partial T}{\partial t} = \lambda\, \Delta T + R'$$

Basics of constitutive modelling

Hydraulic problem

Darcy law

Henri Darcy
(1803–1858)

$$\boldsymbol{q}_l = -\frac{\kappa}{\mu}\left(\text{grad } p_l - \boldsymbol{\gamma}\right)$$

with
μ: dynamic viscosity of water (1 mPa.s at 20 °C)
κ: intrinsic permeability [m^2]

k : hydraulic conductivity [m/s]

Unsaturated case: $\kappa \leftarrow \kappa_{app} = \kappa\, \kappa_{rel}(S_l)$

Basics of constitutive modelling

Mechanical problem

Mechanical constitutive models

Modelling framework: define your needs

- Elasticity vs elastoplasticity
- Cyclic behaviour
- Time and rate effects (viscosity, creep...)
- Humidity effects (capillarity, adsorption)
- Temperature effects
- Damage

Some definitions

- Elasticity: reversibility (energetic point of view)
- Plasticity: irreversible deformation
- Failure ≠ plasticity

Reversible deformations

Reversible behaviour

- the stress-strain relation is unique
- no energy dissipation (no hysteresis cycle)
- no permanent deformation after a loading-unloading cycle

Irreversible behaviour

- the stress-strain relation is no more unique
- energy dissipation $\rightarrow \int \mathrm{d}F = \int \sigma_{ij}\, \mathrm{d}\epsilon_{ij} \geq 0$
- permanent deformation after a loading-unloading cycle $\rightarrow \boldsymbol{\epsilon}^p$: plastic strains

Elasticity

Hooke's law – Isotropic linear elasticity (E, ν) : $\epsilon_{ij} = \dfrac{1+\nu}{E}\sigma_{ij} - \dfrac{\nu}{E}\,\mathrm{tr}(\boldsymbol{\sigma})\delta_{ij}$

with E: Young's modulus and ν: Poisson's ratio.

In vectorial form:

$$\begin{pmatrix} \epsilon_{11} \\ \epsilon_{22} \\ \epsilon_{33} \\ \epsilon_{12} \\ \epsilon_{13} \\ \epsilon_{23} \end{pmatrix} = \frac{1}{E} \begin{pmatrix} 1 & -\nu & -\nu & 0 & 0 & 0 \\ -\nu & 1 & -\nu & 0 & 0 & 0 \\ -\nu & -\nu & 1 & 0 & 0 & 0 \\ 0 & 0 & 0 & 1+\nu & 0 & 0 \\ 0 & 0 & 0 & 0 & 1+\nu & 0 \\ 0 & 0 & 0 & 0 & 0 & 1+\nu \end{pmatrix} \begin{pmatrix} \sigma_{11} \\ \sigma_{22} \\ \sigma_{33} \\ \sigma_{12} \\ \sigma_{13} \\ \sigma_{23} \end{pmatrix}$$

Elasticity

Hooke's law – Isotropic linear elasticity (E, ν) : $\epsilon_{ij} = \dfrac{1+\nu}{E}\sigma_{ij} - \dfrac{\nu}{E}\,\mathrm{tr}(\boldsymbol{\sigma})\delta_{ij}$

with E: Young's modulus and ν: Poisson's ratio.

In the principal stress space:

$$\begin{pmatrix} \epsilon_1 \\ \epsilon_2 \\ \epsilon_3 \end{pmatrix} = \frac{1}{E} \begin{pmatrix} 1 & -\nu & -\nu \\ -\nu & 1 & -\nu \\ -\nu & -\nu & 1 \end{pmatrix} \begin{pmatrix} \sigma_1 \\ \sigma_2 \\ \sigma_3 \end{pmatrix}$$

or, in inverted form:

$$\begin{pmatrix} \sigma_1 \\ \sigma_2 \\ \sigma_3 \end{pmatrix} = \frac{E}{(1+\nu)(1-2\nu)} \begin{pmatrix} 1-\nu & \nu & \nu \\ \nu & 1-\nu & \nu \\ \nu & \nu & 1-\nu \end{pmatrix} \begin{pmatrix} \epsilon_1 \\ \epsilon_2 \\ \epsilon_3 \end{pmatrix}$$

Elastic models

- Isotropic linear elasticity (two constant parameters):
  ex. : E & ν or $E(z)$ & ν or K & G

Elastic models

- Isotropic linear elasticity (two constant parameters):
  ex. : E & ν or $E(z)$ & ν or K & G
- Anisotropic linear elasticity (5 to 21 constant parameters):
  ex. : E_i & ν_i
  ex. : 5 parameters for transverse isotropy

Elastic models

- Isotropic linear elasticity (two constant parameters):
  ex. : E & ν or $E(z)$ & ν or K & G
- Anisotropic linear elasticity (5 to 21 constant parameters):
  ex. : E_i & ν_i
  ex. : 5 parameters for transverse isotropy

$$\mathbb{C} = \begin{pmatrix} 1/E_t & -\nu_t/E_t & -\nu_{lt}/E_t & 0 & 0 & 0 \\ -\nu_t/E_t & 1/E_t & -\nu_{lt}/E_t & 0 & 0 & 0 \\ -\nu_{lt}/E_t & -\nu_{lt}/E_t & 1/E_l & 0 & 0 & 0 \\ 0 & 0 & 0 & 1/G_{lt} & 0 & 0 \\ 0 & 0 & 0 & 0 & 1/G_{lt} & 0 \\ 0 & 0 & 0 & 0 & 0 & 1/G_t \end{pmatrix}$$

with $1/G_t = 2\,(1+\nu_t)/E_t$

j.m. pereira – alert oz & eurad PhD school, 2023 35/87

Elastic models

- Isotropic linear elasticity (two constant parameters):
  ex. : E & ν or $E(z)$ & ν or K & G
- Anisotropic linear elasticity (5 to 21 constant parameters):
  ex. : E_i & ν_i
  ex. : 5 parameters for transverse isotropy
- Non-linear elasticity: $E(\boldsymbol{\sigma})$

Elastic models

- Isotropic linear elasticity (two constant parameters):
  ex. : E & ν or $E(z)$ & ν or K & G
- Anisotropic linear elasticity (5 to 21 constant parameters):
  ex. : E_i & ν_i
  ex. : 5 parameters for transverse isotropy
- Non-linear elasticity: $E(\boldsymbol{\sigma})$
- Hyper-elasticity: $\mathrm{d}\boldsymbol{\sigma} = \dfrac{\partial F}{\partial \epsilon}$

Elastic models

- Isotropic linear elasticity (two constant parameters):
  ex. : E & ν or $E(z)$ & ν or K & G
- Anisotropic linear elasticity (5 to 21 constant parameters):
  ex. : E_i & ν_i
  ex. : 5 parameters for transverse isotropy
- Non-linear elasticity: $E(\boldsymbol{\sigma})$
- Hyper-elasticity: $\mathrm{d}\boldsymbol{\sigma} = \dfrac{\partial F}{\partial \boldsymbol{\epsilon}}$
- Hypo-elasticity: $\mathrm{d}\boldsymbol{\sigma} = \mathbb{D}\,\mathrm{d}\boldsymbol{\epsilon}$ (does not ensure energy conservation)

Factors affecting elastic moduli

- Strain level
  - very small deformation ($\leq 0.001\%$)
  - small deformation ($\geq 0.001\%$ & $\leq 1\%$)
  - large deformation ($\geq 1\%$)
- Stress level
- Stress path

Determining Young modulus

It is advised to determine Young modulus E at strains lower than 0.1%
But, in practice, this depends on the chosen elastoplastic model

Non-linear elasticity (strain dependency of moduli)

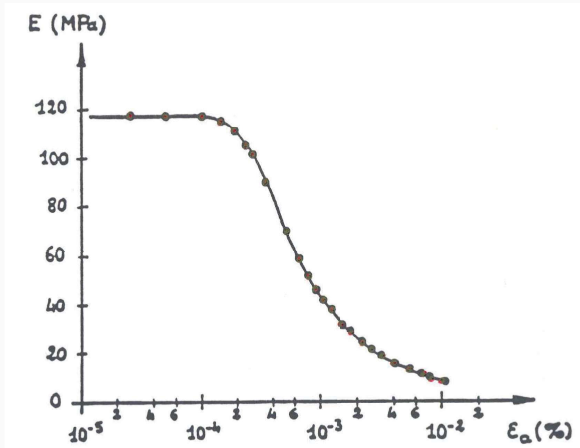

Evolution of the Young's modulus with deformation amplitude (Hicher 1985)

Non-linear elasticity (stress dependency of moduli)

Références	K	G
Burland et Roscoe (1968)	$\frac{1+e_o}{\kappa}p$	G_o
Nelson et Baron (Desai et al., 1984)	$K_o + \alpha_1 p$	$G_o + \alpha_2 q$
Chen et Baladi (Desai et al., 1984)	$\frac{K_o}{1-K_1}(1-K_1 e^{-3K_2 p})$	$\frac{G_o}{1-G_1}(1-G_1 e^{-\sqrt{3}G_2 q})$
Boyce (1980) Cambou et Jafari (1988)	$\frac{K_o p_a \left(\frac{p}{p_a}\right)^{1-n}}{1-(1-n)\frac{K_o}{6G_o}\frac{q^2}{p^2}}$	$G_o p_a \left(\frac{p}{p_a}\right)^{1-n}$
Loret (1981) f est une fonction quelconque	$3r_o f(p^2 + r_o q^2)$	$f(p^2 + r_o q^2)$
Loret (1981) Lade et Nelson (1987)	$\frac{3r_o E_o p_a}{2(1+\nu)}\left[\left(\frac{p}{p_a}\right)^2 + r_o\left(\frac{q}{p_a}\right)^2\right]^n$	$\frac{E_o p_a}{2(1+\nu)}\left[\left(\frac{p}{p_a}\right)^2 + r_o\left(\frac{q}{p_a}\right)^2\right]^n$
Vermeer (1982)	$\frac{2}{3}G$	$G_o\left[\frac{\sqrt{\sigma_1^2+\sigma_2^2+\sigma_3^2}}{3p_0}\right]^{1-\beta}$

p_a est la pression atmosphérique : $K_o, G_o, n, r_o, E_o, \nu, e_o, \kappa, \alpha_1, \alpha_2, K_1, K_2, G_1, G_2$ sont des constantes.

Caution!
Check thermodynamics consistency.

Elasticity? Useful?

Which role for elastic component of behaviour?

- It depends on the application!
- Service Limit State: typically, elastic domain (settlements, etc.)
- Failure analysis: in general, elastic deformation will play a minor role with respect to plastic deformation
- Caution to excavations, for which elastic behaviour is key.
- And never underestimate coupling effects!

Undrained elasticity

Why is this important?

- Short term behaviour of geotechnical structures (foundations, retaining walls, excavations...)
- Some finite element codes offer undrained analyses

How to get undrained elastic moduli from drained elastic moduli?

Undrained elasticity

How to get undrained elastic moduli from drained elastic moduli?

Use the water bulk moduli: $K_w = 2.2$ GPa at 20 °C.
It can be shown that $K_u = K_d + \dfrac{K_w}{n}$ where n is the porosity.
Since water does not transmit shear stresses (good approximation), $G_u = G_d = G$.
Then, one uses the established relations between elastic moduli:

$$E_u = \frac{9K_u G}{3K_u + G} \qquad \nu_u = \frac{3K_u - 2G}{2(3K_u + G)}$$

If $K_u >> G$ (usually the case), then ?

Undrained elasticity

Soil incompressibility:

If $K_u >> G$ (usually the case), then $\nu_u \to 0.5$

$$K_u = \frac{E_u}{3(1 - 2\nu_u)} \qquad G_u = \frac{E_u}{2(1 + \nu_u)}$$

Do not use $\nu_u = 0.5$ in numerical tools, but $\nu = 0.49$ for instance
(remember that $\nu = 0.5$ implies volumetric incompressibility, see K).

j.m. pereira – alert oz & eurad PhD school, 2023 40/87

Elasto-plastic models: main ingredients

Most of elasto-plastic models rely on the strain partition

$$\boldsymbol{\epsilon} = \boldsymbol{\epsilon}^e + \boldsymbol{\epsilon}^p$$

What should we know, beyond elasticity?

1. WHEN?
   plastic criterion – yield surface f
2. HOW?
   increment of plastic strain tensor – flow rule
3. CONSEQUENCE ?
   evolution of the elastic domain – hardening law

Mohr-Coulomb failure criterion

Mohr-Coulomb criterion

$$f(\sigma'_{ij}) \equiv (\sigma'_{max} - \sigma'_{min}) - (\sigma'_{max} + \sigma'_{min}) \sin\varphi' - 2c' \cos\varphi' = 0$$

ϕ': internal friction angle
c': cohesion

- “simply” a failure criterion, not a constitutive model!
- inside the surface (i.e. $f < 0$)? often: isotropic linear elasticity (and thus 4 parameters: E, ν, φ', c')

Something is missing to determine the plastic deformation…

Plastic deformation

- Plasticity theory:
  existence of a plastic potential g such that:

$$d\epsilon_{ij}^{p} = d\Lambda \frac{\partial g}{\partial \sigma_{ij}}$$

  where $d\Lambda \geq 0$: plastic multiplier
- Total strain:

$$d\epsilon_{ij} = d\epsilon_{ij}^{e} + d\epsilon_{ij}^{p}$$

- Particular cases:
  Standard material (or associated flow rule): $g \equiv f$
  In general, geomaterials are non-standard materials: $g \neq f$.

Yield surface and plastic potential

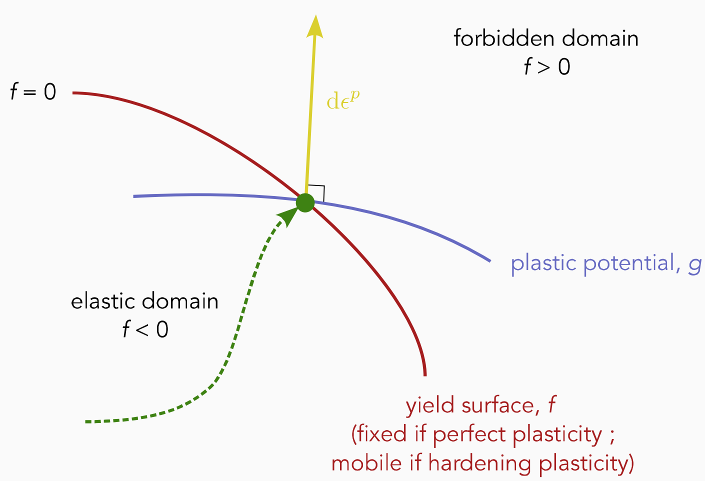

Yield surface and plastic potential

Isotropic linear elastic-perfectly plastic model with Mohr-Coulomb failure criterion a.k.a. "Mohr-Coulomb model"

Mohr-Coulomb criterion

$$f(\sigma'_{ij}) \equiv (\sigma'_{max} - \sigma'_{min}) - (\sigma'_{max} + \sigma'_{min}) \sin\varphi' - 2c' \cos\varphi' = 0$$

$\phi' : internal friction angle$
$c' : cohesion$

Plastic potential

$$g(\sigma'_{ij}) \equiv (\sigma'_{max} - \sigma'_{min}) - (\sigma'_{max} + \sigma'_{min}) \sin\psi$$

ψ: dilatancy angle

How to compute plastic deformation?

Elastic and elastoplastic regimes

- In elastic regime: $\mathrm{d}\boldsymbol{\sigma} = \mathbb{D}^e\,\mathrm{d}\boldsymbol{\epsilon}^e = \mathbb{D}^e\,\mathrm{d}\boldsymbol{\epsilon}$
- In elastoplastic regime: $\mathrm{d}\boldsymbol{\sigma} = \mathbb{D}^e\,\mathrm{d}\boldsymbol{\epsilon}^e = \mathbb{D}^e(\,\mathrm{d}\boldsymbol{\epsilon} - \,\mathrm{d}\boldsymbol{\epsilon}^p)$
- This last equation can be rearranged: $\mathrm{d}\boldsymbol{\sigma} = \mathbb{D}^{ep}\,\mathrm{d}\boldsymbol{\epsilon}$

- By definition, the point representing the stress state must remain on the yield surface (whether perfect plasticity is assumed or hardening/softening is considered)
- This condition writes: $\mathrm{d}f = 0$ and is called **consistency condition**
- Kuhn-Tucker condition (always true, in elastic and elastoplastic regimes): $f \leq 0 \quad \& \quad \mathrm{d}\Lambda \geq 0 \quad \& \quad \mathrm{d}f\,\mathrm{d}\Lambda = 0$

Plastic multiplier

It is obtained using the consistency condition.

Perfect plasticity?

Any interest?

- failure prediction:
  - bearing capacity
  - slope stability...

What are the limitations of "Mohr-Coulomb" model?

- elastic domain unlimited along isotropic and (most of) K_0 loading paths
- fixed elastic domain (no influence of loading history)
- no influence of the intermediate principal stress

Other failure criteria

$$\textbf{Tresca} \quad f(\sigma'_{ij}) \equiv (\sigma'_{max} - \sigma'_{min}) - 2S_u = 0$$

$$\textbf{Mohr-Coulomb} \quad f(\sigma'_{ij}) \equiv (\sigma'_{max} - \sigma'_{min}) - (\sigma'_{max} + \sigma'_{min}) \sin\varphi' - 2c' \cos\varphi' = 0$$

$$f(p', q) \equiv q - \frac{6 \sin\phi'}{3 - \sin\phi'} p' - \frac{6c' \cos\phi'}{3 - \sin\phi'} = q - Mp' - c^* = 0$$

These criteria pose numerical difficulties because of the discontinuities of the surface in the stress space

$$\textbf{von Mises} \quad f(\sigma_{ij}) = \sqrt{J_2} - K \leq 0$$

$$\textbf{Drucker-Prager} \quad f(\sigma_{ij}) = \sqrt{J_2} - \gamma I_1 - K = 0$$

Be careful with sign conventions. Always check it!

Other failure criteria (graphical representation)

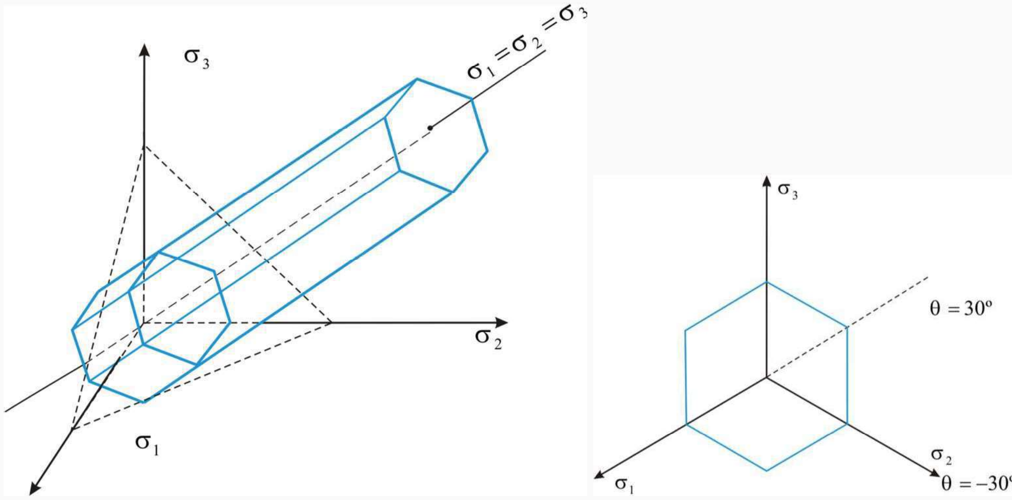

Tresca failure surface

Other failure criteria (graphical representation)

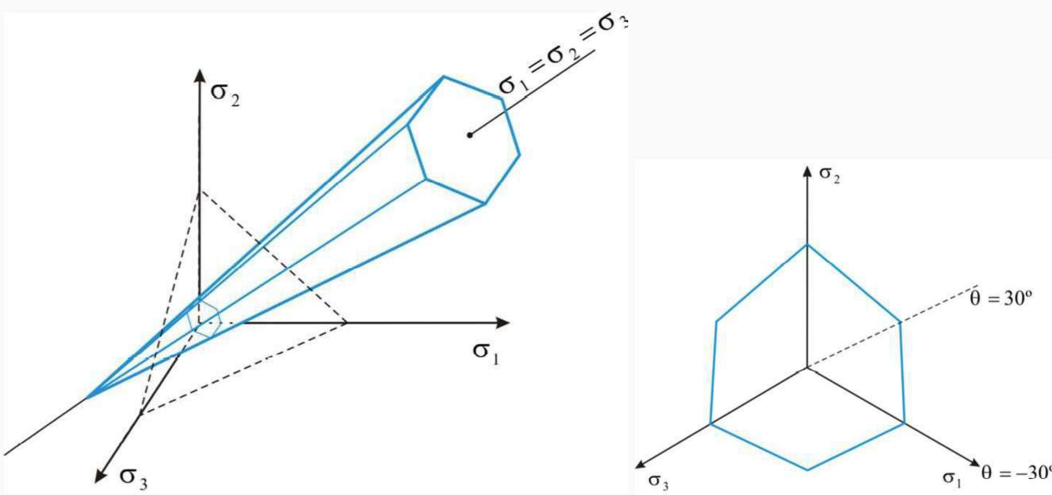

Mohr-Coulomb failure surface

Other failure criteria (graphical representation)

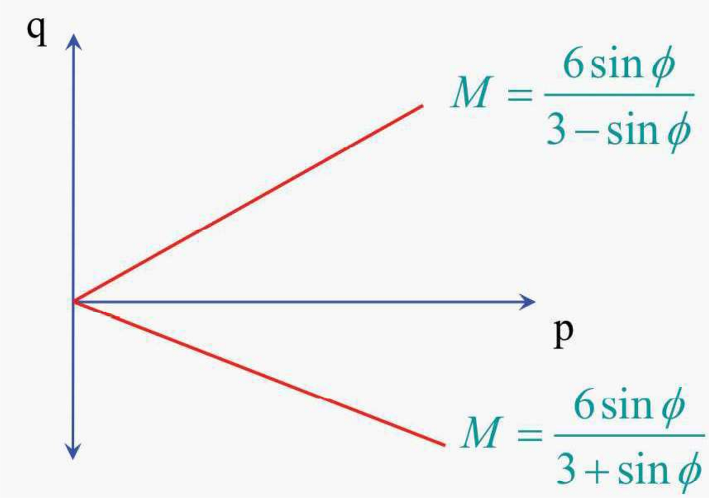

Mohr-Coulomb failure surface (compression vs extension)

Other failure criteria (graphical representation)

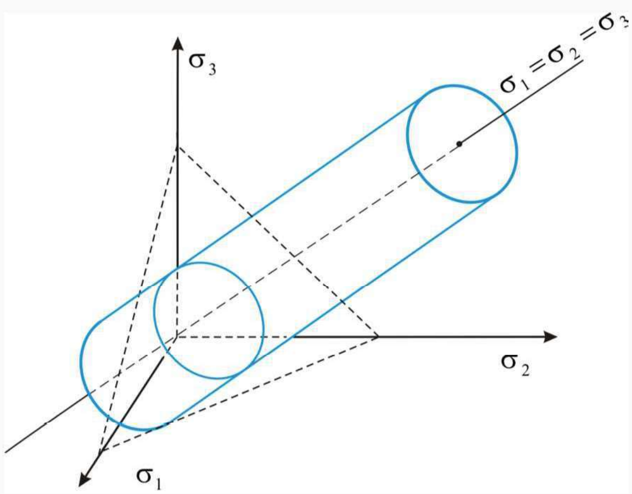

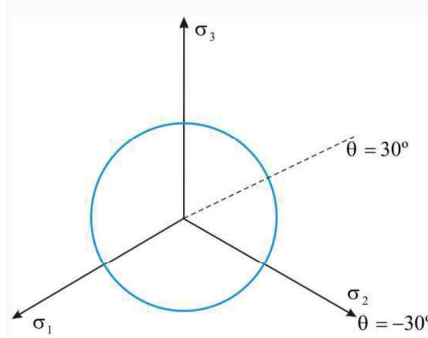

von Mises failure surface

Other failure criteria (graphical representation)

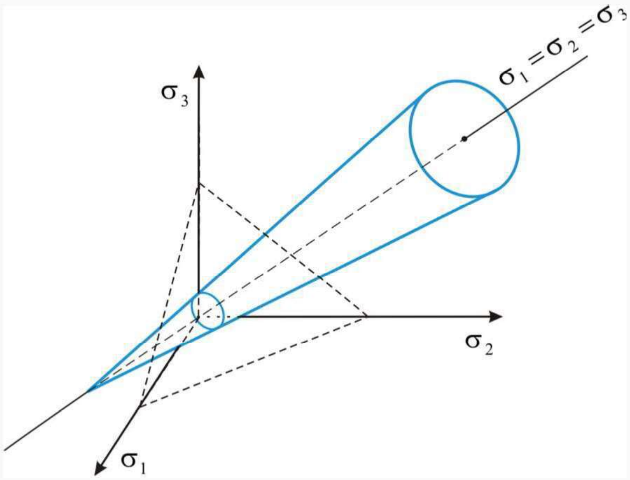

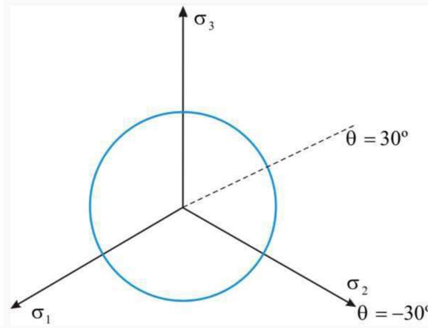

Drucker-Prager failure surface

Other failure criteria (graphical representation)

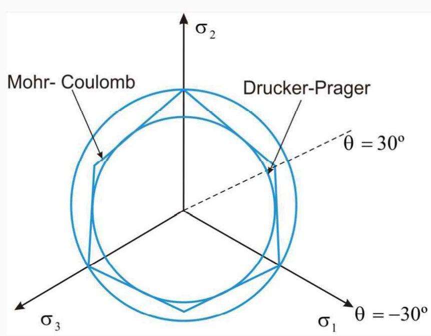

Mohr-Coulomb and Drucker-Prager correspondance

Other failure criteria (graphical representation)

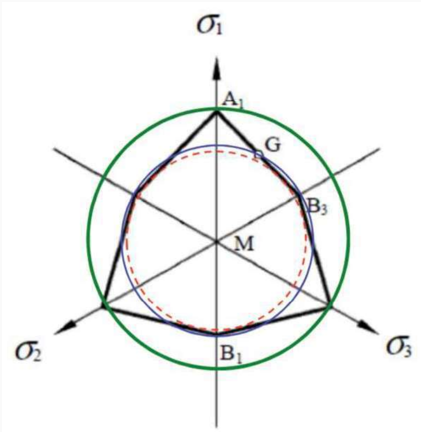

External vertices: $\gamma = \dfrac{2\sin\phi}{\sqrt{3}(3-\sin\phi)}$, $K = \dfrac{6C\cos\phi}{\sqrt{3}(3-\sin\phi)}$

Internal vertices: $\gamma = \dfrac{2\sin\phi}{\sqrt{3}(3+\sin\phi)}$, $K = \dfrac{6C\cos\phi}{\sqrt{3}(3+\sin\phi)}$

Tangent to faces: $\gamma = \dfrac{\sin\phi}{\sqrt{3(3+\sin^2\phi)}}$, $K = \dfrac{3C\cos\phi}{\sqrt{3(3+\sin\phi)}}$

Mohr-Coulomb and Drucker-Prager correspondance

Examples of “real” loading surfaces

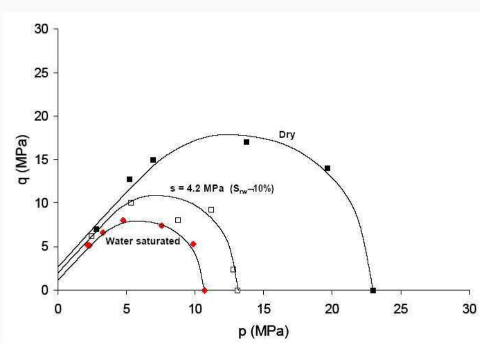

Unsaturated chalk

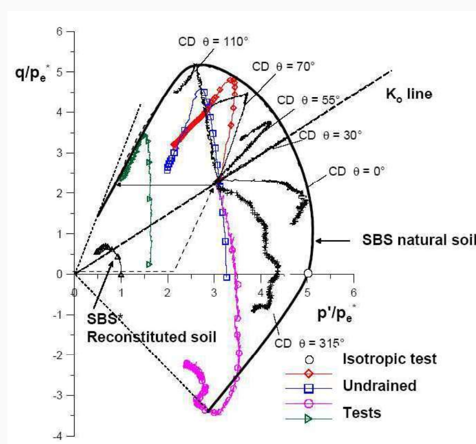

Marine clay

Elastoplastic models

Main ingredients

- Elastic law (linear or not)
- Yield criterion (yield surface) $\rightarrow$ elastic domain
- Flow rule (plastic potential) $\rightarrow$ plastic strain increment
- Hardening law $\rightarrow$ evolution of elastic domain
  (position and size "stored" in hardening variables)

Hardening plasticity

Definition

- The elastic limit is not fixed anymore and will evolve according to the loading history.
- This evolution is tracked through a **hardening variable** ξ, which itself is linked to an **internal variable**. This relation is the so-called **hardening law**.
- A hardening modulus is formally introduced: $\dfrac{\partial f}{\partial \xi}\,\mathrm{d}\xi = -\,\mathrm{d}\lambda\,H$
- $H > 0$ corresponds to positive hardening; reversely, $H < 0$ corresponds to negative hardening (softening); $H = 0$ corresponds to perfect plasticity.

Examples

One can guess that to simulate oedometer tests, the hardening variable will be the preconsolidation pressure and the internal variable, the plastic strain.

Plastic hardening

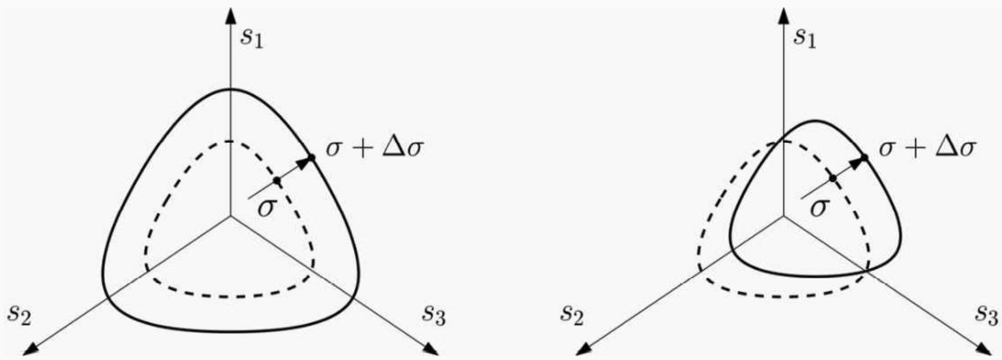

Isotropic and kinematic hardening (require scalar and tensorial hardening variable, resp.)

Cam-clay model – elastic part

- Elastic behaviour

$$\mathrm{d}\epsilon_v^e = -\,\mathrm{d}V/V_0 = \frac{\kappa}{1+e_0}\frac{\mathrm{d}p'}{p'} \qquad \mathrm{d}\epsilon_s^e = \frac{1}{3G}\,\mathrm{d}q$$

- Bulk and shear elastic moduli:

$$K = \frac{\mathrm{d}p'}{\mathrm{d}\epsilon_v^e} = \frac{(1+e_0)\,p'}{\kappa}$$

$$G = \frac{1}{3}\frac{\mathrm{d}q}{\mathrm{d}\epsilon_q^e} = constant$$

2 elastic parameters: κ, G

This is non-linear elasticity!

Cam-clay – yield surface

Original Cam-Clay

$$f \equiv \frac{q}{Mp'} + \ln\left(\frac{p'_0}{p'}\right)^2 = 0$$

Modified Cam-Clay

$$f \equiv \left(\frac{q}{Mp'}\right)^2 - \left(\frac{p'_0}{p'} - 1\right) = 0$$

M: slope of critical state line

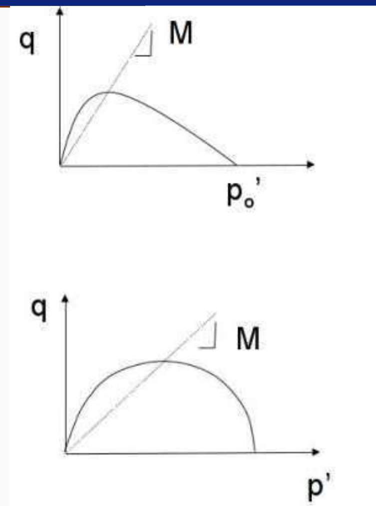

Cam-clay – flow rule & hardening law

- Associated flow rule

$$\mathrm{d}\epsilon^p_{ij} = \mathrm{d}\Lambda \frac{\partial f}{\partial \sigma'_{ij}}$$

$$\mathrm{d}\epsilon^p_v = \mathrm{d}\Lambda \frac{\partial f}{\partial p'} \quad ; \quad \mathrm{d}\epsilon^p_s = \mathrm{d}\Lambda \frac{\partial f}{\partial q}$$

- Hardening law (isotropic elastic limit a.f.o. plastic volumetric strain)

$$\mathrm{d}p'_0 = \frac{(1+e_0)\,p'_0}{\lambda - \kappa}\,\mathrm{d}\epsilon^p_v$$

- Consistency condition

$$\mathrm{d}f(\sigma'_{ij}, p'_0) = \frac{\partial f}{\partial \sigma'_{ij}}\,\mathrm{d}\sigma'_{ij} + \frac{\partial f}{\partial p'_0}\,\mathrm{d}p'_0 = \frac{\partial f}{\partial p'}\,\mathrm{d}p' + \frac{\partial f}{\partial q}\,\mathrm{d}q + \frac{\partial f}{\partial p'_0}\,\mathrm{d}p'_0 = 0$$

Cam-clay model – drained triaxial paths

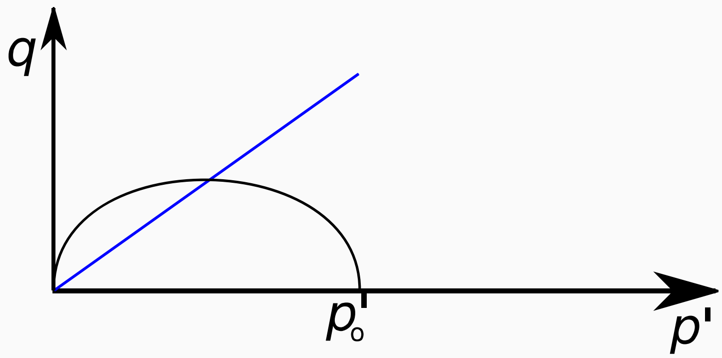

Cam-clay model – drained triaxial paths

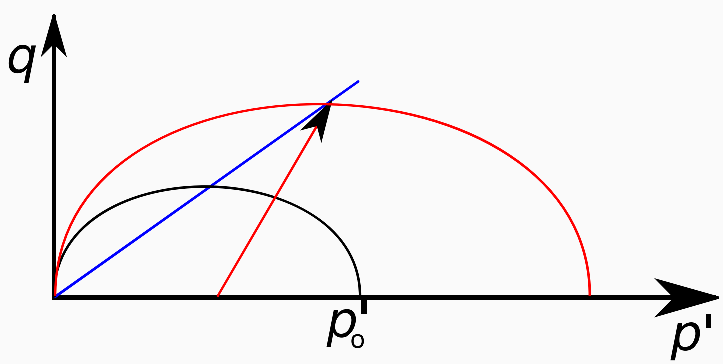

Normally or slightly over- consolidated soils

Cam-clay model – drained triaxial paths

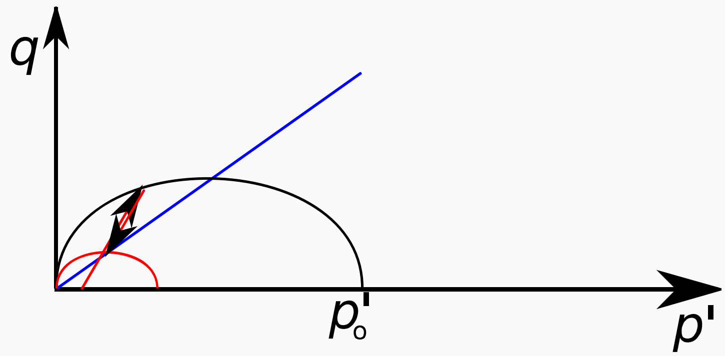

Highly overconsolidated soil ($p' < p'_0/2$)
Elastic behaviour before peak, elastoplastic afterwards

Cam-clay model – undrained triaxial paths

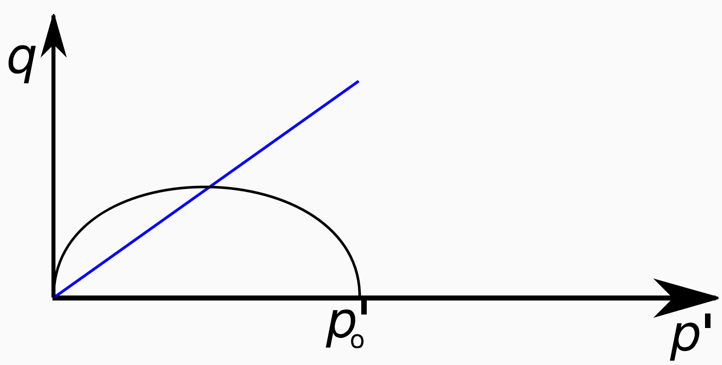

Cam-clay model – undrained triaxial paths

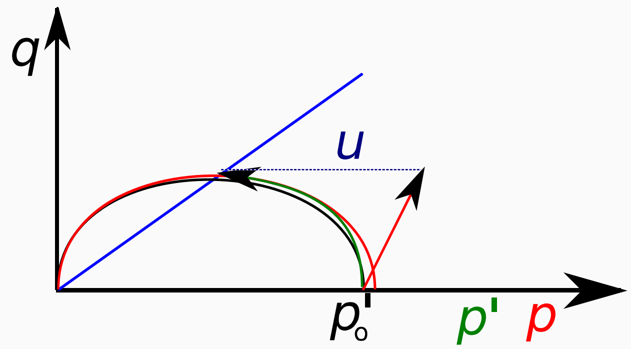

Cam-clay model – undrained triaxial paths

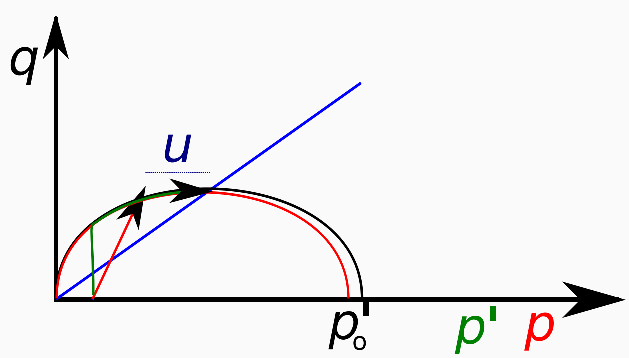

Smooth transition at yield?

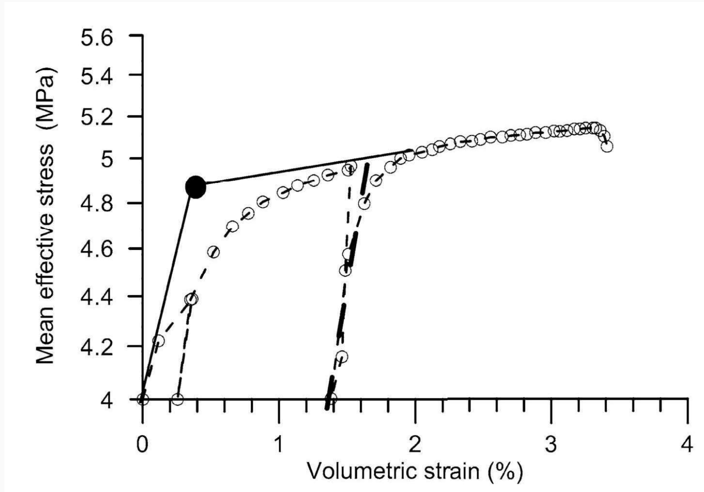

(Hong, Pereira, Tang, et al. 2016)

Smooth transition at yield?

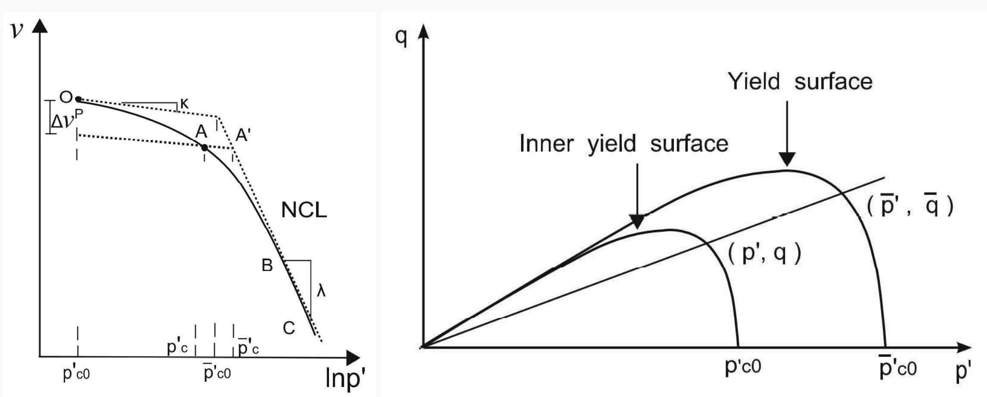

Example of a two-surface model (Hong, Pereira, Tang, et al. 2016)

Smooth transition at yield?

Other approaches

- Generalized plasticity (Pastor, Zienkiewicz, and Chan 1990)
- Bounding surface plasticity (Dafalias and Herrmann 1980, 1986)
- Bubble models (Baudet and Stallebrass 2004)
- Hypoplasticity (Bauer 1996; Gudehus 1996)

Viscoplasticity

Soils generally creep and are sensitive to strain rate:

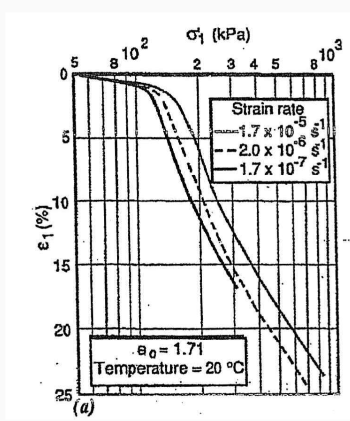

Effects of strain rate on the response of Saint Polycarpe clay (Lerouell and Marques 1996)

Viscoplasticity

Soils generally creep and are sensitive to strain rate:

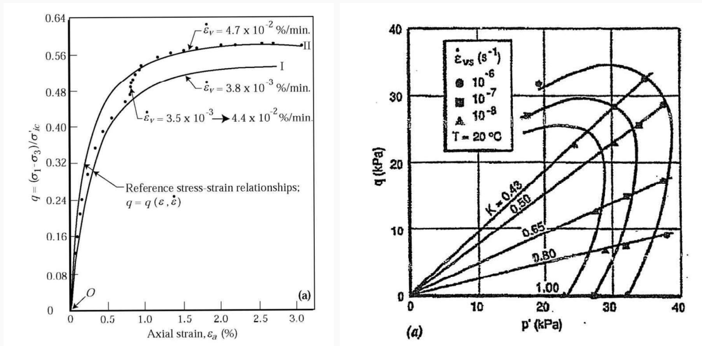

Effects of strain rate on the response of Haney clay (Leroueil and Hight 2003) citing (Vaid and Campanella 1977) and Berthierville clay (Leroueil and Marques 1996)

Viscoplasticity

Soils generally creep and are sensitive to strain rate:

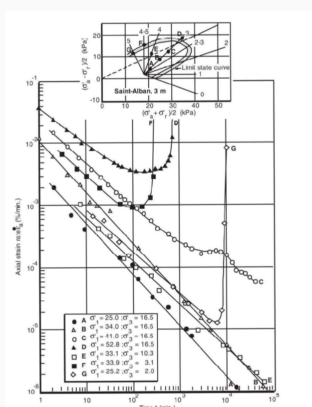

Creep of Saint Alban clay (Leroueil and Hight 2003) citing (Tavenas et al. 1978)

How to account for viscoplasticity?

Usually, soils present inviscid (non-viscous) elasticity and the creep deformation evolves with logarithm of time (slope C_α of secondary consolidation).

How to account for viscoplasticity?

Perzyna's theory (Perzyna 1963)

$$d\epsilon^{vp} = \frac{1}{\eta} < \Phi(f) > \frac{\partial g}{\partial \boldsymbol{\sigma}} \qquad \text{with } \Phi(f) = \left(\frac{p_c^d}{p_c^s} - 1\right)^N \text{ and } \eta\text{: viscosity parameter}$$

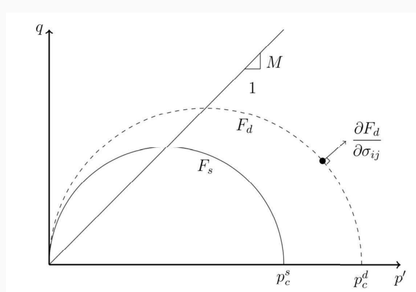

Representation of static F_s and dynamic F_d yield surfaces (Troupel 2017)

How to account for viscoplasticity?

Other theories

- Equivalent time lines (Bjerrum 1967)
- Isotaches (Šuklje 1957)
- Independent viscous strain: $\dot{\epsilon}_v^t = \lambda_\alpha \frac{\dot{t}}{t}$ and $\dot{\epsilon}_v = \dot{\epsilon}_v^e + \dot{\epsilon}_v^p + \dot{\epsilon}_v^t$

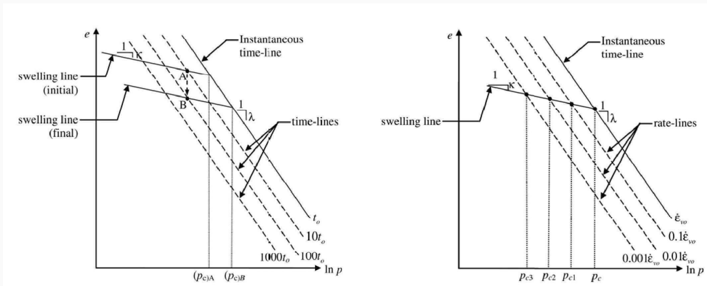

(De Gennaro, Pereira, et al. 2009)

How to account for viscoplasticity?

A simple way to integrate isotach formalism in MCC

$$p_c = p_c(\epsilon_v^p, \dot{\epsilon}_v) = p_c^{ref} \left(\frac{\dot{\epsilon}_v}{\dot{\epsilon}_v^{ref}} \right)^\alpha \exp\left(\frac{1+e_0}{\lambda - \kappa} \epsilon_v^p \right) \qquad \text{with } \alpha = \frac{C_\alpha}{C_c}$$

(De Gennaro and Pereira 2013)

Examples

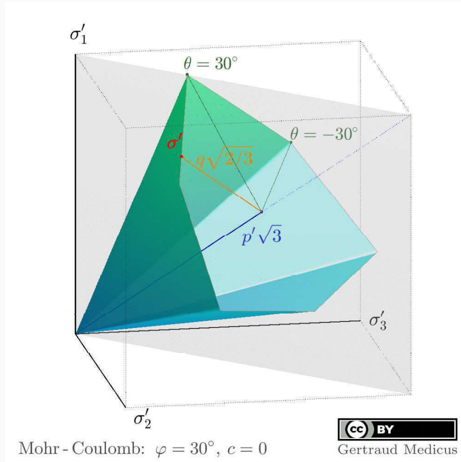

(*https://soilmodels.com/soilanim/*)

THM couplings

About couplings

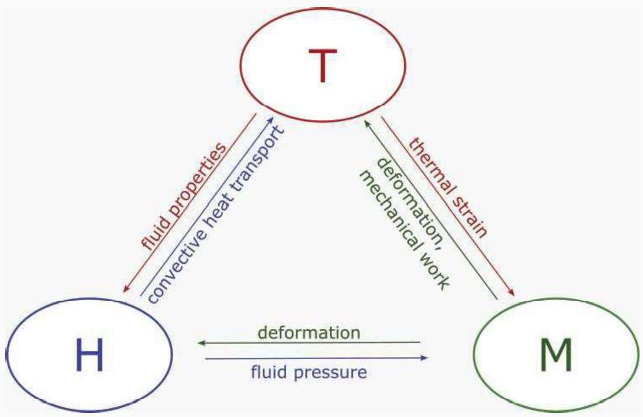

- **Direct couplings**
  between balance equations
- **Indirect couplings**
  affecting material parameters

About couplings – example

Direct coupling
Balance of momentum: $\operatorname{div}\boldsymbol{\sigma} + \rho\boldsymbol{b} = 0$ with $\boldsymbol{\sigma} = \boldsymbol{\sigma}' + p_l\,\mathbf{1}$

Indirect coupling
Darcy law: $\boldsymbol{q}_l = -\frac{\kappa}{\mu}\,(\mathbf{grad}\,p_l - \gamma)$ with $\kappa = \kappa(\phi)$ (e.g. Kozeny-Carman model)
$\rightarrow$ depending on deformation

Question

- What about thermal expansion? Direct or indirect coupling?
- Other examples of indirect coupling?

THM couplings

Transport properties

Transport properties

Possible use of **apparent properties** (macro- or REV scale) obtained experimentally or through back analysis but need for state surfaces (porosity, water saturation, temperature…)

$$\text{e.g. } \pi = \pi(n, S_w, T \dots)$$

Or, use **homogenisation** (upscaling) schemes; they readily account for couplings

Thermal properties and couplings

Volumetric heat capacity easy to estimate

$$C = (1-n)\,\rho_s\,c_s + n\,S_w\,\rho_w\,c_w + n\,(1-S_w)\,\rho_g\,c_g$$

Thermal conductivity? Not so easy

Lazy guess

$$\lambda = (1-n)\lambda_s + n\,S_w\,\lambda_w + n\,(1-S_w)\,\lambda_g$$

Critical review for soils in (Dong, McCartney, and Lu 2015)

Thermal conductivity – homogenisation i

Microstructure must be accounted for (Bergman et al. 1996)

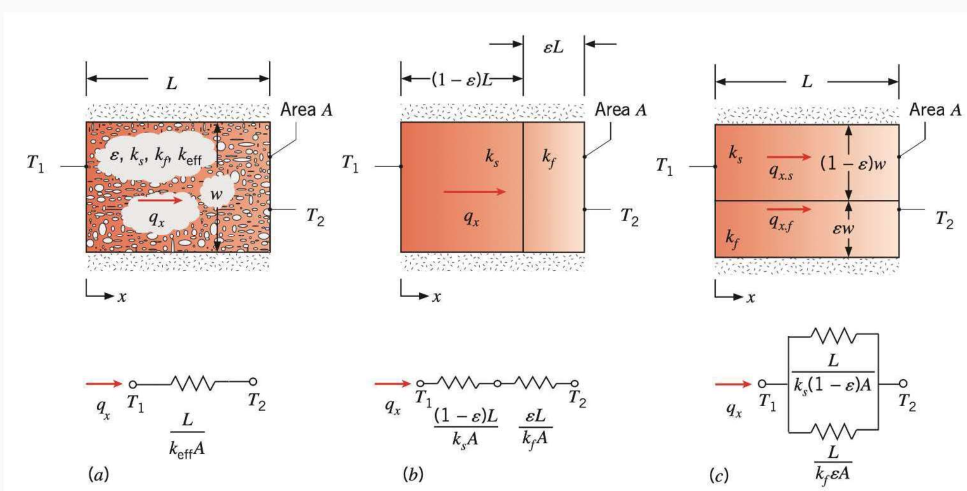

Thermal conductivity – homogenisation ii

More sophisticated homogenisation schemes, e.g. on claystone (Gruescu et al. 2007)

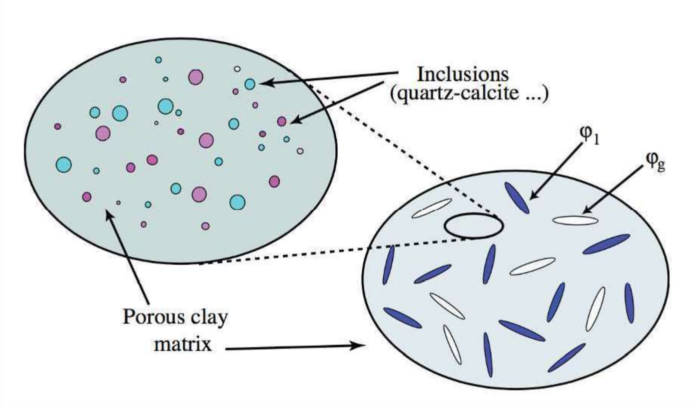

Thermal conductivity – unsaturated case

Thermal conductivity after (Johansen 1975)

$$\lambda_{eff} = \prod_{\alpha} \lambda_{\alpha}^{f_\alpha}$$

Unsaturated cases

$$\lambda(S_w) = (\lambda_{sat} - \lambda_{dry})\,\beta(S_w) + \lambda_{dry}$$

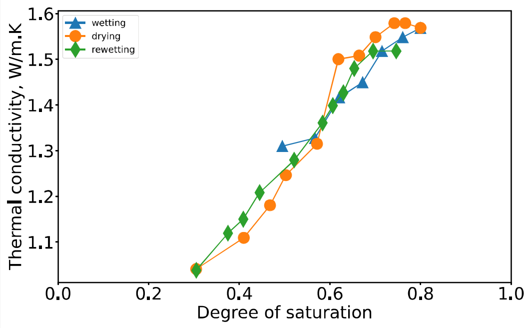

Thermal conductivity of Bapaume loess (Nguyen, Heindl, et al. 2017)

THM couplings

Thermal expansion

Thermal expansion – an introductory example

Triaxial sample, no stress, perfectly drained

Initial void ratio $e_0 = 1.0$

Soil thermal expansion $\alpha = 10^{-2}$ K^{-1}

Temperature increment $\Delta T = 10$ K

Thermal expansion – an introductory example

Triaxial sample, no stress, perfectly drained

Initial void ratio $e_0 = 1.0$

Soil thermal expansion $\alpha = 10^{-2}$ K^{-1}

Temperature increment $\Delta T = 10$ K

Final stress? Final pore pressure?

Thermal expansion – an introductory example

Triaxial sample, no stress, perfectly drained

Initial void ratio $e_0 = 1.0$

Soil thermal expansion $\alpha = 10^{-2}$ K^{-1}

Temperature increment $\Delta T = 10$ K

Final stress? Final pore pressure? $\boldsymbol{\sigma} = \mathbf{0}$ and $p_l = 0$

Thermal expansion – an introductory example

Triaxial sample, no stress, perfectly drained

Initial void ratio $e_0 = 1.0$

Soil thermal expansion $\alpha = 10^{-2}$ K^{-1}

Temperature increment $\Delta T = 10$ K

Final stress? Final pore pressure? $\boldsymbol{\sigma} = \mathbf{0}$ and $p_l = 0$

Final volumetric strain? Final void ratio?

Thermal expansion – an introductory example

Triaxial sample, no stress, perfectly drained

Initial void ratio $e_0 = 1.0$

Soil thermal expansion $\alpha = 10^{-2}$ K^{-1}

Temperature increment $\Delta T = 10$ K

Final stress? Final pore pressure? $\boldsymbol{\sigma} = \mathbf{0}$ and $p_l = 0$

Final volumetric strain? Final void ratio? $\epsilon_v = 0.1$ and $e = 1.0$

Thermal expansion – an introductory example

Triaxial sample, no stress, perfectly drained

Initial void ratio $e_0 = 1.0$

Soil thermal expansion $\alpha = 10^{-2}$ K^{-1}

Temperature increment $\Delta T = 10$ K

Final stress? Final pore pressure? $\boldsymbol{\sigma} = \mathbf{0}$ and $p_l = 0$

Final volumetric strain? Final void ratio? $\epsilon_v = 0.1$ and $e = 1.0$

Plaxis response?

Thermal expansion – an introductory example

Triaxial sample, no stress, perfectly drained

Initial void ratio $e_0 = 1.0$

Soil thermal expansion $\alpha = 10^{-2}$ K^{-1}

Temperature increment $\Delta T = 10$ K

Final stress? Final pore pressure? $\boldsymbol{\sigma} = \mathbf{0}$ and $p_l = 0$

Final volumetric strain? Final void ratio? $\epsilon_v = 0.1$ and $e = 1.0$

Plaxis response? $\epsilon_v = 0.1$ and $e = 1.2$ Why?

Thermal expansion – an introductory example

Triaxial sample, no stress, perfectly drained

Initial void ratio $e_0 = 1.0$

Soil thermal expansion $\alpha = 10^{-2}$ K^{-1}

Temperature increment $\Delta T = 10$ K

Final stress? Final pore pressure? $\boldsymbol{\sigma} = \mathbf{0}$ and $p_l = 0$

Final volumetric strain? Final void ratio? $\epsilon_v = 0.1$ and $e = 1.0$

Plaxis response? $\epsilon_v = 0.1$ and $e = 1.2$ Why?

Probably use of $\Delta e = (1 + e_0) \times \epsilon_v = 0.2$. Why is this wrong?

Thermoporoelasticity

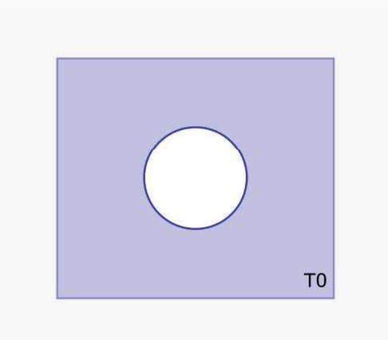

Isotropic behaviour (A. H.-D. Cheng 2016; Coussy 2004)

$$p - p_0 = K\,\epsilon_v - b\,(p_w - p_{w,0}) - 3\alpha\,K\,(T - T_0)$$
$$\phi - \phi_0 = b\,\epsilon_v + \frac{p_w - p_{w,0}}{N} - 3\alpha_\phi\,(T - T_0)$$

Relation with microscopic properties

$$\epsilon_v = (1 - \phi_0)\,\epsilon_s + \phi - \phi_0$$
$$b = 1 - \frac{K}{K_s}; \qquad \frac{1}{N} = \frac{b - \phi_0}{K_s}$$
$$\alpha = \alpha_s; \qquad \alpha_\phi = \alpha\,(b - \phi_0)$$

Thermal expansion i

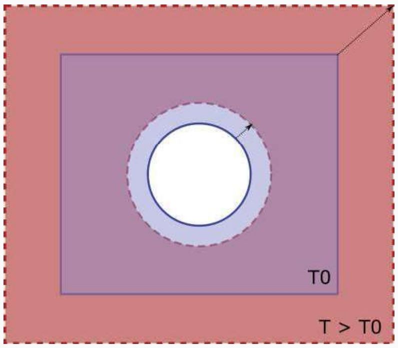

Temperature change assuming matrix incompressibility (drained and stress-free conditions)

$$\epsilon_v = (1-\phi_0)\,\epsilon_s + \phi - \phi_0 \neq \phi - \phi_0$$

$$b = 1 - \frac{K}{K_s} \approx 1; \qquad \frac{1}{N} = \frac{b-\phi_0}{K_s} \approx 0$$

$$\alpha = \alpha_s; \qquad \alpha_\phi = \alpha\,(b-\phi_0) \approx \alpha\,(1-\phi_0)$$

For homogeneous and isotropic solid, solid skeleton and porosity deform homothetically, so that...

Thermal expansion ii

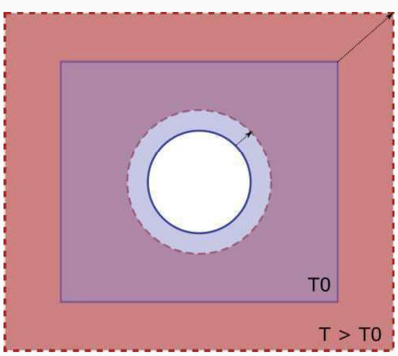

Lagrangian porosity

$$\phi = \frac{V_v}{V_0} \neq \phi_0$$

Eulerian porosity

$$n = \frac{V_v}{V} = n_0$$

(Eulerian by nature) void ratio

$$e = \frac{V_v}{V_s} = e_0$$

...but this is not verified in all numerical codes...

So what?

Even in isothermal conditions

- Usually, no large difference in case of small deformation...
- But, **do use both** lagrangian and eulerian porosities!
  - Eulerian porosity for indirect couplings (updating permeability, thermal conductivity...)
  - Lagrangian porosity tracks deformation of the porous network and should be used to solve the mass balance equation (in a conservative manner)
  - See (Melot et al. 2020) for a study on bitumen, using BIL FEM code (P. Dangla)

THM couplings

Thermal consolidation

Thermal consolidation

Experimental observations (Baldi et al. 1991; Sultan, Delage, and Cui 2002)

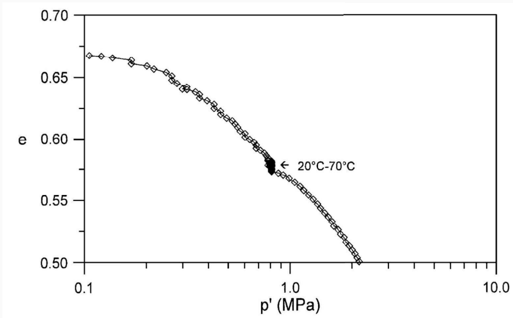

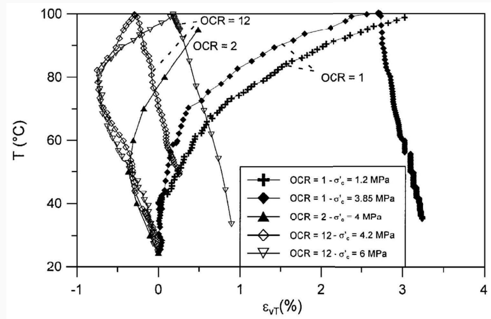

THM models

THM models

Unsaturated geomaterials

Context

Simply (?) wet sand (Sculpture of Sagrada Familia) (photo by SetosPuppy / CC BY-SA)

Context

(courtesy: E. Alonso)

Stress state variables

- Extension of Terzaghi's effective stress
  $\boldsymbol{\sigma}' = \boldsymbol{\sigma} - p_g \mathbf{1} + \chi\, s \mathbf{1}$ (Bishop 1959)
- Two state variables approaches
  - simple (measurable) variables
    $\boldsymbol{\sigma} - p_g \mathbf{1},\ \boldsymbol{\sigma} - p_l \mathbf{1},\ s$ (Coleman 1962; Fredlund and Morgenstern 1977)
  - use of an "effective" stress
    $\boldsymbol{\sigma} + \pi \mathbf{1},\ s$

Stress state variables

- Extension of Terzaghi's effective stress
- Two state variables approaches
  - simple (measurable) variables
  - use of an "effective" stress

Three classes of models (Gens 1995)

$$\begin{cases} \boldsymbol{\Sigma}_1 & = & \boldsymbol{\sigma} - p_g \mathbf{1} + \mu_1(s, S_l)\mathbf{1} \\ \boldsymbol{\Sigma}_2 & = & \mu_2(s, S_l)\mathbf{1} \end{cases}$$

Stress state variables

- Extension of Terzaghi's effective stress
- Two state variables approaches
  - simple (measurable) variables
  - use of an "effective" stress

Three classes of models (Gens 1995)

$$\begin{cases} \boldsymbol{\Sigma}_1 & = & \boldsymbol{\sigma} - p_g \mathbf{1} + \mu_1(s, S_l)\mathbf{1} \\ \boldsymbol{\Sigma}_2 & = & s\mathbf{1} \end{cases}$$

Classe I $\mu_1 = 0$ (Alonso, Gens, and Josa 1990)...
Classe II $\mu_1 = \mu(s)$ (Abou-Bekr 1995; Loret and Khalili 2000)...
Classe III $\mu_1 = \mu(s, S_l)$ (Dangla 2001; Wheeler, Sharma, and Buisson 2003)...

Barcelona Basic Model (BBM)

- First elastoplastic model for unsaturated soils (Alonso, Gens, and Josa 1990)
- Based on modified cam-clay

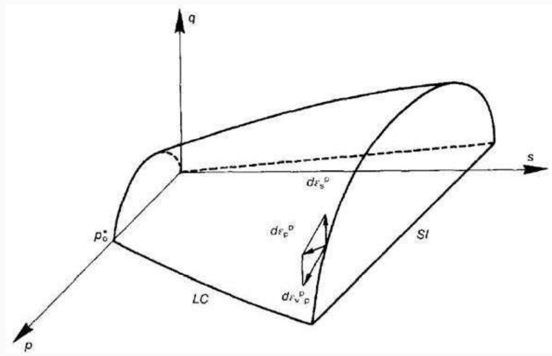

Barcelona Basic Model (BBM)

- First elastoplastic model for unsaturated soils (Alonso, Gens, and Josa 1990)
- Based on modified cam-clay

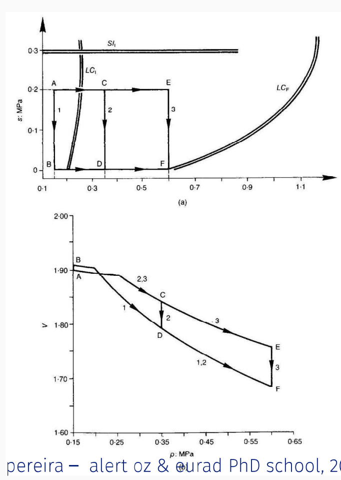

Barcelona Basic Model (BBM)

- First elastoplastic model for unsaturated soils (Alonso, Gens, and Josa 1990)
- Based on modified cam-clay

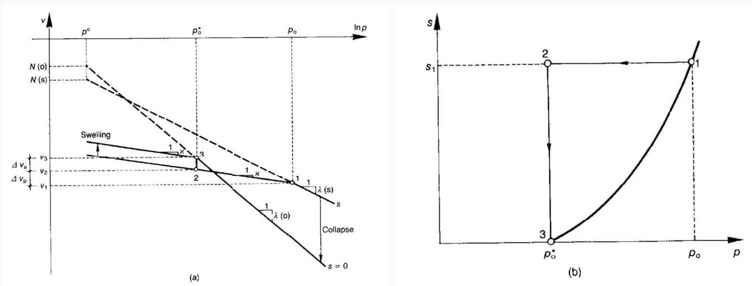

BBM — mathematical formulation I

- Elastic behaviour

$$\mathrm{d}\epsilon_v^e = \frac{\kappa}{v}\frac{\mathrm{d}p}{p} + \frac{\kappa_s}{v}\frac{\mathrm{d}s}{s + p_{atm}}$$

$$\mathrm{d}\epsilon_q^e = \frac{\mathrm{d}q}{3\,G}$$

- Elastic properties

$$K = \left.\frac{\mathrm{d}p}{\mathrm{d}\epsilon_v^e}\right|_s = \frac{(1 + e_0)\,p}{\kappa}$$

$$G = \frac{1}{3}\frac{\mathrm{d}q}{\mathrm{d}\epsilon_q^e} = constant$$

3 elastic parameters: κ, κ_s, G

BBM — mathematical formulation II

Yield surface:

$$f \equiv \left(\frac{q}{Mp}\right)^2 - \left(\frac{p_0}{p} - 1\right)^2 = 0$$

$$\frac{p_0}{p_c} = \left(\frac{p_0^*}{p_c}\right)^{\dfrac{\lambda(0)-\kappa}{\lambda(s)-\kappa}}$$

$$\lambda(s) = \lambda(0)\left[(1-r)\exp(-\beta s) + r\right]$$

$$\mathrm{d}p_0^* = \frac{v\, p_0^*}{\lambda - \kappa}\,\mathrm{d}\epsilon_v^p$$

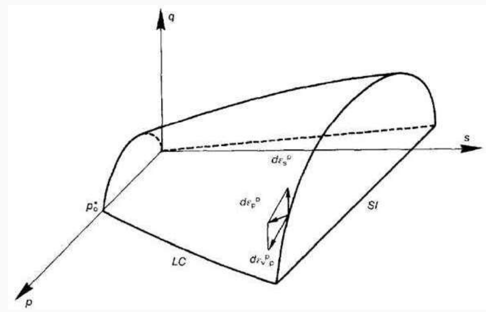

Going further

Accounting for water adsorption effects, osmotic effects…

See for instance:

- On drying induced shrinkage of cement pastes: (Rahoui 2018; Rahoui et al. 2021)
- Recent works by Prof. Ning Lu, e.g. (Wang et al. 2022)

THM models

Thermoporoelastoplastic models

Thermomechanical (elastoplastic) models

What we know

- Little effect of temperature on elastic properties
- Same for failure properties (friction angle and cohesion little affected)
- Yield stress is temperature dependent (cf. thermal consolidation)

See (Abuel-Naga et al. 2009; Cui, Sultan, and Delage 2000; Laloui and Cekerevac 2003) for some founding models

Thermomechanical (elastoplastic) models

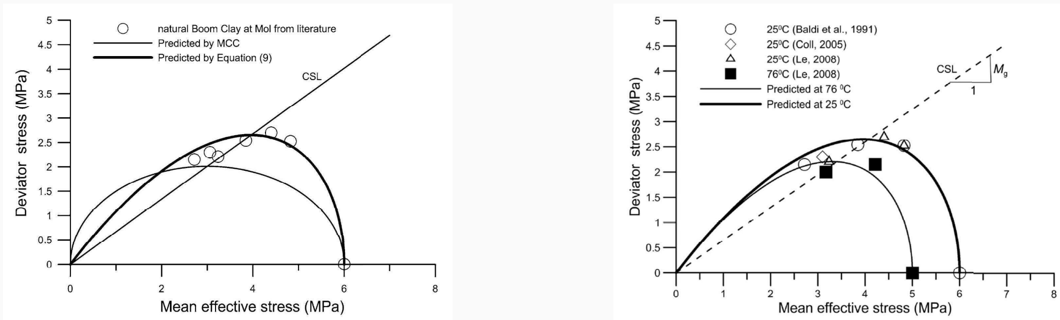

Yield surface for Boom clay and temperature effect
(Hong, Pereira, Cui, et al. 2016; Hong, Pereira, Tang, et al. 2016)

Temperature dependent yield surface

Thermal elastic strain ($\mathrm{d}\epsilon_v^e = \mathrm{d}\epsilon_{v,M}^e + \alpha_T\,\mathrm{d}T$) and temperature dependent yield surface $p_{c0,T} = p_{c0,T}(T)$

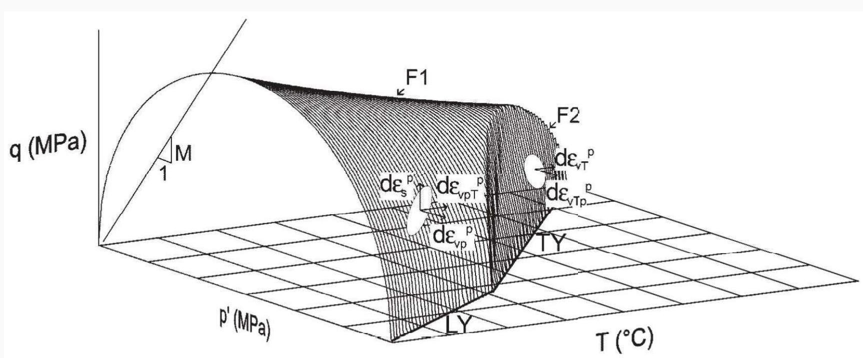

Yield surface in (p', q, T) space (Cui, Sultan, and Delage 2000)

Temperature dependent yield surface

Thermal elastic strain ($d\epsilon_v^e = d\epsilon_{v,M}^e + \alpha_T \, dT$) and temperature dependent yield surface $p_{c0,T} = p_{c0,T}(T)$

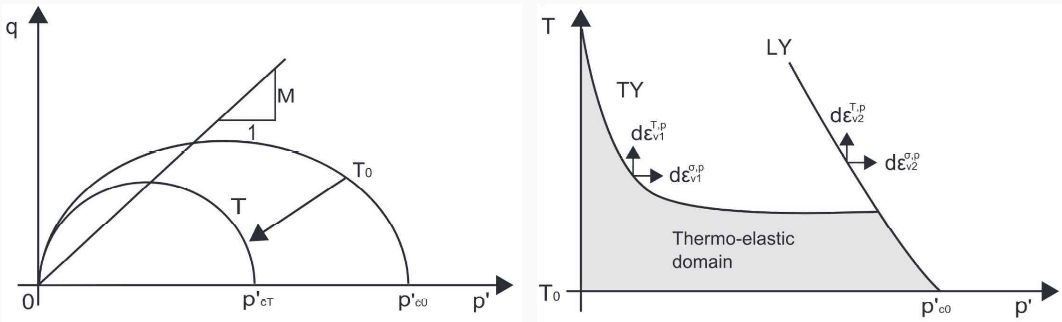

Yield surface in (p', q) and (p', T) space (Hong, Pereira, Cui, et al. 2012)

Temperature dependent yield surface – advanced models

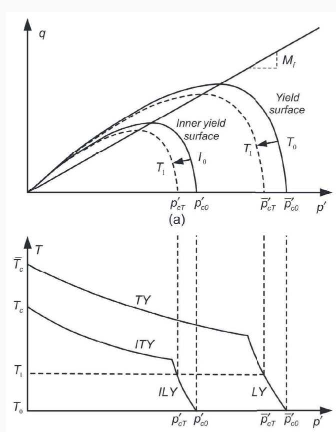

Yield surfaces in (p', q) and (p', T) space (W. Cheng et al. 2020)

Application

Energy geostructures

Piles, diaphragm walls, tunnel support...

What we know?

- Shear strength mostly temperature-independent (Yavari et al. 2016)
- Thermal consolidation in normally consolidated clays: might not be relevant
- Creep? Temperature enhanced

Mainly cyclic and long term effects on vertically (and laterally) loaded piles

Can we keep it simple?

Use of a **”decoupled” strategy** (Yavari et al. 2014) to model in situ and small scale (1g) lab piles: imposed volumetric strain and perfect plasticity

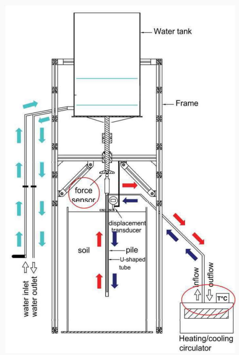

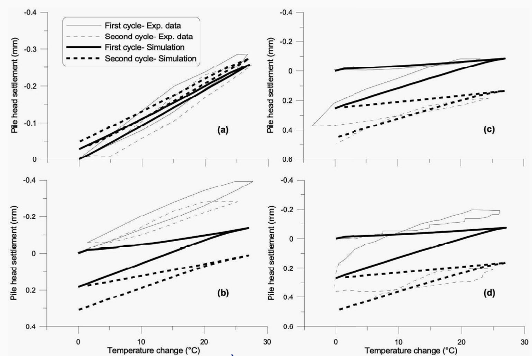

(Kalantidou et al. 2012)

Can we keep it simple?

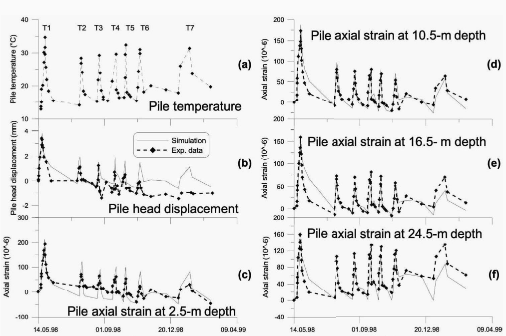

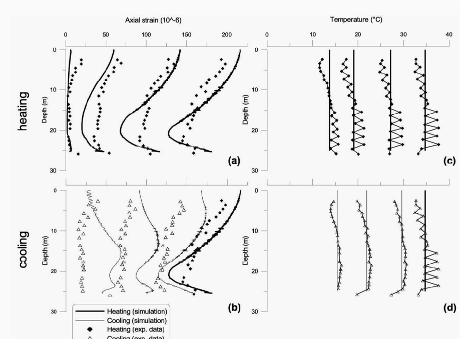

(Laloui, Moreni, and Vulliet 2003)

Essential role played by lateral stress variation on mobilisable shaft friction

Refined THM analysis

More detailed analysis (THM coupled) using rather simple constitutive model (MCC)(Nguyen, Wu, et al. 2020)

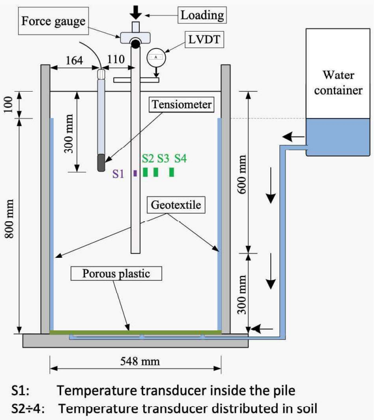

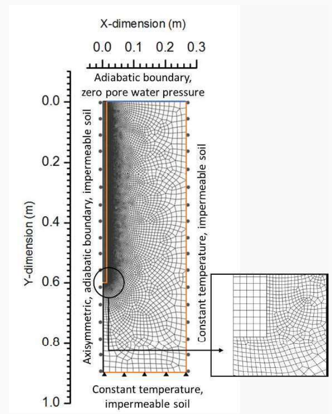

Refined THM analysis

More detailed analysis (THM coupled) using rather simple constitutive model (MCC)(Nguyen, Wu, et al. 2020)

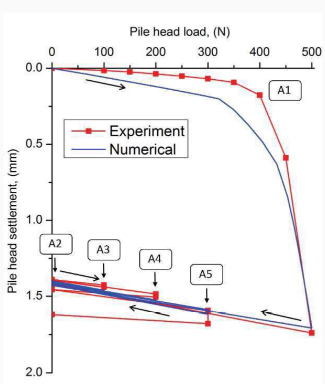

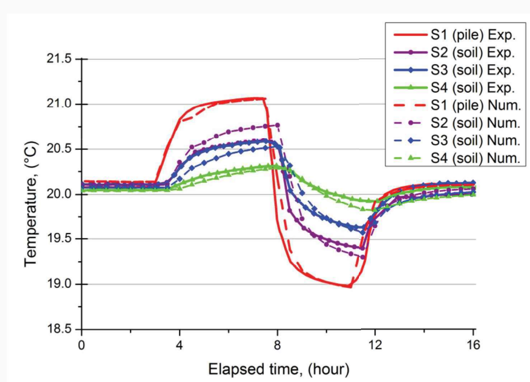

Refined THM analysis

More detailed analysis (THM coupled) using rather simple constitutive model (MCC)(Nguyen, Wu, et al. 2020)

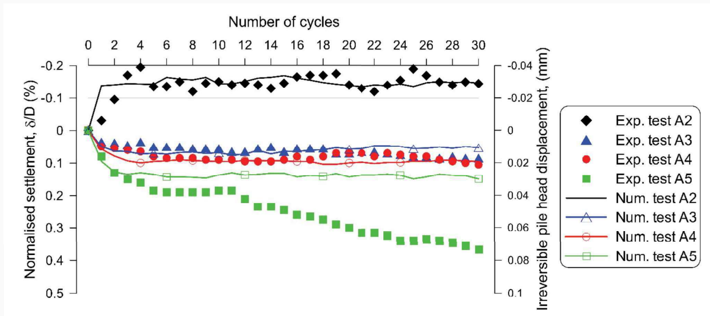

Influence of shaft strength mobilisation
(Bourne-Webb and Bodas Freitas 2020; Pasten and Santamarina 2014)

"All models are wrong but some are useful."
— George Box

Thanks for your attention – Questions?

References i

Abou-Bekr, N. (1995). **"Modélisation Du Comportement Mécanique et Hydraulique Des Sols Partiellement Saturés".** PhD thesis. Ecole Centrale de Paris.

Abuel-Naga, H. M., D. T. Bergado, A. Bouazza, and M. Pender (2009). **"Thermomechanical Model for Saturated Clays".** In: *Géotechnique* 59.3, p. 273.

Alonso, E. E., A. Gens, and A. Josa (1990). **"A Constitutive Model for Partially Saturated Soils".** In: *Géotechnique* 40.3, pp. 405–430.

Baldi, G., T. Hueckel, A. Peano, and R. Pellegrini (1991). ***Developments in Modelling of Thermo-Hydro-Mechanical Behaviour of Boom Clay and Clay-Based Buffer Materials, Vol. 1 and 2, EUR 13365/1 and 13365/2.*** Nuclear Science and Technology, Commission of the European Communities.

Baudet, B. A. and S. Stallebrass (2004). **"A Constitutive Model for Structured Clays".** In: *Géotechnique* 54.4, pp. 269–278.

References ii

- Bauer, E. (1996). **“Calibration of a Comprehensive Hypoplastic Model for Granular Materials”.** In: *Soils and Foundations* 36.1, pp. 13–26.
- Bergman, T. L., A. S. Lavine, F. P. Incropera, and D. P. DeWitt (1996). ***Fundamentals of Heat and Mass Transfer.*** Seventh edition. New York: John Wiley & Sons.
- Bishop, A. W. (1959). **“The Principle of Effective Stress”.** In: *Teknisk Ukeblad* 106.39, pp. 859–863.
- Bjerrum, L. (1967). **“Engineering Geology of Norwegian Normally-Consolidated Marine Clays as Related to Settlement of Buildings”.** In: *Géotechnique* 17, pp. 81–118.
- Bourbié, T., O. Coussy, and B. Zinszner (1987). ***Acoustics of Porous Media.*** Institut Français Du Pétrole Publications. Editions Technip.
- Bourne-Webb, P. and T. Bodas Freitas (2020). **“Thermally-Activated Piles and Pile Groups under Monotonic and Cyclic Thermal Loading–A Review”.** In: *Renewable Energy* 147, pp. 2572–2581.
- Cheng, A. H.-D. (2016). ***Poroelasticity.*** Textbook 37.0. Springer.

References iii

- Cheng, W., P.-y. Hong, J. M. Pereira, Y.-j. Cui, A. M. Tang, and R.-p. Chen (2020). **“Thermo-Elasto-Plastic Modeling of Saturated Clays under Undrained Conditions”.** In: *Computers and Geotechnics* 125 (January), p. 103688.
- Coleman, J. D. (1962). **“Stress Strain Relations for Partly Saturated Soils”.** In: *Géotechnique* 12.4, pp. 348–350.
- Coussy, O. (1991). ***Mécanique Des Milieux Poreux.*** Editions Technip.
- Coussy, O. (2010). ***Mechanics and Physics of Porous Solids.*** Wiley.
- Coussy, O. (1995). ***Mechanics of Porous Continua.*** Chichester: John Wiley & Sons.
- Coussy, O. (2004). ***Poromechanics.*** Chichester: John Wiley & Sons.
- Cui, Y. J., N. Sultan, and P. Delage (2000). **“A Thermomechanical Model for Saturated Clays”.** In: *Canadian Geotechnical Journal* 37.3, pp. 607–620.
- Dafalias, Y. F. and L. R. Herrmann (1980). **“A Bounding Surface Soil Plasticity Model”.** In: *Int. Symp. on Soils under Cyclic and Transient Loading*. Swansea, pp. 335–345.

References iv

- Dafalias, Y. F. and L. R. Herrmann (1986). "Bounding Surface Plasticity. II: Application to Isotropic Cohesive Soils". In: *Journal of Engineering Mechanics* 112.12, pp. 1263–1291.
- Dangla, P. (2001). ***Introduction à La Mécanique Des Milieux Poreux.*** Cours de {DEA} Mécanique des Solides, des Matériaux et des Structures, Ecole doctorale MODES. Laboratoire Central des Ponts et Chaussées.
- De Gennaro, V. and J. M. Pereira (2013). "A Viscoplastic Constitutive Model for Unsaturated Geomaterials". In: *Computers and Geotechnics* 54 (October), pp. 143–151.
- De Gennaro, V., J. M. Pereira, M. S. Gutierrez, and R. J. Hickman (2009). "Viscoplastic Modelling of Fluids Filled Porous Chalks". In: *Italian Geotechnical Journal* 1/09, pp. 44–64.
- Dong, Y., J. S. McCartney, and N. Lu (2015). "Critical Review of Thermal Conductivity Models for Unsaturated Soils". In: *Geotechnical and Geological Engineering* 33.2, pp. 207–221.
- Fredlund, D. G. and N. R. Morgenstern (1977). "Stress State Variables for Unsaturated Soils". In: *Journal of the Geotechnical Engineering Division* 103.5, pp. 447–465.

References v

- Gens, A. (1995). "Constitutive Laws". In: *Modern Issues in Non-Saturated Soils*. Ed. by A. Gens, P. Jouanna, and B. A. Schrefler. Wien: Springer-Verlag, pp. 129–158.
- Gruescu, C., A. Giraud, F. Homand, D. Kondo, and D. P. Do (2007). "Effective Thermal Conductivity of Partially Saturated Porous Rocks". In: *International Journal of Solids and Structures* 44.3, pp. 811–833.
- Gudehus, G. (1996). "A Comprehensive Constitutive Equation for Granular Materials". In: *Soils and Foundations* 36.1, pp. 1–12.
- Hicher, P.-Y. (1985). "Comportement Mécanique Des Argiles Saturées Sur Divers Chemins de Sollicitations Monotones et Cycliques Application à Une Modélisation Élastoplastique et Viscoplastique". Thèse de doctorat d'état ès sciences physiques. Université Paris 6.
- Hong, P. Y., J. M. Pereira, Y. J. Cui, and A. M. Tang (2016). "A Two-Surface Thermomechanical Model for Saturated Clays". In: *International Journal for Numerical and Analytical Methods in Geomechanics* 40.7, pp. 1059–1080.

References vi

- Hong, P. Y., J. M. Pereira, Y. J. Cui, and A. M. Tang (2012). **"Explicit Integration of a Thermo-Mechanical Model for Clays".** In: *Computers and Geotechnics* 46 (November), pp. 13–25.
- Hong, P. Y., J. M. Pereira, A. M. Tang, and Y. J. Cui (2016). **"A Two-Surface Plasticity Model for Stiff Clay".** In: *Acta Geotechnica* 11.4, pp. 871–885.
- Houlsby, G. T. and A. M. Puzrin (2006). ***Principles of Hyperplasticity.*** London: Springer London.
- Johansen, O. (1975). **"Varmeledningsevne Av Jordarter (Thermal Conductivity of Soils)".** US Army Corps of Engineers, Cold Regions Research and Engineering Laboratory, Hanover, N.H. CRREL draft English Translation 637. Trondheim, Norway: University of Trondheim.
- Kalantidou, A., A. M. Tang, J. M. Pereira, and G. Hassen (2012). **"Preliminary Study on the Mechanical Behaviour of Heat Exchanger Pile in Physical Model".** In: *Géotechnique* 62.11, pp. 1047–1051.
- Kaviany, M. (1998). **"Heat Transfer in Porous Media".** In: *Handbook of Heat Transfer*. Ed. by W. M. Rohsenow, J. P. Hartnett, and Y. I. Cho. 3rd edition. McGraw Hill, New York, USA.

References vii

- Laloui, L. and C. Cekerevac (2003). **"Thermo-Plasticity of Clays: Anisotropic Yield Mechanism".** In: *Computers and Geotechnics* 30, pp. 649–660.
- Laloui, L., M. Moreni, and L. Vulliet (2003). **"Comportement d'un Pieu Bi-Fonction, Fondation et Échangeur de Chaleur".** In: *Canadian Geotechnical Journal* 40.2, pp. 388–402.
- Leroueil, S. and D. W. Hight (2003). **"Behaviour and Properties of Natural Soils and Soft Rocks".** In: *Characterisation and Engineering Properties of Natural Soils*. Ed. by T. S. Tan, D. Phoon, D. W. Hight, and S. Leroueil. Vol. 1, pp. 29–254.
- Leroueil, S. and M. E. S. Marques (1996). **"Importance of Strain Rate and Temperature Effects in Geotechnical Engineering".** In: *Measuring and Modeling Time Dependent Soil Behaviour, Proc. of the ASCE Convention*. Vol. 61. Washington, DC, USA, pp. 1–60.
- Loret, B. and N. Khalili (2000). **"A Three-Phase Model for Unsaturated Soils".** In: *International Journal for Numerical and Analytical Methods in Geomechanics* 24.11, pp. 893–927.

References viii

- Melot, G., P. Dangla, S. Granet, S. M'Jahad, J. Champenois, and A. Poulesquen (2020). **"Chemo-Hydro-Mechanical Analysis of Bituminized Waste Swelling Due to Water Uptake: Experimental and Model Comparisons".** In: *Journal of Nuclear Materials* 536, p. 152165.
- Nguyen, V. T., H. Heindl, J. M. Pereira, A. M. Tang, and J. D. Frost (2017). **"Water Retention and Thermal Conductivity of a Natural Unsaturated Loess".** In: *Géotechnique Letters* 7.4, pp. 286–291.
- Nguyen, V. T., N. Wu, Y. Gan, J.-M. Pereira, and A. M. Tang (2020). **"Long-Term Thermo-Mechanical Behaviour of Energy Piles in Clay".** In: *Environmental Geotechnics* 7.4, pp. 237–248.
- Pasten, C. and J. C. Santamarina (2014). **"Thermally Induced Long-Term Displacement of Thermoactive Piles".** In: *Journal of Geotechnical and Geoenvironmental Engineering* 140.5, pp. 1–5.
- Pastor, M., O. C. Zienkiewicz, and A. H. C. Chan (1990). **"Generalized Plasticity and the Modelling of Soil Behaviour".** In: *International Journal for Numerical and Analytical Methods in Geomechanics* 14.3, pp. 151–190.

References ix

- Perzyna, P. (1963). **"The Constitutive Equations for Rate Sensitive Plastic Materials".** In: *Quarterly of Applied Mathematics* 20.4, pp. 321–332.
- Rahoui, H. (2018). **"Contribution to understanding the action of shrinkage reducing admixtures in cementitious materials : experiments and modelling".** PhD thesis. Université Paris-Est.
- Rahoui, H., I. Maruyama, M. Vandamme, J.-M. Pereira, and M. Mosquet (2021). **"Impact of an SRA (Hexylene Glycol) on Irreversible Drying Shrinkage and Pore Solution Properties of Cement Pastes".** In: *Cement and Concrete Research* 143, p. 106227.
- Schofield, A. and P. Wroth (1968). ***Critical State Soil Mechanics.*** London: McGraw-Hill. 310 pp.
- Šuklje, L. (1957). **"The Analysis of the Consolidation Process by the Isotache Method".** In: *Proc. 4th Int. Conf. on Soil Mech. and Found. Engng.* Vol. 1. London, pp. 200–206.
- Sultan, N., P. Delage, and Y. J. Cui (2002). **"Temperature Effects on the Volume Change Behaviour of Boom Clay".** In: *Engineering Geology* 64.2-3, pp. 135–145.

References x

- Tavenas, F., S. Leroueil, P. L. Rochelle, and M. Roy (1978). **“Creep Behaviour of an Undisturbed Lightly Overconsolidated Clay”.** In: *Canadian Geotechnical Journal* 15.3, pp. 402–423.
- Troupel, H. (2017). **“Contribution à l’étude du comportement différé des géomatériaux avec prise en compte des conditions thermo-hydriques”.** PhD thesis. Université Paris-Est.
- Vaid, Y. P. and R. G. Campanella (1977). **“Time-Dependent Behaviour of Undisturbed Clay”.** In: *Journal of Geotechnical Division, ASCE* 103.7, pp. 693–709.
- Wang, Y., L. Hu, S. Luo, and N. Lu (2022). **“Soil Water Isotherm Model for Particle Surface Sorption and Interlamellar Sorption”.** In: *Vadose Zone Journal* 21.5.
- Wheeler, S. J., R. S. Sharma, and M. S. R. Buisson (2003). **“Coupling of Hydraulic Hysteresis and Stress-Strain Behaviour in Unsaturated Soils”.** In: *Géotechnique* 53.1, pp. 41–54.
- Yavari, N., A. M. Tang, J. M. Pereira, and G. Hassen (2014). **“A Simple Method for Numerical Modelling of Mechanical Behaviour of an Energy Pile”.** In: *Géotechnique Letters* 4, pp. 119–124.

References xi

- Yavari, N., A. M. Tang, J. M. Pereira, and G. Hassen (2016). **“Effect of Temperature on the Shear Strength of Soils and the Soil–Structure Interface”.** In: *Canadian Geotechnical Journal* 53.7, pp. 1186–1194.

Appendix E. From Workflows towards Digital Twins: OpenWorkFlow-Project (O. Kolditz)

EURAD GAS#HITEC: PhD School

From Workflows towards Digital Twins: OpenWorkFlow-Project

Olaf Kolditz, Norbert Grunwald, Christoph Lehmann & OpenGeoSys Team

29.08.2023, Liège, Belgium

Workflows

Generic Workflows

"A workflow consists of an orchestrated and **repeatable pattern of activity**, enabled by the systematic organization of resources into processes that transform materials, provide services, or **process information**." (Wikipedia)

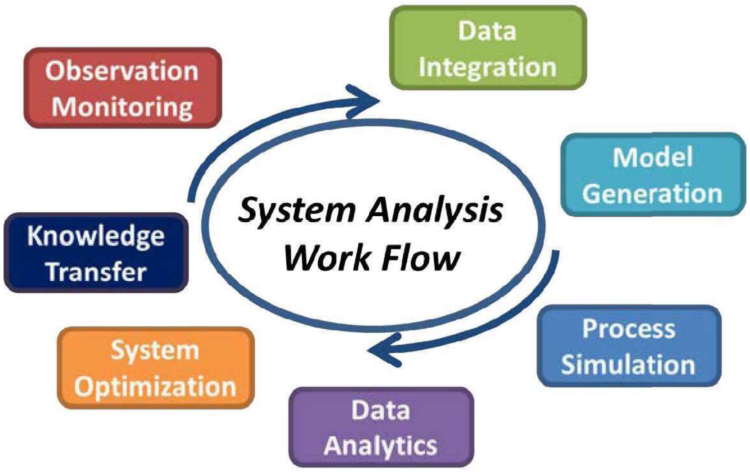

Reference: Ch. Lehmann [LT22], [Kol+19]

Generic Workflows

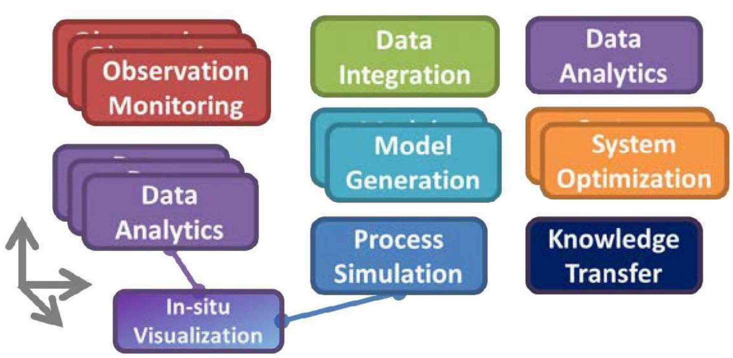

- Exchangeable modules >> Pipelines
- Platform-independent
- Script-based environments (Jupyter, web-browser applications)

Specific Workflows

Geothermal Systems

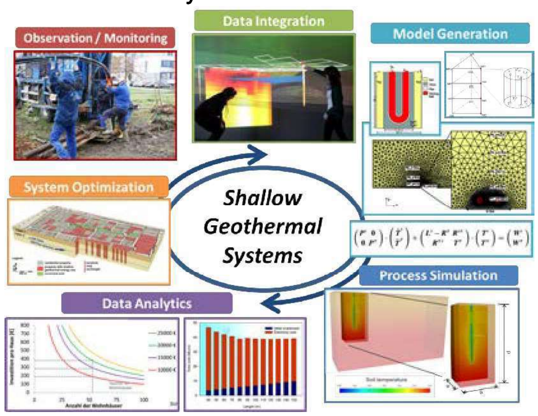

Geotechnical Systems

Specific Workflows

Geothermal Systems

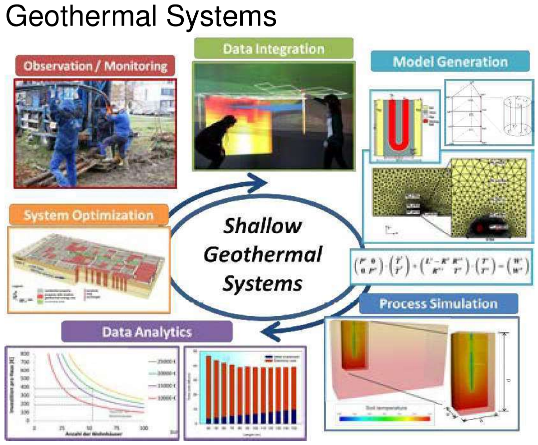

Geotechnical Systems

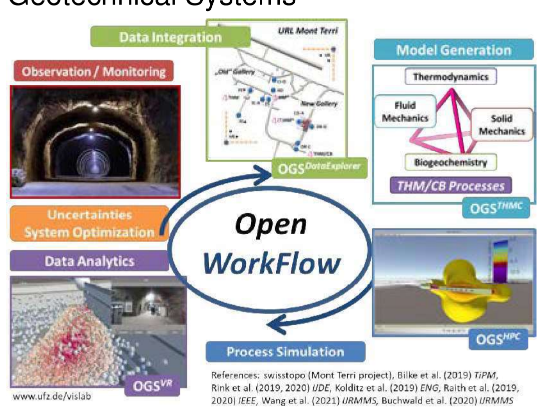

- existing interfaces (OGS DataExplorer), level of automation is low ...

Generic Workflow for the Siting Process #1

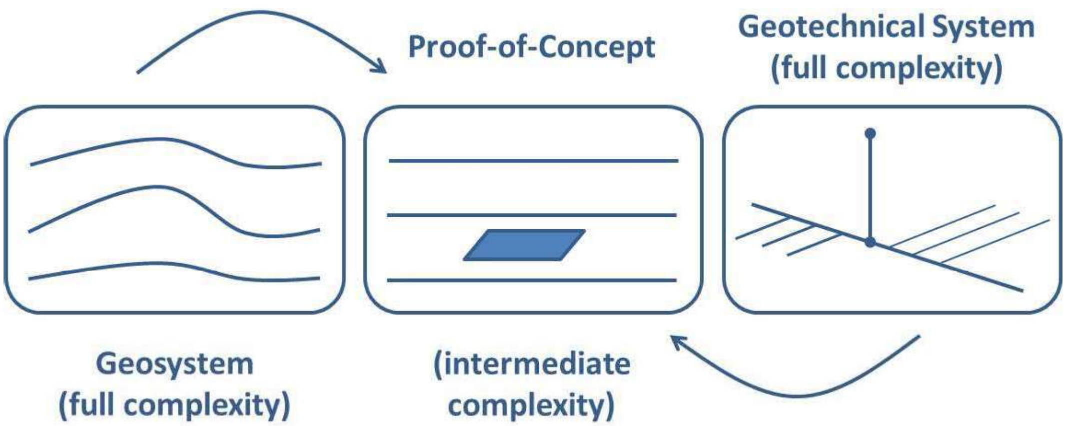

Specific Workflow for the Siting Process #2

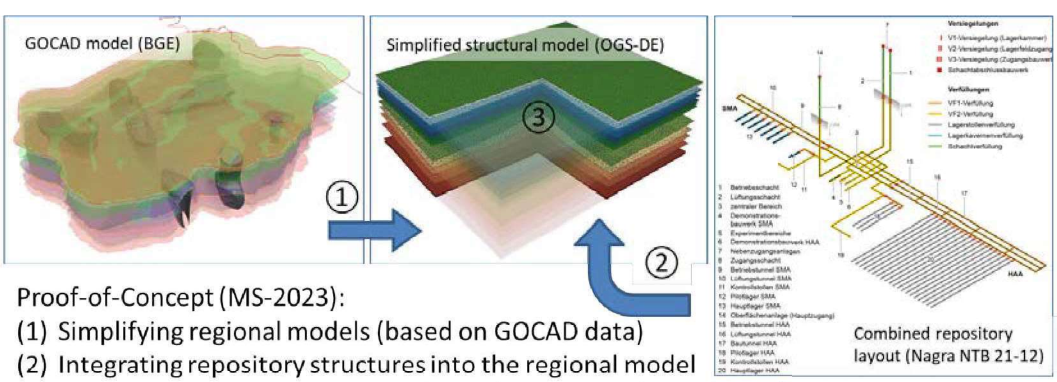

Proof-of-Concept (MS-2023):

(1) Simplifying regional models (based on GOCAD data)
(2) Integrating repository structures into the regional model
(3) THMC simulations at various scales and complexity levels (near/far field processes)

Specific Workflow for the Siting and Repository Concepts #3

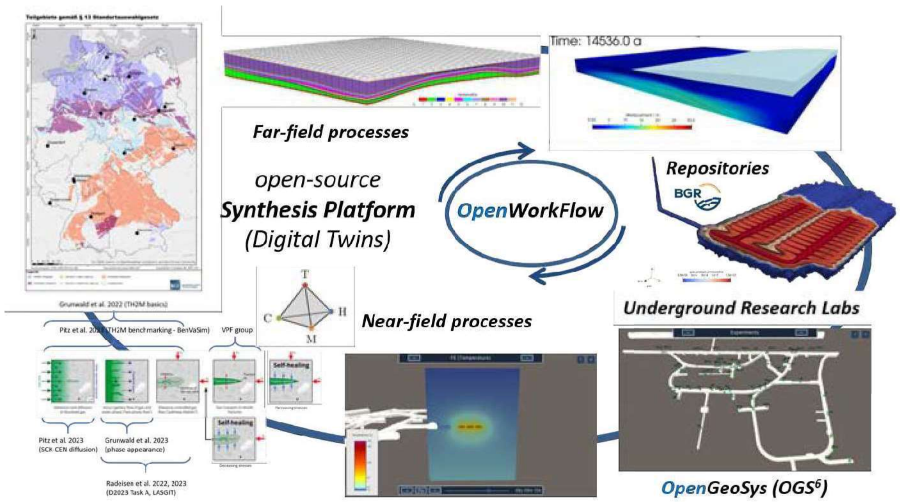

Process Selection: Complexity and Scales

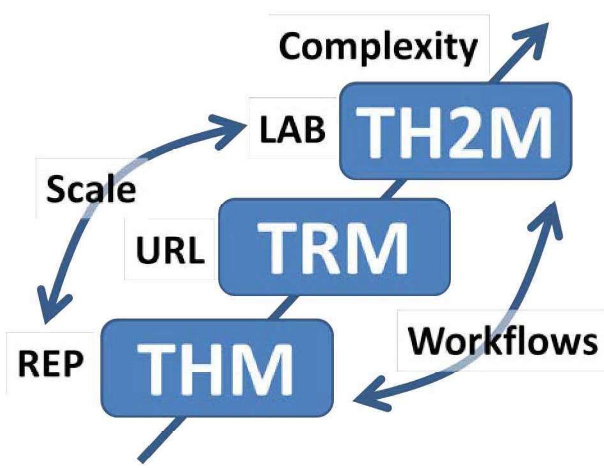

OpenGeoSys (OGS)

OpenGeoSys - THMC/RTP Simulator (`www.opengeosys.org`)

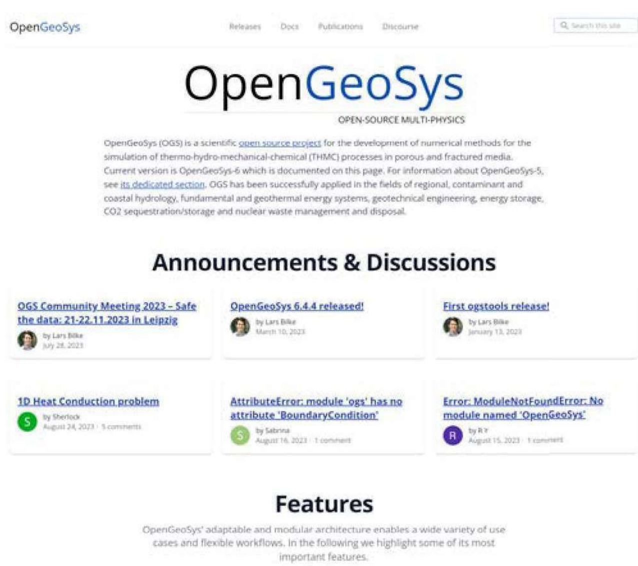

Books & Tutorials (OGS5)

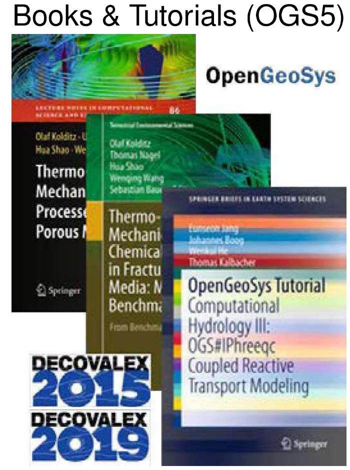

OpenGeoSys - THMC/RTP Simulator (`www.opengeosys.org`)

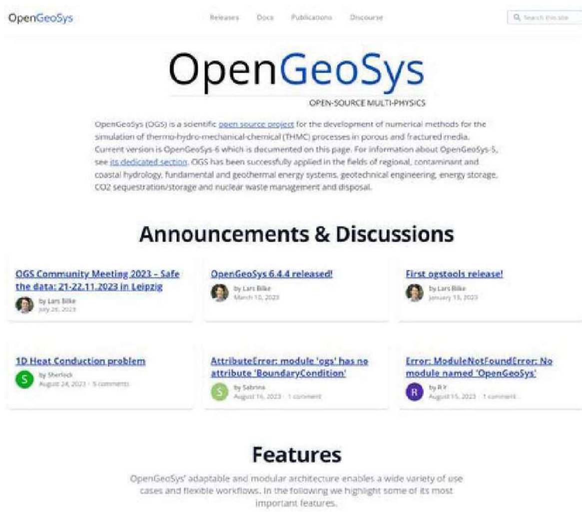

History

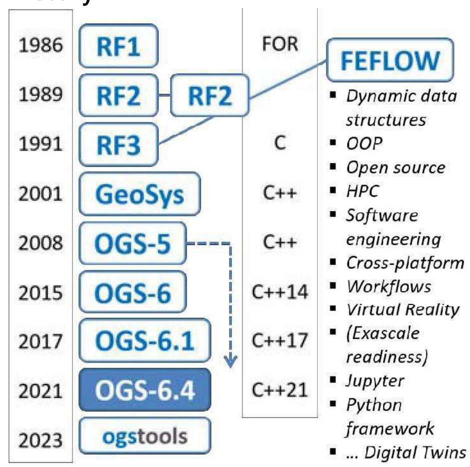

OpenGeoSys - Benchmarking Gallery (JupyterLab)

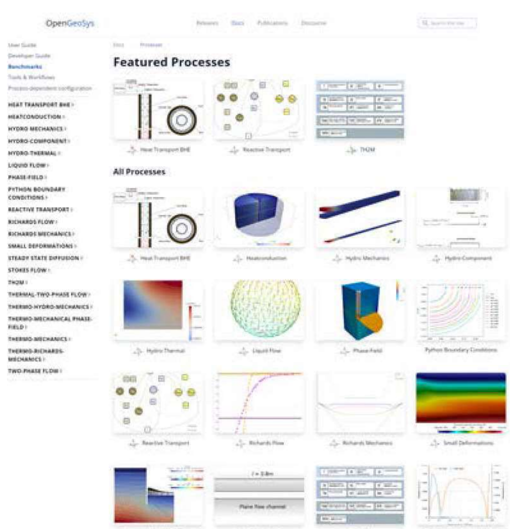

OGS-TH2M Model Class

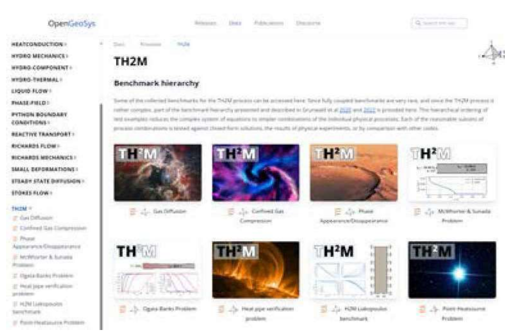

References: [Gru+22], [Pit+23b]

Simulation of Coupled Multiphysics Processes: OpenGeoSys-6 TH2M

TH^2M	• non-isothermal, poro-elastic, multiphase flow • phase change & transition (evaporation&dissolution)

THM	• Point heat source consolidation **Booker | Chaudry** exact solution	TH^2	• Heat pipe problem **Udell | Doughty** benchmark	H^2M	• Poro-elastic soil consolidation **Liakopoulos** benchmark

TH	• Isentropic compression • Advection/ diffusionn **Ogata | Banks** benchmark	TM	• Thermo-elastic plate/cube	HM	• Poro-elastic column consolidation	H^2	• Two-phase flow: **McWhorter** benchmark
T	• Linear/ radial heat conduction	H^G	• Compressible fluid flow	H^L	• Incompressible fluid flow	M	• Linear elastic deformation

References: [Gru+22], [Pit+23b]

OGS participation in DECOVALEX

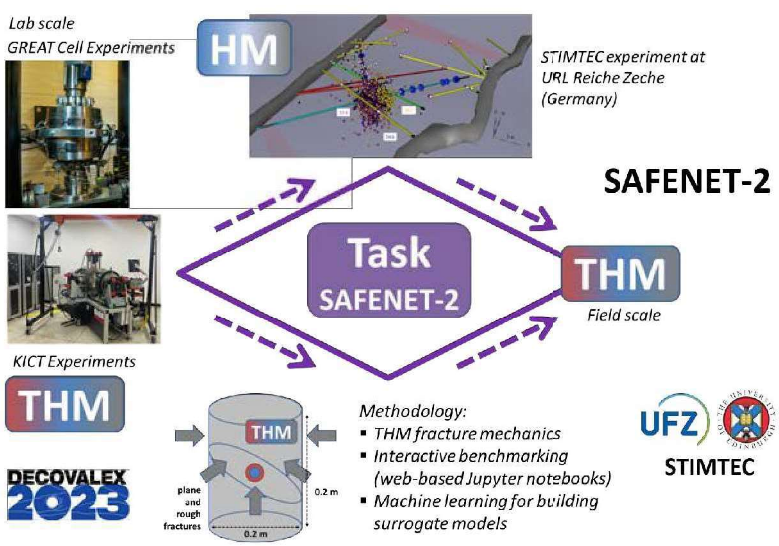

References:
[Mol+23]
[Rad+23a]
[Rad+23b]
[Pit+23a] (BenVaSim)

Simulation of Coupled Multiphysics Processes (>> Norbert)

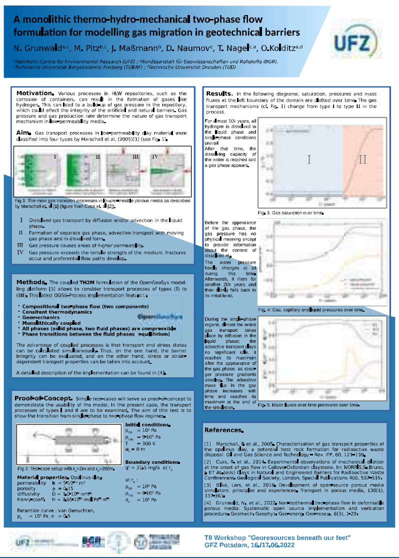

OpenGeoSys-6 TH2M

- Compositional two-phase flow
- Geomechanics (inelastic solids)
- Consistent thermodynamics
- Phase transitions
- Hierarchic benchmarking
- ...

Capable to verify the concept of P. Marschall [MHG05] for various clay types (OPA, COx, Boom)

References: [Gru+22], [Pit+23b]

OpenGeoSys - Applications

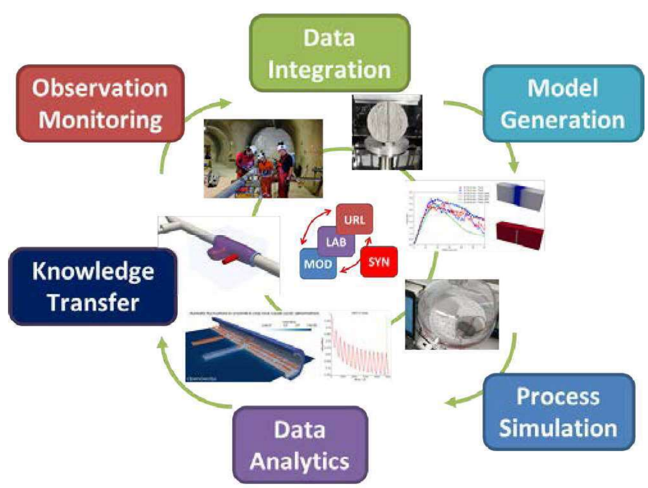

OpenGeoSys - Applications

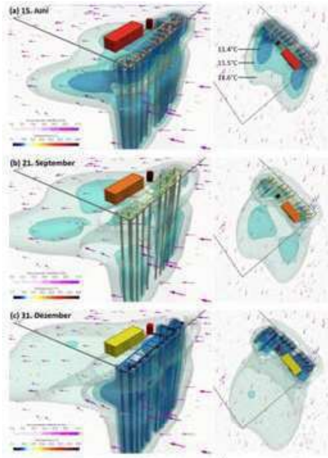

Abbildung 7.6: Visualisierung der Ergebnisse der gekoppelten Simulation von OpenGeoSys und SimulationX. Dargestellt sind die Temperaturentwicklungen in einem Schulgebäude, der zugehörigen Anlage, Wärmesonden und den verbindenden Leitungen via SimulationX sowie von Grundwasserfluss und Temperatur im Untergrund via OpenGeoSys an drei ausgewählten Tagen. Die Transferfunktion der Temperaturdarstellung ist zur besseren Vergleichbarkeit konstant über alle Zeitschritte und dargestellten Komponenten. Die zur Illustration der Temperaturveränderung visualisierten Isotemperaturflächen liegen bei 11.4°C, 11.5°C und 11.6°C (siehe auch Abb. (a) rechts)

Shallow geothermal systems (Leipzig) and ATES (Aquifer Thermal Energy Storage in Kiel)

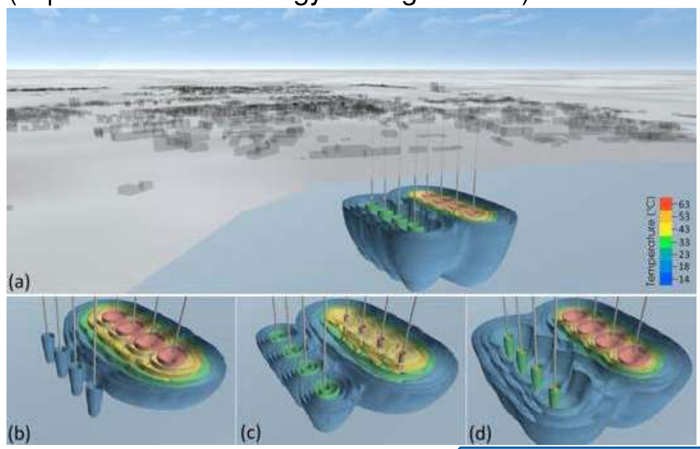

Workflows (cont.)

Specific Workflow for the Siting and Repository Concepts #3a

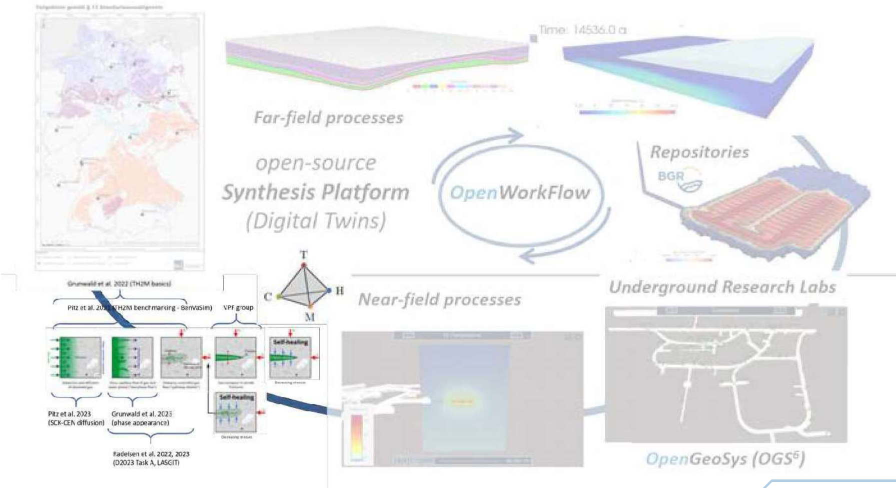

Scale – Lab (EPFL-Experiment, EURAD GAS)

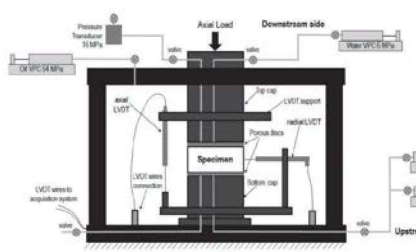

- Aim: Identification of Opalinus Clay properties
- Water Retention behaviour
- Stress-strain relations in recation to gas invasion processes
- Gas transport properties
- Strain dependent permeability model

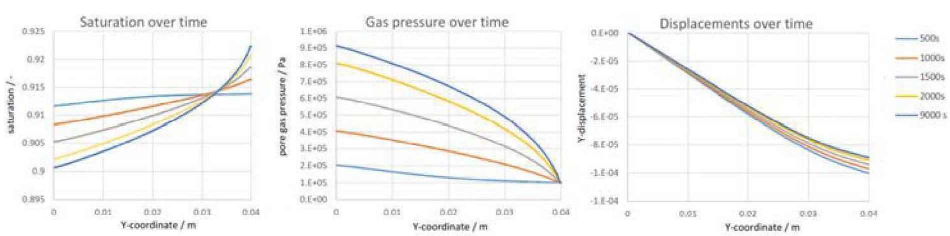

References/Credits: BGR (Michael Pitz [Pit+23b]), EPFL (Alessio Ferrari, Qazim Llabjani)

Specific Workflow for the Siting and Repository Concepts #3b

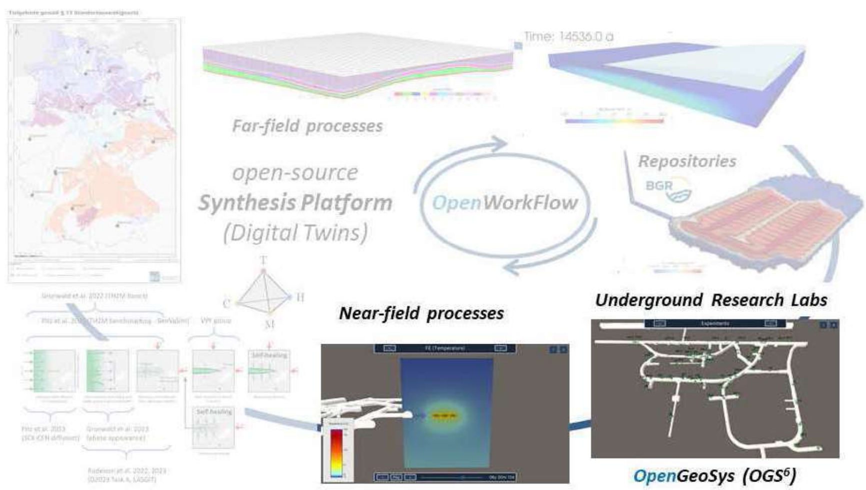

Scale – URL (Mont Terri)

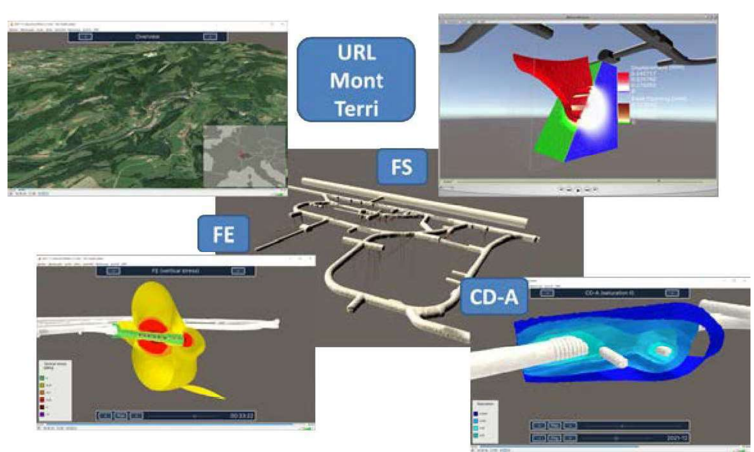

References/Credits: BGR (CD-A, Modeler [Zie+22]), TUBAF (FS, Modeler), UFZ (FE, Wenqing Wang), VIS (Nico Graebling/Karsten Rink) [Gra+22] / GeomInt and iCROSS projects

Specific Workflow for the Siting and Repository Concepts #3c

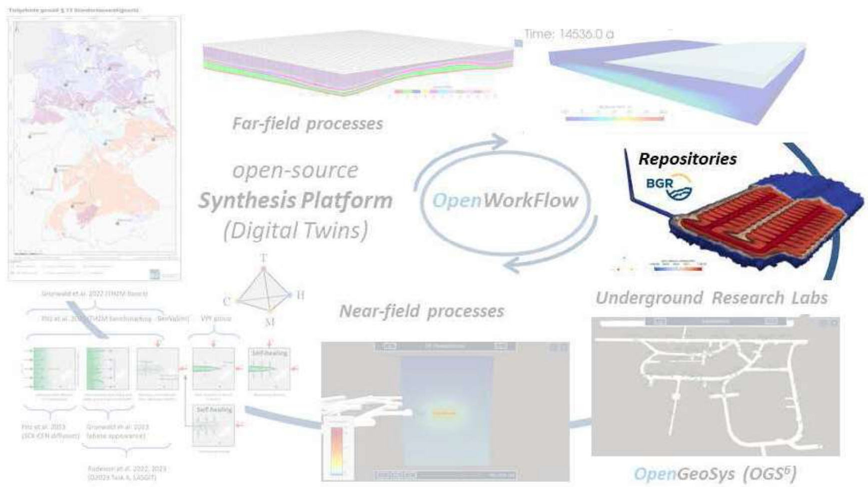

Scale – up to Repository Scale

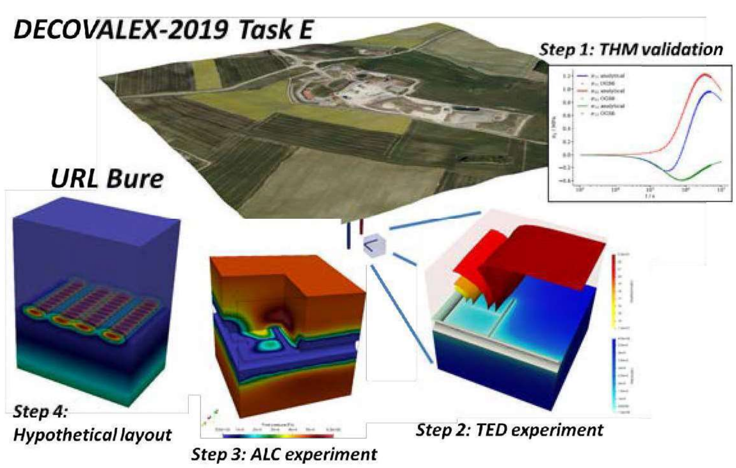

References/Credits: [Wan+21b], [Wan+21a], [Cha+19] / DECOVALEX 2019 project

Specific Workflow for the Siting and Repository Concepts #3d

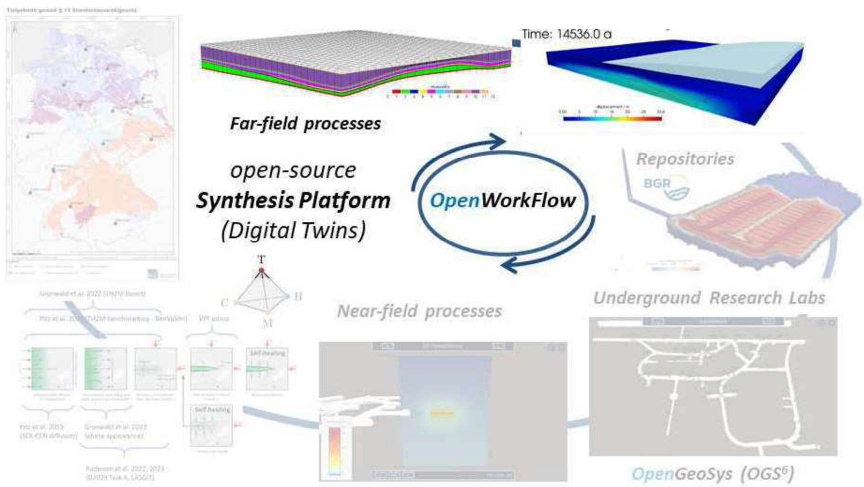

Scale – Far Field Aspects (Glaciation)

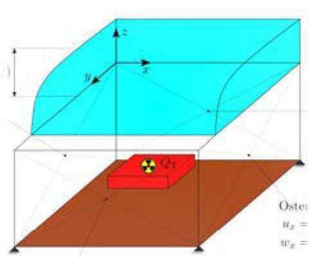

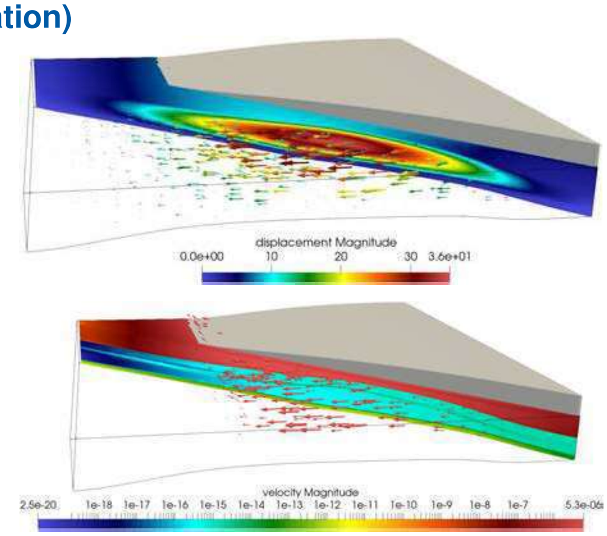

- simulation of several glaciation periods
- clay and salt

References/Credits: Florian Zill [Zil+21], AREHS Team

Digital Twins

Digital Twins

https://commons.wikimedia.org/wiki/File:Oil_rig_Jan_23.jpg

"A digital twin is a virtual representation that serves as the **real-time** digital counterpart of a physical object or process."
(Wikipedia)

- describes all relevant properties of that object/process
- shows all relevant behaviours of that object/process
- provides all necessary data via a uniform interface
- ...

Digital Twin as Workflow Application

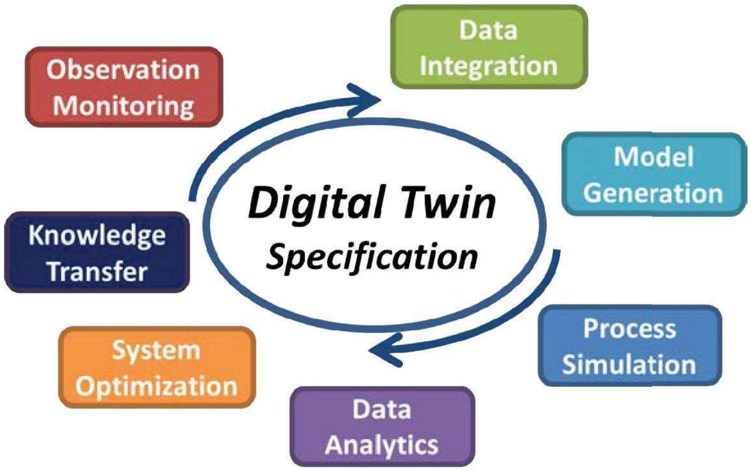

Specifications:

- URL Information System (Mont Terri)
- Repository construction (BIM)
- **Model validation** (DT2)
- ...

Software Engineering (DT1)

References: [Kol+19]

Software Distribution – Container Technology

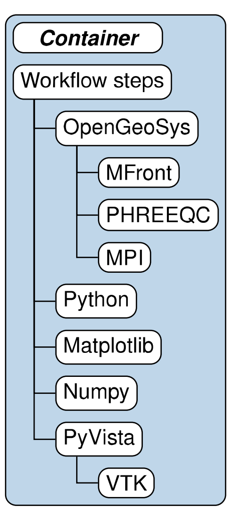

Technical frameworks for DTs

- container = lightweight VM
  - VM = app + 2nd OS files + 2nd OS processes
  - container = app + 2nd OS files
- distribute software along with all dependencies
- unified runtime environment
- executable in many different environments
- facilitates reuse of workflow steps
- simplifies adoption by new users

References: [Bil+19]

Digital Twin for Model Validation (Upscaling)

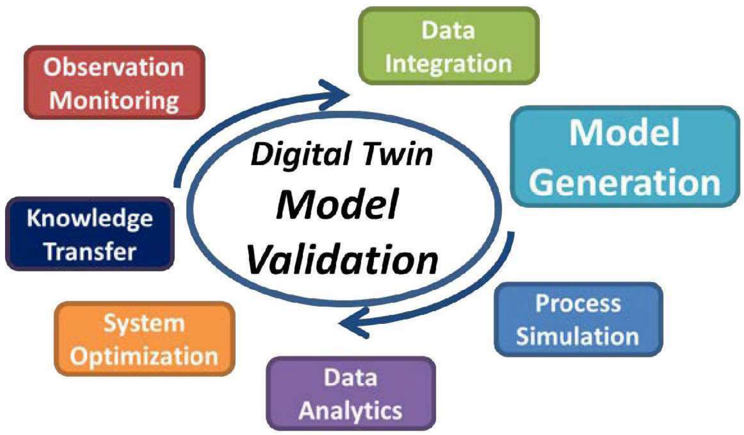

Model validation:

- Model generation
- Benchmarking (data integration, code comparison, ...)
- Model scaling
- ...

From Workflow Application Towards Digital Twins

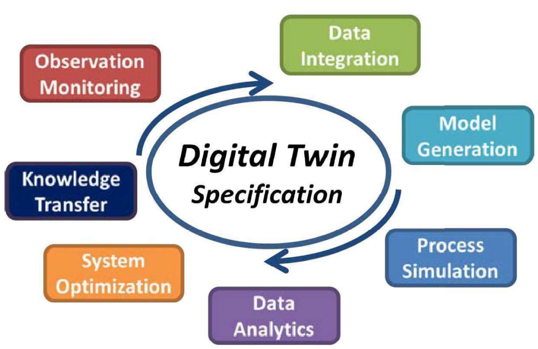

WF Flexibility >> **DT Specification**

- on-the-fly model parameter update
- monitoring of the repository
- continuous model validation
- distributed: multi-agent implementation
- versions
- composability: build more complex twins from a common core
- workflow integration
- need for a robust basis
- . . .

Digital Twin VR Application – URL (Mont Terri)

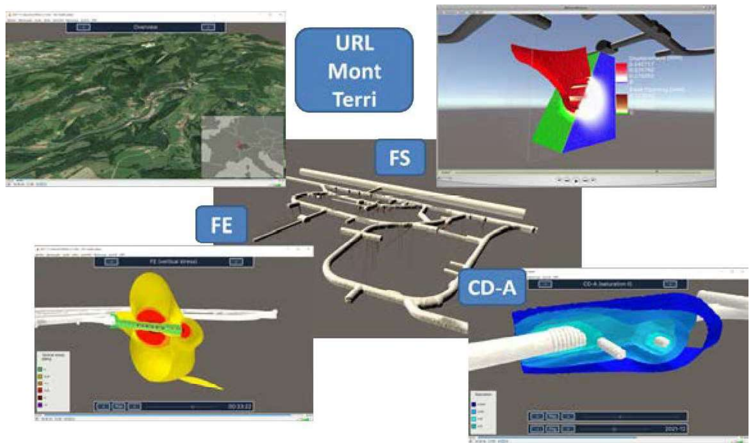

see VISLAB applications and OGS YouTube Channel

Contributors

Lars Bilke
Jörg Buchwald
Aqeel Chaudry
Thomas Fischer
Nico Graebling
Norbert Grunwald
Christoph Lehmann
Renchao Lu
Fabien Magri
Victor Malkovsky
Jobst Maßmann
Tobias Meisel
Thomas Nagel
Dmitri Naumov
Karsten Rink
Ozan Şen
Haibing Shao
Christian Silbermann
Wenqing Wang
Keita Yoshioka
Gesa Ziefle
Florian Zill

Institutions and Acknowledgements

Helmholtz-Zentrum für Umweltforschung – UFZ
TU Bergakademie Freiberg
Bundesgesellschaft für Endlagerung – BGE
Bundesamt für die Sicherheit der nuklearen Entsorgung
Bundesanstalt für Geowissenschafte und Rohstoffe – BGR

References I

[Bil+19] Lars Bilke, Bernd Flemisch, Thomas Kalbacher, Olaf Kolditz, Rainer Helmig, and Thomas Nagel. "Development of Open-Source Porous Media Simulators: Principles and Experiences". In: *Transport in Porous Media* 130.1 (2019). Cited by: 49; All Open Access, Bronze Open Access, pp. 337–361. URL: https://www.scopus.com/inward/record.uri?eid=2-s2.0-85068170902&doi=10.1007%2fs11242-019-01310-1&partnerID=40&md5=33ee985c5c3e4735b93557b9ede5ec1e.

[Cha+19] Aqeel Afzal Chaudhry, Jörg Buchwald, Olaf Kolditz, and Thomas Nagel. "Consolidation around a point heat source (correction and verification)". In: *International Journal for Numerical and Analytical Methods in Geomechanics* 43.18 (2019). Cited by: 10; All Open Access, Hybrid Gold Open Access, pp. 2743–2751. URL: https://www.scopus.com/inward/record.uri?eid=2-s2.0-85073786339&doi=10.1002%2fnag.2998&partnerID=40&md5=4cc9559524aafd722e0ae1082176a8d3.

[Gra+22] Nico Graebling, Ozgür Ozan Şen, Lars Bilke, Tuanny Cajuhi, Dmitri Naumov, Wenqing Wang, Gesa Ziefle, David Jaeggi, Jobst Maßmann, Gerik Scheuermann, Olaf Kolditz, and Karsten Rink. "Prototype of a Virtual Experiment Information System for the Mont Terri Underground Research Laboratory". In: *Frontiers in Earth Science* 10 (2022). Cited by: 1; All Open Access, Gold Open Access. URL: https://www.scopus.com/inward/record.uri?eid=2-s2.0-85135239050&doi=10.3389%2ffeart.2022.946627&partnerID=40&md5=98251ecf01b0027598edbacc49fcd4c0.

[Gru+22] Norbert Grunwald, Christoph Lehmann, Jobst Maßmann, Dmitri Naumov, Olaf Kolditz, and Thomas Nagel. "Non-isothermal two-phase flow in deformable porous media: systematic open-source implementation and verification procedure". In: *Geomechanics and Geophysics for Geo-Energy and Geo-Resources* 8.3 (2022). Cited by: 4; All Open Access, Hybrid Gold Open Access. URL: https://www.scopus.com/inward/record.uri?eid=2-s2.0-85130399620&doi=10.1007%2fs40948-022-00394-2&partnerID=40&md5=6b959574110fc5f4c5df0b773b681be9.

[Kol+19] Olaf Kolditz, Uwe-Jens Gorke, Haibing Shao, Hua Shao, and Thomas Nagel. "Workflows in environmental geotechnics: Status-quo and perspectives". In: *Environmental Science and Engineering* (2019). Cited by: 1, pp. 119–127. URL: https://www.scopus.com/inward/record.uri?eid=2-s2.0-85060653775&doi=10.1007%2f978-981-13-2221-1_6&partnerID=40&md5=9d7f3f14783442ae72089d8e2caef986.

[LT22] Ch. Lehmann and OGS Team. "From Workflows towards Digital Twins". In: *Tage der Standortauswahl* (2022). Keynote talk, Aachen, 08.06.2022.

References II

[MHG05] P. Marschall, S. Horseman, and T. Gimmi. "Characterisation of gas transport properties of the Opalinus Clay, a potential host rock formation for radioactive waste disposal". In: *Oil and Gas Science and Technology* 60.1 (2005), pp. 121–139. URL: https://www.scopus.com/inward/record.uri?eid=2-s2.0-20544436678&doi=10.2516%2fogst%3a2005008&partnerID=40&md5=a6edfc19bc794ad1325c0da667a66397.

[Mol+23] Mostafa Mollaali, Olaf Kolditz, Mengsu Hu, Chan-Hee Park, Jung-Wook Park, Christopher Ian McDermott, Neil Chittenden, Alexander Bond, Jeoung Seok Yoon, Jian Zhou, Peng-Zhi Pan, Hejuan Liu, Wenbo Hou, Hongwu Lei, Liwei Zhang, Thomas Nagel, Markus Barsch, Wenqing Wang, Son Nguyen, Saeha Kwon, Changsoo Lee, and Keita Yoshioka. "Comparative verification of hydro-mechanical fracture behavior: Task G of international research project DECOVALEX–2023". In: *International Journal of Rock Mechanics and Mining Sciences* 170 (2023). Cited by: 0. URL: https://www.scopus.com/inward/record.uri?eid=2-s2.0-85166325287&doi=10.1016%2fj.ijrmms.2023.105530&partnerID=40&md5=3a43688518353d27ce8a084a093cb90c.

[Pit+23a] Michael Pitz, Norbert Grunwald, Bastian Graupner, Kata Kurgyis, Eike Radeisen, Jobst Maßmann, Gesa Ziefle, Jan Thiedau, and Thomas Nagel. "Benchmarking a new TH2M implementation in OGS-6 with regard to processes relevant for nuclear waste disposal". In: *Environmental Earth Sciences* 82.13 (2023). Cited by: 0; All Open Access, Green Open Access, Hybrid Gold Open Access. URL: https://www.scopus.com/inward/record.uri?eid=2-s2.0-85163128056&doi=10.1007%2fs12665-023-10971-7&partnerID=40&md5=b7997c7b6d94abe36397c9606861f5fe.

[Pit+23b] Michael Pitz, Sonja Kaiser, Norbert Grunwald, Vinay Kumar, Jörg Buchwald, Wenqing Wang, Dmitri Naumov, Aqeel Afzal Chaudhry, Jobst Maßmann, Jan Thiedau, Olaf Kolditz, and Thomas Nagel. "Non-isothermal consolidation: A systematic evaluation of two implementations based on multiphase and Richards equations". In: *International Journal of Rock Mechanics and Mining Sciences* 170 (2023). Cited by: 0; All Open Access, Hybrid Gold Open Access. URL: https://www.scopus.com/inward/record.uri?eid=2-s2.0-85167438928&doi=10.1016%2fj.ijrmms.2023.105534&partnerID=40&md5=305d32c2037651ea105488c12ff77d87.

[Rad+23a] Eike Radeisen, Hua Shao, Jürgen Hesser, Olaf Kolditz, Wenjie Xu, and Wenqing Wang. "Simulation of dilatancy-controlled gas migration processes in saturated bentonite using a coupled multiphase flow and elastoplastic H2M model". In: *Journal of Rock Mechanics and Geotechnical Engineering* 15.4 (2023). Cited by: 1; All Open Access, Gold Open Access, pp. 803–813. URL: https://www.scopus.com/inward/record.uri?eid=2-s2.0-85132868396&doi=10.1016%2fj.jrmge.2022.05.011&partnerID=40&md5=d5c9c42b7ddf1da2e7aa9b18fe7e2af6.

References III

[Rad+23b] Eike Radeisen, Hua Shao, Michael Pitz, Jürgen Hesser, and Wenqing Wang. "Derivation of heterogeneous material distributions and their sensitivity to HM-coupled two-phase flow models exemplified with the LASGIT experiment". In: *Environmental Earth Sciences* 82.14 (2023). Cited by: 0; All Open Access, Hybrid Gold Open Access. URL: https://www.scopus.com/inward/record.uri?eid=2-s2.0-85164116109&doi=10.1007%2fs12665-023-11004-z&partnerID=40&md5=28f99fe6795c19f8302ae83eabd4402c.

[Wan+21a] Wenqing Wang, Hua Shao, Thomas Nagel, and Olaf Kolditz. "Analysis of coupled thermal-hydro-mechanical processes during small scale in situ heater experiment in Callovo-Oxfordian clay rock introducing a failure-index permeability model". In: *International Journal of Rock Mechanics and Mining Sciences* 142 (2021). Cited by: 10; All Open Access, Bronze Open Access. URL: https://www.scopus.com/inward/record.uri?eid=2-s2.0-85105047093&doi=10.1016%2fj.ijrmms.2021.104683&partnerID=40&md5=cbcca69cf3806f2de20ecdc4a638ffd6.

[Wan+21b] Wenqing Wang, Hua Shao, Karsten Rink, Thomas Fischer, Olaf Kolditz, and Thomas Nagel. "Analysis of coupled thermal-hydro-mechanical processes in Callovo-Oxfordian clay rock: From full-scale experiments to the repository scale". In: *Engineering Geology* 293 (2021). Cited by: 4; All Open Access, Bronze Open Access. URL: https://www.scopus.com/inward/record.uri?eid=2-s2.0-85111874158&doi=10.1016%2fj.enggeo.2021.106265&partnerID=40&md5=a047b4c01c5a9b9c1ace6b8d9a96bc5c.

[Zie+22] G. Ziefle, T. Cajuhi, N. Graebling, D. Jaeggi, O. Kolditz, H. Kunz, J. Maßmann, and K. Rink. "Multi-disciplinary investigation of the hydraulic-mechanically driven convergence behaviour: CD-A twin niches in the Mont Terri Rock Laboratory during the first year". In: *Geomechanics for Energy and the Environment* 31 (2022). Cited by: 5; All Open Access, Hybrid Gold Open Access. URL: https://www.scopus.com/inward/record.uri?eid=2-s2.0-85126814414&doi=10.1016%2fj.gete.2022.100325&partnerID=40&md5=93000ebc336d62099caa1a7fc9d373a5.

[Zil+21] Florian Zill, Christoph Lüdeling, Olaf Kolditz, and Thomas Nagel. "Hydro-mechanical continuum modelling of fluid percolation through rock salt". In: *International Journal of Rock Mechanics and Mining Sciences* 147 (2021). Cited by: 2; All Open Access, Hybrid Gold Open Access. URL: https://www.scopus.com/inward/record.uri?eid=2-s2.0-85114935462&doi=10.1016%2fj.ijrmms.2021.104879&partnerID=40&md5=25ca33bca708cddce37005049ae37995.

Thank you for your attention.

Appendix F. Introduction to OpenGeoSys (OGS) and Basics of Multiphysics Simulations (O. Kolditz)

TECHNISCHE UNIVERSITÄT BERGAKADEMIE FREIBERG
Die Ressourcenuniversität. Seit 1765.

HELMHOLTZ Zentrum für Umweltforschung

Introduction to OpenGeoSys (OGS) and Basics of Multiphysics Simulations

Norbert Grunwald, Olaf Kolditz & OpenGeoSys Team

Part I: Exploring OGS and Project Setup

29.08.2023, Liège, Belgium

TECHNISCHE UNIVERSITÄT BERGAKADEMIE FREIBERG
Die Ressourcenuniversität. Seit 1765.

HELMHOLTZ Zentrum für Umweltforschung

Discovering the Project Website

TECHNISCHE UNIVERSITÄT BERGAKADEMIE FREIBERG
Die Ressourcenuniversität. Seit 1765.

UFZ HELMHOLTZ Zentrum für Umweltforschung

PROJECT WEBSITE

https://www.opengeosys.org/

- features
  - Releases & Downloads
  - Documentation
  - Guides
  - Benchmarks
  - OGS-Community
  - Publications

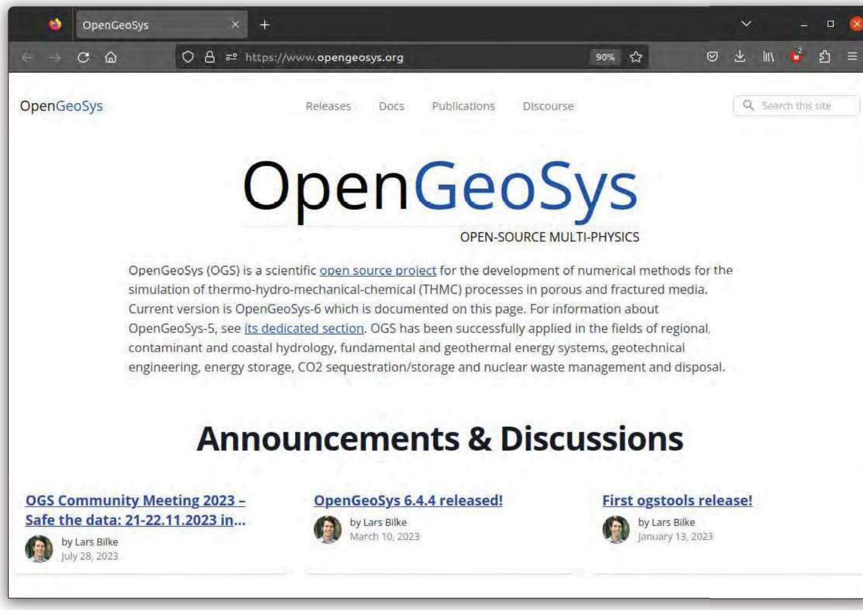

TECHNISCHE UNIVERSITÄT BERGAKADEMIE FREIBERG
Die Ressourcenuniversität. Seit 1765.

UFZ HELMHOLTZ Zentrum für Umweltforschung

GETTING STARTED WITH OpenGeoSyS

- ***Download and Install:***
  - **Precompiled Version:**
    - **Visit website:** `https://www.opengeosys.org/`
    - **Go to Docs -> User Guide**
    - **Follow the provided steps for installation**
- **Contribute and Customize**
  - **Source Code on GitLab:**
    - **Access GitLab repository:** `https://gitlab.opengeosys.org/`
    - **Docs -> Developer Guide contains compilation instructions**
- **Start Using OGS:**
  - **Grab an Example Benchmark Test: Explore our sample benchmark tests in the software package**
  - **Use them as templates for your own projects**

BENCH MARKING

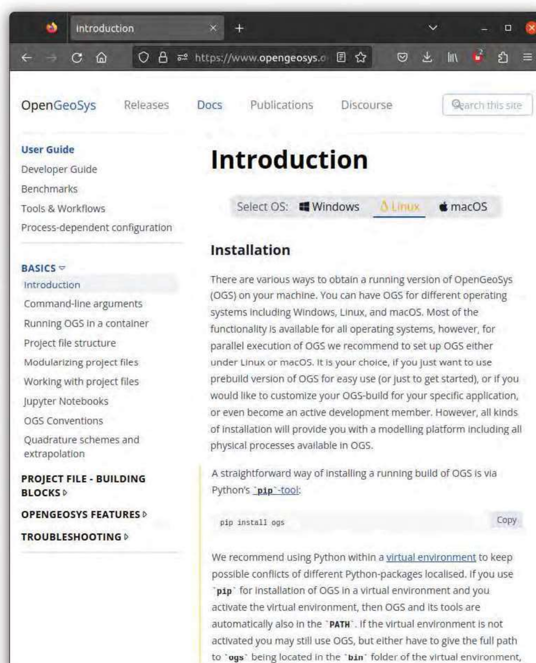

TECHNISCHE UNIVERSITÄT
BERGAKADEMIE FREIBERG
Die Ressourcenuniversität. Seit 1765.

HELMHOLTZ
Zentrum für Umweltforschung

BENCHMARK GALLERY

https://www.opengeosys.org/docs/benchmarks/

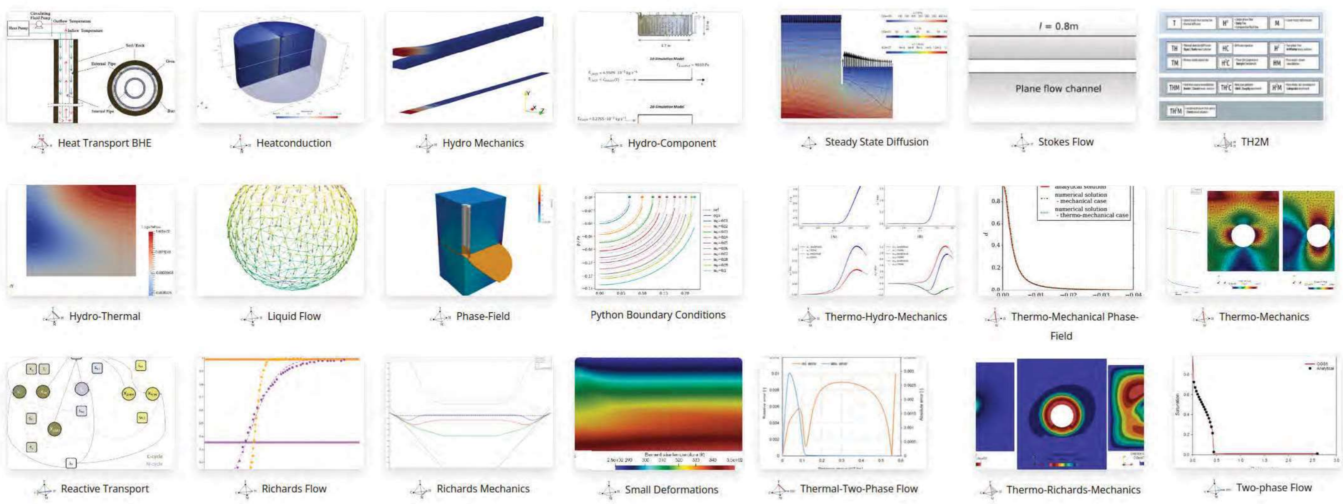

TECHNISCHE UNIVERSITÄT
BERGAKADEMIE FREIBERG
Die Ressourcenuniversität. Seit 1765.

HELMHOLTZ
Zentrum für Umweltforschung

EXPLORING GITLAB REPOSITORY

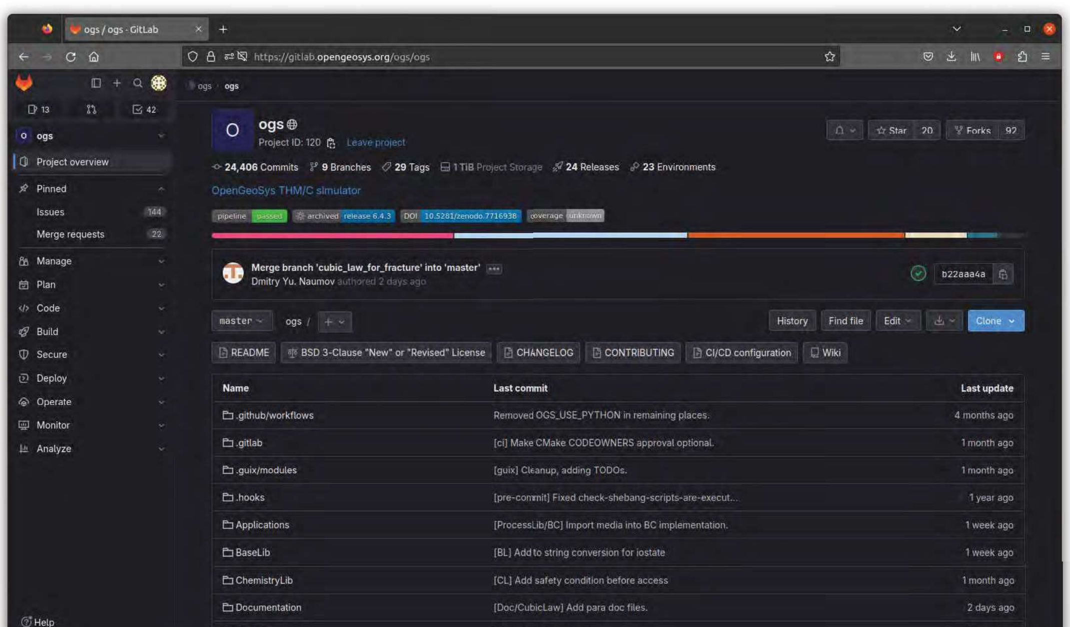

TECHNISCHE UNIVERSITÄT BERGAKADEMIE FREIBERG
Die Ressourcenuniversität. Seit 1765.

HELMHOLTZ Zentrum für Umweltforschung UFZ

ENGAGE WITH THE DEVS ON OUR DISCOURSE

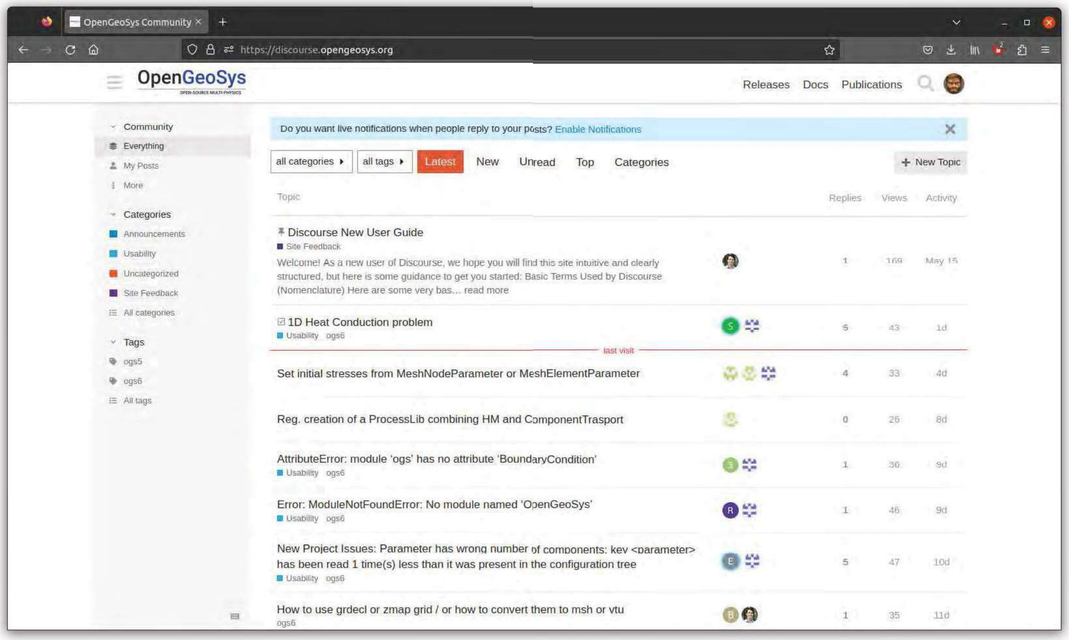

TECHNISCHE UNIVERSITÄT BERGAKADEMIE FREIBERG
Die Ressourcenuniversität. Seit 1765.

HELMHOLTZ Zentrum für Umweltforschung UFZ

Configuring a OGS Project

TECHNISCHE UNIVERSITÄT BERGAKADEMIE FREIBERG
Die Ressourcenuniversität. Seit 1765.

UFZ HELMHOLTZ Zentrum für Umweltforschung

INPUT FILE STRUCTURE

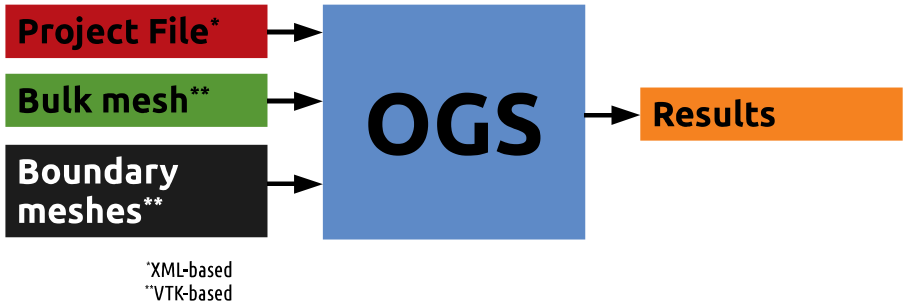

TECHNISCHE UNIVERSITÄT BERGAKADEMIE FREIBERG
Die Ressourcenuniversität. Seit 1765.

UFZ HELMHOLTZ Zentrum für Umweltforschung

INPUT FILE STRUCTURE

Project File *.prj

1. Define XML version and encoding

2. Start a new OpenGeoSys - project

```
<?xml version="1.0" encoding="ISO-8859-1"?>
<OpenGeoSysProject>

...

</OpenGeoSysProject>
```

TECHNISCHE UNIVERSITÄT BERGAKADEMIE FREIBERG
Die Ressourcenuniversität. Seit 1765.

UFZ HELMHOLTZ Zentrum für Umweltforschung

INPUT FILE STRUCTURE

Project File *.prj

3. Define the domain/bulk mesh
4. Define BC/ST-meshes
5. Specify process(es)
6. Specify material properties/ constitutive laws
7. Time Control
8. Set up BC/IC
9. Set solver properties/ convergence criteria

```
<meshes>
    <mesh axially_symmetric="true">domain_quad.vtu</mesh>
    <mesh axially_symmetric="true">boundary_axis.vtu</mesh>
    <mesh axially_symmetric="true">boundary_top.vtu</mesh>
    <mesh axially_symmetric="true">boundary_bottom.vtu</mesh>
    <mesh axially_symmetric="true">boundary_borehole.vtu</mesh>
</meshes>
```

TECHNISCHE UNIVERSITÄT BERGAKADEMIE FREIBERG
Die Ressourcenuniversität. Seit 1765.

UFZ HELMHOLTZ Zentrum für Umweltforschung

INPUT FILE STRUCTURE

Project File *.prj

3. Define the domain/bulk mesh
4. Define BC/ST-meshes
5. Specify process(es)
6. Specify material properties/ constitutive laws
7. Time Control
8. Set up BC/IC
9. Set solver properties/ convergence criteria

```
<meshes>
    <mesh axially_symmetric="true">domain_quad.vtu</mesh>
    <mesh axially_symmetric="true">boundary_axis.vtu</mesh>
    <mesh axially_symmetric="true">boundary_top.vtu</mesh>
    <mesh axially_symmetric="true">boundary_bottom.vtu</mesh>
    <mesh axially_symmetric="true">boundary_borehole.vtu</mesh>
</meshes>
```

DETOUR – *.gml FILE

Geometry File *.gml

- Legacy geometry file

```
<?xml version="1.0" encoding="ISO-8859-1"?>
<OpenGeoSysProject>
    <mesh>square_100x100_quad_1e4.vtu</mesh>
    <geometry>square_100x100.gml</geometry>
```

DETOUR – *.gml FILE

Geometry File *.gml

- Legacy geometry file
- Defines `points`, `polylines` and `surfaces` by coordinates
- Almost obsolete by now*
- Can be used to create boundary meshes from bulk mesh using `constructMeshesFromGeometry`

```
<?xml version="1.0" encoding="ISO-8859-1"?>
<?xml-stylesheet type="text/xsl" href="OpenGeoSysGLI.xsl"?>
<OpenGeoSysGLI xmlns:xsi="http://www.w3.org/2001/XMLSchema-instance"
               xmlns:ogs="http://www.opengeosys.org">
    <name>square_1x1_geometry</name>
    <points>
        <point id="0" x="0" y="0" z="0"/>
        <point id="1" x="100" y="0" z="0"/>
        <point id="2" x="100" y="100" z="0"/>
        <point id="3" x="0" y="100" z="0"/>
    </points>
    <polylines>

        <polyline id="0" name="bottom">
            <pnt>0</pnt>
            <pnt>1</pnt>
        </polyline>
        <polyline id="0" name="right">
            <pnt>1</pnt>
            <pnt>2</pnt>
        </polyline>
        <polyline id="0" name="top">
            <pnt>2</pnt>
            <pnt>3</pnt>
        </polyline>
        <polyline id="0" name="left">
            <pnt>3</pnt>
            <pnt>0</pnt>
        </polyline>

    </polylines>
```

*Although it might be required by some processes(?)

TECHNISCHE UNIVERSITÄT BERGAKADEMIE FREIBERG
Die Ressourcenuniversität. Seit 1765.

HELMHOLTZ Zentrum für Umweltforschung

INPUT FILE STRUCTURE

Project File *.prj

3. Define the domain/bulk mesh
4. Define BC/ST-meshes
5. Specify process(es)
6. Specify material properties/ constitutive laws
7. Time Control
8. Set up BC/IC
9. Set solver properties/ convergence criteria

```
<processes>
    <process>
        <name>THM</name>
        <type>THERMO_HYDRO_MECHANICS</type>
        <integration_order>3</integration_order>
        <dimension>2</dimension>

        ...

        <process_variables>
            <displacement>displacement</displacement>
            <pressure>pressure</pressure>
            <temperature>temperature</temperature>
        </process_variables>

        <secondary_variables>
            <secondary_variable type="static"
                                internal_name="sigma"
                                output_name="sigma"/>
            <secondary_variable type="static"
                                internal_name="epsilon"
                                output_name="epsilon"/>
        </secondary_variables>

        <specific_body_force>0 -9.81</specific_body_force>
    </process>
</processes>
```

TECHNISCHE UNIVERSITÄT BERGAKADEMIE FREIBERG
Die Ressourcenuniversität. Seit 1765.

HELMHOLTZ Zentrum für Umweltforschung

INPUT FILE STRUCTURE

Project File *.prj

3. Define the domain/bulk mesh
4. Define BC/ST-meshes
5. Specify process(es)
6. Specify material properties/ constitutive laws
7. Time Control
8. Set up BC/IC
9. Set solver properties/ convergence criteria

```
<media>
    <medium id="0">
        <phases>
            <phase>
                <type>AqueousLiquid</type>
                <properties>
                    <property>
                        <name>specific_heat_capacity</name>
                        <type>Constant</type>
                        <value>4184.0</value>
                    </property>
                    ...
                </properties>
            </phase>
            <phase>
                <type>Solid</type>
                <properties>
                ...
                </properties>
            </phase>
        </phases>
        <properties>
            <property>
                <property>
                    <name>Permeability</name>
                    <type>Constant</type>
                    <value>1.e-15 0. 0. 1.e-15</value>
                    </property>
                    ...
            </property>
        </properties>
    </medium>
</media>
```

TECHNISCHE UNIVERSITÄT BERGAKADEMIE FREIBERG
Die Ressourcenuniversität. Seit 1765.

HELMHOLTZ Zentrum für Umweltforschung UFZ

DETOUR - MATERIAL PROPERTY HIERARCHY

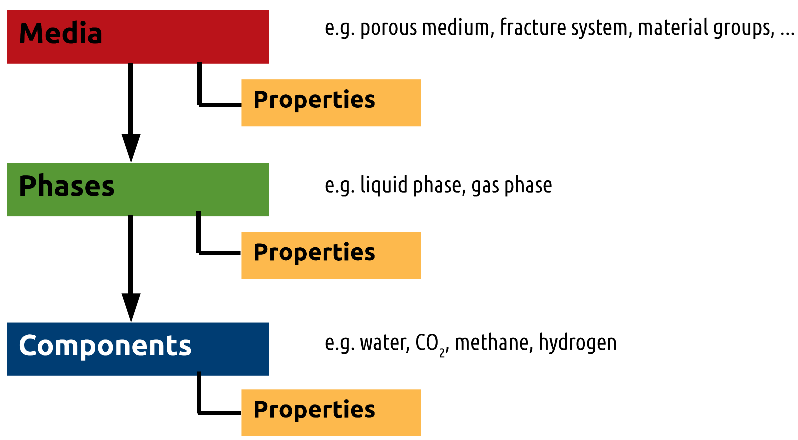

TECHNISCHE UNIVERSITÄT BERGAKADEMIE FREIBERG
Die Ressourcenuniversität. Seit 1765.

HELMHOLTZ Zentrum für Umweltforschung UFZ

DETOUR - MATERIAL PROPERTY HIERARCHY

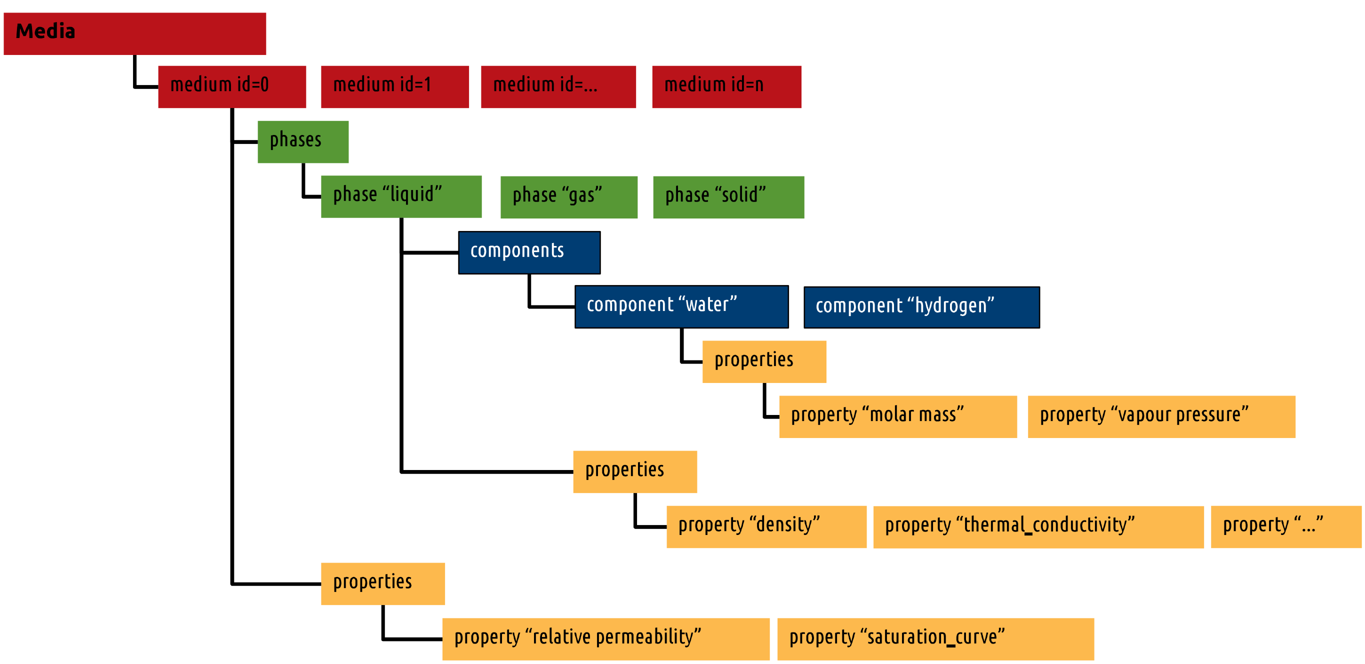

INPUT FILE STRUCTURE

Project File *.prj

3. Define the domain/bulk mesh
4. Define BC/ST-meshes
5. Specify process(es)
6. Specify material properties/ constitutive laws
7. **Time Control**
8. Set up BC/IC
9. Set solver properties/ convergence criteria

```
<time_loop>
    <processes>
        <process ref="THM">
            <nonlinear_solver>basic_newton</nonlinear_solver>
            <convergence_criterion>
            ...
            </convergence_criterion>
            <time_stepping>
                <type>FixedTimeStepping</type>
                <t_initial>0</t_initial>
                <t_end>2.7e8</t_end>
                <timesteps>
                    <pair><repeat>100</repeat><delta_t>86400</delta_t></pair>
                </timesteps>
            </time_stepping>
        </process>
    </processes>
    <output>
        <type>VTK</type>
        <prefix>result</prefix>
        <timesteps>
            <pair><repeat>1</repeat><each_steps>1</each_steps></pair>
        </timesteps>
        <variables>
            <variable>displacement</variable>
            <variable>temperature</variable>
            <variable>sigma</variable>
            ...
        </variables>
    </output>
</time_loop>
```

TECHNISCHE UNIVERSITÄT BERGAKADEMIE FREIBERG
Die Ressourcenuniversität. Seit 1765.
UFZ HELMHOLTZ Zentrum für Umweltforschung

INPUT FILE STRUCTURE

Project File *.prj

3. Define the domain/bulk mesh
4. Define BC/ST-meshes
5. Specify process(es)
6. Specify material properties/ constitutive laws
7. Time Control
8. **Set up BC/IC**
9. Set solver properties/ convergence criteria

```
<process_variables>
    <process_variable>
        <name>displacement</name>
        <components>2</components>
        <order>2</order>
        <initial_condition>displacement0</initial_condition>
        <boundary_conditions>

            <boundary_condition>
                <mesh>boundary_axis</mesh>
                <type>Dirichlet</type>
                <component>0</component>
                <parameter>dirichlet0</parameter>
            </boundary_condition>

            <boundary_condition>
                <mesh>boundary_bottom</mesh>
                <type>Dirichlet</type>
                <component>1</component>
                <parameter>dirichlet0</parameter>
            </boundary_condition>

        </boundary_conditions>
    </process_variable>
    ...
</process_variables>
```

INPUT FILE STRUCTURE

Project File *.prj

3. Define the domain/bulk mesh
4. Define BC/ST-meshes
5. Specify process(es)
6. Specify material properties/ constitutive laws
7. Time Control
8. Set up BC/IC
9. Set solver properties/ convergence criteria

```
<nonlinear_solvers>
    <nonlinear_solver>
        <name>basic_newton</name>
        <type>Newton</type>
        <max_iter>50</max_iter>
        <linear_solver>general_linear_solver</linear_solver>
    </nonlinear_solver>
</nonlinear_solvers>

<linear_solvers>
    <linear_solver>
        <name>general_linear_solver</name>
        <lis>-i bicgstab -p ilu -tol 1e-16 -maxiter 10000</lis>
        <eigen>
            <solver_type>BiCGSTAB</solver_type>
            <precon_type>ILUT</precon_type>
            <max_iteration_step>10000</max_iteration_step>
            <error_tolerance>1e-16</error_tolerance>
        </eigen>
    </linear_solver>
</linear_solvers>
```

TECHNISCHE UNIVERSITÄT BERGAKADEMIE FREIBERG
Die Ressourcenuniversität. Seit 1765.
UFZ HELMHOLTZ Zentrum für Umweltforschung

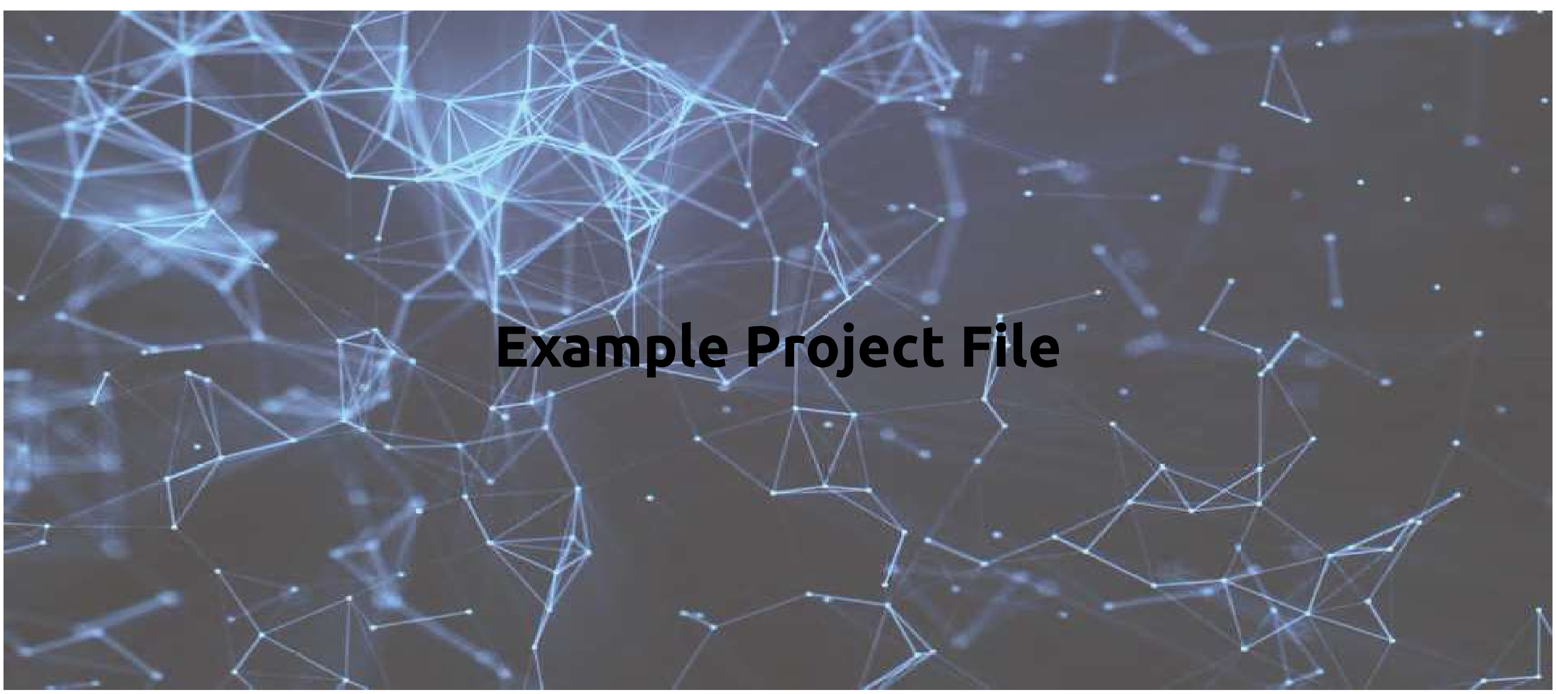

TECHNISCHE UNIVERSITÄT BERGAKADEMIE FREIBERG
Die Ressourcenuniversität. Seit 1765.

UFZ HELMHOLTZ Zentrum für Umweltforschung

POST-PROCESSING

- Evaluate Results using ParaView

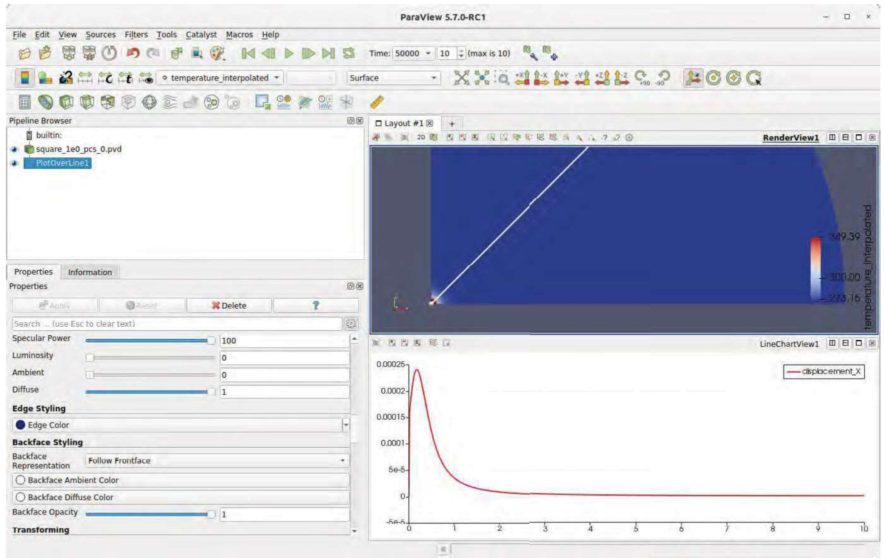

Grunwald, N., Nagel, T., Pitz, M., Kolditz, O. "Extended analysis of benchmarks for gas phase appearance in low-permeable rocks".
Under Review at Geomechanics and Geophysics for Geo-Energy and Geo-Resources, 2023.

TECHNISCHE UNIVERSITÄT BERGAKADEMIE FREIBERG
Die Ressourcenuniversität. Seit 1765.

UFZ HELMHOLTZ Zentrum für Umweltforschung

PYTHON API FOR OGS
ENHANCED WORKFLOW WITH AUTOMATION AND POST-PROCESSING

ogs6py:

- **Automating input file generation and modification.**
- **Change parameters and configurations programmatically.**
- **Ideal for scenario studies and sensitivity analyses.**

vtuIO

- **Advanced post-processing and visualization.**
- **Reads VTU files from the Visualisation Toolkit.**
- **Enables result investigation, further calculations, and plotting.**

TECHNISCHE UNIVERSITÄT BERGAKADEMIE FREIBERG
Die Ressourcenuniversität. Seit 1765.

HELMHOLTZ Zentrum für Umweltforschung

FURTHER DETAILS – INPUT FILE PARAMETERS

Project File *.prj

https://doxygen.opengeosys.org/

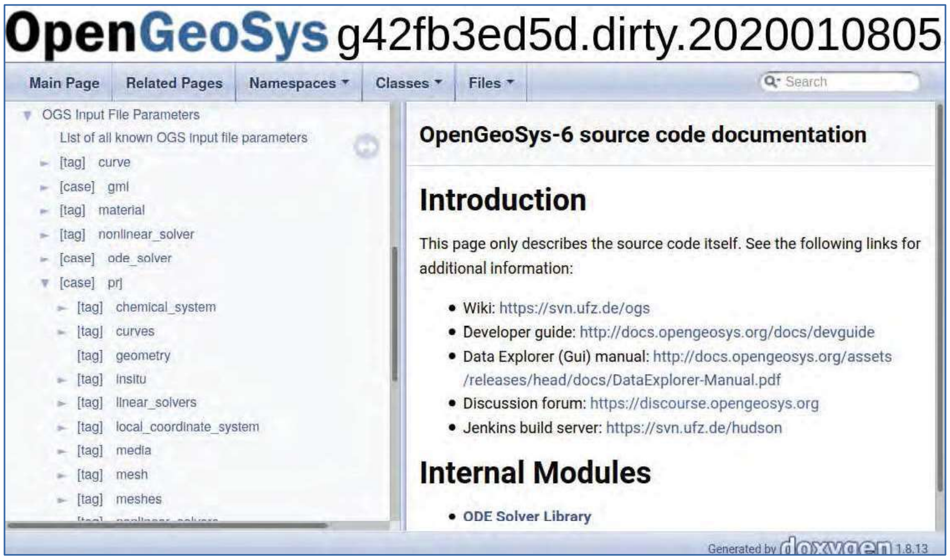

TECHNISCHE UNIVERSITÄT BERGAKADEMIE FREIBERG
Die Ressourcenuniversität. Seit 1765.

HELMHOLTZ Zentrum für Umweltforschung

Introduction to OpenGeoSys (OGS) and Basics of Multiphysics Simulations

Norbert Grunwald, Olaf Kolditz & OpenGeoSys Team

Part II: Basics of Multiphysics Simulations

29.08.2023, Liège, Belgium

TECHNISCHE UNIVERSITÄT BERGAKADEMIE FREIBERG
Die Ressourcenuniversität. Seit 1765.
UFZ HELMHOLTZ Zentrum für Umweltforschung

FOUNDATIONS OF MULTIPHYSICS SIMULATIONS

INTRODUCING THERMO-HYDRAULIC MULTIPHASE MECHANICS (TH2M) SIMULATION

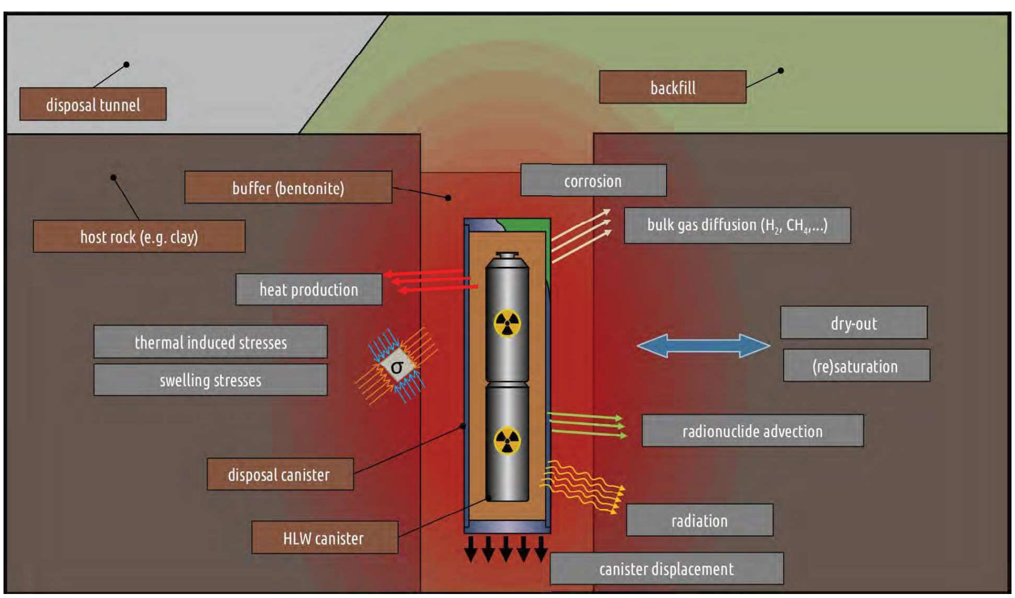

TECHNISCHE UNIVERSITÄT
BERGAKADEMIE FREIBERG
Die Ressourcenuniversität. Seit 1765.

UFZ HELMHOLTZ
Zentrum für Umweltforschung

TH2M Theory

TECHNISCHE UNIVERSITÄT
BERGAKADEMIE FREIBERG
Die Ressourcenuniversität. Seit 1765.

UFZ HELMHOLTZ
Zentrum für Umweltforschung

FOUNDATIONS OF MULTIPHYSICS SIMULATIONS

INTRODUCING THERMO-HYDRAULIC MULTIPHASE MECHANICS (TH2M) SIMULATION

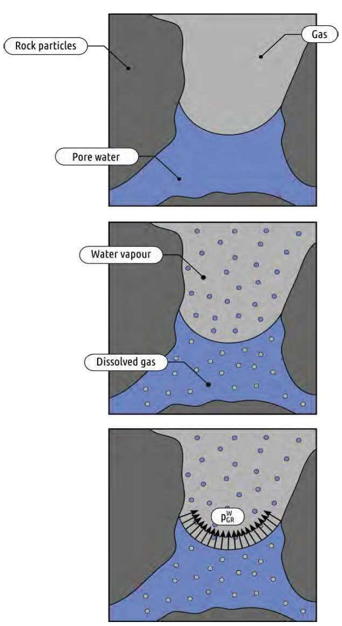

Features

- **Two-phase flow in deformable porous media**
- **Phase transitions among fluid phases**
- **Dissolution of gas in water, water evaporation**
- **Heat transport, non-isothermal behaviour due to various factors**
- **Thermodynamically consistent**
- **Fully, monolithically coupled**

Limitations

- **Local thermal equilibrium**
- **Linear elasticity**
- **Small deformations**
- **Quasi-static behavior**

Grunwald, N., Maßmann, J., Kolditz, O., Nagel, T., 2020. Non-iterative phase-equilibrium model of the H2O-CO2-NaCl-system for large-scale numerical simulations. Mathematics and Computers in Simulation, 178, 46-61.

Grunwald, N., Lehmann, C., Maßmann, J., Naumov, D., Kolditz, O., Nagel, T., 2022. Non-isothermal two-phase flow in deformable porous media: Systematic open-source implementation and verification procedure. Geomechanics and Geophysics for Geo-Energy and Geo-Resources, 8, 107. https://doi.org/10.1007/s40948-022-00394-2

TH2M - THEORY

TH2M is based on the 'Theory of Porous Media' (TPM)

Solid Mechanics → **TPM** ← **Fluid Mechanics**

TPM

- Hybrid combining solid mechanics and fluid mechanics
- "Averaging" of solid and multiple fluid phases with "smeared" properties
- Choice of control volume is essential
- Utilizes volume fractions concept
- Subfields exist in ideal disorder
- Balancing of state variables within the simulation

TECHNISCHE UNIVERSITÄT BERGAKADEMIE FREIBERG
Die Ressourcenuniversität. Seit 1765.
UFZ HELMHOLTZ Zentrum für Umweltforschung

TH2M - THEORY

Control volume:

"The smallest volume of a body whose measurable properties are representative of the properties of the entire body."

Volume fractions:

- At each point of the control volume, there are simultaneously material points of all constituents.
- The control volume is the sum of all partial volumes.

$$\phi_\alpha = \frac{d\Omega_\alpha}{d\Omega} \qquad \sum_\alpha \phi_\alpha = 1$$

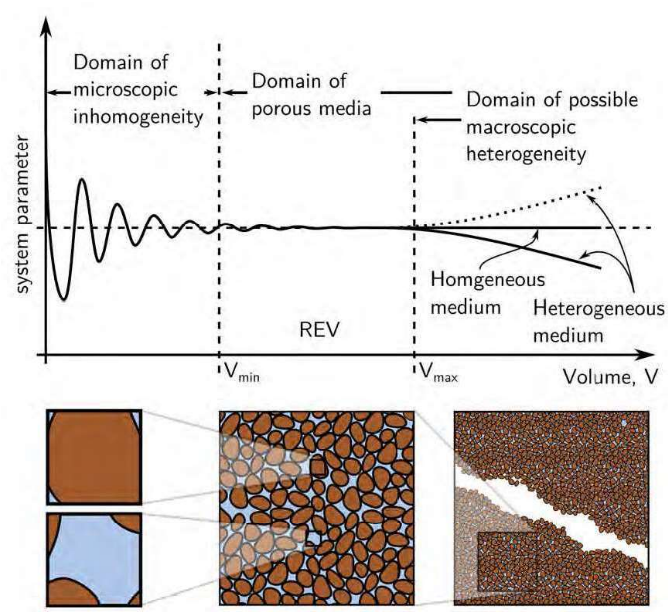

TH2M - THEORY

General Balance Equation for Single-Phase Bodies:

	Change in Ψ	due to: out/inflow	supply	production
Global form:	$\frac{\mathrm{d}}{\mathrm{d}t}\int_{\mathcal{B}} \Psi \,\mathrm{d}v =$	$\int_{\mathcal{S}} (\boldsymbol{\phi}\cdot\mathbf{n})\,\mathrm{d}a$	$+\int_{\mathcal{B}} \sigma\,\mathrm{d}v$	$+\int_{\mathcal{B}} \hat{\Psi}\,\mathrm{d}v$
	$\frac{\mathrm{d}}{\mathrm{d}t}\int_{\mathcal{B}} \boldsymbol{\Psi} \,\mathrm{d}v =$	$\int_{\mathcal{S}} (\boldsymbol{\Phi}\,\mathbf{n})\,\mathrm{d}a$	$+\int_{\mathcal{B}} \boldsymbol{\sigma}\,\mathrm{d}v$	$+\int_{\mathcal{B}} \hat{\boldsymbol{\Psi}}\,\mathrm{d}v$

Local form:

$$\dot{\Psi} + \Psi \,\mathrm{div}\,\dot{\mathbf{x}} = \mathrm{div}\,\boldsymbol{\phi} + \sigma + \hat{\Psi}\,,$$
$$\dot{\boldsymbol{\Psi}} + \boldsymbol{\Psi} \,\mathrm{div}\,\dot{\mathbf{x}} = \mathrm{div}\,\boldsymbol{\Phi} + \boldsymbol{\sigma} + \hat{\boldsymbol{\Psi}}$$

TECHNISCHE UNIVERSITÄT BERGAKADEMIE FREIBERG
Die Ressourcenuniversität. Seit 1765.
UFZ HELMHOLTZ Zentrum für Umweltforschung

TH2M - THEORY

Balance Quantities:

Balance	$\Psi, \boldsymbol{\Psi}$	$\boldsymbol{\phi}, \boldsymbol{\Phi}$	$\sigma, \boldsymbol{\sigma}$	$\hat{\Psi}, \hat{\boldsymbol{\Psi}}$
mass	ρ	$\mathbf{0}$	0	0
momentum	$\rho\,\dot{\mathbf{x}}$	$\mathbf{T}$	$\rho\,\mathbf{b} + \mathbf{b}_e$	$\mathbf{0}$
m. o. m.	$\mathbf{x}\times(\rho\,\dot{\mathbf{x}})$	$\mathbf{x}\times\mathbf{T}$	$\mathbf{x}\times(\rho\,\mathbf{b}+\mathbf{b}_e)+\mathbf{c}_e$	$\mathbf{0}$
energy	$\rho\,\varepsilon + \frac{1}{2}\,\dot{\mathbf{x}}\cdot(\rho\,\dot{\mathbf{x}})$	$\mathbf{T}^T\,\dot{\mathbf{x}} - \mathbf{q}$	$\dot{\mathbf{x}}\cdot(\rho\,\mathbf{b}) + \rho\,r + \varepsilon_e$	0
entropy	$\rho\,\eta$	$\boldsymbol{\phi}_\eta$	σ_η	$\hat{\eta}$
charge	ρ_e	$-\,\boldsymbol{\mathcal{J}}$	0	0
Gauss's law (elec.)	0	$-\,\mathbf{D}$	ρ_e	0
Gauss's law (magn.)	0	$-\,\mathbf{B}$	0	0
Faraday's law	$\mathbf{B}$	$-\,\boldsymbol{\mathcal{E}}$	0	0
Ampère's law	$-\mathbf{D}$	$-\,\boldsymbol{\mathcal{H}}$	$\boldsymbol{\mathcal{J}}$	0

Ehlers, Wolfgang. "Foundations of multiphasic and porous materials." Porous media: theory, experiments and numerical applications. Berlin, Heidelberg: Springer Berlin Heidelberg, 2002. 3-86.

TH2M - THEORY

- **Formulation of:**
  - **Mass balances for two components (e.g. Water and Hydrogen) and for the solid phase**
  - **Energy balances for solid (S), liquid (L), and gaseous (G) phases**
  - **Momentum balances for S, L, G**
- **Evaluation of the entropy inequality**
- **Selection of *Ansatz* functions:**

$$\psi_\mathrm{S} = \psi_\mathrm{S}(\epsilon_\mathrm{S}, T, \rho_\mathrm{SR}) \quad \psi_\mathrm{L} = \psi_\mathrm{L}(T, \rho_\mathrm{LR}, s_\mathrm{L}) \quad \psi_\mathrm{G} = \psi_\mathrm{G}(T, \rho_\mathrm{GR})$$

- **Selection of primary variables:**
  - **Gas phase pressure: p_G, Capillary pressure: p_{cap},**
    Temperature: T, Displacement: $\underline{u}_S$
- **Develop of weak formulations:**

$$\psi \approx \tilde{\psi} = \mathbf{N}\hat{\psi} \qquad\qquad \operatorname{grad}\psi \approx \operatorname{grad}\tilde{\psi} = \nabla\mathbf{N}\hat{\psi}$$

TECHNISCHE UNIVERSITÄT BERGAKADEMIE FREIBERG
Die Ressourcenuniversität. Seit 1765.
HELMHOLTZ Zentrum für Umweltforschung

TH2M - THEORY

- **Implementation:**
  - **Picard formulation**
  - **Numerical Jacobian in Quasi Newton-Raphson by perturbation of primary variables**
- **Quasi Newton-Raphson Method:**
  - **Numerical Jacobian computation**
  - **Perturbation-based approach**
  - **Avoids manual derivation**
  - **Increased runtime**
- **Benefits and Trade-offs:**
  - **Accurate numerical Jacobian**
  - **Trade-off: Longer runtime**

Weak formulation of component mass:

$$
\begin{aligned}
&\underbrace{\int_\Omega \mathbf{N}_p^\mathrm{T} \rho_\mathrm{FR}^\zeta (\alpha_\mathrm{B} - \phi)\, \beta_{p,\mathrm{SR}} \mathbf{N}_p \, \mathrm{d}\Omega}_{\mathbf{M}_\mathrm{pG}^\zeta} (\hat{\boldsymbol{p}}_\mathrm{GR})'_\mathrm{S} - \underbrace{\int_\Omega \mathbf{N}_p^\mathrm{T} \rho_\mathrm{FR}^\zeta (\alpha_\mathrm{B} - \phi)\, \beta_{p,\mathrm{SR}} s_\mathrm{L} \mathbf{N}_p \, \mathrm{d}\Omega}_{\mathbf{M}_\mathrm{pC}^\zeta} \left(\hat{\boldsymbol{p}}_\mathrm{cap}\right)'_\mathrm{S} \\
&+ \underbrace{\int_\Omega \nabla \mathbf{N}_p^\mathrm{T} \left(\rho_\mathrm{GR}^\zeta \frac{k_\mathrm{G}^\mathrm{rel} \boldsymbol{k}_\mathrm{S}}{\mu_\mathrm{GR}^\nu} + \rho_\mathrm{LR}^\zeta \frac{k_\mathrm{L}^\mathrm{rel} \boldsymbol{k}_\mathrm{S}}{\mu_\mathrm{LR}^\nu} + \rho_\mathrm{G} \boldsymbol{D}_\mathrm{G}^\zeta \frac{\partial x_{m,\mathrm{G}}^\zeta}{\partial p_\mathrm{GR}} + \rho_\mathrm{L} \boldsymbol{D}_\mathrm{L}^\zeta \frac{\partial x_{m,\mathrm{L}}^\zeta}{\partial p_\mathrm{GR}} \right) \nabla \mathbf{N}_p \, \mathrm{d}\Omega}_{\mathbf{L}_\mathrm{pG}^\zeta} \hat{\boldsymbol{p}}_\mathrm{GR} \\
&+ \underbrace{\int_\Omega \nabla \mathbf{N}_p^\mathrm{T} \left(\rho_\mathrm{G} \boldsymbol{D}_\mathrm{G}^\zeta \frac{\partial x_{m,\mathrm{G}}^\zeta}{\partial p_\mathrm{cap}} + \rho_\mathrm{L} \boldsymbol{D}_\mathrm{L}^\zeta \frac{\partial x_{m,\mathrm{L}}^\zeta}{\partial p_\mathrm{cap}} - \rho_\mathrm{LR}^\zeta \frac{k_\mathrm{L}^\mathrm{rel} \boldsymbol{k}_\mathrm{S}}{\mu_\mathrm{LR}^\nu} \right) \nabla \mathbf{N}_p \, \mathrm{d}\Omega}_{\mathbf{L}_\mathrm{pC}^\zeta} \hat{\boldsymbol{p}}_\mathrm{cap} + \underbrace{\int_\Omega \mathbf{N}_p^\mathrm{T} \rho_\mathrm{FR}^\zeta \alpha_\mathrm{B} \boldsymbol{m}^\mathrm{T} \mathbf{B}_u \, \mathrm{d}\Omega}_{\mathbf{M}_\mathrm{uS}^\zeta} (\hat{\boldsymbol{u}}_\mathrm{S})'_\mathrm{S} \\
&- \underbrace{\int_\Omega \mathbf{N}_p^\mathrm{T} \rho_\mathrm{FR}^\zeta (\alpha_\mathrm{B} - \phi)\, \beta_{T,\mathrm{SR}} \mathbf{N}_p \, \mathrm{d}\Omega}_{\mathbf{M}_\mathrm{T}^\zeta} \left(\hat{\boldsymbol{T}}\right)'_\mathrm{S} + \underbrace{\int_\Omega \nabla \mathbf{N}_p^\mathrm{T} \left(\rho_\mathrm{G} \boldsymbol{D}_\mathrm{G}^\zeta \frac{\partial x_{m,\mathrm{G}}^\zeta}{\partial T} + \rho_\mathrm{L} \boldsymbol{D}_\mathrm{L}^\zeta \frac{\partial x_{m,\mathrm{L}}^\zeta}{\partial T} \right) \nabla \mathbf{N}_p \, \mathrm{d}\Omega}_{\mathbf{L}_\mathrm{T}^\zeta} \hat{\boldsymbol{T}} \\
&= \underbrace{\int_\Omega \nabla \mathbf{N}_p^\mathrm{T} \left(\rho_\mathrm{GR}^\zeta \frac{k_\mathrm{G}^\mathrm{rel} \boldsymbol{k}_\mathrm{S}}{\mu_\mathrm{GR}^\nu} \rho_\mathrm{GR} + \rho_\mathrm{LR}^\zeta \frac{k_\mathrm{L}^\mathrm{rel} \boldsymbol{k}_\mathrm{S}}{\mu_\mathrm{LR}^\nu} \rho_\mathrm{LR} \right) \boldsymbol{b} \, \mathrm{d}\Omega}_{\boldsymbol{f}_\mathrm{I}^\zeta} - \underbrace{\int_\Omega \mathbf{N}_p^\mathrm{T} \phi \left[s_\mathrm{G} \langle \rho_\mathrm{GR}^\zeta \rangle'_\mathrm{S} + s_\mathrm{L} \langle \rho_\mathrm{LR}^\zeta \rangle'_\mathrm{S} \right] \mathrm{d}\Omega}_{\boldsymbol{f}_\mathrm{II}^\zeta} \\
&- \underbrace{\int_\Omega \mathbf{N}_p^\mathrm{T} \left[\phi \left(\rho_\mathrm{LR}^\zeta - \rho_\mathrm{GR}^\zeta \right) - \rho_\mathrm{FR}^\zeta p_\mathrm{cap} (\alpha_\mathrm{B} - \phi)\, \beta_{p,\mathrm{SR}} \right] \langle s_\mathrm{L} \rangle'_\mathrm{S} \, \mathrm{d}\Omega}_{\boldsymbol{f}_\mathrm{III}^\zeta} + \underbrace{\int_{\partial\Omega} \mathbf{N}_p^\mathrm{T} \dot{m}_\mathrm{AJ}^\zeta \, \mathrm{d}\Gamma}_{\boldsymbol{f}_\mathrm{IV}^\zeta}
\end{aligned}
$$

TECHNISCHE UNIVERSITÄT BERGAKADEMIE FREIBERG
Die Ressourcenuniversität. Seit 1765.

UFZ HELMHOLTZ Zentrum für Umweltforschung

TH2M Benchmarking

TECHNISCHE UNIVERSITÄT BERGAKADEMIE FREIBERG
Die Ressourcenuniversität. Seit 1765.

UFZ HELMHOLTZ Zentrum für Umweltforschung

TH2M BENCHMARK HIERARCHY

1 Primary variable	T	• Linear/ radial heat conduction • thermal diffusion	H^a	• Single-phase flow • **Darcy** flow • Compressible fluid flow	M	• Linear-elastic deformation
2 Primary variables	TH	• Thermal advection/diffusion **Ogata | Banks** exact solution	HC	• Diffusion equation	H^2	• Two-phase flow: **McWhorter** exact solution
	TM	• Thermo-elastic plate/cube	H^2C	• Phase (dis-)appearance **Bourgeat** benchmark	HM	• Poro-elastic column consolidation
3 Primary variables	THM	• Point heat source consolidation **Booker | Chaudry** exact solution	TH^2C	• Heat pipe problem **Udell | Doughty** benchmark	H^2M	• Poro-elastic soil consolidation **Liakopoulos** benchmark
4 Primary variables	TH^2M	• unsaturated point heat source **Cherati** exact solution				

BENCHMARK TEST: HEATPIPE PROBLEM

Heatpipe effect, steady state analytical solution (Udell, 1985)

- Water evaporates at the right edge
- Steam flows to the left edge and condenses, giving off energy in the form of enthalpy of condensation
- The condensate flows back to the right edge.
- High rate of heat transport

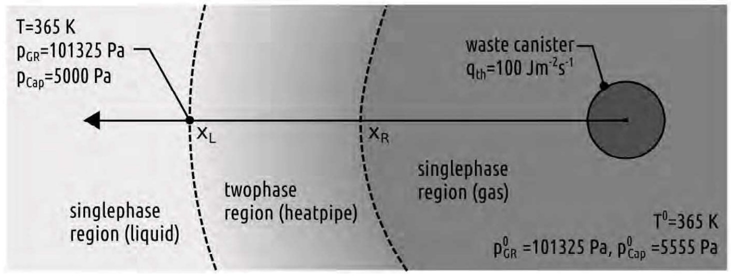

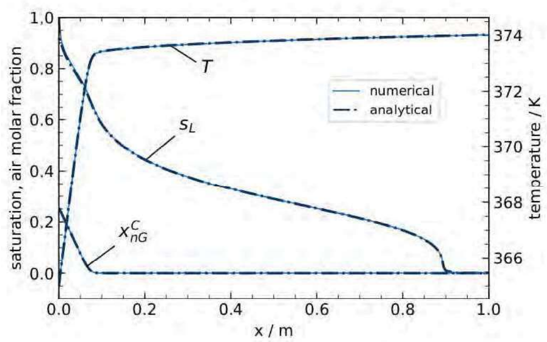

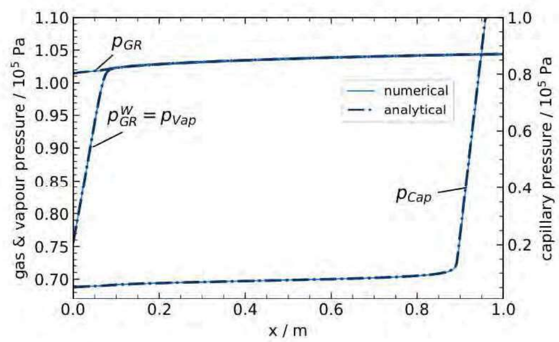

Udell, Kent S. "Heat transfer in porous media considering phase change and capillarity—the heat pipe effect." International Journal of Heat and Mass Transfer 28.2 (1985): 485-495.

TH2M Test Case

TECHNISCHE UNIVERSITÄT BERGAKADEMIE FREIBERG
Die Ressourcenuniversität. Seit 1765.

HELMHOLTZ Zentrum für Umweltforschung

GAS TRANSPORT REGIMES
IN LOW PERMEABLE MEDIA

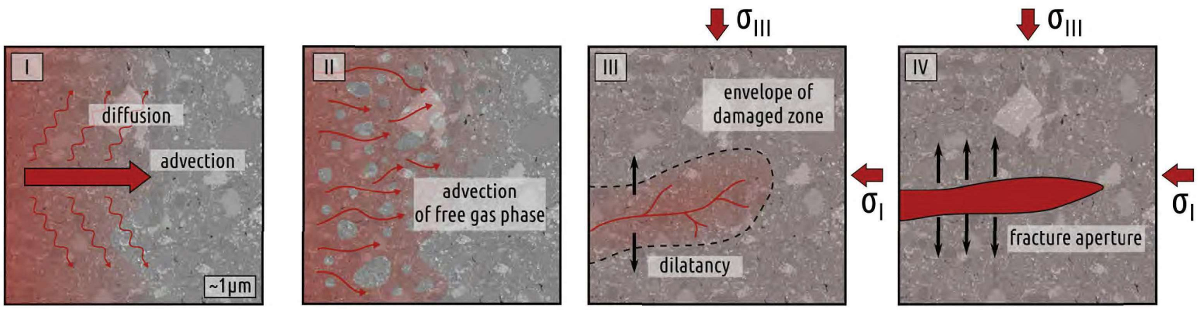

Advection and diffusion of dissolved gases

Visco-capillary flow of gas and liquid phase ("two-phase flow")

Dilatancy controlled gas flow ("pathway dilution")

Gas transport in tensile fractures ("hydro-/ gasfrac")"

Classification of gas transport regimes in clay rock, adapted and modified from Marschall et al. [2005]

Grunwald, N., Nagel, T., Pitz, M., Kolditz, O. "Extended analysis of benchmarks for gas phase appearance in low-permeable rocks". Under Review at Geomechanics and Geophysics for Geo-Energy and Geo-Resources, 2023. in

TECHNISCHE UNIVERSITÄT BERGAKADEMIE FREIBERG
Die Ressourcenuniversität. Seit 1765.

HELMHOLTZ Zentrum für Umweltforschung

PHASE APPEARANCE / DISAPPEARANCE

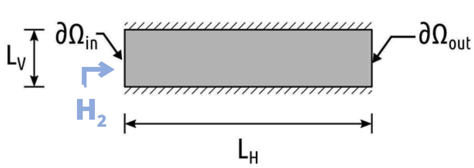

- Benchmark (Bourgeat et al.)
- Continuous H_2-injection at $\partial\Omega_{in}$ at $0 \leq t \leq 500{,}000$a
- Gas phase appears at t≈15,000a
- At t=500,000a rapid drop in water pressure
- Gas phase disappears at t≈700,000a7

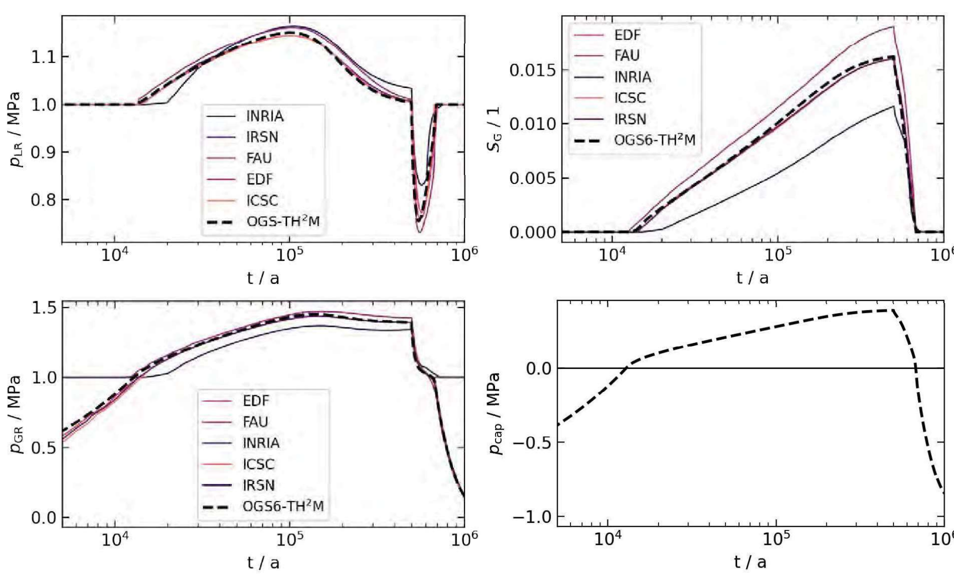

A. **Bourgeat** et al. "Compositional two-phase flow in saturated-unsaturated porous media: benchmarks for phase appearance/ disappearance". In: Simulation of flow in porous media 12 (2013), S. 81–106.

TECHNISCHE UNIVERSITÄT BERGAKADEMIE FREIBERG
Die Ressourcenuniversität. Seit 1765.

UFZ HELMHOLTZ Zentrum für Umweltforschung

APPLICATION: HLWR-SCALE TH2M-SIMULATION I

Motivated by ANSICHT-II* project
created within a cooperation with BGR

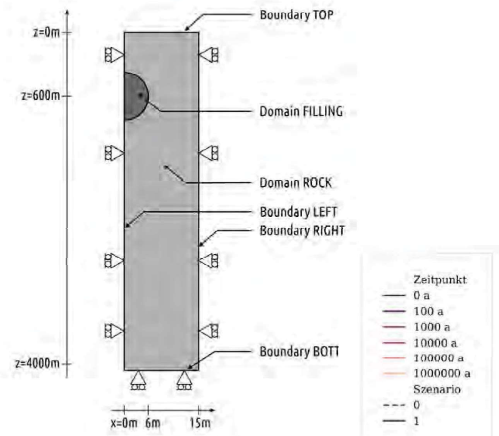

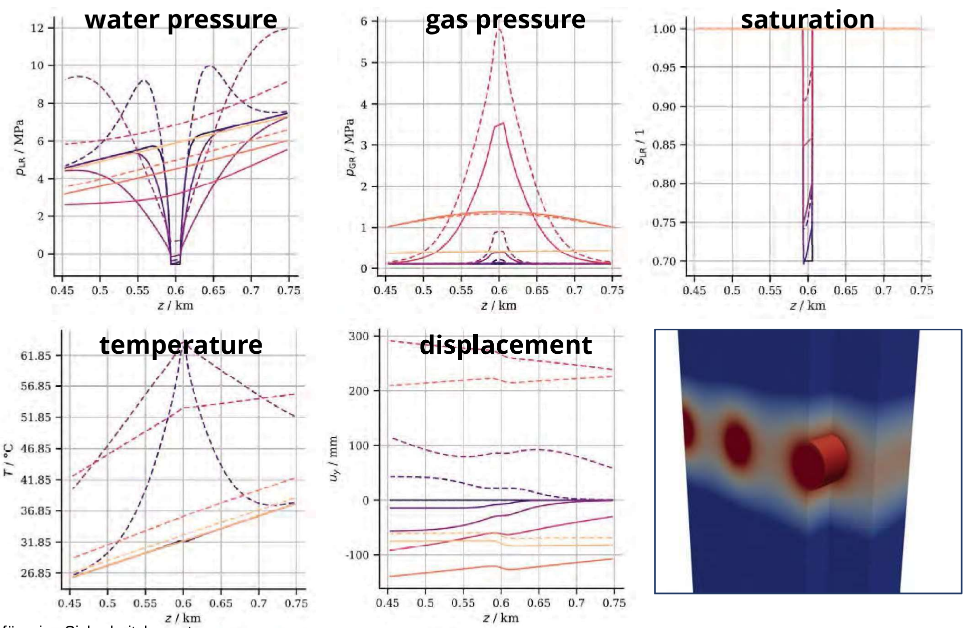

Entry-point for eurad HITEC

*Jobmann, M. et al. (2022, in review): ANSICHT-II: Methodik und Beispiele für eine Sicherheitsbewertung von Endlagersystemen im Tongestein in Deutschland. Synthesebericht. BGR, BGETEC, GRS

TECHNISCHE UNIVERSITÄT BERGAKADEMIE FREIBERG
Die Ressourcenuniversität. Seit 1765.

UFZ HELMHOLTZ Zentrum für Umweltforschung

APPLICATION: HLWR-SCALE TH2M-SIMULATION II

Appendix G. Experimental Multi-Scale Insight into Gas Transport and Self Sealing Capacity: a detailed research methodology on Boom Clay (L. Gonzalez-Blanco)

UNIVERSITAT POLITÈCNICA DE CATALUNYA
BARCELONATECH
Department of Civil and Environmental Engineering
Geotechnical Engineering and Geosciences

CIMNE
EXCELENCIA SEVERO OCHOA

eurad
European Joint Programme on Radioactive Waste Management

EXPERIMENTAL MULTI-SCALE INSIGHT INTO GAS TRANSPORT AND SELF-SEALING CAPACITY
A DETAILED RESEARCH METHODOLOGY ON BOOM CLAY

Laura Gonzalez-Blanco
Enrique Romero
CIMNE / UPC

The project leading to this application has received funding from the European Union's Horizon 2020 research and innovation programme under grant agreement n° 847593.

OUTLINE OF THE LECTURE

1. **Motivation**
2. **Insight into gas transfer and self-sealing**
3. **Some observations regarding gas testing (experimental protocols)**
4. **A detailed research methodology on Boom Clay:**
   - **Material characterization**
   - **Stress paths followed**
   - **Gas test protocols**
   - **Test results at different scales (macroscopic results and microstructural features)**
5. **Final comments. Future challenges**

eurad

WHY GAS TRANSPORT ISSUES ARE OF INTEREST?

Understanding gas transport process is an important issue in the **assessment of radioactive waste repository performance** and other **energy / environmental geotechnics related fields** (shale gas, CO_2 capture, landfill design, ...)

Landfill design (methane, ...)

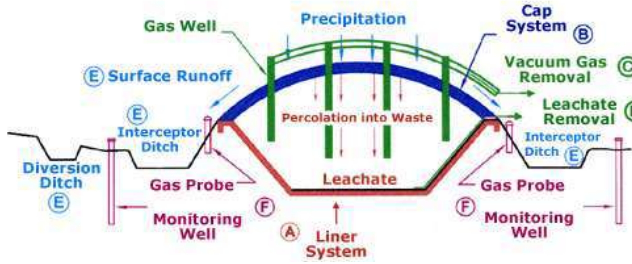

Conventional/unconventional gas reserves

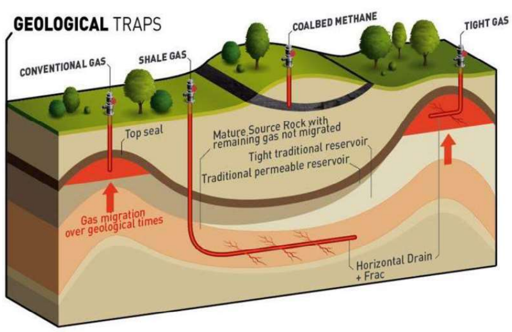

Safely storing CO_2

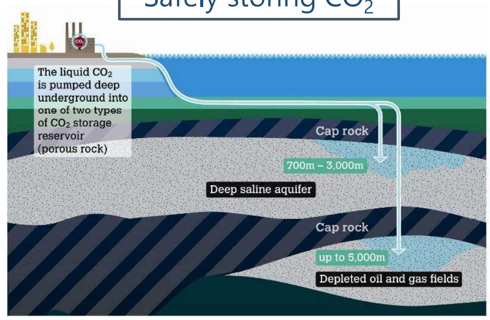

Peterhead CCS Project (UK)

GEOLOGICAL DISPOSAL FACILITIES

Based on the multi-barrier system concept for long-term isolation

- **Artificial barriers:**
  - Waste canister
  - Metallic overpack
  - **Sealing and buffer materials EBS** to prevent / delay the release of radionuclides, gases and other contaminants
- **Natural barriers:**
  - Geosphere: **geological formation** and groundwater (host rock)

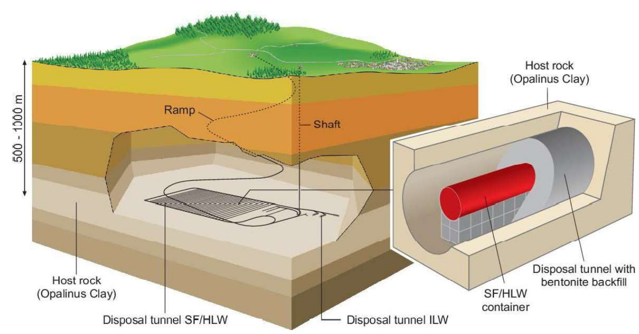

Swiss concept (NAGRA)

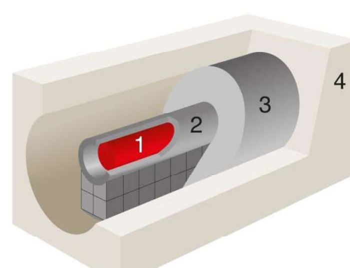

1. Glass matrix, containing radioactive material
2. Metal container
3. **Backfill with bentonite**
4. **Host rock**

GAS GENERATION SOURCES

- Degradation of organic matter: Methane and Carbon Dioxide
- Radiolysis: Hydrogen, Oxygen, Carbon Dioxide, Methane, etc
- Alpha decay process: Helium
- **Anaerobic corrosion of ferrous materials in metallic overpacks** (largest source and production of **Hydrogen**)

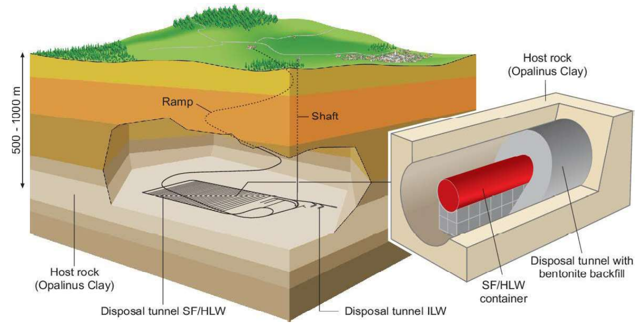

Gas pressure → Gas production rate

Gas pressure → Transport properties of EBS and host formations

Swiss disposal concept for HLW and L/ILW
- Total volume of produced gas: **20 Mio m^3 (STP)**
- Total pore volume of backfilled underground structures: **400000 m^3**
- **Maximum gas overpressure above the hydrostatic pressure: 1-3 MPa**
- **Upper limit of gas pressure: 16 MPa**

Gas pressure build-up may cause the failure of the EBS and the possible release of radionuclides into environment

eurad

MULTI-BARRIER PERFORMANCE

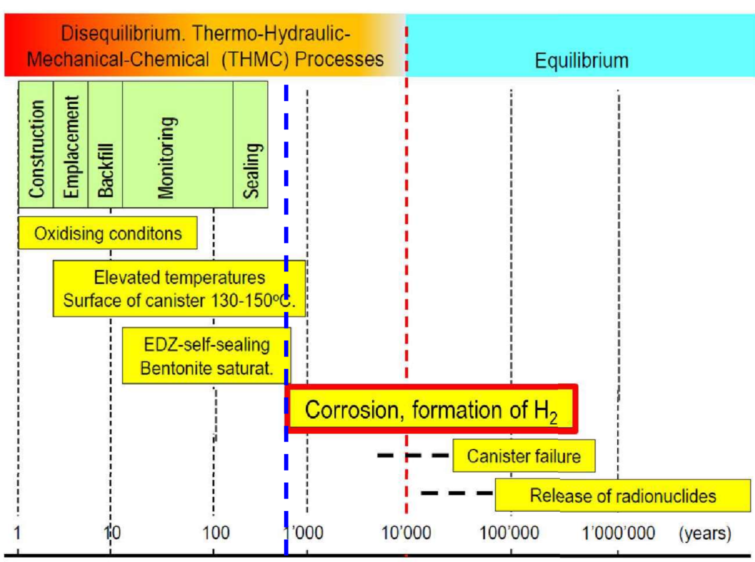

LONG-TERM → Small thermal interactions (thermal history has impact)
EBS and host rock close to saturated conditions (reduced chemical interactions)

NAGRA (www.mont-terri.ch)

- **Large number of past THM-C processes** and phenomena that interact
- **No overlapping with bentonite saturation and EDZ self-sealing**
- Predictions required for **long periods of time**

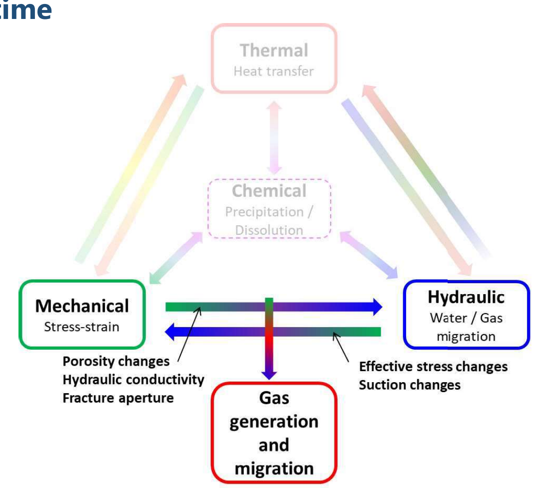

WHAT IS THE MOTIVATION OF THIS LECTURE? SOME COMMENTS

To present an **updated perspective** on the use of multi-scale **laboratory techniques** (multi-physics testing)

Macroscopic (phenomenological) features of advective gas transport and self-sealing in saturated clayey materials. Evaluation of stress paths and effective permeability to water and gas flow for the safety assessment.

Macroscopic laboratory tests are necessary to improve the understanding of the basics and to provide data for the development of predictive tools.

Microstructural tests to evaluate the pore size distribution, reconstruct the fissure/pathway patterns, estimate the total volume of pathways and their connectivity, and observe the closure of the gas pathways upon re-saturation (self-sealing).

Microstructural description of discontinuities, fractures and heterogeneity play an important role and should be to be taken into account for modelling.

WHAT IS THE MOTIVATION OF THIS LECTURE? SOME COMMENTS

- **Experimental techniques** used to study coupled multi-physics process **do not always present the complete picture of understanding** (information on local behavior usually remains unknown). Often, theoretical and/or **numerical models must accompany the interpretation of the physical tests to better exploit the information provided by measurements** and to offer additional confidence on the experimental results (validation of the experimental techniques).

- **Advective gas tests** are associated with so-called **'critical phenomena'** that are at the **verge of predictability** (particularly at specimen scale), and **microstructural features set on compaction / stress paths** affecting pore size distribution and connectivity issues (multiple gas pathways, dominant single cluster, ….) are admitted to **play an important role in the scatter**.

OUTLINE OF THE LECTURE

1. Motivation
2. **Insight into gas transfer and self-sealing**
3. Some observations regarding gas testing (experimental protocols)
4. A detailed research methodology on Boom Clay:
   - Material characterization
   - Stress paths followed
   - Gas test protocols
   - Test results at different scales (macroscopic results and microstructural features)
5. Final comments. Future challenges

GAS MIGRATION IN SATURATED POROUS MEDIA: GAS TRANSPORT MECHANISMS

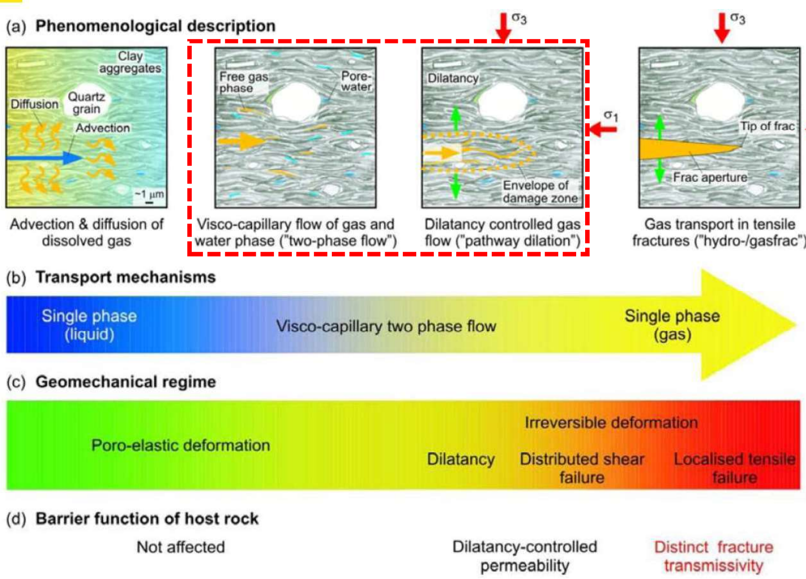

Marschall et al. (2005)

Gas dissolved in water migrates through diffusion (low gas generation rates)

- Gas pressure builds up due to the slow diffusive transport in low permeable media (high gas generation rates)

Gas flow through the matrix partially displacing water (two-phase flow)

- Flow affected by mechanical effects (intrinsic permeability affected by porosity changes)

Gas flow through pressure-dependent pathways/fractures (existing/induced) (microscopic fissuring, macroscopic fracture)

- Flow properties affected by mechanical effects and fracture aperture

GAS TRANSPORT PATHWAYS

Plastic host rock: gas migration along bedding planes or discontinuities in the EDZ that can be initially close

Extension of EDZ in Connecting Gallery
(Boom Clay, HADES URL, Belgium)

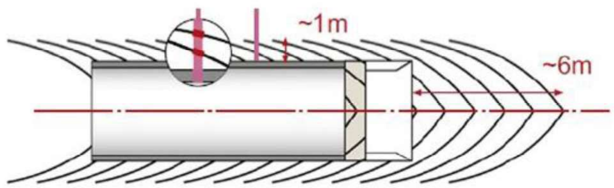

Salehnia et al. (2015)

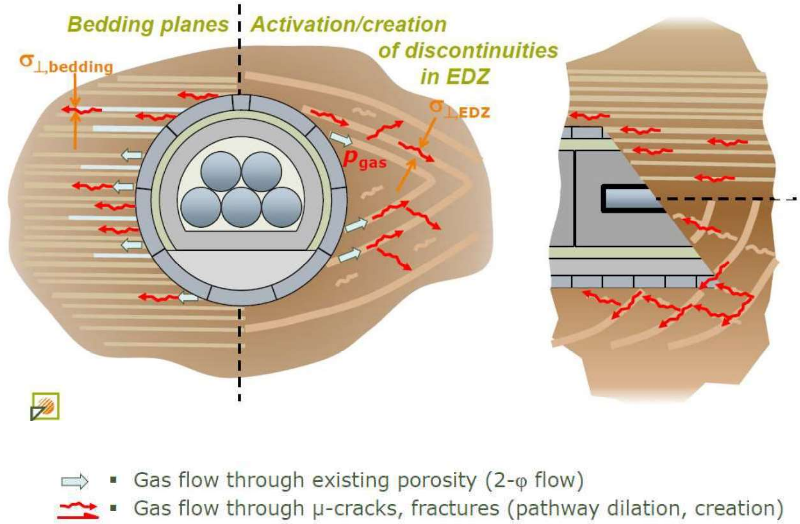

*ONDRAF/NIRAS **(2016)***

eurad

GAS INJECTION EXPERIMENTS

Gas injection tests on Opalinus Clay formation (Switzerland)

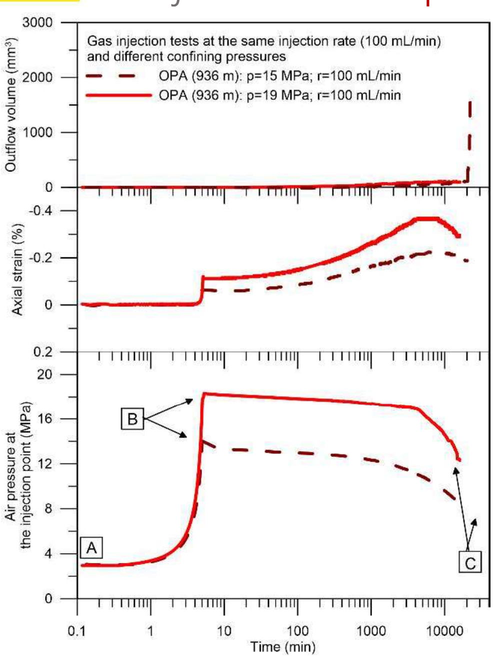

A→B: Gas injection at constant volume rate
B: Shut-off phase (constant injection volume)
B→C: Dissipation phase (constant injection volume)

Volumetric response during gas injection

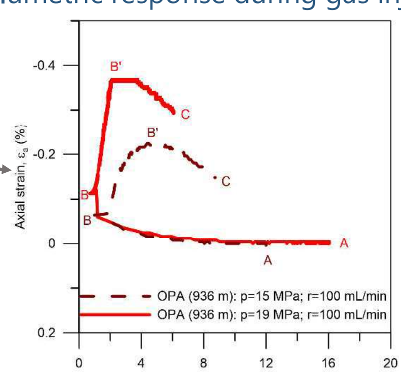

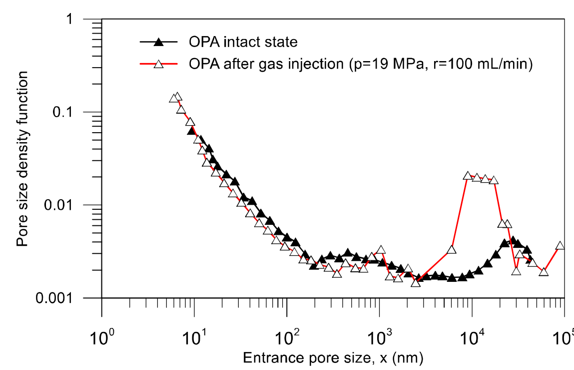

Change in the pore size distribution

Gonzalez-Blanco et al. (2022)

eurad

MICROSTRUCTURE (TECHNIQUES)

Multi-scale characterisation of porosity in Boom Clay
(HADES-level, Mol, Belgium)

Hemes et al. (2015)

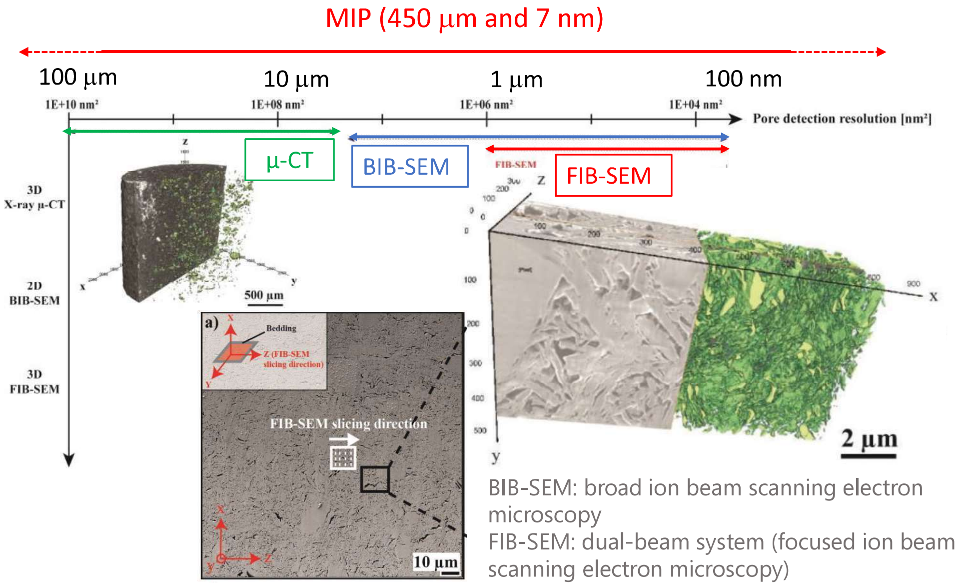

BIB-SEM: broad ion beam scanning electron microscopy
FIB-SEM: dual-beam system (focused ion beam scanning electron microscopy)
MIP: Mercury Intrusion Porosimetry
μ-CT: Micro-focus X-ray computed tomography

Digital image analyses (X-ray μ-CT, BIB-SEM / FIB-SEM tomography) (rendering graphics software ImageJ, Avizo, ...)

3D volume reconstruction from slice-and-view images, and stacking multiple planar images with a known separation

Resolution depending on system and sample size (typically between 0.01 to 100 μm) (1/1000-2000 times the object cross-section diameter)

EXPERIMENTAL DATA AT MULTI-SCALE LEVEL NECESSARY FOR THE DEVELOPMENT AND VALIDATION OF CONSTITUTIVE MODELS

Embedded fracture permeability model
(Olivella & Alonso, 2008)

Fracture aperture $b = \begin{cases} b_0 + \Delta b & b < b_{max} \\ b = b_{max} & b \geq b_{max} \end{cases}$ $\quad \Delta b = a \Delta \varepsilon$

Equivalent permeability $k = k_{matrix} + \dfrac{b^3}{12a}$

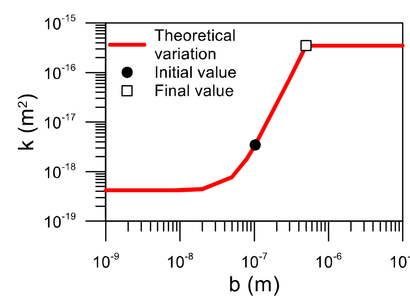

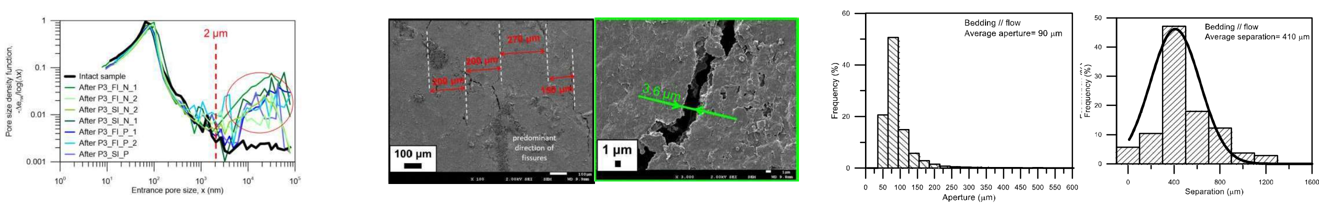

	MIP	FESEM	μ-CT
Aperture: b (μm)	> 2	3 - 10	90// - 150⊥
Separation: a (μm)	-	150 - 270	410// - 560⊥

Gonzalez-Blanco et al. (2016)

APPLICATION OF THE EMBEDDED FRACTURE MODEL

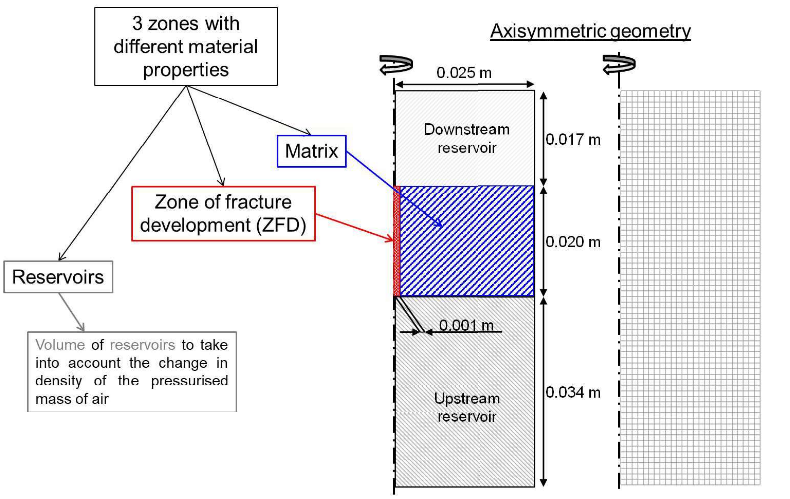

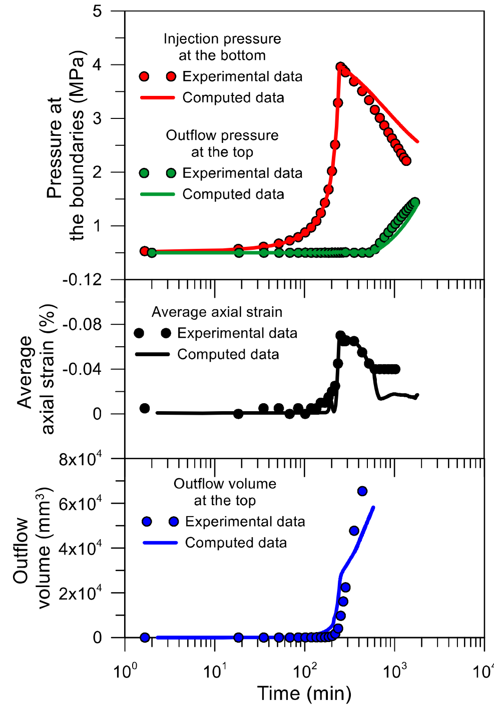

Gonzalez-Blanco et al. (2016)

SIMULATION OF EXPERIMENTAL RESULTS ALLOWED BETTER EXPLOITING THE INFORMATION PROVIDED BY MEASUREMENTS

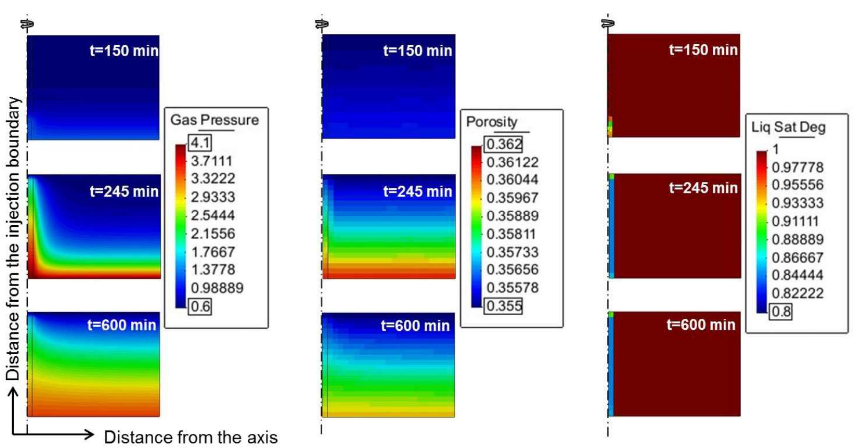

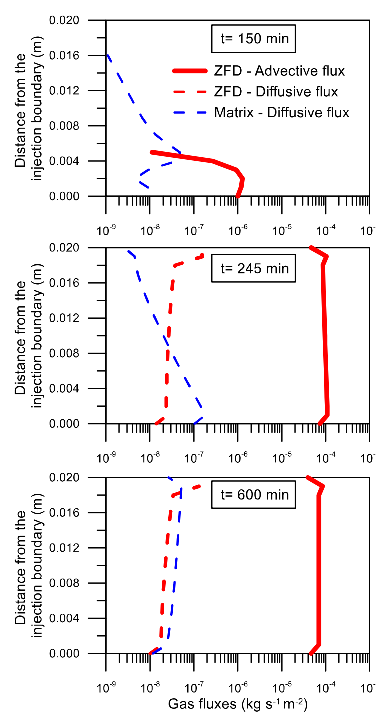

t= 150 min → During gas injection
t= 245 min → At shut-off (end of the injection)
t= 600 min → During gas dissipation

Gonzalez-Blanco et al. (2016)

SELF-SEALING / SELF-HEALING

Sealing → Reduction of fracture permeability by any hydro-mechanical, hydro-chemical or hydro-biochemical processes

Healing → Sealing with loss of memory of the pre-healing state

Self → The process of healing or sealing happens spontaneously in the rock mass without interference by intentional human actions

Possible mechanisms:

- Increase of the stress state
- Pore-pressure changes
- Creep
- Swelling of clay minerals
- Oxidation/precipitation
- Mineralogical changes (crystallisation)
- etc.

Bernier et al. (2007) SELFRAC Project

SELF-SEALING / SELF-HEALING IN ARTIFICIALLY FRACTURED CLAYEY ROCKS

Hydraulic conductivity reduction due to self-sealing

BOOM CLAY

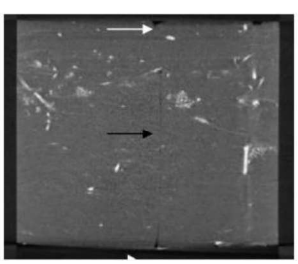

After loading

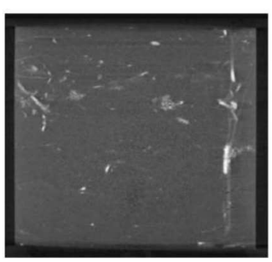

After permeability testing

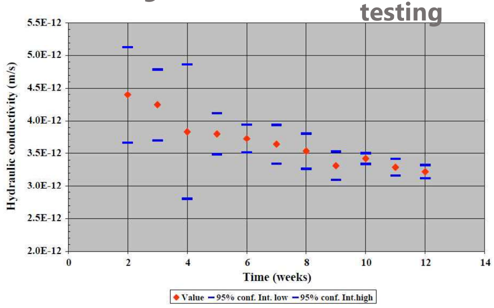

OPALINUS CLAY

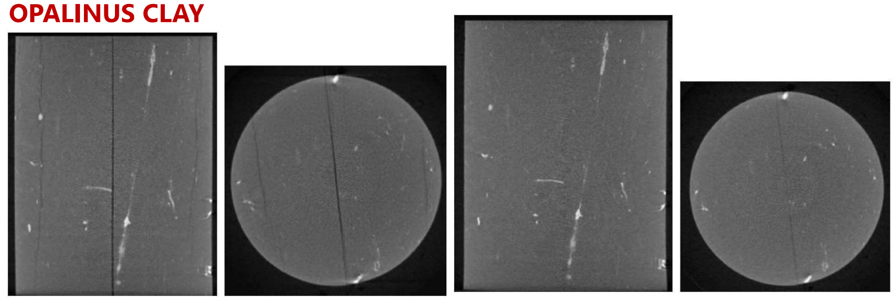

Initial state

After permeability testing

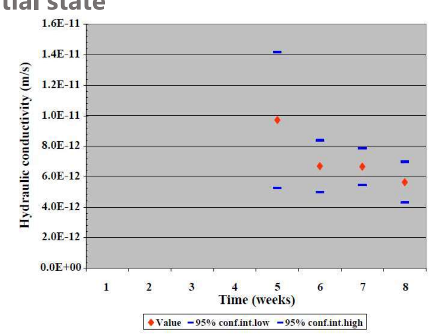

SELFRAC Project
Van Geet et al. (2008)

FRACTURE CLOSURE

CALLOVO-OXFORDIAN CLAY

Artificially-fractured

OPALINUS CLAY

Naturally-fractured

Effect of normal stress on fracture closure

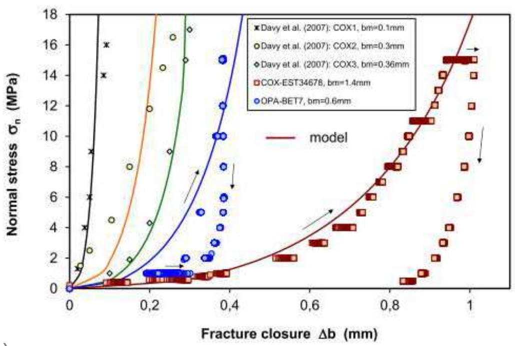

Zhang et al. (2013)

Sealing of fractures in COX claystone during water flowing under various confining stresses

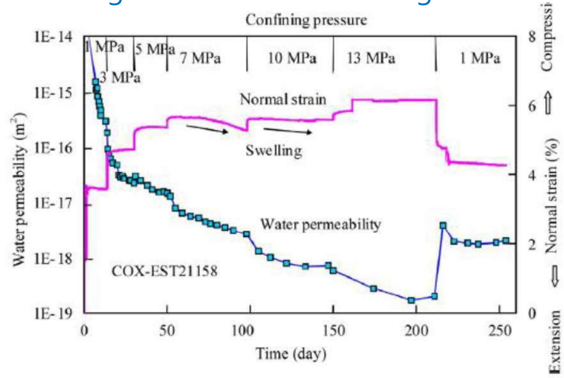

Effects of wetted gas flow on fracture sealing

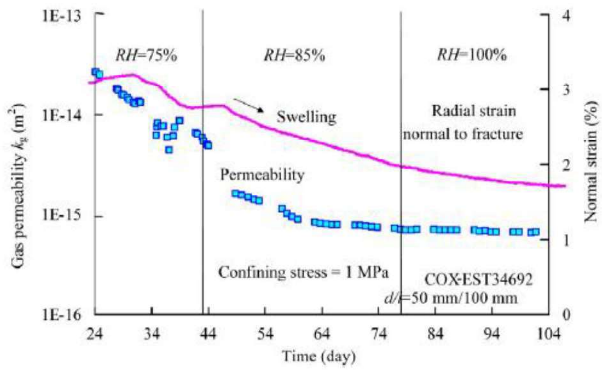

SELF-SEALING / SELF-HEALING IN NATURALLY FRACTURED CLAYEY ROCKS

Water flow while increasing confining pressure

OPALINUS CLAY

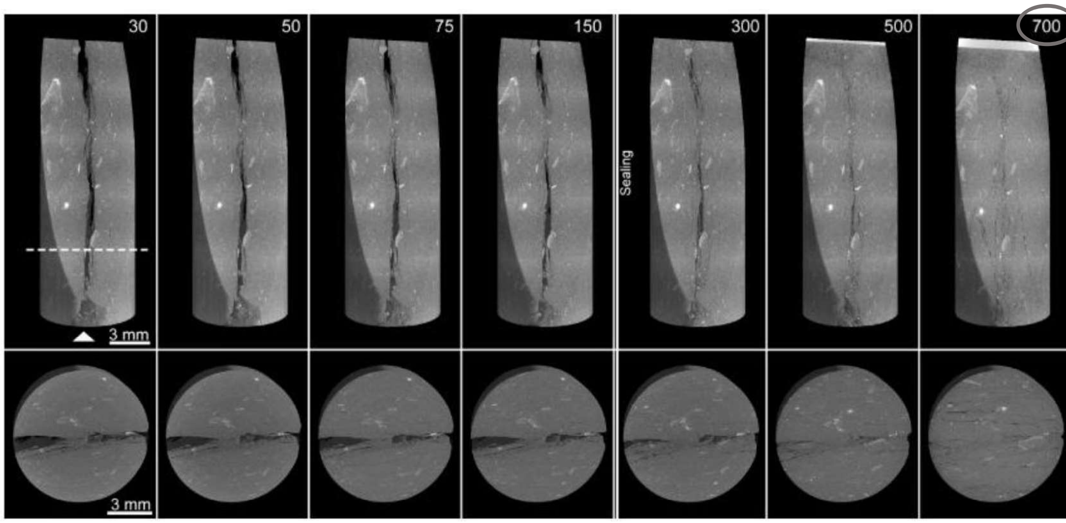

Confining pressure minus back-pressure (psi)

Synchrotron X-Ray Micro-Tomography

Voltolini & Ajo-Franklin (2020)

SELF-SEALING / SELF-HEALING IN ARTIFICIALLY FRACTURED CLAYEY ROCKS

Effect of wetting / drying cycles on fracture closure and re-opening

CALLOVO-OXFORDIAN CLAY

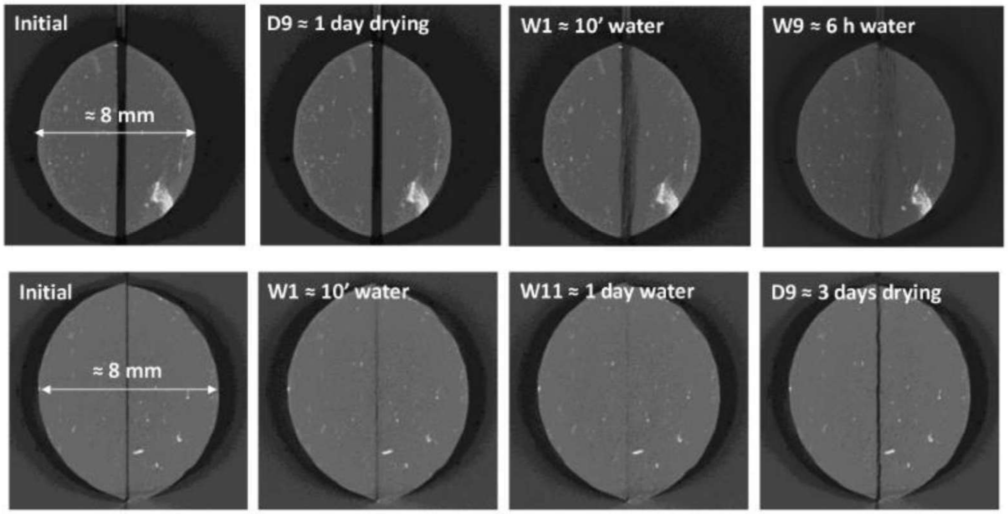

Initial gap 425 μm
Voxel size 15 μm

Initial gap 75 μm
Voxel size 13.5 μm

Di Donna et al (2022)

EFFECT OF GAS INJECTION ON SELF-SEALED FRACTURED CLAYEY ROCKS

Gas invasion in previously fractured and sealed indurated clay samples

CALLOVO-OXFORDIAN CLAY **OPALINUS CLAY**

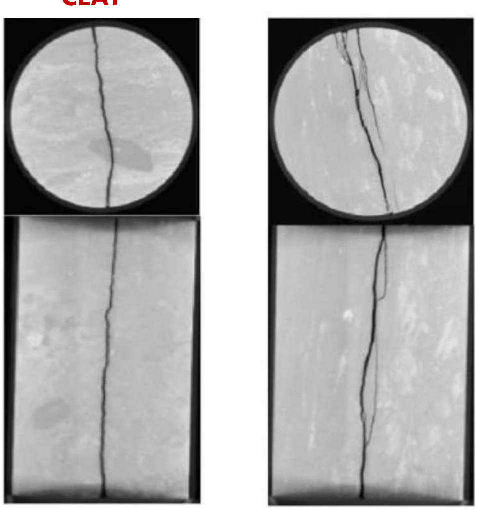

Decrease of water permeability due to fracture closure

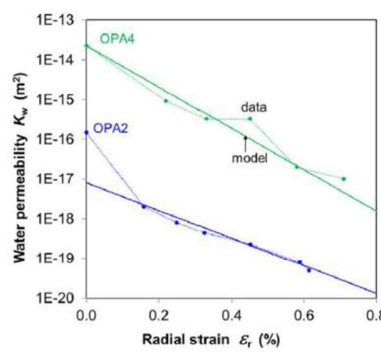

Water permeability **before and after gas invasion**

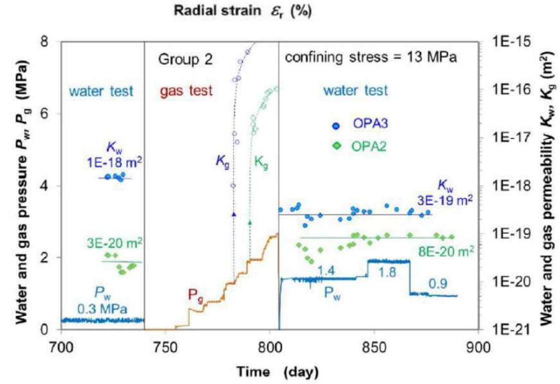

Zhang & Talandier (2022)

OUTLINE OF THE LECTURE

1. Motivation
2. Insight into gas transfer and self-sealing
3. Some observations regarding gas testing (experimental protocols)
4. A detailed research methodology on Boom Clay:
   - Material characterization
   - Stress paths followed
   - Gas test protocols
   - Test results at different scales (macroscopic results and microstructural features)
5. Final comments. Future challenges

eurad

ADVECTIVE GAS EXPERIMENTS AT LAB SCALE: SOME ISSUES OF CONCERN

- Effects of the **stress state** and **stress history (mechanical, saturation, thermal)** on gas migration
- **Volume change behaviour** during the stress history and along gas injection / dissipation (changes in gas and liquid pressures and their impact on gas permeability).
- **Stress changes** during gas injection under constant volume conditions
- Role played by natural **discontinuities and their orientation (anisotropy)**
- **Changes in the pore / fissure network and their connectivity** due to gas injection / dissipation (opening of bedding planes / fissures / pathways)
- **Liquid displacements (desaturation of pathways)** during gas injection / dissipation
- Influence of the **gas injection rate and gas type**
- **Gas migration after re-saturation** (reopening of fissures)

Simple concepts but **not-so-simple tests to perform and interpret**. Need for **coupled modelling to complement the information** not provided by measurements ('boundary value tests')

eurad

HOW TO PERFORM ADVECTIVE GAS INJECTION/DISSIPATION TESTS?

Importance of:

- Hydro-mechanical characterization of tested material (uncertainty / variability assessment)

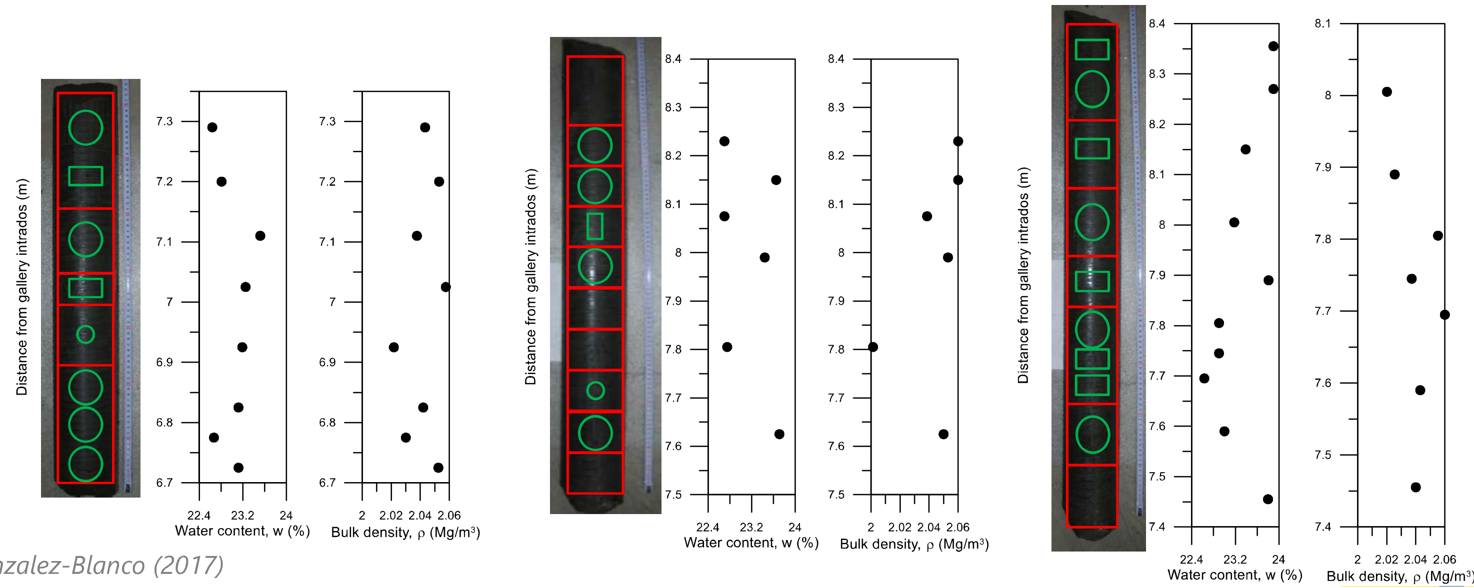

Gonzalez-Blanco (2017)

HOW TO PERFORM ADVECTIVE GAS INJECTION/DISSIPATION TESTS?

Importance of:

- Restoring in situ stress state (effective stress) (natural samples)

Occurrence of (matric) suction despite the nearly saturated state:

- Release of total stresses under water undrained conditions upon retrieval
- Some drying undergone during sampling, transportation, storage and preparation

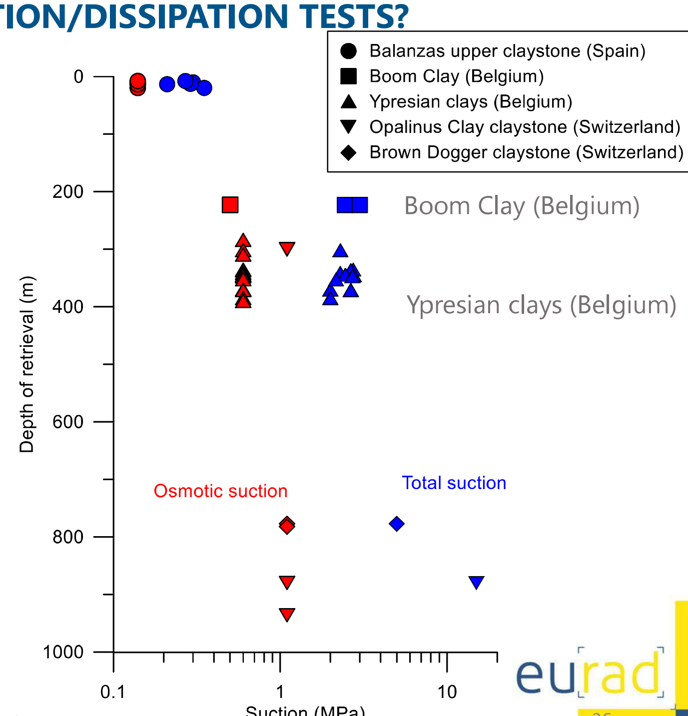

Sau et al. (2019); Sau (2021)

HOW TO PERFORM ADVECTIVE GAS INJECTION/DISSIPATION TESTS?

Importance of:

- Defining the stress paths to follow prior to gas injection (saturation path)

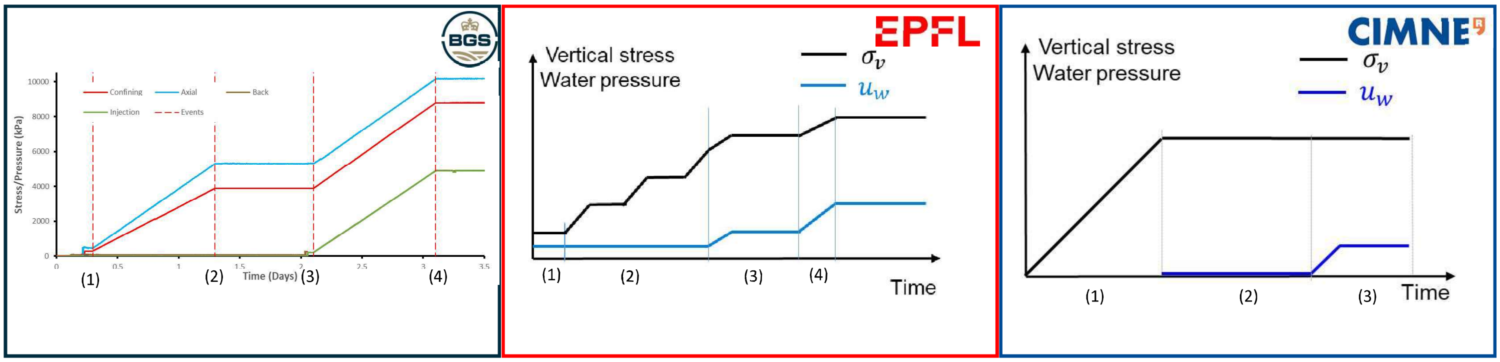

HOW TO PERFORM ADVECTIVE GAS INJECTION/DISSIPATION TESTS?

Importance of:

- Measuring volume changes in stress-controlled tests or stress state under isochoric conditions

Air injection tests under isotropic conditions on Brown Dogger shale formation (Switzerland)

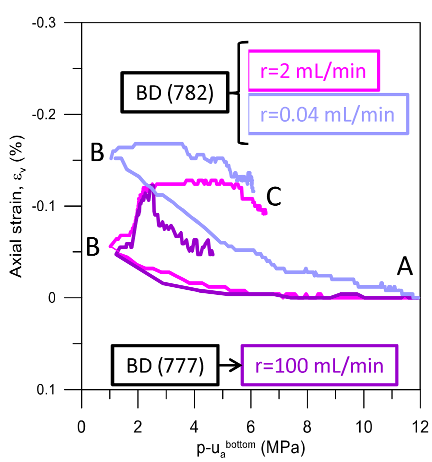

A→B: Gas injection at constant volume rate

B: Shut-off phase (constant injection volume)

B→C: Dissipation phase (constant injection volume)

Gonzalez-Blanco et al. (2022)

HOW TO PERFORM ADVECTIVE GAS INJECTION/DISSIPATION TESTS?

Importance of:

- Gas injection protocol: some decisions to make

Air injection test on Opalinus Clay

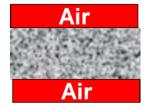

- Progressive desaturation of the sample
- Air injection pressure decays
- Breakthrough process does not occur

➢ Gas type (air / N_2 / He ...)

➢ Type of fluid at the boundaries (gas – gas) / (gas – liquid)

➢ Relative humidity of gas (dry gas / wet gas)

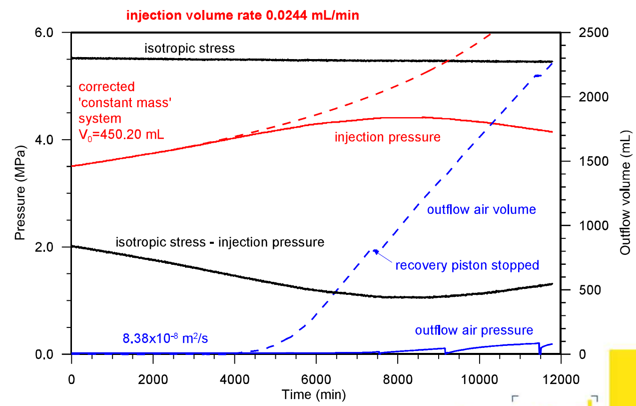

Romero et al (2010)

HOW TO PERFORM ADVECTIVE GAS INJECTION/DISSIPATION TESTS?

Importance of:

- Gas injection protocol:

➢ Flow direction with respect to bedding orientation (anisotropy features)

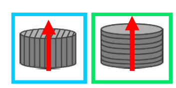

➢ Surface to apply gas injection (gas on entire sample surface, point injection)

➢ Gas injection method (pressure ramp / pressure steps / volumetric ramp / ...)

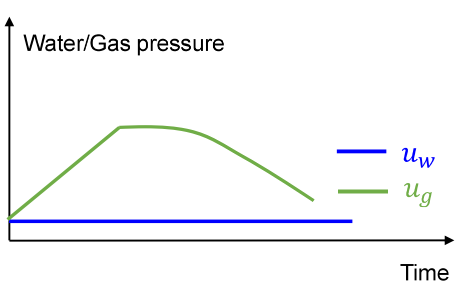

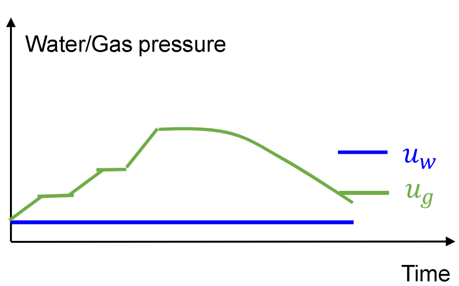

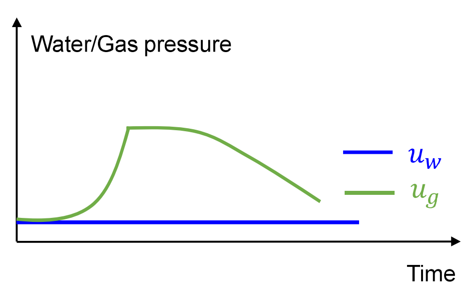

HOW TO PERFORM ADVECTIVE GAS INJECTION/DISSIPATION TESTS?

Importance of:

- Gas injection protocol:

➢ Gas injection rate (slow – fast) (dynamic effects on water retention curve)

➢ Information on system volumes (inflow/outflow volumes, dead volume up to valves, gaps)

Air injection test on Opalinus Clay

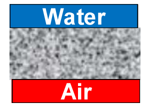

Air diffusion phenomena are important to consider when the injection rate is too slow

Injection volume rate: 0.1 mL/min

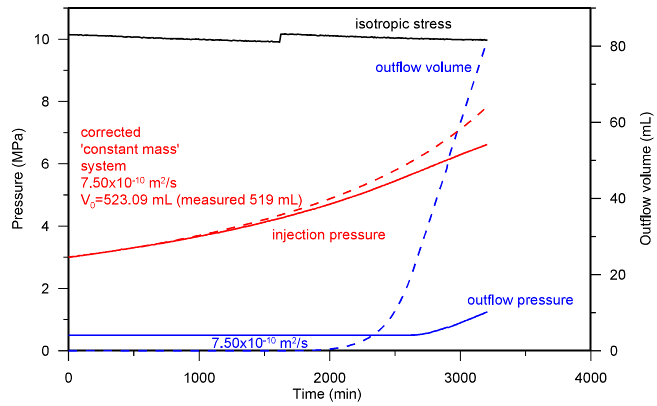

Romero et al. (2010)

HOW TO PERFORM ADVECTIVE GAS INJECTION/DISSIPATION TESTS?

Importance of:

- Gas injection protocol:

➢ Type of test ('soft breakthrough' with maximum pressure close to AEV / 'hard breakthrough' until gas outflow close to the minimum total stress)

$u_{g\ ini}$ → > AEV / < AEV

➢ Stress state and gas pressure (maximum gas pressure)

$\sigma_1 - u_{g\ max}$ → < 1 MPa (flow through interface) / > 1 MPa (flow through sample)

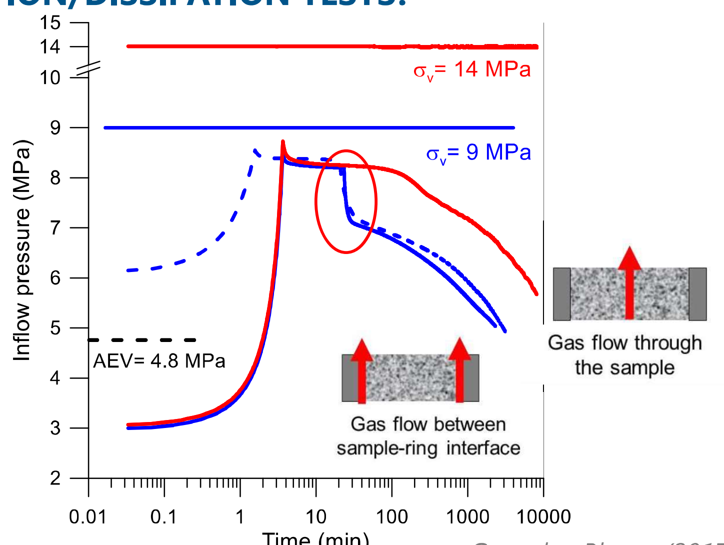

Gonzalez-Blanco (2017)

$\sigma_1 - u_{g\ max}$ > 1 MPa to avoid air passage between sample-ring interface

⇩

Development of oedometer cell with lateral stress measurement

OUTLINE OF THE LECTURE

1. Motivation
2. Insight into gas transfer and self-sealing
3. Some observations regarding gas testing (experimental protocols)
4. A detailed research methodology on Boom Clay:
   - Material characterization
   - Stress paths followed
   - Gas test protocols
   - Test results at different scales (macroscopic results and microstructural features)
5. Final comments. Future challenges

BOOM CLAY

Marine sediment of the Cenozoic (Rupelian age, 30 My)

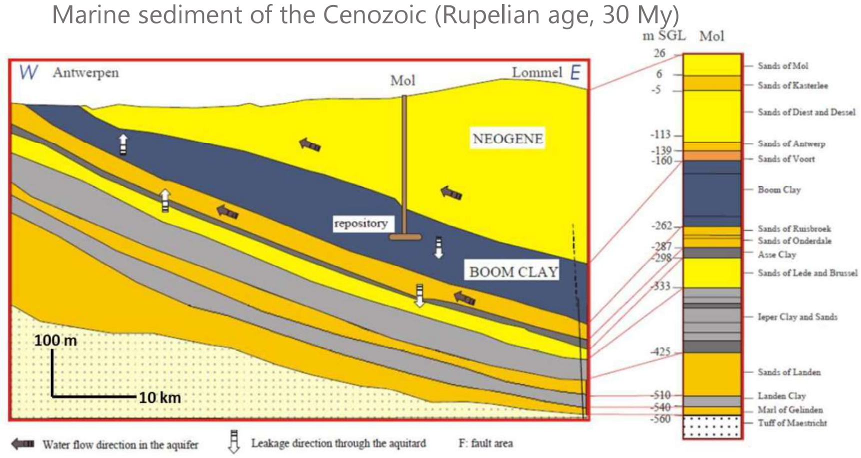

Sillen & Marivoet (2007)

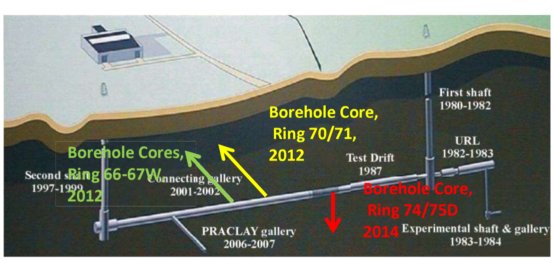

Samples retrieved at **HADES URL** level (223 m depth) in boreholes horizontally drilled

EXPERIMENTAL CHARACTERIZATION

Parameter	Value
Geotechnical properties	
Density of soils, ρ_s (Mg/m^3)	2.67
Liquid limit w_L (%)	67
Plasticity index, I_P (%)	38
Initial conditions	
Density, ρ (Mg/m^3)	2.02-2.06
Dry density, ρ_d (Mg/m^3)	1.63-1.69
Porosity, n	0.37-0.39
Void ratio, e	0.58-0.63
Water content, w (%)	22.6-24.0
Degree of saturation	close to 1
Total suction after retrieval, Ψ (MPa)	2.45
Air-entry value from MIP (MPa)	4.8
Dominant pore mode from MIP(nm)	70

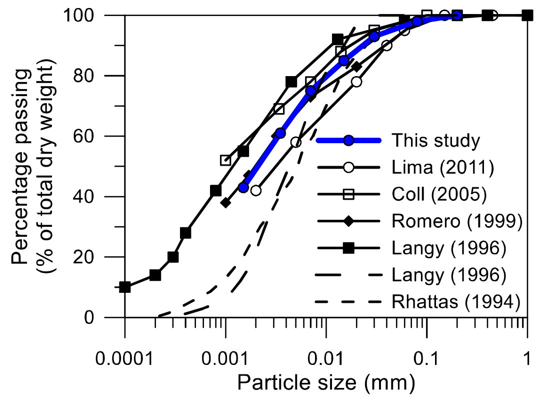

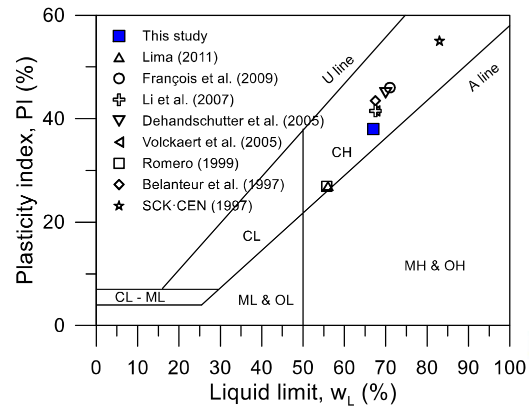

EXPERIMENTAL CHARACTERIZATION

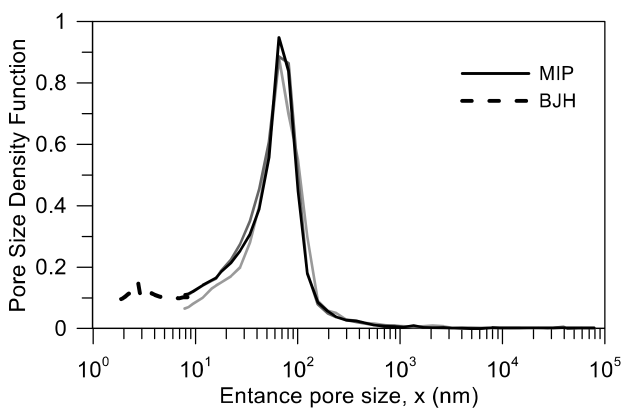

Mono-modal pore size distribution from MIP:

- dominant pore mode around 70 nm
- AEV ~ 4.8 MPa

Drying path of the water retention curve:

- initial total suction after retrieval 2.45 MPa
- AEV ~ 4.5 MPa

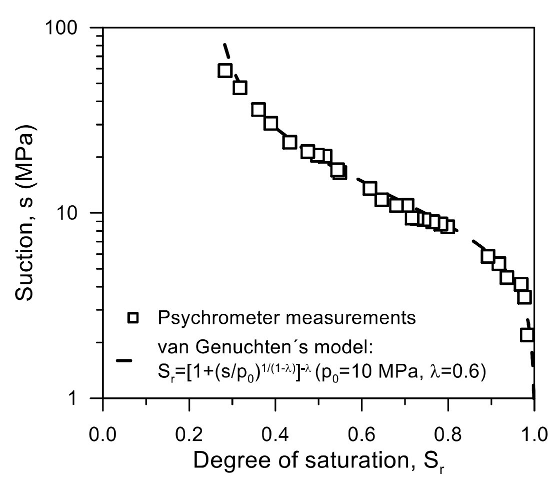

EXPERIMENTAL SET-UPS

Old oedometer cell

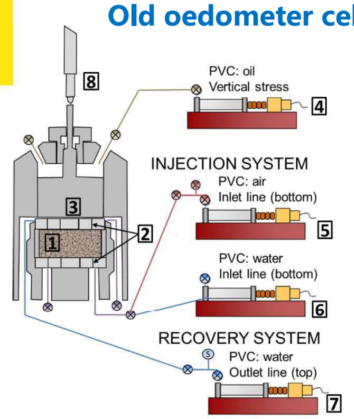

Sample size
- 20 mm in height
- 50 mm in diameter

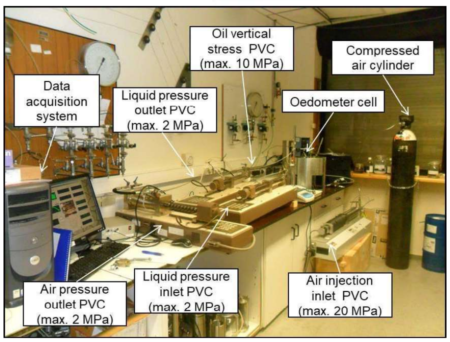

New oedometer cell with lateral stress measurement

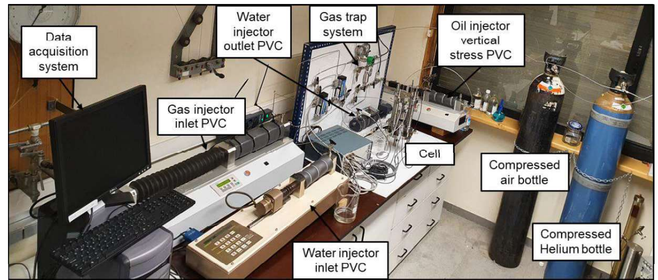

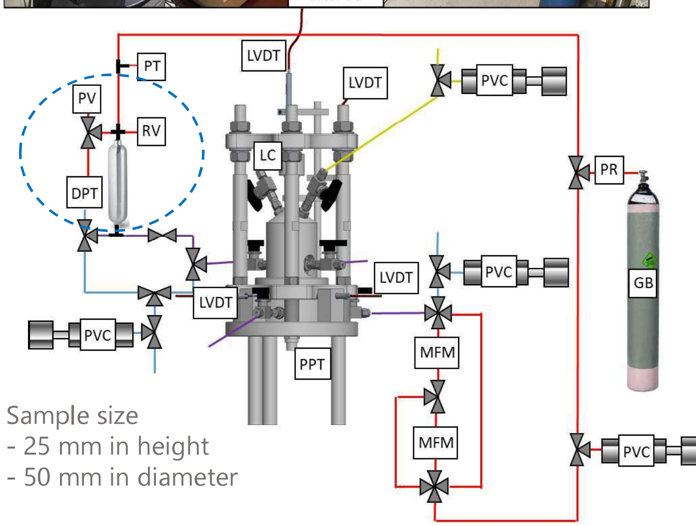

Sample size
- 25 mm in height
- 50 mm in diameter

EXPERIMENTAL SET-UPS

New oedometer cell with lateral stress measurement

Deformable Ring to indirectly measure the lateral stress

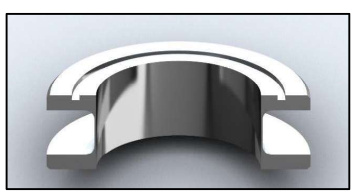

Lateral displacement measurement with **2 LVDTs**
- Measure range: ± 1 mm
- Accuracy: 0.3% FS
- Resolution: 0.15 µm

Maximum lateral displacement 35 µm ⟹ LVDT measures 233 steps

0.14% (some small loss of K_0 condition) between 0.02% and 0.15% for semi-rigid systems

Resolution in terms of **lateral stress** = Full Scale (≈ 4000 kPa) / steps ≈ **20 kPa**

eurad

TEST PROTOCOL

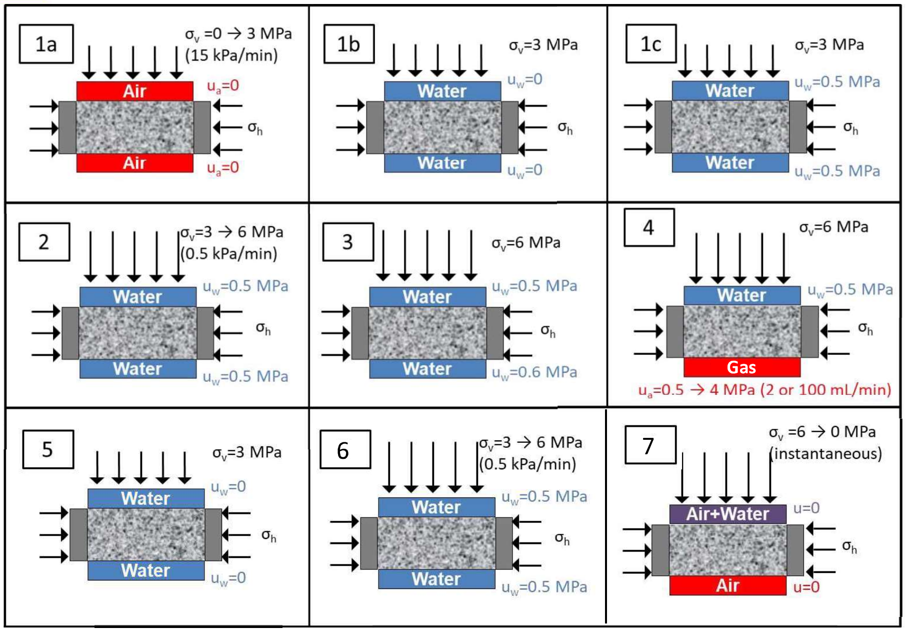

1. Pre-conditioning path
   1a. Undrained loading
   1b. Contact with water
   1c. Water pressurization
2. Drained loading
3. Water permeability
4. Gas injection/dissipation
5. Re-saturation for self-sealing
6. Water permeability
7. Undrained unloading

Additional tests:
- to study the K_0 evolution
- to analyse the post-yield behaviour
- to determine the water permeability variation with porosity
- to see the effect of a second gas injection

PRE-CONDITIONING STAGE

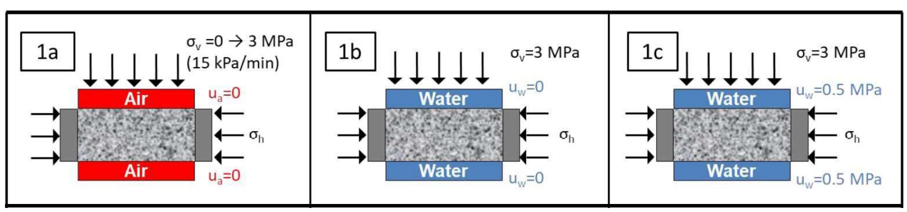

Objectives:
- to apply similar stress state than *in situ*
- to reduce initial suction
- to avoid expansion and degradation of the sample induced by suction reduction at low stress levels

At 223 m depth (*in situ* conditions)

$$\sigma_{1v} = 4.50\ MPa$$
$$u_{wi} = 2.25\ MPa$$
$$\sigma'_{1i} = 2.25\ MPa$$
$$\sigma_1'^{max} = 5.2\ MPa$$

After retrieval (undrained unloading)

$$\Delta\sigma_1; \Delta\sigma_3 \rightarrow \Delta u_w = B\left[\Delta\sigma_3 + \frac{1}{3}A(\Delta\sigma_1 - \Delta\sigma_3)\right]$$
$$B = 1;\ A = 1/3$$
$$\Delta u_w = \frac{\Delta\sigma_1 + 2\Delta\sigma_3}{3} = \Delta p = -4.5\ MPa$$
$$u_{wf} = u_{wi} + \Delta u_w = -2.25\ MPa$$

Post-storage

$$\Psi = 2.45\ MPa$$
$$S_r \backsim close\ to\ 1$$

High initial suction due to stress relief

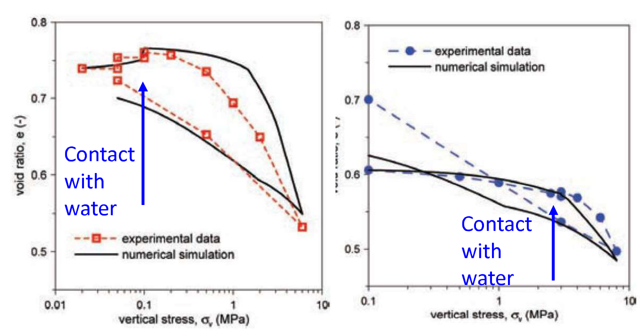

Large deformation when soaking at 0.02 MPa

Soaking at 3 MPa

Della Vecchia et al (2011)

PRE-CONDITIONING STAGE: AXIAL STRESS-STRAIN

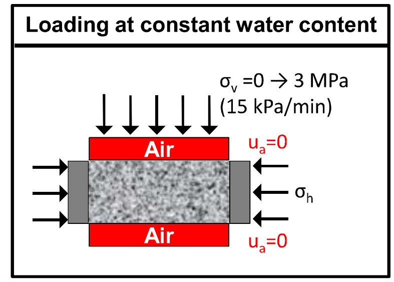

Some deformation occurred:

→ Deformation due to suction changes and stress changes

Slightly higher compressibility on loading of sample with bedding planes orientated normal to the axis (**anisotropy in the elastic domain**)

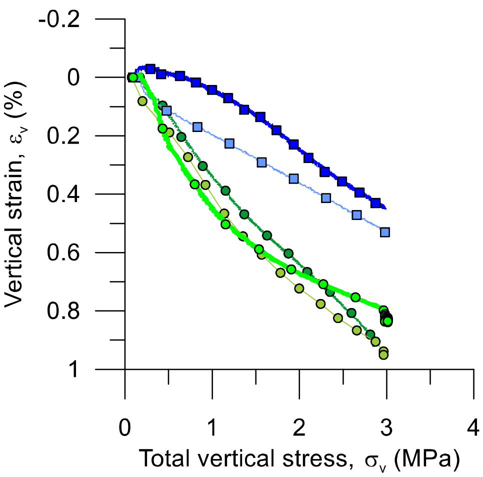

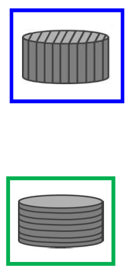

$\Delta\sigma_1 = 3\ MPa$

$\Delta\Psi \simeq -2.3\ MPa$

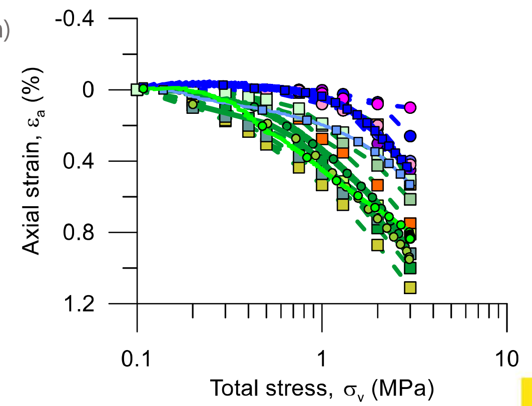

*Values of initial compressibility have been corrected after the new calibration of the cell compressibility

PRE-CONDITIONING STAGE: HORIZONTAL STRESS

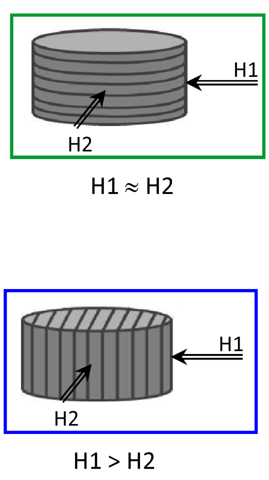

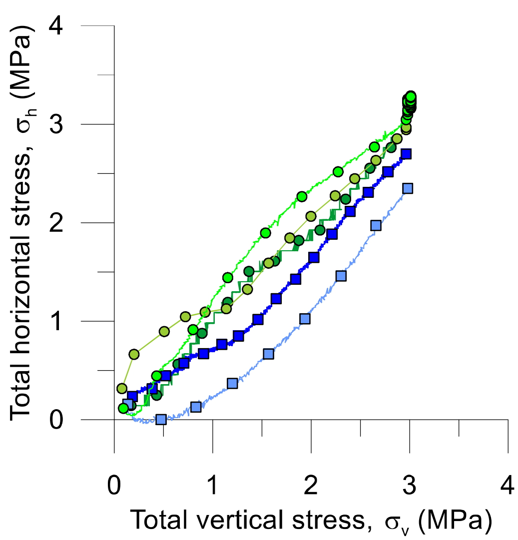

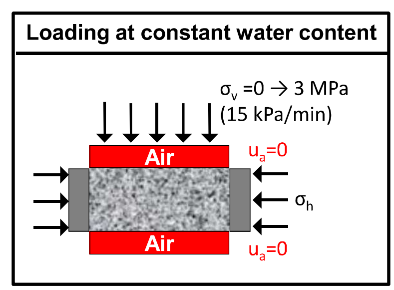

Initial total horizontal stress calibrated:
$\sigma_{h0} \approx 150\ kPa$

*Total horizontal stress computed as the average stress measured at both sensors

PRE-CONDITIONING STAGE: SWELLING STRAIN

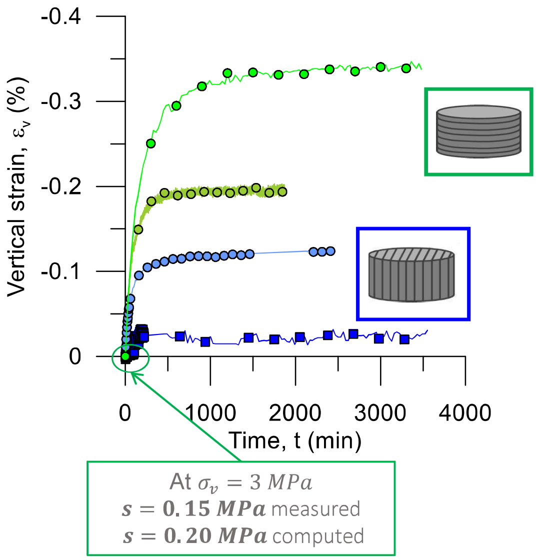

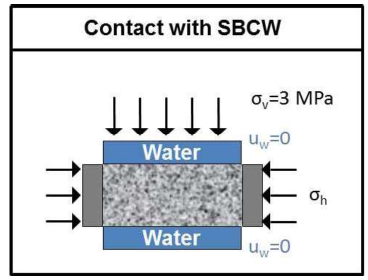

Swelling strains recorded during soaking due to some remaining suction

Samples with bedding planes normal to flow underwent higher swelling (anisotropy in the elastic domain)

eurad

PRE-CONDITIONING STAGE: HORIZONTAL STRESS

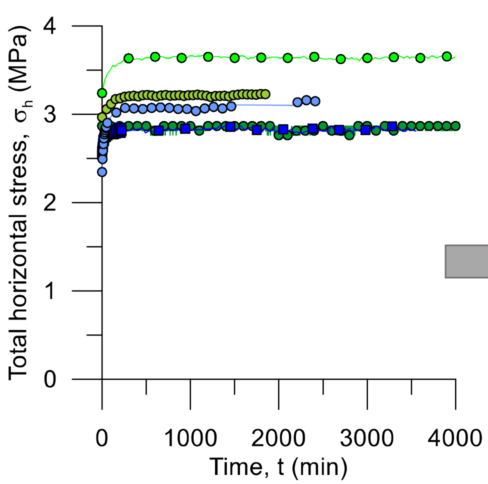

Values after restoring the in situ conditions*

$K_0 = 1.20$ $\sigma_h = 3.64$

$K_0 = 0.99$ $\sigma_h = 2.97$

$K_0 = 1.08$ $\sigma_h = 3.24$

$K_0 = 0.95$ $\sigma_h = 2.85$

$K_0 = 1.03$ $\sigma_h = 3.09$

*Slightly affected by the initial horizontal stress and very sensitive to the sensor location with respect to bedding planes

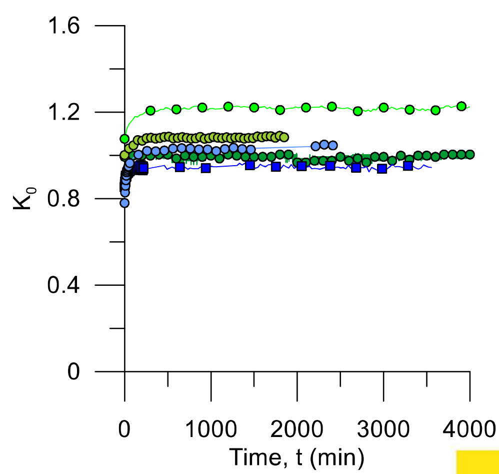

eurad

DRAINED LOADING

- Small anisotropy in elastic domain

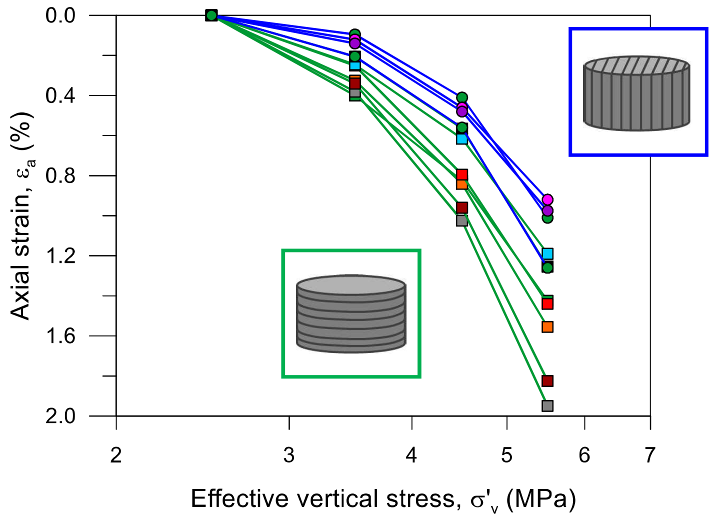

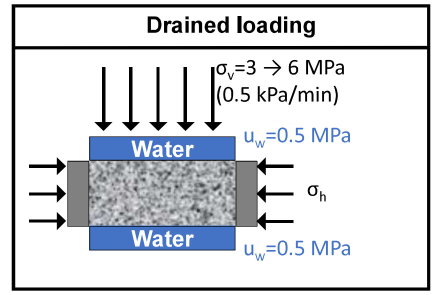

ADDITIONAL HYDRO-MECHANICAL PATHS TO STUDY K_0

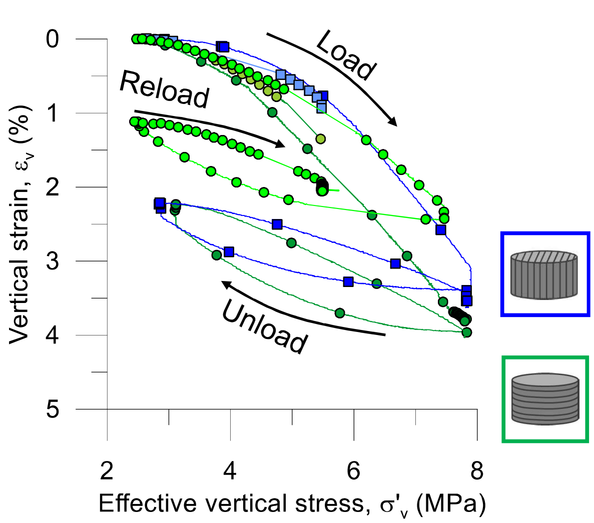

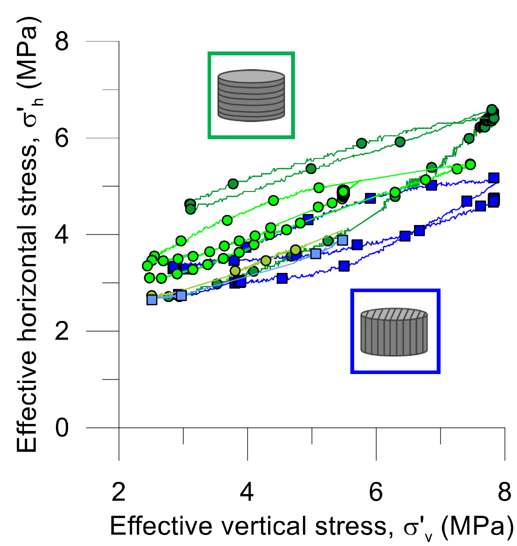

ADDITIONAL HYDRO-MECHANICAL PATHS TO STUDY K_0

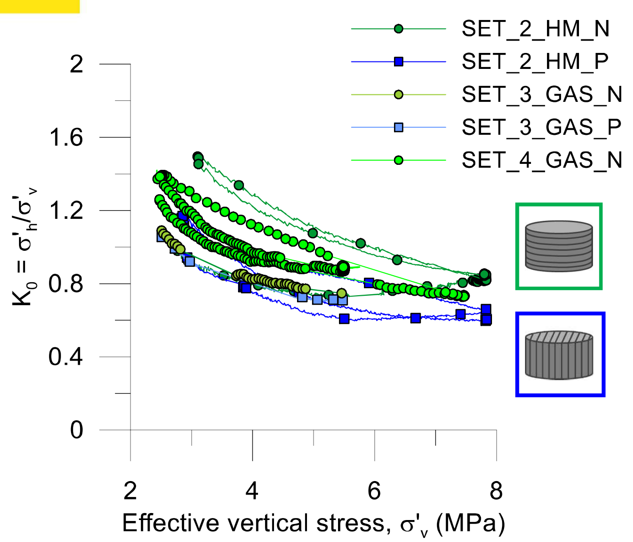

Drained unload stage

$$K_0^{OC} = K_0^{NC} \cdot OCR^n$$

$n = \sin(\phi') = 0.326$ with $\phi' = 19°$

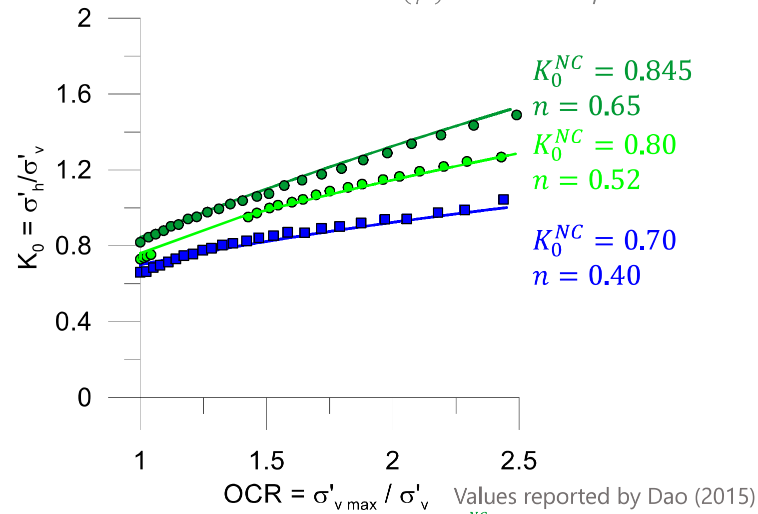

Values reported by Dao (2015)

$K_0^{NC} = 0.78 - 0.86$

$K_0^{NC} = 0.65 - 0.7$

OCR is computed in terms of the vertical effective stress, but it can be also expressed in terms of mean effective stresses

ADDITIONAL HYDRO-MECHANICAL PATH

❖ **SET2_HM_N**

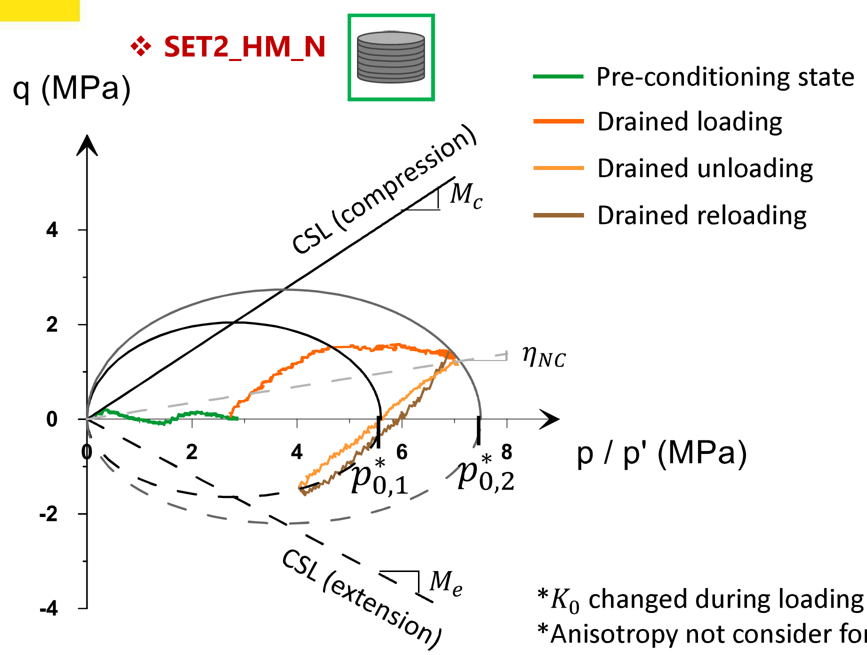

*K_0 changed during loading

*Anisotropy not consider for M_c and M_e

❖ Barcelona Basic Model Parameters:

- $\phi' = 19°$
- $M_c = 0.73$
- $M_e = 0.58$
- $p^*_{0,1} = 5.6\ MPa$
- $p^*_{0,2} = 7.5\ MPa$

$$p = \frac{1}{3}(\sigma_1 + 2\sigma_3) \qquad p' = \frac{1}{3}(\sigma'_1 + 2\sigma'_3)$$

$$q = (\sigma_1 - \sigma_3)$$

$$M_c = \frac{6\sin(\phi')}{3 - \sin(\phi')} \qquad M_e = \frac{6\sin(\phi')}{3 + \sin(\phi')}$$

$$\eta_{NC} = \frac{3(1 - K_0)}{(1 + 2K_0)}$$

ADDITIONAL HYDRO-MECHANICAL PATH

❖ **SET2_HM_P**

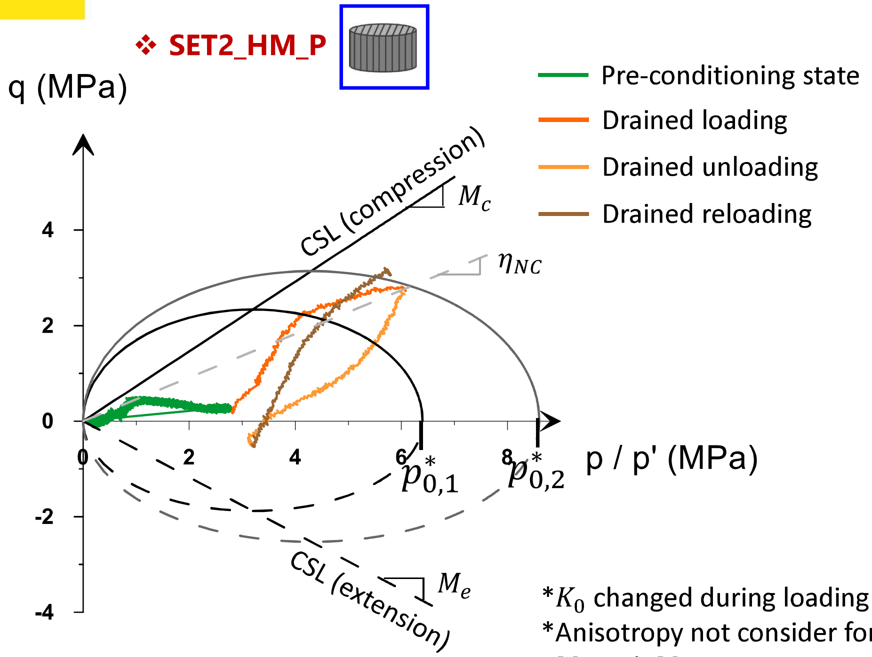

*K_0 changed during loading

*Anisotropy not consider for M_c and M_e

❖ Barcelona Basic Model Parameters:

- $\phi' = 19°$
- $M_c = 0.73$
- $M_e = 0.58$
- $p^*_{0,1} = 6.4\ MPa$
- $p^*_{0,2} = 8.6\ MPa$

$$p = \frac{1}{3}(\sigma_1 + 2\sigma_3) \qquad p' = \frac{1}{3}(\sigma'_1 + 2\sigma'_3)$$

$$q = (\sigma_1 - \sigma_3)$$

$$M_c = \frac{6\sin(\phi')}{3 - \sin(\phi')} \qquad M_e = \frac{6\sin(\phi')}{3 + \sin(\phi')}$$

$$\eta_{NC} = \frac{3(1 - K_0)}{(1 + 2K_0)}$$

ADDITIONAL HYDRO-MECHANICAL PATH TO ANALYSE THE POST-YIELD BEHAVIOUR

- Slope of post-yield compression line similar for both orientations

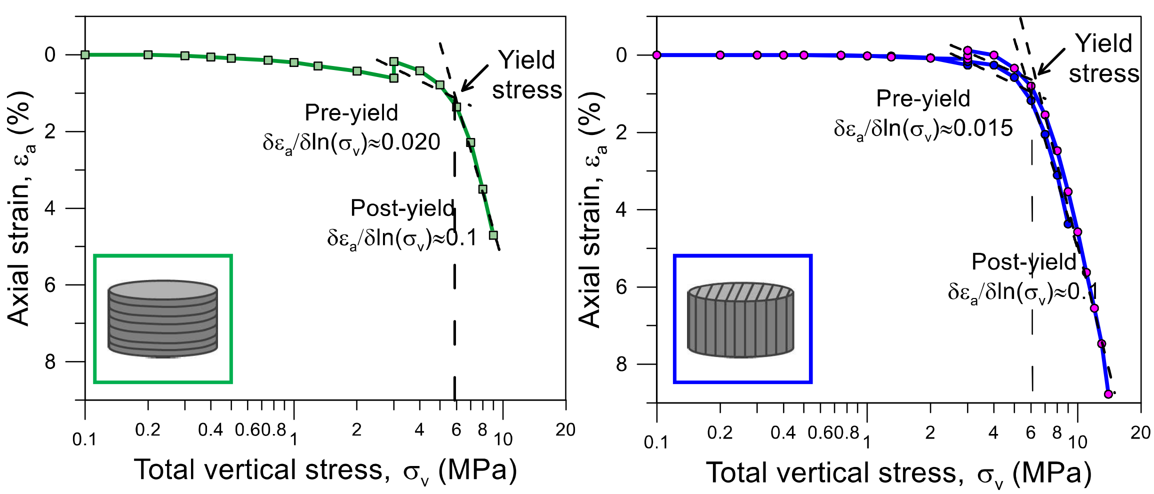

WATER PERMEABILITY

- Dependence of water permeability on porosity
- Higher water permeability with flow parallel to bedding planes (**anisotropy**)
- Loading to 8 MPa and unloading to 6 MPa causes a significant decrease in water permeability

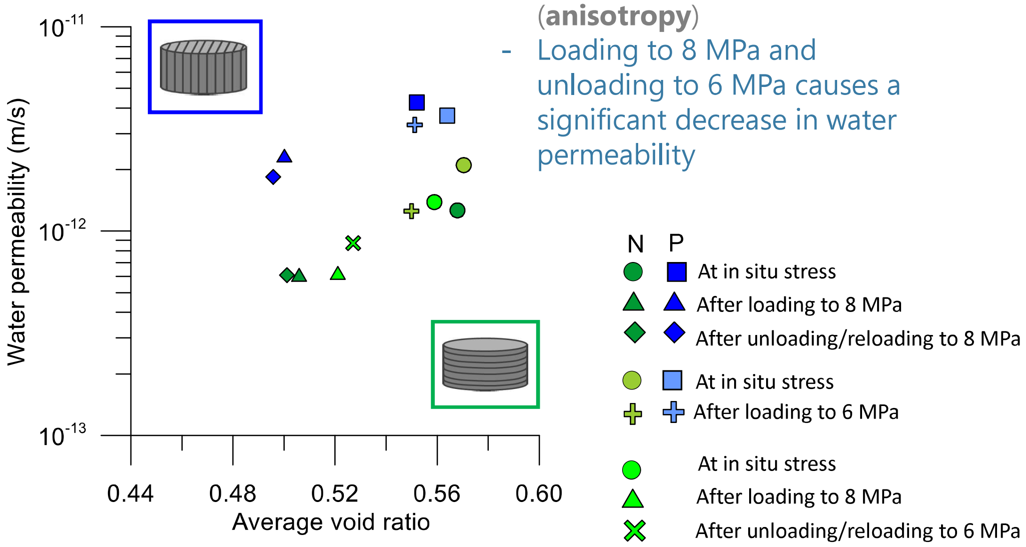

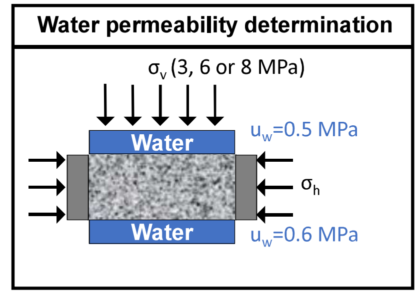

GAS INJECTION STAGES

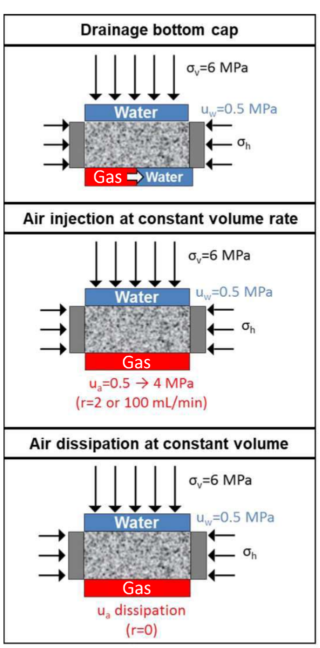

A→B: Gas injection at constant volume rate
B: Shut-off of the injection system
B→C: Gas dissipation at constant gas injection volume

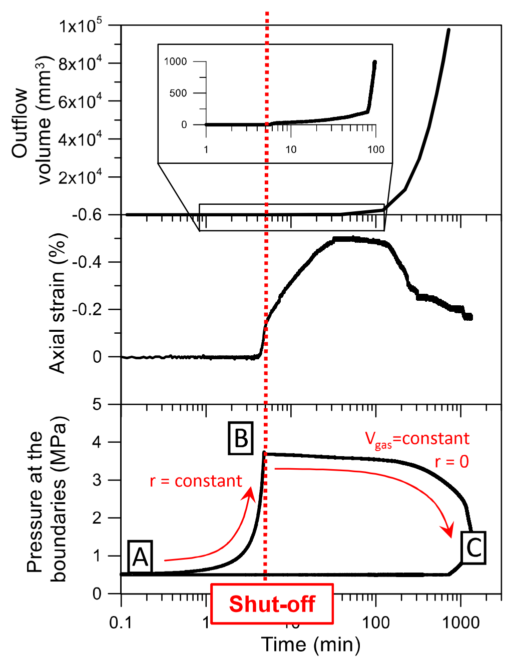

Tests performed:

Two orientations:
- flow normal to bedding planes
- flow parallel to bedding planes

Two volumetric rates:
- fast (r= 100 mL/min)
- slow (r= 2 mL/min)

Two gases:
- Air
- Helium

GAS INJECTION AND DISSIPATION
EFFECT OF BEDDING ORIENTATION AND INJECTION RATE

A→B: Fast air injection at constant volume rate 100 mL/min up to 4 MPa
- No important expansion detected
- No outflow detected

B→B': Shut-off and dissipation phase at constant injection volume
- Expansion while air pressure front propagates (constitutive stress decreases)

B'→C: Dissipation phase at constant injection volume
- When outflow volume rate increases, air pressure decreases and samples undergo compression (constitutive stress increases)

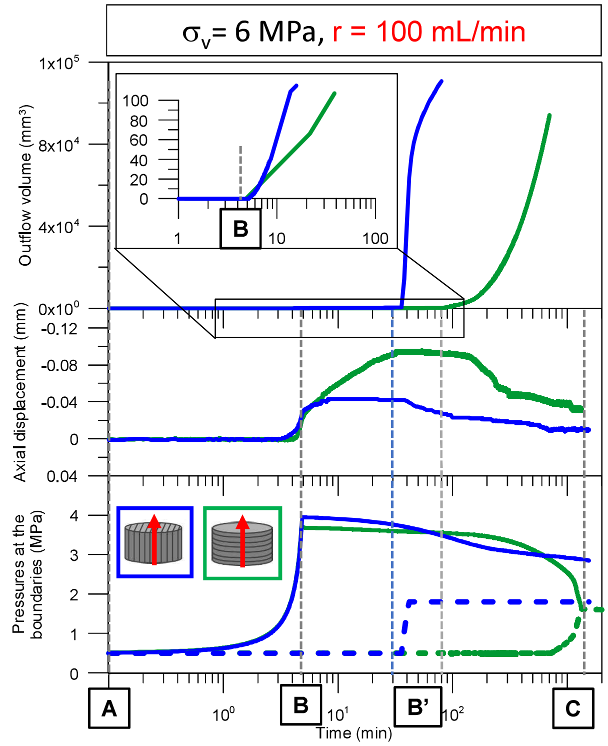

GAS INJECTION AND DISSIPATION
EFFECT OF BEDDING ORIENTATION AND INJECTION RATE

A→B: Slow air injection at constant volume rate 2 mL/min up to 4 MPa
- Expansion while air pressure front propagates (constitutive stress decreases)
- First outflow detected during the injection

B→C: Shut-off and dissipation phase at constant injection volume
- Immediately after shut-in, the outflow volume rate increases, the air pressure decreases and samples undergo compression (constitutive stress increases)

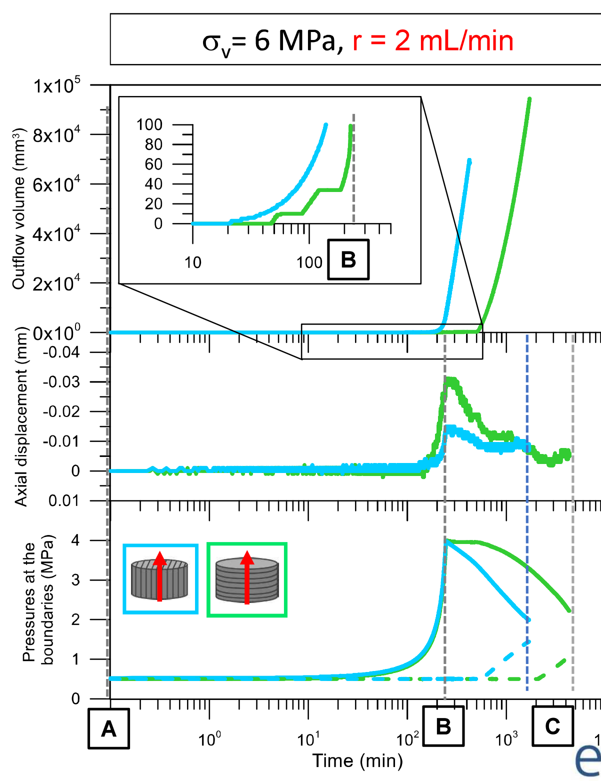

GAS INJECTION AND DISSIPATION
VOLUMETRIC BEHAVIOUR

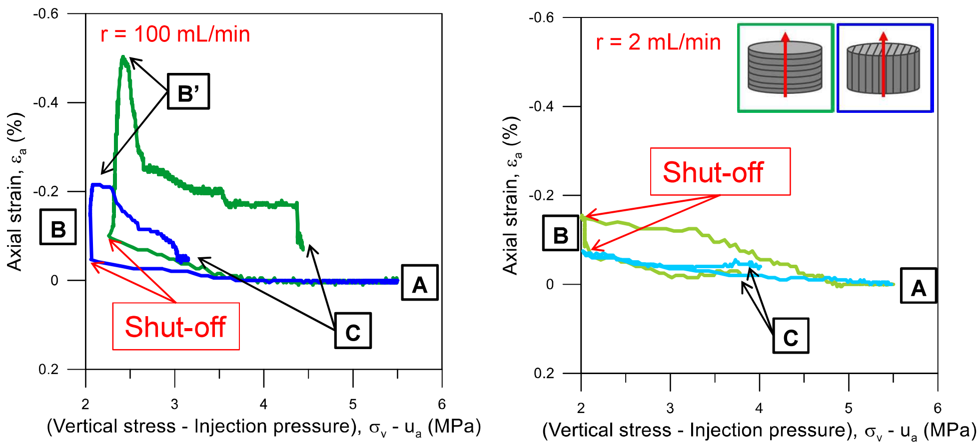

Significant effect of injection rate

Faster injections → higher expansions (samples expanded after shut-off during pressure front propagation)

Pore pressure nearly equilibrated during slower injections (no expansion after shut-off)

Important influence of bedding orientation under oedometer conditions

Samples with bedding planes normal to flow underwent higher expansions on air equalisation and larger compressions on the air dissipation stage (anisotropy)

GAS INJECTION AND DISSIPATION
AIR VS HELIUM

Similar behaviour found when Helium was used as injected gas in comparison with air:

- Slightly faster dissipation
- Slightly higher expansion

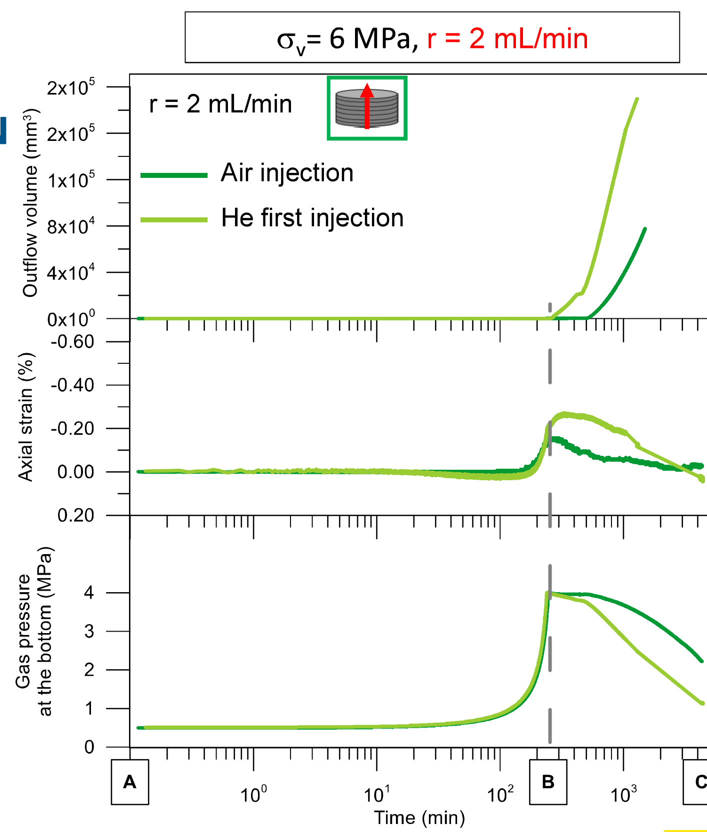

GAS INJECTION AND DISSIPATION
SUCCESSIVE INJECTION STAGES

The response during the second injection is rather similar to the first injection.

- Slightly higher expansion

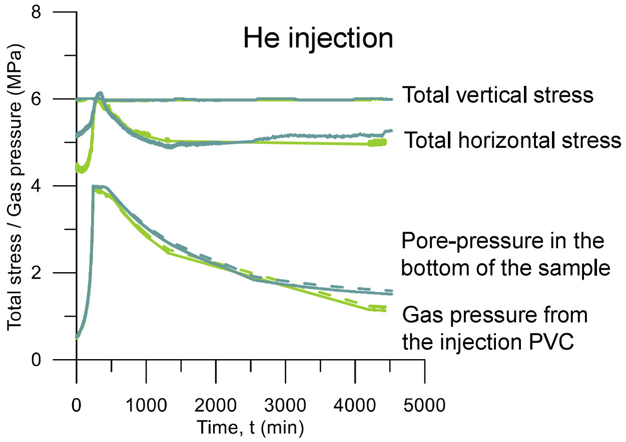

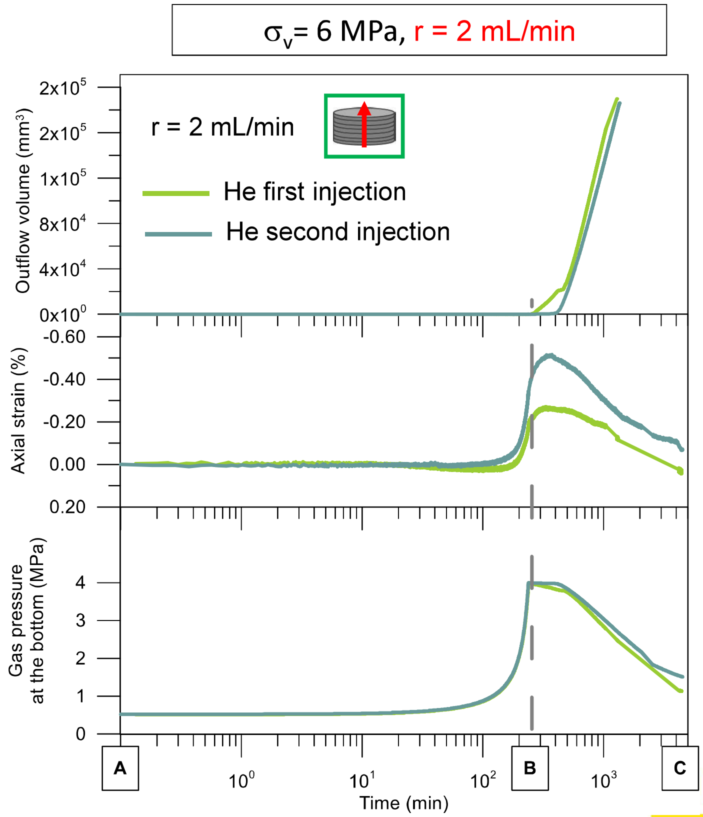

GAS INJECTION AND DISSIPATION
GAS PERMEABILITY FROM INJECTION PRESSURE DECAY DATA

$$K = -\frac{2LV_{in}\mu_g}{A((u_{in}(t))^2 - (u_{out}(t))^2)}\frac{du_{in}}{dt}$$

u_{in}: Injection pressure
u_{out}: pressure at recovery point
V_{in}: constant gas injection volume
L: height of sample
A: sample area
μ_g: gas viscosity

Assumptions:

- Steady-state conditions at high degrees of saturation (gas pathways desaturated)
- Flow cross-section equal to sample area
- Negligible gas diffusion though water

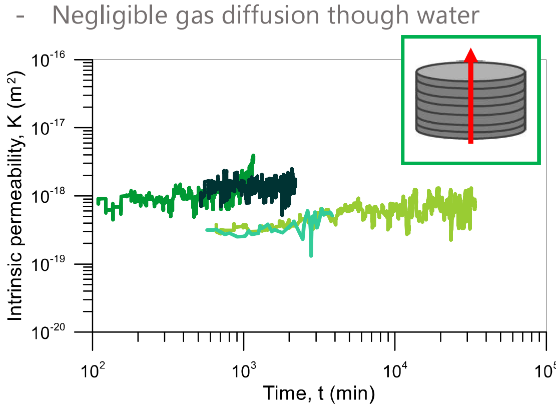

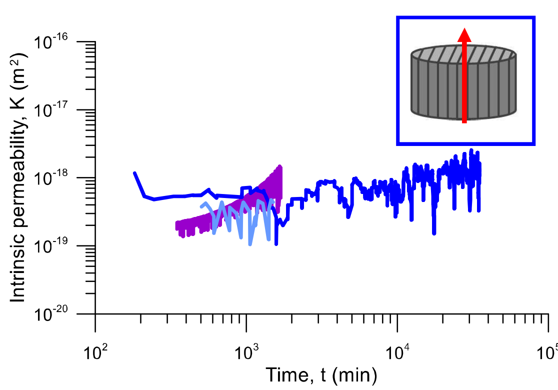

RE-SATURATION AFTER GAS INJECTION

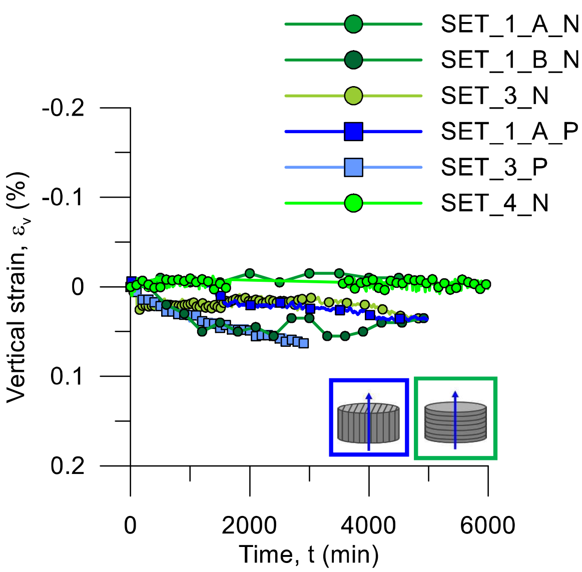

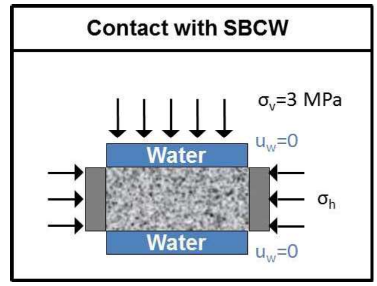

Very small deformations were recorded during the re-saturation stage, which indicated no important desaturation during gas migration

Bedding orientation	Injection stage	Volume of water expelled (mL)	Sr at the end of the injection
Bedding ⊥ flow	1st injection	2.22	0.87
	2nd injection	2.60	0.85
Bedding ⊥ flow	1st injection	2.82	0.83
	2nd injection	2.75	0.83

WATER PERMEABILITY AFTER GAS INJECTION

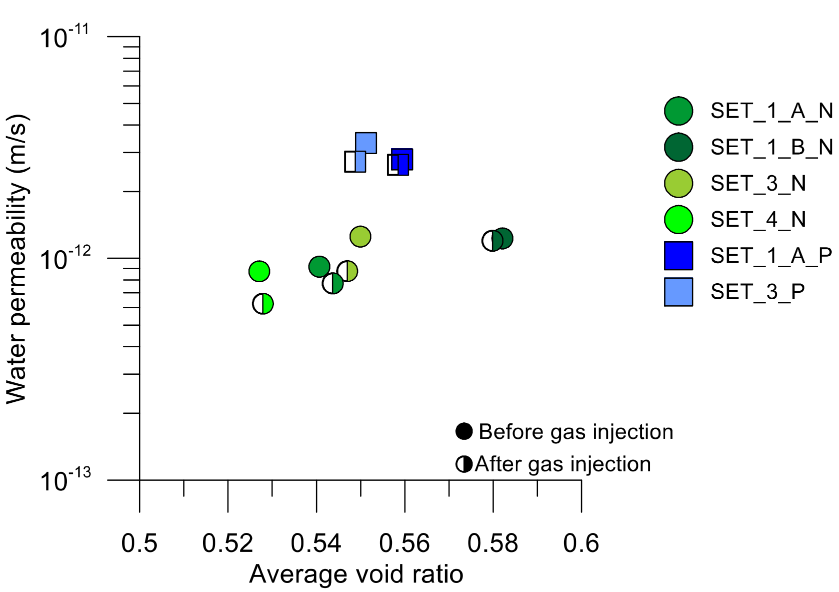

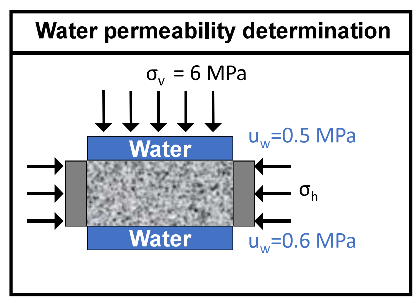

Water permeability before and after the gas injection does not present significant changes in either bedding orientations

Self-sealing of gas pathways due to the re-saturation process

WATER VS GAS PERMEABILITY

(Effective) permeability to gas determined during the dissipation stages was found to be higher than the (intrinsic) permeability to water.

No important anisotropic features were detected in the permeability to gas (it was not the case of the permeability to water with higher values with bedding planes parallel to flow).

(Effective) permeability to gas after re-saturation (2nd injection) is slightly higher than for the 1st injection. Although, after unloading/reloading this difference is insignificant.

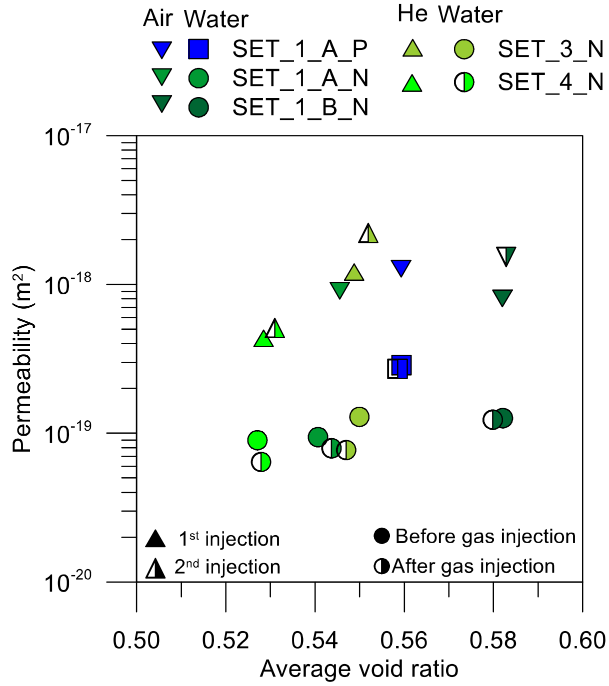

MICROSTRUCTURAL CHANGES INDUCED BY GAS MIGRATION: TECHNIQUES

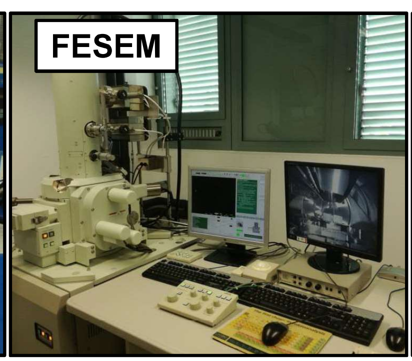

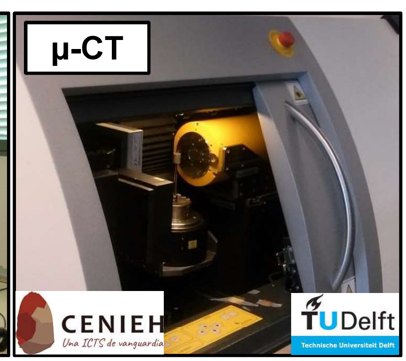

MIP
- Quantitative technique
- Intruded (connected) porosity
- Discerning different scales
- Pore size detection: 7 nm - 100 µm
- Shape through fractal analysis

FESEM
- Qualitative/quantitative technique
- Morphology of the surface
- Resolution depending on magnification (1 µm in this study)
- Image analysis (measuring distances, pores, aggregates, orientation etc.)

µ-CT
- Qualitative/quantitative technique
- 3D volume reconstruction
- Resolution depending on sample size (20 µm in this study)
- Image analysis (fissure volume through filtering process, connectivity, …)

Equivalent sizes and drying protocols (freeze-drying) to allow comparing techniques

MIP: PORE SIZE DISTRIBUTION AFTER GAS INJECTION

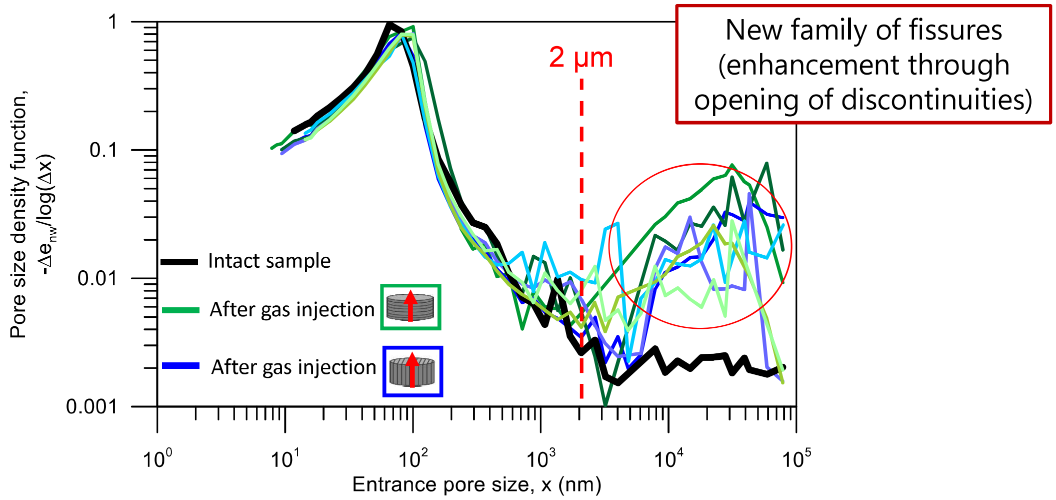

Bi-modal pore size distribution after air tests:
natural pores (matrix) and fissures (damage/degradation)

eurad

MIP: PORE SIZE DISTRIBUTION AFTER SELF-SEALING AND SECOND GAS INJECTION

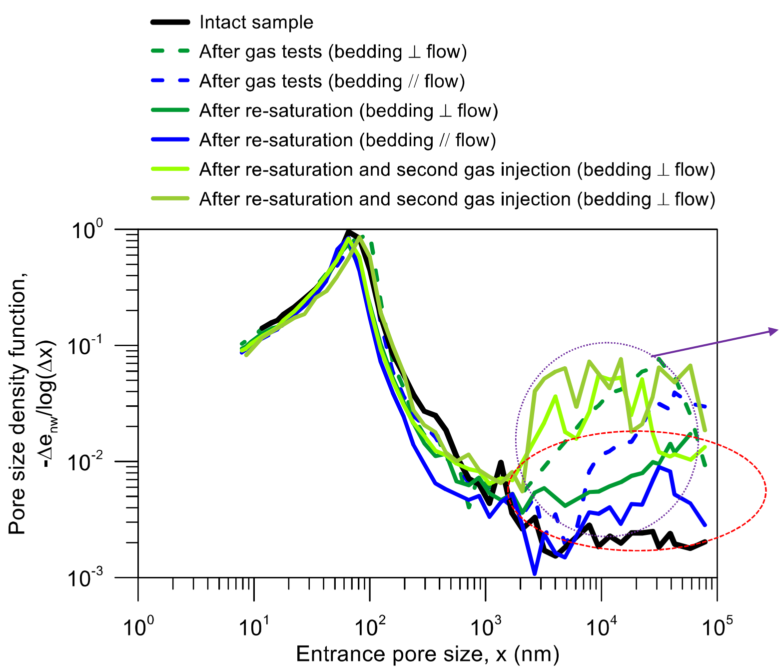

Small volume increase after the second gas injection

Lower volumes at the macro-scale after re-saturation, but slightly higher than on the intact sample

eurad

MIP: INFLUENCE OF THE UNLOADING PROCESS IN PORE SIZE DISTRIBUTION

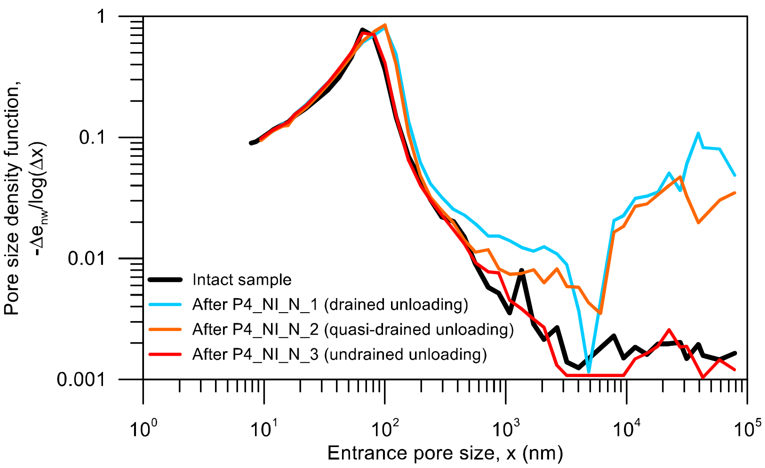

Influence of the unloading process on the final pore size distribution:

- Drained unloading process induces damage (opening of fissures) equivalent to air pressurization process
- Undrained unloading process does not modify the microstructure

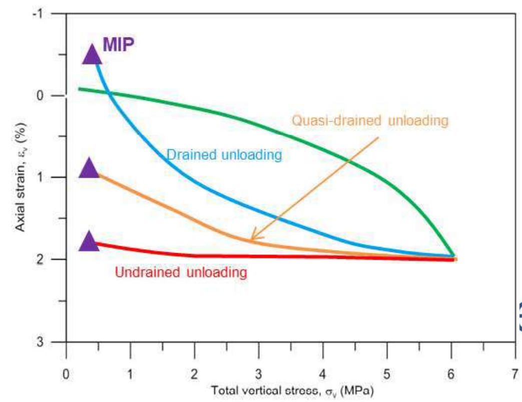

MICRO-CT: IMAGE TREATMENT

Procedure for μ-CT image analysis:

- Define Region of Interest (ROI)
- Identify features
- Volume reconstruction
- Filtering process (if required)
- Connectivity filter (if required)

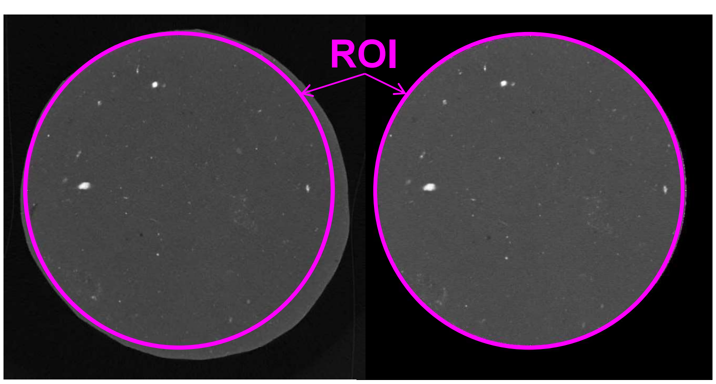

3D volume reconstruction (rendering) of intact sample

Bedding direction not visible

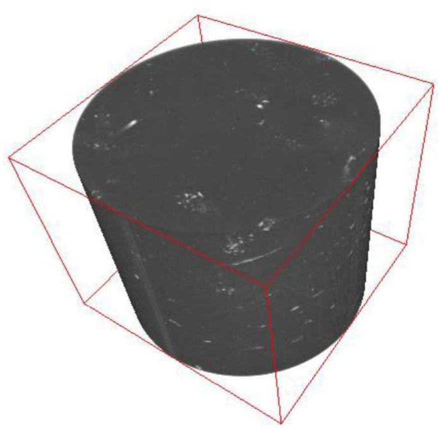

Software ImageJ

(Schneider et al, 2012)

MICRO-CT: FEATURES IDENTIFICATION

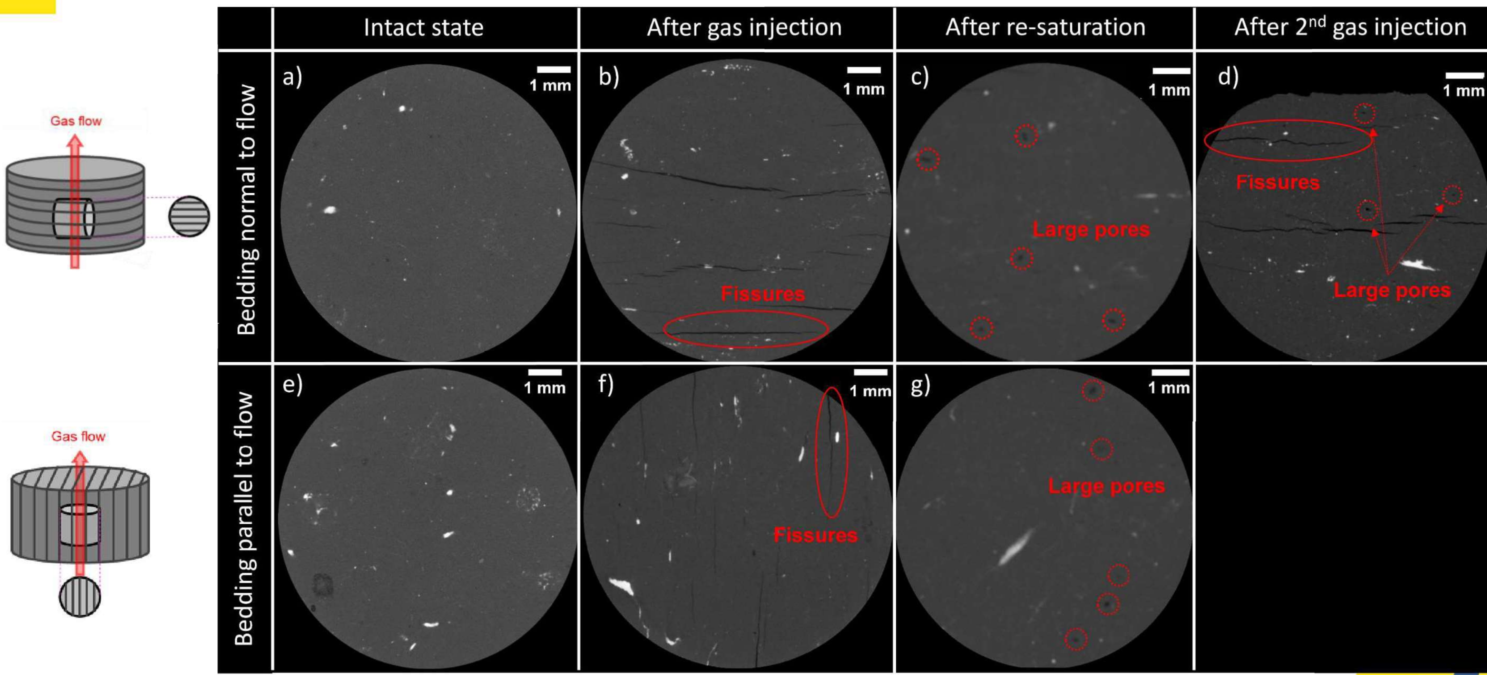

MICRO-CT: AFTER GAS INJECTION

Fissure filtering

Isolation of fissure pattern by using: Multiscale Hessian fracture filtering *(Voorn et al., 2013)*

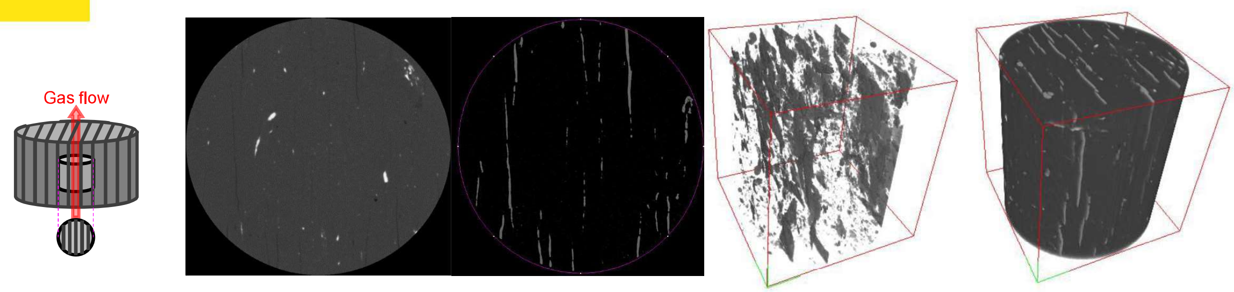

V_{sample} = 1900 mm^3
$V_{pores+fissures}$ = 712 mm^3
$V_{fissures}$ = 34.5 mm^3

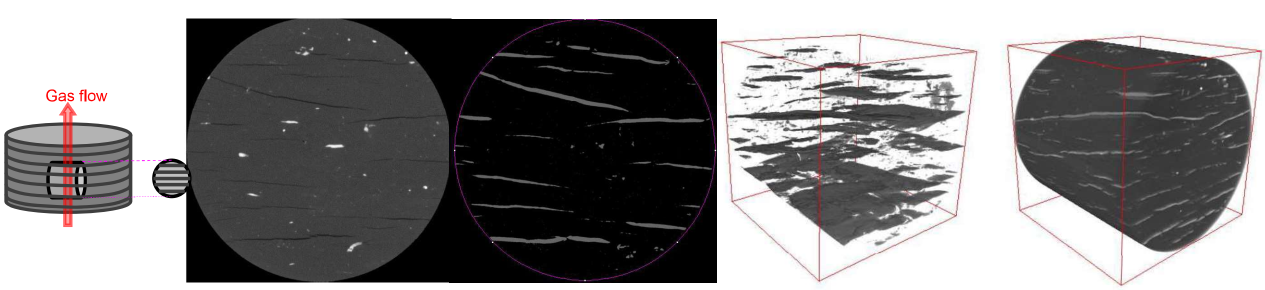

V_{sample} = 1600 mm^3
$V_{pores+fissures}$ = 960 mm^3
$V_{fissures}$ = 23.9 mm^3

MICRO-CT: FISSURE APERTURE

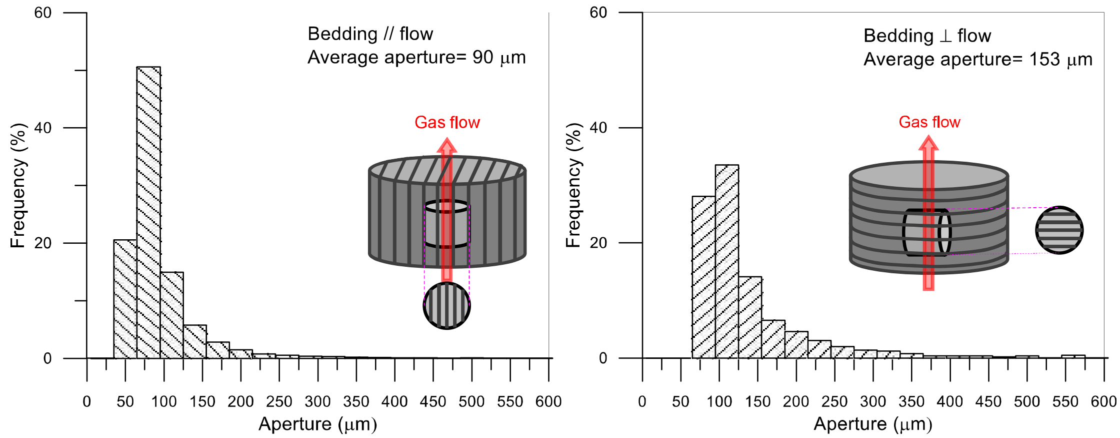

Fissures on the sample with bedding planes orientated parallel to gas flow were thinner than those with bedding planes oriented normal to flow

eurad

MICRO-CT: FISSURE SEPARATION

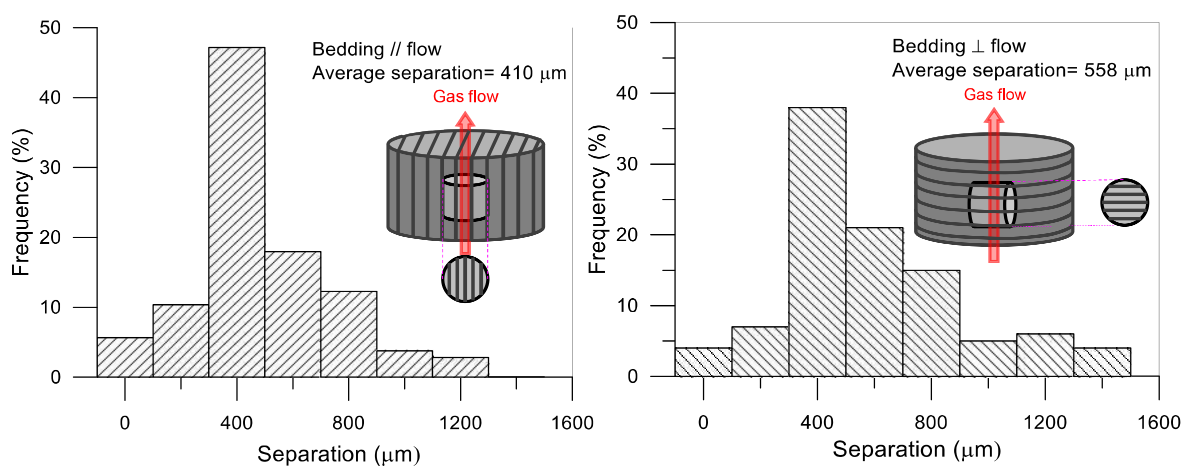

Fissures on the sample with bedding planes orientated parallel to gas flow were slightly closer than those with bedding planes oriented normal to flow

eurad

MICRO-CT: AFTER RE-SATURATION

After re-saturation

SET_1_A_P

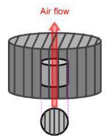

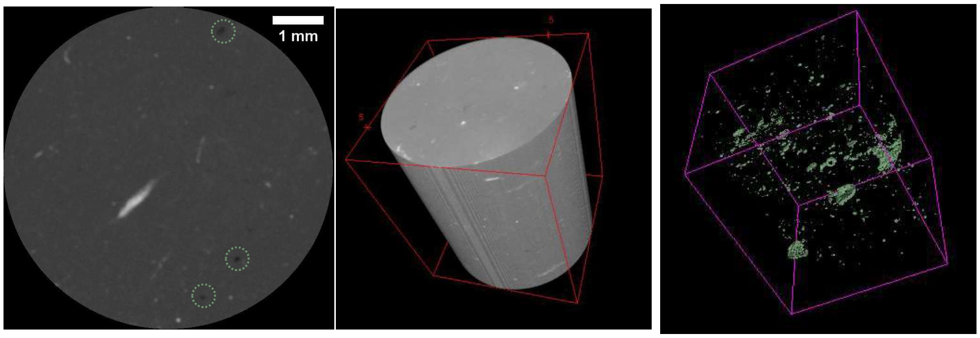

SET_1_A_N

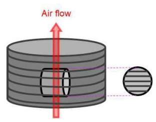

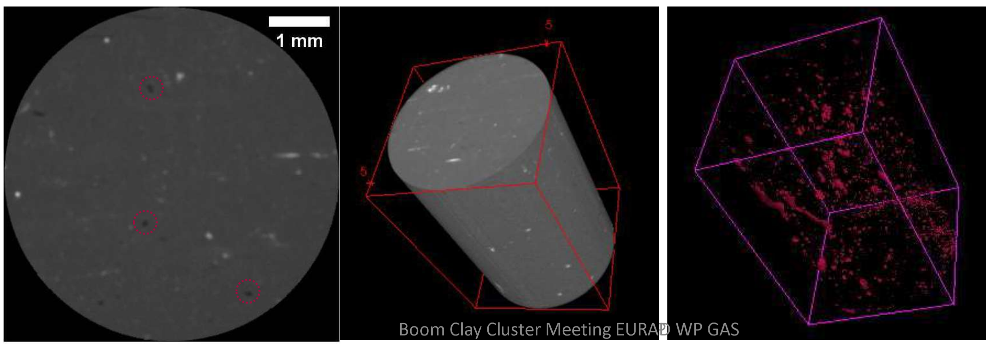

Large pores not detected at the intact state, are identified at both orientations, possibly due to gas entrapment during re-saturation and gas exsolution / gas bubble coalescence during the undrained unloading

The connectivity between these large pores was not detected by μ-CT (< 40 μm)

Pixel size 20 μm

MICRO-CT: AFTER SECOND GAS INJECTION

After second gas injection

SET_1_B_N

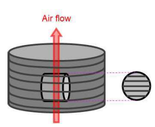

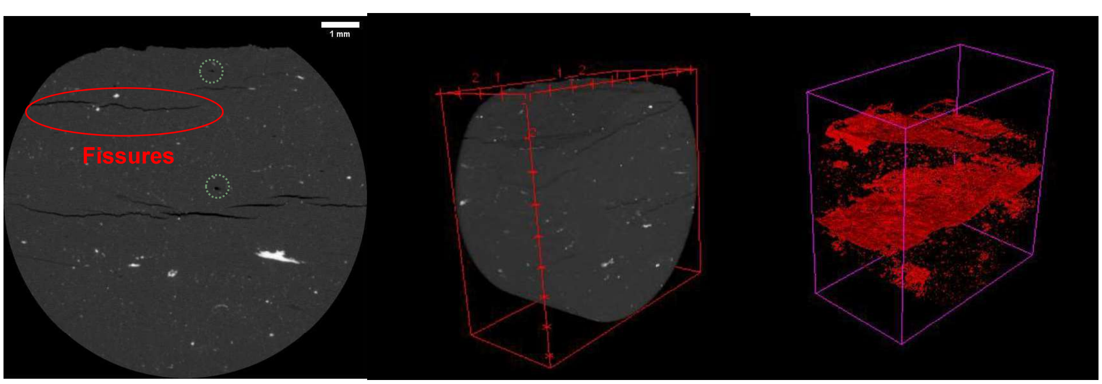

Large-aperture fissures and **large pores** are detected after the second gas injection. However, neither low-aperture fissures bridging bedding planes nor connection paths between large pores were detected (< 40 μm)

Pixel size 20 μm

MICRO-CT: AFTER SECOND GAS INJECTION

SET_3_N

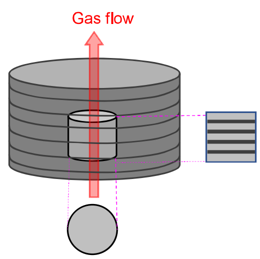

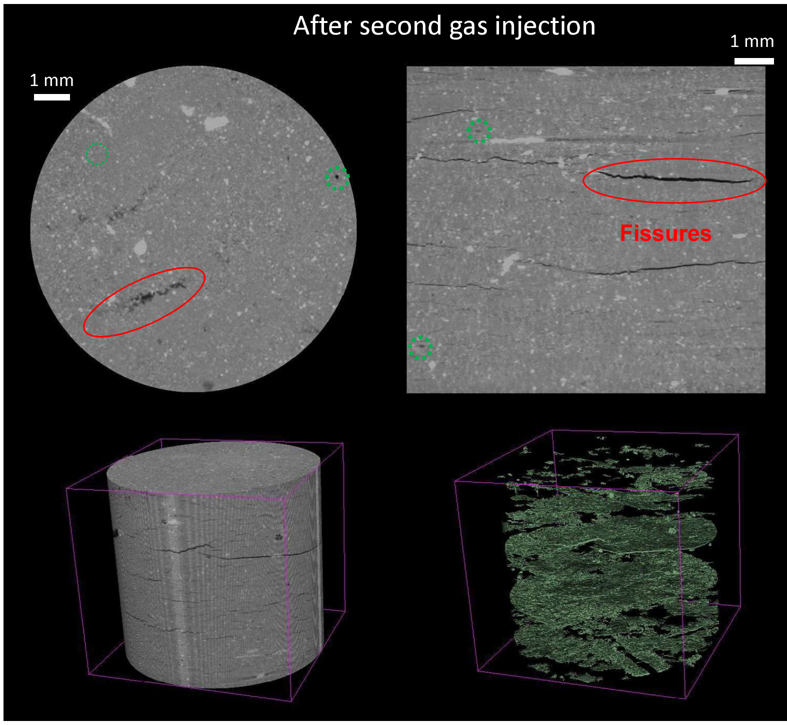

Large-aperture fissures and **large pores** are detected after the second gas injection. Low-aperture fissures bridging bedding planes can be discern, despite still unconnected (not continuous) (< 20 μm)

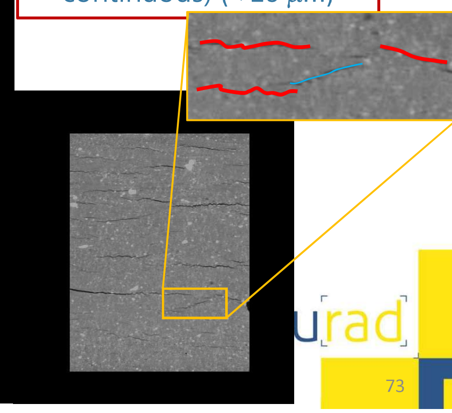

Pixel size 10 μm

FESEM: IMAGE BEFORE AND AFTER TESTS

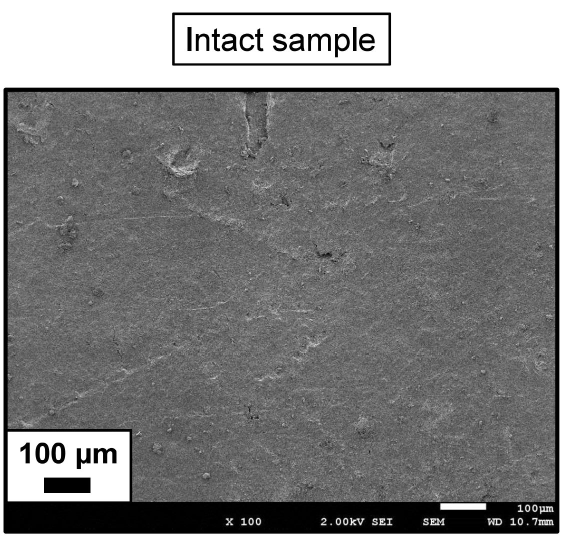

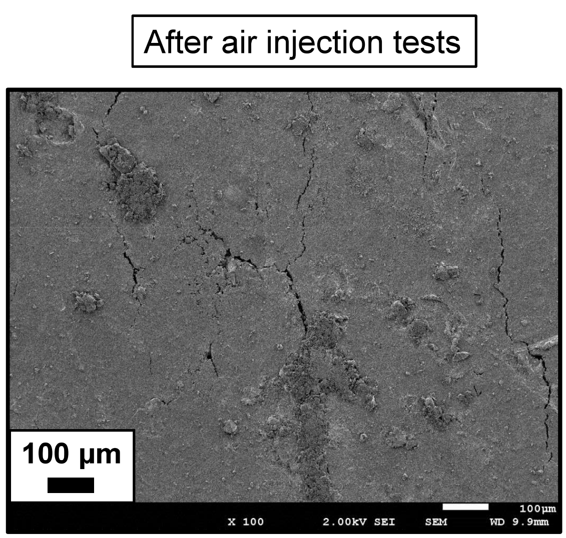

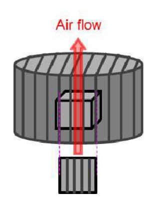

FESEM: IMAGE BEFORE AND AFTER TESTS

Intact sample

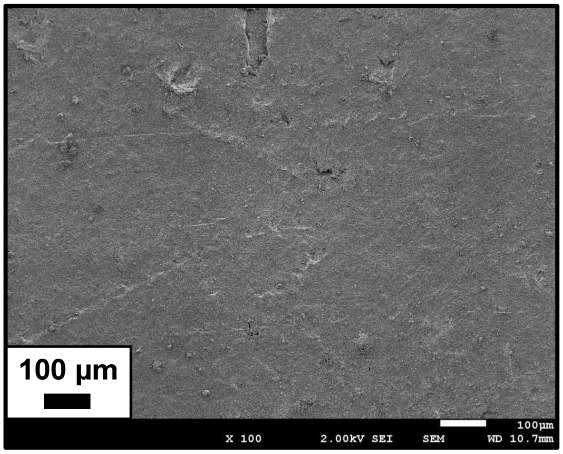

After air injection tests

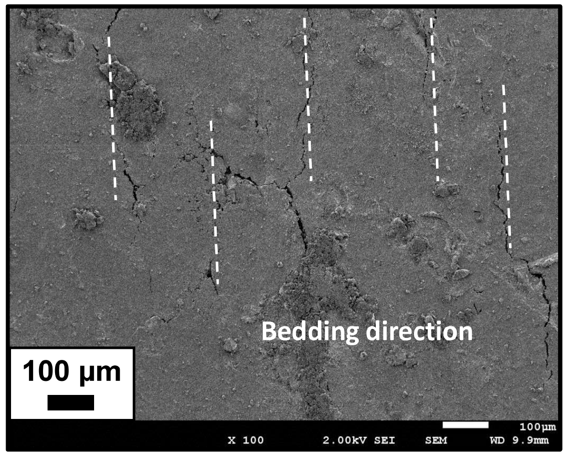

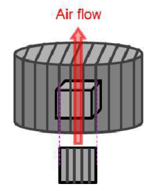

FESEM: IMAGE BEFORE AND AFTER TESTS

Intact sample

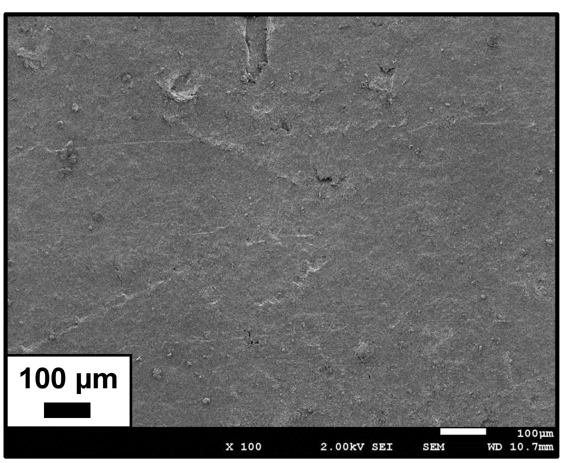

After air injection tests

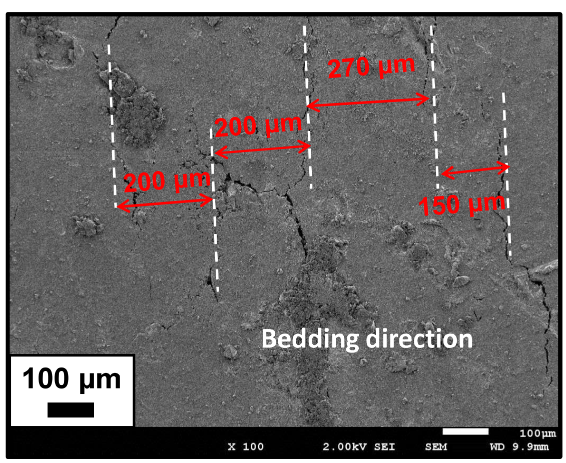

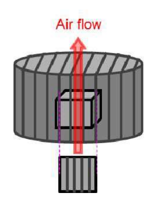

FESEM: IMAGE AFTER TESTS

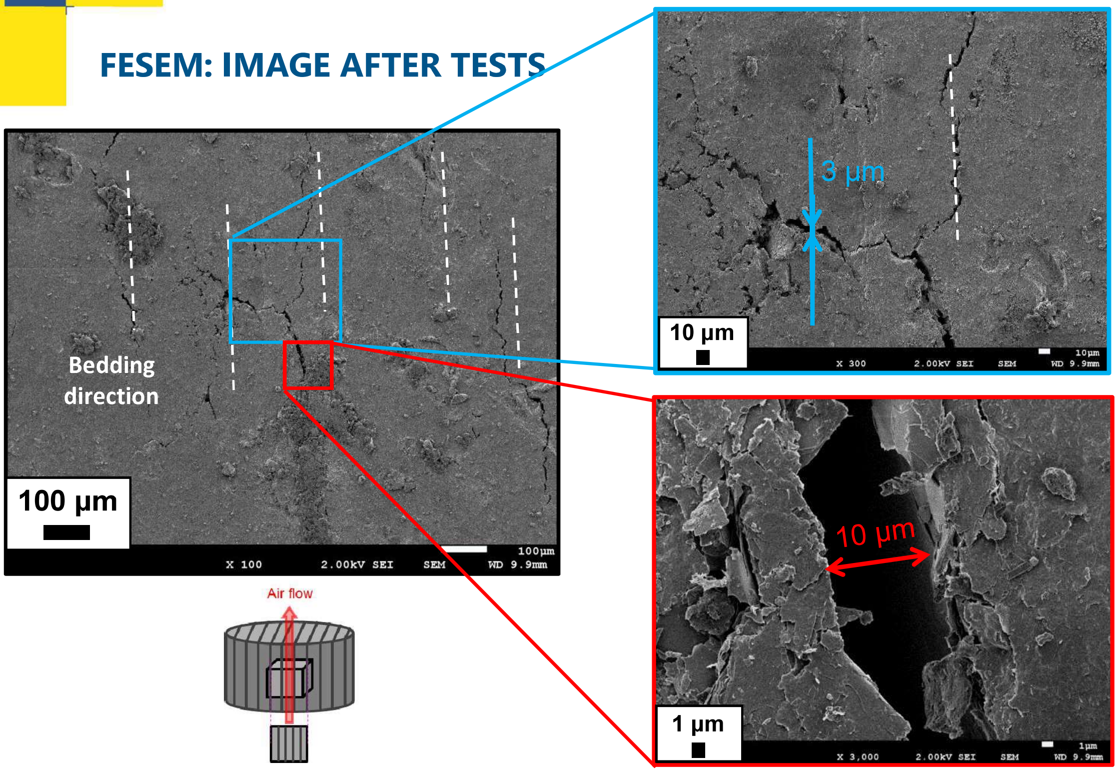

Low-aperture fissures bridging bedding planes

Large-aperture fissures following bedding direction

MICROSTRUCTURAL ANALYSIS: EVOLUTION OF PORE SIZE DISTRIBUTION

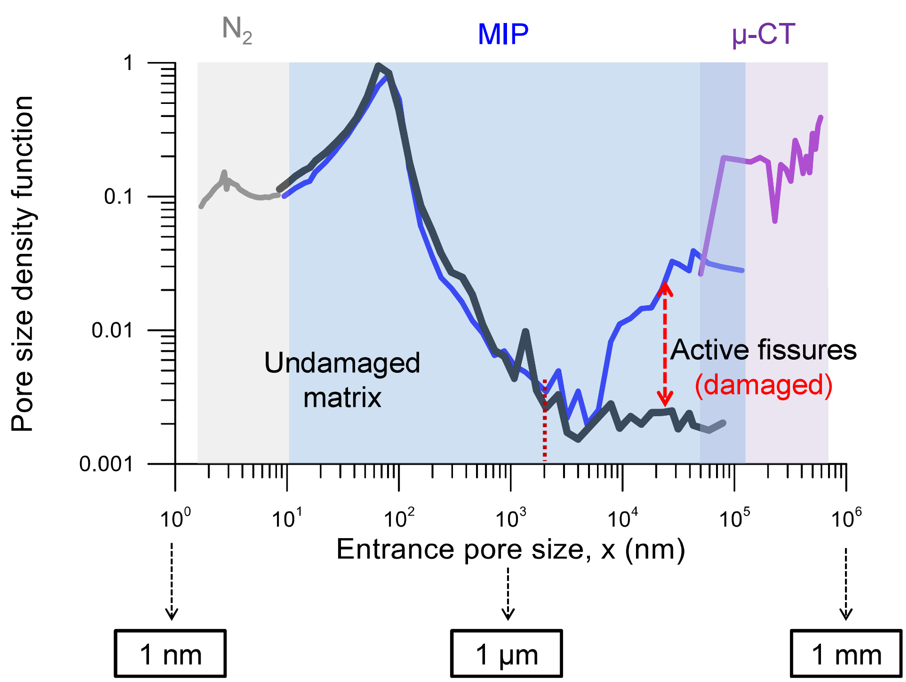

CONCEPTUAL MODEL

a) Water permeability: $k_{initial\ P} > k_{initial\ N}$

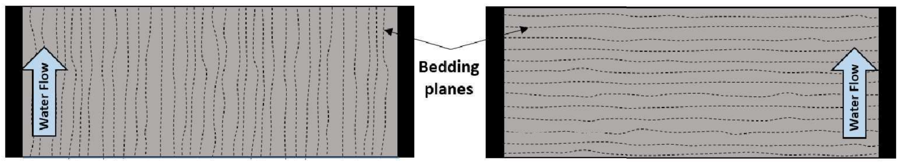

b) Gas injection: $k_P \approx k_N$ & $k_P/k_{initial\ P} < k_N/k_{initial\ N} \rightarrow \alpha_P < \alpha_N$

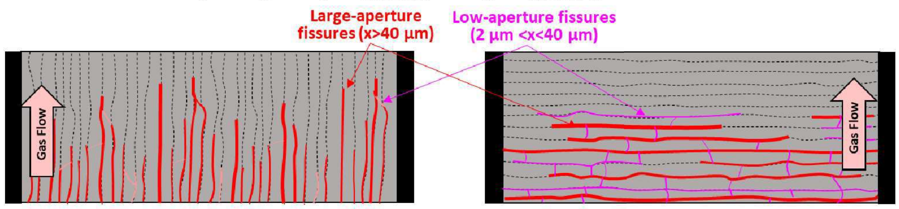

c) Re-saturation: $k_P \approx k_{initial\ P} > k_N \approx k_{initial\ N}$

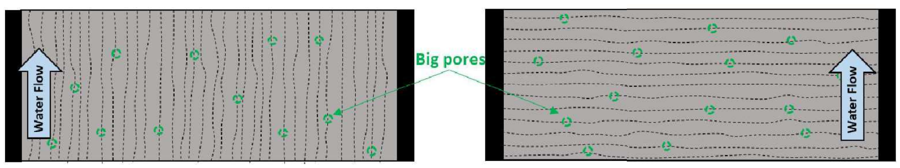

MACRO-FISSURED RATIO DETECTED AND FINAL DEGREE OF SATURATION

Void ratio: $e = \dfrac{V_m + V_M + V_f}{V_s}$

Macro void ratio:

$$e_M = \frac{V_M}{V_s}$$

e_M includes the 'connected' volume of large pores associated with (possible) gas entrapment / gas exsolution

Fissured void ratio:

$$e_f = \frac{V_{fissures}}{V_{solid}}$$

e_f includes the 'connected' volume of **large-aperture fissures** detected in the direction of the bedding planes with the µ-CT and low-aperture fissures bridging bedding planes which were not detected by µ-CT (< 40 µm)

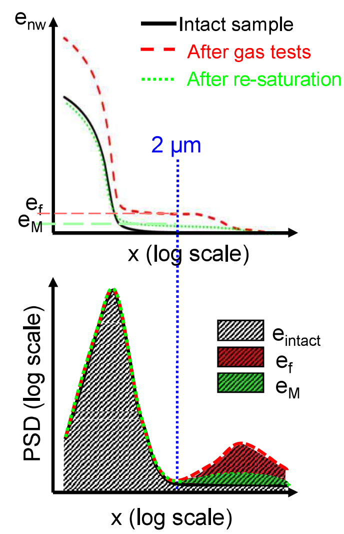

Macro-fissured ratio $\boxed{f = \dfrac{e_f + e_M}{e}}$

Final degree of saturation*

$\boxed{S_r = 1 - f}$

*Assuming all the fissures are unsaturated

MICROSTRUCTURAL ANALYSIS: INTERPRETATION

Sample	Orientation	Technique	$e_f + e_M$	f	S_r
After gas injection (e=0.560)	Bedding // flow	MIP (b>2 μm)	0.039	0.069	0.931
		MIP (b>40 μm)	0.025	0.044	0.956
		μ-CT (b>40 μm)	0.028	0.050	0.950
After gas injection (e=0.563)	Bedding ⊥ flow	MIP (b>2 μm)	0.041	0.070	0.930
		MIP (b>40 μm)	0.020	0.034	0.966
		μ-CT (b>40 μm)	0.014	0.024	0.976
After re-saturation (e=0.559)	Bedding // flow	MIP (b>2 μm)	0.015	0.028	0.972
		MIP (b>40 μm)	0.011	0.019	0.981
		μ-CT (b>40 μm)	0.011	0.020	0.98
After re-saturation (e=0.540)	Bedding ⊥ flow	MIP (b>2 μm)	0.024	0.044	0.956
		MIP (b>40 μm)	0.017	0.031	0.969
		μ-CT (b>40 μm)	0.019	0.035	0.965
After second gas injection (e=0.582)	Bedding ⊥ flow	MIP (b>2 μm)	0.087	0.149	0.851
		MIP (b>40 μm)	0.032	0.056	0.944
		μ-CT (b>40 μm)	0.034	0.059	0.941
After second gas injection (e=0.565)	Bedding ⊥ flow	MIP (b>2 μm)	0.086	0.152	**0.848**
		MIP (b>20 μm)	0.043	0.076	0.924
		μ-CT (b>20 μm)	0.038	0.067	0.933

MULTI-SCALE ANALYSES

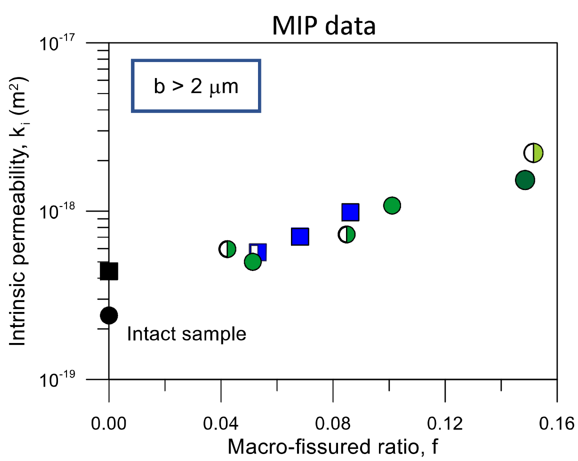

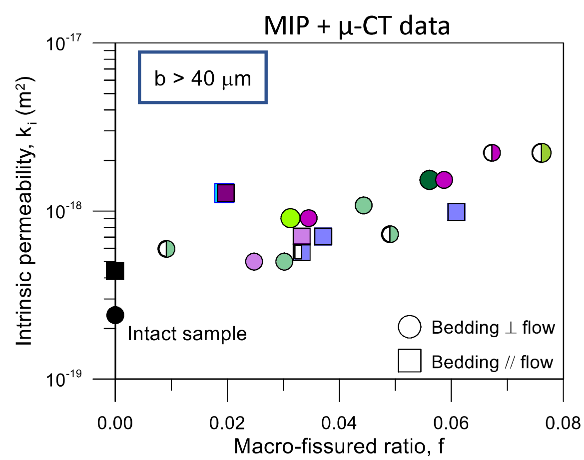

Macro-fissured ratio

$$f = \frac{e_f + e_M}{e}$$

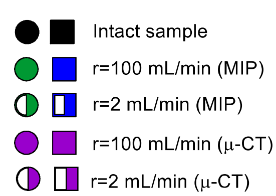

MULTI-SCALE MODEL

Permeability determined in the last stage (water or gas) is normalised with respect to the initial permeability to water (before any injection) to obtain a permeability ratio.

Model parameters

$$f_0 = \frac{e_M}{e} = 0.02$$ → Volume of macropores at the intact state (MIP data)
Independent of the bedding orientation

$$\boxed{\frac{k_i}{k_{ini}} = [\alpha(f - f_0) + 1]}$$

$$\alpha \begin{cases} \alpha_\perp = 84 \\ \alpha_{//} = 20 \end{cases}$$ → Fitting parameter with experimental data
Dependent of bedding orientation

Permeability to water before gas injection → **Anisotropy** at the initial state is taken into account with k_{ini}

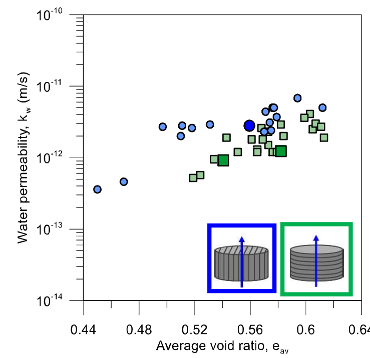

MULTI-SCALE MODEL

The permeability ratio relates linearly to the macro-fissured ratio for each orientation

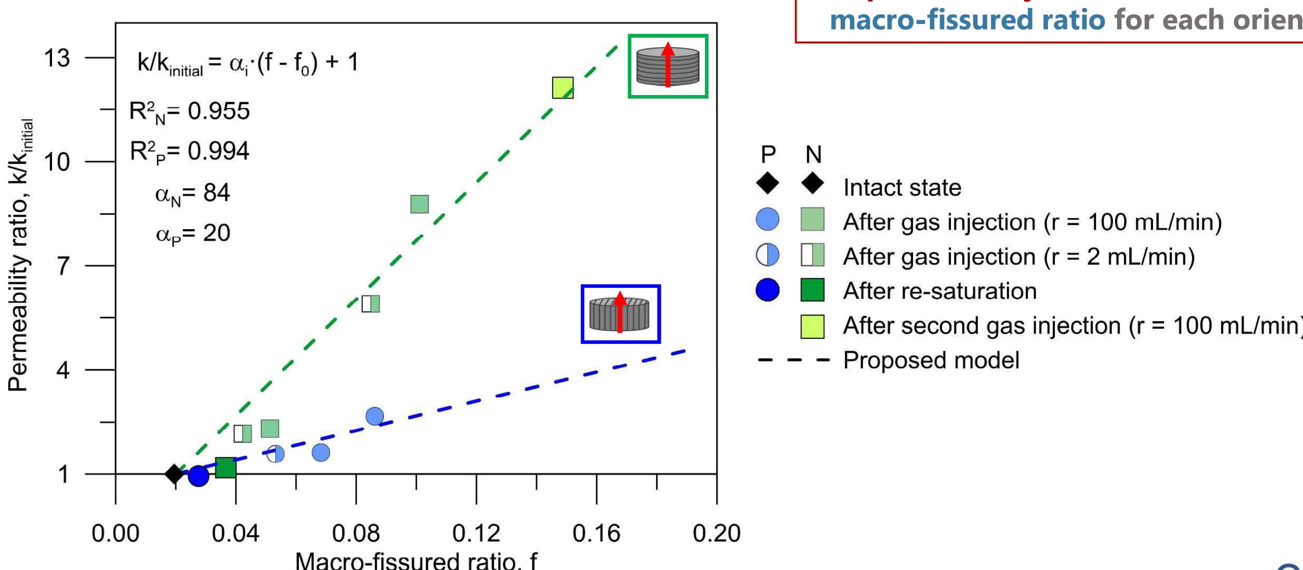

REFERENCES OF THIS WORK

- Gonzalez-Blanco, L., Romero, E., Jommi, C., Li, X. & Sillen, X. (2016). Gas migration in a cenozoic clay: Experimental results and numerical modelling. *Geomechanics for Energy and the Environment*, 6, pp.81–100.
- Gonzalez-Blanco, L., Romero, E., Li, X., Sillen, X., Marschall, P. & Jommi, C. (2016) Air injection tests in two argillaceous rock formations: experimental results and modelling. *1st International Conference on Energy Geotechnics ICETG, Kiel, Germany, Wuttke, Bauer & Sánchez (Eds.).*
- Gonzalez-Blanco, L., Romero, E., Jommi, C. Li, X. & Sillen, X. (2017). Exploring fissure opening and its connectivity in a Cenozoic clay during gas injection. Chapter in Springer Series in Geomechanics and Geoengineering, January, 2017 In book*: Advances in Laboratory Testing and Modelling of Soils and Shales (ATMSS)*, 288-295.
- Gonzalez-Blanco, L., (2017). Gas migration in deep argillaceous formations: Boom Clay and indurated clays. *PhD Thesis, Universitat Politècnica de Catalunya, Barcelona, Spain.*
- Gonzalez-Blanco, L., Romero, E., Marschall, P & Levasseur, S. (2022) Hydro-mechanical response to gas transfer of deep argillaceous host rocks for radioactive waste disposal. *Rock Mechanics and Rock Engineering*, 55, 1159-1177.
- Gonzalez-Blanco, L. & Romero, E. (2022) A multi-scale insight into gas migration in a deep Cenozoic clay. *Géotechnique*. Ahead of print
- Gonzalez-Blanco, L., Romero, E. & Levasseur, S. (2023) Self-sealing of Boom Clay after gas transport. *Rock Mechanics and Rock Engineering* (accepted)

OUTLINE OF THE LECTURE

1. **Motivation**
2. **Insight into gas transfer and self-sealing**
3. **Some observations regarding gas testing (experimental protocols)**
4. **A detailed research methodology on Boom Clay:**
   - **Material characterization**
   - **Stress paths followed**
   - **Gas test protocols**
   - **Test results at different scales (macroscopic results and microstructural features)**
5. **Final comments. Future challenges**

eurad

FUTURE CHALLENGES

Multi-scale experimental research is needed to comprehend the gas transport and self-sealing phenomena in saturated argillaceous rocks.

Macroscopic behaviour:
- Effect of stress state
- Gas transport mechanisms
- Gas effective permeability
- Recovery of hydraulic function

Microscopic observation:
- Opening of gas pathways
- Role of bedding planes
- Quantification of microstructural changes
- Effectiveness of self-sealing

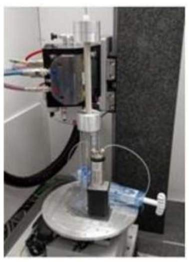

On-site tomography

- Real tracking of gas pathways during gas invasion
- No influence of unloading process or sample pre-treatment (freeze-drying)

eurad

eurad

European Joint Programme on Radioactive Waste Management

THANK YOU FOR YOUR ATTENTION!!

Financial support of ONDRAF/NIRAS (Belgium) and NAGRA (Switzerland) with CIMNE/UPC (Spain) through several research projects is greatly acknowledged

ONDRAF/NIRAS
Belgian Agency for Radioactive Waste and enriched Fissile materials

nagra.

REFERENCES

- Bernier, F, Li, X.L., Bastiaens, W., Ortiz, L., Van Geet, M., Wouters, L., Frieg, B., Blümling, P., Desrues, J., Viaggiani, G., Coll, C., Chanchole, S., De Greef, V., Hamza, R., Malinsky, L., Vervoort, A., Vanbrabant, Y., Debecker, B., Verstraelen, J., et al. (2007) Fractures and Self-healing within the Excavation Disturbed Zone in Clays (SELFFRAC). Final Report.
- Dao, L.Q. (2015) Etude du comportement anisotrope de l'argile de Boom. *PhD Thesis*, Université Paris-Est, France.
- Della Vecchia, G., Jommi, C., Lima, A., & Romero, E. (2011) Some remarks on the hydro-mechanical constitutive modelling of natural and compacted Boom clay. *International Conference of Unsaturated Soils*, Barcelona, Spain, Taylor & Francis Group, London.
- Di Donna, A., Charrier, P., Dijkstra, J., Andò, E. & Bésuelle, P. (2022) The contribution of swelling to self-sealing of claystone studied through x-ray tomography. *Physics and Chemistry of the Earth*, 127, 103191.
- Hemes, S., Desbois, G., Urai, J.L., Schröppel, B. & Schwarz, J.O. (2015) Multi-scale characterization of porosity in Boom Clay (HADES-level, Mol, Belgium) using a combination of X-ray μ-CT, 2D BIB-SEM and FIB-SEM tomography. *Microporous and Mesoporous Materials*, 208, 1–20.
- Marschall, P., Horseman, S., & Gimmi, T. (2005) Characterisation of Gas Transport Properties of the Opalinus Clay, a Potential Host Rock Formation for Radioactive Waste Disposal. *Oil & Gas Science and Technology*, 60(1), 121–139.
- ONDRAF/NIRAS (2016) Conceptualisations of gas related issues. *Workshop on gas related issues in clay based repository programmes.*
- Pineda, J., Alonso, E.E. & Romero, E. (2014) Environmental degradation of claystones. *Géotechnique*, 64(1), 64–82.

REFERENCES

- Pineda, J., Romero, E., Alonso, E. Pérez, T. (2014) A New High-Pressure Triaxial Apparatus for Inducing and Tracking Hydro-Mechanical Degradation of Clayey Rocks. *Geotechnical Testing Journal*, 37 (6), 1-15.
- Romero, E. & Gonzalez-Blanco, L. (2019) Hydro-mechanical processes associated with gas transport in MX-80 Bentonite in the context of Nagra's RD&D programme. Nagra Technical Report NAB 19-06.
- Romero, E., Arnedo, D., Alonso, E.E., & Marschall, P. (2010) Gas Injection Laboratory Experiments on Opalinus Clay. *In: Clays in Natural & Engineered Barriers for Radioactive Waste Confinement,* 4th International Meeting, March 2010, Nantes, France, pp. 113–114.
- Salehnia, F., Collin, F., Li, X., Dizier, A., Sillen, X. & Charlier, R. (2015) Coupled modeling of Excavation Damaged Zone in Boom clay: Strain localization in rock and distribution of contact pressure on the gallery's lining. *Computers and Geotechnics*, 69, 396-410.
- Sau, N. (2021) THM coupled behavior of a deep indurated argillaceous formation. *PhD Thesis*, Universitat Politècnica de Catalunya, Spain.
- Sau, N., Romero, R. & Van Baelen, H. (2020) Restoring initial conditions in a deep argillaceous formation with induced suction on retrieval. *E3S Web of Conferences* 195, 04012.
- Schneider, C.A., Rasband, W.S., & Eliceiri, K.W. (2012) NIH Image to ImageJ: 25 years of image analysis. *Nature Methods*, 9 (7), 671–675.

REFERENCES

- Sillen, X. & Marivoet, J. (2007) Thermal impact of a HLW repository in clay. *External Report SCK·CEN-ER-38*.
- Van Geet, M., Baestiaens, W. & Ortiz, L. (2008) Self-sealing capacity of argillaceous rocks: Review of laboratory results obtained from the SELFRAC project. *Physics and Chemistry of the Earth*, 33 (1), S396-S406.
- Voltolini, M. & Ajo-Franklin, J.B., 2020. The Sealing Mechanisms of a Fracture in Opalinus Clay as Revealed by in situ Synchrotron X-Ray Micro-Tomography. *Frontiers in Earth Science*, 8, 207.
- Voorn, M., Exner, U. & Rath, A. (2013) Multiscale Hessian fracture filtering for the enhancement and segmentation of narrow fractures in 3D image data. *Computers & Geosciences* 57, 44-53.
- Zhang, C.L. & Talandier, J. (2022) Self-sealing of fractures in indurated claystones measured by water and gas flow. *Journal of Rock Mechanics and Geotechnical Engineering*, 15(1), 227-238.
- Zhang, C.L. (2013) Sealing fractures in claystone. *Journal of Rock Mechanics and Geotechnical Engineering*, 5, 214-220.

Appendix H. Experimental Testing of BCV Bentonite (J. Svoboda)

EXPERIMENTAL TESTING OF BCV BENTONITE
WP HITEC AND GAS

JIŘÍ SVOBODA

CTU IN PRAGUE

This project has received funding from the European Union's Horizon 20 research and innovation programme 2014-2018 under grant agreement N°847593

European Joint Programme on Radioactive Waste Management

BCV

- BCV = Bentonite Černý Vrch
- Reference bentonite for research in Czech Republic
- Mg-Ca Bentonite

Wt.%	Anatase	Quartz	Montmorillonite	Mg-calcite	Goethite	Hematite	Kaolinite	Ankerite	Siderite	Illite
Original BCV	2.3	11.4	69.7	3.7	3.1	-	5	0.6	0.5	3.7

Wt.%	SiO_2	TiO_2	Al_2O_3	Fe_2O_3	FeO	MgO	MnO	CaO	Na_2O	K_2O	P_2O_5	F	CO_2	C	S	$H_2O(+)$	Total
BCV	51.86	2.34	15.56	11.41	0.14	2.82	0.2	2.83	0.37	1.02	0.51	0.12	1.68	0.17	< 0.010	9.06	100.09

	BCV_2017
Na^+ (%)	**11**
Ca^{2+} (%)	**23**
K^+ (%)	2
Mg^{2+} (%)	**64**
CEC_{Cu-VIS} ($mmol^+ \cdot 100\ g^{-1}$)	60.9

BENTONITE

- Bentonite is the name for a claystone which contains as main component the clay mineral Montmorillonite.
- The name bentonite comes from the „Fort Benton“ in the US state Wyoming, where geologists found at the end of the 19th century a plastic soil with unusual properties, which they called Bentonite.
- Bentonite was used already by the old indians as a kind of soap for washing their clothes.

MONTMORILLONITE

- Near the town Montmorillon (SW part of France) a plastic clay deposit had been discovered by French geologists, at the end of 19th century.
- Montmorillonite is the most important representative of the group of swellable three-layer minerals, which are called Smectites.
- The content of Montmorillonite is one of the most important quality parameter for raw bentonite as well as for processed bentonite products.

wikipedia

3.3 Clay minerals

3.3.1 Main minerals

Common clay mineral types are /2/:

- Halloysite
- Kandites (kaolinites, dickite, nacrite)
- Smectites (montmorillonite, saponite, nontronite, beidellite)
- Illite
- Vermiculite
- Chlorites
- Palygorskite group (attapulgite, sepiolite)

SKB: Buffer and Backfill handbook

SMECTITE STRUCTURE

Li < Na < K < Ca < Mg < NH_4

”Ca/ Mg/ Na bentonite”

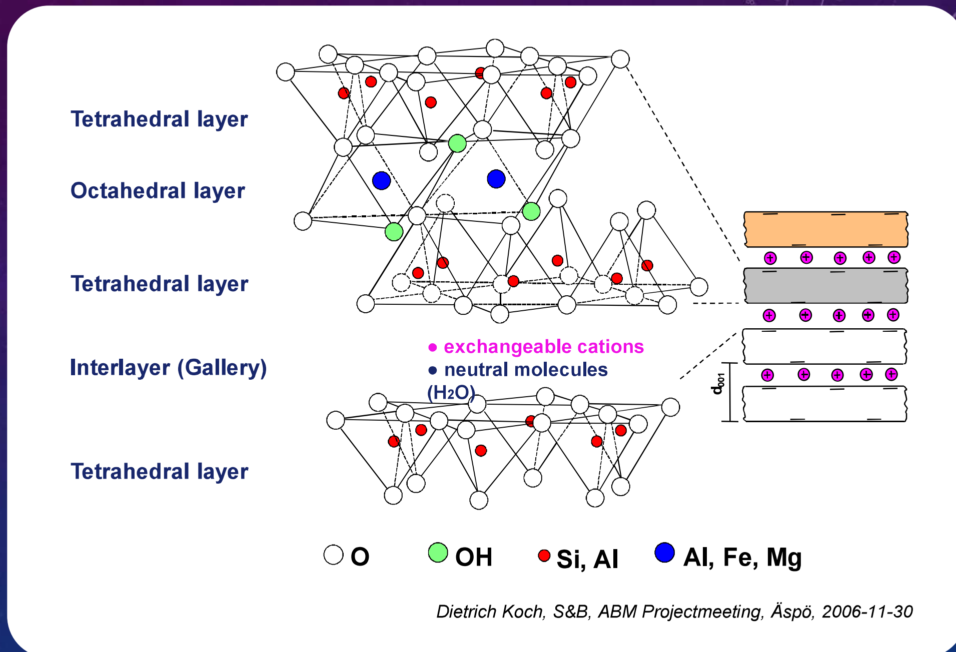

Dietrich Koch, S&B, ABM Projectmeeting, Äspö, 2006-11-30

BENTONITE

- Naturally occurring material → Inhomogeneities → Uncertainty/**Natural spread** in material properties, accessory minerals – ***known unknown***
- Industrially processed for most needs (including DGR)

- Various forms
  - Natural form
  - Processed
    - **Powder**
    - **Pellets**
    - **Compacted blocks**

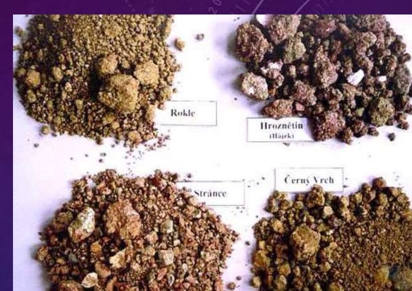

SKB: TR-17-06

ROLE OF BENTONITE IN EBS

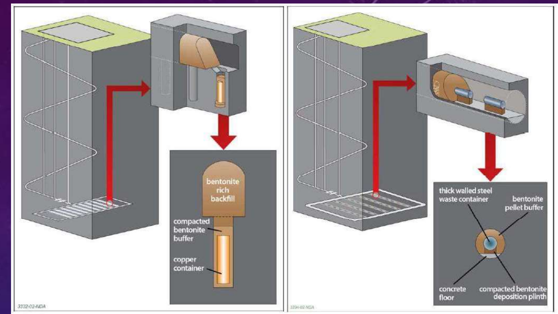

Figure 2-26. RWM illustrative designs for a higher strength rock (based upon KBS-3V, left) and lower strength sedimentary rock type (based upon NAGRA concept, right) after RWM (2016)

Bentonite is main material of buffer and backfill

- Buffer – surrounds waste package
  - Waste package protection (from host rock movements,…)
  - Isolation of waste (physical, hydraulic, chemical,…)
  - Minimise radionuclide release to environment (limit water movement, sorption,…)
  - Heat transfer
- Backfill – (back)filling of all empty spaces in DGR (galleries, tunnels, shafts,…)
  - Hydraulic isolation of EBS system
  - Support for backfill

Requirements on properties of EBS system/materials → **bentonite**

REQUIREMENTS ON BENTONITE

- **Long-term stability** — **- properties shall be predictable for the lifetime of repository**

  Hint: Natural analogues
- Extremely low permeability - limitation of water movement (corrosion, pollutant transfer)
- Extremely high plasticity - mechanical protection and sealing
- Swelling - sealing
- Self-healing - sealing, recovery after damage
- High thermal conductivity - cooling of waste package
- …

Note: Performance of bentonite (properties) depend on density and water content

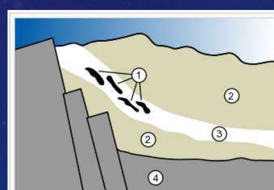

Geological situation in Gabon leading to natural nuclear fission reactors

1. Nuclear reactor zones
2. Sandstone
3. Uranium ore layer
4. Granite

wikipedia

EBS ERECTION

Bentonite has to be emplaced – technological process

→ Unknowns due to technology/installation of EBS

- Gaps/joints between blocks & layers
- Free space between pellets

- Unfilled voids (or less material) due to technological reasons
  - Space for tools and manipulation
  - Emplacement accuracy
  - Tolerances/Uneven surfaces
  - Too small space to access/fill
  - Errors…

Note: the installation method has influence on average density of emplaced component

SKB: TR-17-06

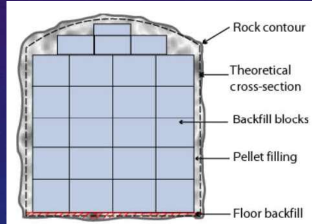

Figure 1-2. Cross section of a backfilled KBS-3V deposition tunnel showing the three main components of the backfill. 1) precompacted blocks, 2) pellet fill and 3) material placed under the blocks to provide stable foundation for the blocks (Keto et al. 2009a).

Figure 2-12. Placement trials of tunnel fill using twin-auger technique. (De Bock et al. 2008: Note NAGRA canister-sized cylinder placed in tunnel.)

SKB: P-11-44

WHAT SHOULD WE TEST AND WHY?

- Material properties and composition
  - Density dependent
  - Water content dependent

- System properties
  - Heterogenous materials
  - Material in various form in one system
  - Discontinuities, gaps, …

- Influence of:
  - Temperature
  - Water (flow, composition,…)
  - Disturbing events (gas breakthrough, seismic activity,…)
  - …

GAS

MECHANISTIC UNDERSTANDING OF GAS TRANSPORT IN CLAY MATERIALS

GAS – TYPICAL AND ALTERNATIVE APPROACH (DILATANT FLOW/FRACTURATION)

- Typical - Gas breakthrough test
  - Slow injection of gas until the pathway is created
  - Slow increase of gas pressure
  - Pressure at gas breakthrough obtained
  - Very, very slow…
- Alternative - Fast gas breakthrough test
  - High gas pressure applied **immediately**
  - Time to breakthrough measured
  - **Fast test. Easy repetition.**
  - Gas breakthrough pressure NOT obtained
  - Qualitative result (in terms of breakthrough event)

WHAT WE WANT TO KNOW?

- At what pressure does a breakthrough happen
- What happens to the EBS performance
- What are the influences of material density, heterogeneity, discontinuities,…

WP GAS - CTU OVERVIEW

Task 2 – "Slow"

- Material: BCV - homogeneous samples
- Permeameter: hydraulic cond., swell. pressure
- Long-term air injection tests – via injection needle or sintered steel plates
- Incremental pressure increase until breaktrough

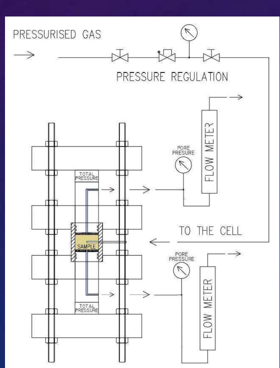

Air injection system

Permeameter

Task 3 – "Fast" and repeated

- Material: BCV - homogeneous and inhomogeneous samples
- Permeameter: hydraulic cond., swell. pressure
- Short-term air injection tests, high pressures
- Repeated cycles of gas injection and resaturation

Air injection system

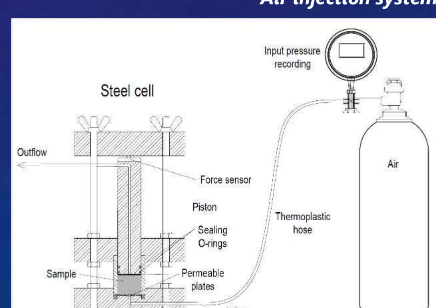

SLOW TESTS

T2

A TALE OF LOST NEEDLE…

The first idea was to inject gas into centre of sample via needle and try measure the desaturation (water outflow).

6 months of sample saturation, then test. It didn't work out 3 times…

- Port leaked
- Gas escaped around needle
- Needle corroded out
- Outflow (water) measurement not sensitive enough

→ Time for Plan B

- Additional cell
- Test from bottom
- Improved setup – replacement of needle by PTFE tube

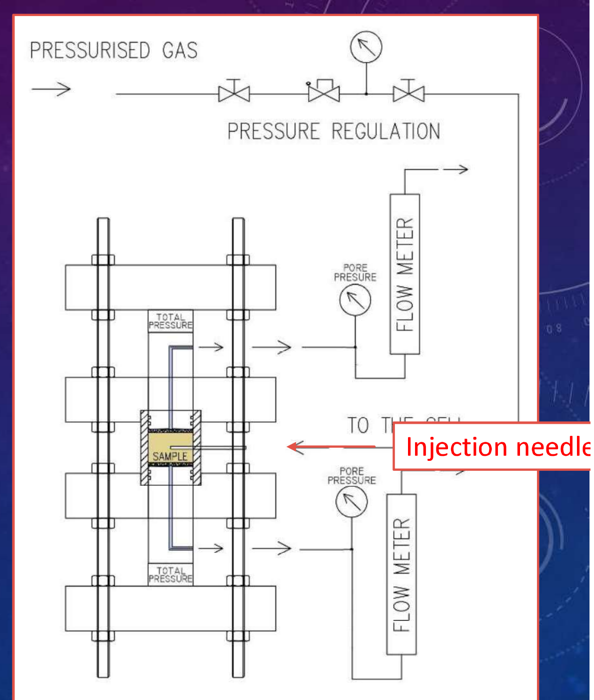

sample no.	target ρ_d [kg/m^3]	preparation of sample	saturation/resaturation phase [days]	plan of gas pressure test	gas test no.	start of the gas pressure test	end of the gas pressure test	note	gas injection point	total pressure - top sensor [MPa]	total pressure - bottom sensor [MPa]	initial injection pressure - in first step [MPa]	loading step [kPa]/time [days]	duration of gas injection [days]	breakthrough pressure [MPa]
P766	1300	20.08.2020	168	12.02.2021	PN069	26.04.2021	26.04.2021	unsuccessful test - technical problems with needle at the centre of the sample	Injection needle	0,45	-	0,6	50/14	0,5	---
P805	1345	10.05.2021	168	26.10.2021	PN077	26.10.2021	26.10.2021	unsuccessful test - gas passes through testing cell, technical problems with the injection needle	Injection needle	0,40	-	0,2	50/14	5	---
			50	22.12.2021	PN082	22.12.2021	24.03.2022	resaturation of the sample after unsuccessful test	to base	0,38	0,18	0,07	50/14	84	**0,37**
P815	1394	06.09.2021	93	14.03.2022	PN081	14.03.2022	14.06.2022	unsuccessful test - technical problems with gas leakage during the test	Injection needle	2,21	1,14	0,38	50/14 than 50/7 (after 3rd step)	98	**0,84**
			80	15.09.2022	PN092	23.09.2022	14.03.2023		to base	2,03	1,10	0,57	50/7	172	**2,5**
P823	1473	09.11.2021	168	26.04.2022	PN086	26.04.2022	14.03.2023	simple measuring apparatus (with one piston) and with gas injection to the base of the sample	to base	3,00	-	1,54	50/7	322	**4,43**
P840	1500	20.04.2022	168	07.10.2022	PN107	21.03.2023	11.07.2023	1st step - 2.35 MPa	Injection needle	3,76	2,74	2,35	50/7	110	**3,26**

BCV 1345 – TEST PN082

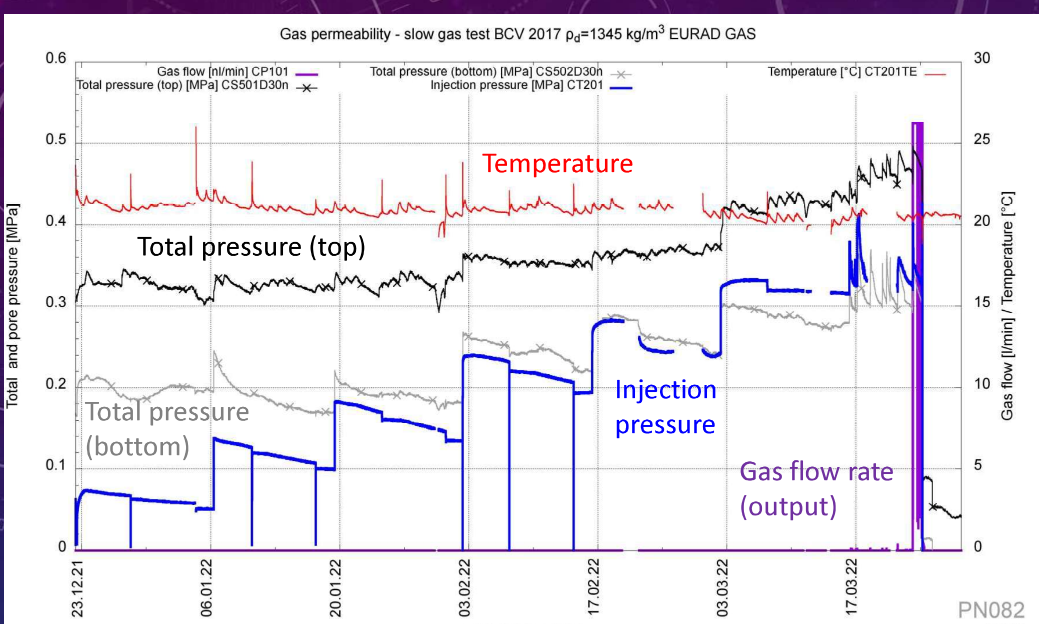

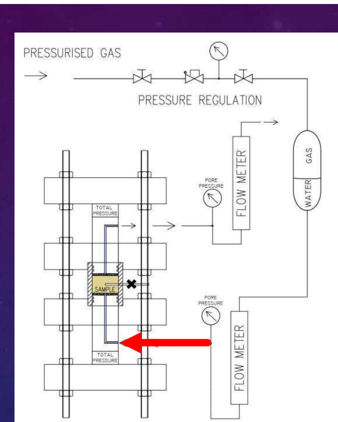

Start: 22-12-2021 End: 24-03-2022

Saturation: 168 + 50 days
Total (swelling) pressure:
Top sensor 0.38 MPa
Bottom sensor 0.18 MPa

Initial pressure step: 0.07 MPa
Pressure increments:
50 kPa (14 days)
Breaktrough pressure: 0.37 MPa
Theoretical swelling pressure:
1.5 – 2.1 MPa for 1400 kg/m^3

BCV 1345 – TEST PN082 _BT EPISODE

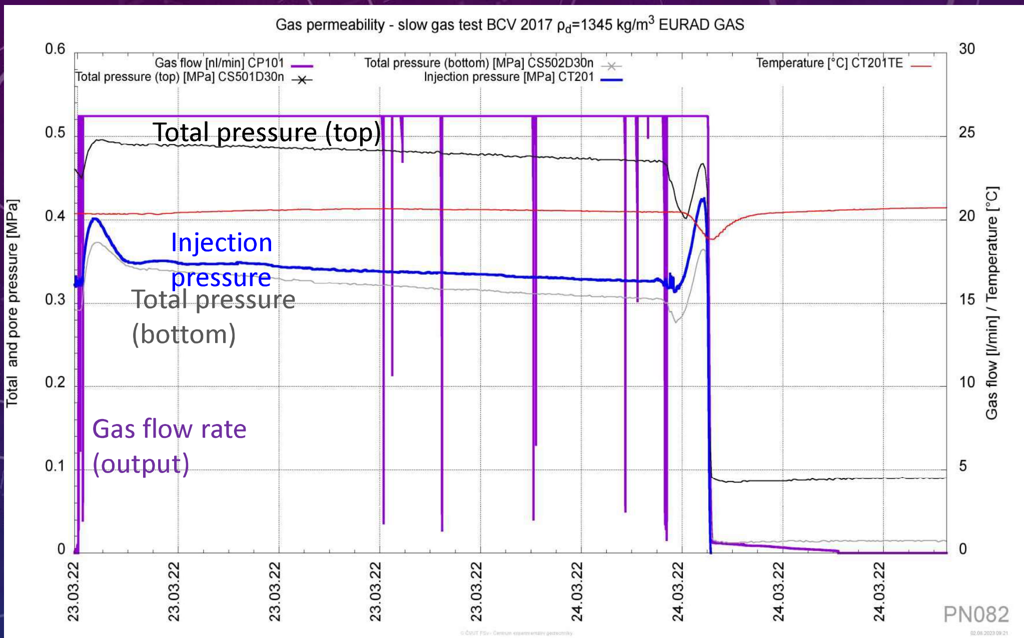

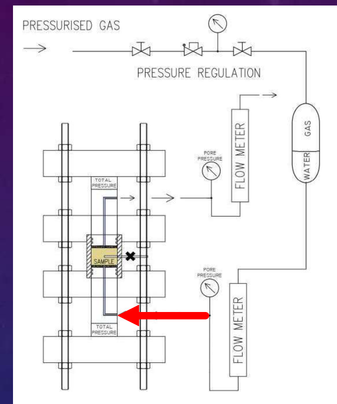

Start: 22-12-2021 End: 24-03-2022

Saturation: 168 + 50 days
Total (swelling) pressure:
Top sensor 0.38 MPa
Bottom sensor 0.18 MPa

Initial pressure step: 0.07 MPa
Pressure increments:
50 kPa (14 days)
Breaktrough pressure: 0.37 MPa
Theoretical swelling pressure:
1.5 – 2.1 MPa for 1400 kg/m^3

BCV 1395 – TEST PN092

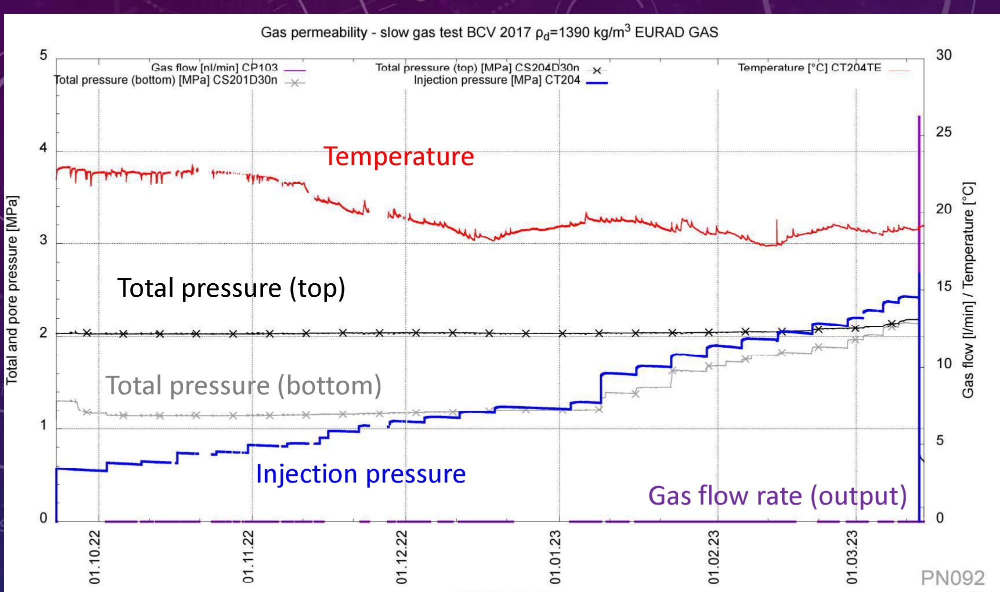

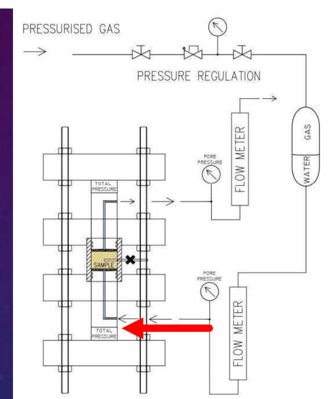

Start: 23-09-2022 End: 14-03-2023

Initial saturation: 80 days
Total (swelling) pressure:
Top sensor 2.03 MPa
Bottom sensor 1.10 MPa

Initial pressure step: 0.6 MPa
Pressure increments:
50 kPa (7 days)
Breaktrough pressure: 2.5 Mpa

Theoretical swelling pressure: 1.5 – 2.1 MPa for 1400 kg/m^3

BCV 1395 – TEST PN092 - BT EPISODE

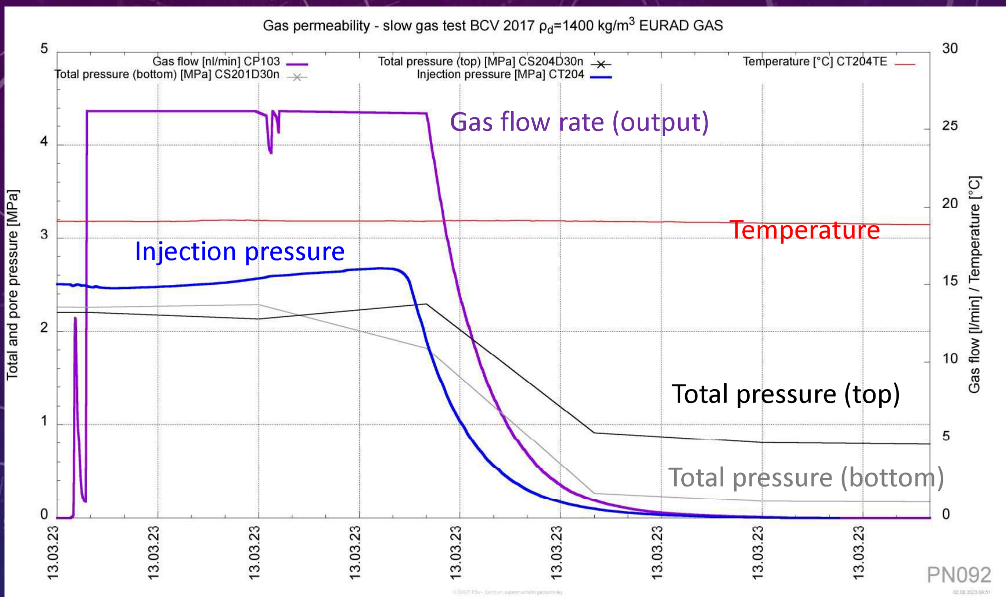

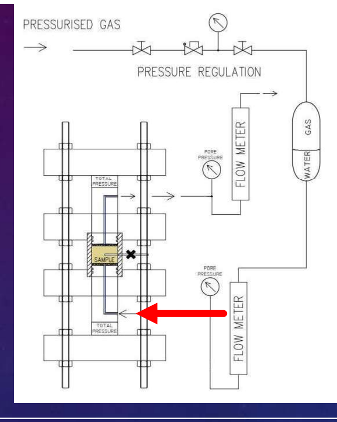

Initial saturation: 80 days
Total (swelling) pressure:
Top sensor 2.03 MPa
Bottom sensor 1.10 MPa

Initial pressure step: 0.6 MPa
Pressure increments:
50 kPa (7 days)
Breaktrough pressure: 2.5 MPa

Theoretical swelling pressure: 1.5 – 2.1 MPa for 1400 kg/m^3

Start: 23-09-2022 End: 14-03-2023

BCV 1475 – TEST PN086

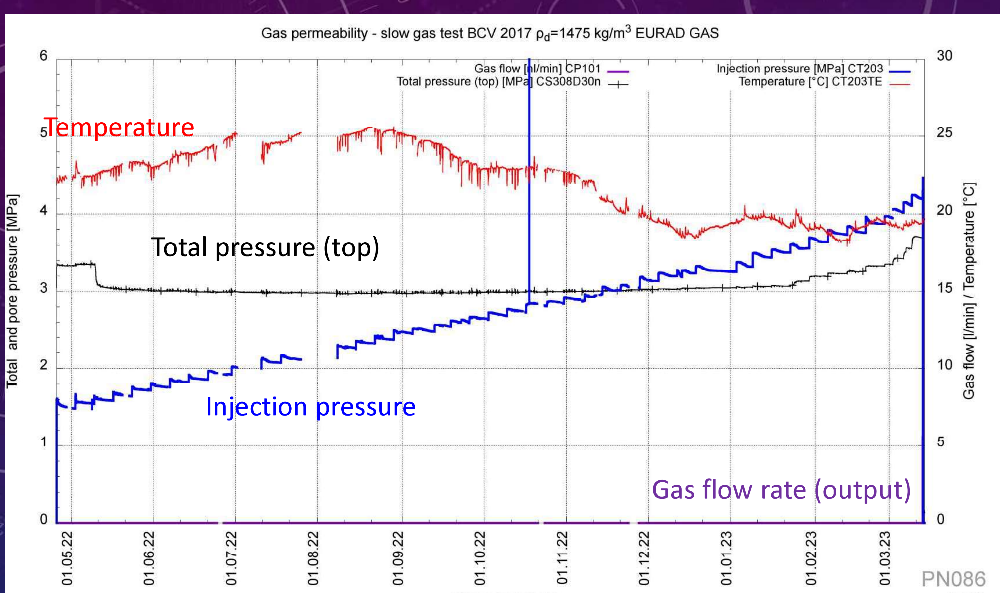

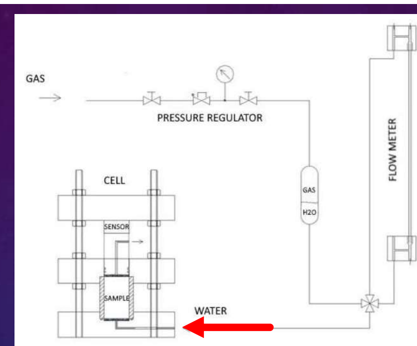

Initial saturation: 168 days
Total (swelling) pressure:
Top sensor 3.00 MPa

Initial pressure step: 1.5 MPa
Pressure increments:
50 kPa (7 days)
Breakthrough pressure: 4.43 MPa

Theoretical swelling pressure: 2.1 – 3.0 MPa for 1450 kg/m^3

Start: 26-04-2022 End: 14-03-2023

BCV 1475 – TEST PN086 – BT EPISODE

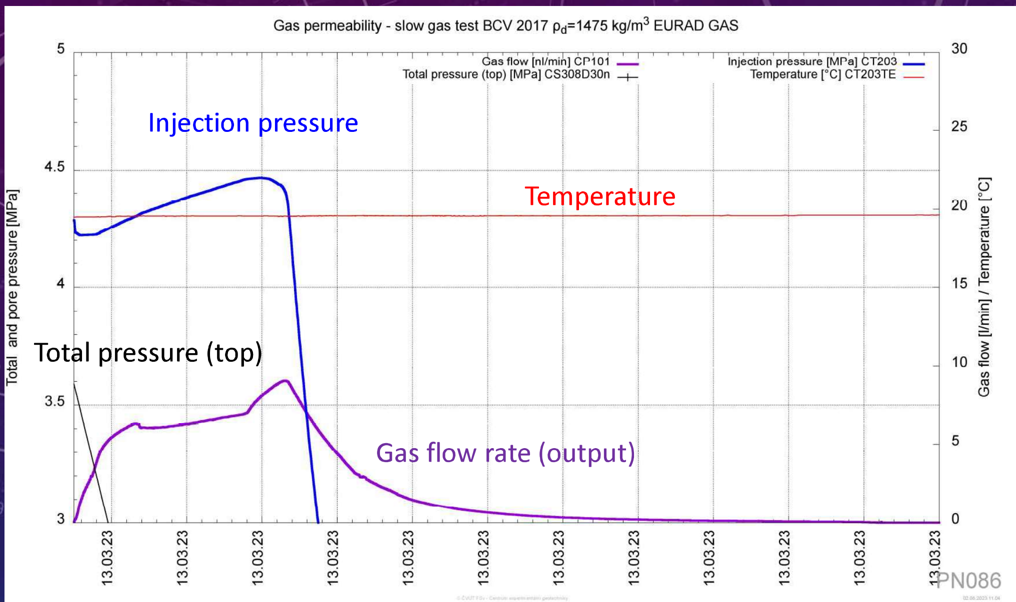

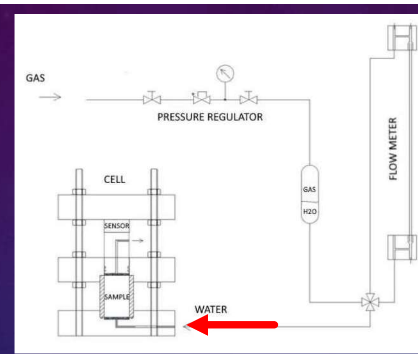

Initial saturation: 168 days
Total (swelling) pressure:
Top sensor 3.00 MPa

Initial pressure step: 1.5 MPa
Pressure increments:
50 kPa (7 days)
Breaktrough pressure: 4.43 MPa

Theoretical swelling pressure: 2.1 – 3.0 MPa for 1450 kg/m^3

Start: 26-04-2022 End: 14-03-2023

BCV 1500 – TEST PN107

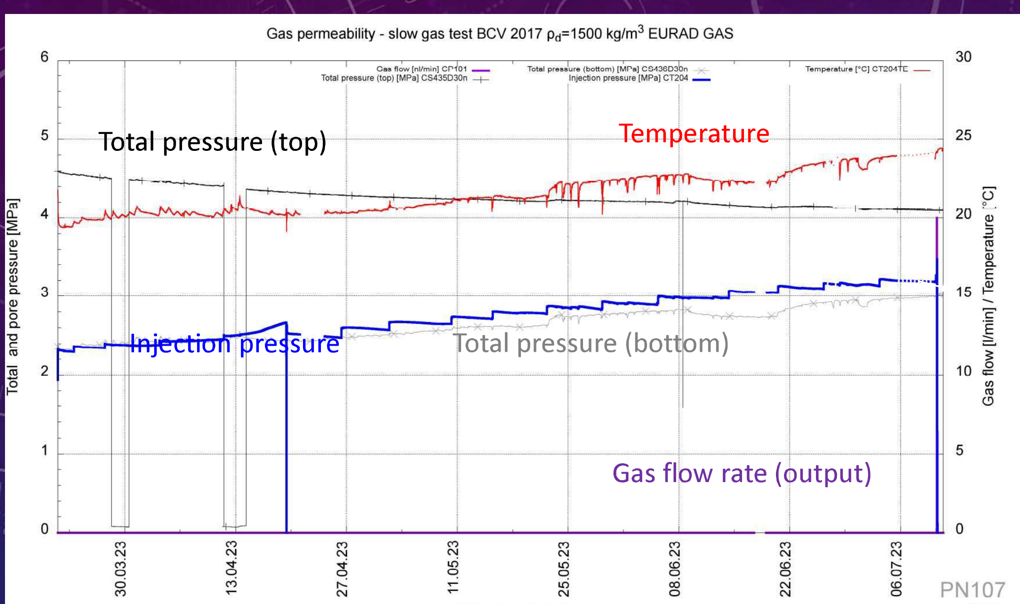

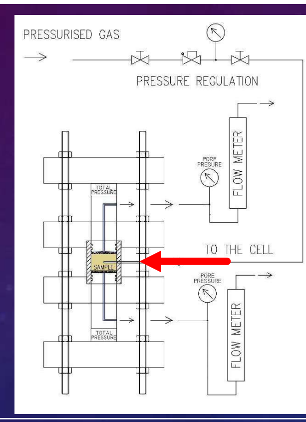

Saturation: 168 days
Total (swelling) pressure:
Top sensor 3.76 MPa
Bottom sensor 2.74 MPa

Initial pressure step: **2.35** MPa
Pressure increments:
50 kPa (7 days)
Breakthrough pressure:
3.26 MPa
Theoretical swelling pressure:
1.9 – 5.2 MPa for 1500 kg/m^3

Start: 21-03-2023 End: 11-07-2023

BCV 1500 – TEST PN107 – BT EPISODE

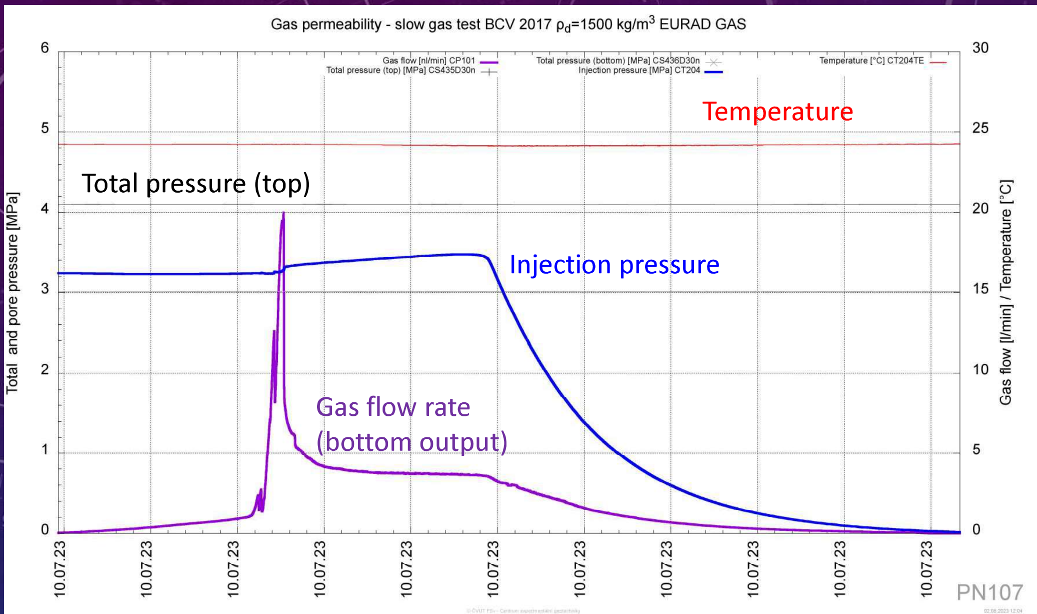

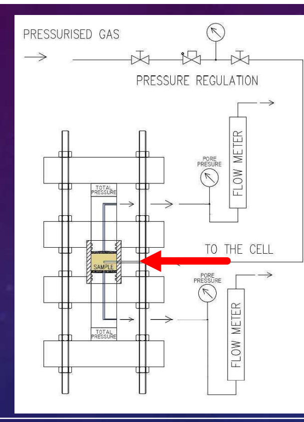

Saturation: 168 days
Total (swelling) pressure:
Top sensor 3.76 MPa
Bottom sensor 2.74 MPa

Initial pressure step: **2.35** MPa
Pressure increments:
50 kPa (7 days)
Breaktrough pressure: 3.26 MPa
Theoretical swelling pressure: 1.9 – 5.2 MPa for 1500 kg/m^3

Start: 21-03-2023 End: 11-07-2023

CT SCAN P840

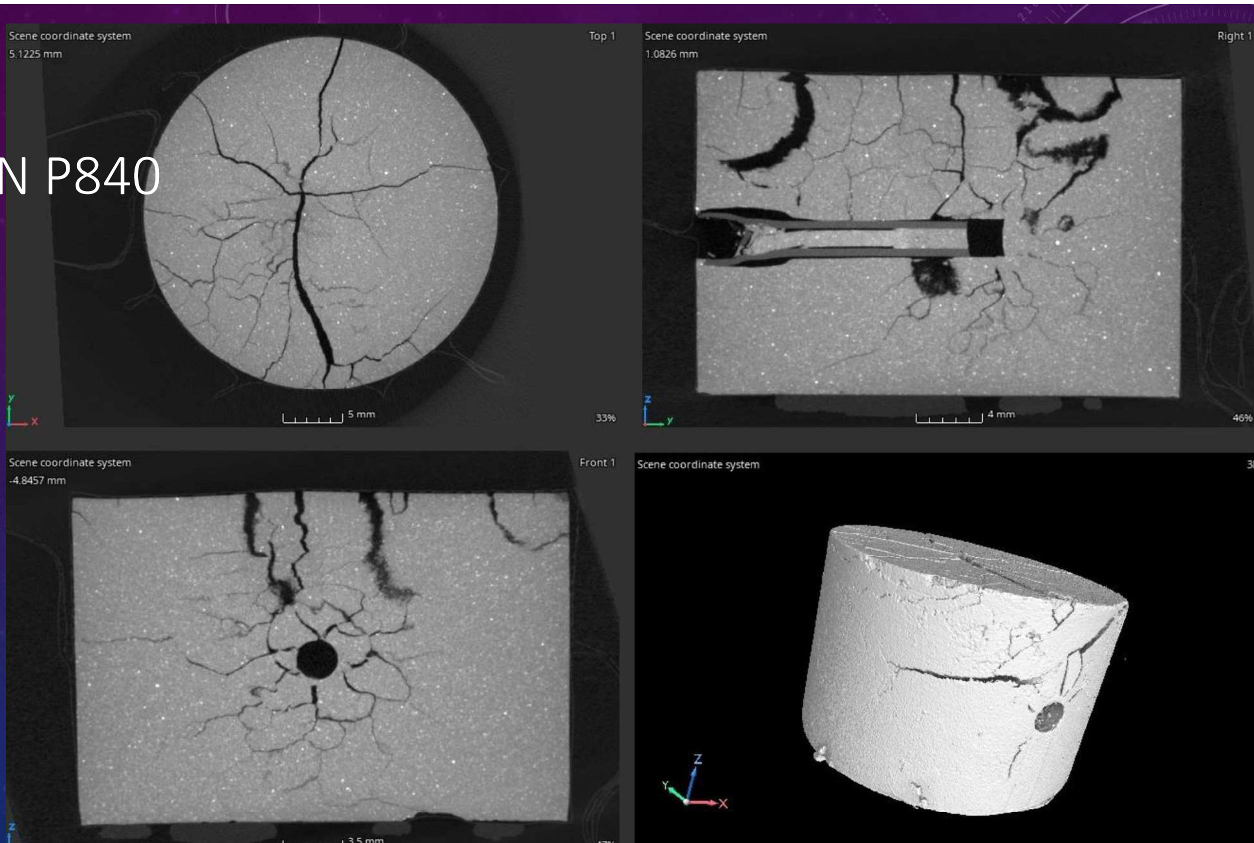

SLOW TESTS - CONCLUSION

A lot of technical problems…

Tests with gas injection into the base of the cylindrical sample

- The total pressure sensors react to the injection pressure – mechanical behaviour of the sample – a combination of the „plastic“ state of the sample and friction
- The breakthrough events registered for values of pressures above the swelling pressure

Tests with injection needle

- The breakthrough events registered for values of pressures above the swelling pressure

Air vs Hydrogen

- The results of test with air are giving similar results to tests with hydrogen (tests by UJV)

FAST TESTS

T3.1 - GAS-INDUCED IMPACTS ON BARRIER INTEGRITY

T3.2 - PATHWAY CLOSURE AND SEALING PROCESSES

FAST TESTS

How it works?

- **Initial saturation (hydraulic conductivity, swelling pressure)**
- **Gas breakthrough test**
  Monitoring: input gas pressure, total pressure, flow rate at output
- **Re-saturation (hydraulic conductivity, swelling pressure)**
- ……(5 repeated cycles)
- **Dismantling**

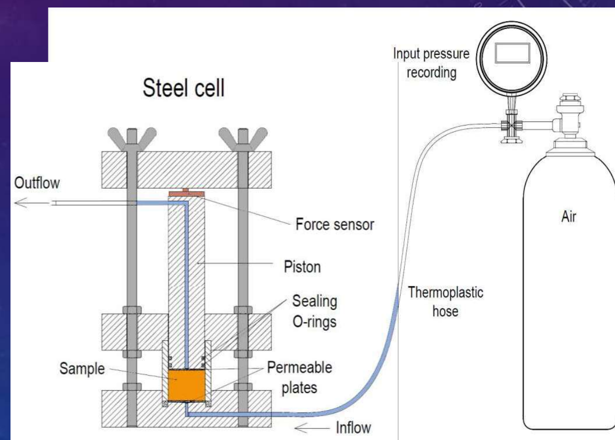

FAST TESTS

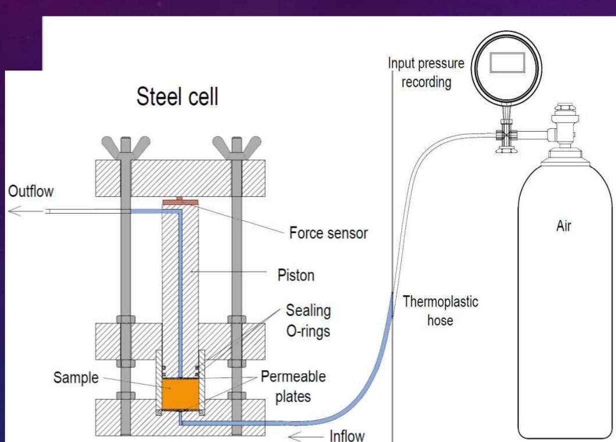

Evaluation

Comparison (between cycles of one sample and between samples) of:

- Time to breakthrough
- Evolution of outflow rate after breakthrough
- Input pressure decay curve after breakthrough (the input line is kept open after breakthrough)
- **Swelling pressure and hydraulic conductivity**

COMPARISON OF REPEATED CYCLES

Bentonite B75 (Czech Ca-Mg bentonite) – project for the Czech Science Foundation (2015)

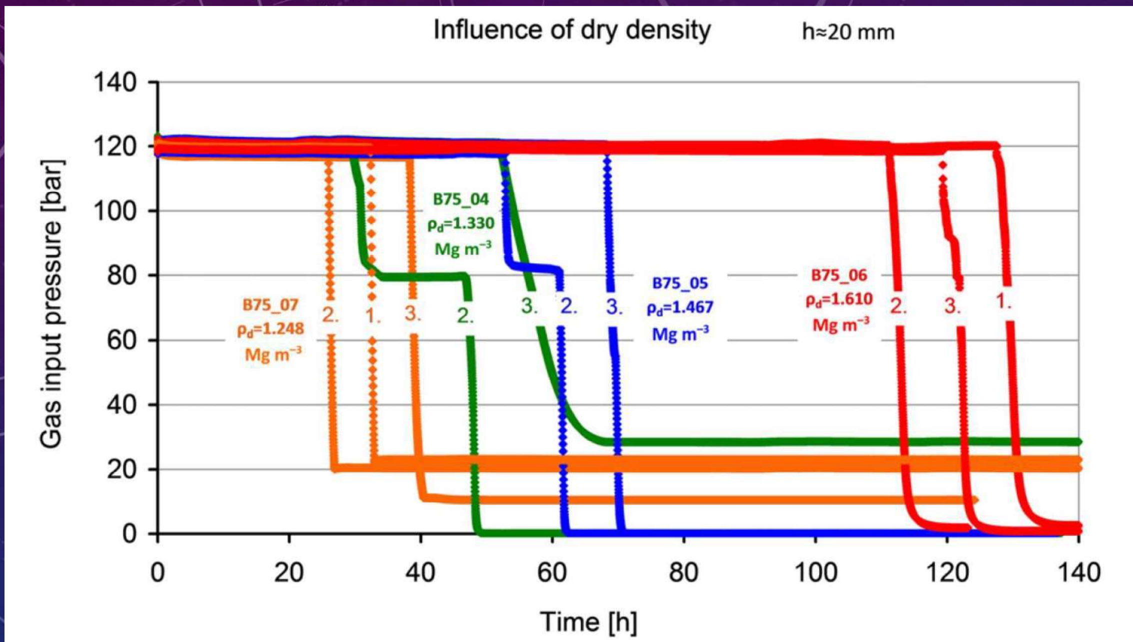

Smutek, J., Hausmannová, L., Svoboda, J. The gas permeability, breakthrough behaviour and re-sealing ability of Czech Ca–Mg bentonite. Geological Society, London, Special Publications. 2017, 443(1), 333-348. ISSN 0305-8719. DOI:10.1144/SP443.5.

INPUT PRESSURE DECAY CURVE

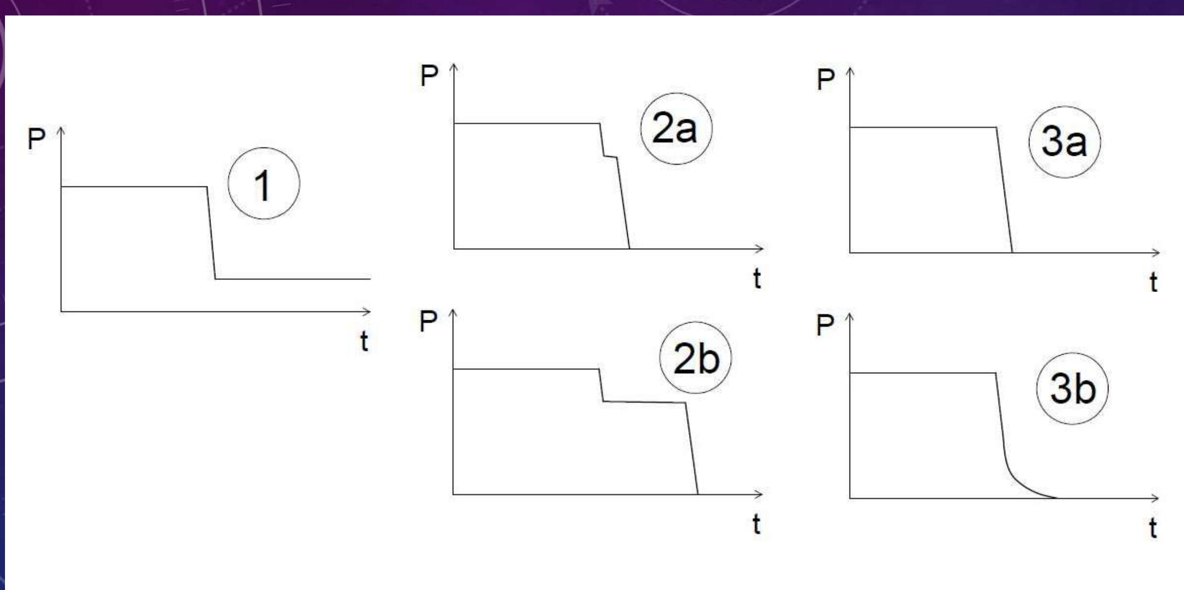

COMPARISON OF REPEATED CYCLES

Bentonite B75 (Czech Ca-Mg bentonite) – project for the Czech Science Foundation (2015)

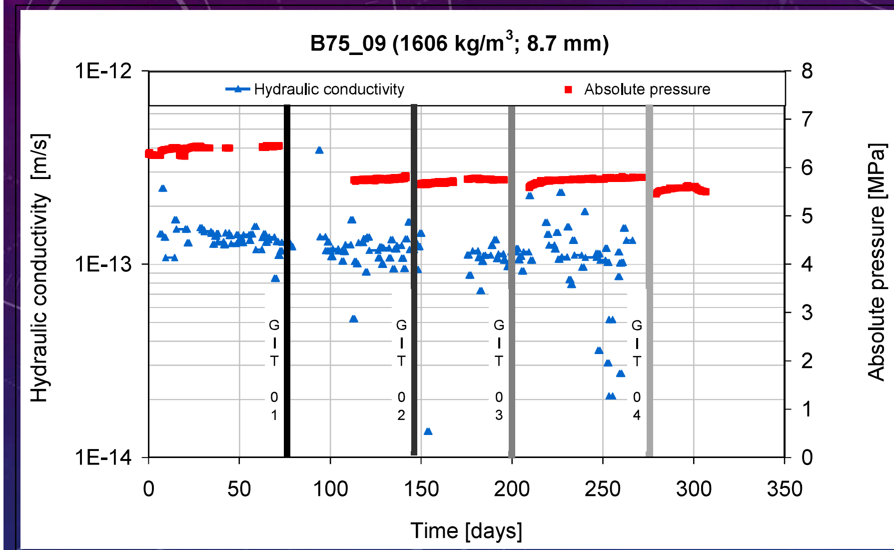

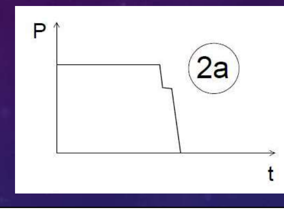

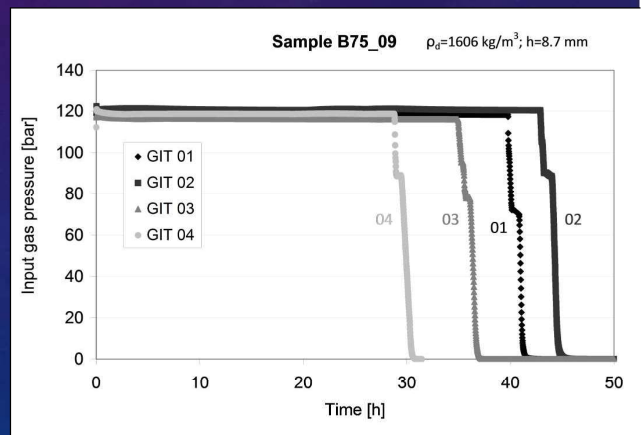

COMPARISON OF REPEATED CYCLES

Bentonite B75 (Czech Ca-Mg bentonite) – project for the Czech Science Foundation (2015)

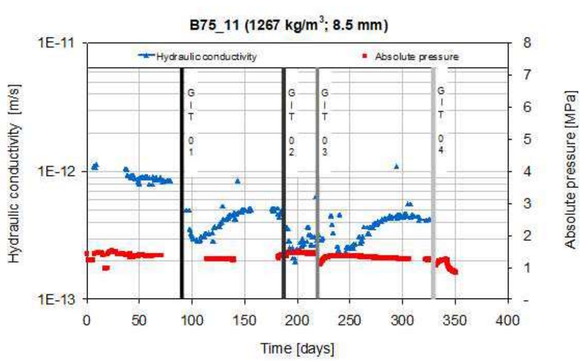

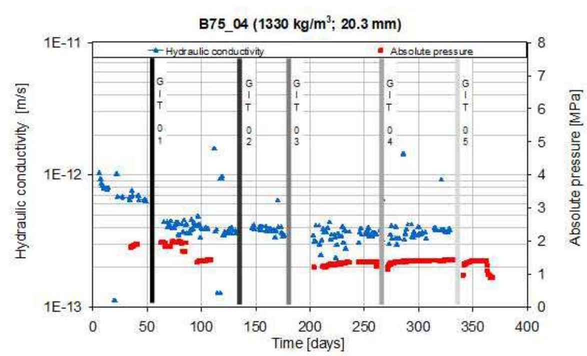

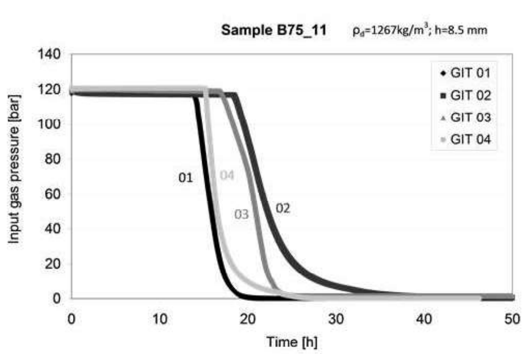

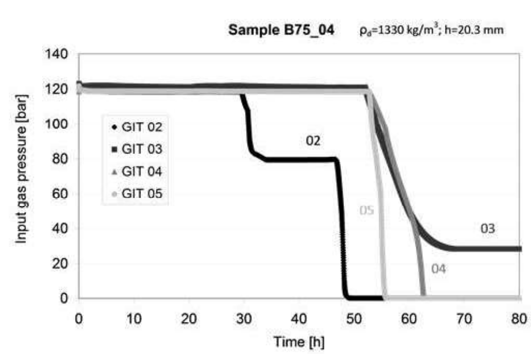

WP GAS

T3.1 - Gas-induced impacts on barrier integrity
T3.2 - Pathway closure and sealing processes

- Homogeneous compacted bentonite samples
  - BCV bentonite
  - 5 samples: dry density 1300 - 1610 kg/m^3
  - Completed (5 cycles of gas injection and resaturation)
- Inhomogeneous samples (artificial joint)
  - BCV bentonite
  - 4 samples: dry density 1450 - 1610 kg/m^3
  - Ongoing, max. 3 cycles finished
  - The next breakthrough test series planned to June 2023

HOMOGENEOUS SAMPLES

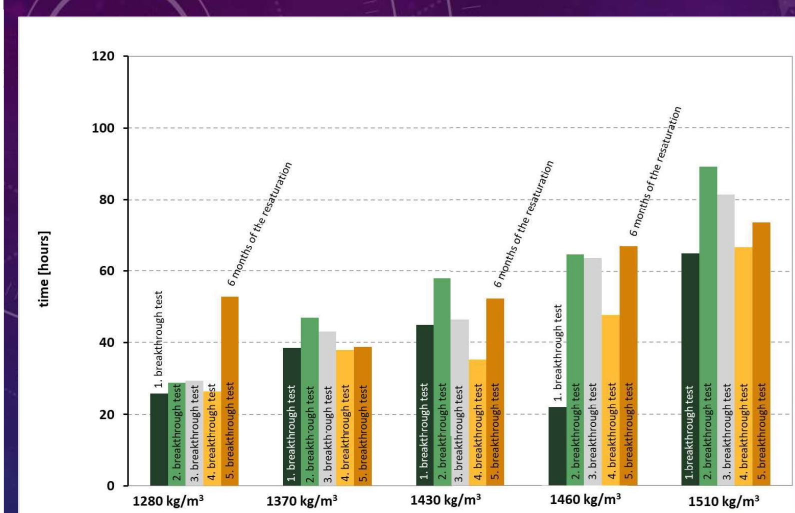

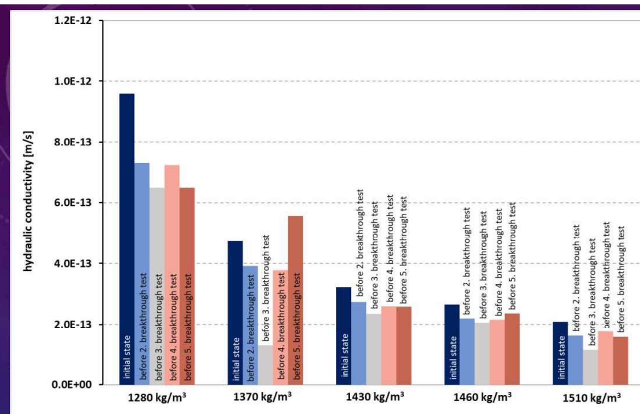

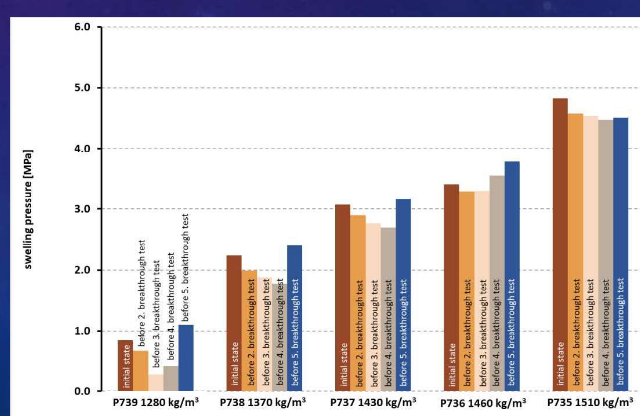

HOMOGENEOUS SAMPLES – BREAKTHROUGH EPISODES

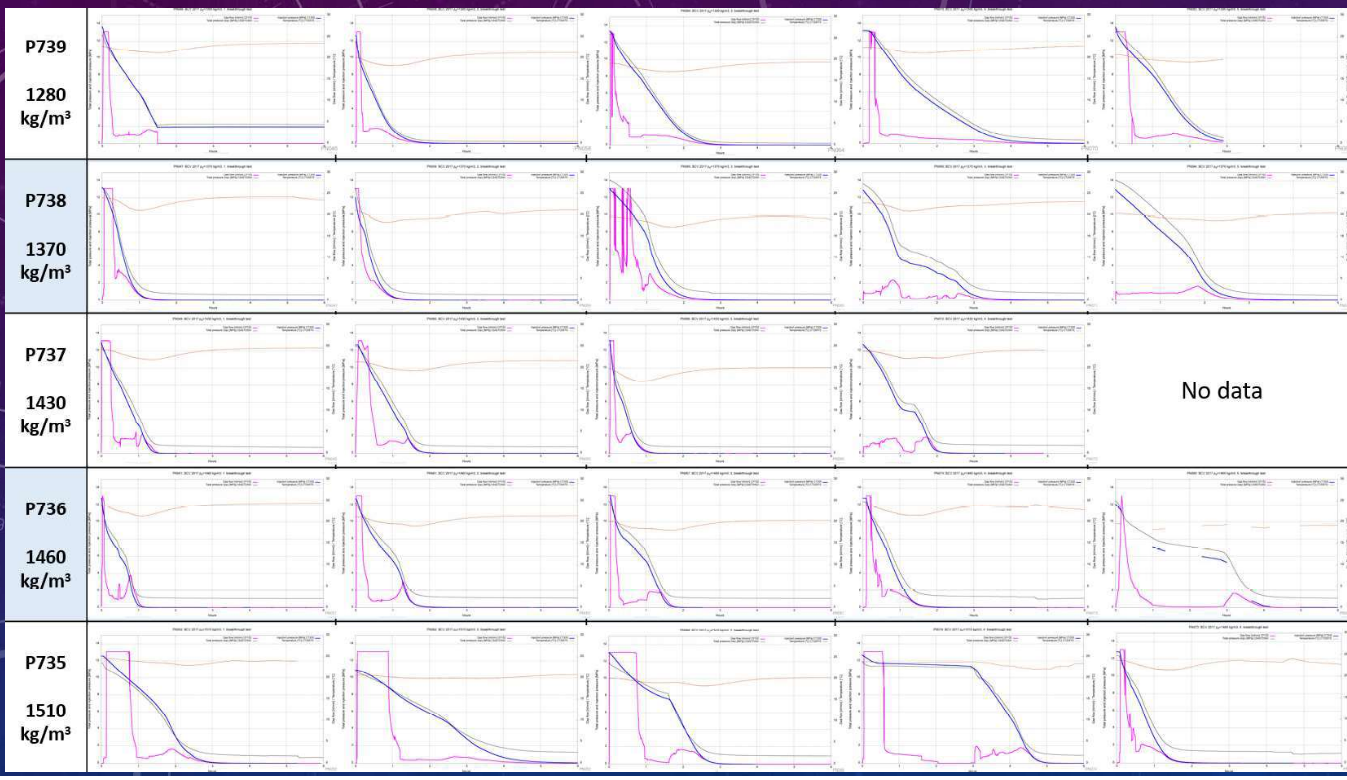

INHOMOGENEOUS SAMPLES

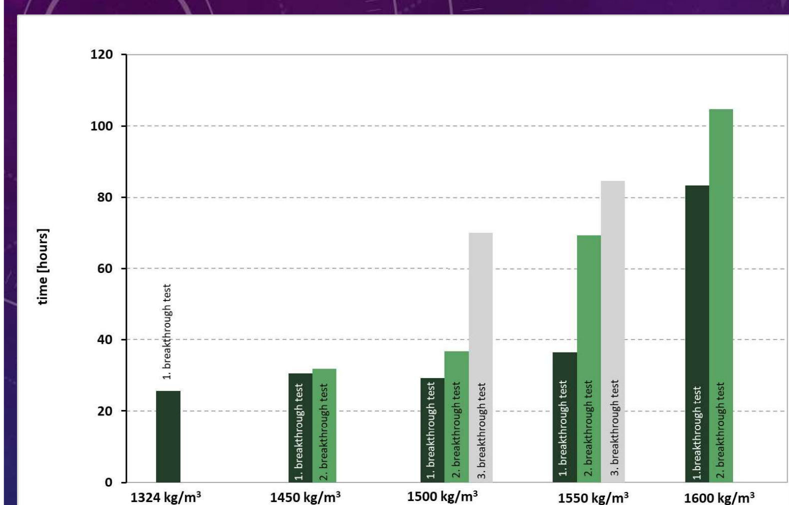

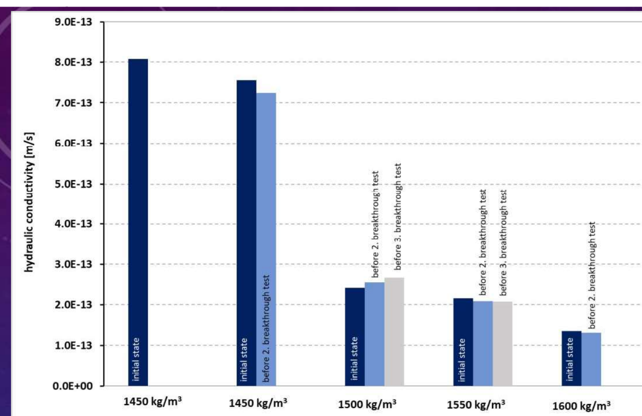

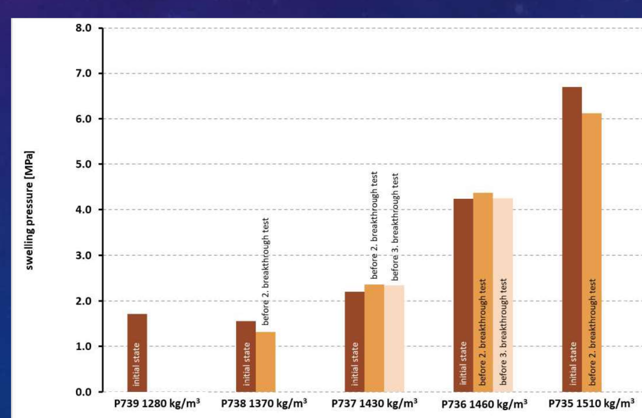

CONCLUSIONS

- Integrity of barrier seems to hold after gas breakthrough given enough time (resaturation)
- Duration of saturation has an impact on the self-healing of the sample
- Fast test can be used to check EBS state and resilience. The endurance in the fast test is a qualitative indication of the EBS state
- Gas tests show clearly that bentonite evolves long time even whet hydraulic conductivity and pressure is stable

LET'S CONTINUE WITH HITEC - TEMPERATURE

The overall objective is to evaluate whether an increase of temperature is feasible and safe by applying (i) existing and (ii) the within the task newly produced knowledge about the behaviour of clay buffer materials at elevated temperatures.

The increase of temperature may result in strong evaporation near the heater and vapour movement towards the external part of the buffer. As a consequence, part of the barrier, or all of it, depending on the particular disposal concept, will remain unsaturated and under high temperatures during periods of time that can be very long. Moreover the high temperature gradient (and pore pressure) even crossing boiling point of water will lead to several adverse effects as Sauna effects.

The aim is to gain knowledge to hydro-mechanical behaviour at high temperature. The temperature impact on important processes will be measured either while the clay is at the high temperature or after a high temperature exposure. Processes that may have a temperature dependence are swelling pressure, hydraulic conductivity, erosion properties, transport of solutes etc.

- T3.1 Characterization of material treated by high temperature
- T3.2 Determination of parameters at temperatures >100°C
- T3.3 Small scale experiments, model development and verification

HITEC – T3.1 MATERIAL TREATED BY HIGH TEMPERATURE

- Swelling
  - Free swelling
  - Swelling pressure
- Hydraulic conductivity
- Atterberg limits
- Composition

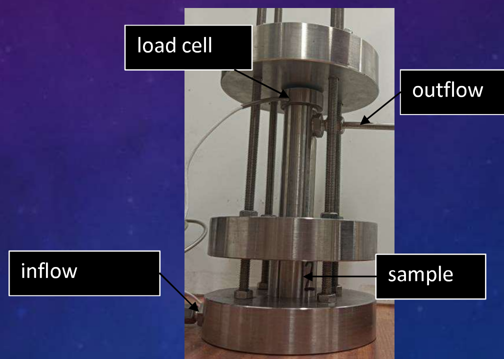

CTU cell

The sample after the test,
d = 30 mm, h = 20 mm

BCV MATERIAL

HITEC – influence of high temperature

- Dry material @150°C
- Suspension @150°C

Sampling:

- 6 months
- 12 months
- 24 months

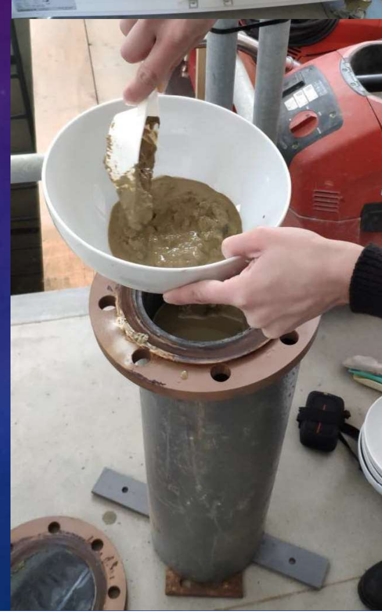

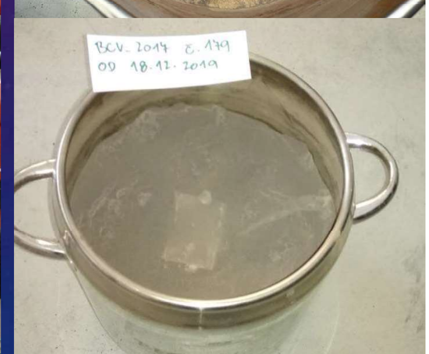

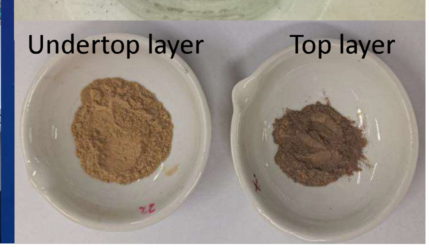

HYDRAULIC CONDUCTIVITY

- Hydraulic conductivity of thermally treated BCV in dry state is systematically above the trend line of untreated BCV
- No difference between *k* of dry treated BCV after 6m of treatment and *k* after 12m of treatment is observed
- No impact of elevated temperature on wet treated BCV is observed. In part of low densities the measured values are under the trend line of untreated BVC

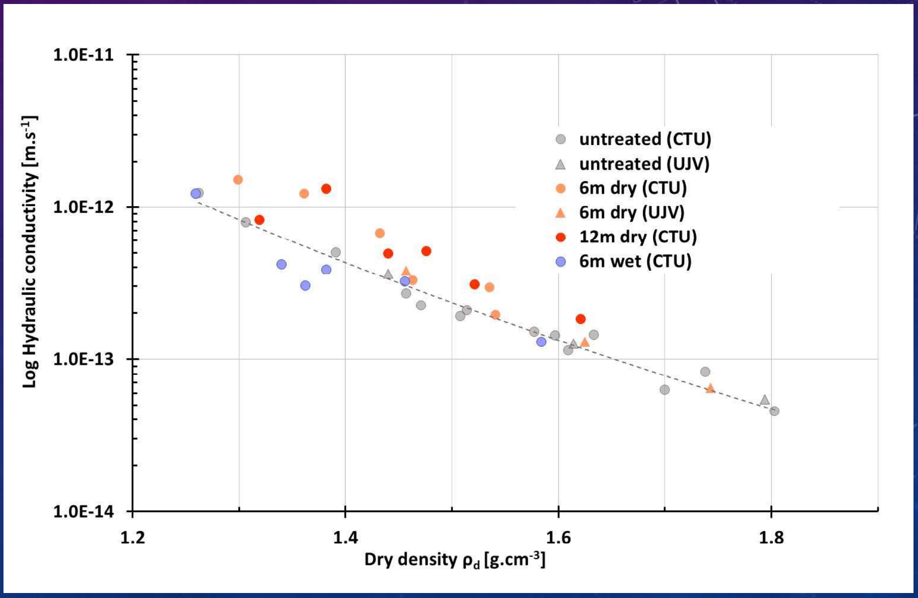

SWELLING PRESSURE

- Consistent decrease of swelling pressure is observed on set of samples of dry treated bentonite
- No impact of duration of thermal treatment is observed on dry treated bentonite
- No significant difference in swelling pressure is observed between wet treated and untreated bentonite

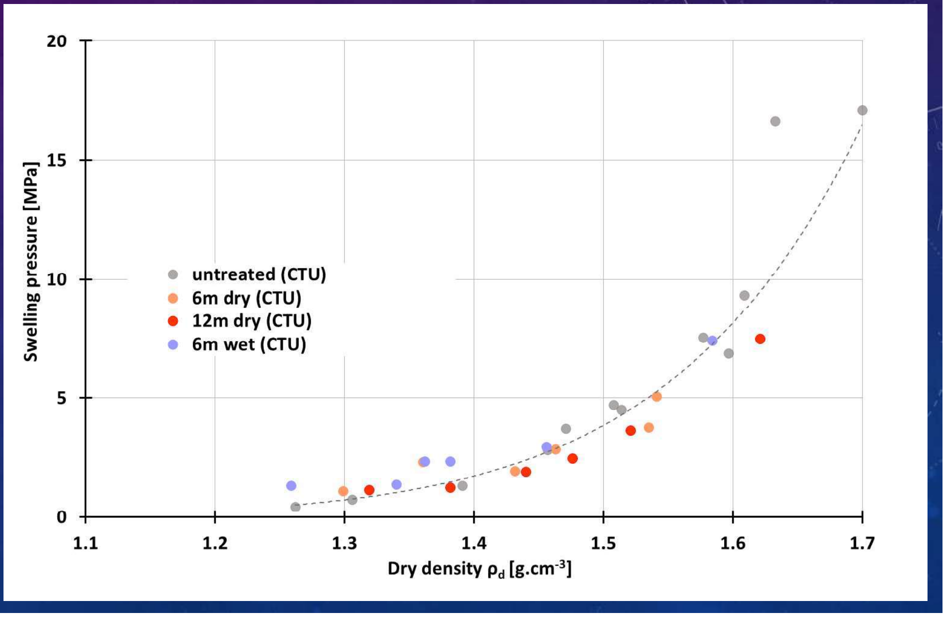

WL, CEC, SSA AFTER THERMAL TREATMENT @150 °C

- Same trend observed for liquid limit (cone method), cation exchange capacity (Cu-trien method), specific surface area (EGME) and hydraulic conductivity

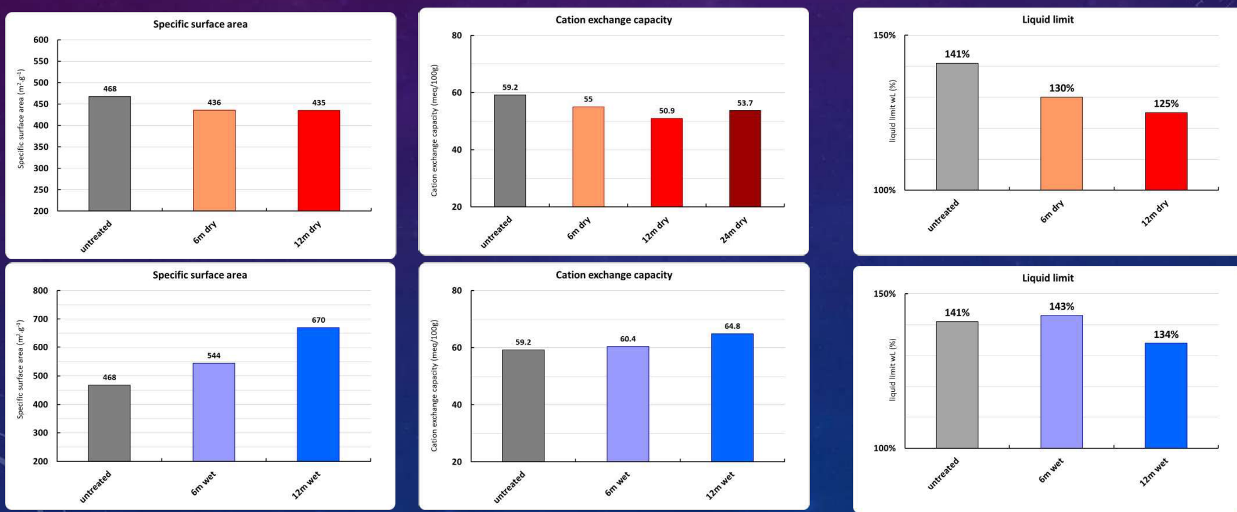

DRY treated

WET treated

HITEC – T3.2 DETERMINATION OF PARAMETERS AT TEMPERATURES >100°C

- Swelling pressure
- Hydraulic conductivity

- Temperature up to 130°C
- Start at laboratory temperature

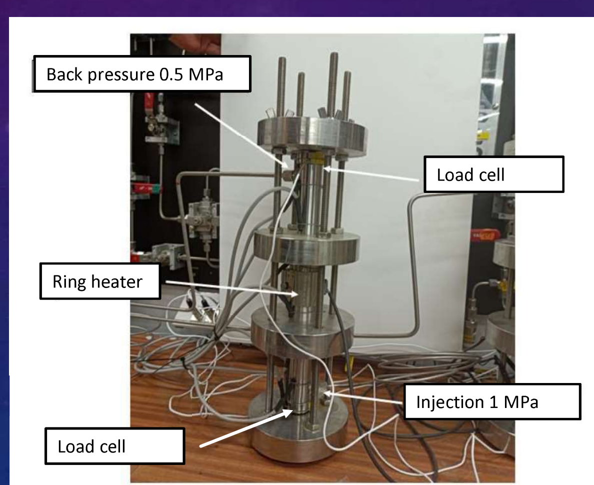

BCV @130 °C

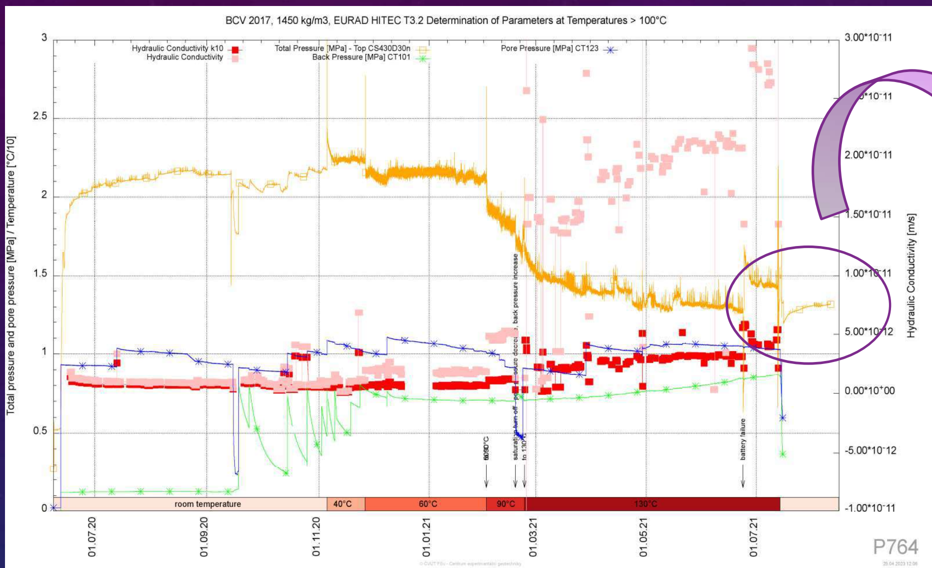

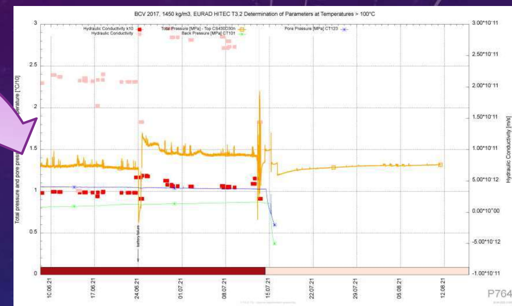

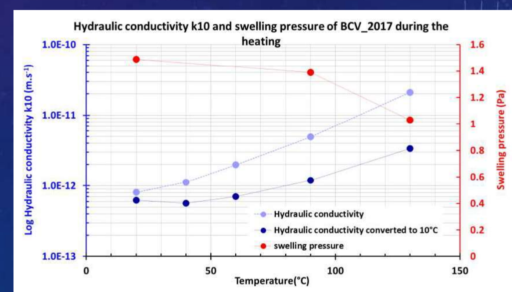

- Continuous decrease of total pressure
- Swelling pressure does not recover to the values of untreated material

BCV @130 °C

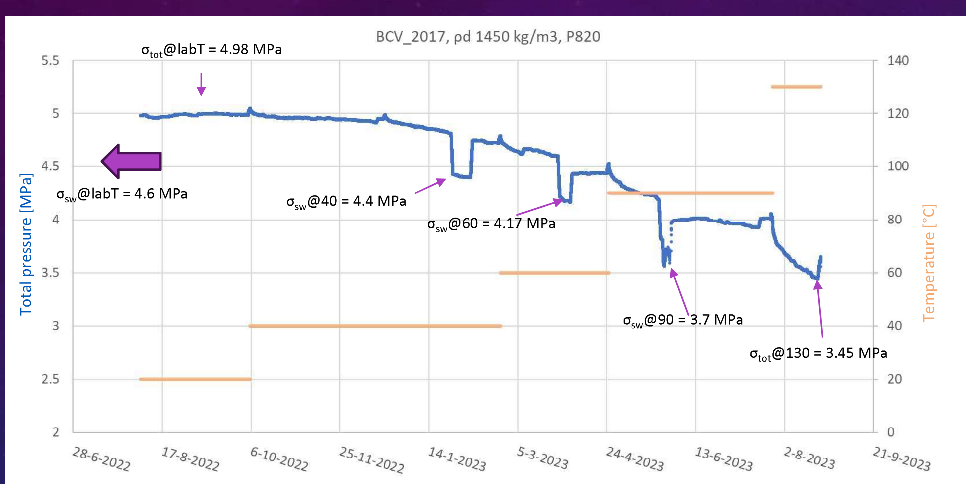

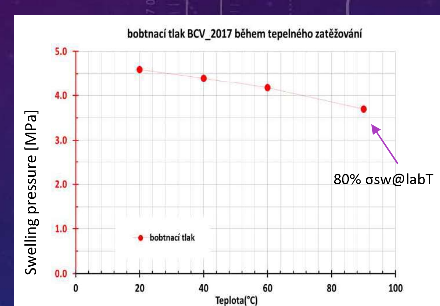

- Continuous decrease of total pressure

BCV @130 °C

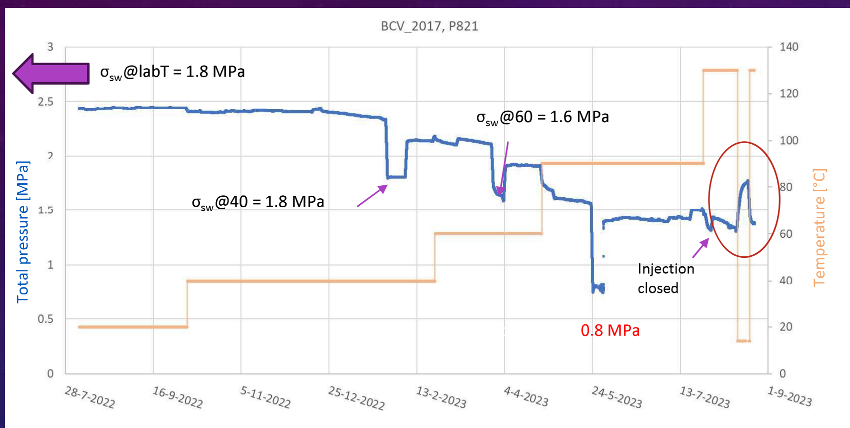

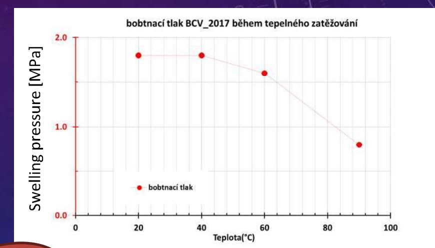

σ_{tot}@labT after themal load = 1.76 MPa

σ_{tot}@labT before thermal load = 2.43 MPa

T	σ_{sw} (MPa)	%σ_{sw}@labT
lab	1.8	100
40 °C	1.8	100
60 °C	1.6	89
90 °C	0.8	44

- Continual decrease of total pressure

T3.3 SMALL SCALE EXPERIMENTS, MODEL DEVELOPMENT AND VERIFICATION

First run

- Powdered BCV, 900 kg/m^3
- 1. Phase – saturation by 6 bar
- 2. Phase – gradual heating up to 150 °C
- Heating and the saturation at the same time
- No boiling

Second run

- Peletized BCV, 1400 kg/m3
- 1. Phase – heating right up to 150 °C – simulation of the condition of the repository
- 2. Phase – start of saturation by the pressure ensuring boiling in the middle of the vessel
- Heating and the saturation at the same time
- Boiling

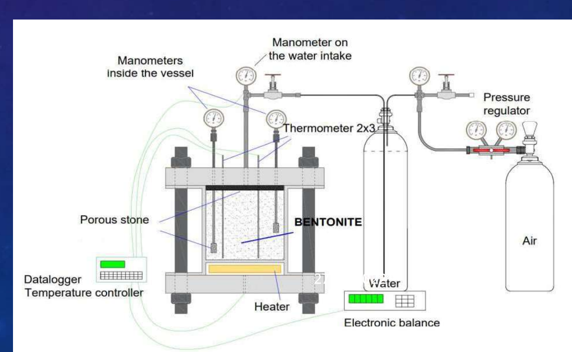

FIRST RUN

Initial dry density = 0,84 g/cm³

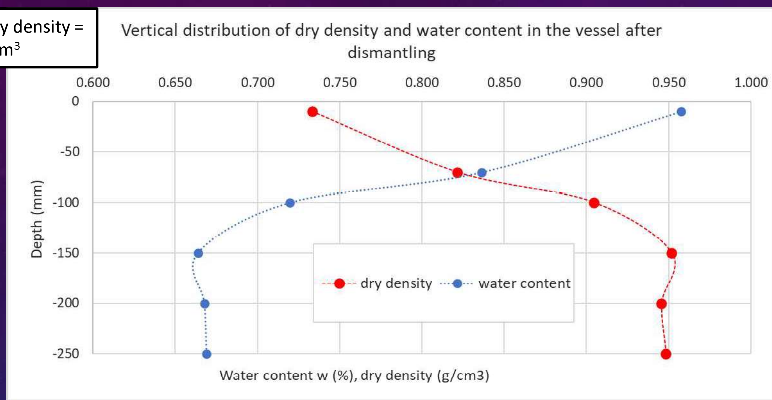

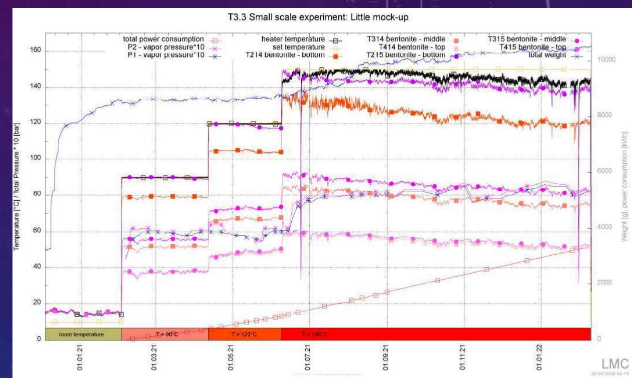

depth (mm)	w (%)	ρ (g/cm3)	ρd (g/cm3)
0			
-10	98%	1.388	0.733
-70	84%	1.507	0.821
-100	72%	1.559	0.904
-150	66%	1.584	0.951
-200	67%	1.568	0.945
-250	67%	1.578	0.948

3nd layer
(-100 mm)

MAIN RESULTS – NUMERICAL MODELLING

- FE model – axisymmetric domain with the same geometry for the first and the second runs

axis of symmetry

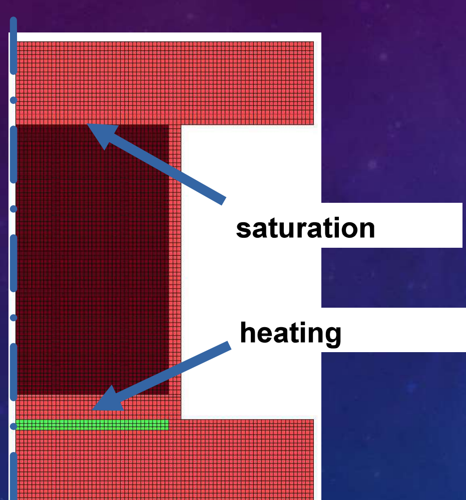

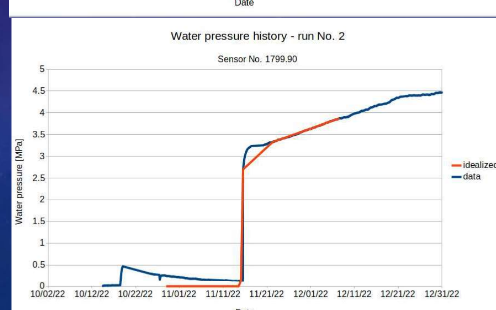

NUMERICAL VS REAL

First run

Second run

- Temperature

- Pressure

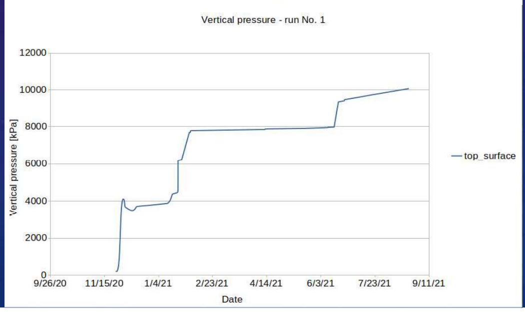

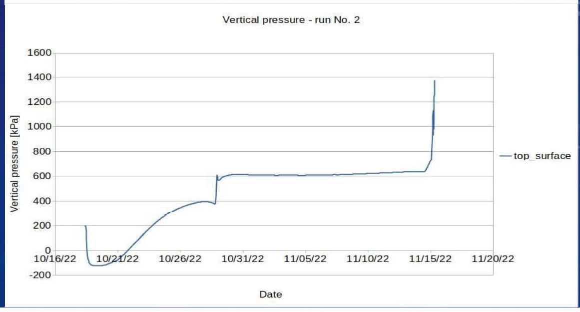

COMBINATION OF TEMPERATURE AND GAS?

Under investigation…

- First results show that fast tests have lower time to breakthrough. Probably coinciding with observed decrease of swelling pressure.

THANK YOU FOR YOUR ATTENTION

END OF PRESENTATION

ACKNOWLEDGEMENT

This project has received funding from the European Union´s Horizon 2020 research and Innovation programme 2014-2018 under grant agreement N°847593

BCV testing was also supported by the Euratom research and training programme 2014-2018 under contract no. 745942 Bentonite Mechanical Evolution

And more testing of BCV was supported by the project Engineered barrier 200C (no. TK01030031) from the Technology Agency of the Czech Republic

B75 testing was supported by Czech Science Foundation (project 14-19655S)

Appendix I. Visualising gas flow in the laboratory (A. Wiseall)

Visualising gas flow in the laboratory

EURAD Summer School

Andrew Wiseall – Geoscience Research Manager at Nuclear Waste Services

Acknowledgements: R. Cuss, J. Harrington, C. Graham at the British Geological Survey)

All laboratory results and images courtesy of the British Geological Survey

Contents

- Why do we need to understand gas flow for nuclear waste disposal?
- How is gas produced in a repository?
- What methods can we use to investigate this in the laboratory?
- Recent results from the EURAD GAS study
- Main results and knowledge gaps for the future

Experimental results were all measured and recorded at the British Geological Survey. Work was predominantly carried out as part of the EURAD GAS project, with work being partially funded by NWS and other European WMO's (EC project number 847593)

Gas generation in a GDF

- In a repository for **heat emitting** radioactive waste gas will be generated through a number of processes including:
  - **Corrosion** of metals (H_2)
  - Radioactive **decay of the waste** (Rn…)
  - **Radiolysis** of water (H_2)
- If production exceeds diffusion capacity a discrete gas phase forms.
- Gas will accumulate until its pressure becomes sufficiently large to enter the engineered barrier or host rock
- Understanding gas generation and migration (**in clay-based systems**) is a key issue in the assessment of **repository performance**

- Also relevant to **shale gas**, **hydrocarbon migration**, **carbon capture storage** and **landfill design**…

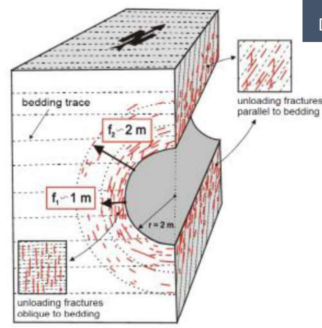

From: Bossart *et al.* (2002)

Induced Engineering Damage Zone fractures

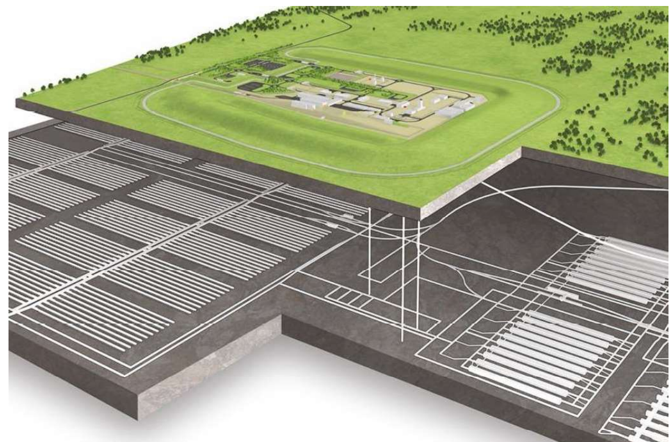

Gov.uk

Introduction to low permeability materials

"*There are few problems in geoscience more complex than the quantitative prediction of gas migration fluxes through an argillaceous rock formation*" (Rodwell et al. 1999)

A number of key features distinguish clay-rich media from other rock-types such as:

- sub-microscopic dimensions of the interparticle spaces
- very large specific surface of the mineral phases
- strong physico-chemical interactions between water molecules and surfaces
- very low permeability
- generally low tensile strength
- deformable matrix
- very pronounced coupling between the hydraulic and mechanical response

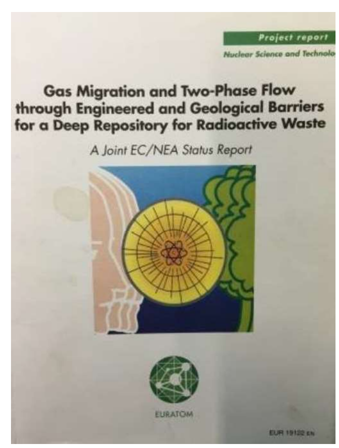

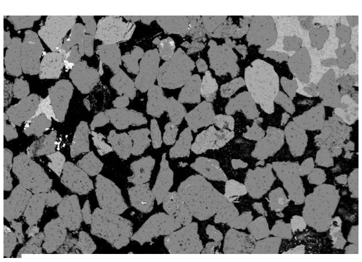

Sherwood sandstone

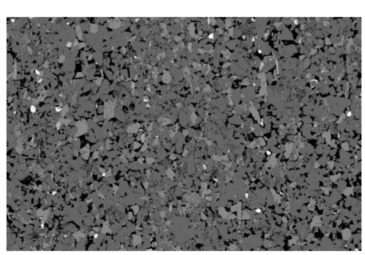

Siltstone

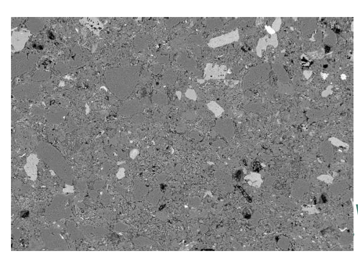

Permian Marl

How does gas flow?

Movement of gas will occur by the combined processes diffusion and bulk advection.

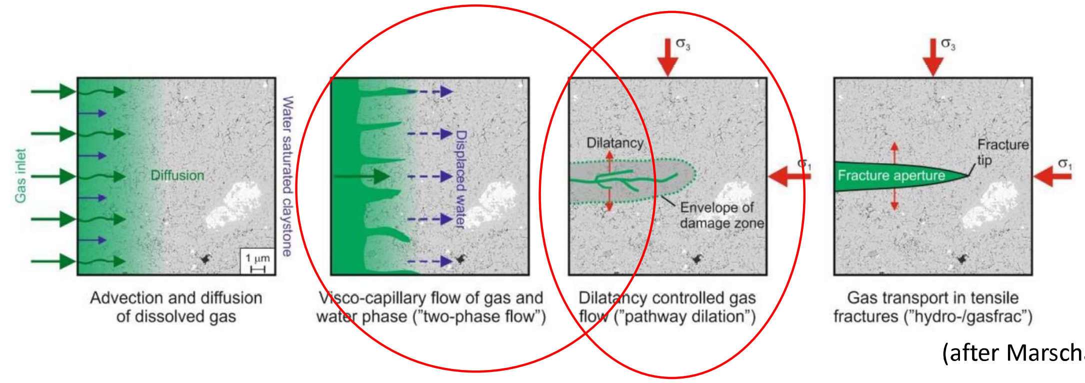

(after Marschall et al. 2005)

EURAD GAS aiming to look at controls on gas flow in these low permeability materials.

- Mineralogy
- Stress state
- Orientation
- Influence of Engineering Damaged Zone

Importance of workflow and sample quality

- Preservation of samples is an important part of testing on mudrocks
- Laboratory testing should be carried out as close to *in situ* conditions as possible.
- Sample preservation, preparation and storage techniques are especially important for low permeability materials.
- Laboratory workflow should be conscious of this at all times
- Pre and post test quantification of properties, e.g. geotechnical and petrological, are vital to give sample and data context

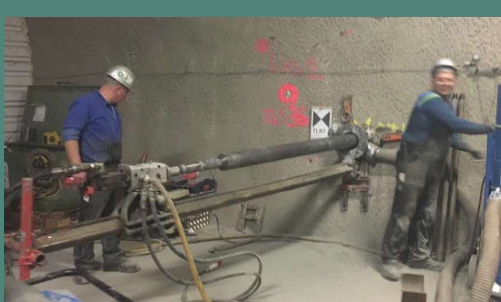

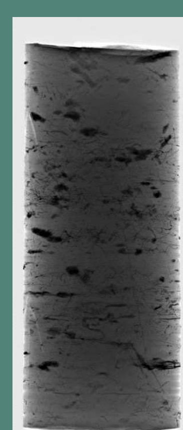

GDF

Nuclear Waste Services

Things to consider?

Aims & hypothesis

- What specific questions are we aiming to answer?
- Do we have a conceptual model to prove or disprove?

Apparatus

- What apparatus is available?
- Does this suit the questions we want to answer?
- Do any modifications need to be done?

Workflow (pre and post test)

- Sample preservation, preparation, characterisation, installation and post test analysis.

Boundary conditions

- What are the boundary conditions we want to test under? E.g. pressure, temperature, salinity, pH
- Are these suitable to the question we want to answer?
- Do we have the apparatus for these conditions?

Workflow

Pre-test

- Sample preparation
- Sample characterisation
- Calibration/leak testing of apparatus

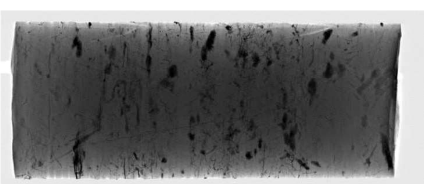

CT image of core barrel for sample selection

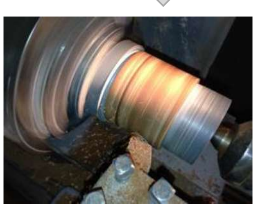

Sample manufacture by machine lathing

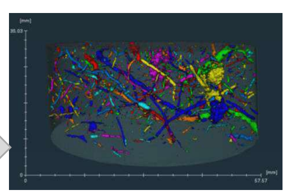

CT image of sample

Test

- E.g. gas injection test with a clear aim and boundary conditions

Post-test

- Careful dismantling of apparatus
- Sample characterisation

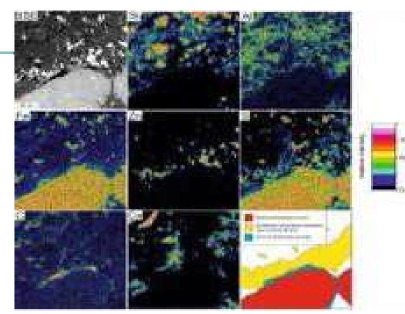

Triaxial apparatus

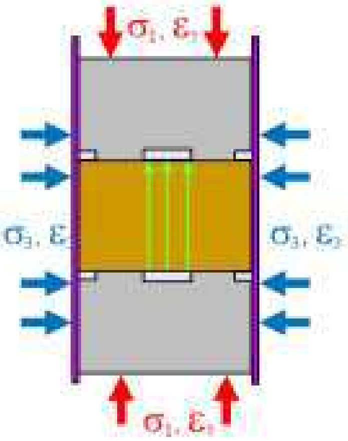

- Axial stress
- Confining stress
- Injection and Backpressure system
- 3 Radial sensors
- Axial sensors

Testing carried out at *in situ* pressure conditions

Within EURAD programme tests carried out on Boom Clay, Opalinus Clay and Callovo-Oxfordian Claystone

Triaxial gas injection tests

Rationale

- Displacement versus dilatant gas flow (natural material)
  - undertake a series of triaxial measurements examining the mechanisms governing gas flow through intact samples of Boom Clay and Cox
  - Tests performed parallel and perpendicular to bedding
- Experiments consist of a baseline hydraulic test followed by gas injection at one end of the sample

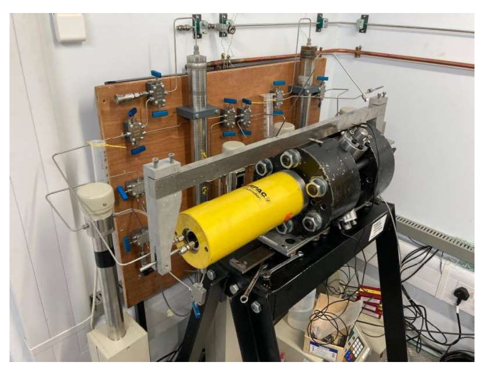

Test	Apparatus	Rock type	Stages	Boundary	Direction
1	Triax	COx	HY, GE, PP	In situ	//
2	Triax	Boom Clay	HY, GE, PP	In situ	⊥
3	Triax	Boom Clay	HY, GE, PP	Low/high confining	⊥
4	Triax	COx	HY, GE, PP	Low/high confining	//

Gas test 1 COx // (sample 21-043)

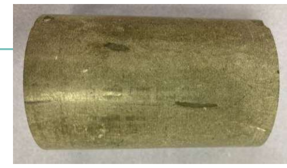

- A simple two-step gas injection ramp performed [1]
- During ramp 1 a small outflow seen as water was expelled from the injection filter [2]
- During first gas ramp the sample showed dilation from swelling [3]

[1]

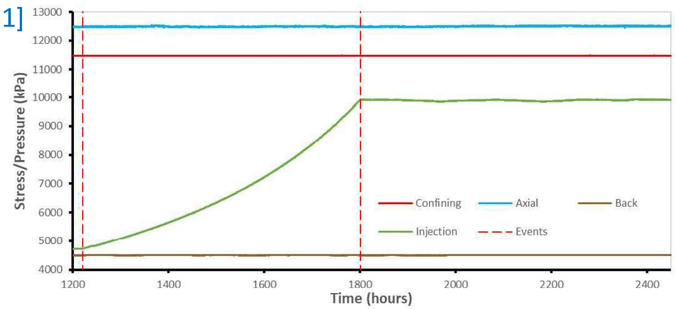

[3]

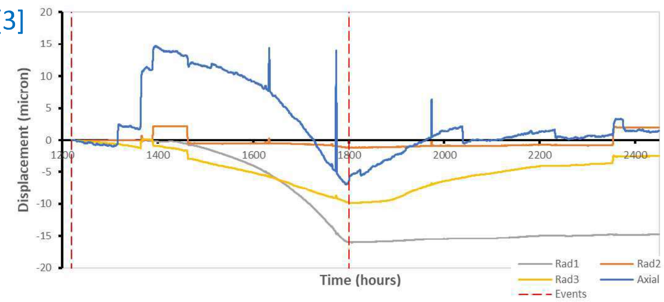

[2]

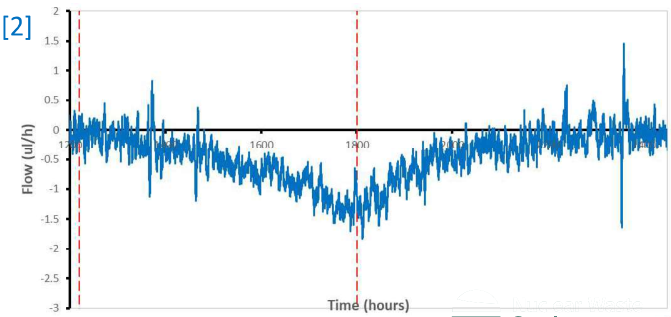

Gas test 1 COx // (sample 21-043)

[1]

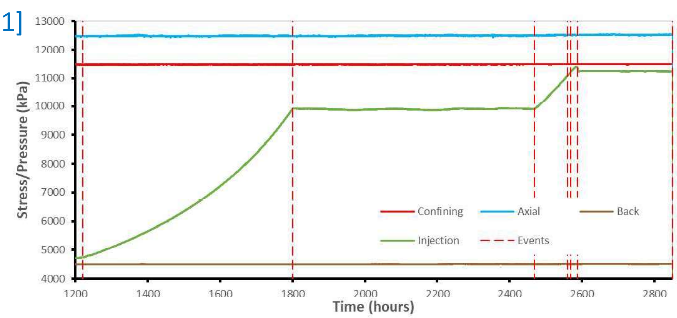

[3]

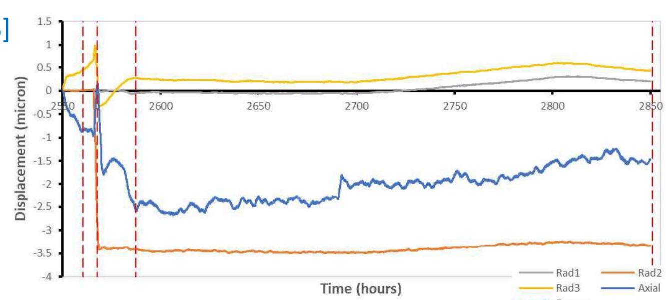

[2]

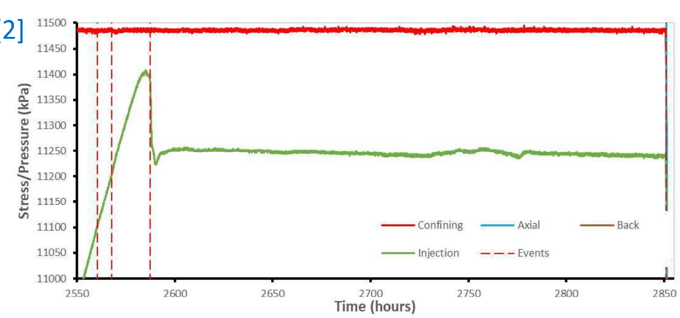

[4]

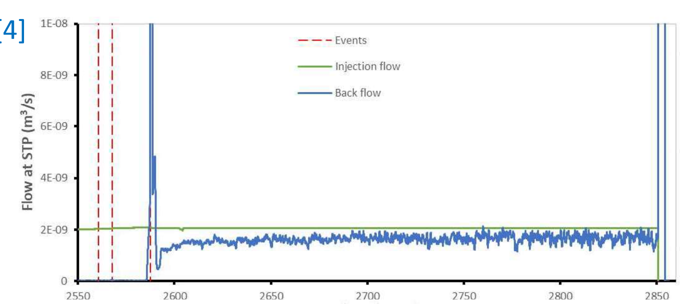

Similar gas outflow results seen in Boom Clay and Opalinus Claystone

Comparison to previous results

COx - EURAD

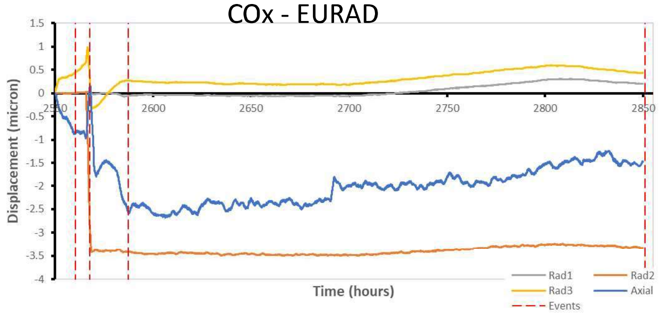

Boom Clay - EURAD

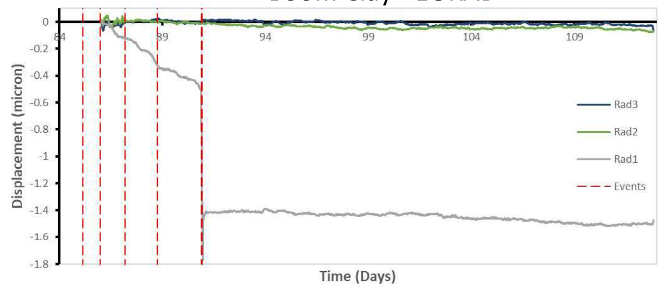

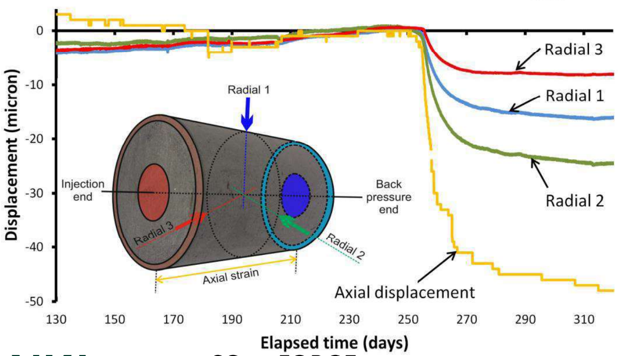

COx - FORGE

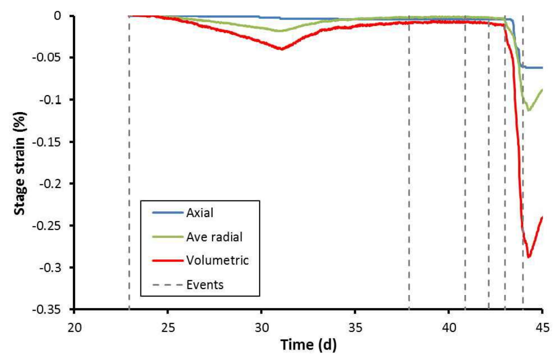

Boom Clay - OPERA

What do these results mean?

- As gas enters and moves through the sample we see very small amounts of strain until a rapid gas breakthrough event occurs. Strain does not occur evenly throughout the sample, suggesting dilation flow.
- In previous tests, using a smaller injection filter, this breakthrough event occurred over a much longer time.

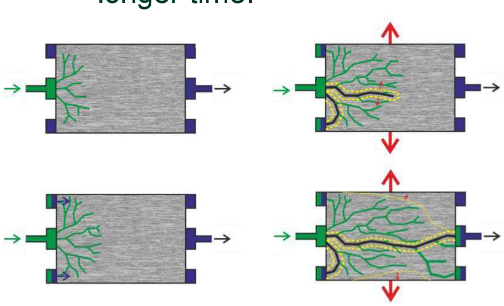

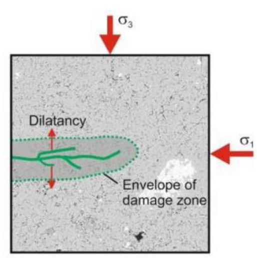

Dilatancy controlled gas flow ("pathway dilation")

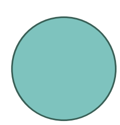

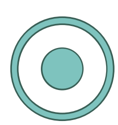

- Test geometry different. Are the current tests exploiting damage on the outside of the sample
- Sidewall flow test conducted as part of GT. Saw dilation << 1 μm

How can we visualise this process in the laboratory?

Visualising gas flow

- Apparatus constructed with 50mm thick, 150mm diameter UV fused silica glass window.
- Normal load applied via steel platens and torque on screws, up to 3 MPa.
- Capable of gas injection pressure ranging from 0.5-15 MPa, controlled by 260D Teledyne Isco syringe pump.
- Pump flow rate can range from 1 µl/min to 107 ml/min
- Helium, Hydrogen, CO_2, Nitrogen, Compressed air & water capability for injection
- Time-lapse macro photography.

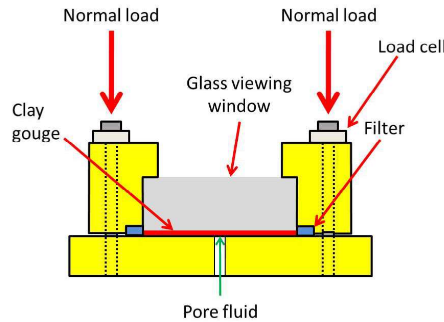

Callovo-Oxfordian

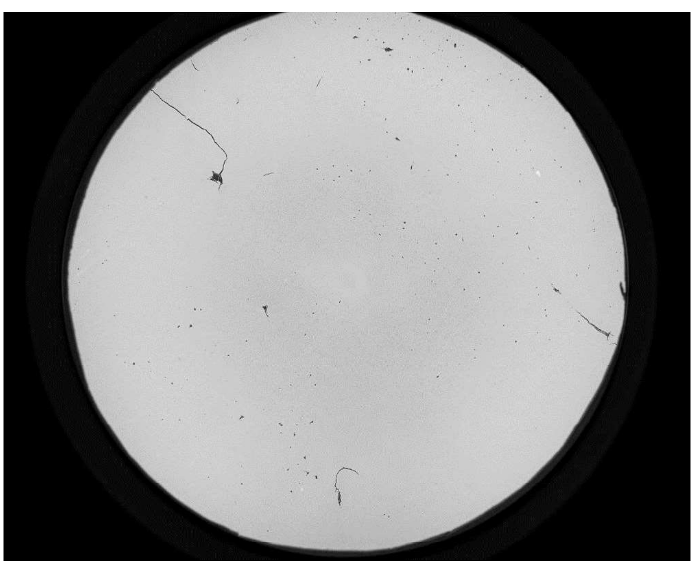

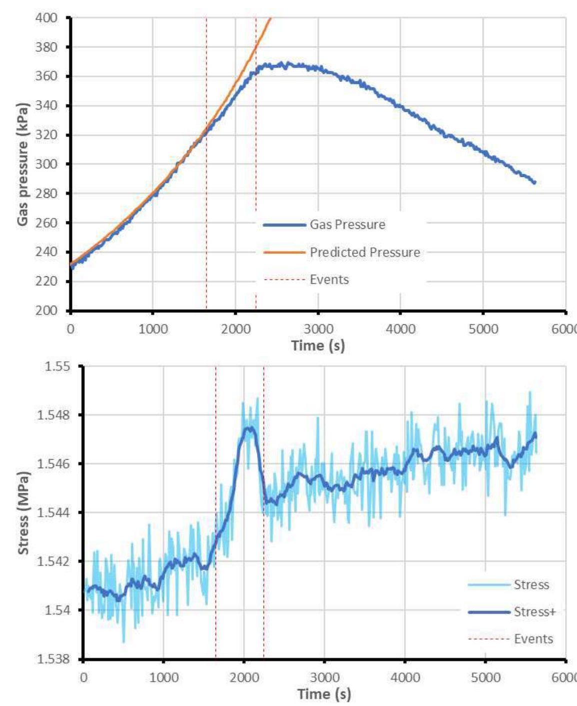

- 675s video

Evidence of Self-sealing – COx

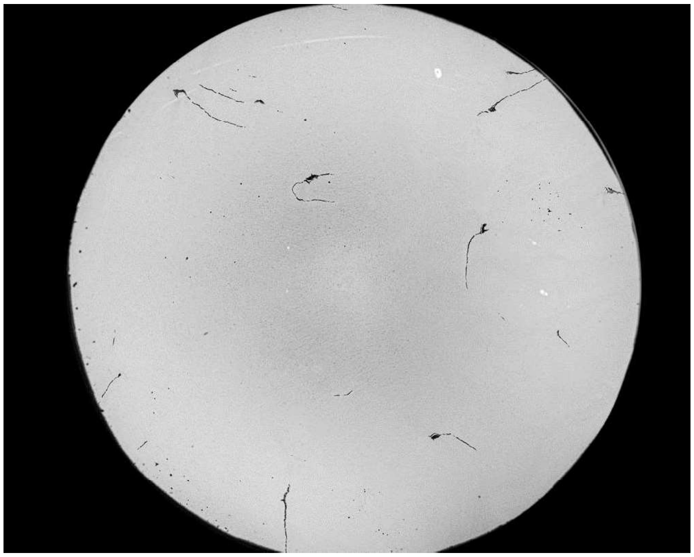

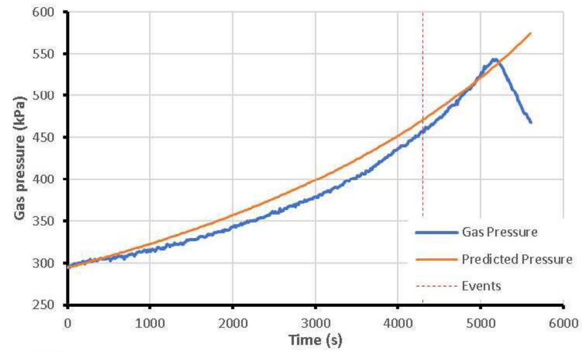

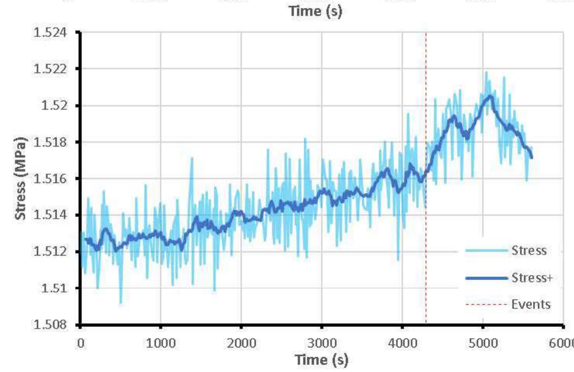

Gas flow via dilation pathways

- Pathways appear to be stochastic and do not always take advantage of what appear to be natural weaknesses in the analogue samples
- Clear deformation of local surrounding matrix
- Do not always appear to exploit apparent weaknesses in the matrix, e.g. pre-existing features
- Branching of pathways, searching for route of least resistance
- Only visible in analogue samples. Previous work has examined other ways of visualising these features
- How would these features be modelled?

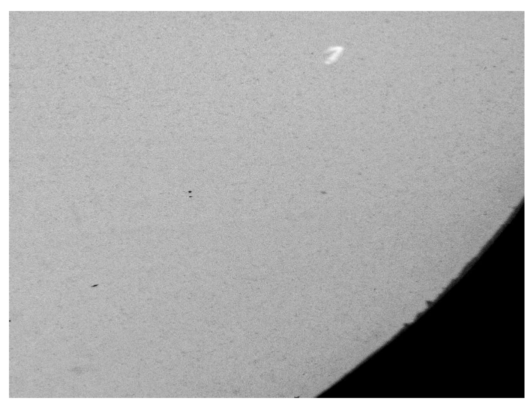

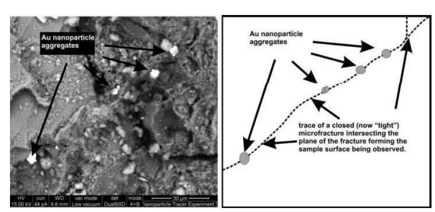

- Nano particle injection provided definitive proof of dilatant flow in BC
- Gas permeability is a dependent variable related to the number and geometry of pressure-induced pathways

GDF

Nuclear Waste Services

Conclusions and lessons learnt

- In these clay-rich, low permeability materials gas flows via dilation pathways (where advection flow is occurring)
- Complex to model stochastic nature and small scale of pathways – research needed to understand controls
- What controls the pathway route?
- How do these processes upscale to field scale?

- Combination of methods often needed to build evidence base for claims
- Tests on both intact and analogue materials can be important
- Need to be aware of impact of test arrangement on results
- Detailed and constantly developed workflows allow results to be put into context and details on physical processes to be understood

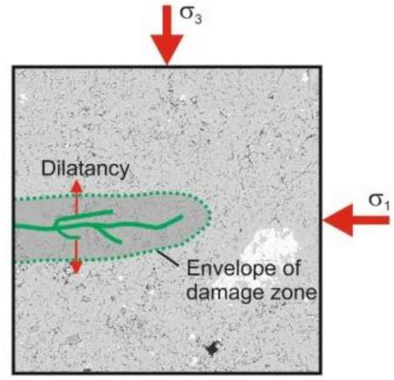

Dilatancy controlled gas flow ("pathway dilation")

Overlapping research areas

- Carbon Capture and Storage
- Compressed Air Energy Storage / Hydrogen Storage
- Engineering geology

GDF

Nuclear Waste Services

Any questions?

Acknowledgements: Jon Harrington, Rob Cuss, Caroline Graham, Katherine Daniels and NWS AS+R team

GDF

Nuclear Waste Services

Appendix J. Advanced multiphysics modelling of geomaterials: Introduction (A-C Dieudonné)

ALERT Geomaterials
Alliance of Laboratories in Europe for Education, Research and Technology
http://alertgeomaterials.eu

eurad
European Joint Programme
on Radioactive Waste Management

Advanced multiphysics modelling of geomaterials: multiscale approaches and heterogeneities

Join at vevox.app

ID: 177-435-608

Pierre BÉSUELLE[1], Frédéric COLLIN[2], **Anne-Catherine DIEUDONNÉ**[3]

[1] Université Grenoble Alpes – 3SR laboratory
[2] University of Liège – UEE Research Unit
[3] Delft University of Technology – Faculty of Civil Engineering and Geosciences

This project has received funding from the European Union's Horizon 2020 research and innovation programme under grant agreement N°847593

Modelling approaches for geomaterials generally substitute the real discontinuous porous medium by idealized homogeneous continua

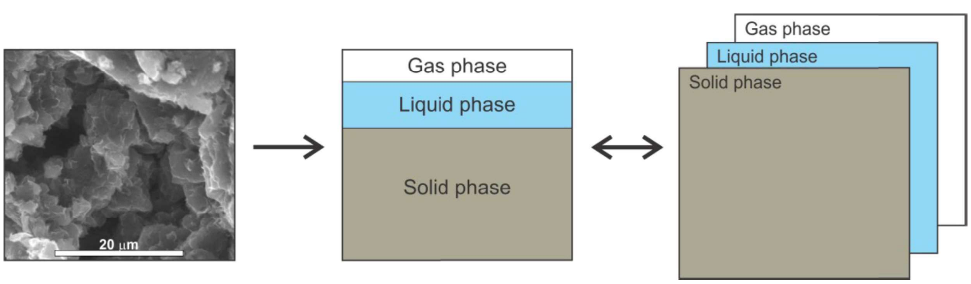

Unknowns:
- Solid phase: $\boldsymbol{u}$
- Liquid phase: u_w
- Gas phase: u_g

Balance equations:
- Solid mass
- Water mass
- Air mass
- Momentum

Constitutive equations:
- Water retention model: S_r
- Multiphase flow model: $\boldsymbol{f}_l^w, \boldsymbol{f}_g^w \ldots$
- Mechanical model: $\boldsymbol{\sigma}'$

eurad

MECHANICAL CONSTITUTIVE BEHAVIOUR

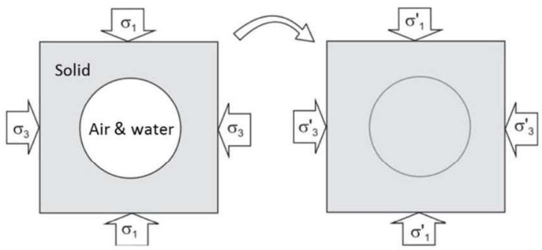

Mechanically equivalent

- Single phase
- Single stress

Constitutive relationships

$$d\boldsymbol{\sigma}' = \boldsymbol{D}: d\boldsymbol{\varepsilon} = \boldsymbol{D}(\boldsymbol{\sigma}, \dot{\boldsymbol{\sigma}}, \boldsymbol{\kappa}, \boldsymbol{t}): d\boldsymbol{\varepsilon}$$

These features reflect processes that take place at a small scale but which, **for convenience**, are modelled at the macro/continuous scale

- **Macroscopic and continuous approaches are generally sufficient in many cases, where the material behaviour follows stress paths which are well represented by the model**

  (the behaviour of geomaterials is strongly nonlinear and path dependent!)

… BUT

- Model parameters are not always measurable quantities, but should be calibrated
- Macroscopic approaches suffer from limitations upon complex stress paths and/or when the behaviour is extrapolated over time

➔ In this case, multi-scale modelling is a way of enriching the description of the material behaviour by explicitly accounting for the smaller-scale characteristics behaviour

BENTONITE

Experimental observations: wetting under constant volume and free-swelling conditions

MX-80 bentonite/sand (7/3 in dry mass) (Gatabin et al. 2016)

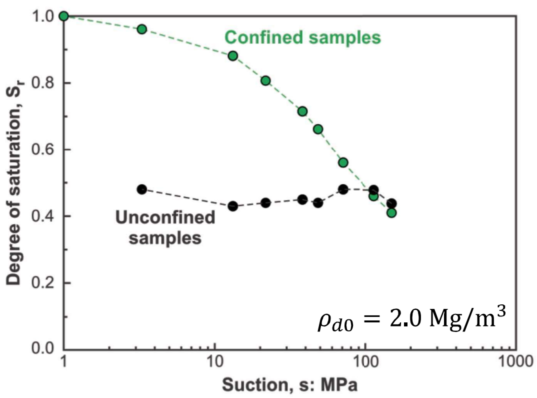

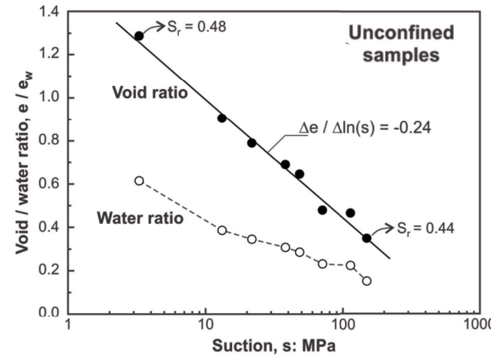

$$S_r = \frac{V_w}{V_v} = \frac{e_w}{e}$$

⇨ **Competing effects** of

- Water uptake (e_w)
- Swelling (e)

BENTONITE

$$e_w = S_r \, . \, e = e_{wm} + e_{wM}$$

(Dieudonné et al, 2017)

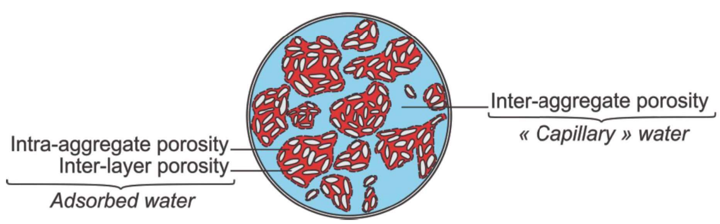

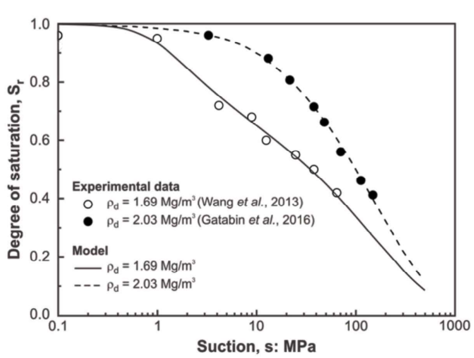

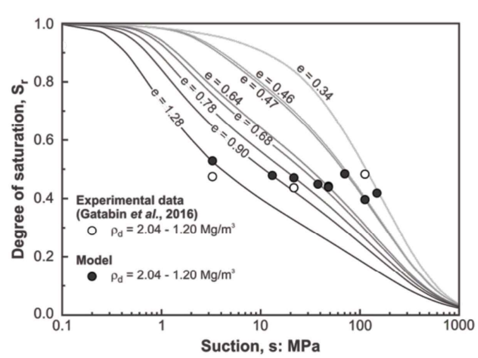

BIO-CEMENTED SOILS (Zhang & Dieudonné, 2023)

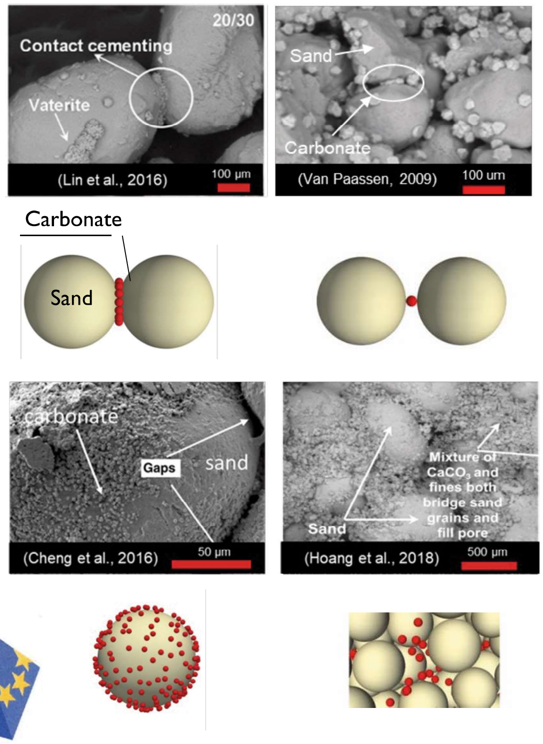

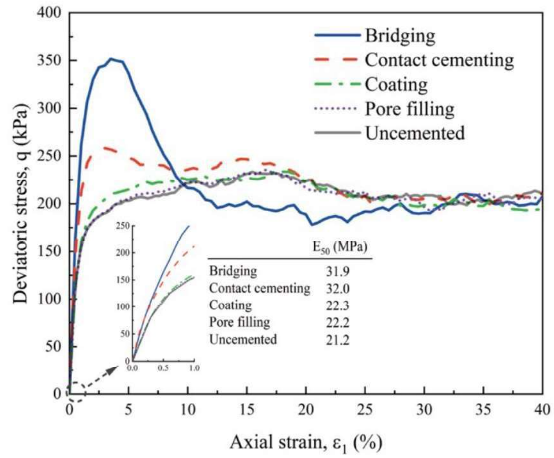

WHAT IS A MULTISCALE MODELLING APPROACH?

A multi-scale modelling approach includes:

- **A description of the microstructure**
  - Can be discrete, continuous or hybrid
- **A coupling strategy between micro- and macro-scales**
  - Can be analytical or computational

Remark: a model is, by definition, a simplification of reality (even multi-scale approaches!). For a given problem, a multi-scale approach is not always necessary for all aspects of the multiphysics behaviour !

REFERENCES

- Dieudonné A.C., Della Vecchia G., Charlier R. (2017) Water retention model for compacted bentonites. Canadian Geotechnical Journal 54(7), 915-925.
- Gatabin C., Talandier J., Collin F., Charlier R. & Dieudonné A.C. (2016) Competing effects of volume change and water uptake on the water retention behaviour of a compacted MX-80 bentonite/sand mixture. Applied Clay Science 121-122, 57-62.
- Zhang A. & Dieudonné A.C. (2023) Effects of carbonate distribution pattern on the mechanical behaviour of bio-cemented sands: A DEM study. Computers and Geotechnics 154, 105152.

Appendix K. Advanced multiphysics modelling of geomaterials: multiscale approaches and heterogeneities (P. Bésuelle)

ALERT Geomaterials
Alliance of Laboratories in Europe for Education, Research and Technology
http://alertgeomaterials.eu

European Joint Programme on Radioactive Waste Management

Multiphysics and multiscale coupled processes in geomaterials.

Focus on thermal effects and gas transfer impact on the behaviour of geomaterials.

Advanced multiphysics modelling of geomaterials: multiscale approaches and heterogeneities

Pierre **BESUELLE**
Nicolas **ZALAMEA**
Univ. Grenoble Alpes and CNRS – 3SR

This project has received funding from the European Union's Horizon 2020 research and innovation programme under grant agreement N°847593

Outline

1. Motivations
2. Methods
3. Couplings
4. Strain localisation
5. Model calibration
6. Parallelisation
7. Conclusions and perpectives

Motivations

Propose an alternative approach to phenomenological models :

- which take into account the microstructure of the material
- which ensures a bridge with the macroscopic scale (multiscale)
- which allows the introduction of multiphysical couplings at the small scale
- that is operational for engineering calculations

3SR

Motivations

Last few decades evolution of experimental characterization :

- High resolution imaging methods
- Full field measurement (DIC improvements)
- *in operando* tests (4D imaging)
- Multiscale imaging (local and global)

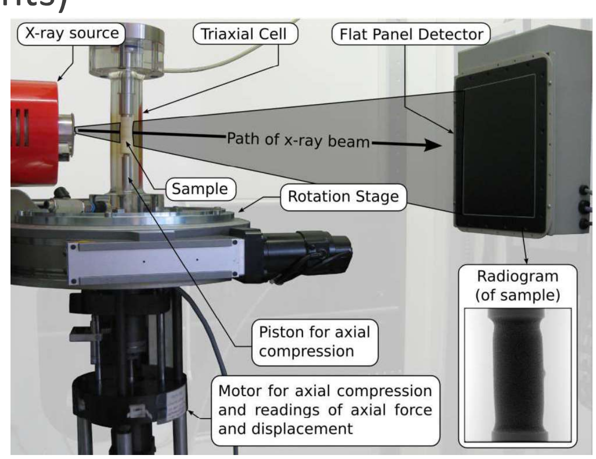

3SR

Motivations

Granular material

(Hostun sand)

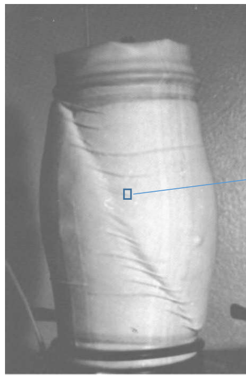

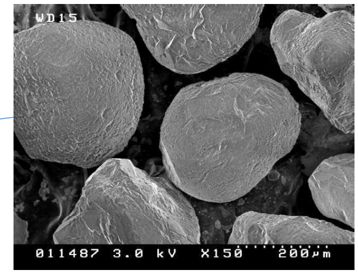

Multiscale x-ray CT (3SR)
Voxel size 7 μm
+ discrete DIC

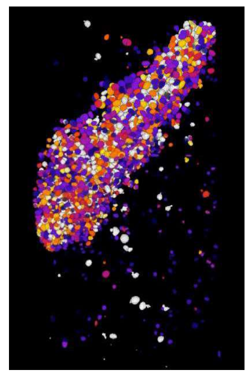

PhD thesis Ando, 2013

Grain rotation

Motivations

Clay rock

(Callovo-Oxfordian clay rock)

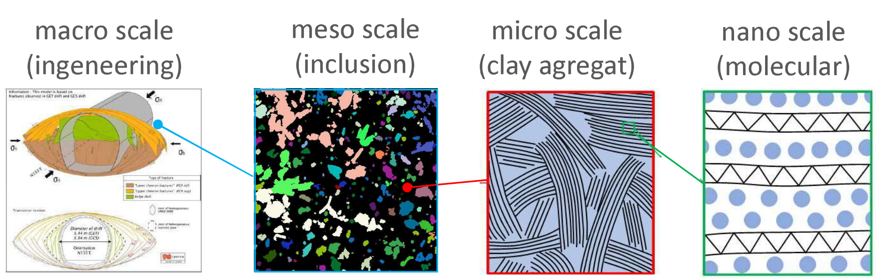

Motivations

Clay rock

(Callovo-Oxfordian clay rock)

macro scale (engineering)

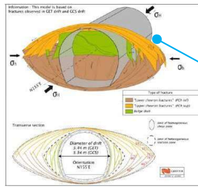

meso scale (inclusion)

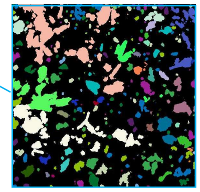

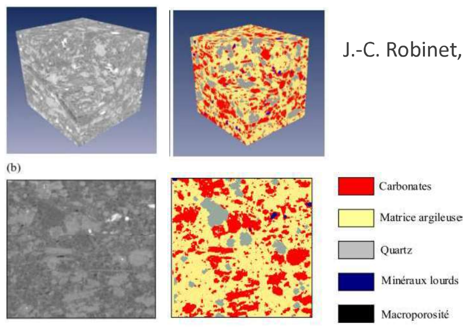

10µm

J.-C. Robinet, 2008

BIB-SEM

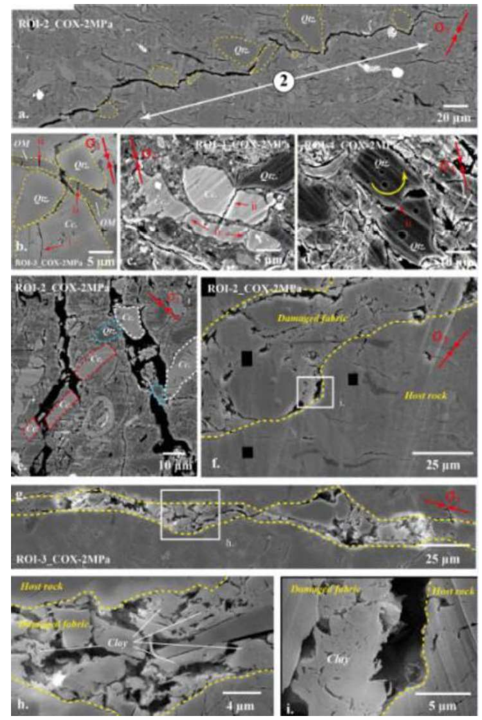

G. Desbois *et al.*, 2017

Motivations

Clay rock

(Callovo-Oxfordian clay rock)

in operando test + η-X-ray CT synchrotron + DIC

Triaxial test

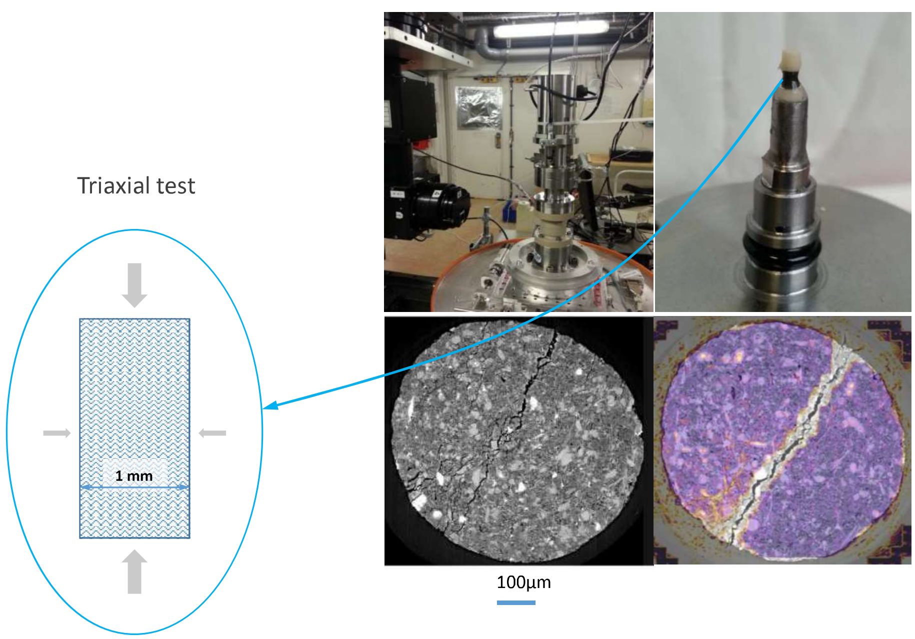

100µm

Bésuelle *et al.*

Motivations

Clay rock

(Callovo-Oxfordian clay rock)

Evolution of a vertical slice during axial loading

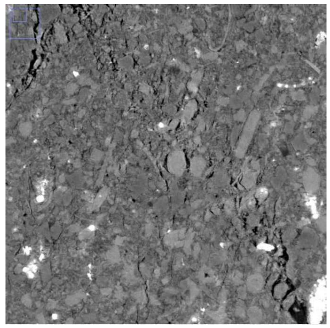

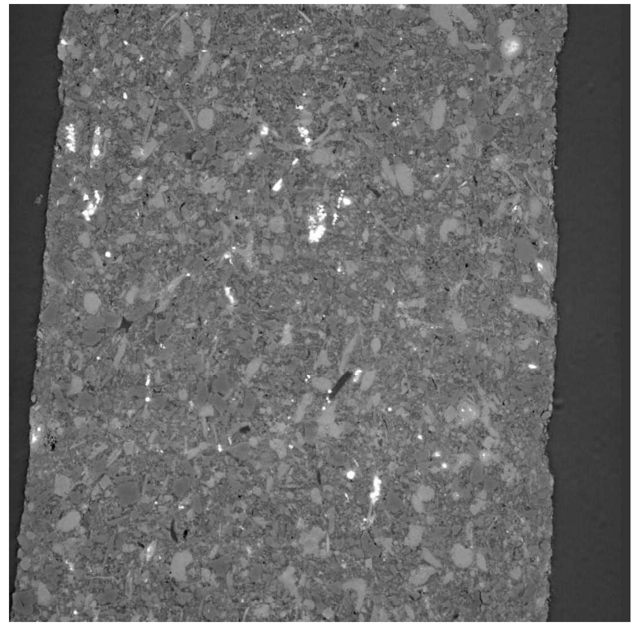

10µm

Bésuelle *et al.*

Motivations

Clay rock

(Callovo-Oxfordian clay rock)

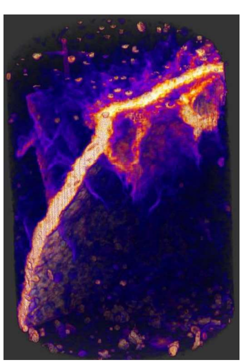

Combined continuous & discrete DIC

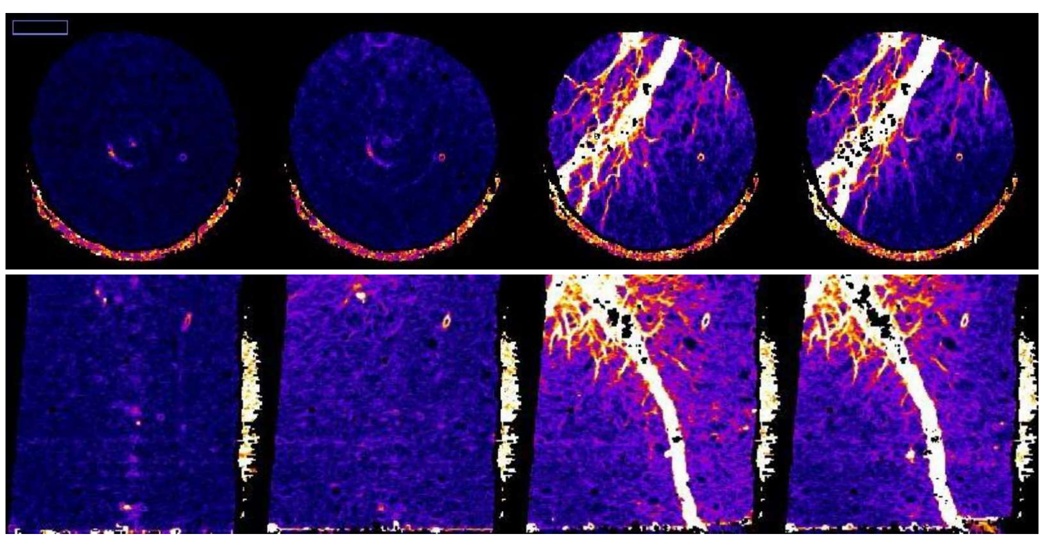

Bésuelle *et al.*

Motivations

Macro scale (continuum) : FEM	Meso scale (heterogeneous)
☺ well suited to Real scale problem ☹ CAN NOT realistically model their heterogeneous nature	Reproduces « naturally » the complex behaviour at mesoscale: • granular material (DEM): cyclic response, anisotropy, strain path dependency, ☺ • brittle materials (FEM): damage, anisotropy, strain path dependency, multiphysical couplings ☺ • Computation time depends on the number of grains -> high CPU costs ☹ > limitation to small problems
Bridging between scale: FEMxDEM or FEMxFEM (FEM^2) ☺ ☺	

Outline

1. Motivations
2. Methods
3. Couplings
4. Strain localisation
5. Model calibration
6. Parallelisation
7. Conclusions and perpectives

Methods

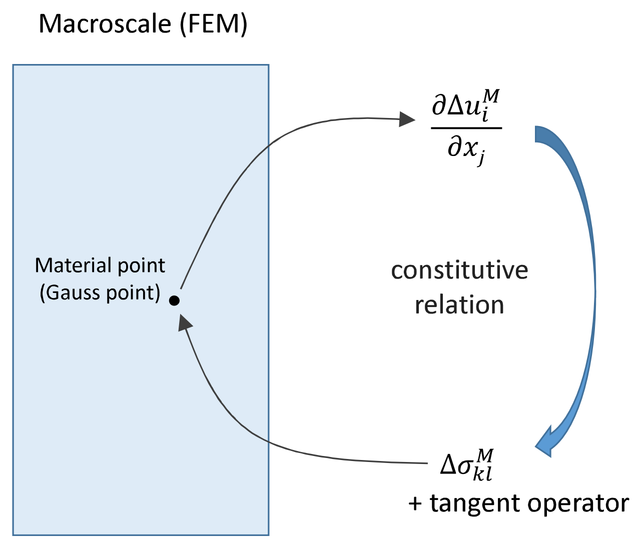

Methods

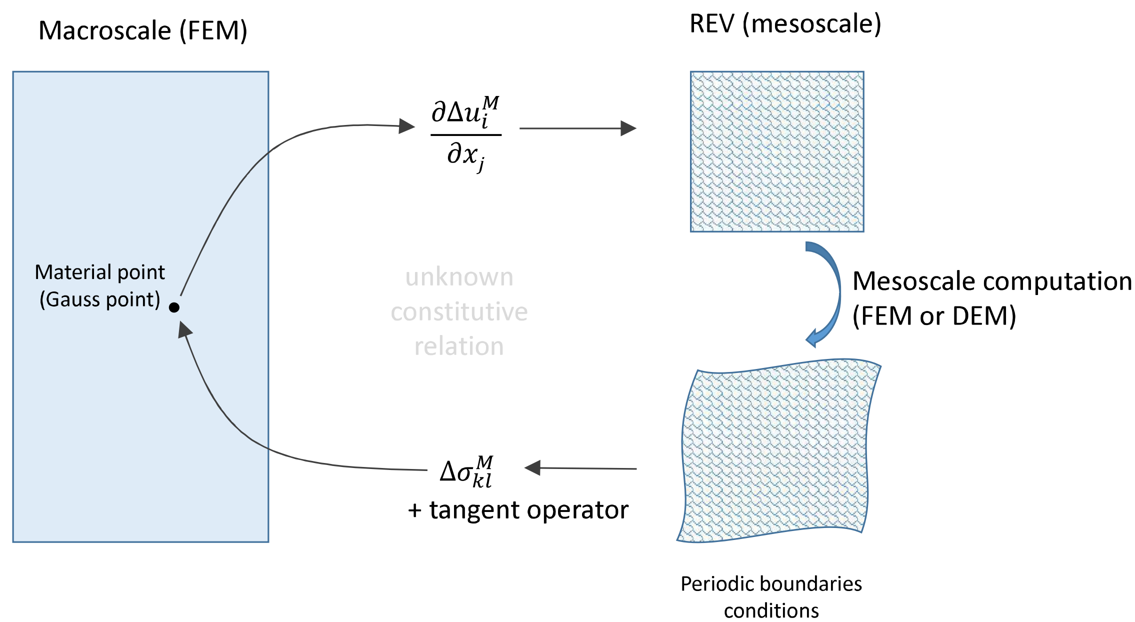

Methods

Example of a brittle material modeled by FEM:

Field equation (macro): $\int_{\Omega^t} \left(\sigma_{ij} \frac{\partial u_i^*}{\partial x_j^t} \right) dV - \int_{\Gamma^t} \left(t_i u_i^* \right) dS = 0$

Macro strain increment: $\frac{\partial \Delta u_i^M}{\partial x_j}$ $\left(F_{ij}^M = R_{ik}^M U_{kj}^{REV} \right)$

Periodic conditions (meso): $\Delta(u^+ - u^-) = \frac{\partial \Delta u_i^M}{\partial x_j}(x^+ - x^-)$

Macro stress: $\sigma_{ij}^M = \frac{1}{\Omega} \int_{\Gamma^{REV}} (\sigma_{ik}^m n_k)\, x_j \, d\Gamma$

Tangeant operator: $\delta \sigma_{ij}^M = C_{ijkl} \frac{\partial \delta u_i^M}{\partial x_j}$

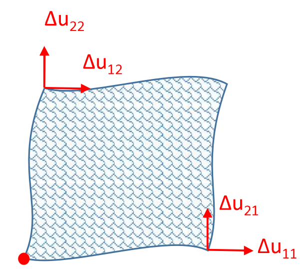

Methods

- a mesostructure is associated to each Gauss point
- the mesostructure follows the full loading path of the material point

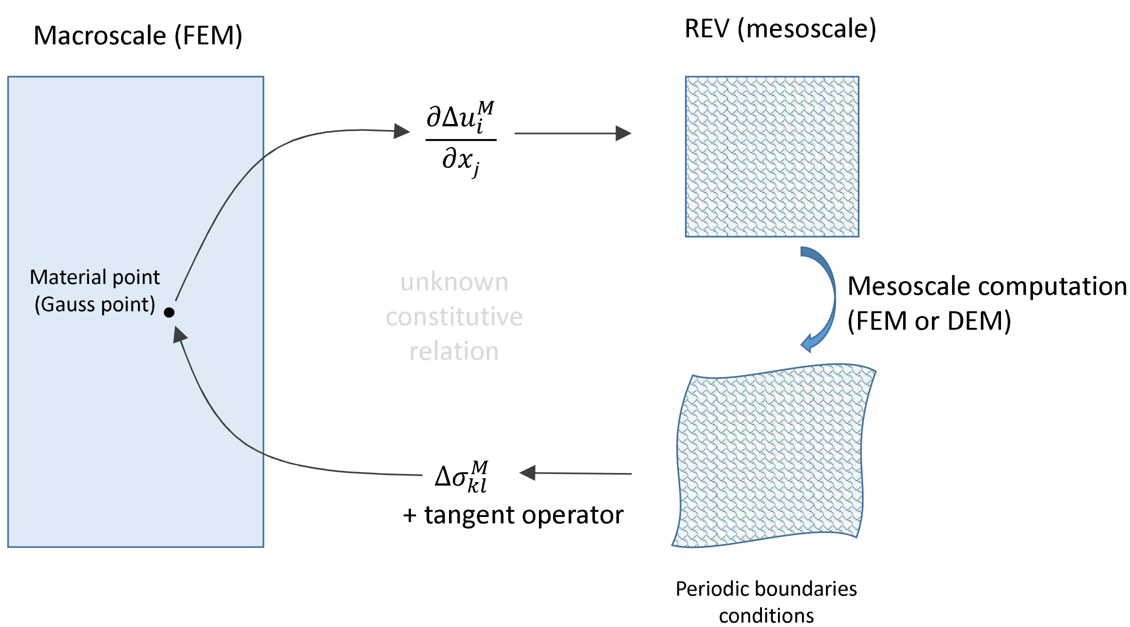

Outline

3SR

Methods

Example of a brittle material with fluid modeled by FEM:

Field equation (macro): $$\int_{\Omega^t} \left(\sigma_{ij} \frac{\partial u_i^*}{\partial x_j^t} \right) dV - \int_{\Gamma^t} \left(t_i u_i^* \right) dS = 0$$

$$\int_{\Omega^t} \left(m_j \frac{\partial p^*}{\partial x_j^t} - \dot{M} p^* \right) dV - \int_{\Gamma^t} q p^* dS = 0$$

Macro strain increment: $\frac{\partial \Delta u_i^M}{\partial x_j}, p^M, \nabla p^M$

Periodic conditions (meso): $\Delta(u^+ - u^-) = \frac{\partial \Delta u_i^M}{\partial x_j}(x^+ - x^-)$

$$\Delta(p^+ - p^-) = \frac{\partial \Delta p^M}{\partial x_j}(x^+ - x^-)$$

$w^+ - w^+ = 0$

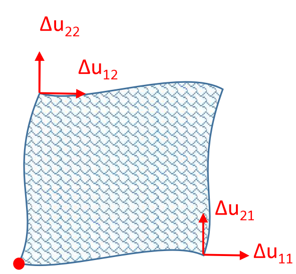

Frey *et al.*, 2012
van den Eijnden *et al.*, 2015

3SR

Methods

Example of a brittle material with fluid modeled by FEM:

Macro stress: $\sigma_{ij}^{M} = \frac{1}{\Omega}\int_{\Gamma^{solid}} (\sigma_{ik}^{m}\, n_k)\, x_j \, d\Gamma$

Fluid flux: $m_i = \frac{1}{\Omega}\int_{\Gamma^{fluid}} w\, x_i \, d\Gamma$

Fluid mass content: $M = V^{fluid}\, \rho^{fluid}$

Tangeant operator:
$$\begin{Bmatrix} \delta\sigma_{ij}^{M} \\ \delta M \\ \delta m_i^{M} \end{Bmatrix} = \begin{bmatrix} C_{ijkl} & A_{ij} & B_{ijl} \\ D_{kl} & E & G_l \\ I_{ikl} & J_i & L_{il} \end{bmatrix} \begin{Bmatrix} \frac{\partial \delta u_k^{M}}{\partial x_l} \\ \delta p^{M} \\ \frac{\partial \delta p^{M}}{\partial x_l} \end{Bmatrix}$$

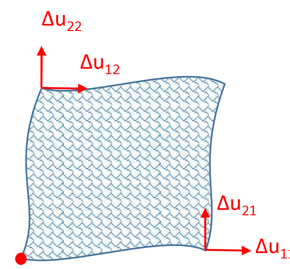

Frey *et al.*, 2012
van den Eijnden *et al.*, 2015

Methods

Example of a brittle material with fluid modeled by FEM:

Consistant tangeant operator:
$$\begin{Bmatrix} \delta\sigma_{ij}^{M} \\ \delta M \\ \delta m_i^{M} \end{Bmatrix} = \begin{bmatrix} C_{ijkl} & A_{ij} & B_{ijl} \\ D_{kl} & E & G_l \\ I_{ikl} & J_i & L_{il} \end{bmatrix} \begin{Bmatrix} \frac{\partial \delta u_k^{M}}{\partial x_l} \\ \delta p^{M} \\ \frac{\partial \delta p^{M}}{\partial x_l} \end{Bmatrix}$$

- by perturbations
- by static condensation

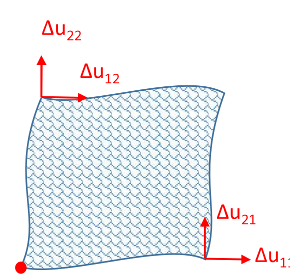

Frey *et al.*, 2012
van den Eijnden *et al.*, 2015

Methods

Assumptions:

- Macro: large transformations, meso: small transformations
- Macro solid rotation is treated out of the small scale problem. Only stretching determined the limit conditions of the small scale problem

$$F_{ij}^{M} = R_{ik}^{M} U_{kj}^{REV} \qquad \nabla_i^{M} p = R_{ik}^{M} \nabla_i^{REV} p$$

$$\sigma_{ij}^{M} = R_{ik}^{M} \sigma_{kl}^{REV} R_{jl}^{M} \qquad m_i^{M} = R_{ij}^{M} m_j^{REV}$$

- Scale separation: mesoscale characteristic time very smaller than at macro scale. Small scale problem is treated in its steady state

Methods

Sequential decomposition:

- Newton-Raphson iterative routine for solving the mechanical system (uniform pressure): FEM
- Direct routine for solving hydraulic problem (known configuration): Balance of mass fluxes on interface nodes,
- Homogenization and tangent operators (perturbation or static condensation).

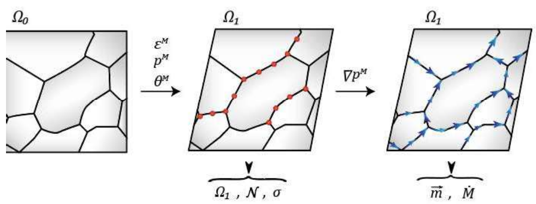

Methods

Example of a brittle material with fluid modeled by FEM:

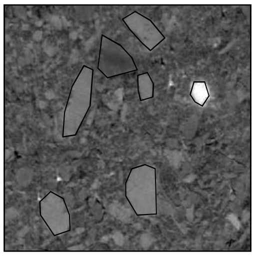

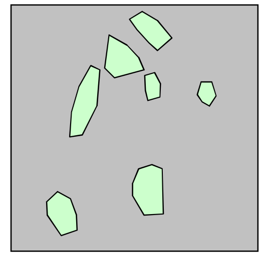

Representative elementary volume (REV)

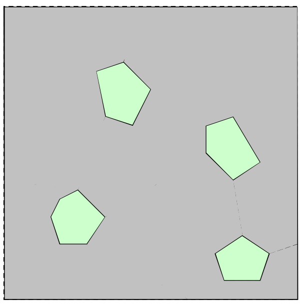

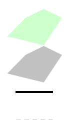

inclusion
clay matrix
interface inclusion/clay
potential cracks in clay matrix

Frey *et al.*, 2012
van den Eijnden *et al.*, 2015

Methods

Example of a brittle material with fluid modeled by FEM:

Mechanics

- Grains: linear elastic solid phases

$$\sigma_{ij} = 2\mu\varepsilon_{ij} + \lambda\varepsilon_{kk}\delta_{ij}$$

- Cohesive interfaces: damage laws

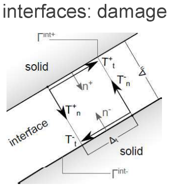

Normal

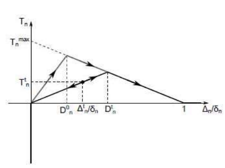

Tangential

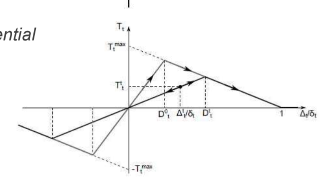

Fluid flow

- Cohesive interfaces (coupling M → H)
  - Interface opening defines channel hydraulic conductivity ($\kappa \propto \Delta h^3$)
- Flow assumptions
  - Laminar flow between smooth parallel platens
  - Network of 1D channels between grains
- Fluid forces (coupling H → M)
  - Fluid pressure acting normally on solids boundaries
- Fluid compressibility
  - $\rho^w = \rho^0 e^{k_w(p - p_0)}$

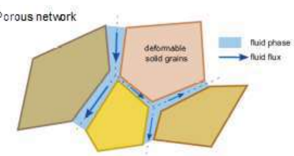

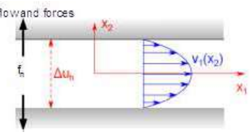

Frey *et al.*, 2012
van den Eijnden *et al.*, 2015

Methods

Example of a brittle material with fluid modeled by FEM:

- Laminar flow in parallel plates (cubic law)

$$\vec{m} = \rho_w \frac{\Delta {u_h}^3}{12\eta} \frac{dp}{ds}$$

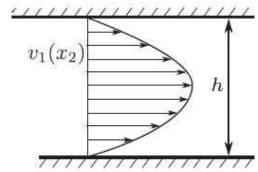

- Fluid aperture *vs.* mechanical aperture

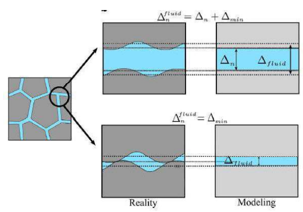

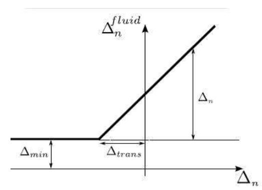

Marinelli *et al.*, 2013

Methods

A model for brittle material modeled by FEM:

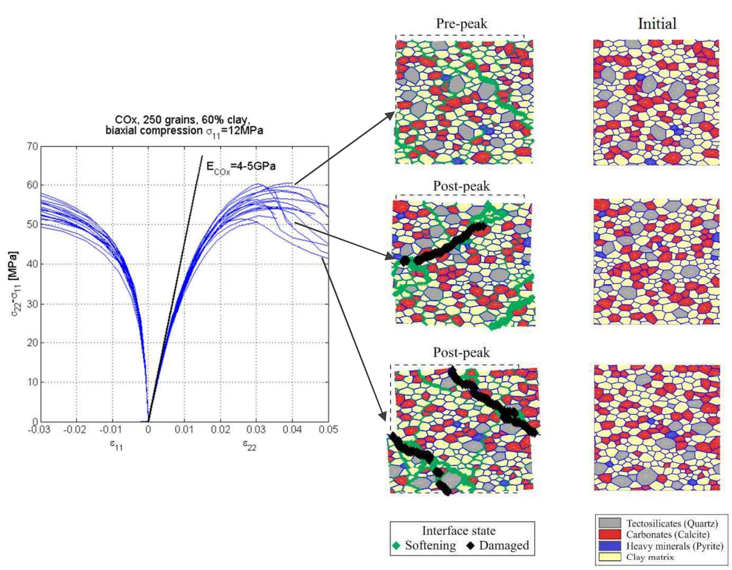

Deformation of a REV following vertical compression and horizontal confining pressure (12 MPa)

Pardoen *et al.*, 2020

Methods

Example of a brittle material with fluid and temperature modeled by FEM:

Field equation (macro):

$$\int_{\Omega^t}\left(\sigma_{ij}\frac{\partial u_i^*}{\partial x_j^t}\right)dV - \int_{\Gamma^t}\left(t_i u_i^*\right)dS = 0$$

$$\int_{\Omega^t}\left(m_j\frac{\partial p^*}{\partial x_j^t} - \dot{M}p^*\right)dV - \int_{\Gamma^t} q_w p^* dS = 0$$

$$\int_{\Omega^t}\left(h_j\frac{\partial \theta^*}{\partial x_j^t} - \dot{H}\theta^*\right)dV - \int_{\Gamma^t} q_h \theta^* dS = 0$$

Macro strain increment: $\frac{\partial \Delta u_i^M}{\partial x_j}, p^M, \nabla p^M, \theta^M, \nabla\theta^M$

Methods

Example of a brittle material with fluid and temperature modeled by FEM:

Periodic conditions (micro):

$$\Delta(u^+ - u^-) = \frac{\partial \Delta u_i^M}{\partial x_j}(x^+ - x^-)$$

$$\Delta(p^+ - p^-) = \frac{\partial \Delta p^M}{\partial x_j}(x^+ - x^-)$$

$$q_w{}^+ - q_w{}^+ = 0$$

$$\Delta(\theta^+ - \theta^-) = \frac{\partial \Delta \theta^M}{\partial x_j}(x^+ - x^-)$$

$$q_h{}^+ - q_h{}^- = 0$$

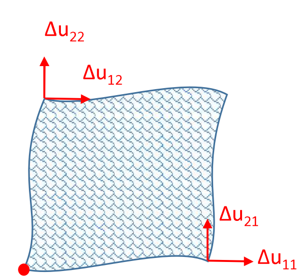

Zalamea *et al.*, 2023

Methods

Example of a brittle material with fluid and temperature modeled by FEM:

Macro stress: $\sigma_{ij}^{M} = \frac{1}{\Omega} \int_{\Gamma solid} (\sigma_{ik}^{m}\, n_k)\, x_j \, \mathrm{d}\Gamma$

Fluid flux: $m_i = \frac{1}{\Omega} \int_{\Gamma fluid} w\, x_i \, \mathrm{d}\Gamma$

Fluid mass content: $M = \frac{1}{\Omega} \int_{S} \rho_w{}^{m}\, \mathrm{d}S = V^{fluid} \rho^{fluid}$

Thermal flux: $h_i = \frac{1}{\Omega} \int_{\Gamma} q_h\, x_i \, \mathrm{d}\Gamma$

Internal energy: $H = \frac{1}{\Omega} \int_{S} \rho^m\, c_p{}^m\, \theta^m \, \mathrm{d}S$

Tangeant operator:

$$\begin{Bmatrix} \delta\sigma_{ij}^{M} \\ \delta M \\ \delta m_i^{M} \\ \delta H \\ \delta h_i^{M} \end{Bmatrix} = \begin{bmatrix} C_{ijkl} & A_{ij} & B_{ijl} & N_{ij} & O_{ijl} \\ D_{kl} & E & G_l & P & R_l \\ I_{ikl} & J_i & L_{il} & S_i & T_{il} \\ U_{kl} & V & W_l & X & Y_l \\ Z_{ikl} & F_i & K_{il} & Q_i & H_{il} \end{bmatrix} \begin{Bmatrix} \frac{\partial \delta u_k^{M}}{\partial x_l} \\ \delta p^{M} \\ \frac{\partial \delta p^{M}}{\partial x_l} \\ \delta\theta^{M} \\ \frac{\partial \delta\theta^{M}}{\partial x_l} \end{Bmatrix}$$

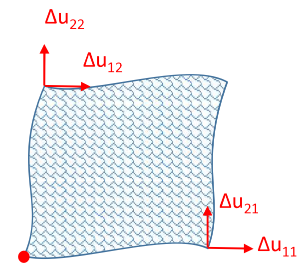

Zalamea *et al.*, 2023

Methods

A model for brittle material with fluid and temperature modeled by FEM:

Mechanics

- Grains: linear elastic solid phases

  $\sigma_{ij} = 2\mu\varepsilon_{ij} + \lambda\varepsilon_{kk}\delta_{ij}$ + thermal terms

- Cohesive interfaces: damage laws

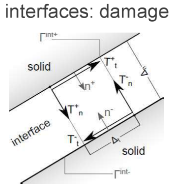

Normal

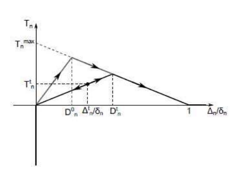

Tangential

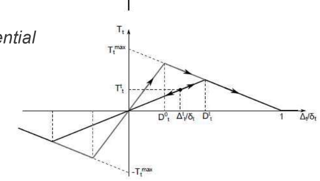

Fluid flow

- Cohesive interfaces (coupling M → H)
  - Interface opening defines channel hydraulic conductivity ($\kappa \propto \Delta h^3$)
- Flow assumptions
  - Laminar flow between smooth parallel platens
  - Network of 1D channels between grains
- Fluid forces (coupling H → M)
  - Fluid pressure acting normally on solids boundaries
- Fluid compressibility
  - $\rho^w = \rho^0 e^{k_w (p - p_0)}$

Porous network

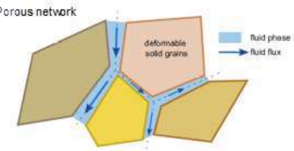

Fluid flow and forces

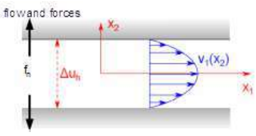

Frey *et al.*, 2012
van den Eijnden *et al.*, 2015

Methods

A model for brittle material with fluid and temperature modeled by FEM:

Thermal coupling

- Fluid dilation

$$\rho^w = \rho^0 e^{k_w (p - p_0)} + \int_{to}^{t} \alpha_w(T)dT$$

- Viscosity reduction

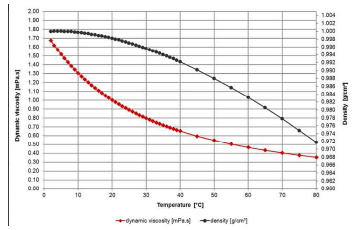

- Thermal exchanges

In solid grains: conduction

$$\vec{q} = -\gamma \, \nabla \theta^s$$

At interfaces:

Advection with fluid flow

$$\vec{q}_{adv} = \vec{m} \, c_p \, \frac{\partial \theta^i}{\partial s}$$

where θ^i is an averaged temperature of the fluid through the interface aperture

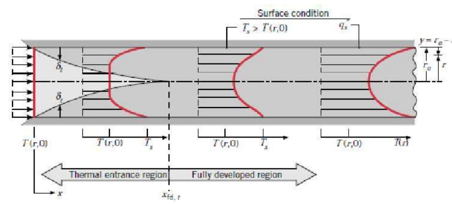

Incropera *et al.*, 2007

Convection from grains surface

$$\vec{q}_{conv} = h \, (\theta^s - \theta^i)$$

where θ^s is the grain surface temperature

Neglecting conduction parallel to the interface:

$$\vec{m} \, c_p \, \frac{\partial \theta^i}{\partial s} = h^+ \left(\theta^{s+} - \theta^i\right) + h^- \left(\theta^{s-} - \theta^i\right)$$

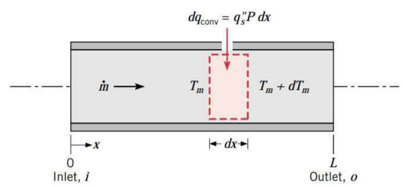

Zalamea *et al.*, 2023

Methods

A model for brittle material with fluid and temperature modeled by FEM:

Equivalent Thermal Resistance Model (ETRM)

$$\sum_{k=\alpha_1}^{\alpha_m} Q_{ik} = \sum_{k=\alpha_1}^{\alpha_m} \frac{\theta_k - \theta_i}{R_{ik}} = 0$$

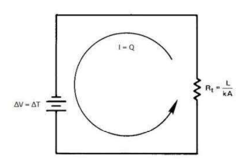

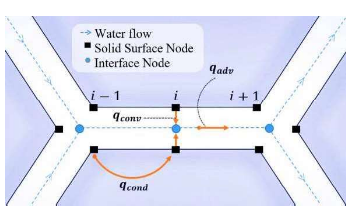

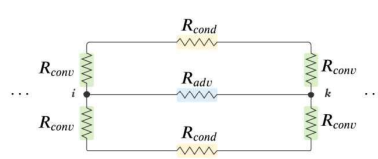

$$\left[\sum_{k=\alpha_1}^{\alpha_n} \frac{1}{R_{conv,i} + R_{cond,ik} + R_{conv,k}} + \sum_{k^*=\beta_1}^{\beta_{n^*}} \frac{1}{R_{adv,ik^*}}\right] (\theta_i - \theta_k) = 0$$

$$R_{cond} = \frac{1}{K_{cond}}$$

$$R_{conv} = \frac{1}{h}$$

$$R_{adv} = \frac{1}{C_p m}$$

Zalamea *et al.*, 2023

Methods

A model for brittle material with fluid and temperature modeled by FEM:

$$\begin{bmatrix} K_{adv} + 2K_{conv} & -K_{conv} \\ K_{adv} & K_{cond} \end{bmatrix} \begin{bmatrix} \theta^i \\ \theta^s \end{bmatrix} = \begin{bmatrix} 0 \\ Q^{REV} \end{bmatrix}$$

where Q^{REV} are the thermal flow on the boundaries of the REV

Zalamea *et al.*, 2023

Methods

Sequential decomposition:

- Newton-Raphson iterative routine for solving the mechanical system (uniform pressure and temperature fields): FEM
- Direct routine for solving hydraulic problem (known configuration, uniform temperature field): Balance of mass fluxes on interface nodes,
- Direct routine for solving thermal problem (known configuration, known water flow): Equivalent Thermal Resistance Model.
- Homogenization and tangent operators (perturbation or static condensation).

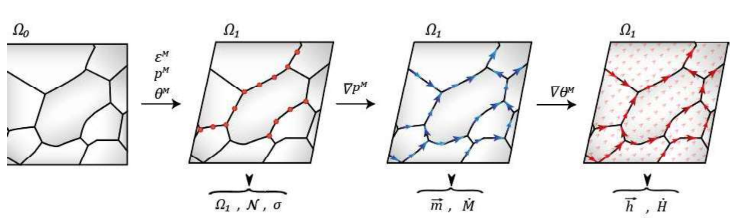

Methods

A model for brittle material with fluid and temperature modeled by FEM:

Example of thermal pressurisation (undrained heating)

Material		COx	Clay	Calcite	Quartz	Pyrite	
Composition	-	100%	50%	30%	18%	2%	Pardoen, 2019
Bulk density	kg/m3	2450	-	-	-	-	
Porosity	-	0,18	-	-	-	-	
Isotropic intrinsic permeability	m2	2,30E-20	-	-	-	-	
Isotropic Young's modulus	MPa	7000	2300	84000	95000	305000	Roberson,2012
Poisson's Ratio	-	0,3	0,11	0,317	0,074	0,154	Roberson,2012
Isotropic thermal conductivity	W/mK	1,67	1,2*	3,4	6,0	4,0**	Horai,1971;de Vries, 1985
Linear thermal expansion coefficient	1/K	1,25E-05	8,30E-06	5,00E-06	1,10E-05	4,00E-06	Braun, 2019
Solid phase specific heat	J/kgK	978	878	710	1100	748	NIST, SRD 69

Conditions		
σ	12,5	Mpa
P_0	4,7	MPa
T_0	20	C

- Application of initial confinement stress and pore pressure.
- Undrained Heating to 80°C at constant confining.

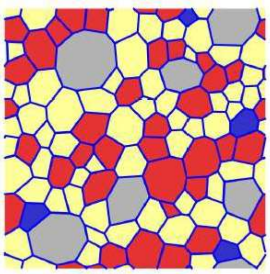

- Clay- Yellow (47,95%)
- Calcite - Gray (32,93%)
- Quartz – Red (16,51%)
- Pyrite – Blue (2,62%)

100 GRAINS

Interfaces	
D_t,crit	0,05
D_n,crit	0,05
D_t,0	0,001
D_n,0	0,001
T_t,max [MPa]	5,5
T_n,max [MPa]	2
Δu_min	1,4e-5
Δu_trans	-1,4e-5

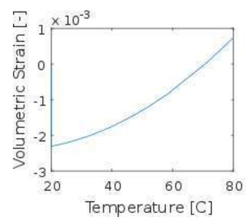

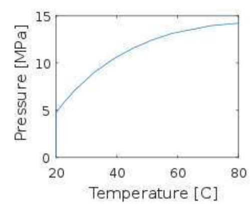

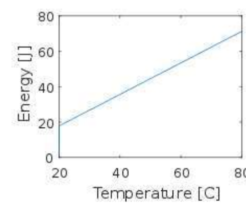

Zalamea *et al.*, 2023

Methods

A model for brittle material with fluid and temperature modeled by FEM:

Example of thermal pressurisation (undrained heating)

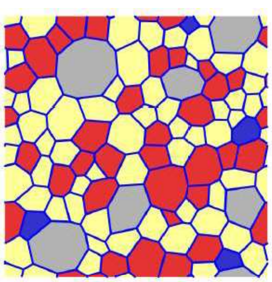

- Clay- Yellow (47,95%)
- Calcite - Gray (32,93%)
- Quartz – Red (16,51%)
- Pyrite – Blue (2,62%)

100 GRAINS

Conditions		
σ	12,5	Mpa
P_0	4,7	MPa
T_0	20	C

- Application of initial confinement stress and pore pressure.
- Undrained Heating to 80°C at constant confining.

Interfaces before heating

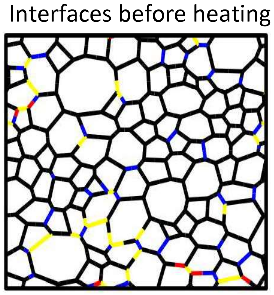

Interfaces after heating

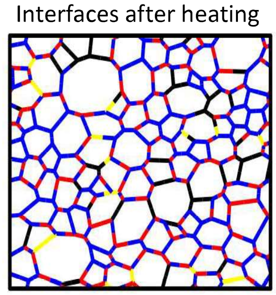

Thermal induced damage of the interfaces.

- **black**, no damage to the interface.
- **blue,** damage only in normal direction.
- **yellow**, damage only in tangential direction.
- **red,** damage on both directions.

Zalamea *et al.*, 2023

Methods

A model for brittle material with fluid and temperature modeled by FEM:

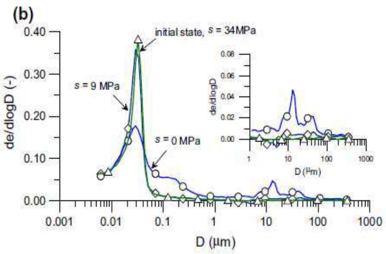

Porosity distribution

- Interface porosity: Influence the permeability evolution during loading
- Meso-porosity: influence the effective fluid storage of REV and introduce mechanical weakness
- Nano-porosity in clay grains: influence the effective fluid storage and the effective Biot coefficient

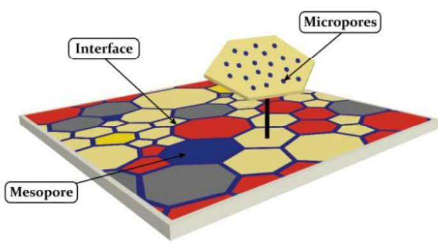

- Porous materials on clay matrix
  - Computation of the variation of pore space.
  - Possible to include a Biot coefficient of the clay matrix.

$$\sigma_{ij} = C_{ijkl}(\varepsilon_{kl} - \alpha_{kl}(T - T_o)) + p$$

$$\delta V_{\phi} = tr(\varepsilon - \alpha(T - T_o)) * V_o$$

- Meso pores in the REV

Zalamea *et al.*, 2023

Outline

1. Motivations
2. Methods
3. Couplings
4. Strain localisation
5. Model calibration
6. Parallelisation
7. Conclusions and perpectives

Strain localisation

Failure by strain concentration inside shear bands

- Sand

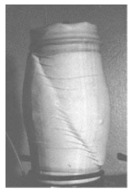

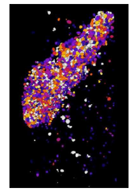

- Clay rock

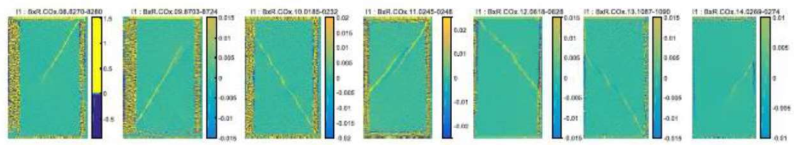

- Sandstone

Strain localisation

Characteristic lengths

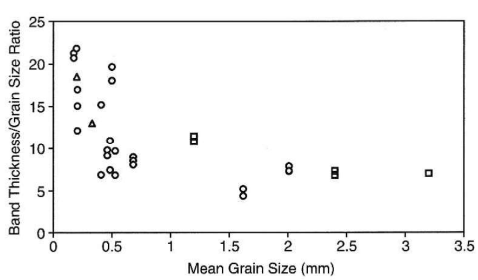

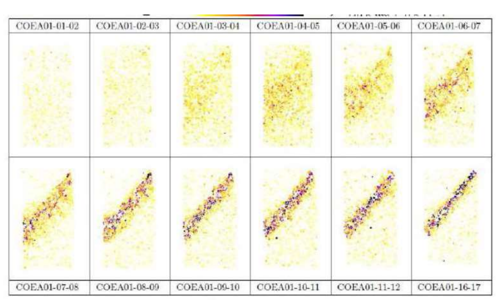

Ando *et al.* 2015
(sand)

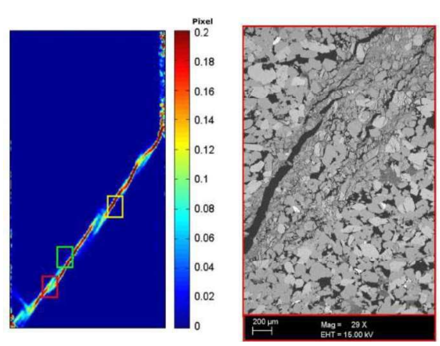

Lanata *et al.* 2014
(sandstone)

Strain localisation

Mesh size dependance

Example of a plane strain compression test (using classical continuum)

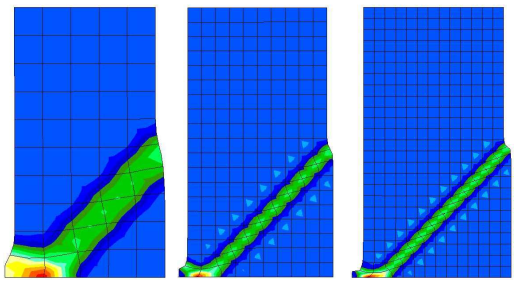

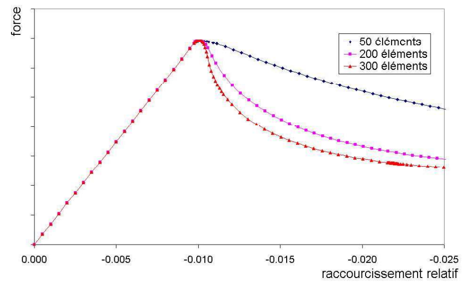

50 elements 200 elements 300 elements axial force versus shortening

enriched continuum (internal length)

Strain localisation

Regularization by enriched continuum

Continuum with microstructure (Germain *et al.* 1973)

Second gradient continuum (Chambon *et al.* 2001)

$$\int_{\Omega^t}\left(\sigma_{ij}\frac{\partial u_i^*}{\partial x_j^t}+\Sigma_{ijk}\frac{\partial^2 u_i^*}{\partial x_j^t\partial x_k^t}\right)dV-\int_{\Gamma^t}\left(t_i u_i^*+T_i\frac{\partial u_i^*}{\partial x_k^t}n_k\right)dS=0$$

Balance equation

$$\frac{\partial\sigma_{ij}}{\partial x_j}-\frac{\partial^2\Sigma_{ijk}}{\partial x_j\,\partial x_k}+G_i=0,$$

Boundary conditions

$$\sigma_{ij}n_j-n_k n_j D\Sigma_{ijk}-\frac{D\Sigma_{ijk}}{Dx_k}n_j-\frac{D\Sigma_{ijk}}{Dx_j}n_k+\frac{Dn_l}{Dx_l}\Sigma_{ijk}n_j n_k-\frac{Dn_j}{Dx_k}\Sigma_{ijk}=p_i,$$

$$\Sigma_{ijk}n_j n_k=P_i,$$

Strain localisation

Regularization by enriched continuum

Continuum with microstructure (Germain *et al.* 1973)

Second gradient continuum (Chambon *et al.* 2001)

$$\int_{\Omega^t} \left(\sigma_{ij} \frac{\partial u_i^*}{\partial x_j^t} + \Sigma_{ijk} \frac{\partial^2 u_i^*}{\partial x_j^t \partial x_k^t} \right) dV - \int_{\Gamma^t} \left(t_i u_i^* + T_i \frac{\partial u_i^*}{\partial x_k^t} n_k \right) dS = 0$$

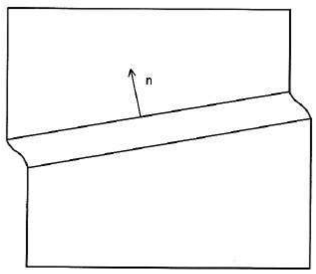

Second gradient formalism constitutive relation — *decoupling assumption*

Classical part: $\delta\sigma_{ij}^M \leftrightarrow \frac{\partial \delta u_k}{\partial x_l}$

Second gradient part: $\delta\Sigma_{ijk} \leftrightarrow \frac{\partial^2 \delta u_l}{\partial x_m \partial x_n}$

Strain localisation

Bifurcation analysis

Continuum with microstructure (Germain *et al.* 1973)

Second gradient continuum (Chambon *et al.* 2001)

$$\int_{\Omega^t} \left(\sigma_{ij} \frac{\partial u_i^*}{\partial x_j^t} + \Sigma_{ijk} \frac{\partial^2 u_i^*}{\partial x_j^t \partial x_k^t} \right) dV - \int_{\Gamma^t} \left(t_i u_i^* + T_i \frac{\partial u_i^*}{\partial x_k^t} n_k \right) dS = 0$$

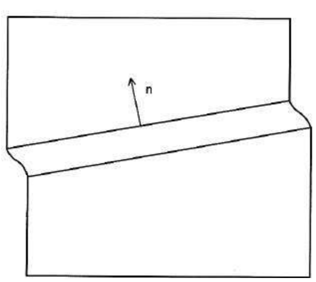

Classical part $\dot{\sigma}_{ij} = K^e_{ijkl} \frac{\partial \dot{u}_k}{\partial x_l}$ or $\dot{\sigma}_{ij} = K^{ep}_{ijkl} \frac{\partial \dot{u}_k}{\partial x_l}$ depending on $\frac{\partial \dot{u}_k}{\partial x_l}$,

Second gradient part $\dot{\Sigma}_{ijk} = A_{ijklmn} \frac{\partial^2 \dot{u}_l}{\partial x_m \partial x_n}$.

Kinematic assumption $\frac{\partial \dot{u}_i^\zeta}{\partial x_j} = \frac{\partial \dot{U}_i}{\partial x_j} + g_i^\zeta n_j$,

Internal length $\det(\mathcal{A})\Lambda_a \ \Lambda_b \ \Lambda_c = \det(\mathcal{K}^{ep})$.

Bésuelle *et al.* 2006

Strain localisation

Numerical implementation

Second gradient continuum (Chambon *et al.* 2001)

$$\int_{\Omega^t}\left(\sigma_{ij}\frac{\partial u_i^*}{\partial x_j^t}+\Sigma_{ijk}\frac{\partial^2 u_i^*}{\partial x_j^t\partial x_k^t}\right)dV-\int_{\Gamma^t}\left(t_i u_i^*+T_i\frac{\partial u_i^*}{\partial x_k^t}n_k\right)dS=0$$

Second gradient continuum using Lagrange multipliers (Matsushima *et al.* 2002)

$$\int_{\Omega^t}\left(\sigma_{ij}\frac{\partial u_i^*}{\partial x_j^t}+\Sigma_{ijk}\frac{\partial v_{ij}^*}{\partial x_k^t}+\lambda_{ij}\left(\frac{\partial u_i^*}{\partial x_j^t}-v_{ij}^*\right)\right)dV-\int_{\Gamma^t}\left(t_i u_i^*+T_i\frac{\partial u_i^*}{\partial x_k^t}n_k\right)dS=0$$

$$\int_{\Omega^t}\lambda_{ij}^*\left(\frac{\partial u_i}{\partial x_j^t}-v_{ij}\right)dV=0$$

Strain localisation

Numerical implementation

Second gradient continuum using Lagrange multipliers (Matsushima *et al.* 2002)

$$\int_{\Omega^t}\left(\sigma_{ij}\frac{\partial u_i^*}{\partial x_j^t}+\Sigma_{ijk}\frac{\partial v_{ij}^*}{\partial x_k^t}+\lambda_{ij}\left(\frac{\partial u_i^*}{\partial x_j^t}-v_{ij}^*\right)\right)dV-\int_{\Gamma^t}\left(t_i u_i^*+T_i\frac{\partial u_i^*}{\partial x_k^t}n_k\right)dS=0$$

$$\int_{\Omega^t}\lambda_{ij}^*\left(\frac{\partial u_i}{\partial x_j^t}-v_{ij}\right)dV=0$$

u : displacement

v : displacement gradient

λ : Lagrange multipliers

■ $u_1\ u_2$ *Q8*

● $v_{11}\ v_{12}\ v_{21}\ v_{22}$ *Q4*

▲ $\lambda_{11}\ \lambda_{12}\ \lambda_{21}\ \lambda_{22}$ *Q1*

→ 36 DOF by element

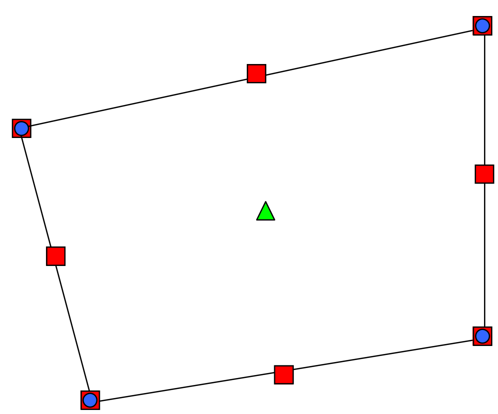

Bésuelle *et al.* 2006

Strain localisation

Numerical implementation

Second gradient continuum with fluid (Collin *et al.* 2006)

$$\int_{\Omega^t}\left(\sigma_{ij}\frac{\partial u_i^*}{\partial x_j^t}+\Sigma_{ijk}\frac{\partial^2 u_i^*}{\partial x_j^t\partial x_k^t}\right)dV-\int_{\Gamma^t}\left(t_i u_i^*+T_i\frac{\partial u_i^*}{\partial x_k^t}n_k\right)dS-\int_{\Omega^t}\rho^{mix,t}g_i u_i^* dV=0$$

$$\int_{\Omega^t}\left(m_j\frac{\partial p^*}{\partial x_j^t}-\dot{M}p^*\right)dV-\int_{\Gamma^t}qp^*dS=0$$

$$\rho^{mix,t}=\rho^{s,t}(1-\phi^t)+\rho^{w,t}\phi^t$$

Strain localisation

Numerical implementation

Validation

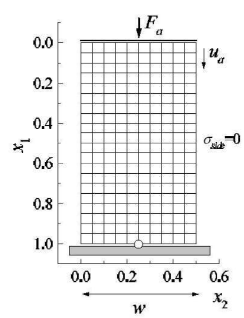

example of a plane strain compression

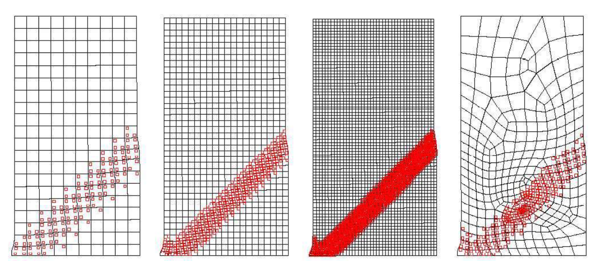

Gauss points in the plastic regime

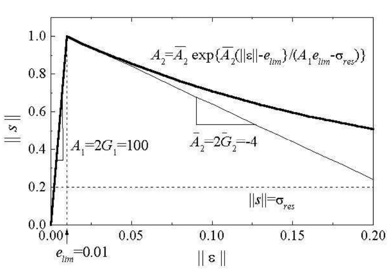

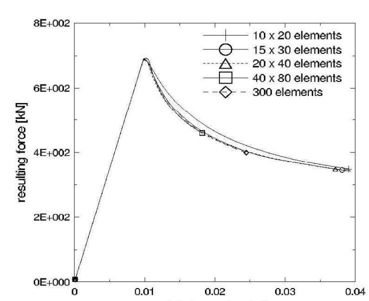

Strain localisation

Enriched continuum and computational homogeneisation

Second gradient continuum (Chambon *et al.* 2001)

$$\int_{\Omega^t}\left(\sigma_{ij}\frac{\partial u_i^*}{\partial x_j^t}+\Sigma_{ijk}\frac{\partial^2 u_i^*}{\partial x_j^t \partial x_k^t}\right)dV-\int_{\Gamma^t}\left(t_i u_i^*+T_i\frac{\partial u_i^*}{\partial x_k^t}n_k\right)dS=0$$

Second gradient formalism constitutive relation

decoupling assumption

Classical part

$$\delta\sigma_{ij}^M \leftrightarrow \frac{\partial \delta u_k}{\partial x_l}$$

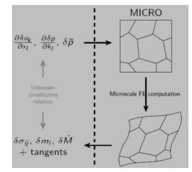

Computational homogeneisation

Second gradient part

$$\delta\Sigma_{ijk} \leftrightarrow \frac{\partial^2 \delta u_l}{\partial x_m \partial x_n}$$

$$\Sigma_{ijk} = [D]\,\frac{\partial^2 \delta u_l}{\partial x_m \partial x_n}$$

Phenomenological law (elastic isotrope linear relation with one parameter)

Strain localisation

Enriched continuum and computational homogeneisation (FEM^2)

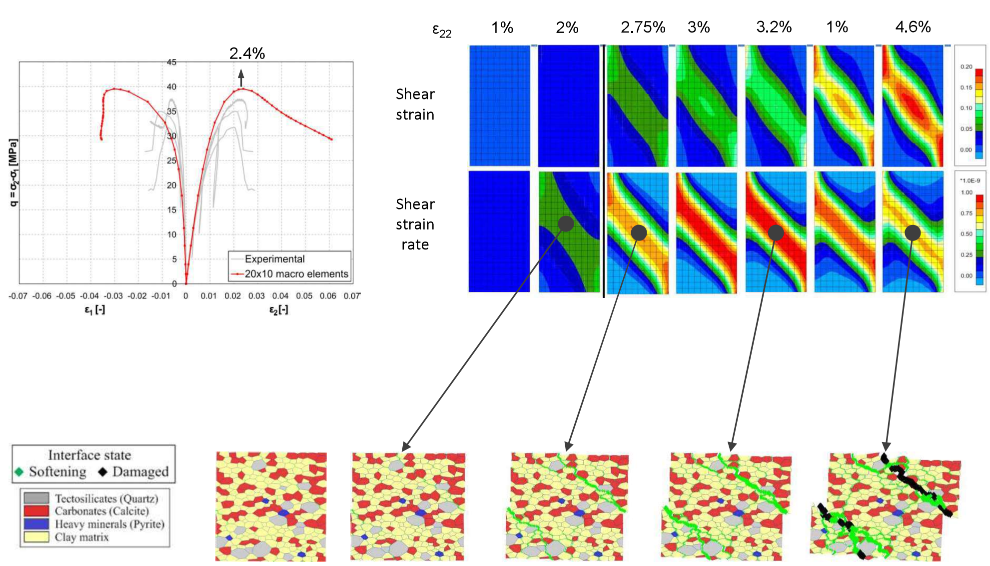

Pardoen *et al.* 2020

Outline

1. Motivations
2. Methods
3. Couplings
4. Strain localisation
5. Model calibration
6. Parallelisation
7. Conclusions and perpectives

Model calibration

The constitutive description of the model concern 'exclusively'* the description of micro-model

Micro-inspired

- morphology, heterogeneity, constitutive parameters, etc…
- micro-experiments
- smaller-scale modeling

Macro-inspired

- unknown micro-properties are fitted from macro-experiments responses

Other

- Size of the REV (number of grains), etc…

* Influenced by the boundaries conditions of the REV (periodic conditions, preferential orientations)

Model calibration

Micro-inspired: morphology, heterogeneity, constitutive parameters, etc…

Brittle material
• Mineralogies distribution • Grains size distribution • Grain morphology (elongation, preferential distribution, etc…) • Spatial distributions
• Heterogeneity, anisotropy, permeability

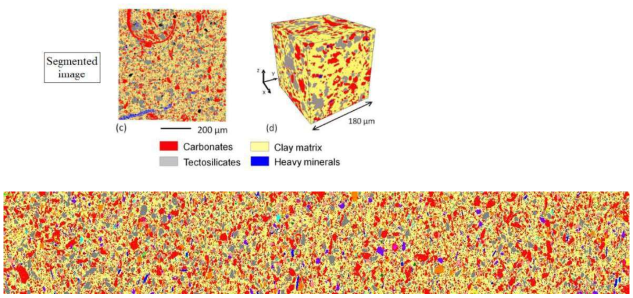

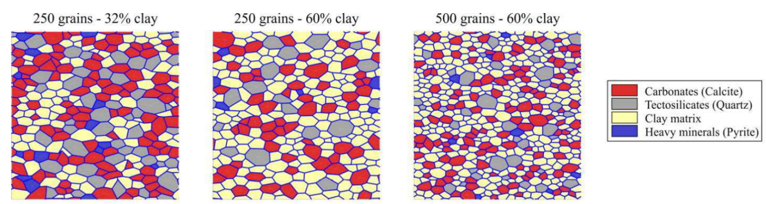

Pardoen *et al.*, 2019

Model calibration

Micro-inspired: morphology, heterogeneity, constitutive parameters, etc…

Numerical EV, 250 grains
18% quartz, 30% calcite, 2% pyrite, 50% clay

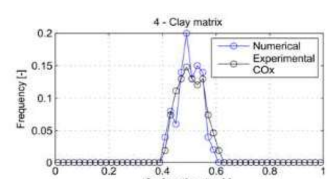

Grains elongation
(circumscribed ellipse)

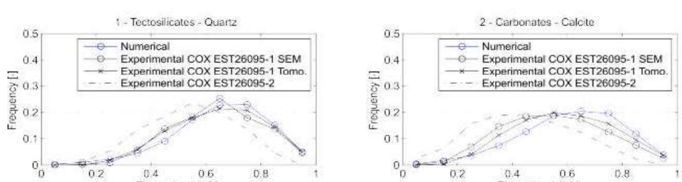

Grains orientation
(circumscribed ellipse)

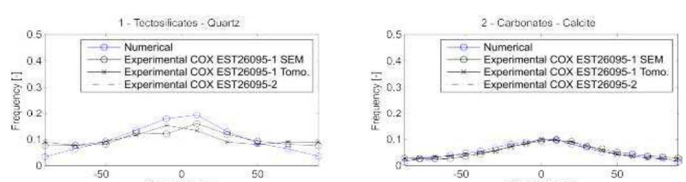

Pardoen *et al.*, 2019

Model calibration

- Micro-inspired: micro-experiments
  - Mechanisms of deformation (qualitative information)

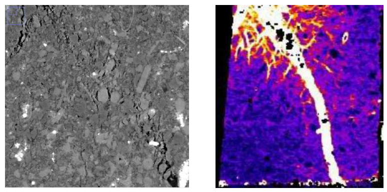

- Micro-inspired: smaller scale modelling

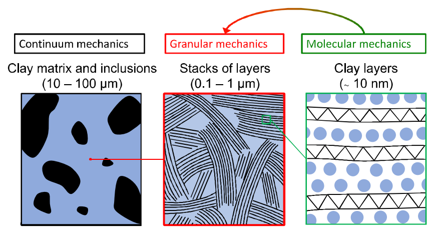

Model calibration

Macro-inspired

- unknown micro-properties are fitted from macro-experiments responses (hiden assumptions)

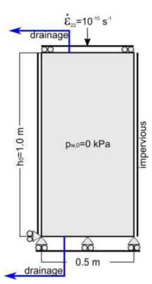

	E [GPa]	ν [-]	Surf. density [%]	
Quartz	95	0.074	12	
Carbonate	84	0.317	27	
Pyrite	305	0.154	1	
Clay	2.3	0.110	60	
	$\delta_c^{t/n}$ [-]	$D_0^{t/n}$ [-]	c_0^t [MPa]	c_0^n [MPa]
Interfaces	0.1	0.001	2.5	1.

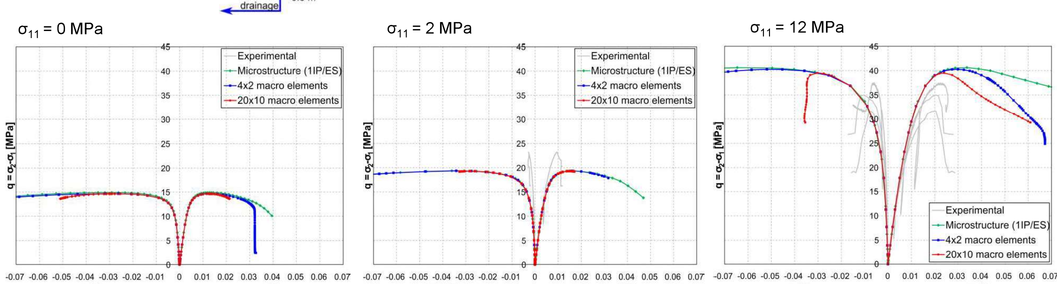

Effect of the confining pressure on the stress peak

Pardoen *et al.*, 2019

Model calibration

REV variability

Non homogeneity of the material at intermediate scales between macro and meso

Examples:

- Variability of the porosity
- Variability of preferential orientations
- Variability of the clay content (random, structured)
- etc…

Model calibration

REV variability

- Numerical experiments with FEM^2 suggest that REV variability can influence the final pre-peak response (pre-peak diffuse localisation)
- Some similarity with experimental observations (random distribution with two REV)

Numerical modeling of a biaxial compression test in a clay rock (FEM^2)
random distribution of orientation of one REV

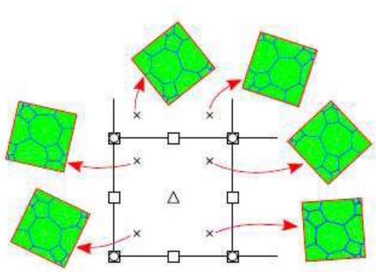

van den Eijnden *et al.* 2015

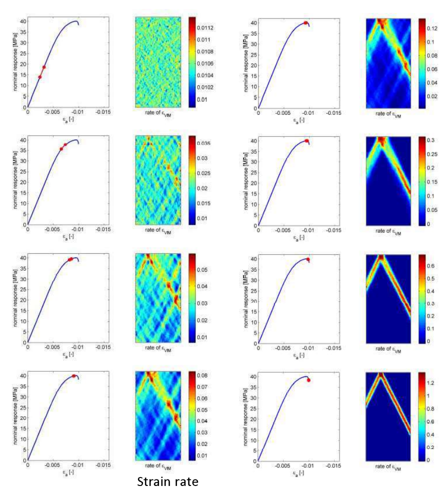

Biaxial compression test on COx at 12 MPa confining pressure

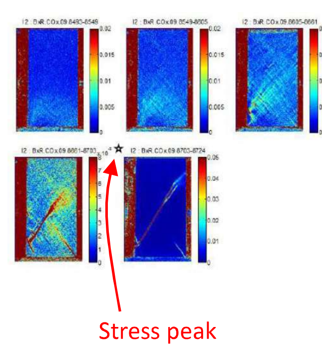

Model calibration

REV variability

- Numerical experiments with FEM^2 suggest that REV variability can influence the final pre-peak response (pre-peak diffuse localisation)
- Some similarity with experimental observations (random distribution with two REV)

Gallery excavation with a single REV

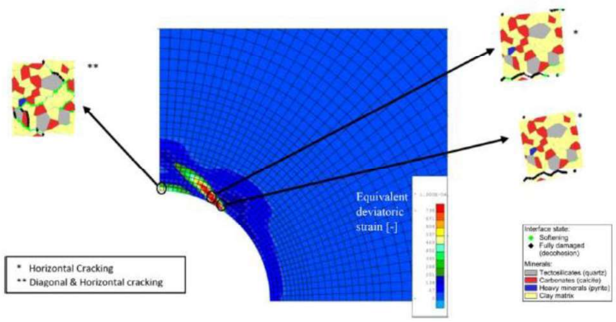

with multiple REV

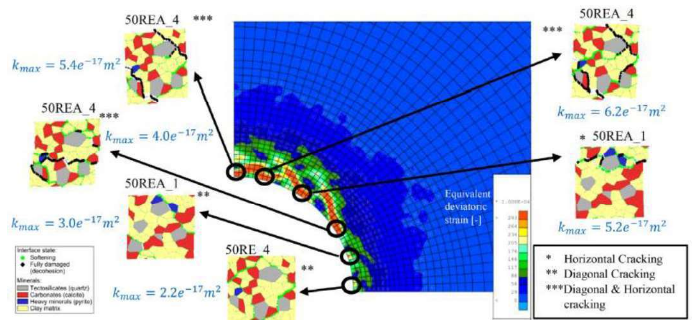

Outline

1. Motivations
2. Methods
3. Couplings
4. Strain localisation
5. Model calibration
6. Parallelisation
7. Conclusions

Conclusions

Conclusions

- Computational double scale homogenization approach for geomaterials has been developed
  - For brittle material, a FEM^2 scheme is selected, with multiphysical (THM) couplings introduced at the small scale
- The approache is compatible with the second gradient continuum for strain localization (mesh independent)
- Calibration is both micro-inspired and macro-inspired
- Massive parallelization has been adapted to the double scale approach, which implies a modification of the FEM code architecture
- The double scale approach is used for large scale boundaries values problems

Appendix L. Advanced multiphysics modelling of geomaterials: numerical modelling of discrete gas pathways and cracking (A-C Dieudonné)

ALERT Geomaterials
Alliance of Laboratories in Europe for Education, Research and Technology
http://alertgeomaterials.eu

European Joint Programme on Radioactive Waste Management

Advanced multiphysics modelling of geomaterials: multiscale approaches and heterogeneities

Pierre BÉSUELLE[1], Frédéric COLLIN[2], **Anne-Catherine DIEUDONNÉ**[3]

[1] Université Grenoble Alpes – 3SR laboratory
[2] University of Liège – UEE Research Unit
[3] Delft University of Technology – Faculty of Civil Engineering and Geosciences

This project has received funding from the European Union's Horizon 2020 research and innovation programme under grant agreement N°847593

ALERT Geomaterials
Alliance of Laboratories in Europe for Education, Research and Technology
http://alertgeomaterials.eu

European Joint Programme on Radioactive Waste Management

Advanced multiphysics modelling of geomaterials: numerical modelling of discrete gas pathways and cracking

Anne-Catherine DIEUDONNÉ, Joaquín Liaudat

Delft University of Technology – Faculty of Civil Engineering and Geosciences

This project has received funding from the European Union's Horizon 2020 research and innovation programme under grant agreement N°847593

GAS MIGRATION MECHANISMS IN CLAYS

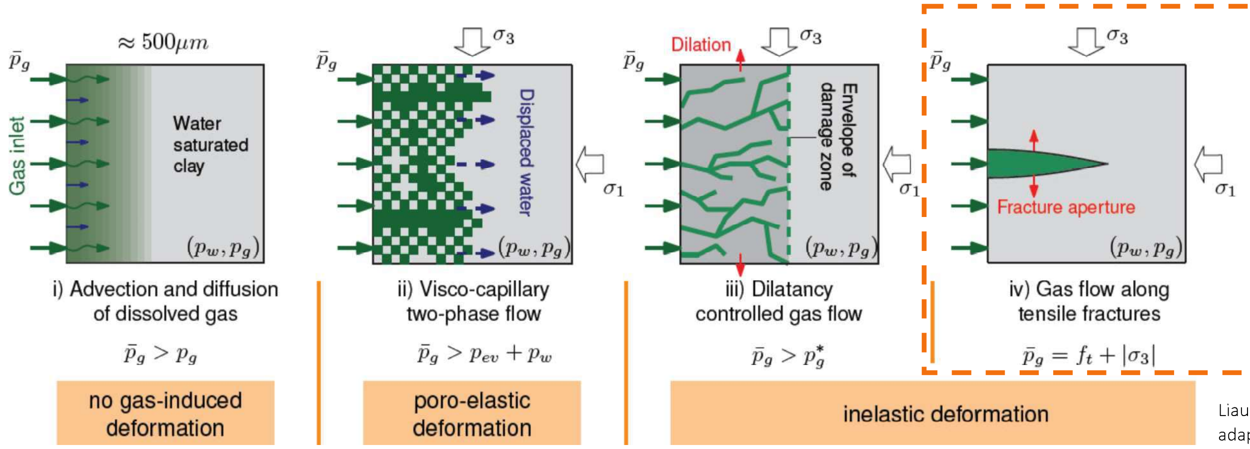

Liaudat *et al.* (2023), adapted from Marschall et al. (2005)

p_w, p_g : water and gas pressures in the REV
$\bar{p}_g$: gas injection pressure
p_{ev} : clay gas entry value
f_t : tensile strength
σ_1, σ_3 : principal stresses

FEM+Z MODELLING APPROACH (LIAUDAT *ET AL.*, 2023)

1. **Continuum elements** with classical two-phase flow in porous media formulation
2. Explicit representation of gas cracking via **zero-thickness interface elements ("+Z")** equipped with a cohesive fracture constitutive model
    - Interface elements are introduced a priori in between continuum elements as potential cracking paths
    - Closed interface elements do not influence the overall response of modelled material

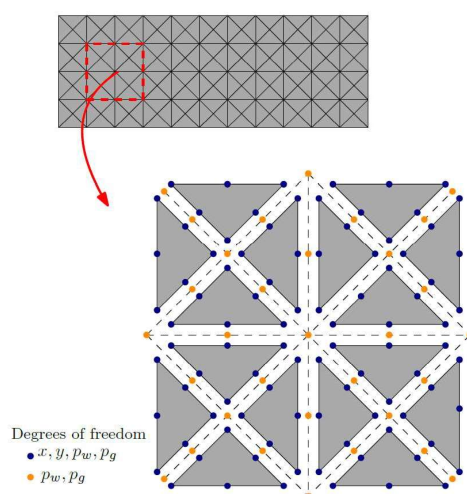

PNEUMO-HYDRO-MECHANICAL INTERFACE (PHMI) ELEMENT (LIAUDAT *ET AL.*, 2023)

3-node zero-thickness interface element

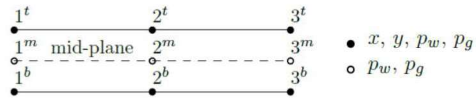

Mechanical Governing equations

- Basic variables:
  - normal and tangential stress components on mid-plane
  - conjugate relative displacements

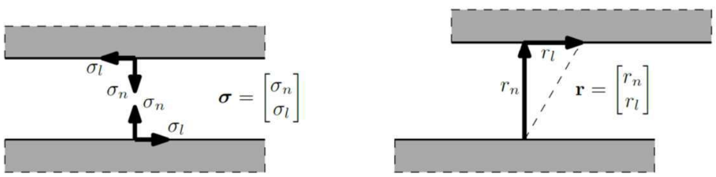

Flow governing equations

- Two-phase flow
- Diffusion-advection of dissolved gas
- Longitudinal and transversal flows
- Longitudinal transmissivity and diffusivity dependent on normal aperture

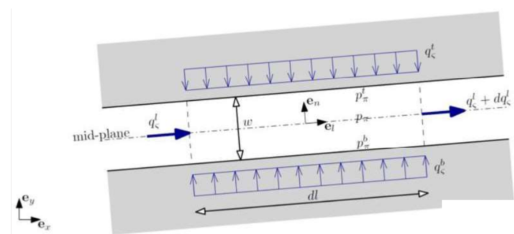

MECHANICAL CONSTITUTIVE FORMULATION

Crisfield's cohesive zone model

- Bilinear damage model
- Unique damage variable for shear and tension (coupled damage)
- No damage is produced by compression (negative) normal displacements.
- Normal stiffness in compression is affected by a penalty term to prevent significant overlapping in compression.
- Frictional effects are not accounted for (strictly valid only for a purely cohesive material)

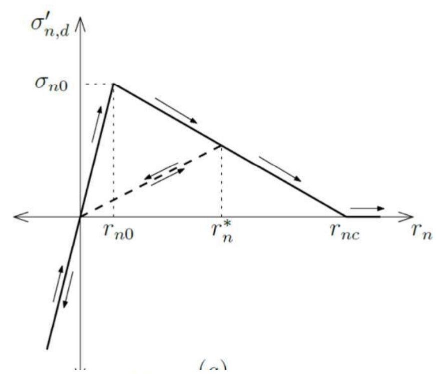

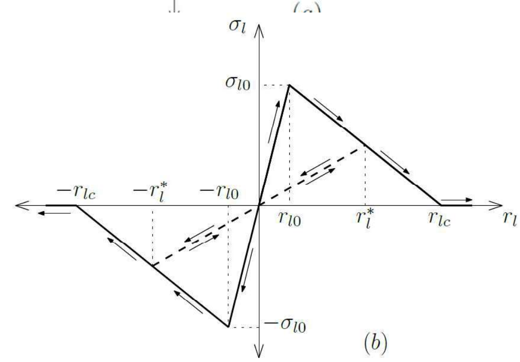

RETENTION CURVES

- For solid elements:

$$S_w = (1 - S_{wr})\left[1 + \left(\frac{p_c}{p_b}\right)^{\frac{1}{1-\lambda}}\right]^{-\lambda} + S_{wr}$$

- For interface elements:

$$\bar{S}_w = (1 - \bar{S}_{wr})\left[1 + \left(\frac{p_c}{\bar{p}_b}\right)^{\frac{1}{1-\lambda}}\right]^{-\lambda} + \bar{S}_{wr}$$

$$\text{with } \bar{p}_b(r_n) = \frac{d}{d + 2\langle r_n\rangle} p_b \text{ and } \bar{S}_{wr}(r_n) = \frac{nd}{nd + \langle r_n\rangle} S_{wr}$$

where n and d [m] are the porosity and the characteristic
pore size of the continuum porous medium.

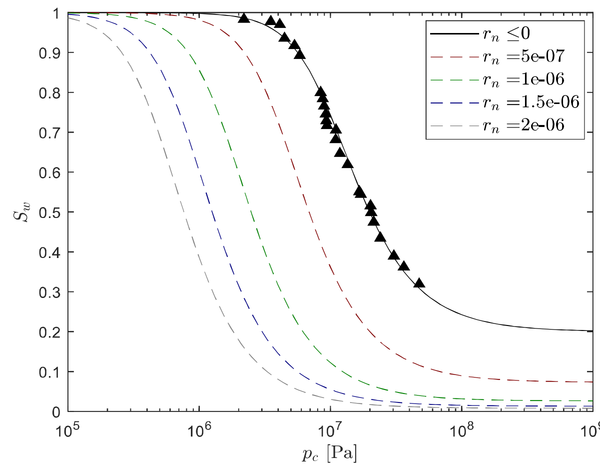

Solid line: retention curve for continuum medium and closed fractures
Dashed lines: retention curves for increasing fracture aperture
Markers: Experimental data (Boom Clay) from Gonzalez-Blanco et al. (2016)

RELATIVE PERMEABILITY CURVES

- The same power laws are adopted for solid and interface elements:

$$k_{w,r} = S_e^{n_w}\;; \quad k_{g,r} = (1 - S_e)^{n_g}$$

where n_w and n_g are shape parameters, and S_e is the effective saturation degree.

- For solid elements,

$$S_e = \frac{S_w - S_{wr}}{1 - S_{wr}}$$

- For interface elements,

$$S_e = \frac{S_w - \bar{S}_{wr}}{1 - \bar{S}_{wr}}$$

$$\text{with } \bar{S}_{wr}(r_n) = \frac{nd}{nd + \langle r_n\rangle} S_{wr}$$

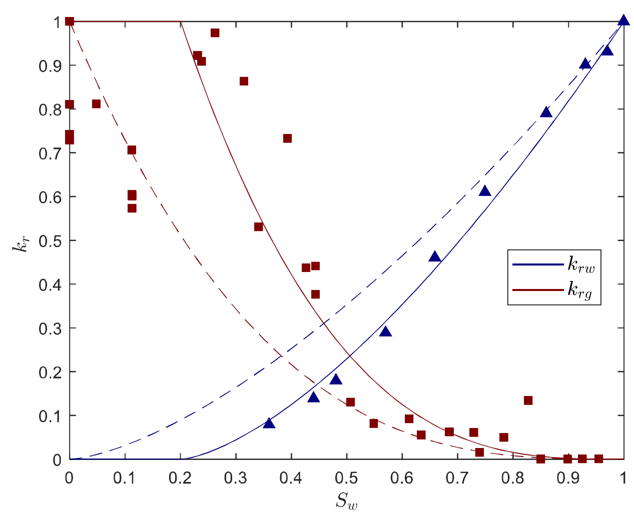

Solid line: continuum medium and closed fractures
Dashed lines: fracture with large aperture
Markers: Experimental data (Boom Clay) from Volkaert et al. (1995)

MODELLING RESULTS

1D gas injection under isochoric conditions

This project has received funding from the European Union's Horizon 2020 research and innovation programme under grant agreement N°847593

MODEL GEOMETRY AND FE MESH

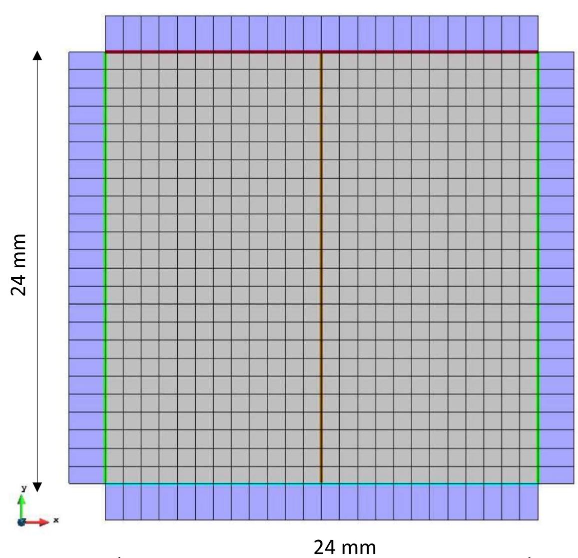

- Very stiff, impervious loading plates
- Boom clay sample (linear elastic)

- Bottom contact
- Lateral contact
- Top contact
- Potential fracture path

INITIAL AND BOUNDARY CONDITIONS

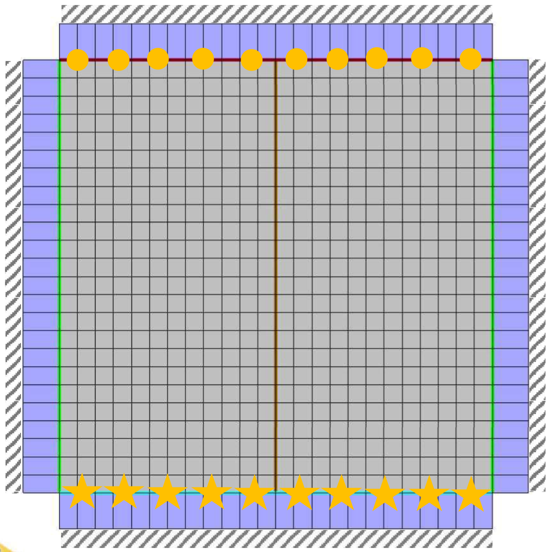

Initial conditions

Isotropic initial stress state: $\sigma_x = \sigma_y = 4.5$ MPa

Initial pore pressure $p_g = p_w = 2.2$ MPa ($S_w = 1$)

Boundary conditions

Isochoric conditions

- Gas and water pressure fixed at the top contact
- Gas injection at the bottom contact ($f_g = 1.0\times10^{-9}$ kg/s)

EFFECT OF THE GAS INJECTION RATE: Time evolution curves

Gas injection pressure

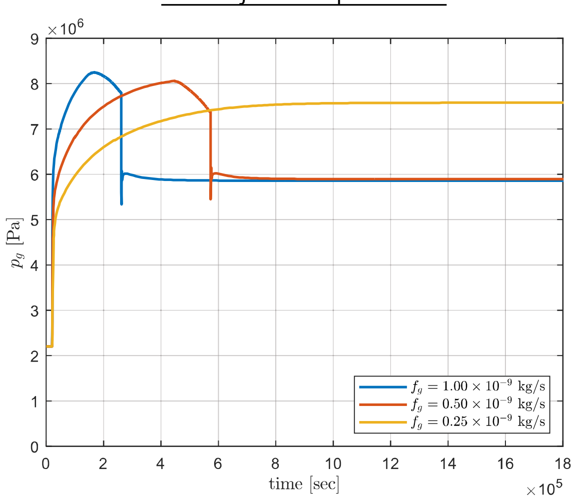

Gas outflow

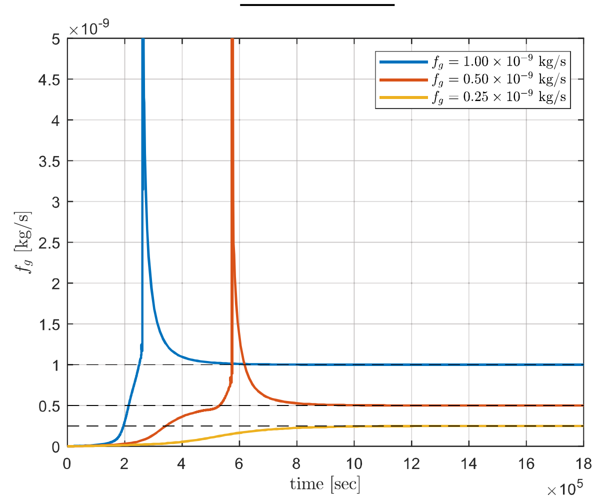

Initial stress and pore pressure for all cases: $\sigma = 4.50$ MPa, $p_w = p_g = 2.2$ MPa

EFFECT OF THE GAS INJECTION RATE: p_g and S_r at the end of the simulation (steady state)

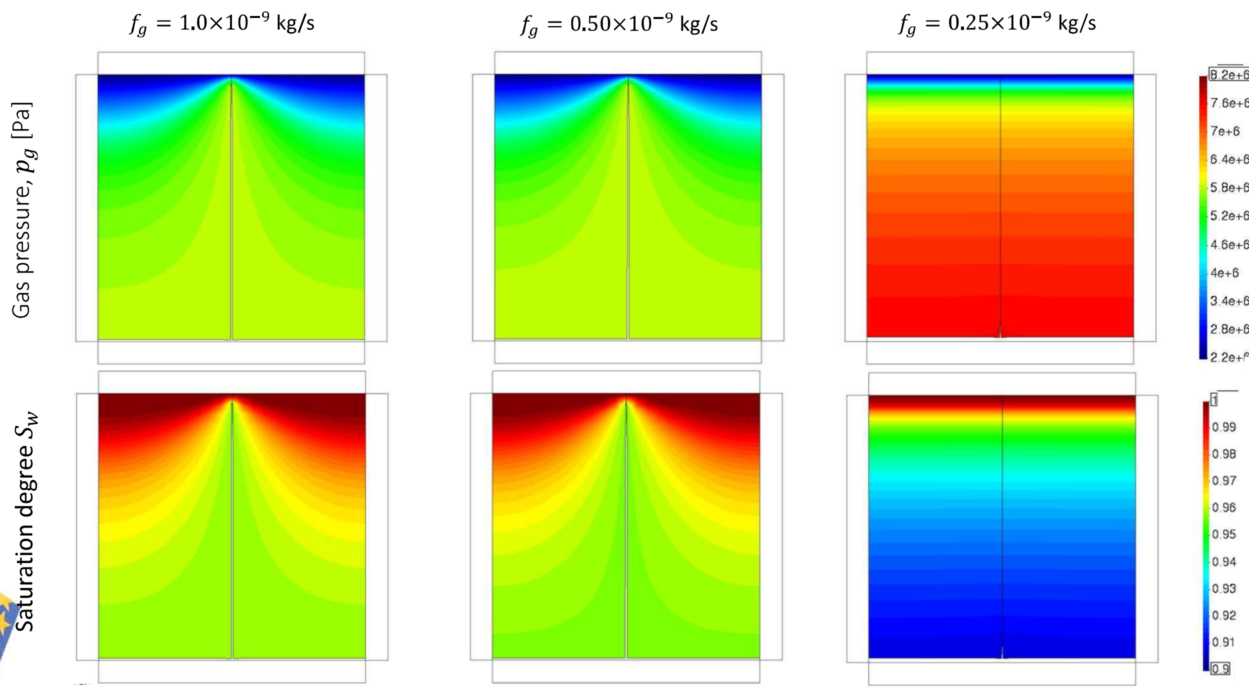

FREE CRACKING PATH

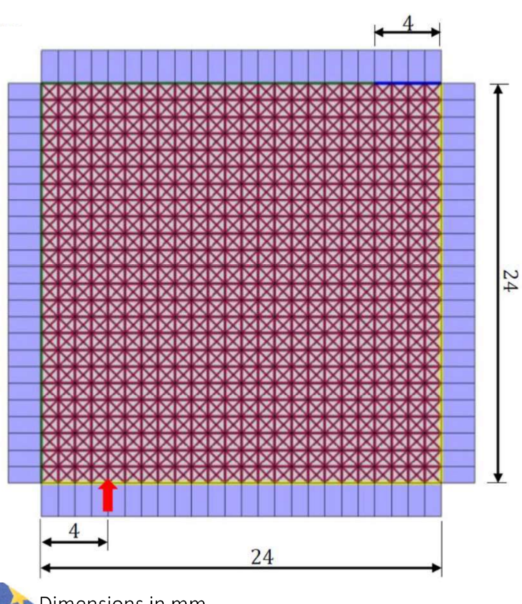

Very stiff, impervious loading plates

Boom clay sample (linear elastic)

Clay-cell interface (impervious bottom side)

Clay-cell interface (impervious top side)

Back-pressure filter

Potential cracking paths

Initial conditions

Isotropic initial stress state: $\sigma_x = \sigma_y = 4.5$ MPa

Initial pore pressure $p_g = p_w = 2.2$ MPa ($S_w = 1$)

Boundary conditions

Isochoric conditions

Gas and water pressure fixed at the sink

Gas injection $f_g = 1.0\times10^{-9}$ kg/s

FREE CRACKING PATH

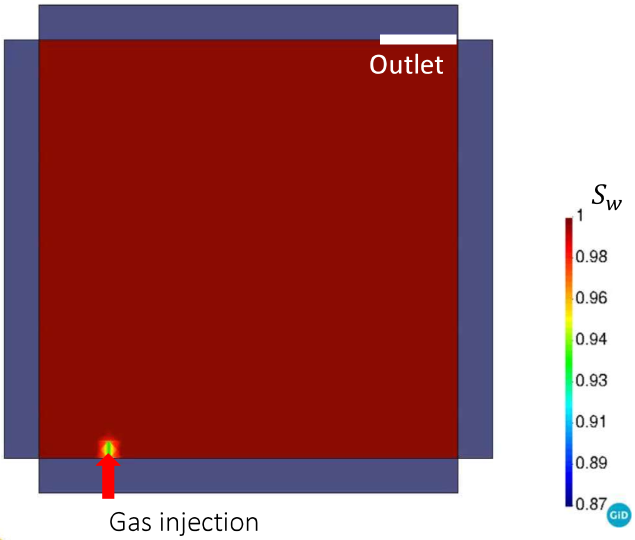

Gas injection pressure

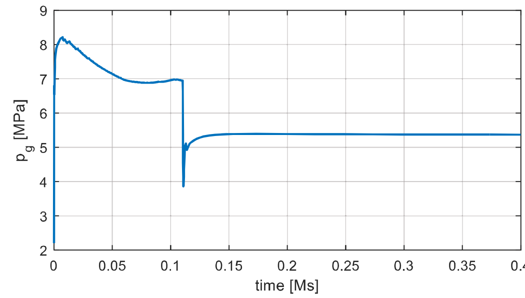

Gas outflow

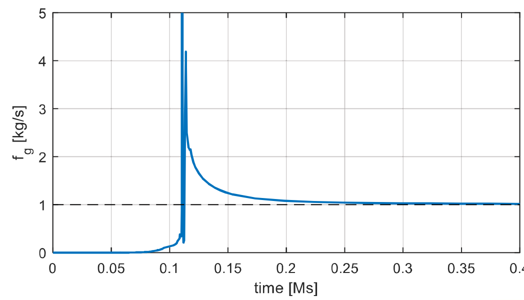

FREE CRACKING PATH

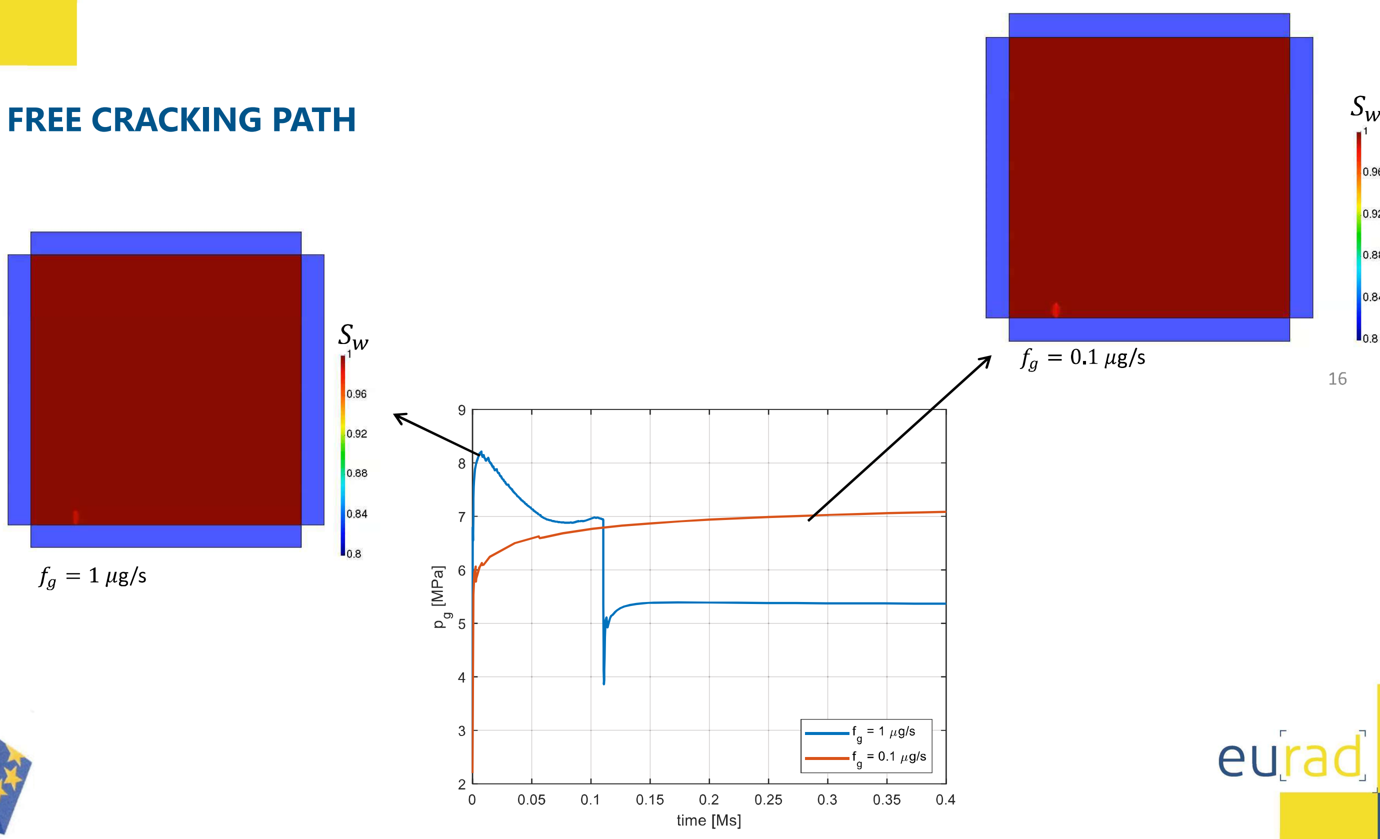

eurad

FREE CRACKING PATH: MESH SENSITIVITY

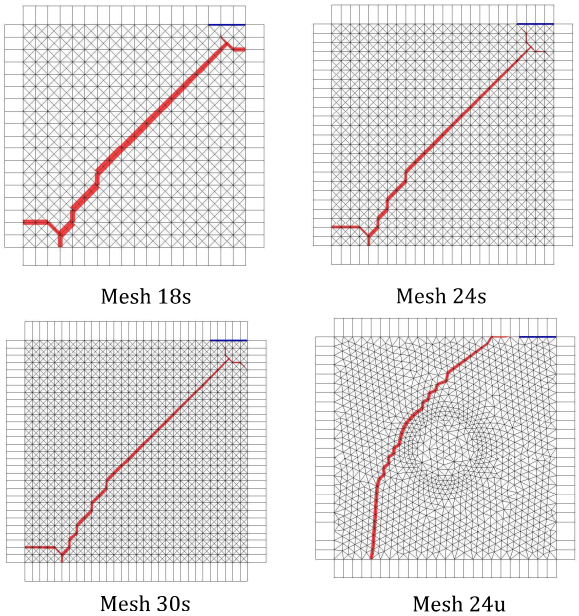

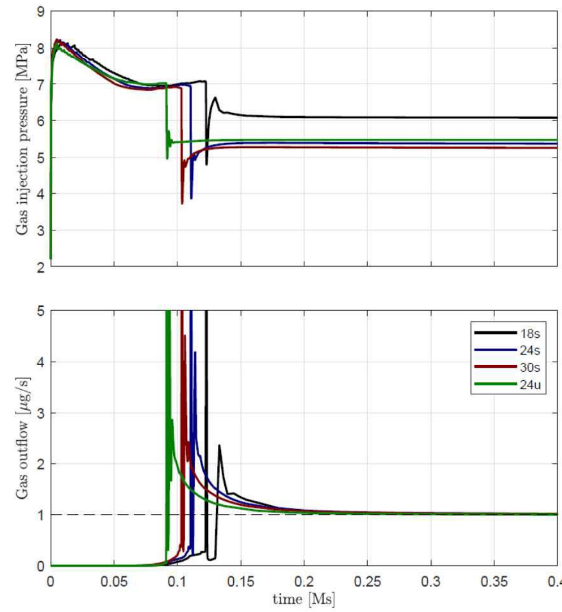

ALERT Geomaterials
Alliance of Laboratories in Europe for Education, Research and Technology
http://alertgeomaterials.eu

eurad
European Joint Programme on Radioactive Waste Management

MODELLING RESULTS

“2D” Gas fracturing tests (BGS)

This project has received funding from the European Union’s Horizon 2020 research and innovation programme under grant agreement N°847593

BGS FRACTURE VISUALIZATION RIG Wiseall, Cuss, Graham & Harrington (2015)

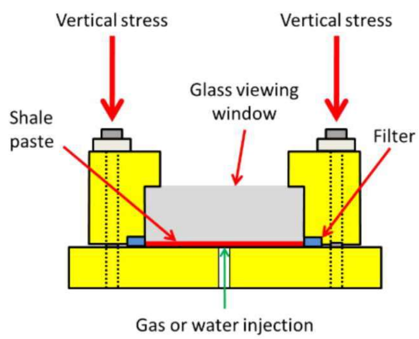

- Gas fractures developed under approx. plane strain conditions
- Crack propagation can be observed as gas is injected

MODEL GEOMETRY, FE MESH AND INITIAL CONDITIONS

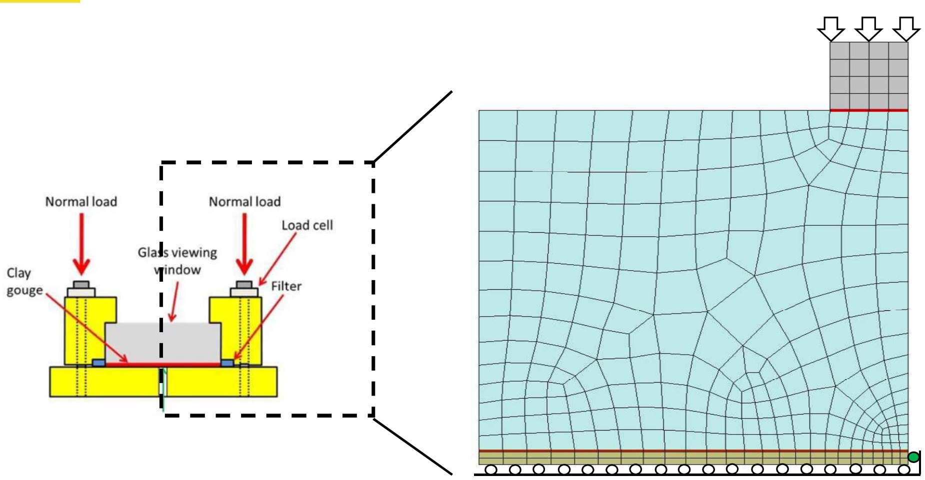

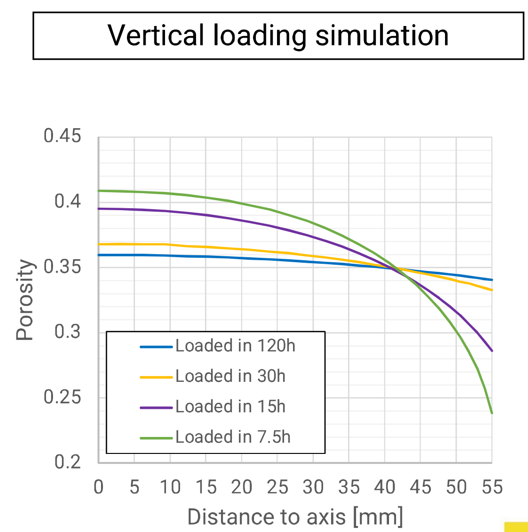

GAS FRACTURING SIMULATIONS

Back-pressure

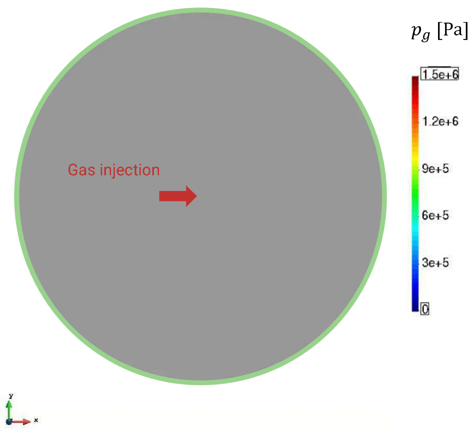

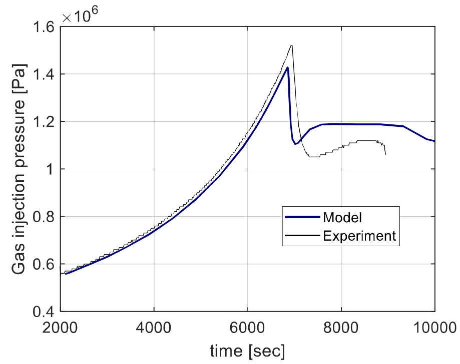

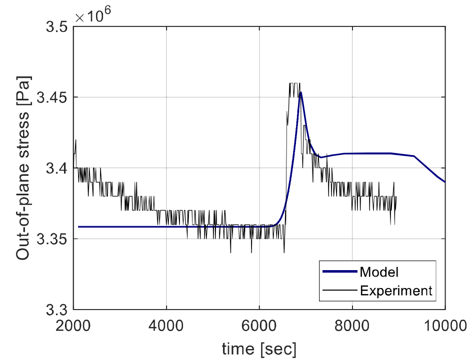

CONCLUSIONS

- The proposed FEM+z approach can simultaneously simulate
  - Diffusion/advection of dissolved gas and two-phase flow both in the continuous porous medium

  and
  - Gas flow along/across macroscopic cracks induced and propagated by the gas pressure.
- Self-sealing is achieved automatically when the induced cracks close as the gas pressure is reduced.
- Experimental observations are qualitatively reproduced by the model.
- The explicit representation of discontinuities (e.g., fractures, joints, faults, material interfaces, etc.) allows a more detailed study of the effect of these features in the overall pneumo-hydro-mechanical behaviour of the clay barriers.

REMARK

Dialogue between experimentalists and modellers is crucial to better understand the observed behaviour and the impact of testing equipment and protocols… especially when dealing with gas!

- Realistic representation of clay-experimental device interfaces and boundary conditions is important as these may have a significant influence on the results.
- In addition to the gas injection, simulation of the initial conditioning of the sample, as well as the dismantling process may be necessary to explain experimental observations.

REFERENCES

- Liaudat J., Dieudonné A.C. and Vardon P.J. (2023) Modelling gas fracturing in saturated clay samples using triple-node zero-thickness interface elements. Computers and Geotechnics 154, 105128.

Appendix M. Advanced multiphysics modelling of geomaterials: Multiscale modelling of gas flow (F. Collin)

Advanced multiphysics of geomaterials: multiscale approaches and heterogeneities

ALERT OZ / EURAD GAS & HITEC Summer School
28 August – 01 September 2023 • Liège (Belgium)

Pierre BÉSUELLE, Frédéric COLLIN,
Anne-Catherine DIEUDONNÉ, Sebastia OLIVELLA

The project leading to this application has received funding from the European Union's Horizon 2020 research and innovation programme under grant agreement n° 847593.

Advanced multiphysics of geomaterials: Multiscale modelling of gas flow

ALERT OZ / EURAD GAS & HITEC Summer School
28 August – 01 September 2023 • Liège (Belgium)

Gilles Corman, Frédéric COLLIN

The project leading to this application has received funding from the European Union's Horizon 2020 research and innovation programme under grant agreement n° 847593.

Context

Geological disposal of radioactive wastes

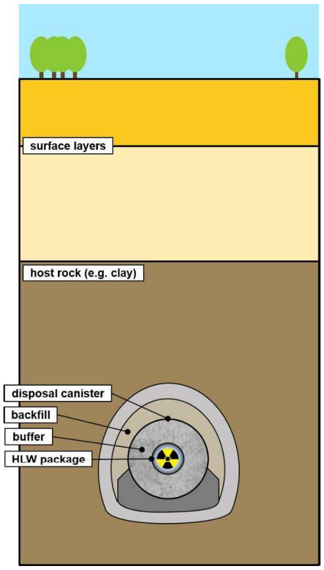

Conceptual scheme of a deep geological repository.

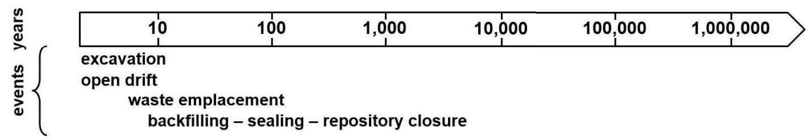

Context

Geological disposal of radioactive wastes

► Complex multi-physical (**THMC**) processes

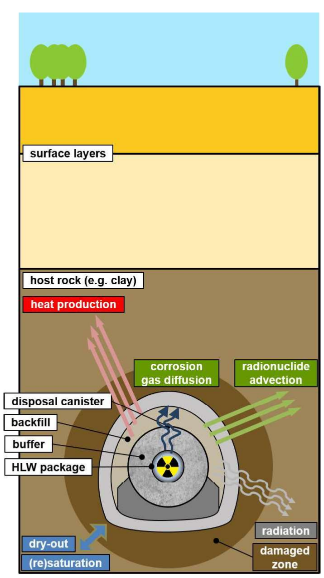

Conceptual scheme of a deep geological repository.

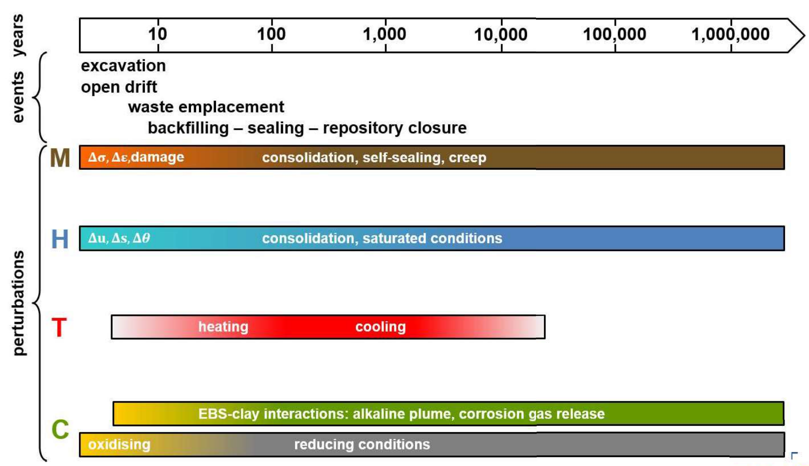

Major perturbations of the host rock over the lifetime of a geological repository, adapted from *Sillen (2012)*.

Context

Geological disposal of radioactive wastes

- ► Complex multi-physical (THMC) processes
- ► Interactions between processes

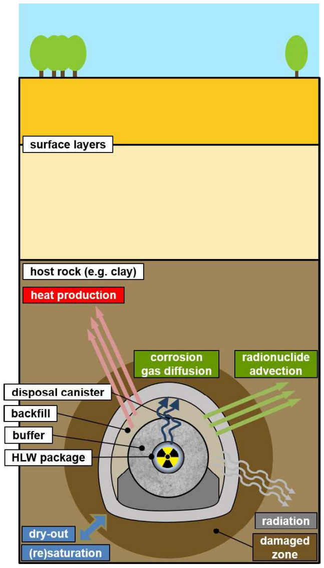

Conceptual scheme of a deep geological repository.

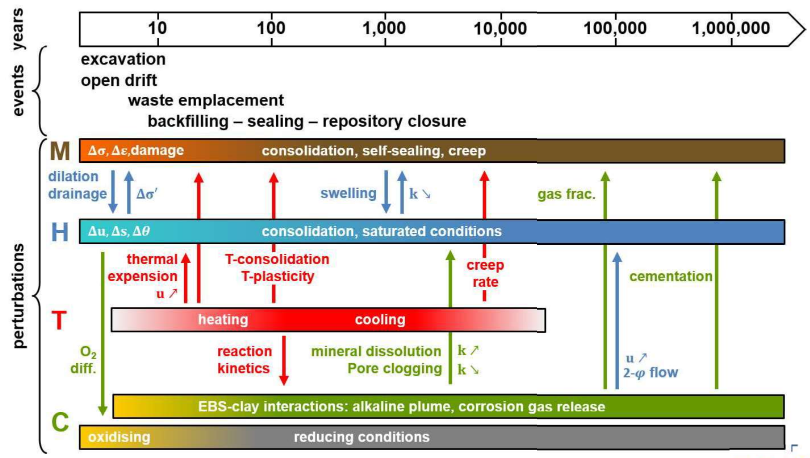

Major perturbations of the host rock over the lifetime of a geological repository, adapted from *Sillen (2012)*.

Context

Geological disposal of radioactive wastes

- ► Complex multi-physical (THMC) processes
- ► Interactions between processes

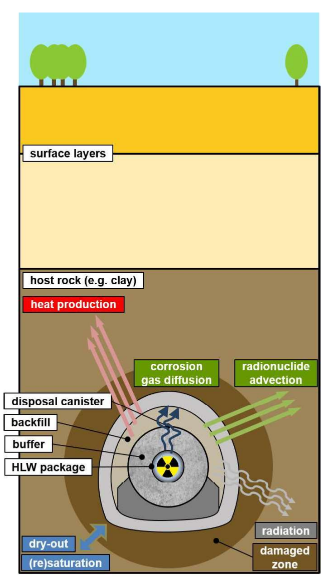

Conceptual scheme of a deep geological repository.

1st aspect: short-term

2nd aspect: long-term

Predictions: numerical modelling

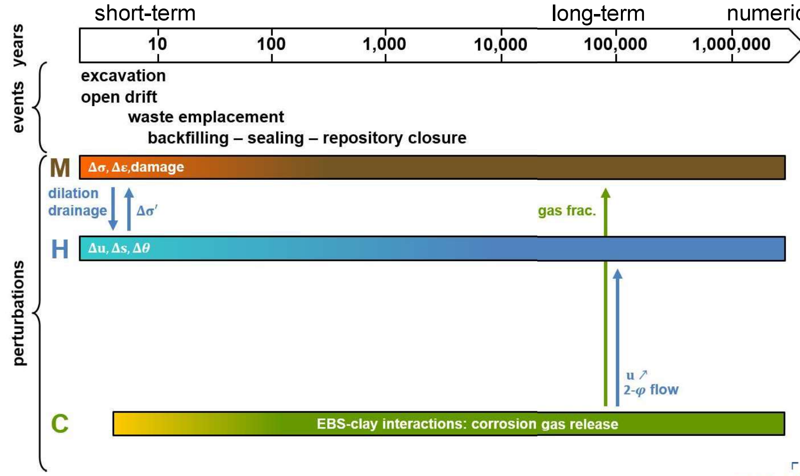

Major perturbations of the host rock over the lifetime of a geological repository, adapted from *Sillen (2012)*.

Context

Gas migration issue

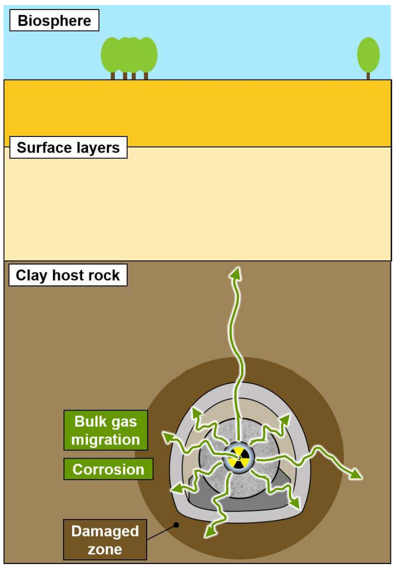

Conceptual scheme of a deep geological repository focussing on the gas generation process.

Corrosion

↓

Gas release

↓

Gas pressure build-up

↓

Potential gas migrations through the barrier

Context

Gas migration issue

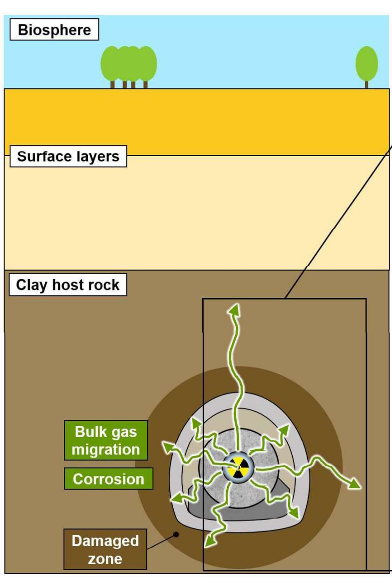

Conceptual scheme of a deep geological repository focussing on the gas generation process.

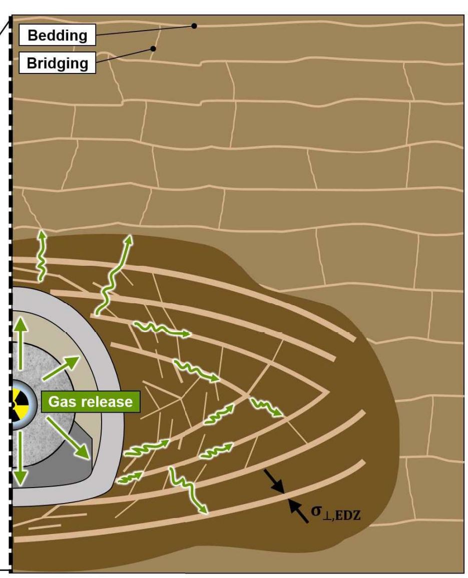

Expected gas transport modes in the EDZ and the sound rock, *from ONDRAF/NIRAS (2016).*

Excavation damaged zone (EDZ)

- Governed by the hydraulic properties modifications induced by fracturation

Context

Gas migration issue

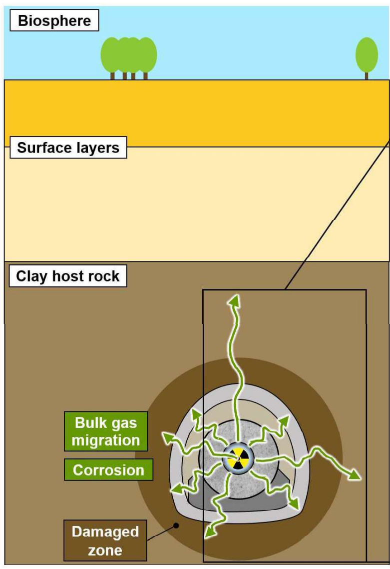

Conceptual scheme of a deep geological repository focussing on the gas generation process.

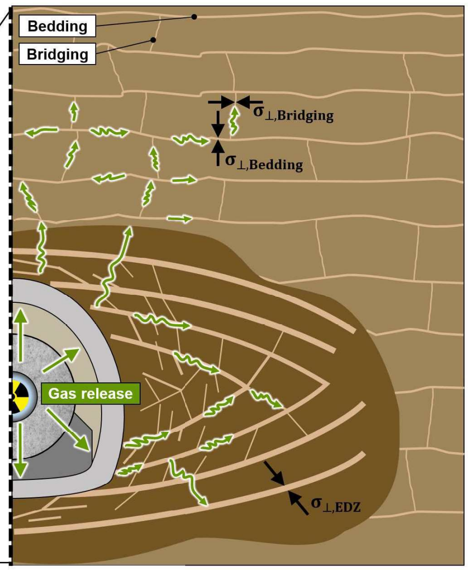

Expected gas transport modes in the EDZ and the sound rock, *from ONDRAF/NIRAS (2016).*

Sound rock layers

- ► Governed by the rock structure **at a micro-level**
- ► Multi-Scale Model

Excavation damaged zone (EDZ)

- ► Governed by the hydraulic properties modifications induced by fracturation

Content

From experimental evidence to modelling

Background

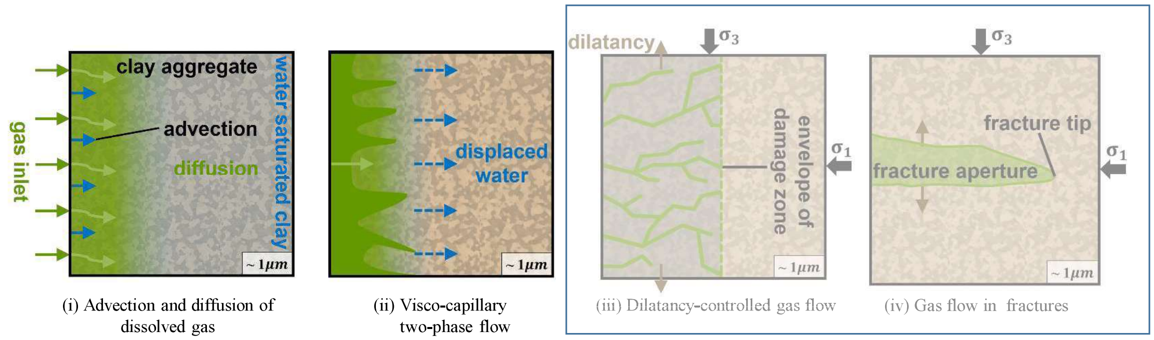

Phenomenological description of the gas transport processes relevant to low-permeable clayey rocks, *adapted from Marschall et al. (2005).*

Classical HM two-phase flow models

From experimental evidence to modelling

Classical HM two-phase flow models

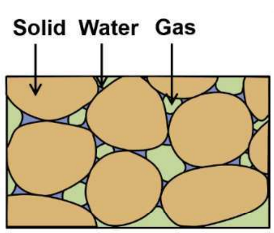

Triphasic porous medium

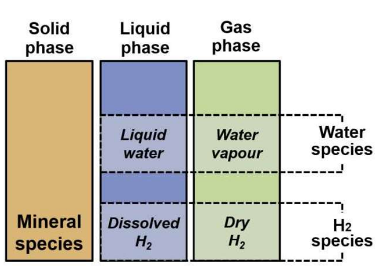

Phases and species

Bright, Aster, Lagamine, OpenGEOSys, Though2/3

From experimental evidence to modelling

Background

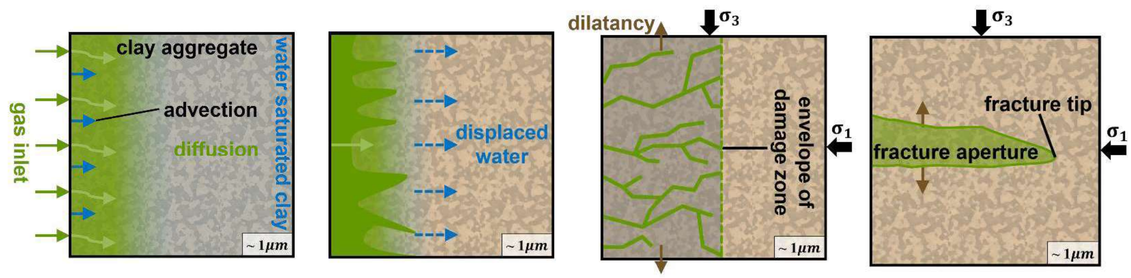

(i) Advection and diffusion of dissolved gas

(ii) Visco-capillary two-phase flow

(iii) Dilatancy-controlled gas flow

(iv) Gas flow in fractures

Phenomenological description of the gas transport processes relevant to low-permeable clayey rocks, *adapted from Marschall et al. (2005).*

Classical HM two-phase flow models

Supported by experimental data

From experimental evidence to modelling

Laboratory experiments

Clay-rich material

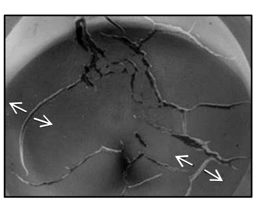

Gas-induced fracturing, *Wiseall et al. (2015)*

Callovo-Oxfordian claystone

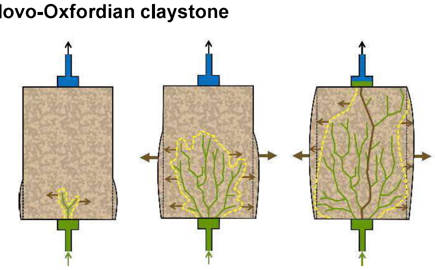

Onset of gas flow, *modified after Cuss et al. (2014)*

Boom Clay

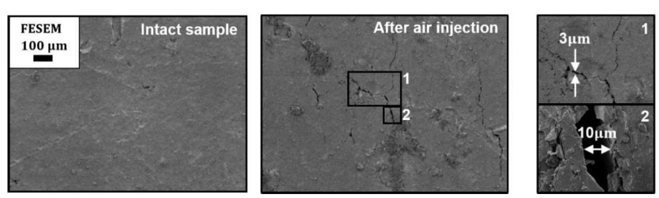

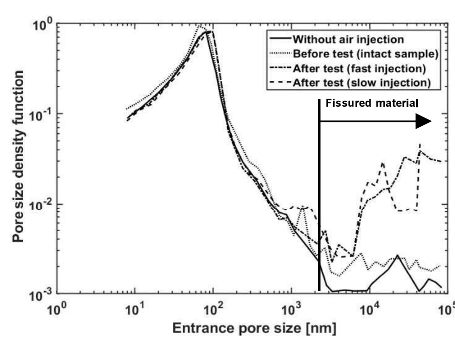

Changes in Boom Clay pore size distribution after air injection, and corresponding FESEM images with zooms on the detected fissures, *modified after Gonzalez-Blanco et al. (2022)*

From experimental evidence to modelling

Background

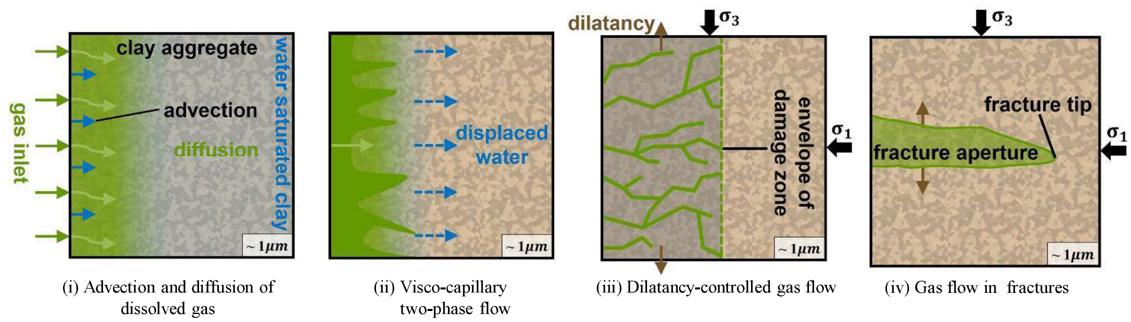

Phenomenological description of the gas transport processes relevant to low-permeable clayey rocks, *adapted from Marschall et al. (2005).*

Classical HM two-phase flow models

Supported by experimental data

- Natural heterogeneities represent preferred weaknesses for the process of opening discrete gas-filled pathway
- Introduce stronger coupling between gas flow and mechanical behaviour into the models.

► **Advanced HM models**

From experimental evidence to modelling

Advanced HM models

Macroscopic models

► No direct representation of local phenomena

► Enriched with micromechanical effects

► Examples:

- Natural heterogeneity based models Olivella and Alonso (2008)
- Intrinsic permeability based models Pardoen et al. (2016)
- Embedded fracture models Alonso et al. (2006)
- Explicit fracture based models Cerfontaine et al. (2015)

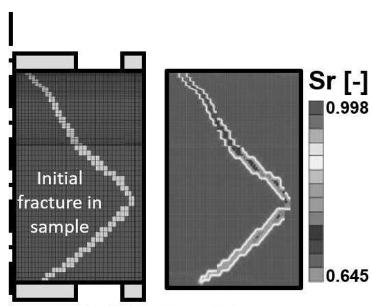

Embedded fracture model, from *Gerard et al (2014).*

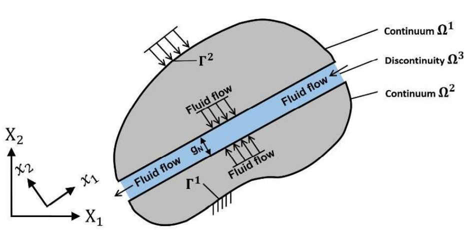

Conceptual scheme of the explicit fracture based model, *after Cerfontaine et al. (2015)*

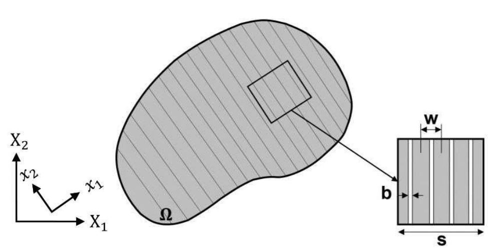

Conceptual scheme of the embedded fracture model, *after Olivella et al. (2008)*

From experimental evidence to modelling

Advanced HM models

Microscopic models

- Direct modelling of all the microstructure complexity at very low scale
- Useful for modelling at the process scale
- High computational expense at the scale of a repository

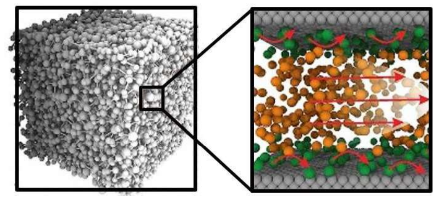

From pore network to molecular model, from *Yu et al. (2019)*.

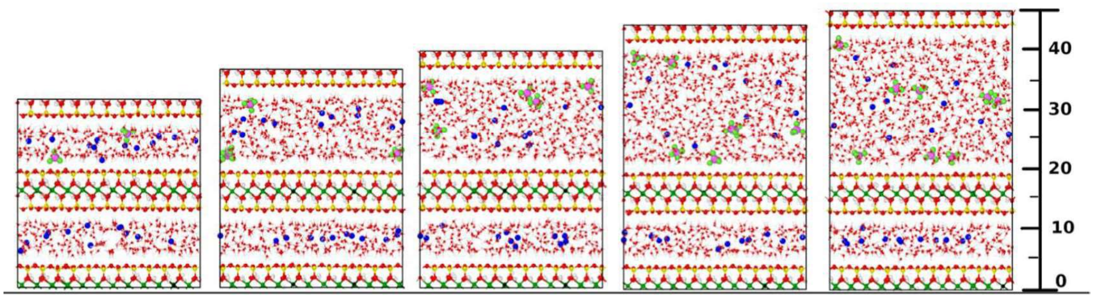

Study of the the physico-chemical properties of dissolved gases in several configurations of a hydrated clay system, from Owusu et al. *(2022)*.

From experimental evidence to modelling

Advanced HM models

Micro-macro based models

- Combines the benefits from large- and small-scale modelling strategies
- Explicit description of all the constituents on their specific length scale through a REV definition

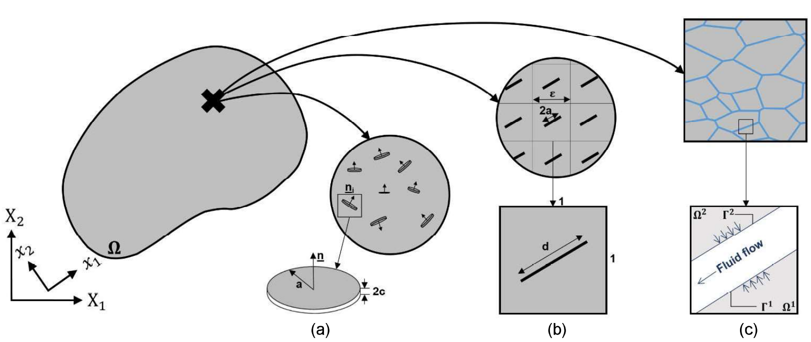

Conceptual scheme of micro-macro based models, with microstructure definitions of a microcracked material, *after (a) Levasseur (2013), (b) François (2010), and (c) van den Eijnden (2016).*

Content

Multi-scale modelling approach

Overview

- Macro-to-micro scale transition: Localisation of the macro-scale deformations to the micro-scale
- Resolution of the boundary value problem at the micro-scale
- Micro-to-macro scale transition: Homogenisation of the micro-scale stresses to compute the macroscopic quantities
- Resolution of the boundary value problem at the macro-scale

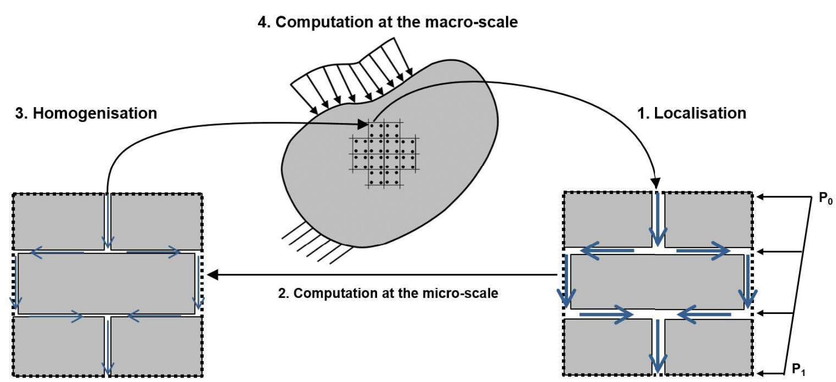

Conceptual scheme of the iterative process for the multiscale model

Hybrid developed tool

- Complete hydraulic system implemented and solved at the micro-scale
- Mechanical effects addressed at the macro-scale and implicitly integrated at the lower scale through HM couplings

Multi-scale modelling approach

Model formulation at the macroscopic scale

Clay material treated as a porous medium

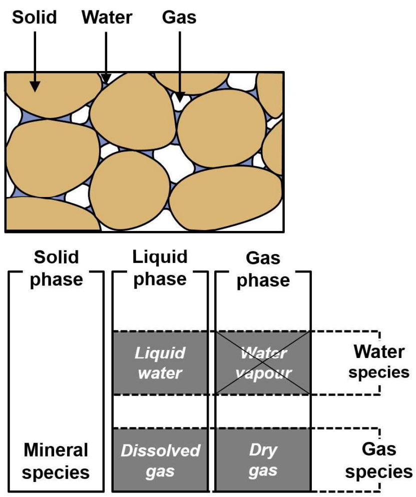

Unsaturated triphasic porous medium and definition of phases and species

Balance equations

- Momentum

$$\frac{\partial \sigma_{ij}}{\partial x_j} + \rho g_i = 0$$

- Water

$$\underbrace{\dot{M}_w + \frac{\partial f_{w,i}}{\partial x_i}}_{\text{Liquid water}} - Q_w = 0$$

- Gas

$$\underbrace{\dot{M}_g + \frac{\partial f_{g,i}}{\partial x_i}}_{\text{Dry gas}} + \underbrace{\dot{M}_{dg} + \frac{\partial f_{dg,i}}{\partial x_i}}_{\text{Dissolved gas}} - Q_g = 0$$

Constitutive equations

- Total stress definition

$$\sigma_{ij} = \sigma'_{ij} + b_{ij}\left[S_{r_w} p_w^M + (1 - S_{r_w}) p_g^M\right]\delta_{ij}$$

- Variation of solid density

$$\frac{\dot{\rho}_s}{\rho_s} = \frac{(b_{ij} - \phi)(S_r^w \dot{p}_w + S_r^g \dot{p}_g) + \dot{\sigma}'}{(1 - \phi)K_s}$$

Multi-scale modelling approach

Macro-to-micro scale transition: Localisation

Decomposition of the micro-kinematics:

- Macro-pressure fields $(\square^M)$ of water and gas must be identical to the micro-quantities $(\square^m)$ for any point of the material

$$p_w^M(\hat{P}) = p_w^m(\hat{P}) \qquad p_g^M(\hat{P}) = p_g^m(\hat{P})$$

- For any point P close to $\hat{P}$,
  at the macroscopic scale:

$$p_w^M(P) \approx p_w^M(\hat{P}) + \frac{\partial p_w^M(\hat{P})}{\partial x_j}\left(x_j - \hat{x}_j\right) \qquad p_g^M(P) \approx p_g^M(\hat{P}) + \frac{\partial p_g^M(\hat{P})}{\partial x_j}\left(x_j - \hat{x}_j\right)$$

Higher-order terms neglected

at the microscopic scale:

$$p_w^m(P) \approx p_w^M(\hat{P}) + \frac{\partial p_w^M(\hat{P})}{\partial x_j}\left(x_j - \hat{x}_j\right) + p_w^f(\hat{P}) \qquad p_g^m(P) \approx p_g^M(\hat{P}) + \frac{\partial p_g^M(\hat{P})}{\partial x_j}\left(x_j - \hat{x}_j\right) + p_g^f(\hat{P})$$

Fluctuation fields to replace higher-order terms

Separation of scales

- Approach restricted to situations where the variations of the macroscopic fields is large compared to the variations of micro-scale fields

$$\frac{\partial p_w^M(\hat{P})}{\partial x_j}\left(x_j - \hat{x}_j\right) + p_w^f(\hat{P}) \ll p_w^M(\hat{P})$$

$$\frac{\partial p_g^M(\hat{P})}{\partial x_j}\left(x_j - \hat{x}_j\right) + p_g^f(\hat{P}) \ll p_g^M(\hat{P})$$

Multi-scale modelling approach

Micro-scale boundary value problem

REV generation in general

- Representative of the microstructure
    - Large enough to represent the microstructure
    - Small enough to satisfy the principle of scale separation
- Spatial repetition of a very small part of the whole microstructure
    - Relevant statistical representation of any random part of the micro-scale
    - Not a unique choice

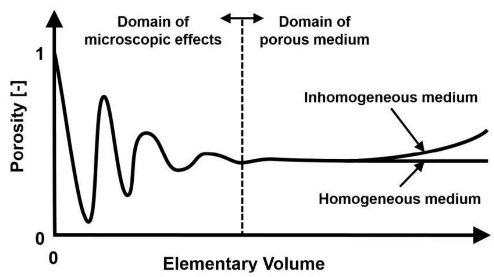

Representativeness of an elementary volume applied to the concept of porosity, *Bear (1972).*

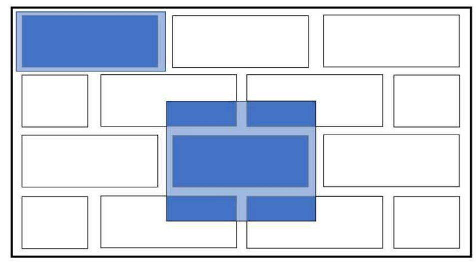

Examples of two rectangular unit cells, *Anthoine (1995).*

Multi-scale modelling

Micro-scale boundary value problem

Multi-scale model supported by experimental data

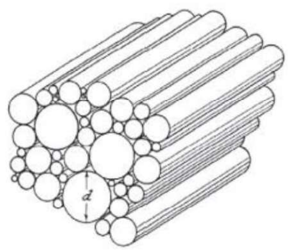

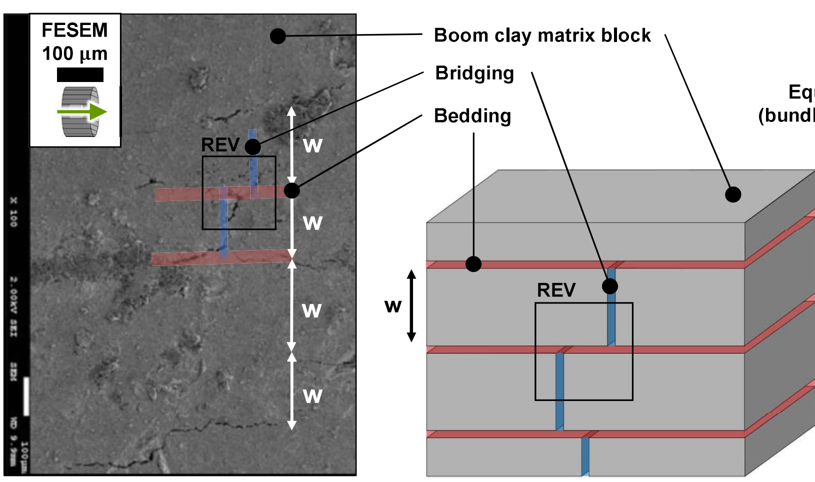

Internal visualisation of a Boom Clay sample using FESEM, *from Gonzalez-Blanco (2017).*

Physical idealisation of the microstructure.

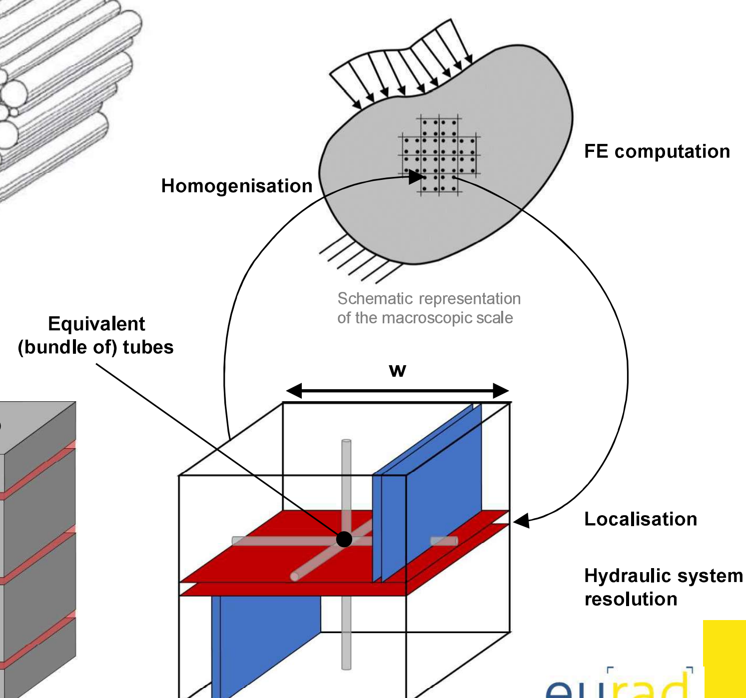

Definition of the representative element volume (REV)

Multi-scale modelling approach

Micro-scale boundary value problem

Balance equations at the micro-scale

- Gas

$$\cancel{\dot{M}_g^m} + \frac{\partial f_{g_i}^m}{\partial x_i} + \cancel{\dot{M}_{dg}^m} + \frac{\partial f_{dg_i}^m}{\partial x_i} = 0$$

- Water

$$\cancel{\dot{M}_w^m} + \frac{\partial f_{w_i}^m}{\partial x_i} = 0$$

$\dot{M}_g^m \; \dot{M}_{dg}^m \; \dot{M}_w^m$: Variations of fluid contents

$$f_{w_i}^m = \rho_w q_{w_i}$$
$$f_{g_i}^m = \rho_g q_{g_i}$$
$$f_{dg_i}^m = \rho_{dg} q_{w_i} + i_{dg_i}$$

Mass flows

- Mechanical effects: computed at the macro-scale and transferred to the micro-scale through HM couplings

eurad

Multi-scale modelling approach

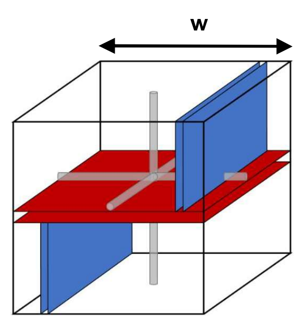

Micro-scale boundary value problem

Constitutive equations: Hydraulic problem considering a channel flow model (Navier-Stokes equations)

- Advective component:

$$q_{\alpha_i} = -\frac{k_{r\alpha}}{\mu_\alpha}\frac{1}{A}\kappa_{frac}\frac{\partial p_\alpha}{\partial x_i} = -\frac{k_{r\alpha}}{\mu_\alpha}\frac{h_b^3}{12w}\frac{\partial p_\alpha}{\partial x_i}$$

$$q_{\alpha_i} = -\frac{k_{r\alpha}}{\mu_\alpha}\frac{1}{A}\kappa_{tube}\frac{\partial p}{\partial x_i} = -\frac{k_{r\alpha}}{\mu_\alpha}\pi\frac{D^4}{128w^2}\frac{\partial p}{\partial x_i}$$

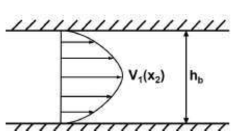

Laminar fluid flow profiles between two parallel plates

$$\kappa_{frac} = -\frac{h_b^2}{12}h_b \cdot w$$

$$\kappa_{tube} = -\pi\frac{D^4}{128}$$

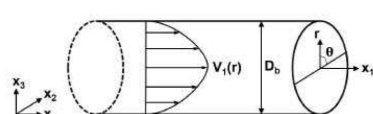

Laminar fluid flow profiles in a circular pipe

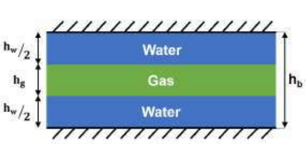

Gas flow in between of water flows in a fracture space

$$k_{r_w} = \frac{S_r^2}{2}(3-S_r)$$
$$k_{r_g} = (1-S_r)^3$$

$$k_{r_w} = S_r^2$$
$$k_{r_g} = (1-S_r)^2$$

Gas flow in between of water flows in a circular pipe

- Diffusive component

$$i_{dg_i} = -S_{r_w}\,\tau\,D_{dg/w}\,\rho_w\frac{\partial}{\partial x_i}\left(\frac{\rho_{dg}}{\rho_w}\right)$$

eurad

Multi-scale modelling approach

Micro-scale boundary value problem

Constitutive equations: Hydro-mechanical couplings

- Stress-dependent evolution of micro-elements aperture

$$\Delta\sigma' = K_n \, \Delta h \qquad \Delta\sigma' = K \, \Delta D_b$$

$$K_n = \frac{K_n^0}{\left(1+\frac{\Delta h}{h_0}\right)^2} \qquad K = \frac{2G}{D_0}$$

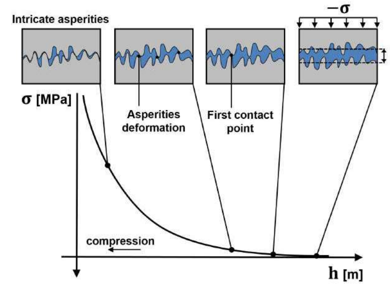

Constitutive law describing the normal behaviour of a rough rock joint, *Cerfontaine (2015)*

- Stress-dependent formulation of the transmissivity and the entry pressure of micro-elements

$$\kappa_{frac} = -\frac{h_b^2}{12} h_b \cdot w \qquad \kappa_{tube} = -\pi \frac{D^4}{128}$$

$$p_e = p_{e_0}\left(\frac{h_{b_0}}{h_b}\right)^m \qquad p_e = p_{e_0}\left(\frac{D_{b_0}}{D_b}\right)^m$$

$$p_{e_0} = \frac{2\sigma_{GL} cos\theta}{h_b} \qquad p_{e_0} = \frac{2\sigma_{GL} cos\theta}{D_b/2}$$

$$h_b = h_0 + h \qquad D_b = D_0 + D$$

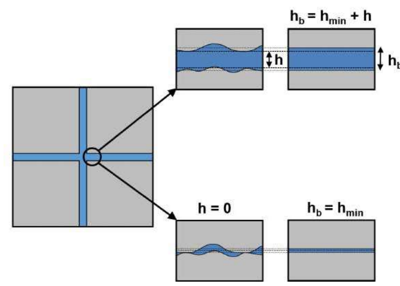

Definitions of the hydraulic and the mechanical aperture in reality (left) and in the modelling (right), *Marinelli (2016)*

Multi-scale modelling approach

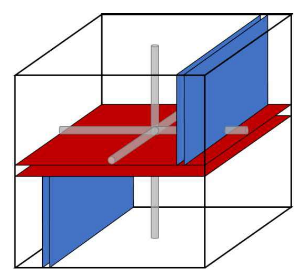

Micro-scale boundary value problem

General principles for numerical resolution of the hydraulic system

- Hydraulic network respecting these conditions:
  - Anti-symmetric boundary fluxes
  - Macroscopic pressure gradient between the boundaries
- Hydraulic problem established through mass balance on each node (j)
- Hydraulic problem solved
  - For a given configuration
  - Under steady-state conditions
  - By applying the macro-pressure to one node

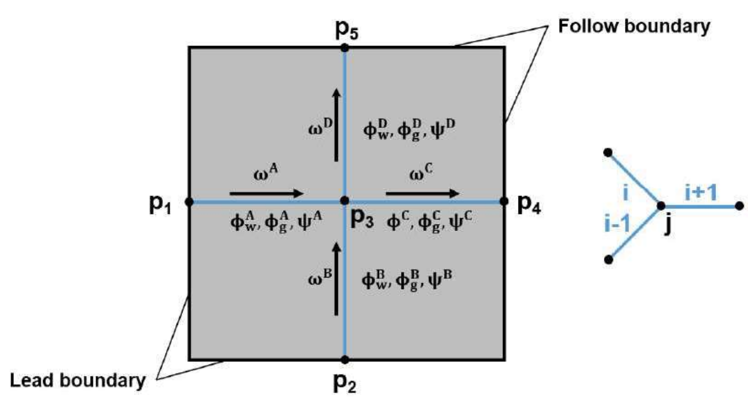

Example of a channel network with the mass balance on node j

Multi-scale modelling approach

Micro-scale boundary value problem

General principles for numerical resolution of the hydraulic system

- Hydraulic network respecting these conditions:
  - Anti-symmetric boundary fluxes
  - Macroscopic pressure gradient between the boundaries

=> Channel (fracture or tube) mass fluxes of water and gas

$$\omega_w = -\underbrace{\frac{\rho_w k_{r_w}}{\mu_w}\kappa\frac{\partial p_w^m}{\partial s}}_{\text{Advection of liquid water}}$$

$$\omega_g = -\underbrace{\frac{\rho_g k_{r_g}}{\mu_g}\kappa\frac{\partial p_g^m}{\partial s}}_{\text{Advection of gaseous gas}} - \underbrace{H_g\frac{\rho_g k_{r_w}}{\mu_w}\kappa\frac{\partial p_w^m}{\partial s}}_{\text{Advection of dissolved gas}}$$

$$\underbrace{-S_{r_w}\bar{\tau}D_{dg/w}\frac{H_g}{\rho_w}\left(\frac{\rho_w\rho_{g,0}}{\rho_{g,0}}\frac{\partial p_g^m}{\partial s} - \frac{\rho_g\rho_{w,0}}{\chi_w}\frac{\partial p_w^m}{\partial s}\right)}_{\text{Diffusion of dissolved gas}}$$

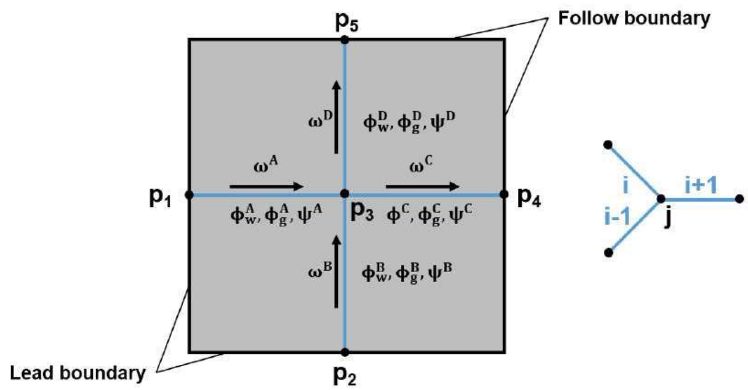

Example of a channel network with the mass balance on node j

Multi-scale modelling approach

Micro-scale boundary value problem

General principles for numerical resolution of the hydraulic system

- Hydraulic problem established through mass balance on each node (j)
  - Mass conservation principle, *i.e.* for each node of the network, the sum of the input flows is equal to the sum of the output flows

$$\frac{d\omega_\alpha^i}{ds^i} = 0 \quad \Leftrightarrow \quad \omega_\alpha^{i-1} + \omega_\alpha^i + \omega_\alpha^{i+1} = 0$$

$\alpha = w, g$ Liquid or gaseous phase

- Well-posed hydraulic system to solve

$$[G_{ww}]\{p_w^m\} = 0 \qquad [G_{gg}]\{p_g^m\} + [G_{gw}]\{p_w^m\} = 0$$

  - For a given configuration
  - Under steady-state conditions
  - By applying the macro-pressure to one node

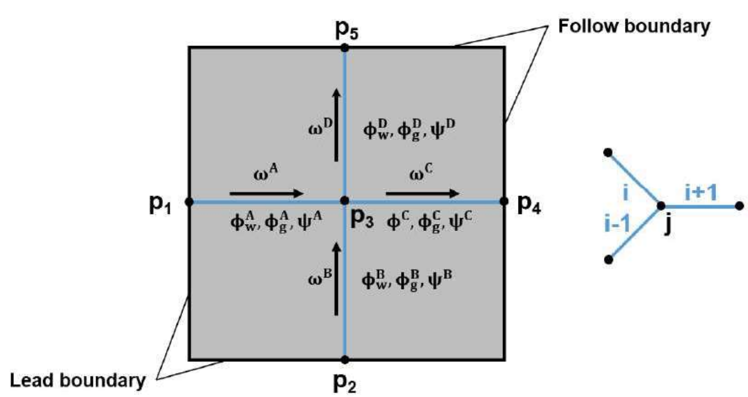

Example of a channel network with the mass balance on node j

Multi-scale modelling approach

Micro-to-macro scale transition: Homogenisation

- Fluid fluxes

$$
\begin{aligned}
f_{w_i}^{M}\frac{\partial p_w^{\star,M}}{\partial x_i} &= \frac{1}{\Omega}\int_{\Omega} f_{w_i}^{m}\frac{\partial p_w^{\star,M}}{\partial x_i} d\Omega = \frac{1}{\Omega}\int_{\Gamma}\bar{q}_w^m p_w^{\star,M} d\Gamma \\
&= \frac{1}{\Omega}\frac{\partial p_w^{\star,M}}{\partial x_i}\int_{\Gamma}\bar{q}_w^m x_i d\Gamma \\
&= \frac{1}{\Omega}\int_{\Gamma}\bar{q}_w^m x_i d\Gamma
\end{aligned}
$$

$$
f_{g_i}^{M} + f_{dg_i}^{M} = \frac{1}{\Omega}\int_{\Gamma}\bar{q}_g^m x_i d\Gamma
$$

- Fluid masses: total amount of fluids inside the fractures and tubes

$$
\begin{aligned}
M_w^M &= \frac{1}{\Omega}\int_{\Omega_w^{int}} \rho_w d\Omega \\
&= \rho_w S_{r_w}\phi_n
\end{aligned}
$$

$$
\begin{aligned}
M_g^M &= M_g^m + M_{dg}^m \\
&= \frac{1}{\Omega}\left(\int_{\Omega_g^{int}} \rho_g d\Omega + \int_{\Omega_w^{int}} \rho_{dg} d\Omega\right) \\
&= \rho_g\left(1 - S_{r_w}\right)\phi_n + \rho_{dg} S_{r_w}\phi_n
\end{aligned}
$$

Multi-scale modelling approach

Macro-scale boundary value problem

- Under matrix form:

$$
\begin{bmatrix}
\left[K_{ww}^M\right]_{(3\times3)} & \left[K_{wg}^M\right]_{(3\times3)} \\
\left[K_{gw}^M\right]_{(3\times3)} & \left[K_{gg}^M\right]_{(3\times3)}
\end{bmatrix}
\begin{Bmatrix}
\begin{Bmatrix} \delta\nabla p_w^M \\ \delta p_w^M \end{Bmatrix}_{(3)} \\
\begin{Bmatrix} \delta\nabla p_g^M \\ \delta p_g^M \end{Bmatrix}_{(3)}
\end{Bmatrix}
=
\begin{Bmatrix}
\begin{Bmatrix} \delta f_w^M \\ \delta \dot{M}_w^M \end{Bmatrix}_{(3)} \\
\begin{Bmatrix} \delta f_g^M \\ \delta \dot{M}_g^M \end{Bmatrix}_{(3)}
\end{Bmatrix}
$$

Summarized as:

$$
\left[A^M\right]_{(10\times10)}\left\{\delta U^M\right\}_{(10)} = \left\{\delta\Sigma^M\right\}_{(10)}
$$

Content

Preliminary modelling

One-element simulation

Bedding plane separation:

- $300\mu m$

Bedding plane aperture:

- $0.1\mu m$

Tubes diameter
→ Distribution curve

Bridging plane aperture
→ not considered

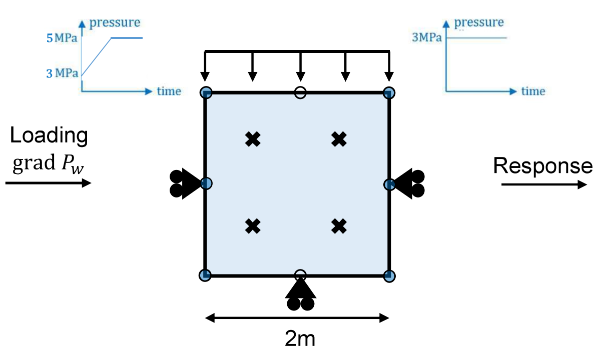

Injection test

- Mechanically blocked
- Water pressure increase
  - 3MPa to 5MPa
- Gas pressure imposed at 3MPa

Preliminary modelling

One-element simulation

Bedding plane separation:
- $300\mu m$

Bedding plane aperture:
- $0.1\mu m$

Tubes diameter
→ Distribution curve

Bridging plane aperture
→ not considered

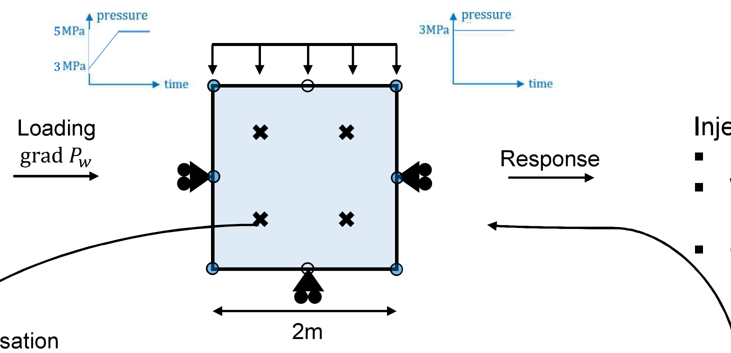

Injection test
- Mechanically blocked
- Water pressure increase from 3MPa to 5MPa
- Gas pressure imposed at 3MPa

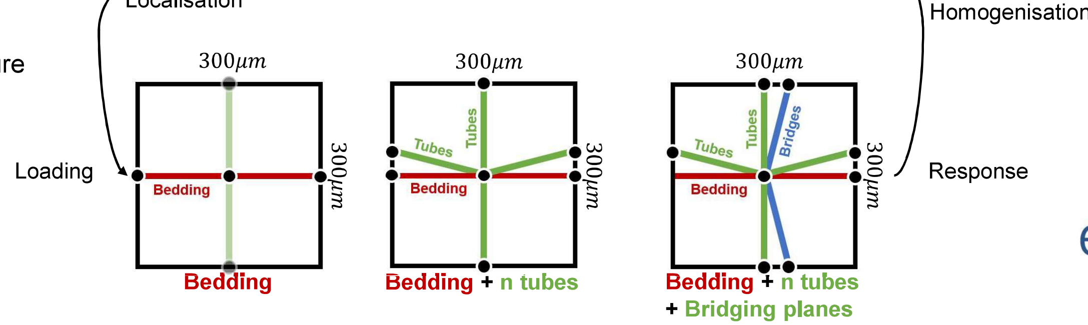

Preliminary modelling

One-element simulation

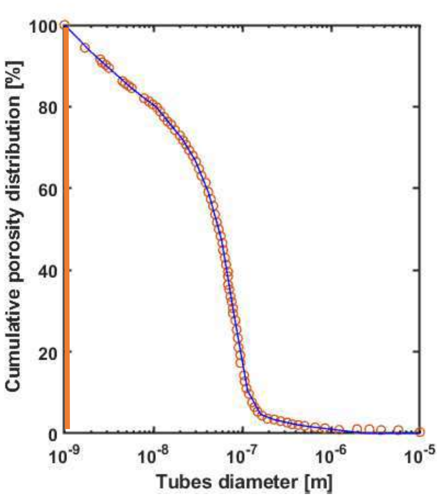

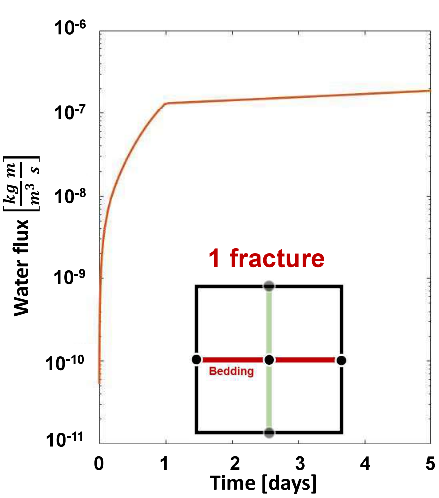

$$\mathrm{k_{int}} = \frac{\mu_w}{\rho_w} Flux \frac{\Delta x}{\Delta p} \quad with \quad \begin{aligned} \Delta x &= 2m \\ \Delta p &= 2\ MPa \end{aligned}$$

$\mathrm{Aperture} = 2.0 \cdot 10^{-6} m$

Number of tubes	Flux $\left[\frac{\mathrm{kg\ m}}{\mathrm{m^3\ s}}\right]$	$\mathrm{k_{int,x}}\ [\mathrm{m^2}]$
0	$1.581 \cdot 10^{-7}$	$1.581 \cdot 10^{-19}$

Preliminary modelling

One-element simulation

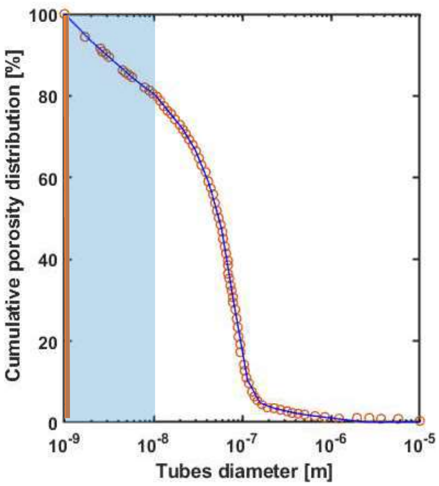

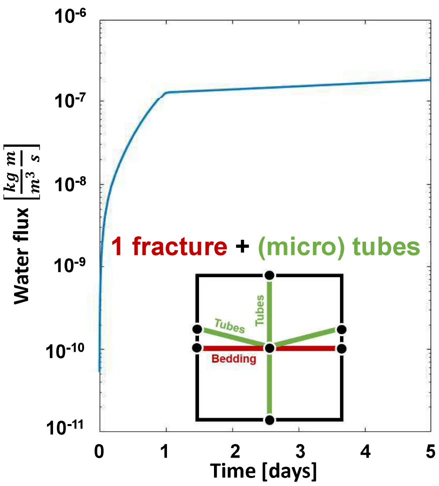

$$\mathrm{k_{int}} = \frac{\mu_w}{\rho_w} Flux \frac{\Delta x}{\Delta p} \quad with \quad \begin{array}{l} \Delta x = 2m \\ \Delta p = 2\ MPa \end{array}$$

$\text{Aperture} = 2.0 \cdot 10^{-6} m$

Number of tubes	Flux $\left[\frac{\mathrm{kg\ m}}{\mathrm{m^3\ s}}\right]$	$\mathrm{k_{int,x}}\ [\mathrm{m^2}]$
0	$1.581 \cdot 10^{-7}$	$1.581 \cdot 10^{-19}$
770	$1.643 \cdot 10^{-7}$	$1.643 \cdot 10^{-19}$

eurad

Preliminary modelling

One-element simulation

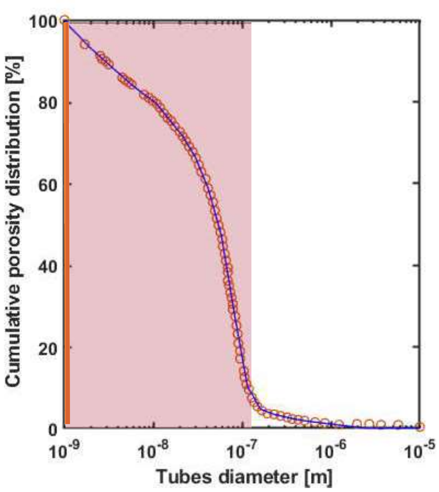

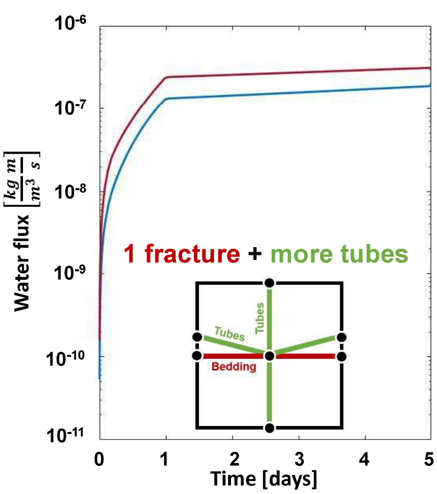

$$\mathrm{k_{int}} = \frac{\mu_w}{\rho_w} Flux \frac{\Delta x}{\Delta p} \quad with \quad \begin{array}{l} \Delta x = 2m \\ \Delta p = 2\ MPa \end{array}$$

$\text{Aperture} = 2.0 \cdot 10^{-6} m$

Number of tubes	Flux $\left[\frac{\mathrm{kg\ m}}{\mathrm{m^3\ s}}\right]$	$\mathrm{k_{int,x}}\ [\mathrm{m^2}]$
0	$1.581 \cdot 10^{-7}$	$1.581 \cdot 10^{-19}$
770	$1.643 \cdot 10^{-7}$	$1.643 \cdot 10^{-19}$
6394	$3.057 \cdot 10^{-7}$	$3.057 \cdot 10^{-19}$

Fracture-controlled flow

eurad

Preliminary modelling

One-element simulation

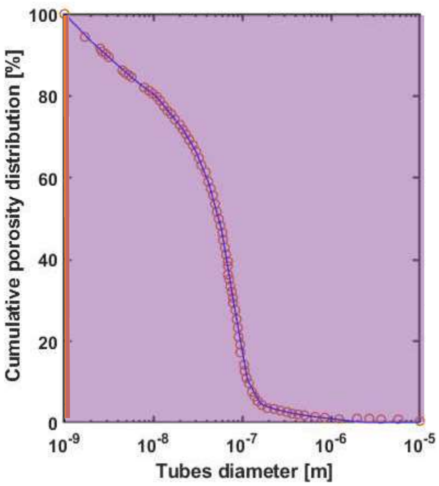

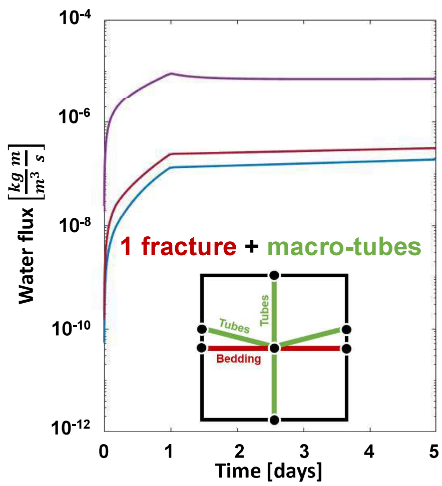

$$\mathrm{k_{int}} = \frac{\mu_w}{\rho_w} Flux \frac{\Delta x}{\Delta p} \quad with \quad \begin{array}{c} \Delta x = 2m \\ \Delta p = 2\ MPa \end{array}$$

$\text{Aperture} = 2.0 \cdot 10^{-6} m$

Number of tubes	Flux $\left[\frac{\text{kg m}}{\text{m}^3 \text{ s}}\right]$	$\mathrm{k_{int,x}}$ [m²]
0	$1.581 \cdot 10^{-7}$	$1.581 \cdot 10^{-19}$
770	$1.643 \cdot 10^{-7}$	$1.643 \cdot 10^{-19}$
6394	$3.057 \cdot 10^{-7}$	$3.057 \cdot 10^{-19}$
		Fracture-controlled flow
9995	$7.200 \cdot 10^{-6}$	$7.200 \cdot 10^{-18}$

Effect of large pores

Preliminary modelling

One-element simulation

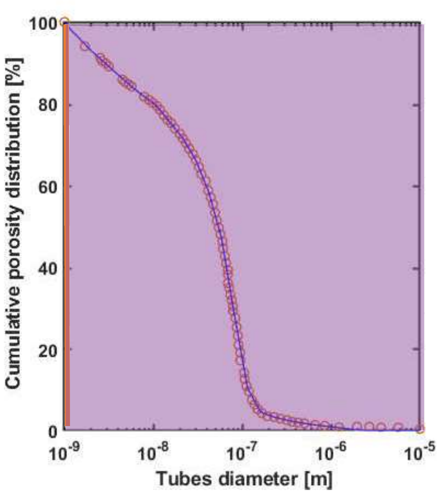

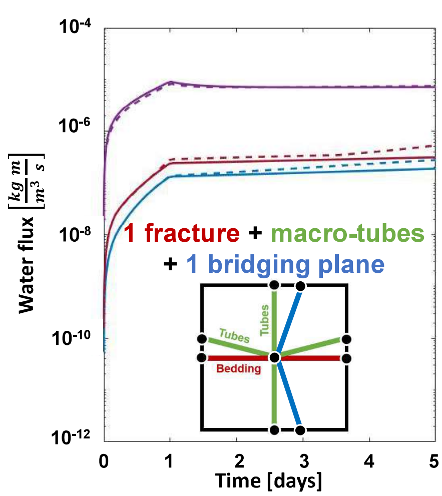

$$\mathrm{k_{int}} = \frac{\mu_w}{\rho_w} Flux \frac{\Delta x}{\Delta p} \quad with \quad \begin{array}{c} \Delta x = 2m \\ \Delta p = 2\ MPa \end{array}$$

$\text{Aperture} = 2.0 \cdot 10^{-6} m$

Number of tubes	Flux $\left[\frac{\text{kg m}}{\text{m}^3 \text{ s}}\right]$	$\mathrm{k_{int,x}}$ [m²]
0	$1.581 \cdot 10^{-7}$	$1.581 \cdot 10^{-19}$
770	$1.643 \cdot 10^{-7}$	$1.643 \cdot 10^{-19}$
6394	$3.057 \cdot 10^{-7}$	$3.057 \cdot 10^{-19}$
		Fracture-controlled flow
9995	$7.200 \cdot 10^{-6}$	$7.200 \cdot 10^{-18}$

Effect of large pores

Model verification

Comparison with a macro-scale THM coupled model

Geometry

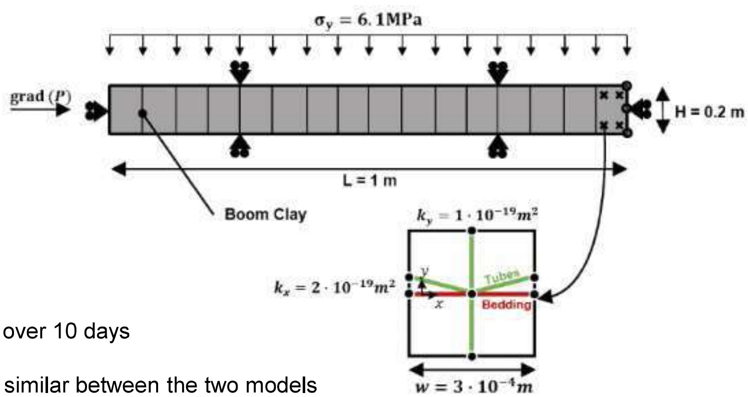

P_{w0}=0.6MPa
P_{g0}=0.1MPa → P_g = 1.0MPa over 10 days

All the parameters are taken similar between the two models

Model verification

Comparison with a macro-scale THM coupled model

Water-related results

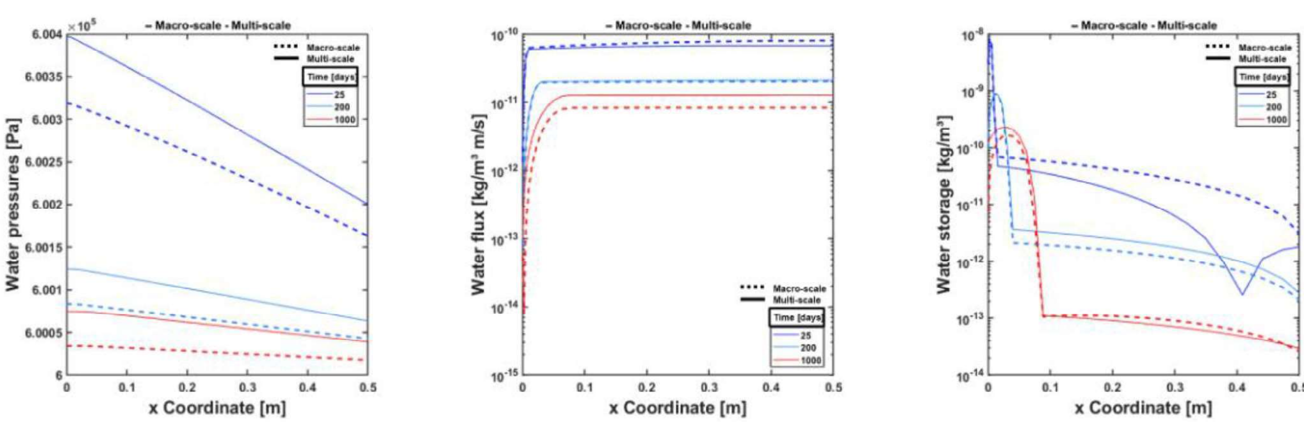

Model verification

Comparison with a macro-scale THM coupled model

Gas-related results

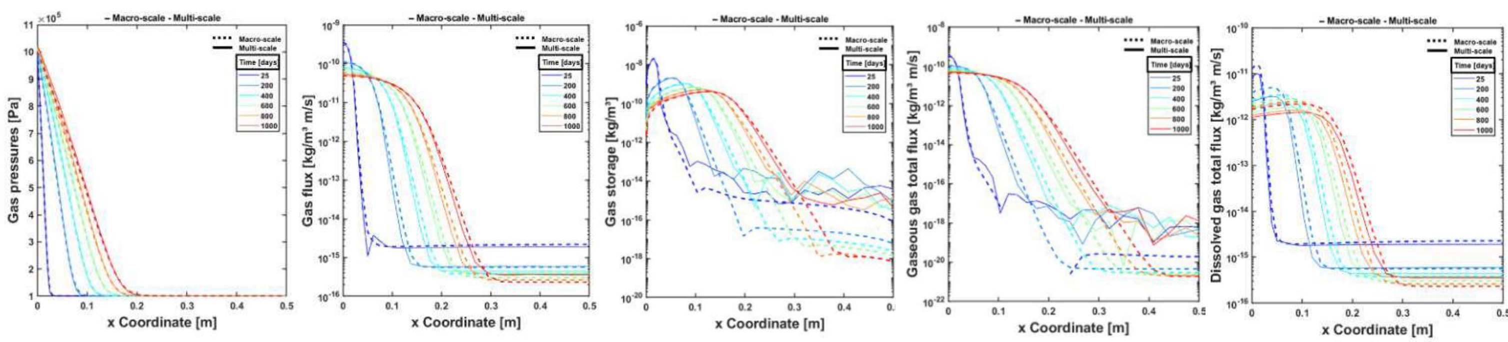

Content

❶ Context

❷ From experimental evidence to modelling

❸ Multi-scale modelling approach

❹ Preliminary modelling

❺ Modelling gas injection experiment

❻ Conclusions

Gas injection experiment

Characterisation of the microstructure parameters

► **1. Size of the REV** Bedding plane separation
$w = 300\ \mu m$

Experimental estimations of bedding plane separation, from *Gonzalez-Blanco (2017)*

FESEM	μ-CT
$150 - 270\ \mu m$	$410 - 560\ \mu m$

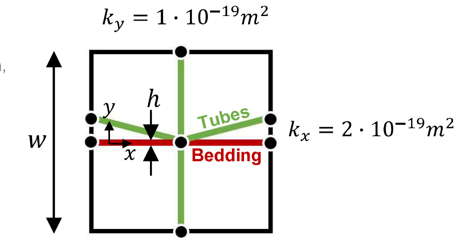

► **2. Macroporosity** Fitting of the pore size distribution

Effect of small-size pores
(Tortuosity = Calibration factor)

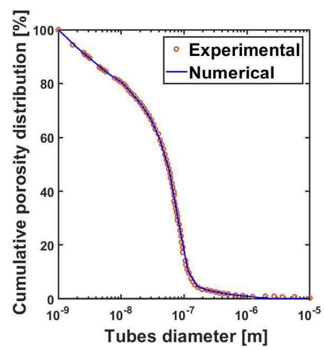

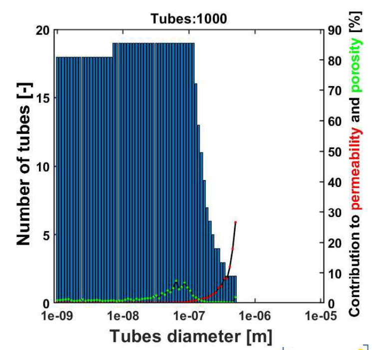

Gas injection experiment

Characterisation of the microstructure parameters

► **1. Size of the REV** Bedding plane separation
$w = 300\ \mu m$

Experimental estimations of bedding plane separation, from *Gonzalez-Blanco (2017)*

FESEM	μ-CT
$150 - 270\ \mu m$	$410 - 560\ \mu m$

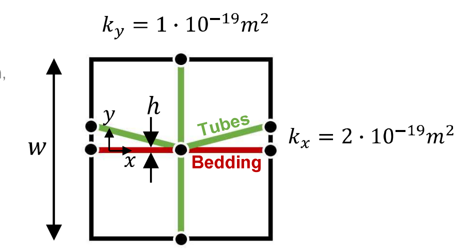

► **2. Macroporosity** Fitting of the pore size distribution

Effect of small-size pores
(Tortuosity = Calibration factor)

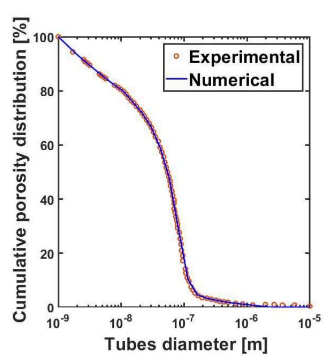

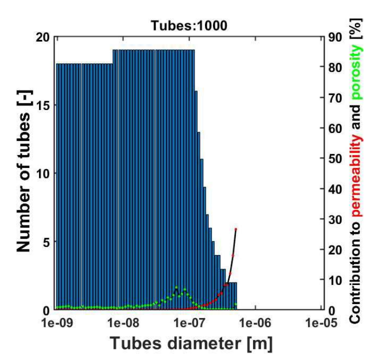

► **3. Intrinsic permeability** Effect of large-size pores

Fracture aperture

$k_{x,frac,0} = 10^{-19} m^2$

$\rightarrow h_0 = \sqrt[3]{12\, w\, k}$

Macropores

$$k_x = \frac{\pi}{8}\left(\frac{D}{2}\right)^4\left(\frac{1}{w^2}\right) + \overbrace{\frac{h^2(\cdot\, w)}{12}\left(\frac{h}{w}\right)}^{k_{x,frac}}$$

$$k_y = \frac{\pi}{8}\left(\frac{D}{2}\right)^4\left(\frac{1}{w^2}\right)$$

Gas injection experiment

Characterisation of the microstructure parameters

► **4. Relative permeability curves**

Yuster et al. (1951)

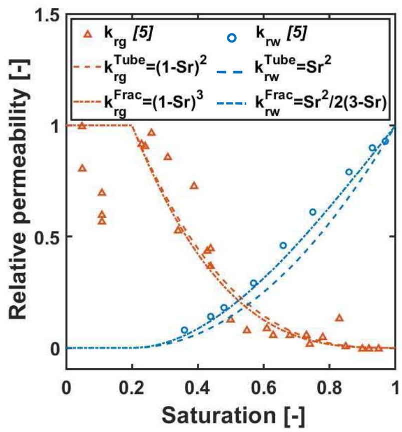

► **5. Retention curve**

Van Genuchten (1980)

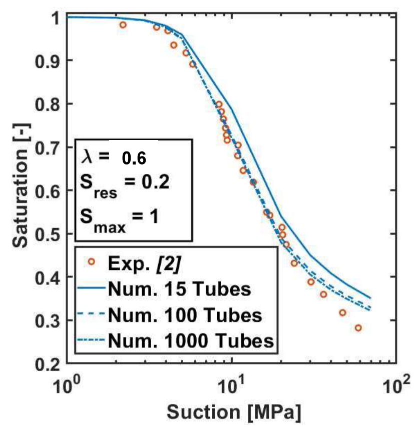

$$S_r = S_{res} + (S_{max} - S_{res})\left(1 + \left(\frac{s}{P_e}\right)^{\frac{1}{1-\lambda}}\right)^{-\lambda}$$

► **6. Normal stiffness of the fracture**

Goodman (1976)

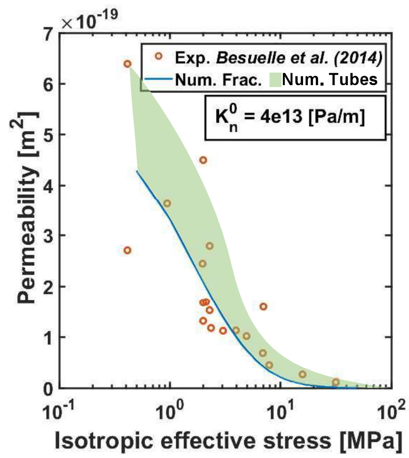

$$\Delta\sigma' = K_n \Delta h \quad \text{with} \quad K_n = \frac{K_n^0}{\left(1 + \frac{\Delta h}{h_0}\right)^2}$$

Gas injection experiment

Geometry and boundary conditions

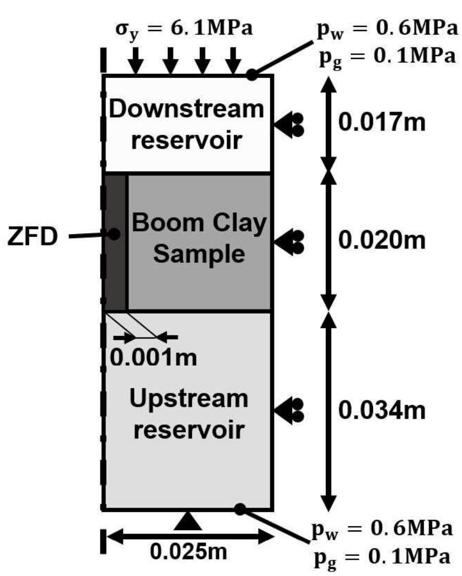

Parameters

Reservoirs

- Stiff elements: $E = 10000MPa$ $\nu = 0.3$
- Highly conductive: $n = 0.5$ $k = 10^{-10}m^2$
- Flat retention curve: $P_{entry} = 0.01MPa$

Boom Clay matrix

- Mechanical: $E = 200 - 400MPa$ $\nu = 0.33$
- Hydraulic:
  - Initial aperture: $0.80 - 1.27 \cdot 10^{-7}m$
  - Initial permeability: $2.0 - 4.0 \cdot 10^{-19}m^2$
  - Initial porosity: 0.363

Boom Clay Zone of Fracture Development (ZFD)

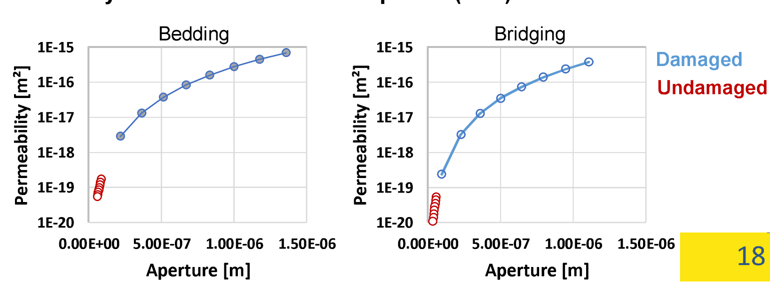

Gas injection experiment

Simulation stages

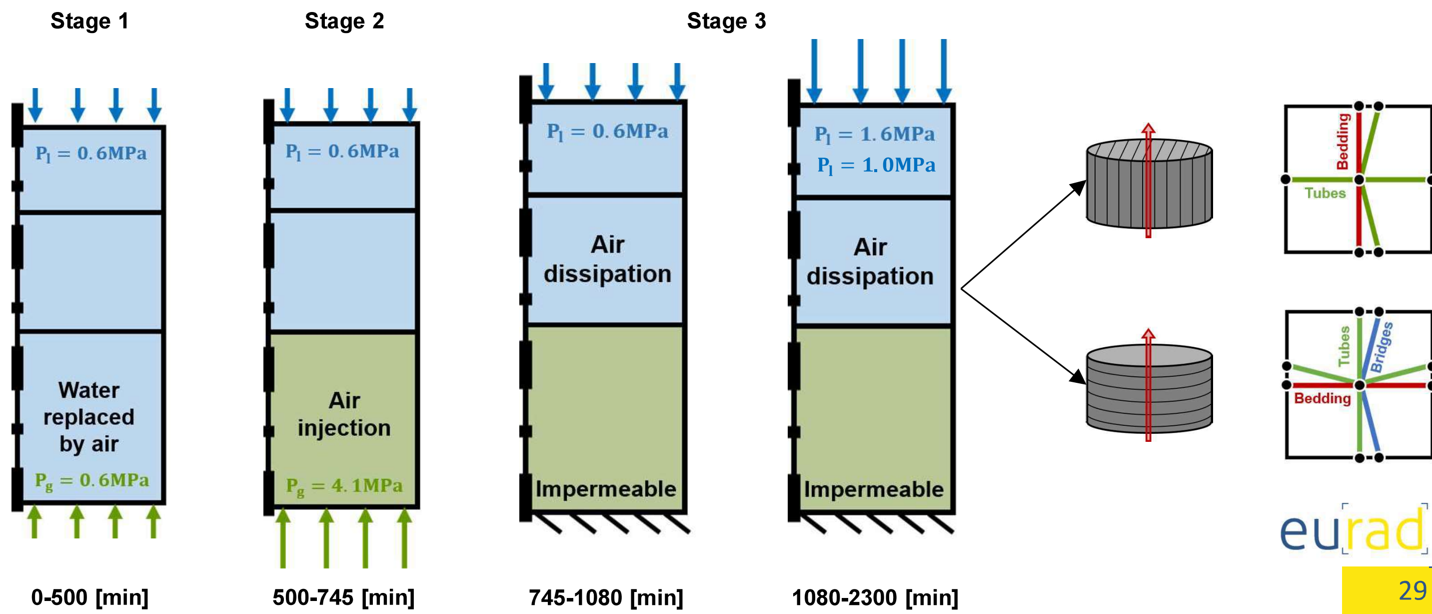

Gas injection experiment

Average axial strain

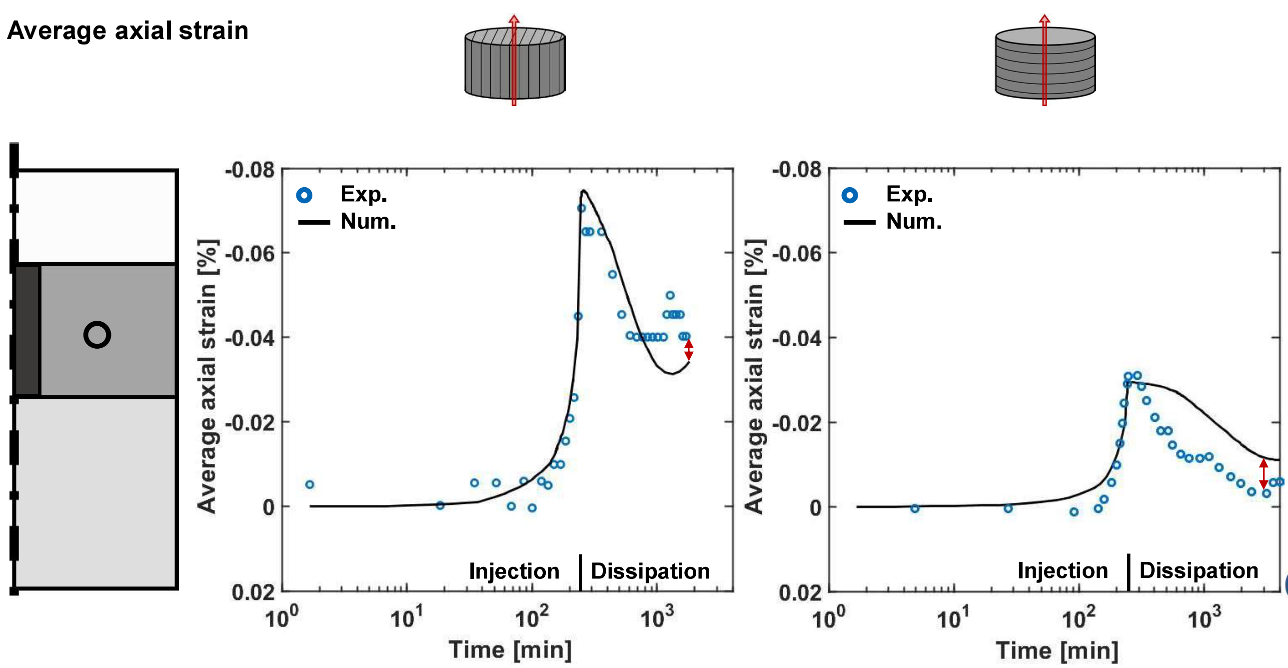

Gas injection experiment

Outflow volume

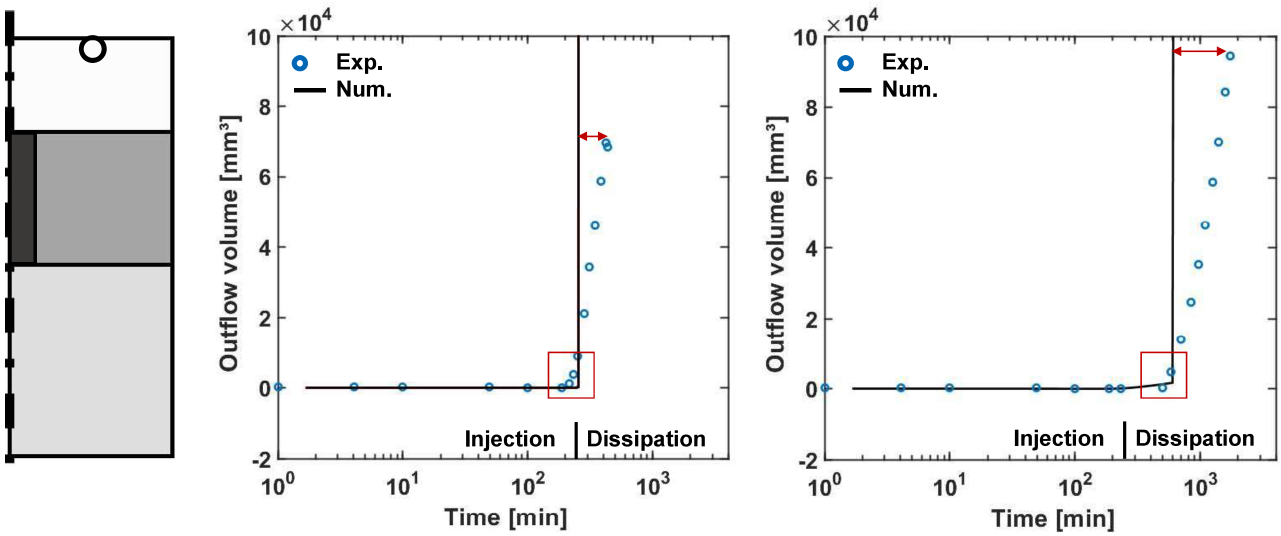

Gas injection experiment

Injection and recovery pressures

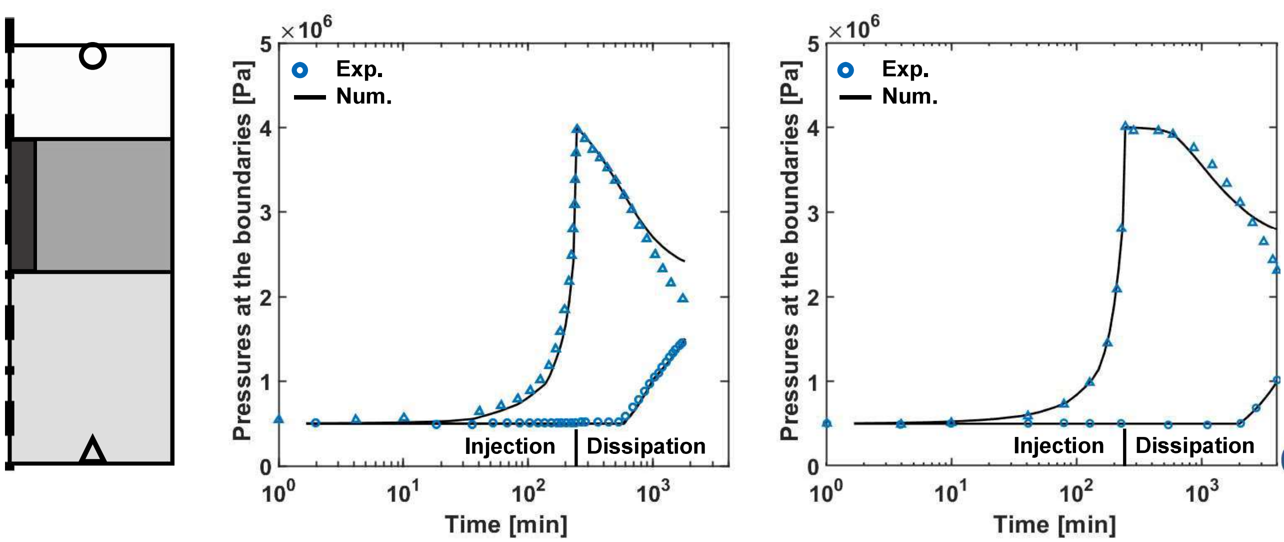

Gas injection experiment

Fracture aperture

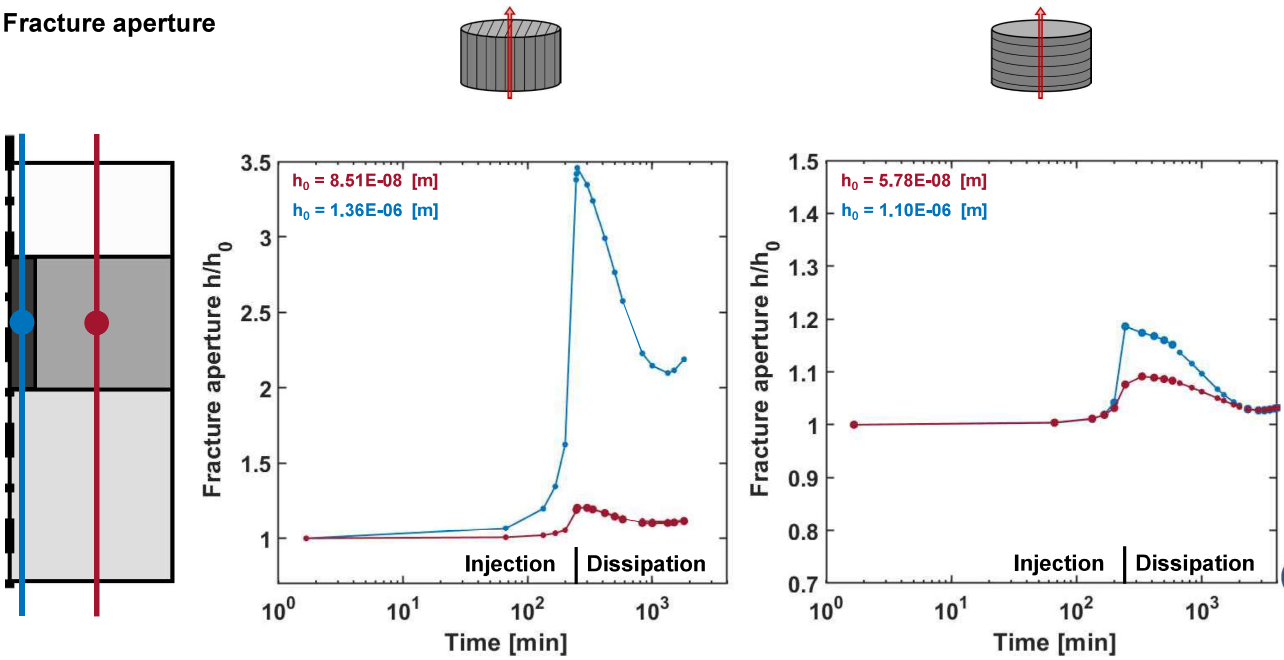

Gas injection experiment

Fracture aperture

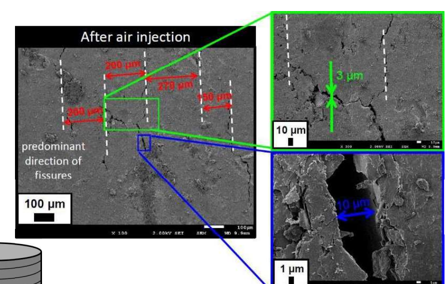

Experimental observations:
Opened fractures after injection

Gonzalez-Blanco & Romero (2022)

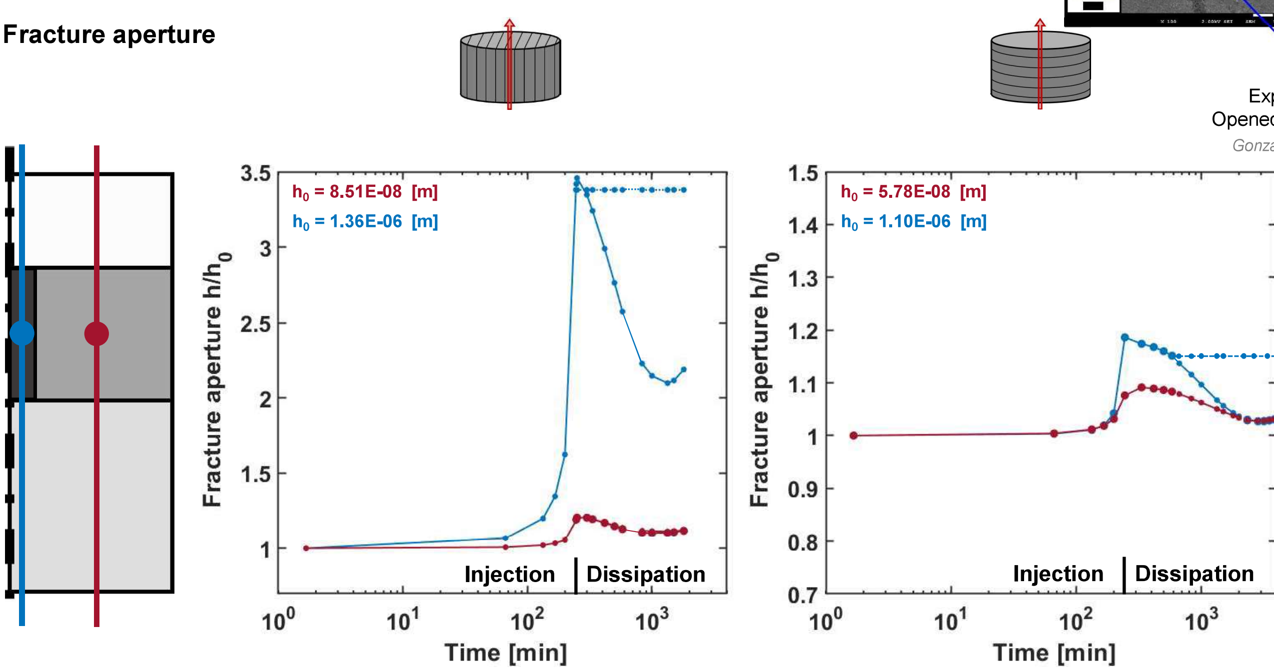

Gas injection experiment

Injection and recovery pressures

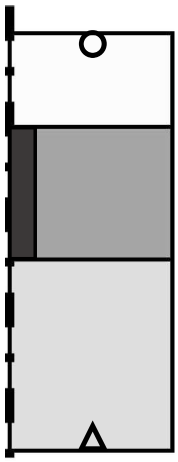

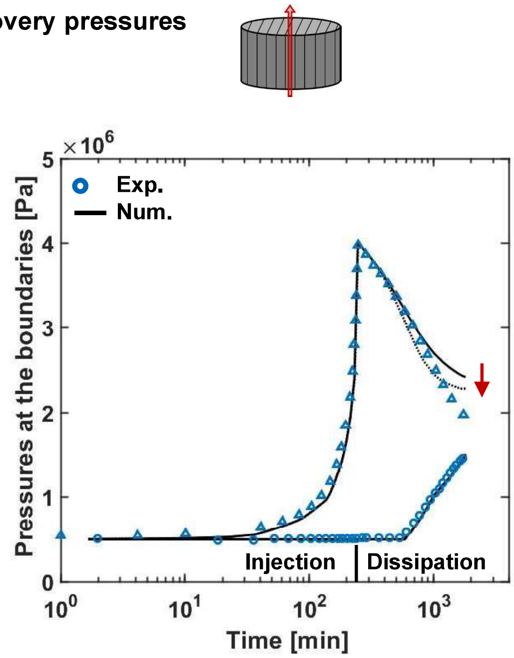

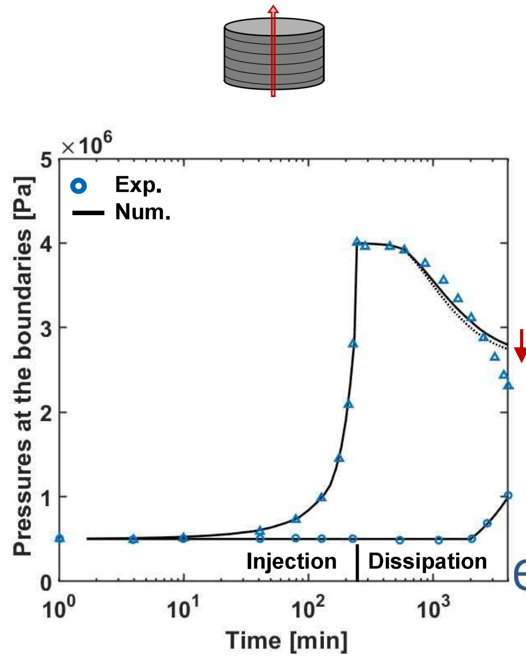

Gas injection experiment

Injection and recovery pressures

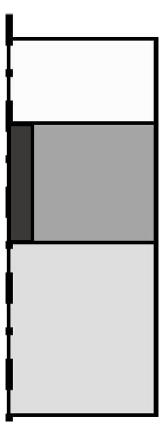

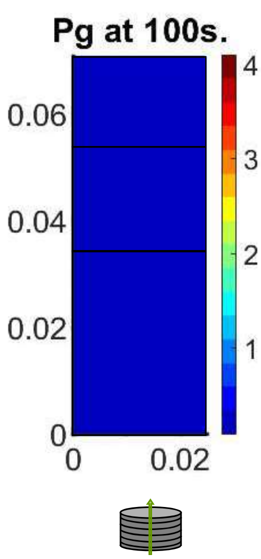

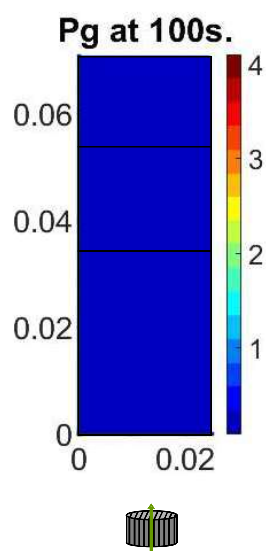

Gas injection experiment

Injection and recovery pressures

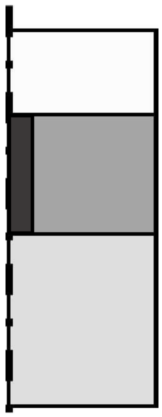

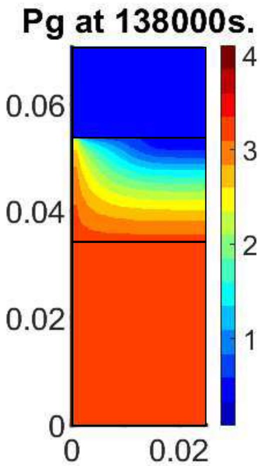

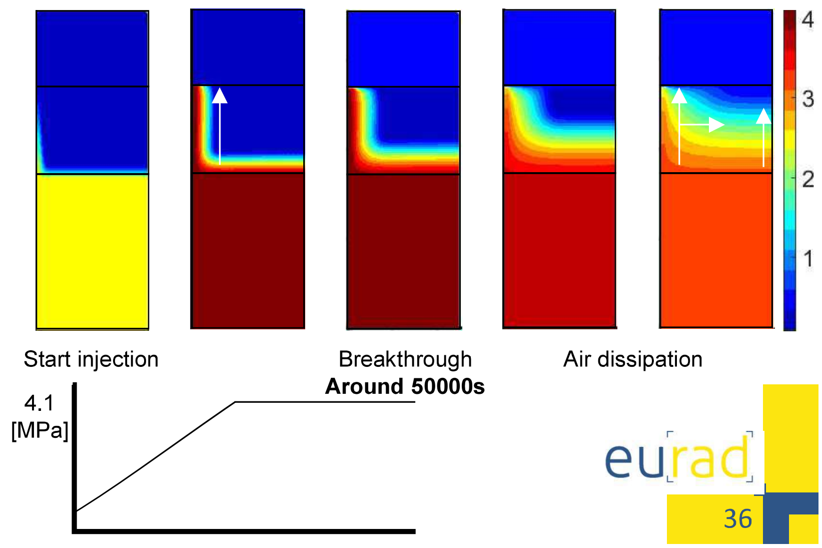

Gas injection experiment

Effect of the connectivity of the planes

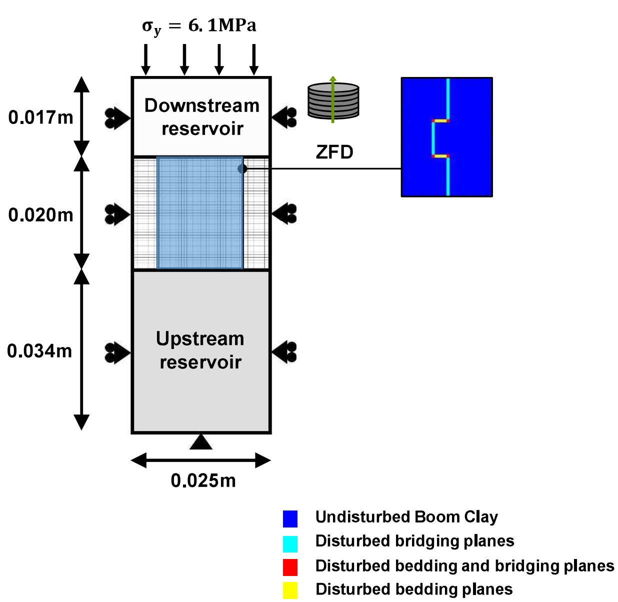

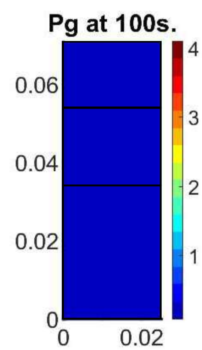

Gas injection experiment

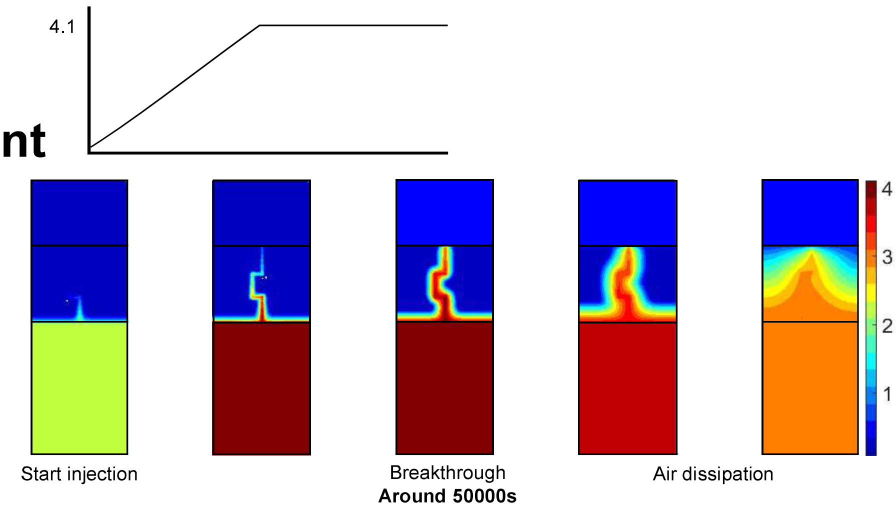

Effect of the <u>connectivity</u> of the planes

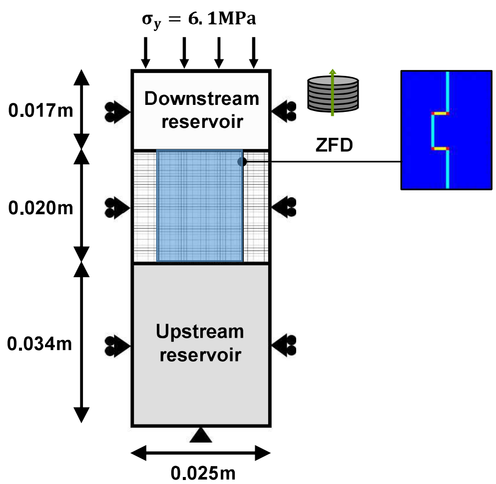

- Undisturbed Boom Clay
- Disturbed bridging planes
- Disturbed bedding and bridging planes
- Disturbed bedding planes

Gas injection experiment

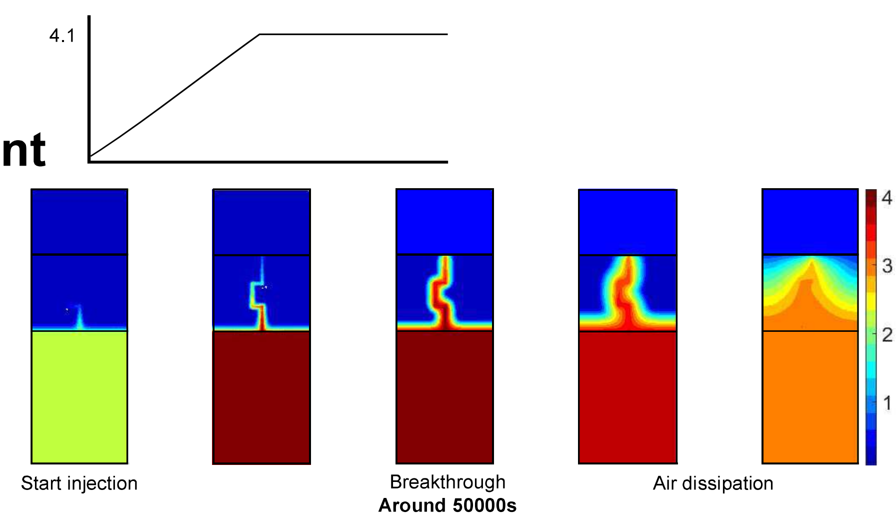

Effect of the <u>connectivity</u> of the planes

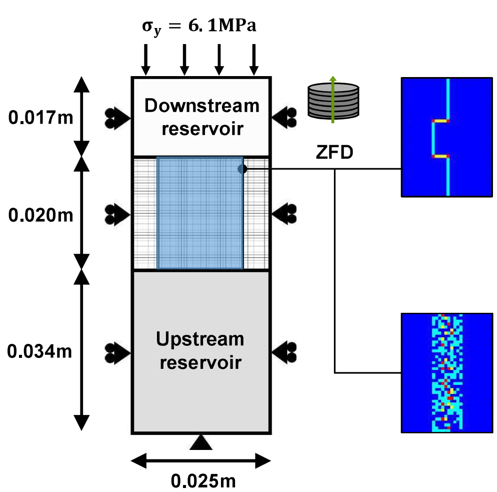

- Undisturbed Boom Clay
- Disturbed bridging planes
- Disturbed bedding and bridging planes
- Disturbed bedding planes

Gas injection experiment

Effect of the connectivity of the planes

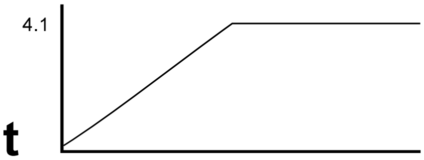

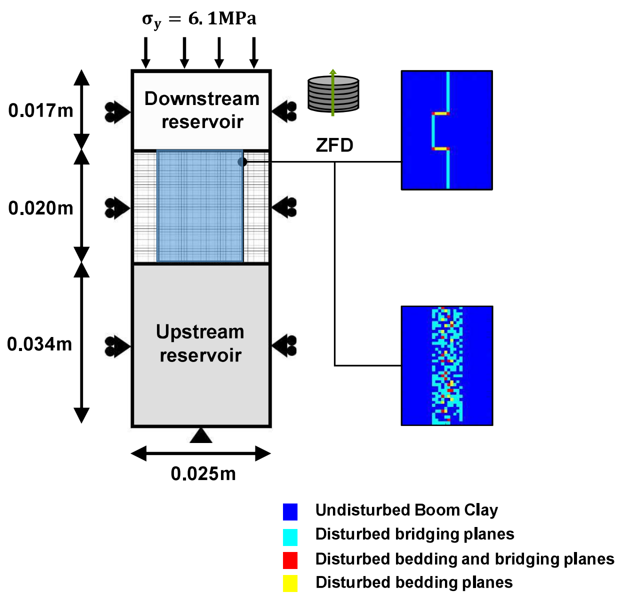

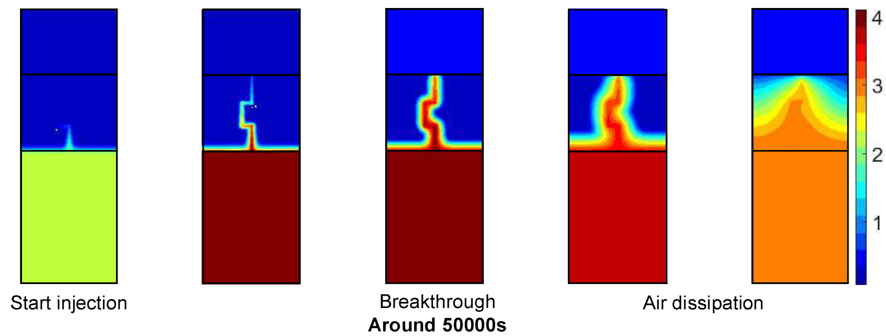

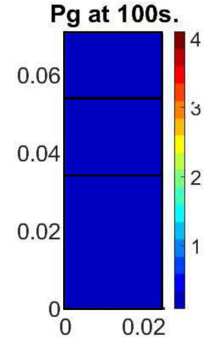

Gas injection experiment

Effect of the connectivity of the planes

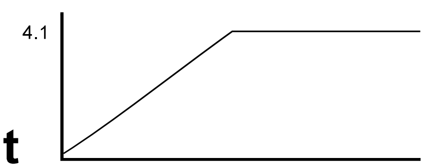

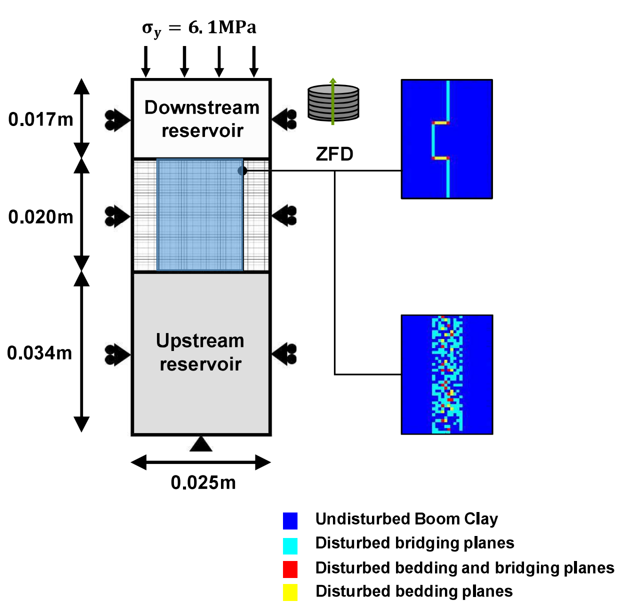

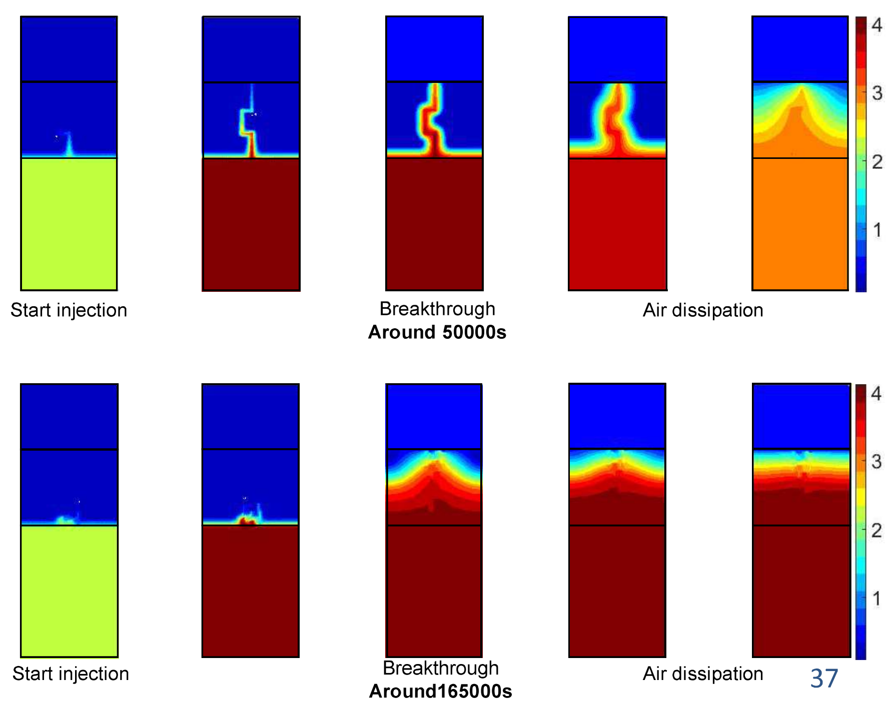

Gas injection experiment

Effect of the connectivity of the planes under up-scaling

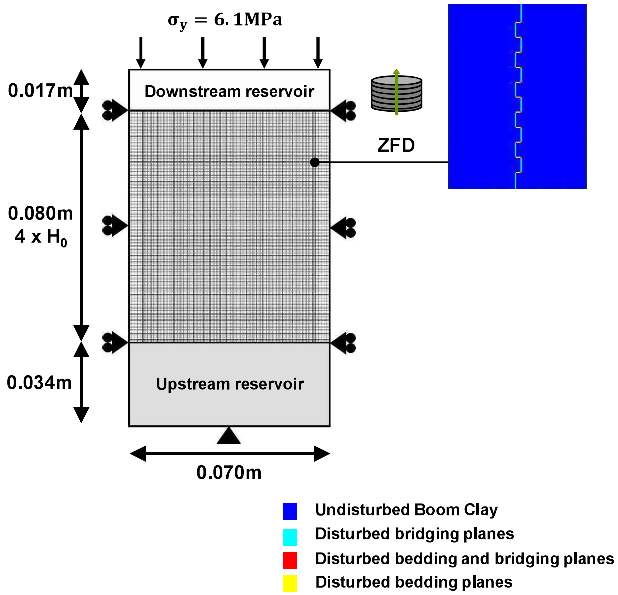

Gas injection experiment

Effect of the connectivity of the planes under up-scaling

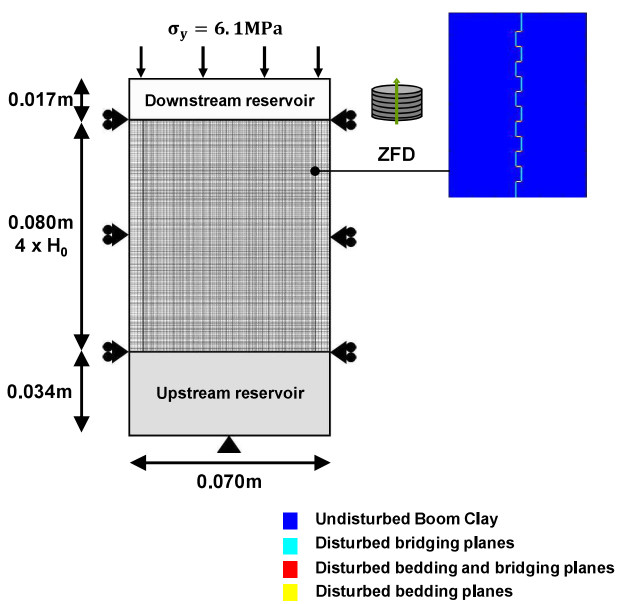

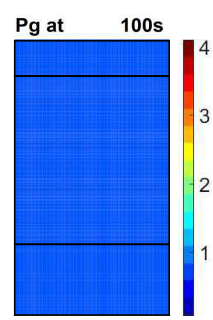

Gas injection experiment

Effect of the connectivity of the planes under up-scaling

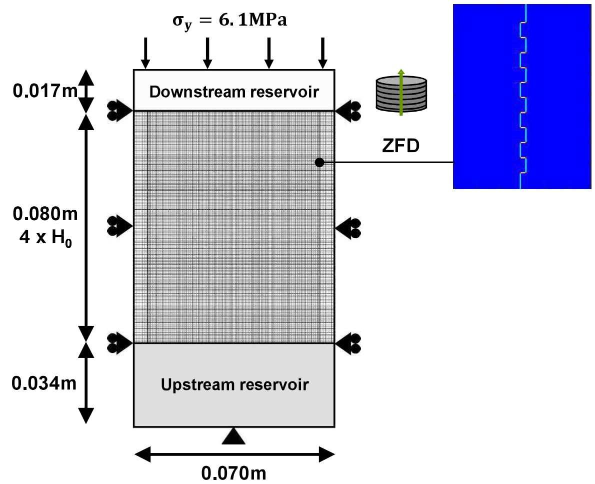

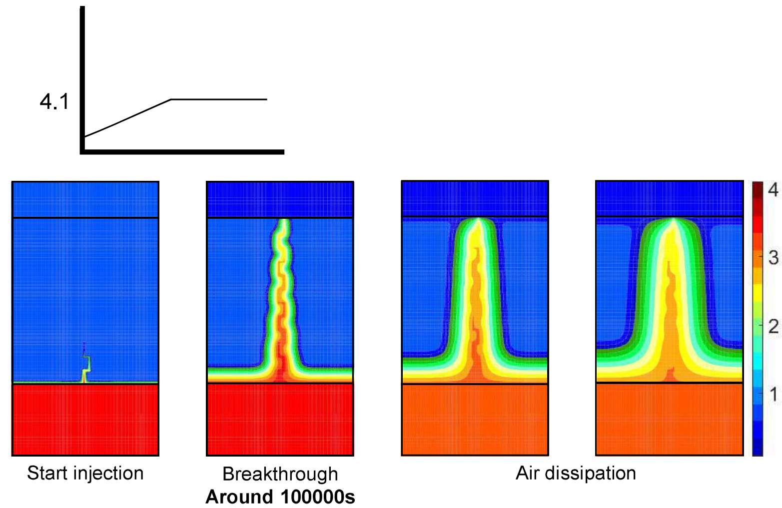

- Undisturbed Boom Clay
- Disturbed bridging planes
- Disturbed bedding and bridging planes
- Disturbed bedding planes

Gas injection experiment

Effect of the connectivity of the planes under up-scaling

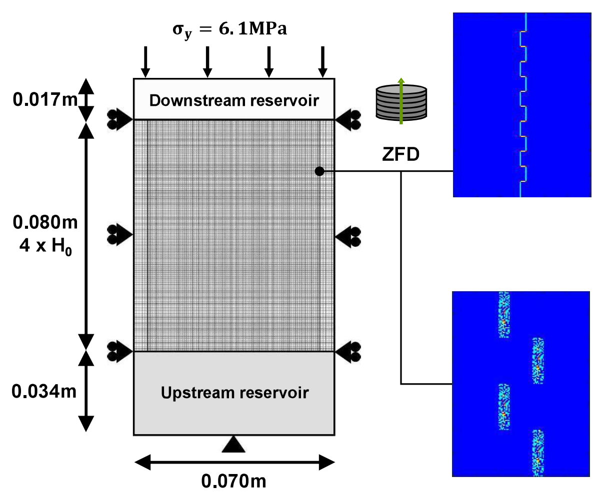

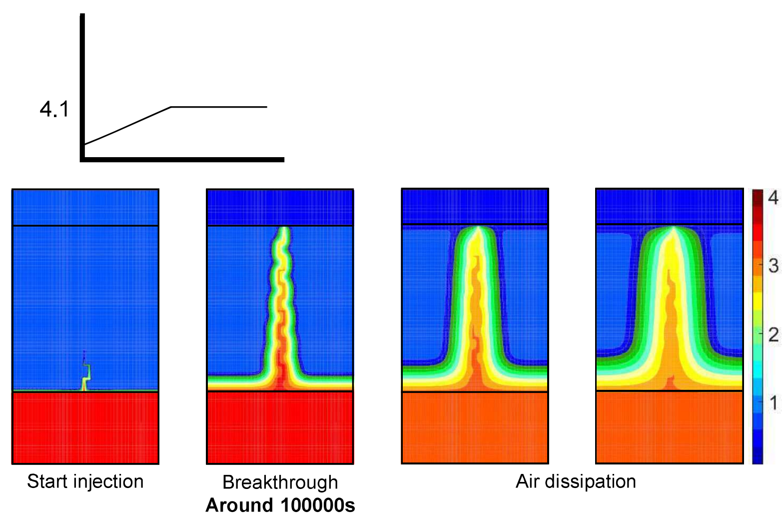

- Undisturbed Boom Clay
- Disturbed bridging planes
- Disturbed bedding and bridging planes
- Disturbed bedding planes

Gas injection experiment

Effect of the connectivity of the planes under up-scaling

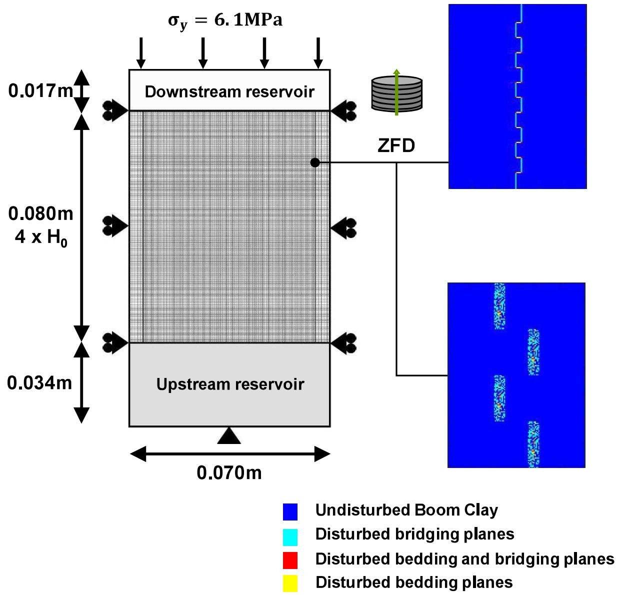

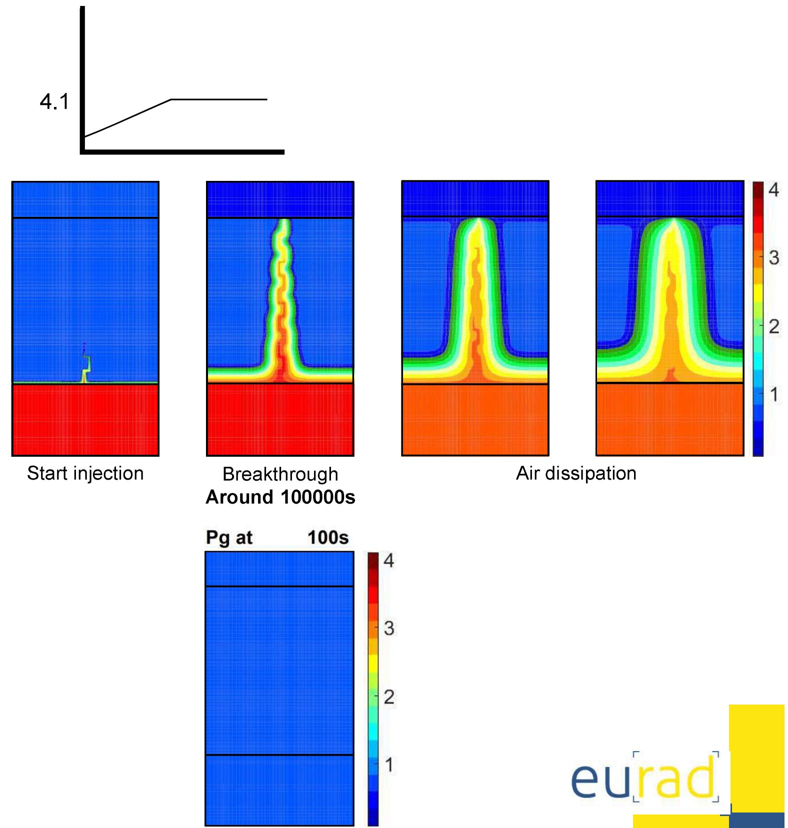

Gas injection experiment

Effect of the connectivity of the planes under up-scaling

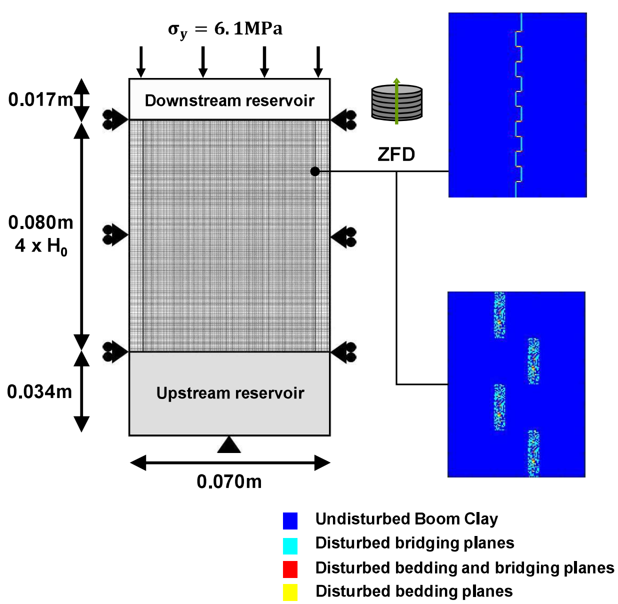

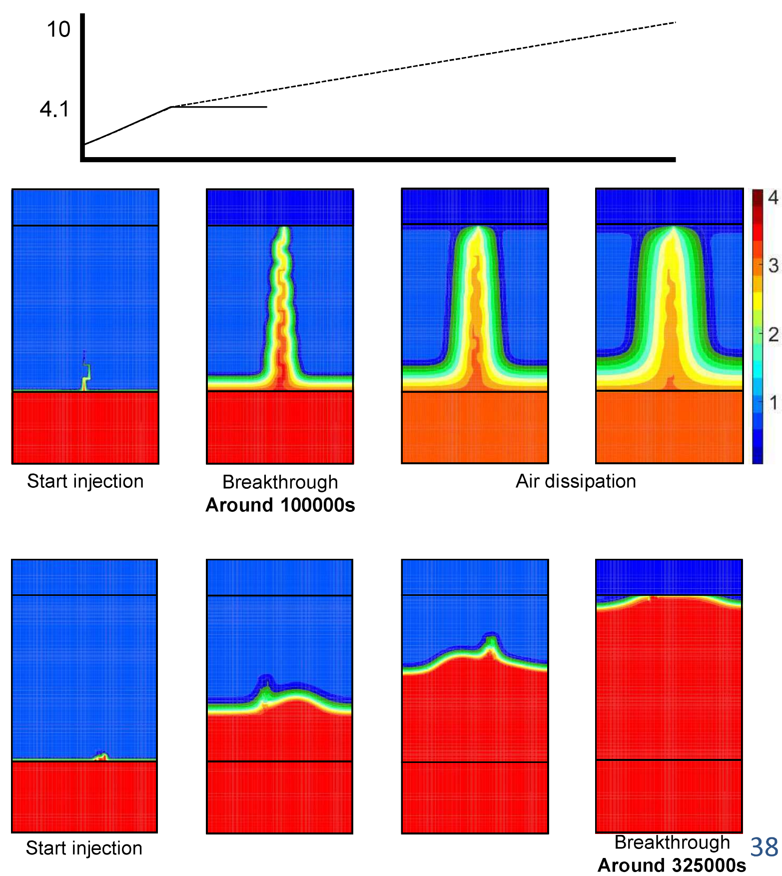

Content

Conclusions

We **developed** a multi-scale model able to

1. Simply idealise the microstructure of the rock with fractures and tubes
2. Reproduce mechanisms inherent to gas migrations in sound rock layers

We **showed** that

1. Macro-pores, bedding planes and bridging planes play different roles in gas flows
2. Preferential flow paths can be generated through fractures with weaker properties
3. Different gas mechanisms occur in the presence of weaker bridging planes

Advanced multiphysics of geomaterials: multiscale approaches and heterogeneities

ALERT OZ / EURAD GAS & HITEC Summer School
28 August – 01 September 2023 • Liège (Belgium)

Pierre BÉSUELLE, Frédéric COLLIN,
Anne-Catherine DIEUDONNÉ, Sebastia OLIVELLA

The project leading to this application has received funding from the European Union's Horizon 2020 research and innovation programme under grant agreement n° 847593.

Appendix N. In situ THM testing at high temperature: Poorly indurated clays (Boom clay) (A. Dizier)

IN SITU THM TESTING AT HIGH TEMPERATURE

Poorly indurated clays (Boom Clay)

August 31, 2023 • Arnaud Dizier, Jan Verstricht, Temenuga Georgieva, Mieke De Craen, S. Levasseur (O/N) and ESV EURIDICE GIE Technical Team

The project leading to this application has received funding from the European Union's Horizon 2020 research and innovation programme under grant agreement n° 847593.

ESV EURIDICE GIE

European Underground Research Infrastructure for Disposal of radioactive waste in Clay Environment

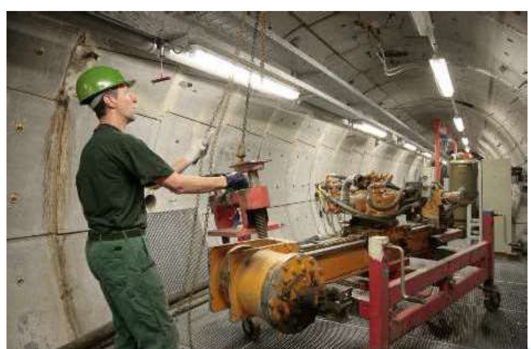

ESV EURIDICE GIE

sck cen

ONDRAF/NIRAS

ESV EURIDICE GIE

GEOLOGOCAL DISPOSAL OF RADIOACTIVE WASTE IN BELGIUM

- Disposal in galleries located in low permeable geological layers (poorly indurated clays)
- Engineering Barrier System (EBS) for high level and long-lived radioactive wastes (Belgian concept)

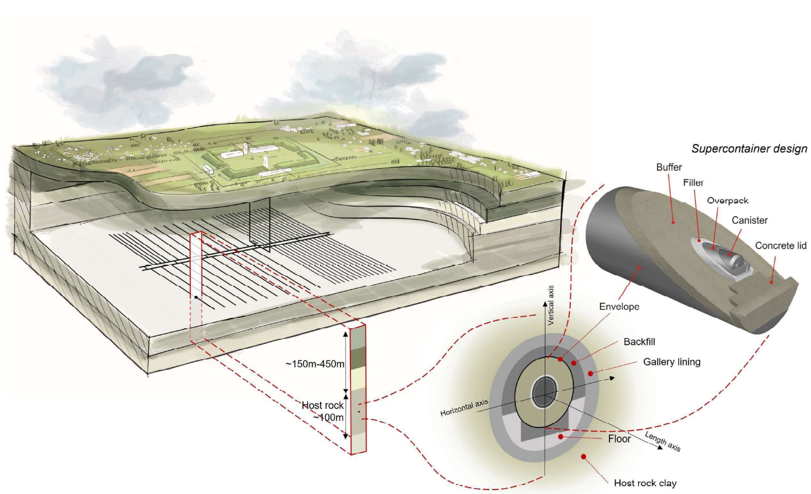

Vertical cross-section of the disposal gallery for C-waste

HADES URL IN POORLY INDURATED BOOM CLAY

- Thickness of ~ 100 m, depth 185 – 287 m
- HADES URL: depth 225 m

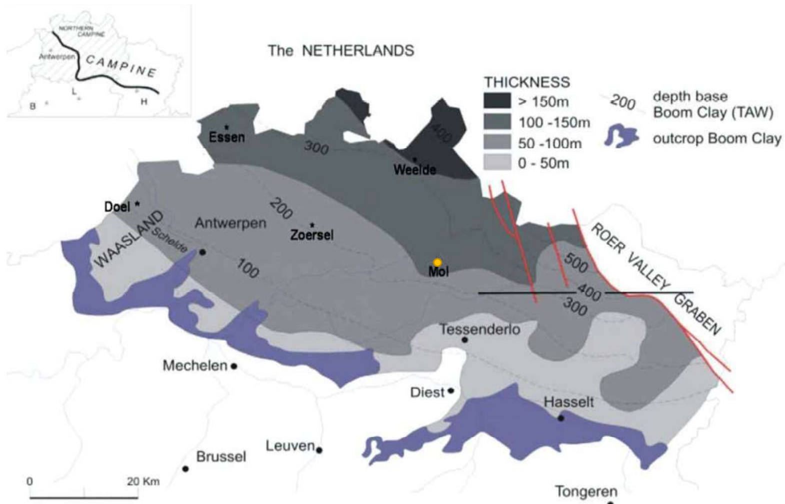

HADES – Underground Research Laboratory

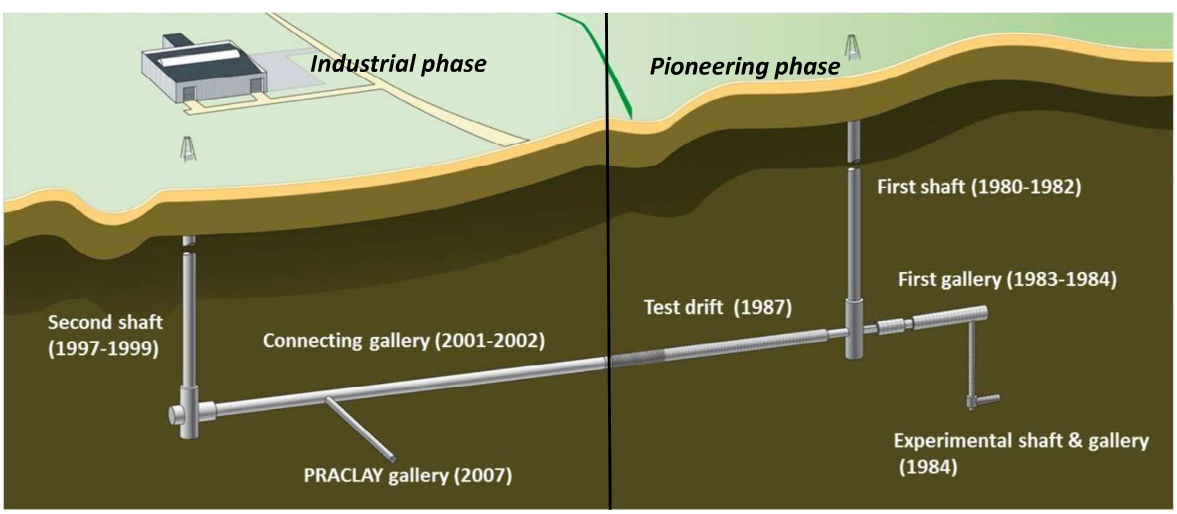

HADES – Underground Research Laboratory

Industrial phase (after 2000)

Pioneering phase (1980 – 1990)

BOOM CLAY: POTENTIAL HOST CLAY FORMATION ?

- Geology: low seismic activities, no volcanic activities, limited tectonic activities
- Plastic clay, self-sealing
- Good hydrogeological conditions
- Good geochemical conditions

➔ limit and delay the migration of radionuclides

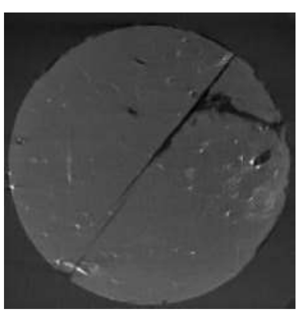

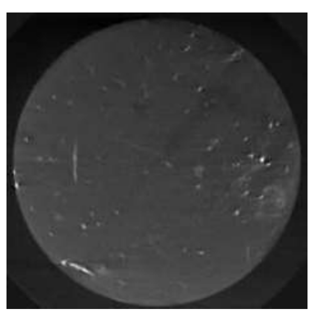

BOOM CLAY: PHYSICAL CHARACTERISATION

- Geotechnical properties:
  - Porosity : 0.39
  - Soil density : 1900 - 2100 [kg/m³]
  - Plastic limit : 13 – 26.5 %
  - Liquid limit : 55 - 80 %
  - Water content : 20 – 30 wt% (dry weight)
- Hydraulical characteristics:
  - Hydraulic conductivity $K = 2 - 4.10^{-12}$ m/s
- Thermal characteristics:
  - Thermal conductivity $\lambda = \pm 1.35$ W.m^{-1}.K^{-1}

eurad

BOOM CLAY: PHYSICAL CHARACTERISATION

- Geotechnical characteristics (Bernier et al., 2007)
  - Poisson's coefficient ν' : 0.125
  - Young Modulus E': 300 MPa
  - Cohesion c': 300 kPa
  - Friction angle ϕ': 18°
  - Dilatancy angle ψ': 0° - 10°

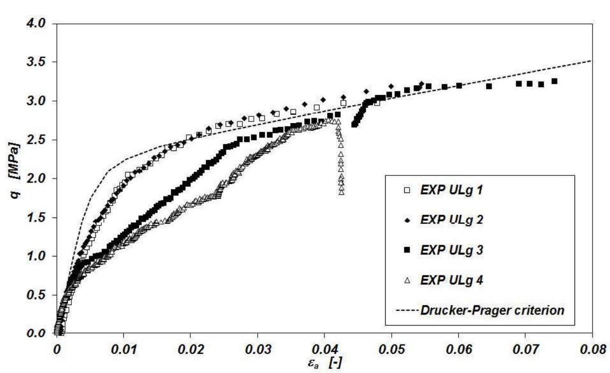

eurad

LONG HISTORY OF IN SITU TEMPERATURE TESTING

- First test aiming at simulating a vitrified high level waste canister in a clay quarry in Terhagen before 1980
- In the URL:
  - BACCHUS I, II (1988 - 1995)
  - CERBERUS (1985 - 1999)
  - CACTUS I, II (1990 - 1994)
  - ATLAS I, II, III, IV (1992 -…)
  - PRACLAY (2014-...)

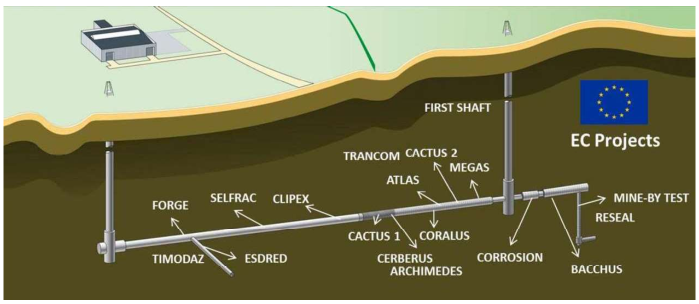

THM EXPERIMENTS IN HADES – ATLAS (1992 - ...)

- Small scale heater tests ATLAS I-II, III & IV (*Admissible Thermal Loading for Argillaceous Storage*)
  - Assess/ confirm the thermal properties of Boom Clay
  - T→HM coupling in Boom Clay

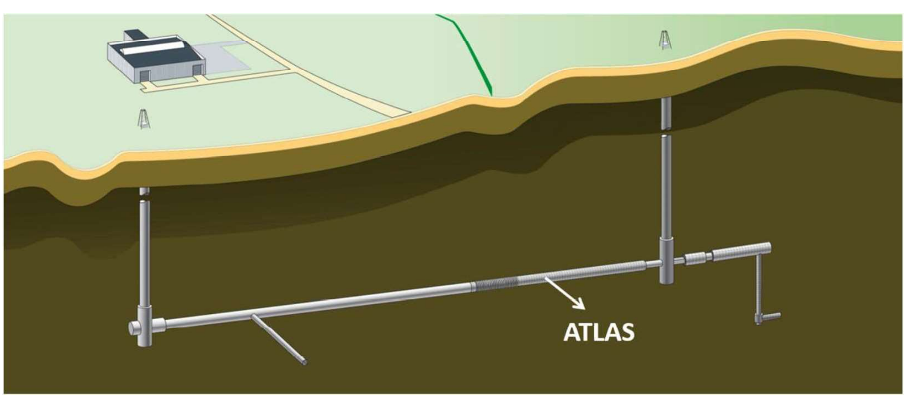

THM EXPERIMENTS IN HADES – ATLAS (1992 - …)

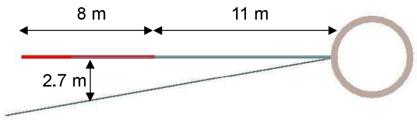

Test drift
Heater
Observation boreholes

Illustration ATLAS III experiment

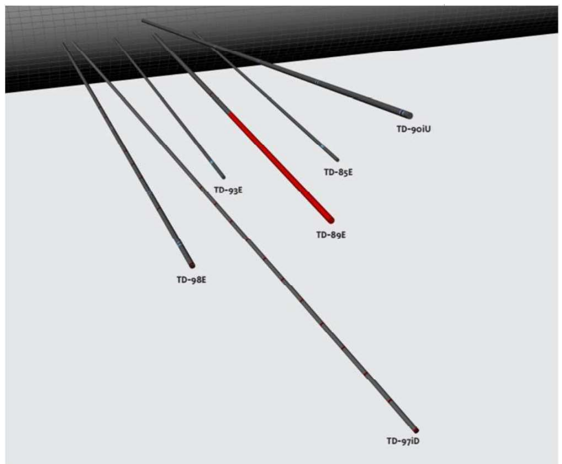

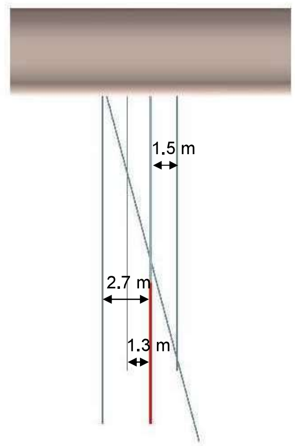

THM EXPERIMENTS IN HADES – ATLAS (1992 - …)

- ATLAS instrumentation :
  - Kulite pressure sensors on the heating probe
  - Piezometer filter
  - Flat-jacks and biaxial stressmeter

Central borehole with the heating probe

Illustration of a piezometer filter with twin tube connection

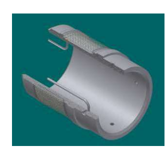

Illustration of an instrumented casing

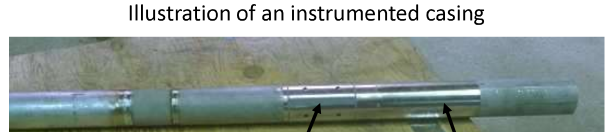

Flat-jacks

Biaxial Stressmeter

THM EXPERIMENTS IN HADES – ATLAS III (2007)

- ATLAS III: Temperature and pore water pressure evolution (exp. + num. results)
  - Anisotropic thermo-hydro-poro-elastic model: transverse isotropic elasticity
  - Heat transport (conduction)
  - Transverse anisotropy of intrinsic permeability $K_h \approx 2 \times K_v$

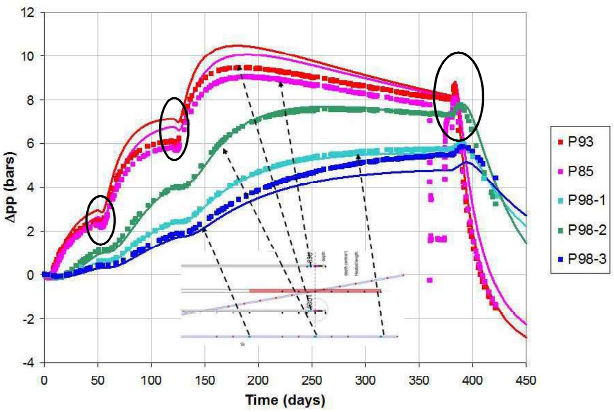

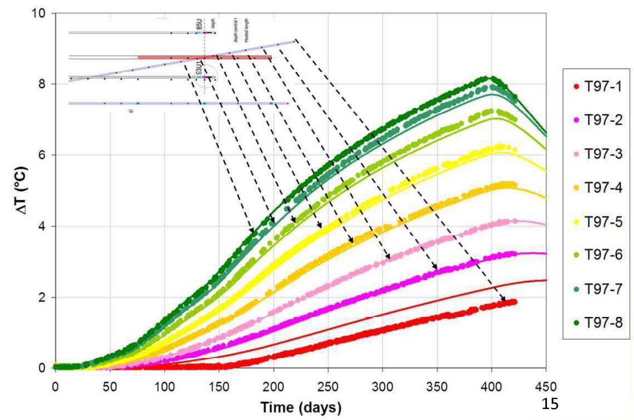

THE LARGE-SCALE PRACLAY HEATER TEST

- Demonstrating the feasibility of geological disposal of high-level radioactive waste in clay formation

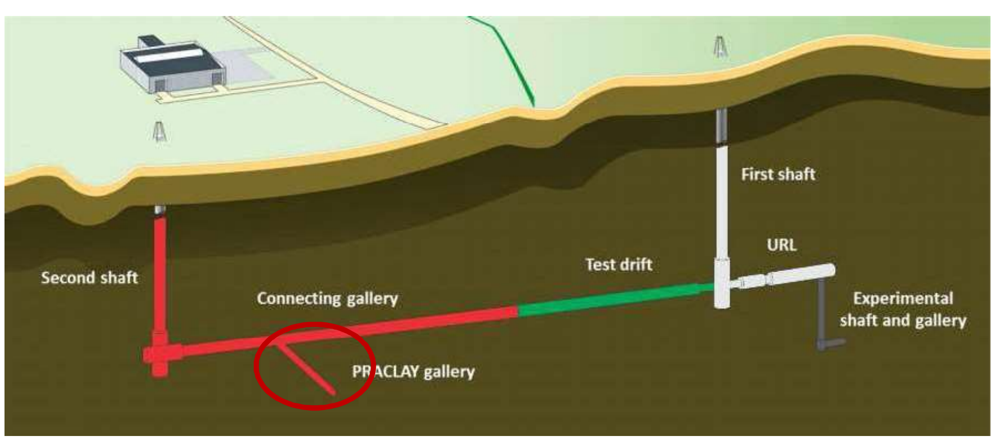

eurad

THE PRACLAY EXPERIMENT – OBJECTIVES AND DESIGN

- Feasibility of construction gallery and crossing
- Seal test ➔ Design and installation of the hydraulic seal
- Large scale-heater test ➔ Simulate the heat-emitting high-level radioactive waste

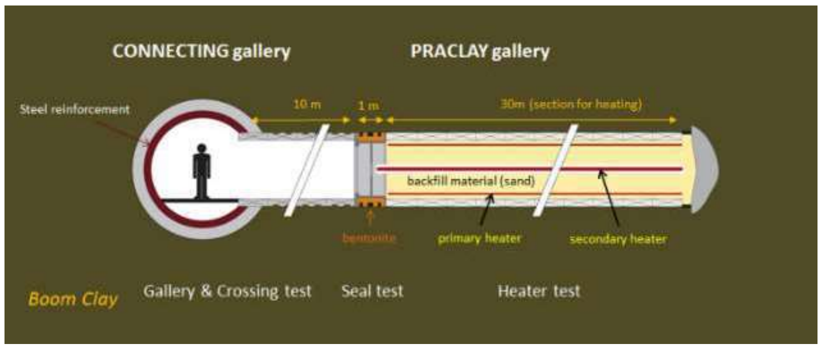

THE PRACLAY EXPERIMENT - PHASES

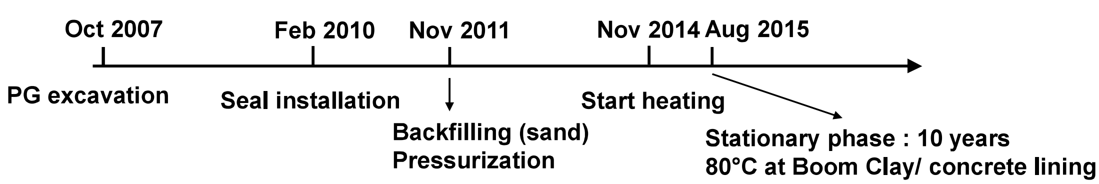

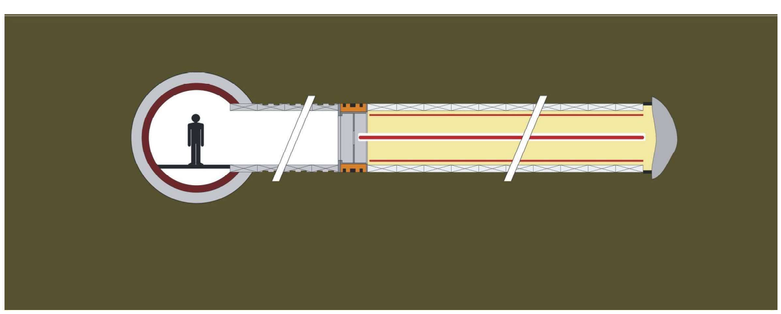

PRACLAY GALLERY EXCAVATION (2007)

- Designed for geotechnical and thermal loads
- Segmental tunnel lining
- Compressive materials

PRACLAY GALLERY EXCAVATION (2007)

- Installation of foam panels

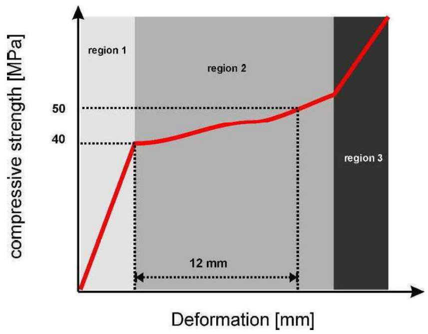

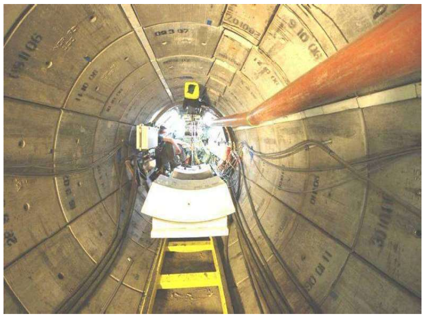

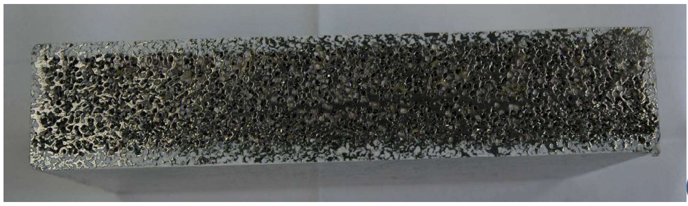

PRACLAY GALLERY EXCAVATION (2007)

- Open-face tunnel boring machine with a roadheader
- Segment erector for the placement of the segment blocks

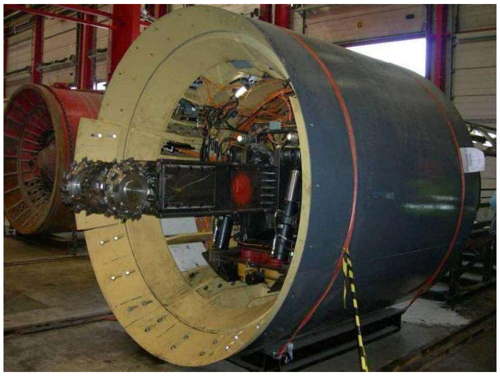

PRACLAY GALLERY EXCAVATION (2007)

- Crossing with the installation of a steel reinforcement ring

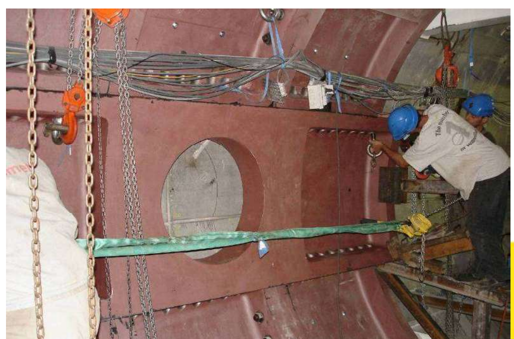

PRACLAY GALLERY EXCAVATION (2007)

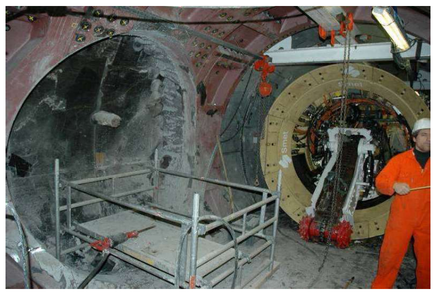

PRACLAY GALLERY EXCAVATION (2007)

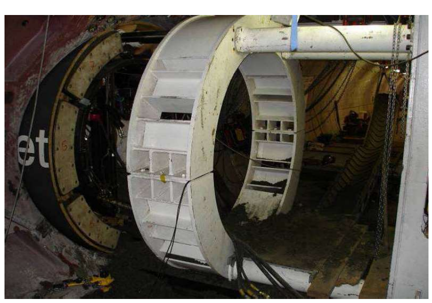

PRACLAY GALLERY EXCAVATION (2007)

PRACLAY GALLERY EXCAVATION (2007)

Excavation induced fractures: gallery side-wall

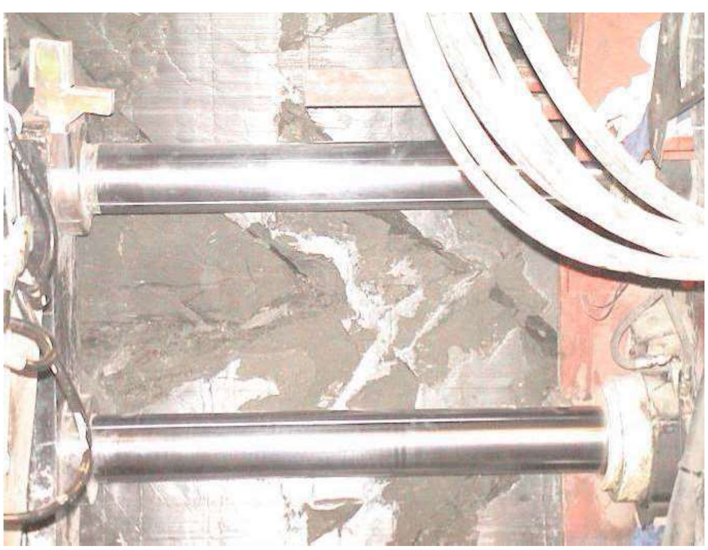

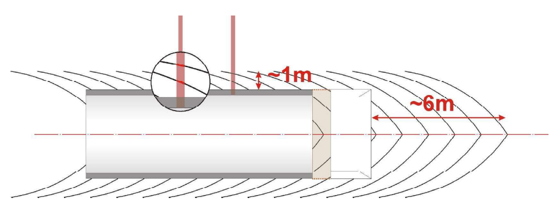

Observations during the excavation of the Connecting gallery

PRACLAY GALLERY EXCAVATION (2007)

- Installation of a temporary lining for the hydraulic seal

PRACLAY GALLERY – HYDRAULIC SEAL INSTALLATION

PRACLAY GALLERY – HEATER SYSTEM, BACKFILLING

THE PRACLAY EXPERIMENT – OBJECTIVES

- Boom Clay retains its ability to contain radioactive waste when heated?
- Study combined disturbances :
  - hydro-mechanical caused by gallery construction
  - large-scale thermal load on the Boom Clay due to heat-emitting high-level waste

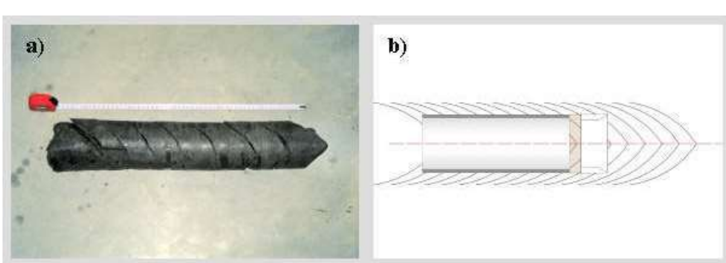

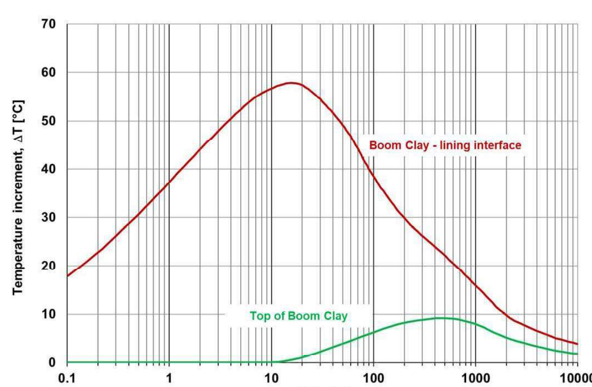

THE PRACLAY EXPERIMENT – DESIGN – THERMAL CONDITIONS

- Temperature at gallery extrados = 80°C
- Faster temperature increase

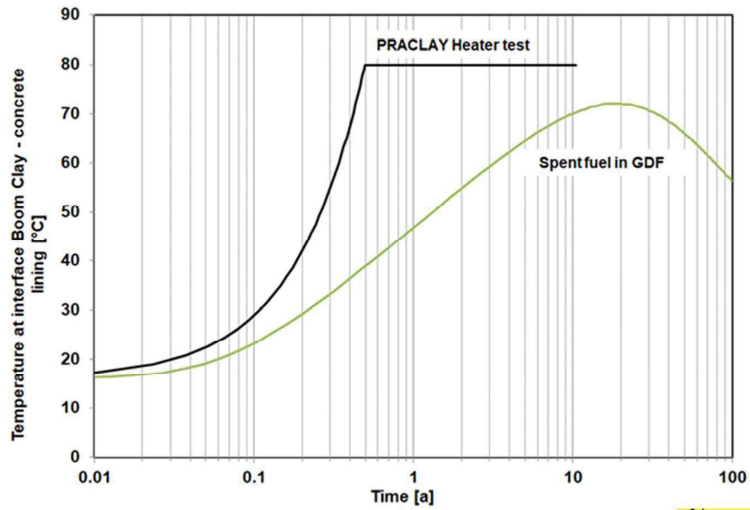

THE PRACLAY EXPERIMENT – DESIGN – HYDRAULIC CONDITIONS

- More penalizing conditions ➔ as much undrained as possible

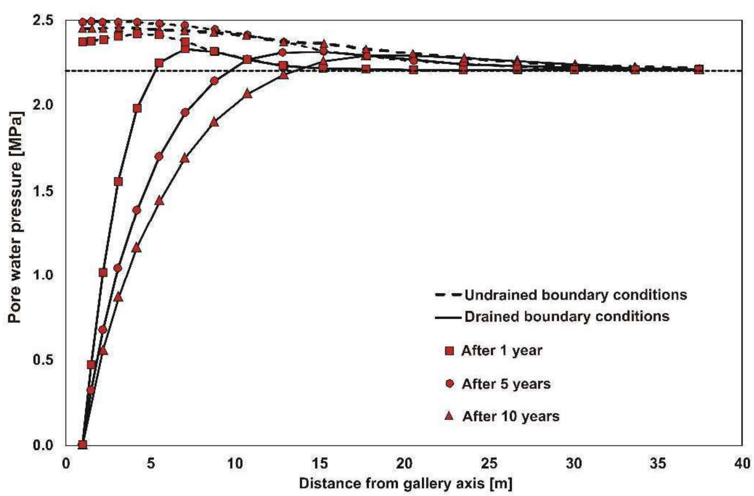

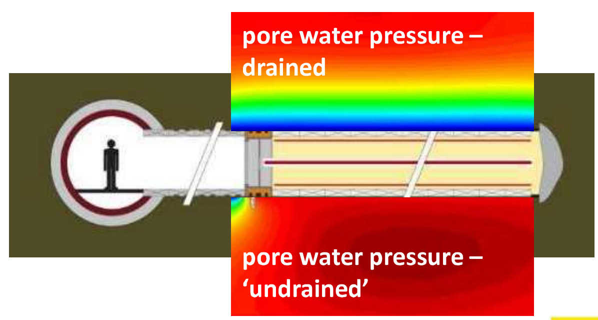

THE PRACLAY EXPERIMENT - MONITORING

- Number of sensors (1100): temperature, pore water pressure, stresses, displacements

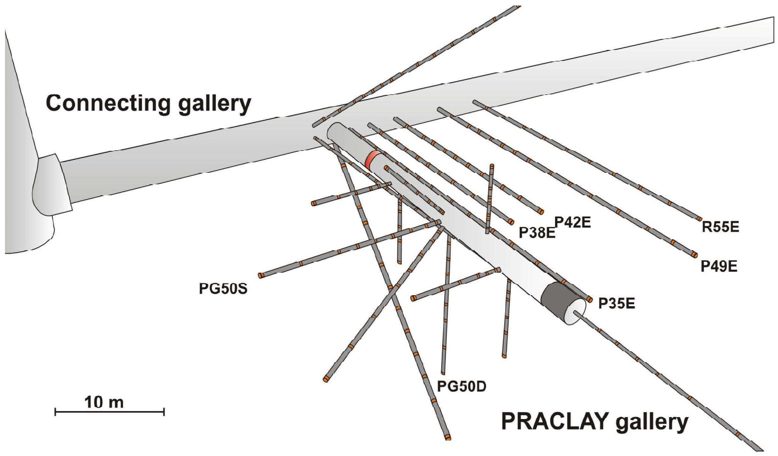

THE PRACLAY EXPERIMENT – THERMAL LOADING PLAN

- 3 heating steps to reach 80°C at Boom Clay/ concrete lining interface (250 W/m representative from geological disposal facility)

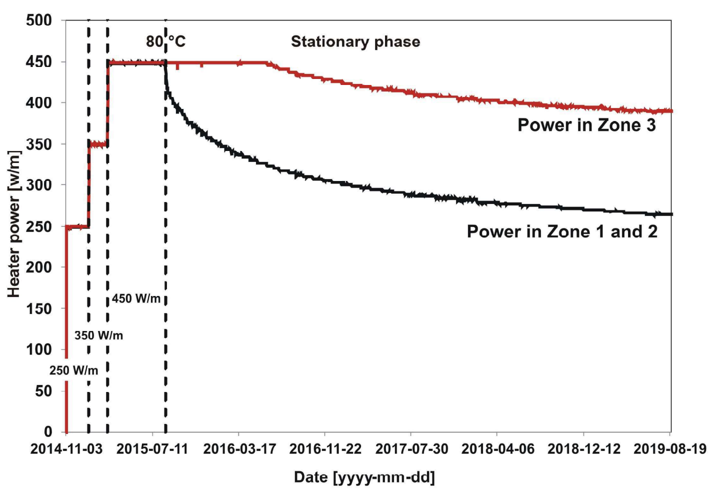

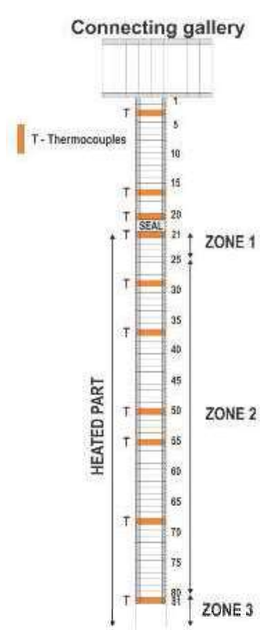

THE PRACLAY EXPERIMENT - THERMAL LOADING PLAN

- Increase of the temperature in the concrete lining
- Current situation: 80°C at Boom Clay/ lining interface

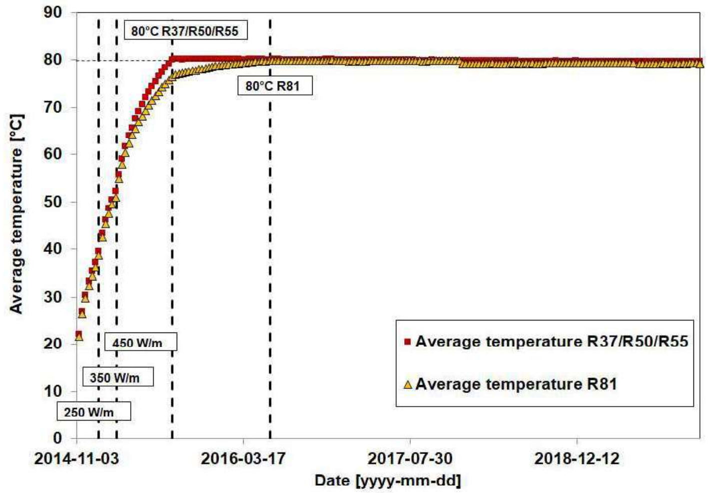

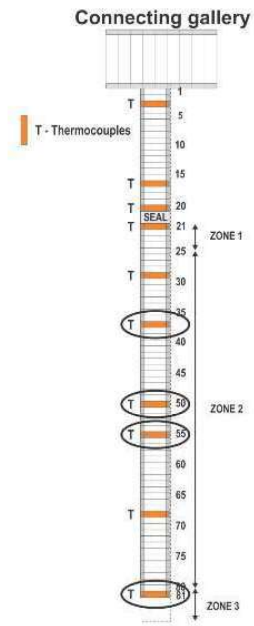

THE PRACLAY EXPERIMENT – PORE PRESSURE INSIDE THE GALLERY

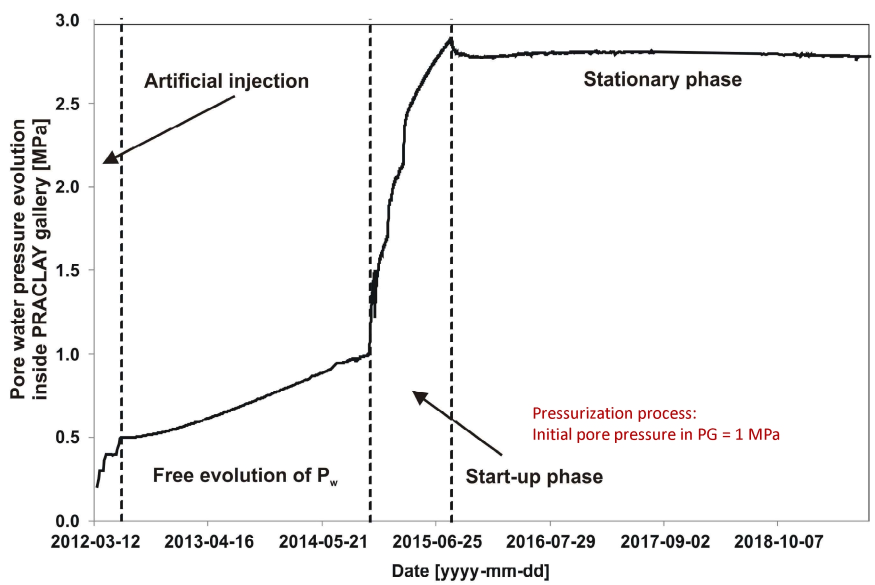

THE PRACLAY EXPERIMENT – TEMPERATURE OBSERVATIONS

- Temperature evolution

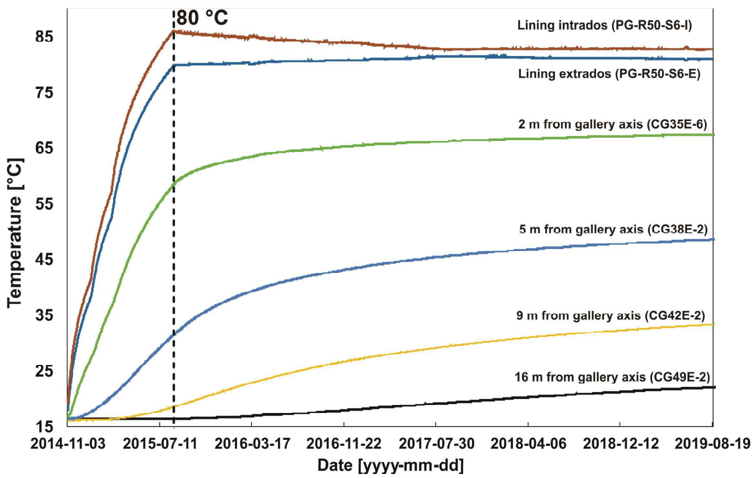

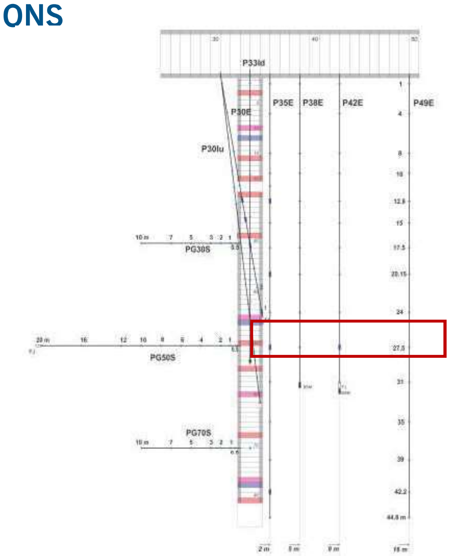

Extension of the thermally affected zone : > 16 m

THE PRACLAY EXPERIMENT – TEMPERATURE OBSERVATIONS

- **Profiles // to PRACLAY gallery in CG35E**

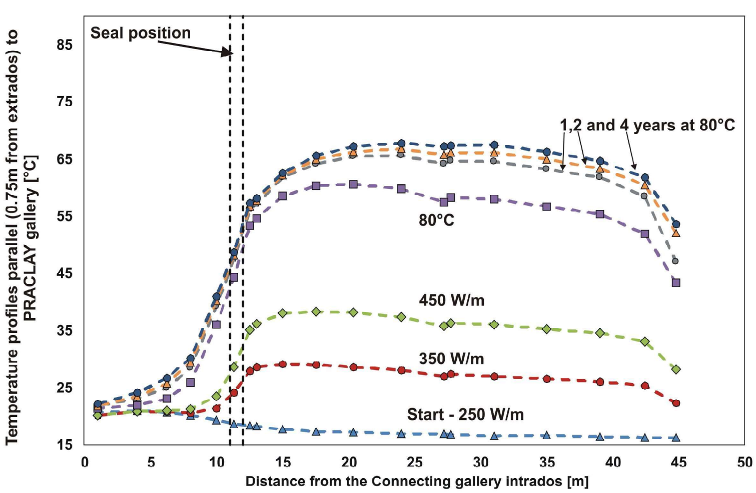

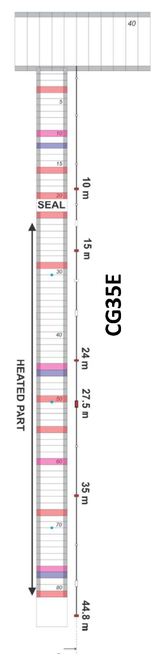

THE PRACLAY EXPERIMENT – TEMPERATURE OBSERVATIONS

- Temperature profiles in different directions

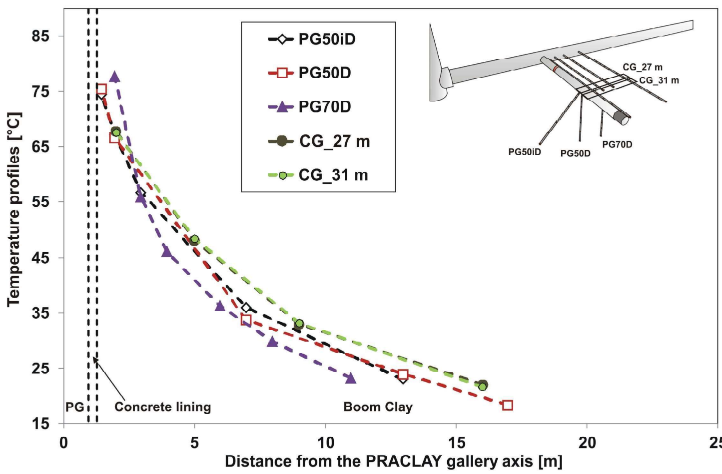

THE PRACLAY EXPERIMENT - PORE WATER PRESSURE OBSERVATIONS

- Pore pressure evolution

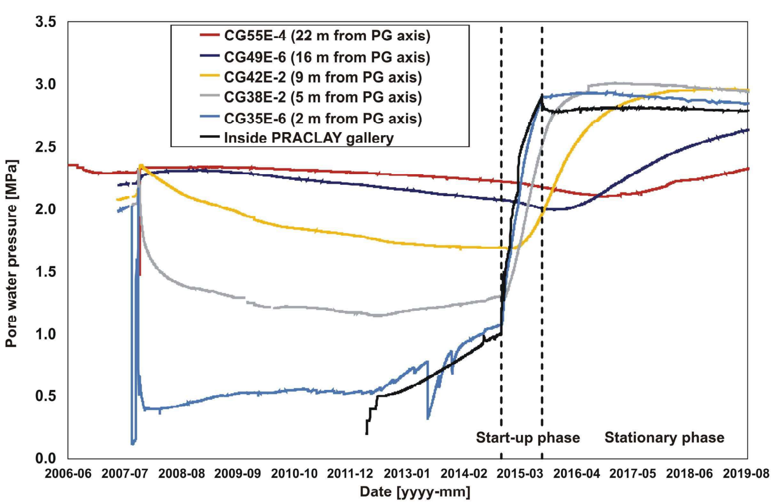

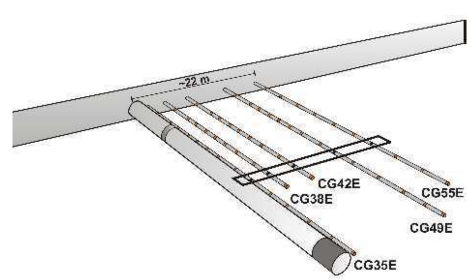

THE PRACLAY EXPERIMENT – PORE WATER PRESSURE OBSERVATIONS

- Pore pressure evolution in CG55E

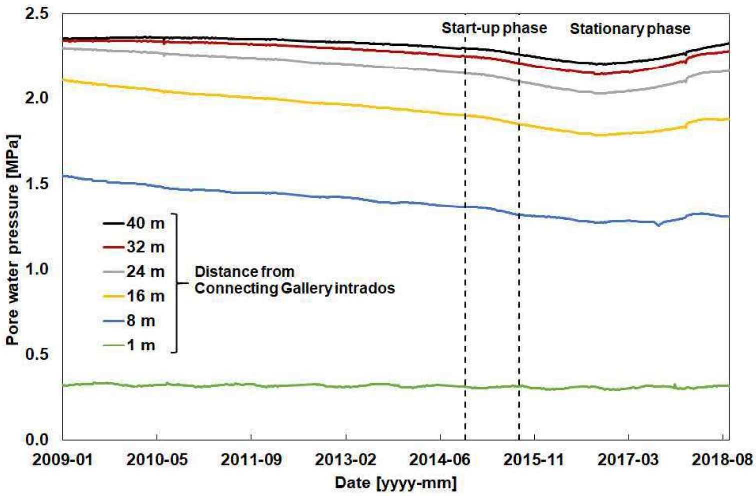

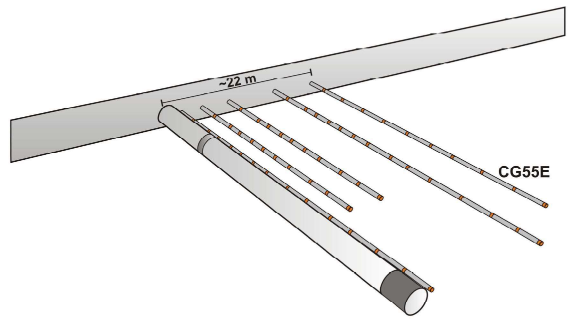

THE PRACLAY EXPERIMENT - PORE WATER PRESSURE OBSERVATIONS

- Pore water distribution in Boom Clay

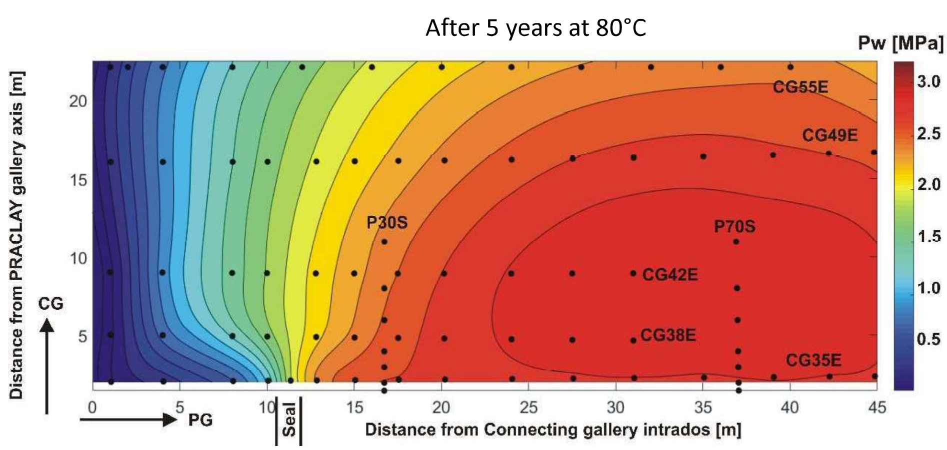

THE PRACLAY EXPERIMENT – NUMERICAL INTERPRETATION

- Comparison between measurements and modelling results

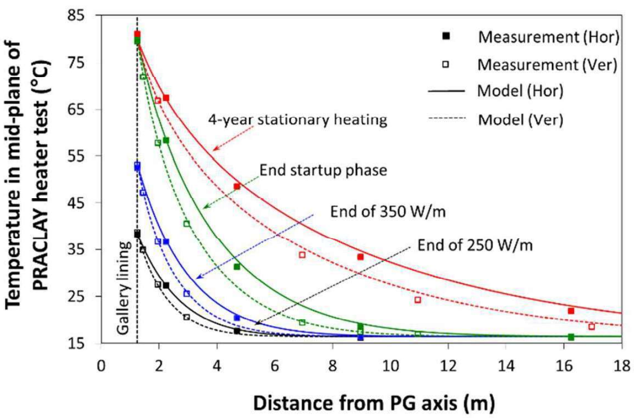

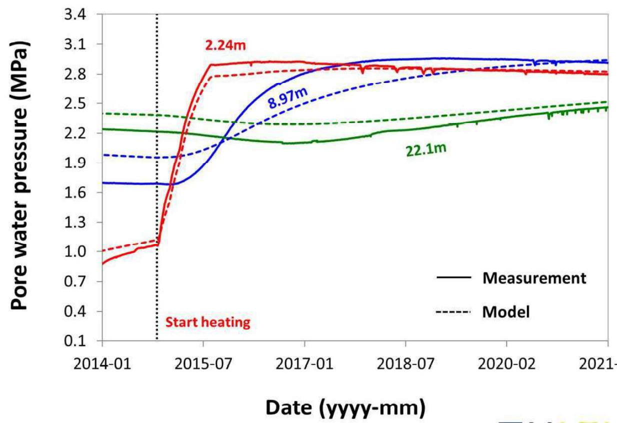

FINITE ELEMENT ANALYSIS OF A GEOLOGICAL DISPOSAL FACILITY

- Fully coupled THM finite element simulations with COMSOL© of a geological disposal facility in poorly indurated clay formation

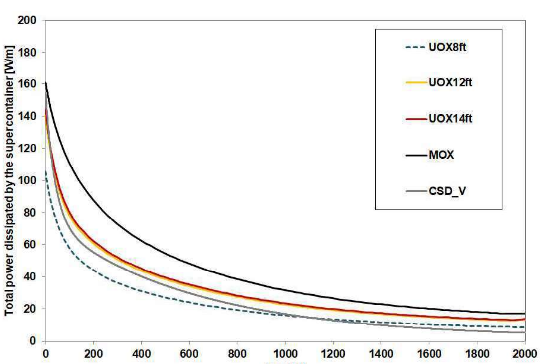

Heat input

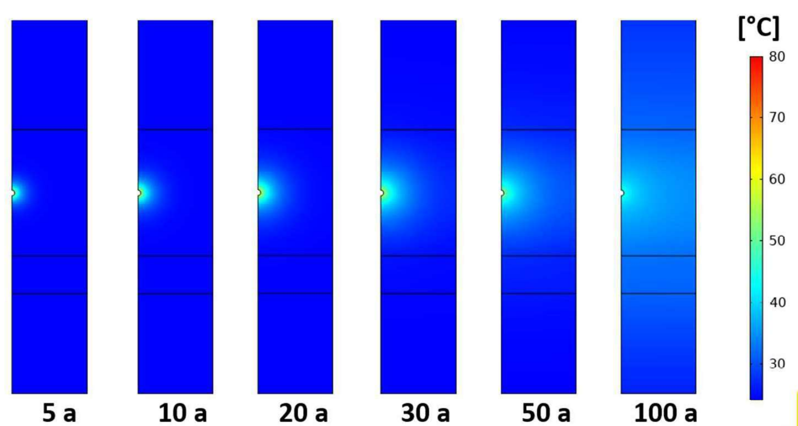

Temperature distribution

FINITE ELEMENT ANALYSIS OF A GEOLOGICAL DISPOSAL FACILITY

- Fully coupled THM finite element simulations with COMSOL© of a geological disposal facility in poorly indurated clay formation

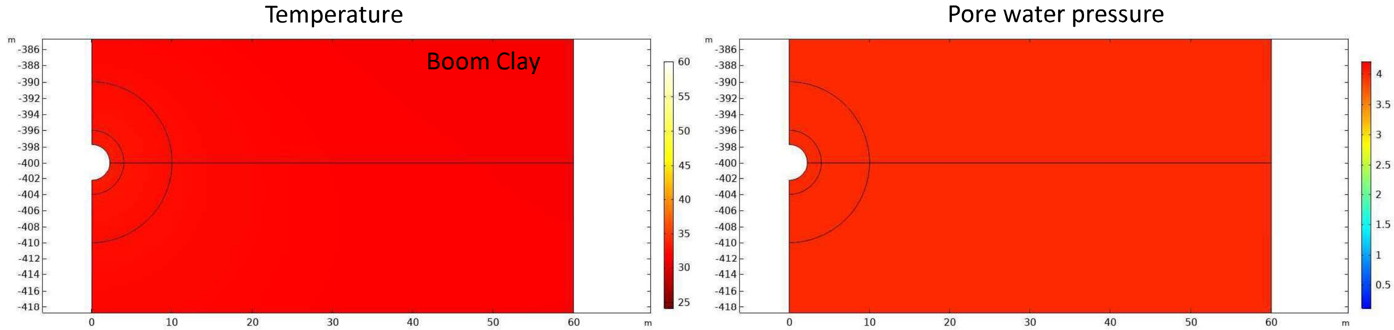

After 2000 years of heating

FINITE ELEMENT ANALYSIS OF A GEOLOGICAL DISPOSAL FACILITY

- Fully coupled THM finite element simulations with COMSOL© of a geological disposal facility in poorly indurated clay formation

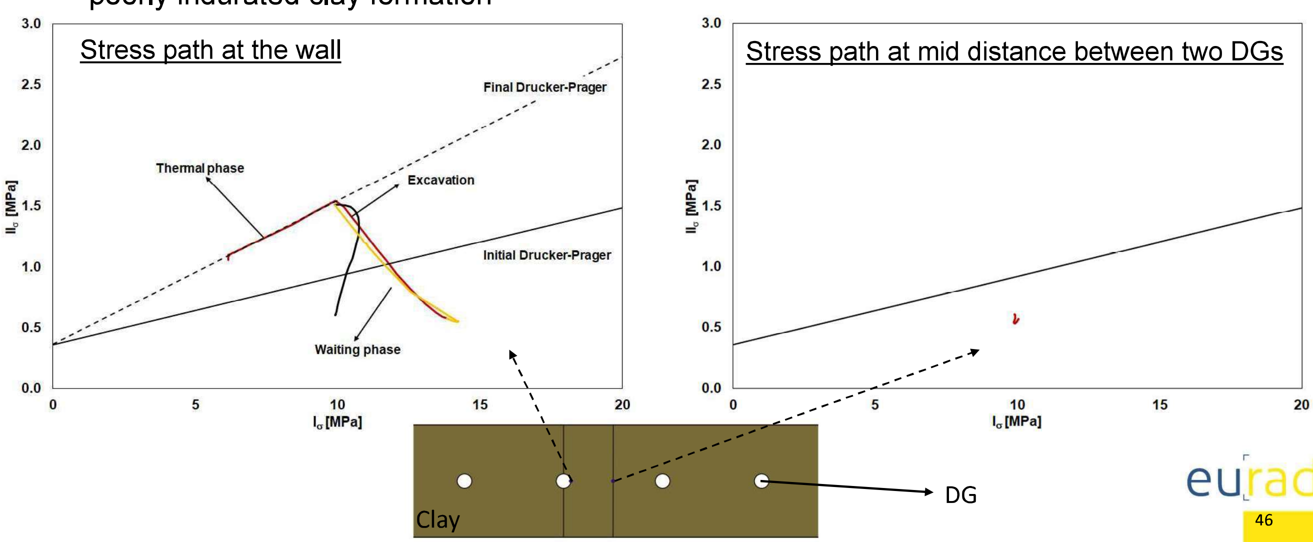

CONCLUSIONS

Long term investigation in THM coupled processes in poorly indurated clay

- Large scale in situ PRACLAY heater test:
  - Boom Clay is able to sustain the thermal load
    - ✓ Anisotropic responses, as expected (vertical vs horizontal profiles)
    - ✓ No indication of abrupt changes in pore water pressure nor large displacement
  - No interruption of the heater system
  - Good performance of the test set-up
  - Seal fulfils its role as a hydraulic cut-off

- Interpretation by back-analysing the measurements of heater tests
  - Determination of a set of THM properties/ parameters
  - Important input for the design/ optimization of a future GDF

Li et al., 2023. Geological Disposal of Radioactive Waste in Deep Clay Formations: 40 Years of RD&D in the Belgian URL HADES. Geological society, special publication 536 (open access https://doi.org/10.1144/SP536**)**

VISIT OF THE HADES URL (1ST SEPTEMBER)

7:30 Departure to Mol

9:00 – 9:30 Transfer from Tabloo to EURIDICE

9:30 – 12.15 Visit of the HADES URL

12:30 – 13:15 Sandwich lunch Bistroo (in Tabloo)

13:15 – 15:30 Visit of the Tabloo expositions

Tabloo : Gravenstraat 3, 2480 Dessel

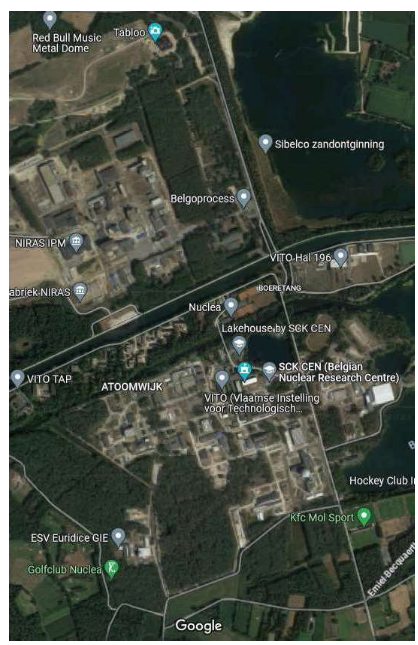

EIG EURIDICE

European Underground Research Infrastructure for Disposal of Nuclear Waste in Clay Environment

Boeretang 200 – BE-2400 MOL

ESV EURIDICE GIE

eurad

Appendix O. FE-G (and a pinch of FE) In Situ THM and GAS experiments (E. Stopelli)

FE-G (AND A PINCH OF FE) IN SITU THM AND GAS EXPERIMENTS

EURAD GAS+HITEC DOCTORAL SCHOOL, Liège, 31.08.23

E. Stopelli, PM Hydrochemistry, ISP Nagra

nagra

KEY TOPICS

- Full Scale Emplacement experiment (FE)
- Some THM data from FE
- FE-G: gases as proxy for chemistry
  - 9 years of monitoring
    - Oxygen
    - Helium
    - Methane
  - Summary of observations for safety
  - Work in progress

FE- THM

FE OBJECTIVES AND SET UP

1:1 Full Scale simulation of HLW waste generic Emplacement in Opalinus Clay

- Simulation of construction and emplacement techniques – feasibility
- Investigation of repository induced thermo-hydro-mechanical (THM) coupled effects on the host rock

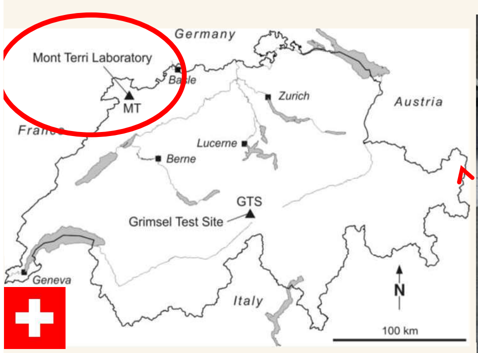

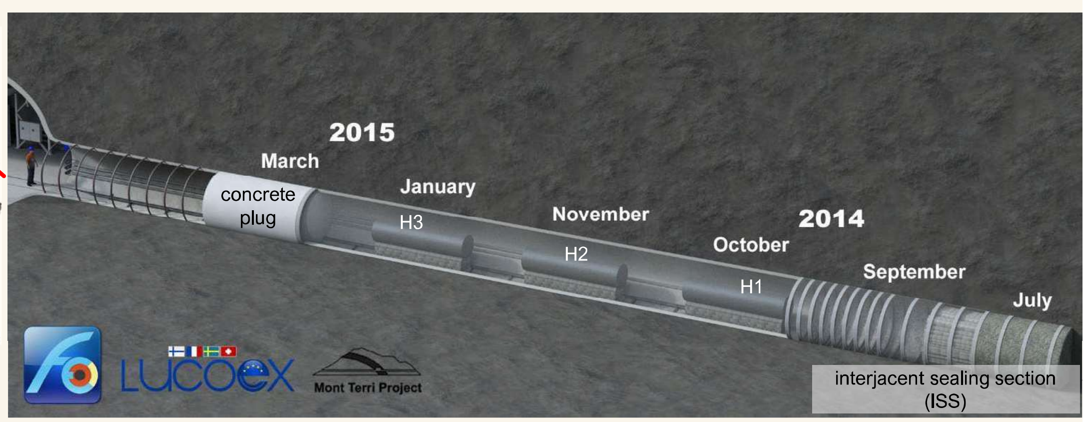

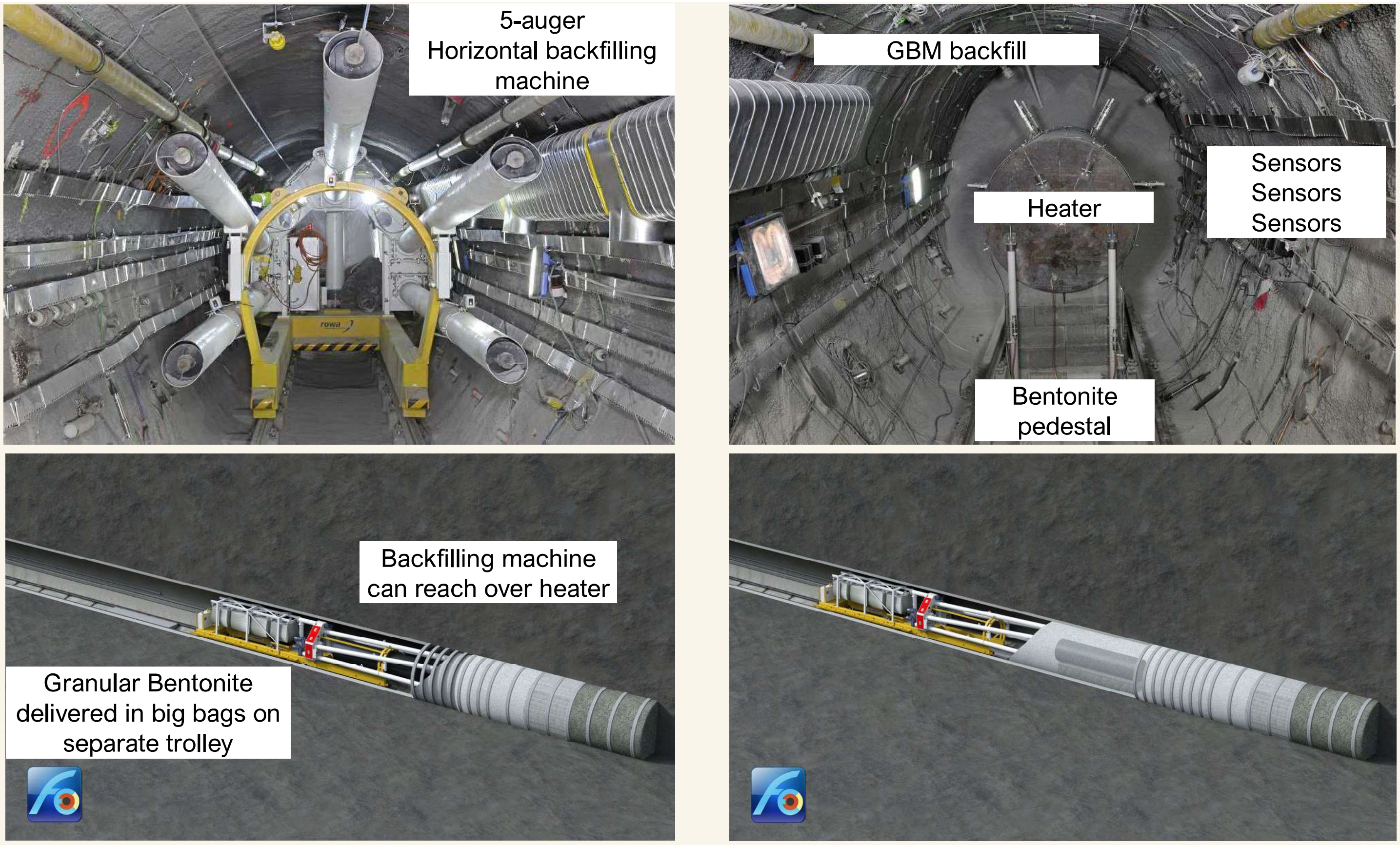

FE DATA - TEMPERATURE

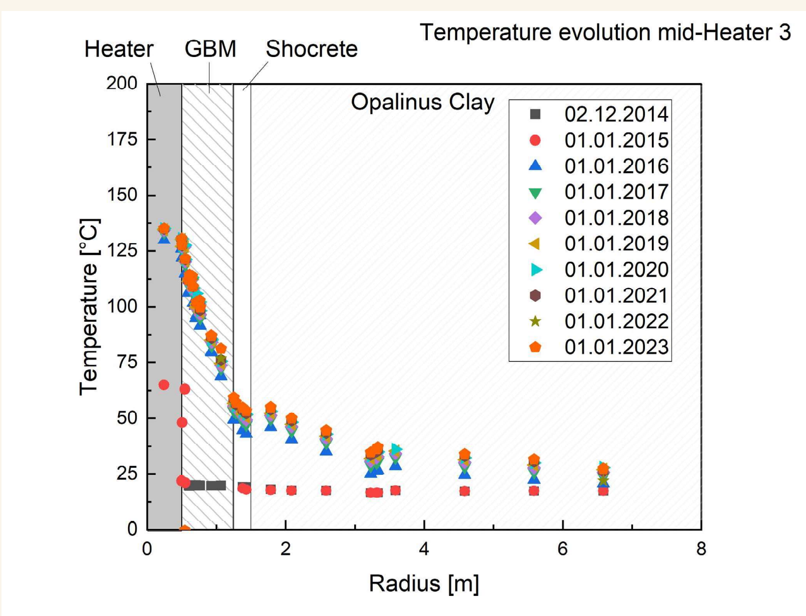

- Heater
  - Top: ~135°C
  - Centre: ~133-135°C
  - Bottom: ~126°C
- Gap: ~55-60°C
- GBM from 125 to ~50°C
- Tunnel wall
  - SC: ~50°C
- Near field from 50 to ~25°C

FE DATA – RELATIVE HUMIDITY

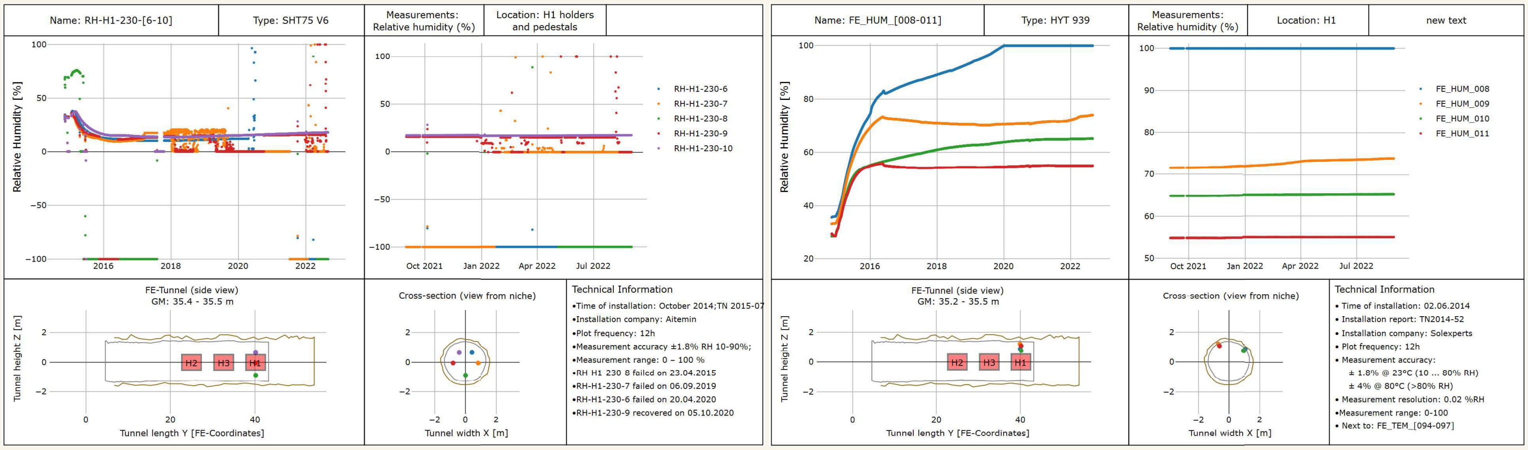

- 65% sensors in operation
- RH close to Heaters shows increase of RH in 2015, drying, then slight increase in RH
- RH at tunnel wall shows increase, mostly in 2015 (initial 20-30%, current 60-90%, wet spots 100%)

FE MODELLING TASK FORCE

Mission:

- Elaborate models of the FE with THM codes, capable to mimic the complete history of the experiment
- Elaborate workflows for predictive modelling of temperature, pore pressure evolution and stress-strain behavior in the bentonite buffer and the host rock

Tasks:

1. Code-to-code comparison / Code & Calculation Verification – C&CV (CodeBright / CodeAster / OpenGeoSys)
2. Back-analyses of FE monitoring data
3. Prediction evaluation exercise

FE-G THE GASES

eawag aquatic research

ANDRA

Mont Terri Project

Nuclear Waste Services

nwmo NUCLEAR WASTE MANAGEMENT ORGANIZATION

nagra

FE-G OBJECTIVES AND SET UP

Processes controlling gas phase evolution in an emplacement tunnel for HLW/SF (FE)

Monitoring and modelling gas evolution for long term safety (pressure build up, reactions)

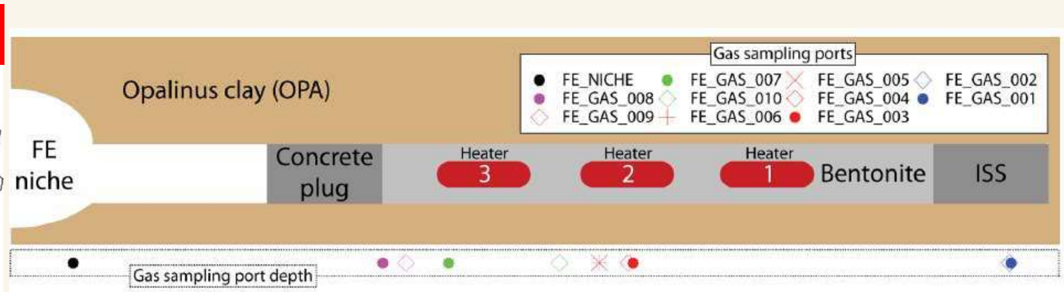

- Measurements
  - 6 in-situ O_2 sensors emplaced within the tunnel
  - Twice per year gas sampling of 10 port lines for off-site analyses – gases, isotopes
  - On-site mass spectrometer miniRUEDI for monitoring

FE-G CAVEATS

Concrete plug is not gas tight

Excavation Damaged Zone (EDZ) in contact with air - resaturation

Material set up:

- Metallic components – corrosion
- H_2S not collectable

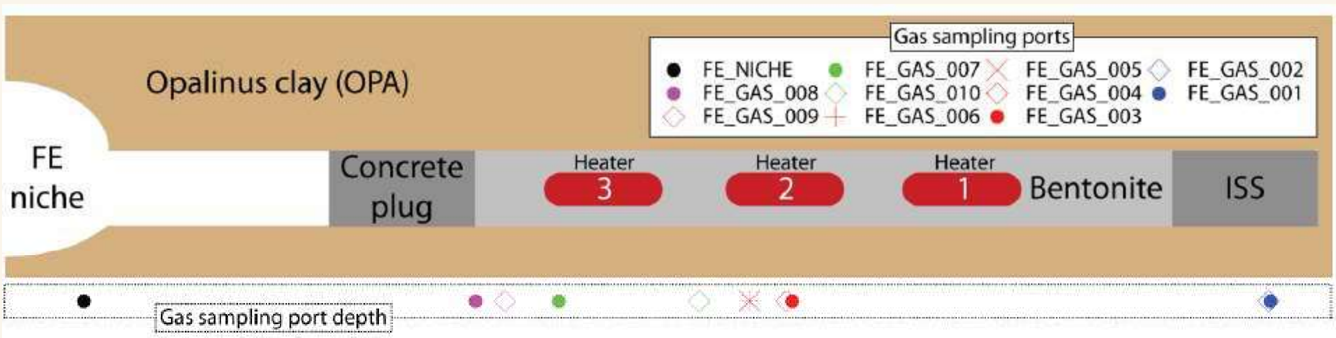

FE-G - OXYGEN

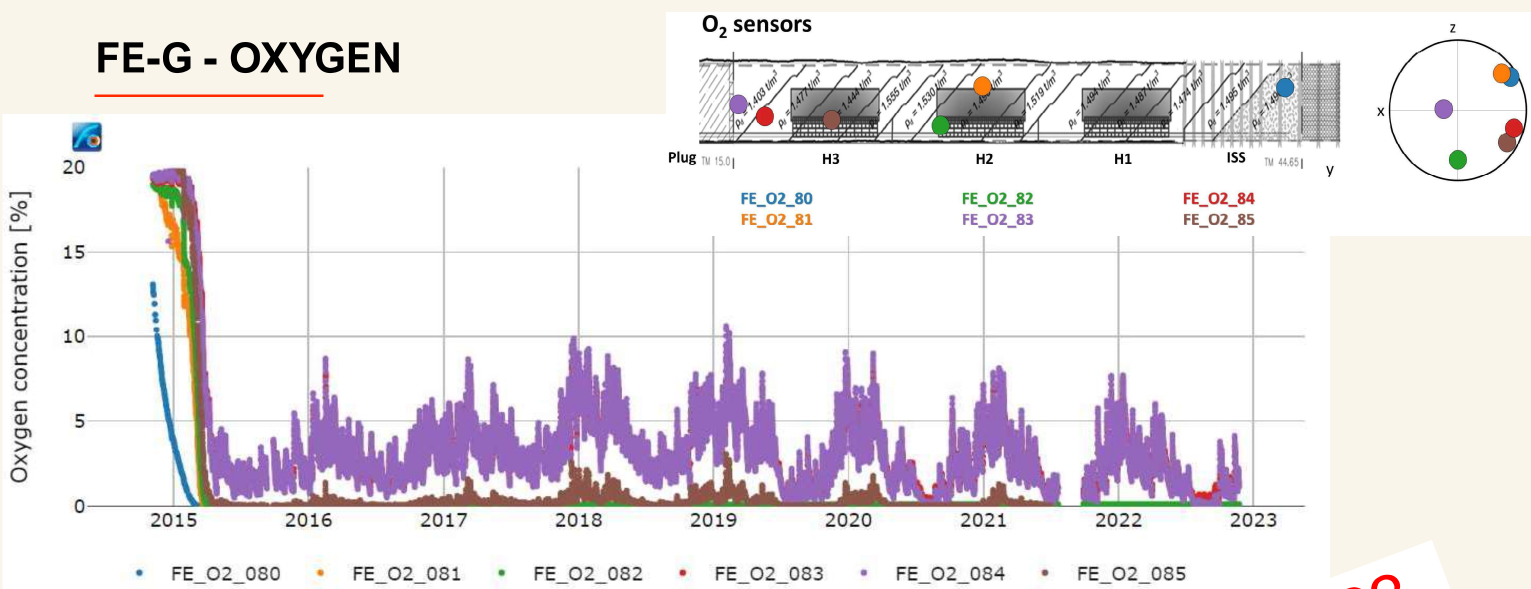

- Rapid O_2 loss at early stages of emplacement
- O_2 exchange with niche - ongoing
- O_2 decrease between concrete plug and heater 3 - ongoing

Any ideas???

FE-G - OXYGEN MODELLING

Extended 3D COMSOL model for early evolution of O_2

- First O_2 budgeting in model

Narrowed down the processes impacting early O_2 budget

- O_2 reversible sorption onto dry bentonite
- O_2 reactions where RH is high enough – also only locally

Current work:

Polynomial fit, canisters, mesh refinement, EDZ

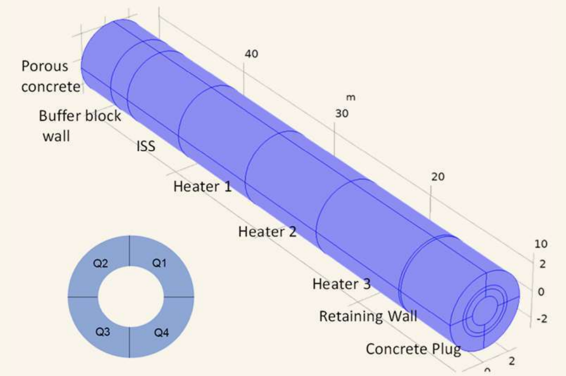

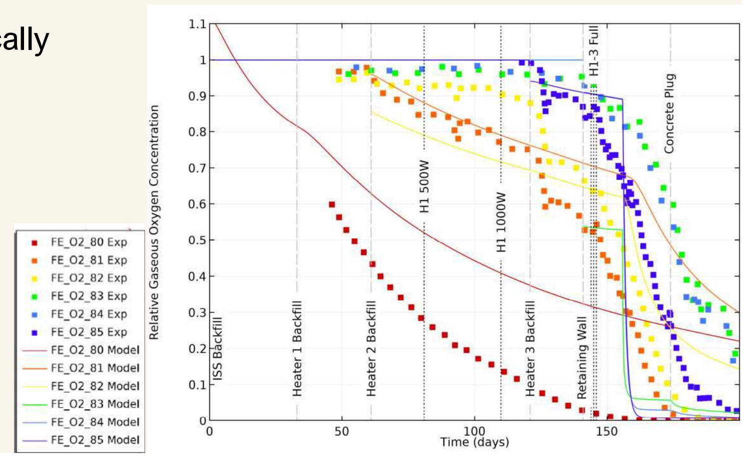

FE-G - HELIUM

- Indicates terrigenic ^4He gas exchange with OPA pore water
- Slight temporal accumulation
- Some decrease of concentrations towards the plug – air mixing

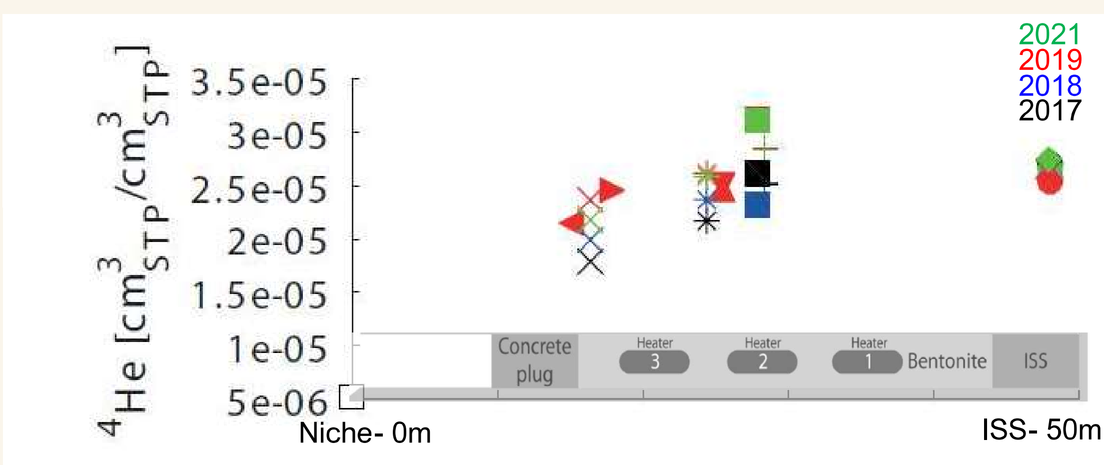

FE-G - METHANE

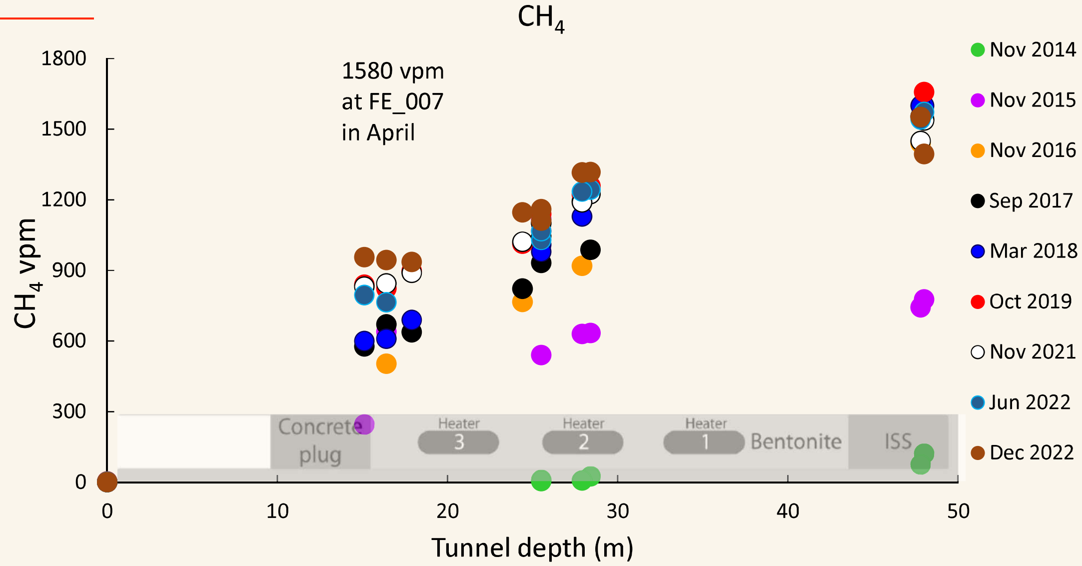

- CH_4 accumulation from OPA pore water
  - Concentrations compatible with OPA pore water (Vinsot et al., 2017)
  - More marked decrease across the tunnel compared to ^4He – lower atmospheric abundance + air dilution

FE-G - METHANE ISOTOPES

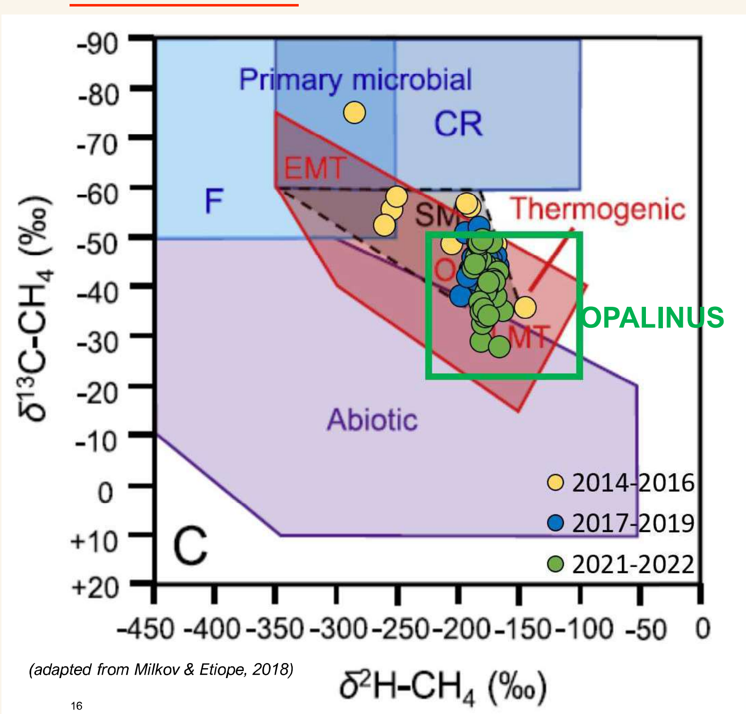

(adapted from Milkov & Etiope, 2018)

After variability at the beginning of the emplacement, when methane concentrations were low, values stabilised towards a range typical of OPA pore water

FE-G - SUMMARY FOR SAFETY

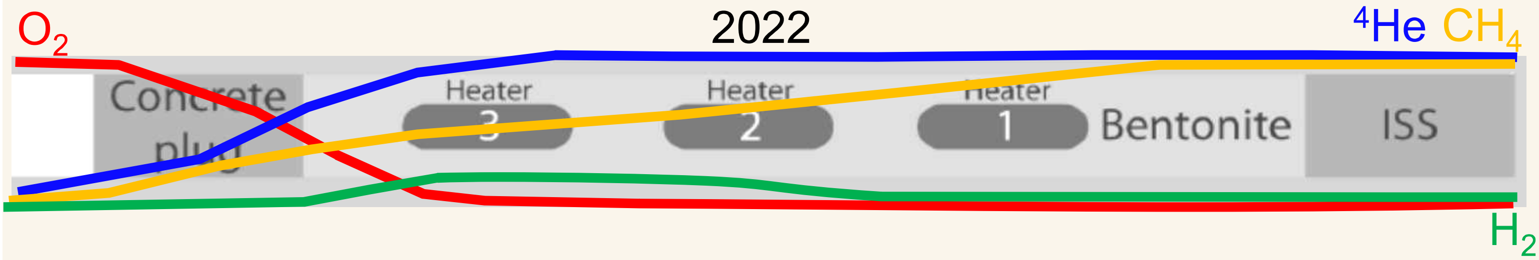

- No gas pressure build up or anomalous gas observed (plug and EDZ!!)
- Ongoing temporal gas changes and dynamic system during heating phase
  - O_2 budget at early emplacement phase for corrosion, ongoing O_2 diffusion/advection
  - He accumulation from OPA
  - CH_4 later emplacement phase from OPA

FE-G: INTERPRETATION STRATEGIES AND WORK IN PROGRESS

- O_2 at early emplacement for budget
  - Implementation of COMSOL model #4 (fits, canisters, RH of pedestal sensors, refined mesh)
- Gas fluxes – conservative steady state conditions
  - Noble gases data and P sensors
  - Diffusion/advection (air) model based on ^4He and P
  - Role of EDZ
- CH_4 and hydrocarbons investigations
- Comparison with similar emplacement studies (i.e. HotBENT experiment)

FE-G recent reports

TN 2022-13 – model COMSOL #3
TN 2022-11 - lab results offsite analyses
TN 2022-09 – noble gases offsite analyses
NAB 19-36
Giroud et al., App. Geochem., 2018
Tomonaga et al., App. Geochem., 2019

Thanks

FE and FE-G Project Partners
FE and FE-G Contractors
You for your attention

emiliano.stopelli@nagra.ch

Appendix P. In Situ gas fracturing experiments conducted in the Callovo Oxfordian claystone (C. Plua)

In situ gas fracturing experiments conducted in the Callovo-Oxfordian claystone

Carlos Plúa, Rémi de La Vaissière and Gilles Armand

PHD SCHOOL

EURAD Training course

28 August – 1 September 2023, Liège

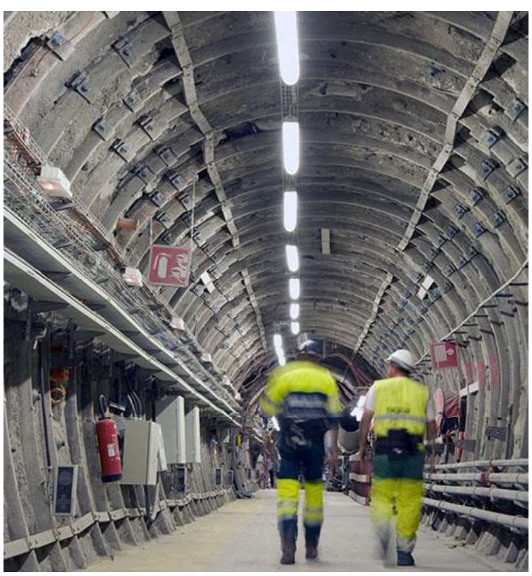

Context

Context
The Cigéo project

- **Andra** is in charge of the management and disposal of radioactive waste in France
- **Cigéo** is the French Industrial Center for **Geological Disposal** for **HLW** and **ILW**
  - Licence application in December 2022
  - Location in the eastern part of the Paris basin into a claystone formation
- **Callovo-Oxfordian (COx)**
  - Depth of 500 m
  - Favorable characteristics
    - very low hydraulic conductivity
    - low molecular diffusion
    - high retention capacity for radionuclides

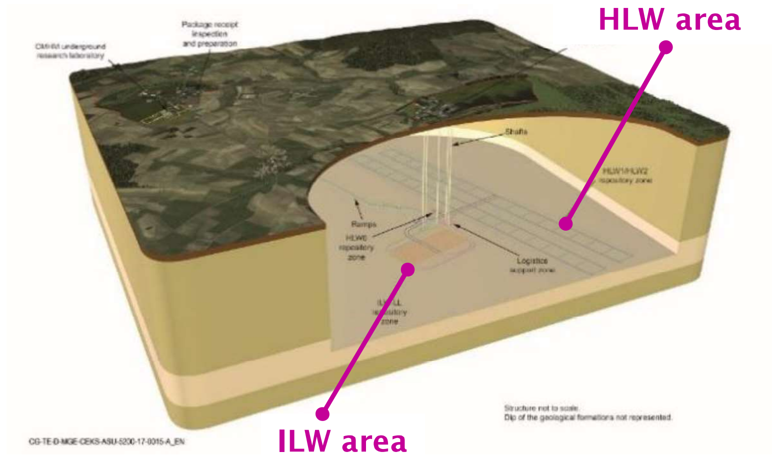

Context
The Meuse/Haute-Marne URL

- Enables scientific and technological research to be carried out directly within the COx
- Objectives in geomechanics
  - To study **hydro mechanical** behavior
  - To characterize the **Thermo Hydro Mechanical** behavior
  - To perform **sealing experiments**
  - To characterize the **E**xcavation **D**amaged **Z**one
    - Shape depends on the excavation orientation wrt to σh or σH

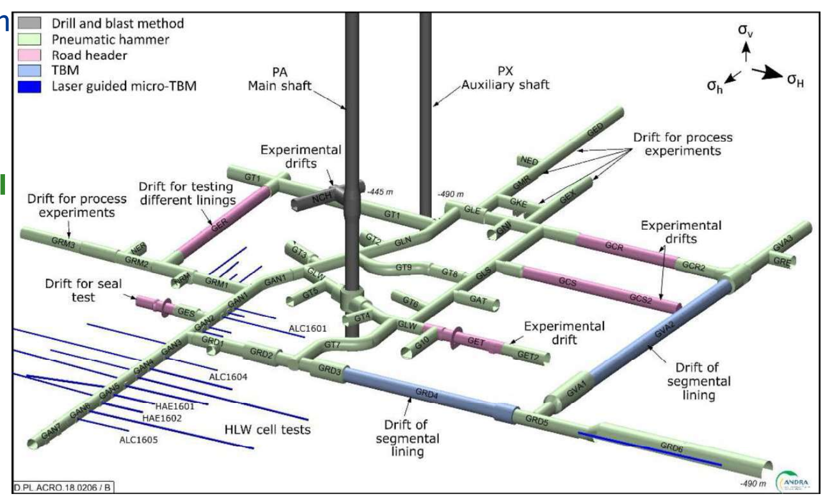

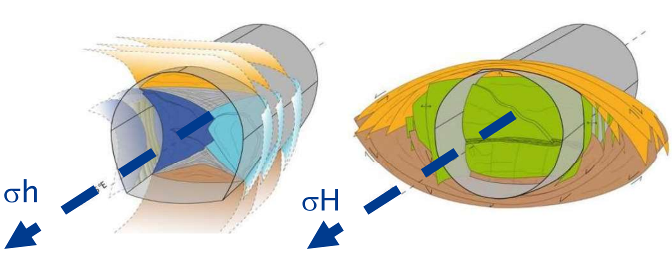

Context
Gas migration in the repository

- To investigate the **initiation** and **propagation** of a **gas-driven fracture** through the COx
    - Hydrogen generation in the repository in the post-closure phase could lead to gas pressure large enough to cause a vertical gas-driven fracture to propagate upwards through the COx formation

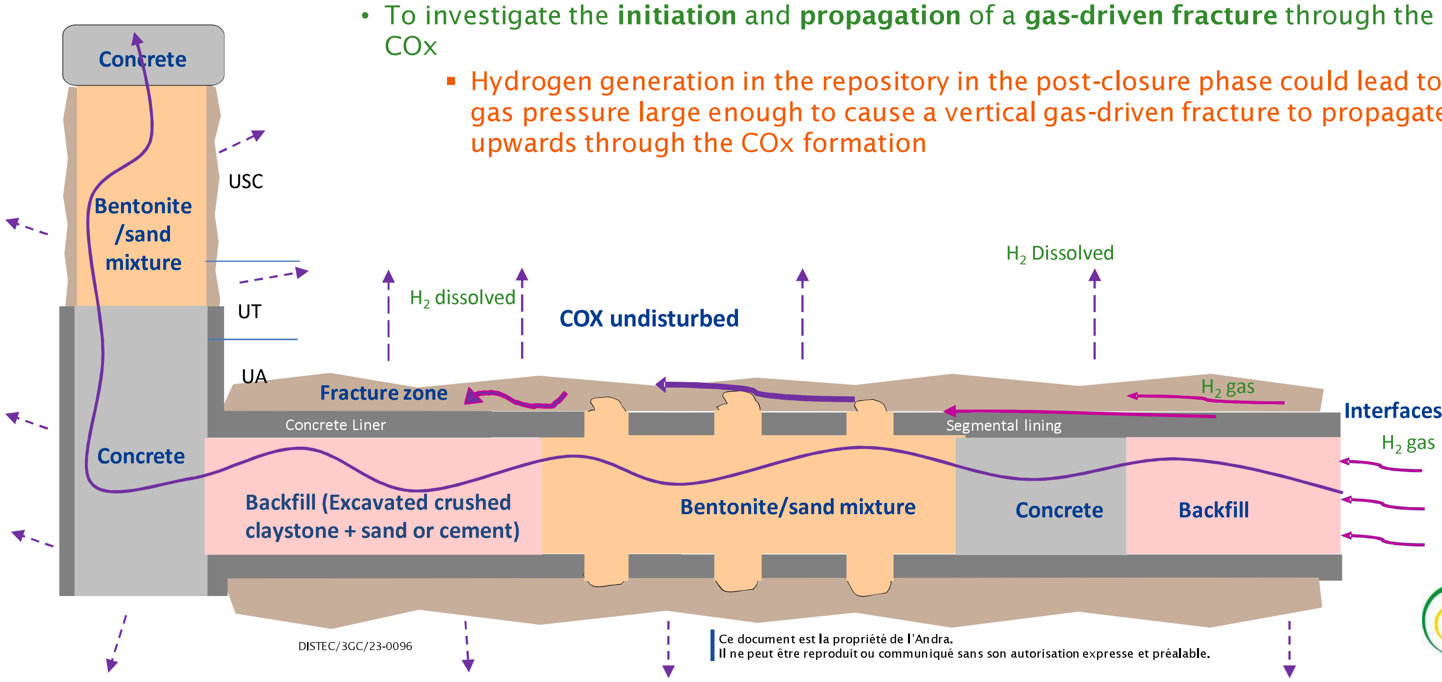

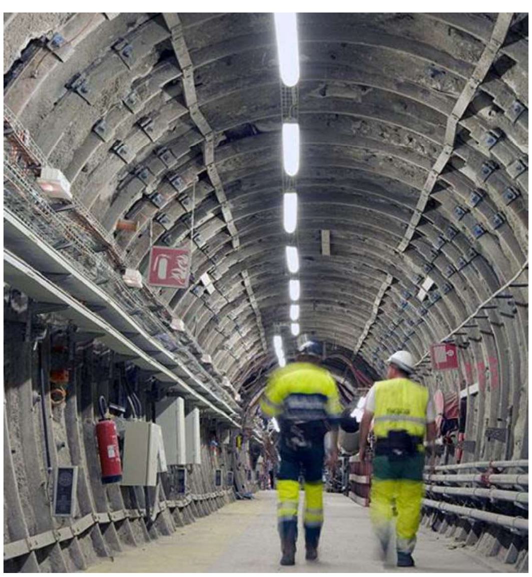

PGZ1 experiment

DISTEC/3GC/23-0096

Ce document est la propriété de l'Andra.
Il ne peut être reproduit ou communiqué sans son autorisation expresse et préalable.

PGZ1
Objective

- PGZ1 is dedicated to identify **gas migration mechanisms** into the COx claystone at different pressure levels
  - Series of gas injection tests at different flow rates
  - Gas: Nitrogen
- 3 instrumented boreholes drilled and equipped in July 2009

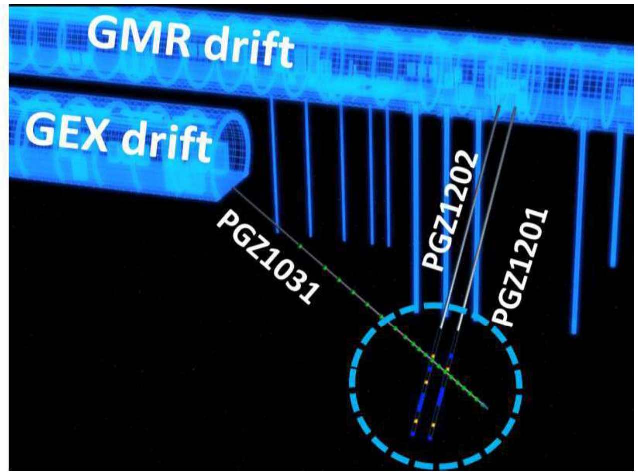

PGZ1
Borehole characteristics

- **PGZ1201** & **PGZ1202** drilled from the GMR drift
  - Length: 28 m, spacing: 0.9 m
  - Oriented parallel to σH
  - Equipped with a multipacker system to monitor water/gas pressure in 3 intervals: PGZ120x_01, 02 & 03

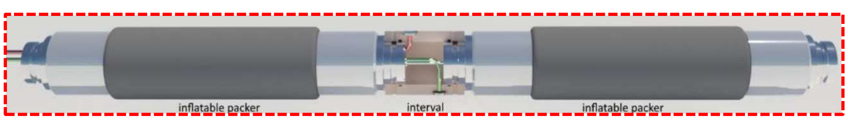

- **PGZ1031** drilled from the GEX drift
  - Equipped with a multiple magnetic extensometers probe (MagX system®) to monitor axial deformation

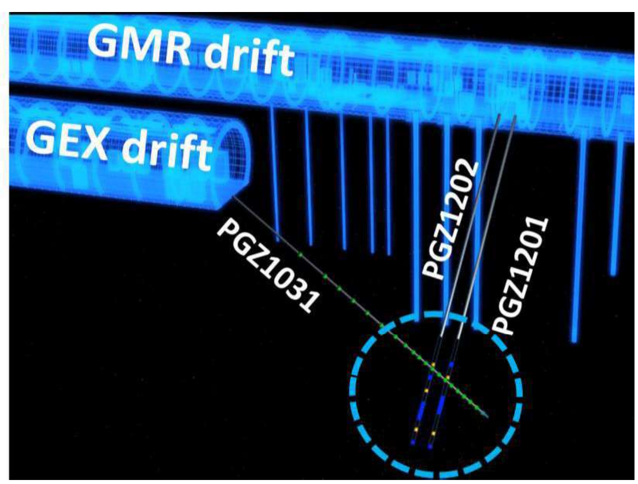

PGZ1
Overview

- 10 years of water/gas pressure monitoring
  - Pore pressure in intervals
  - Mechanical pressure in packers
- PGZ1201_02
  - **HYDROx**: Water permeability tests
  - **GASx**: gas injection tests at low rate (slow test)
  - **HYDO-FRAC**: water injection test to measure σh
- PGZ1202_02
  - **GAS-FRAC**: gas injection test at high flow rate (fast test)

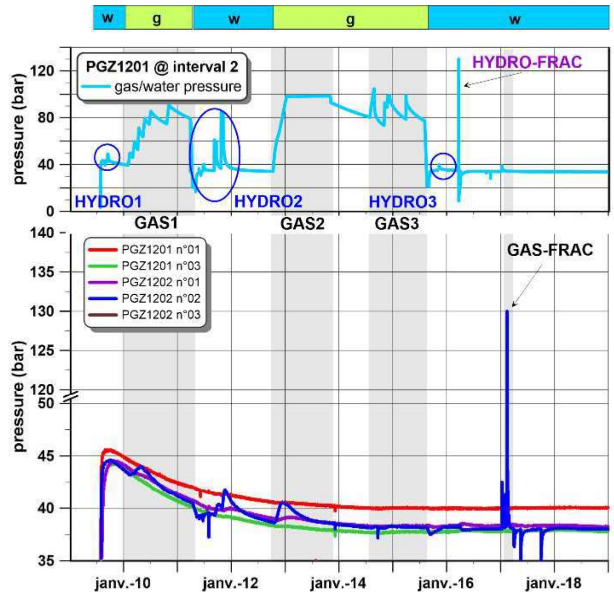

PGZ1
PGZ1201 - GAS1 (slow test)

- 6 constant gas flow steps (GRIx) followed by pressure recovery periods (GRISx):
  - maximal pressure = 9.1 MPa
- Classical two-phase flow model reproduces reasonably well observations
  - Two separate zones with different gas entry pressure are required:
    - Inner zone corresponds to the Borehole Damage Zone with a very low gas entry pressure (≤ 2 MPa)
    - Outer zone corresponds to the sound claystone with a high gas entry pressure

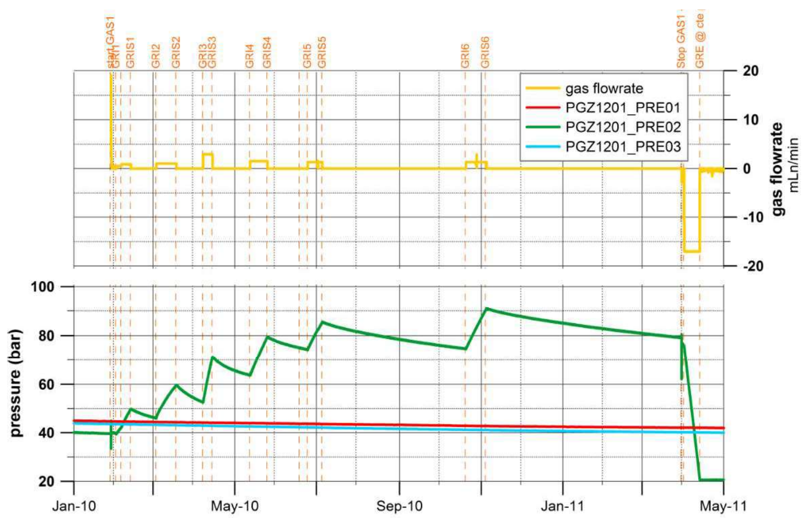

PGZ1
PGZ1201 - GAS1 (slow test)

Université de Liège

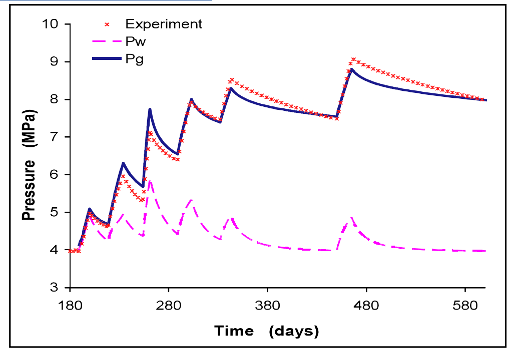

- 6 constant gas flow steps (GRIx) followed by pressure recovery periods (GRISx):
  - maximal pressure = 9.1 MPa
- Classical two-phase flow model reproduces reasonably well observations
  - Two separate zones with different gas entry pressure are required:
    - Inner zone corresponds to the Borehole Damage Zone with a very low gas entry pressure (≤ 2 MPa)
    - Outer zone corresponds to the sound claystone with a high gas entry pressure

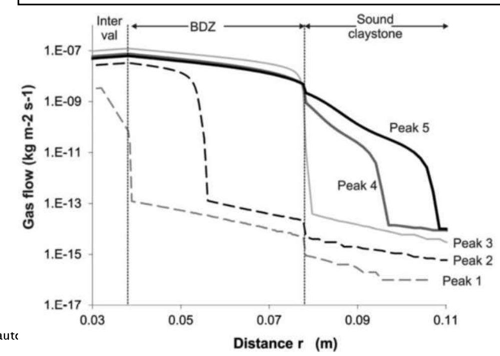

PGZ1
PGZ1201 – GAS3 (slow test)

- Constant injection flow rate test until reaching 10.45 MPa
- Then injection was turned to constant injection pressure
  - A sudden gas breakthrough was observed at 10.45 MPa
    - the gas pressure suddenly dropped in the test interval and the flow meter has reached simultaneously its maximum value
- A gas fracture was created with a gas pressure value well **below** the minimum principal stress component (σh ~ 12.5 MPa)
  - an overall rigid motion is detected on the extensometer string in borehole PGZ1031

It was not possible to locate the position of the fracture

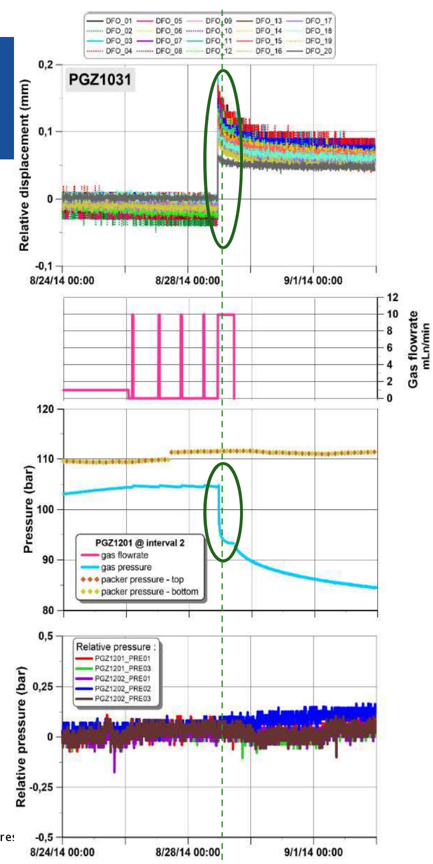

PGZ1
PGZ1201 – GAS3 (slow test)

- A new gas injection step was performed a few months later with a gas mixture (nitrogen + helium) and high gas flow rate
  - Helium is used as a gas tracer
    - Detection of helium is done on PGZ1031 head
  - A maximal gas pressure is reached at 9.99 MPa
- During this test, no displacement was detected by the extensometer string
  - The recorded motion is due to human action

This is evidence that a fracture was created in the rock

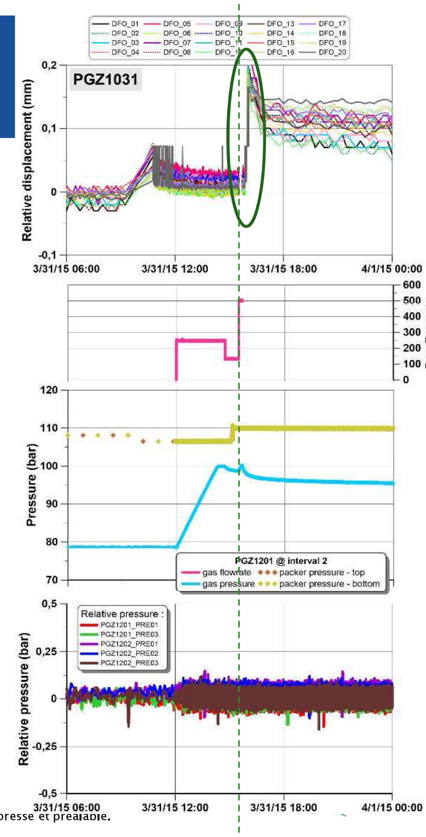

PGZ1
PGZ1202 – GAS-FRAC (fast test)

- GAS-FRAC started with an injection at high constant flow rate @ 500 mLn/min that lasted about 2 hours
- The interval pressure reached progressively 14.18 MPa when the injection line was closed in order to monitor the pressure drop
  - Six minutes after the injection line was closed a sudden pressure drop was observed with:
    - a simultaneous increase in pressure in PGZ1202_03
    - a sudden differential displacements recorded by the PGZ1031
- A gas fracture was created with a gas pressure value well **above** the minimum principal stress component ($\sigma h \sim 12.5$ MPa)

One packer starts to leak : the testing program has been abandoned

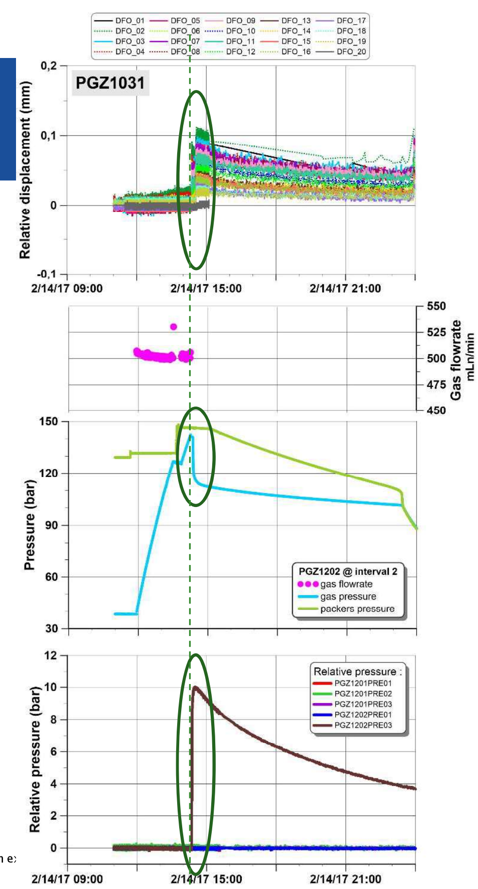

PGZ1
Summary

- Different gas injection tests at various flow rates (from 1 mLn/min to 500 mLn/min) have been conducted
- GAS1 reveals that generalized Darcy's law allows for the correct modelling of measurements up to 9.1 MPa
  - Gas first percolates radially into the BDZ and then starts to migrate into the sound claystone (with a high gas entry pressure above 4 MPa)
  - Analysis of the different gas injection phases reveals that generalized Darcy's law allows for the correct modelling of measurements up to 9.1 MPa
- During GAS3 & GAS-FRAC, a relationship between gas flow rate and gas fracturing pressure is highlighted
  - Some hypothesis
    - Drained/undrained boundary condition
    - Geometry of the cavity (shape and size of the BDZ)
    - The stress applied by the packers

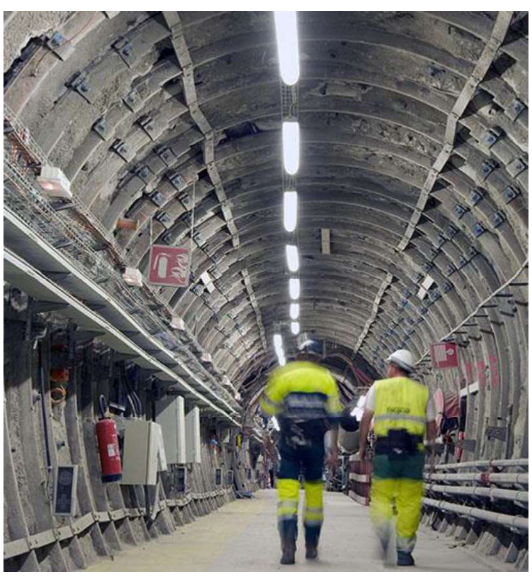

PGZ3 experiment

DISTEC/3GC/23-0096
Ce document est la propriété de l'Andra.
Il ne peut être reproduit ou communiqué sans son autorisation expresse et préalable.

PGZ3
Objectives

- Study the gas fracturing pressure at different injection flow rates
- New boreholes have been drilled since 2020
  - Length 35 m
  - Oriented according to the horizontal principal stresses
    - **PGZ1002** & **PGZ1003** drilled from the GEX drift
    - **PGZ3001, PGZ3002** & **PGZ3004** drilled from the GRM drift
    - **PGZ5301** drilled from the GMA drift

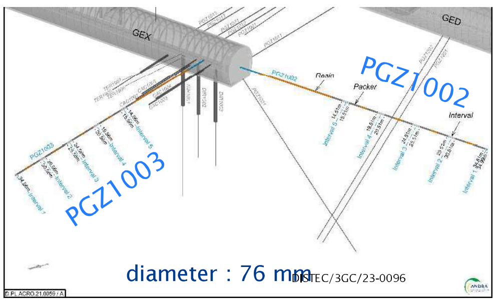

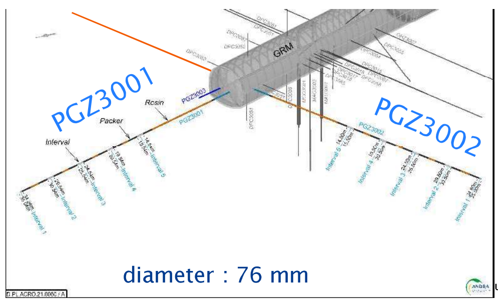

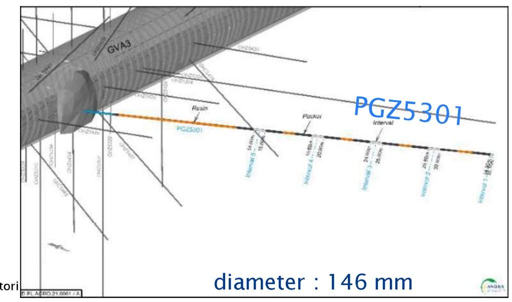

PGZ3
PGZ1002 & PGZ1003 - (fast tests)

- Injection inteval 4:
  - Located at 20 m from the drift wall
- 3 phases of gas injection tests (~ 500 mLn/min)
  - Phase 1 (December 2020):
    - to reach the breaking point of the rock
  - Phase 2 (February 2021):
    - To reopen the fracture
  - Phase 2 (March 2021):
    - to stimulate and reopen the fracture

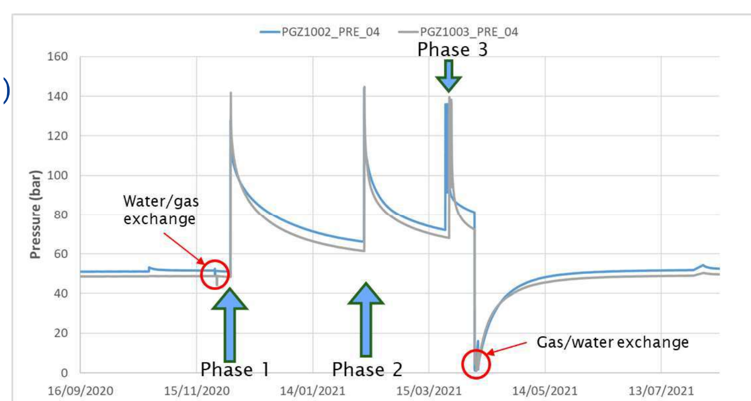

PGZ3
PGZ1002 - fast test (Phase 1)

- Gas injection test : ~ 90 min
- Max. gas pressure : 13.01 MPa
- Interferences:
  - Packers @ interval 3
  - Interval 3 : much deeper (25 m)
    - Interface leakage ?
    - Possible creation of a opening along the borehole?

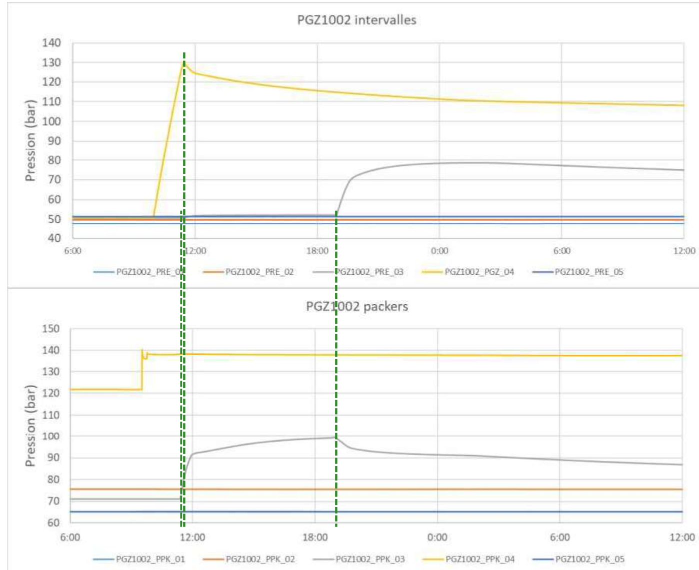

PGZ3
PGZ1002 - fast test (Phase 1)

- Pressure build-up
  - Not perfectly linear
    - Gas volume variation
  - Inflection observed towards dP = 74.83 bar or 12.78 MPa in absolute pressure
    - correlated with the reaction of packers (interval n° 3)
- Gas volume variation
  - ideal gas law with gas deviation correction (Z factor: compressibility factor)
    - Volume of ~530 mL at the start of the injection (value greater than the volume of water extracted)
  - Slow increase in gas volume until inflection

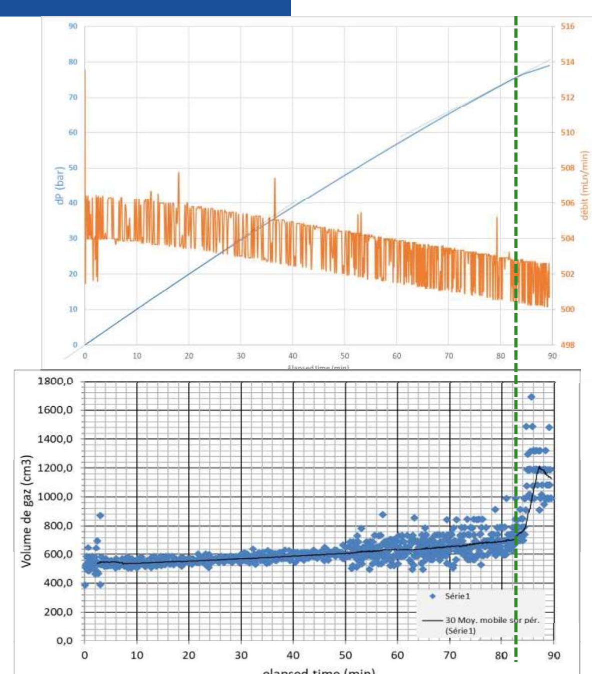

DISTEC/3GC/23-0096

Ce document est la propriété de l'Andra.
Il ne peut être reproduit ou communiqué sans son autorisation expresse et préalable.

PGZ3
PGZ1003 - fast test (Phase 1)

- First step : ~ 90 min
  - Gas pressure end ~ 13.01 MPa
- Second step: ~ 35 min
  - Max. gas pressure : 14.28 MPa
- Interferences:
  - Packers @ interval 3 + interval 5
  - Interval 5 : shallower (15 m)
    - Interface leakage ?
    - Possible creation of a opening along the borehole?

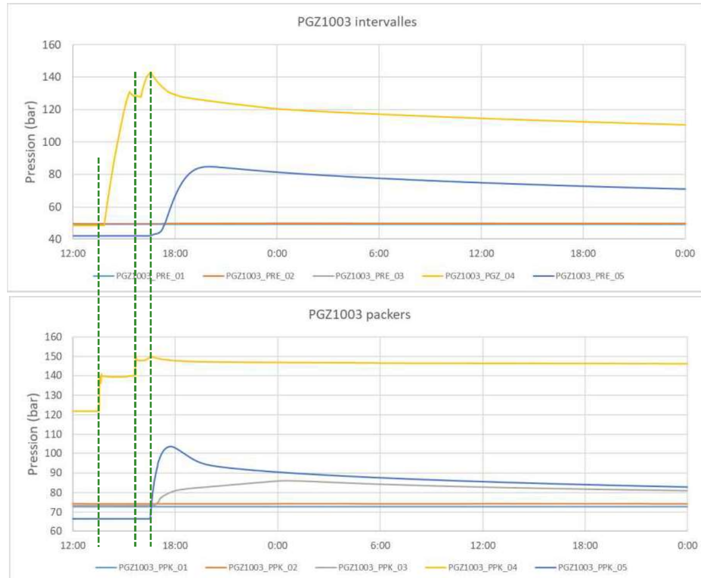

PGZ3
PGZ1003 - fast test (Phase 1)

- First step
  - Not perfectly linear pressure build-up
  - Gas volume variation
    - Volume of ~415 mL at the start of the injection (value greater than the volume of water extracted)
    - Slow increase in gas volume until inflection
  - Inflection observed towards dP = 79,87 bar i.e. 12,5 MPa in absolute pressure

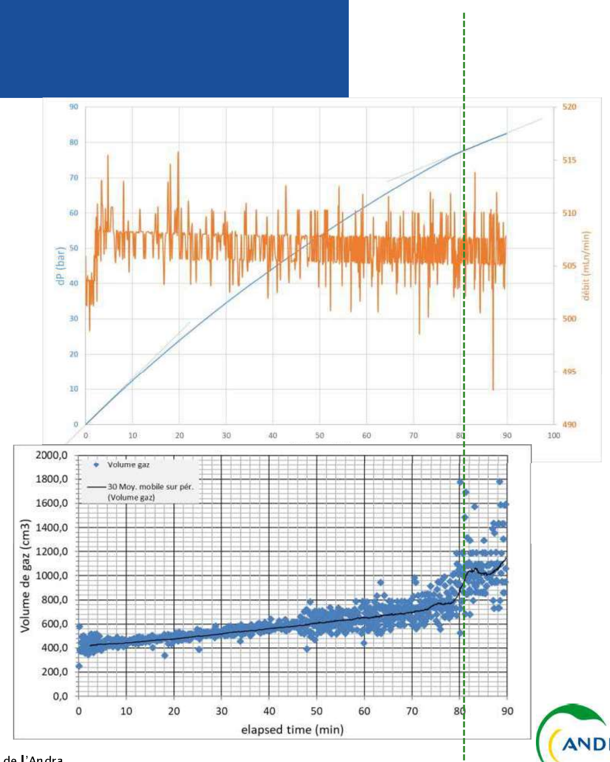

DISTEC/3GC/23-0096

Ce document est la propriété de l'Andra.
Il ne peut être reproduit ou communiqué sans son autorisation expresse et préalable.

PGZ3
PGZ1003 - fast test (Phase 1)

- Second step
  - Not perfectly linear pressure build-up
  - Gas volume variation
    - Volume of ~655 mL at the start of the injection (value lower than the volume at the end of the previous step)
    - Slow increase in gas volume until inflection
  - 2 inflection points observed at :
    - 14.05 MPa
    - 14.25 MPa
  - Max gas pressure : 14.28 MPa

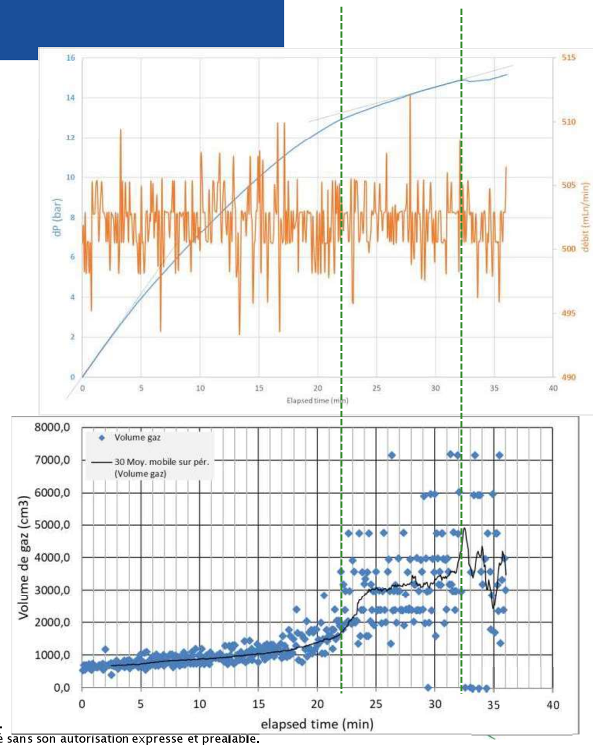

DISTEC/3GC/23-0096

PGZ3
PGZ3001 - slow test

- RI2 :
  - gas started to percolate along borehole wall
- RI3:
  - Sudden drop in pressure at 90,9 bars
  - Correlated with a slight peak in packer pressure PPK01
    - This suggests abrupt detachment at an interface along the borehole wall
- RI4 & RI5:
  - interferences are observed surrounding the packers 01-03-04 and into the intervals 01-03-04
  - Difficult to increase the pressure
- RI7:
  - Fracturing occurred at 131 bars
  - Drop of 6 bars

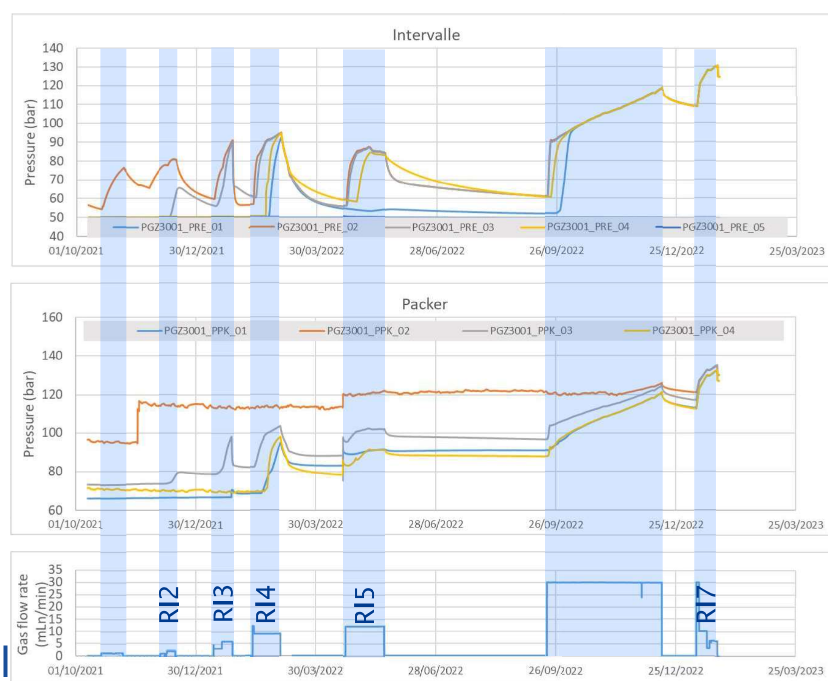

DISTEC/3GC/23-0096

PGZ3
PGZ3002 - slow test

- After RI2 and during RI3 : gas percolates along borehole wall
  - Interferences are observed surrounding the packers (01-03-04) and into the intervals (01-03-04)
- RI4 & RI5
  - The gas flow rate was increased to compensate for gas leakage along the borehole
    - Max injection rate: 90 mLn/min
    - Difficult to increase the pressure

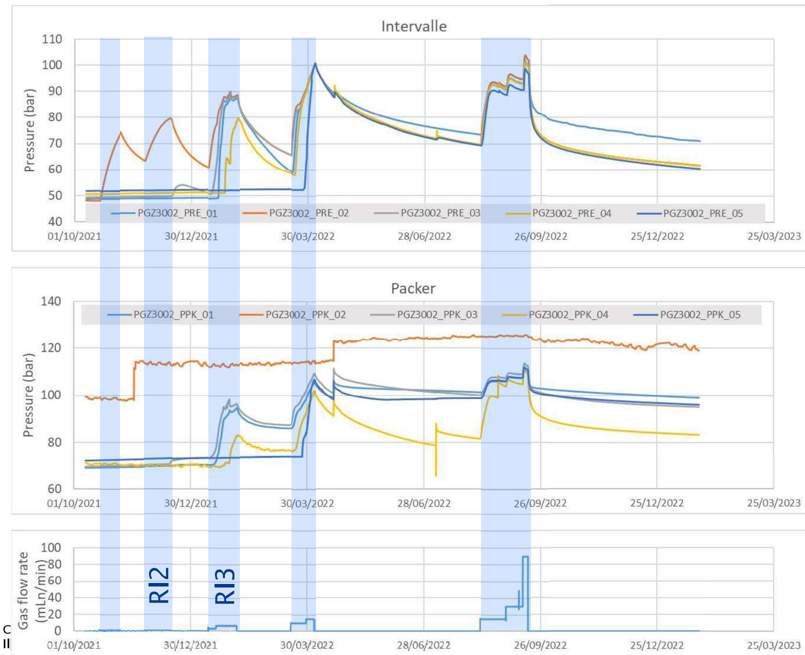

PGZ3
Summary

Fast injection flow rate (500 mLn/min) in PGZ1002 and PGZ1003

- a fracture was initiated and spread along borehole wall :
  - @ PGZ1002 : 12,78 MPa
  - @ PGZ1003 : 14,28 MPa
- A gas fracture was created with a gas pressure value well **above** the minimum principal stress component (~ 12.5 MPa)

Slow gas injection flow rate in PGZ3001 and PGZ3002

- Fracturing pressure was only reached in PGZ3002
  - 13.1 MPa
- It is difficult to increase the pressure in the testing interval
  - Gas could easily percolate along horizontal boreholes at low pressure

PGZ1 vs PGZ3
Where does the gas flow ?

In PGZ3 boreholes: gas easily percolates along borehole wall or within the BDZ

- Horizontal boreholes
  - Breakouts along borehole wall
    - No perfect circular cavity
    - Tightness between packers and rock
      - Water => YES due to self-sealing
      - Gas => No
    - Tightness between resin and rock
- It is very likely that gas percolates along the interfaces (packer-rock and resin-rock)

In PGZ1 (PGZ1201): no gas flows along borehole

- PGZ1201 is oriented // to sigma H but inclined
  - Less breakouts ?
    - Better gas tightness between packers and rock ?

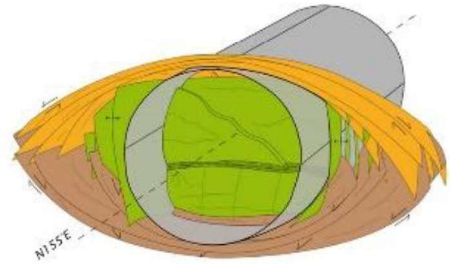

Shape of the excavation damaged zone for drift oriented along sigma H

breakout along horizontal borehole (oriented sigma H) => cavity is not perfectly circular

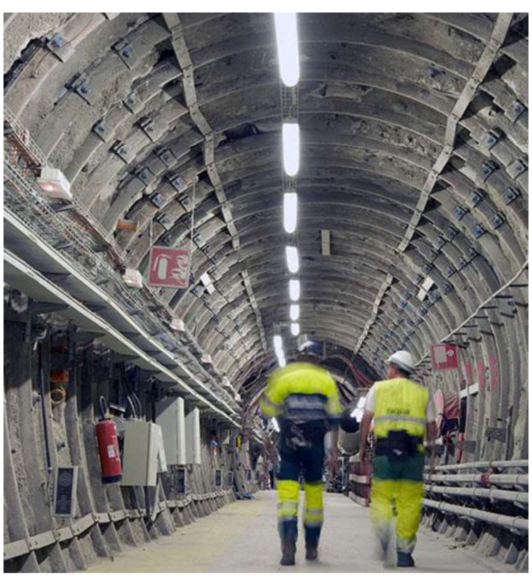

Thank you for your attention

Ce document est la propriété de l'Andra.
Il ne peut être reproduit ou communiqué sans son autorisation expresse et préalable.

References

- Armand, G. et al. (2014). Geometry and Properties of the Excavation Induced Fractures at the Meuse/Haute-Marne URL Drifts. International Journal of Rock Mechanics and Mining Sciences 27(1): 21-41
- Cuss, R. J. et al. (2014). Experimental observations of mechanical dilation at the onset of gas flow in Callovo-Oxfordian claystone. Geological Society, London, Special Publications, 400, 507–519
- de La Vaissière, R. et al. (2014). Gas injection test in the Callovo-Oxfordian claystone: data analysis and numerical modelling. Geological Society, London, Special Publications, 400, 427-441
- de La Vaissière, R., et al. (2019). From Two-Phase Flow to Gas Fracturing into Callovo-Oxfordian Claystone. ARMA. Proceedings of the 53rd U.S. Rock Mechanics/Geomechanics Symposium, 23-26 June, New York, USA
- de La Vaissière, R., et al. (2019). Effect of gas flow rate on gas fracturing in Callovo-Oxfordian claystone. ISRM. Proceedings of the 14th International Congress on Rock Mechanics and Rock Engineering, September 13-18, Foz do Iguassu, Brazil
- Harrington, Jon F. et al. (2017). Gas transport properties through intact and fractured Callovo-Oxfordian mudstones. Geological Society, London, Special Publications, 454.
- Marschall, P. et al. (2005). Characterisation of Gas Transport Properties of the Opalinus Clay, a Potential Host Rock Formation for Radioactive Waste Disposal. Oil & gas science & technology 60 (1): 121-139.
- Senger , R. et al. (2006). Design and analysis of a gas threshold pressure test in a low-permeability clay formation at Andra's Underground Research Laboratory, Bure (FRANCE). Proceedings, TOUGH Symposium 2006, Lawrence Berkeley National Laboratory, Berkeley, California, May 15–17, USA

Appendix Q. The FEBEX In Situ Test: An 18-year long Simulation of an engineered barrier (M. V. Villar)

THE FEBEX IN SITU TEST: AN 18-YEAR LONG SIMULATION OF AN ENGINEERED BARRIER

María Victoria Villar
CIEMAT, Madrid

DOCTORAL SCHOOL
EURAD WP GAS & WP HITEC
28 August – 1 September 2023, Liege (BE)

GOBIERNO DE ESPAÑA
MINISTERIO DE CIENCIA E INNOVACIÓN
Ciemat
Centro de Investigaciones Energéticas, Medioambientales y Tecnológicas
UE 23
eurad
European Joint Programme on Radioactive Waste Management

Outline

- Introduction: geological disposal of nuclear waste and engineered barriers
- The FEBEX project and the in situ test
- Partial dismantling of the in situ test after 5 years
- FEBEX-DP: dismantling of the in situ test after 18 years operation
- Postmortem analysis of some THM properties

Buffer/backfill in HLW repositories

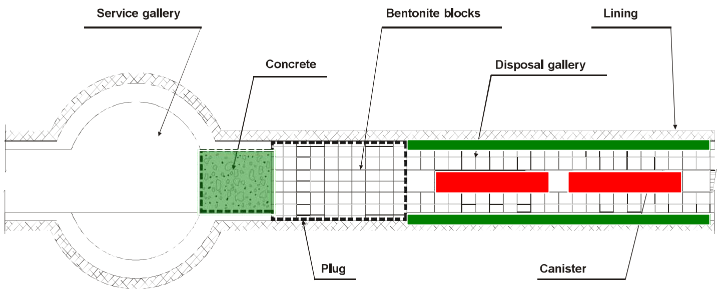

ENRESA: clay host rock

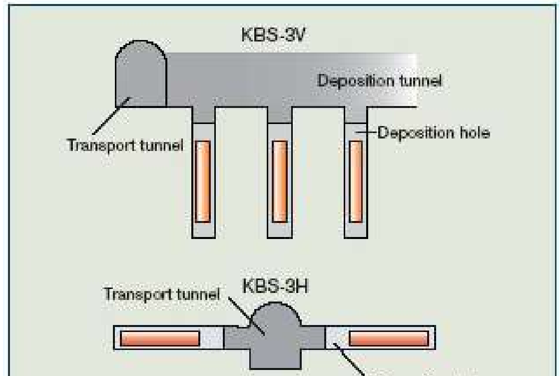

SKB: crystalline host rock

	FUNCTIONS	MATERIALS	
BUFFER	limit the entry of water, contribute to radionuclide retention and heat dissipation, provide mechanical protection for the canisters	Bentonite (expansive, smectite-rich material, can retain elements in its structure) Mixtures of bentonite and aggregates: crushed granite, basalt, quartz, zeolytes, graphite	

The barrier during the transient stage

PROCESSES: hydration + heating + radiation

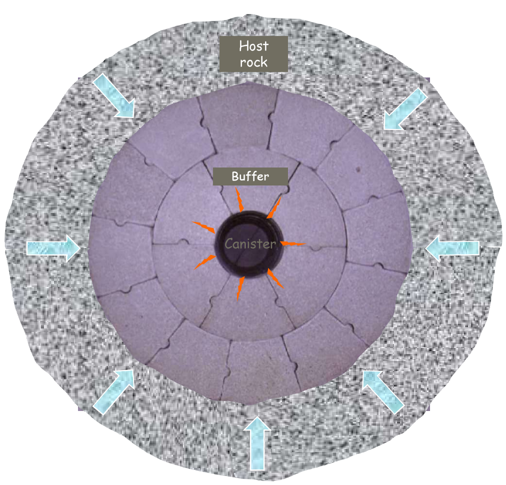

Hydration with groundwater:

Development of swelling pressure

Sealing of voids, microstructural reorganisation

Compression of air in pores

Chemical changes

Heating from the canister:

Drying near the heater: cracking?

Vapour diffusion/advection

Chemical and mineralogical changes

Gas generation and transport

SPANISH CONCEPT FOR DISPOSAL IN GRANITE

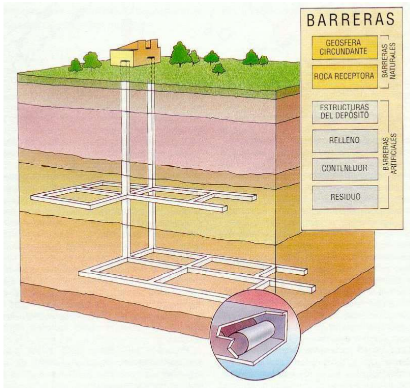

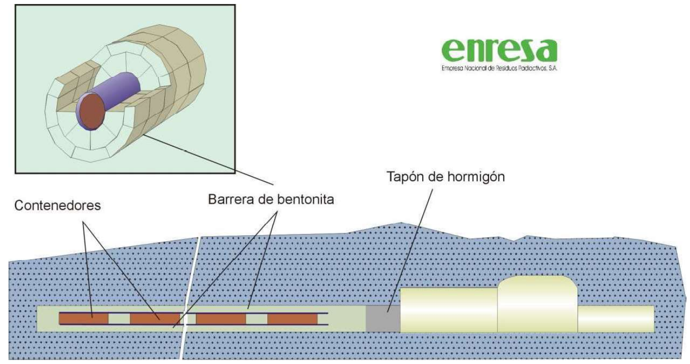

- Barrier thickness: 0.75 m
- Barrier dry density: 1.65 g/cm^3, initial water content: hygroscopic
- Initial degree of saturation: 50-60 %
- Maximum temperature at canister surface: 100ºC

FEBEX PROJECT

Study of the behaviour of the near-field components of a high level radioactive waste repository in crystalline rock

1. *In situ* test under natural conditions and at full scale (Grimsel, Switzerland)

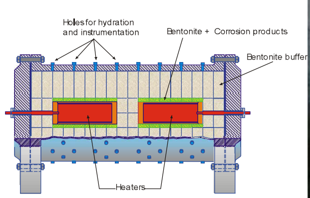

2. Mock-up test at almost full scale (CIEMAT, Madrid)

3. **A series of laboratory tests to complement the information from the two large-scale tests: process understanding, determination of parameters**
4. **THM-THG modelling: model development, data interpretion, prediction**

FEBEX IN SITU TEST AT GRIMSEL UNDERGROUND LABORATORY (GTS)

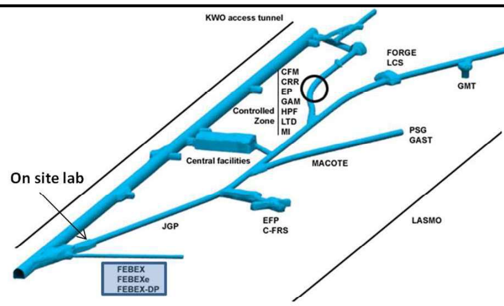

- Underground laboratory excavated in granite at 1730 m.a.s.l. and depth 500 m
- The FEBEX in situ test simulated at a large scale the components of the near field of an underground repository of nuclear waste
- Natural hydration from the host rock and two heaters simulating the waste containers
- Engineered barrier of compacted bentonite blocks

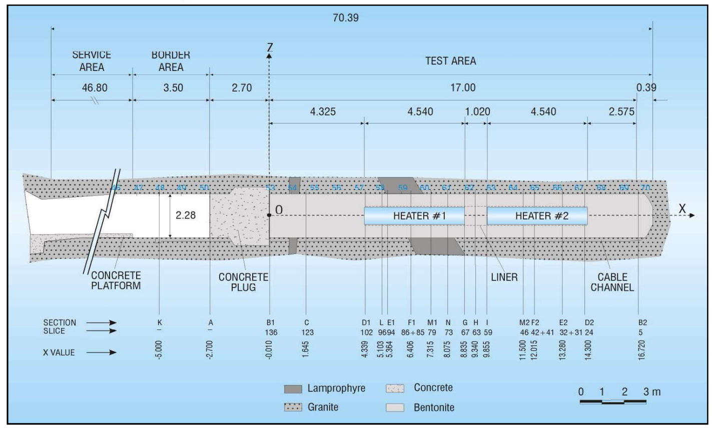

FEBEX IN SITU TEST: INITIAL DESIGN

FEBEX

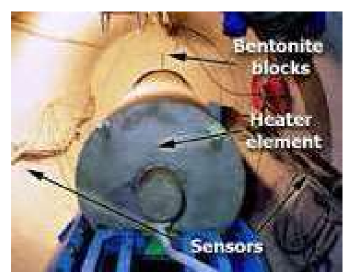

- Full-scale in situ test at GTS
- Barrier of FEBEX bentonite blocks, natural hydration, two heaters at 100°C
- Steal perforated liner to align the heaters along the gallery
- Sensors in bentonite and rock
- Instrumented boreholes in granite to follow hydrogeological evolution
- Tracers
- Concrete plug to close the gallery
- In operation since 1997
- Partial dismantling in 2002
- Final complete dismantling in 2015

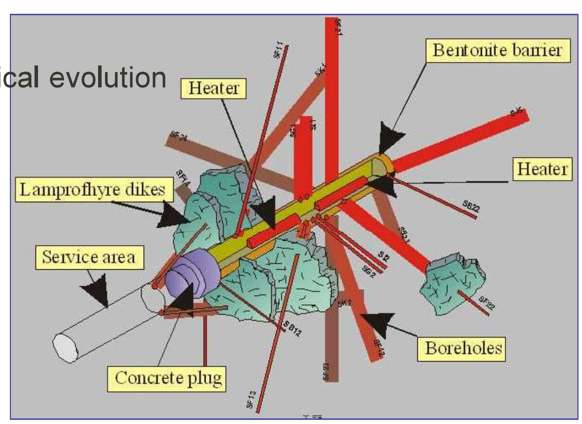

FEBEX IN SITU TEST: PREPARATION AND ASSEMBLY (1996-1997)

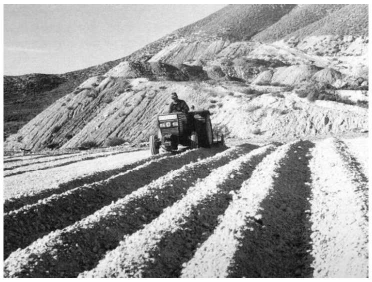

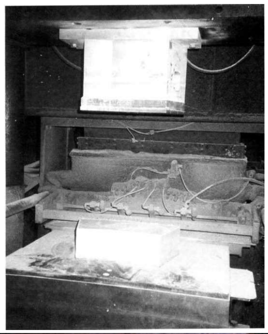

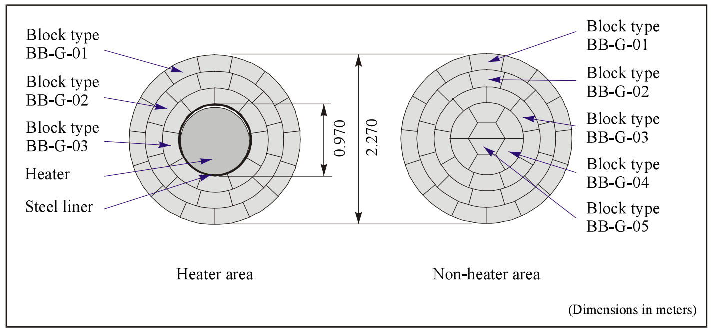

•The FEBEX bentonite came from the Cortijo de Archidona quarry (Almería, SE Spain), it consists of >90% of montmorillonite and Ca, Mg and Na as exchangeable cations

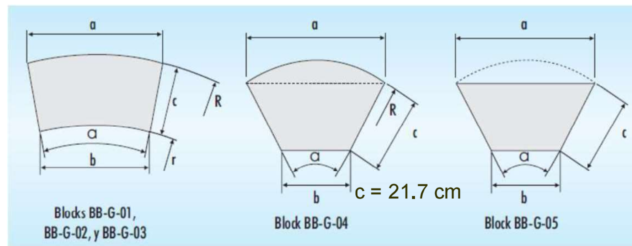

The sealing material was a barrier of bentonite blocks. The bentonite was compacted at a dry density of 1.70 g/cm^3 with its hygroscopic water content (14%): resulting barrier density 1.60 g/cm^3 (gap volume ~6%)

FEBEX IN SITU TEST: PREPARATION AND ASSEMBLY (1996-1997)

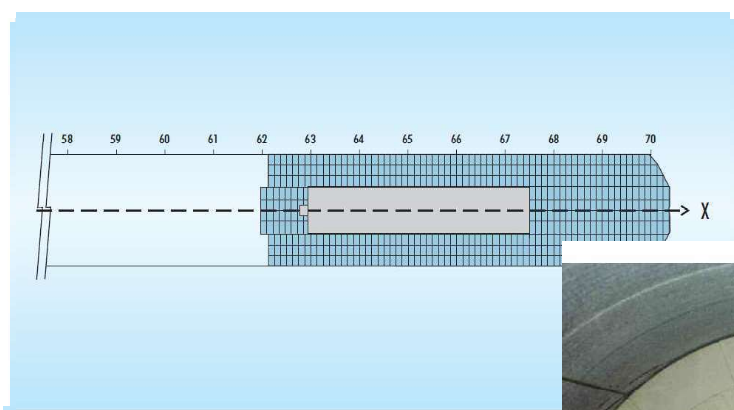

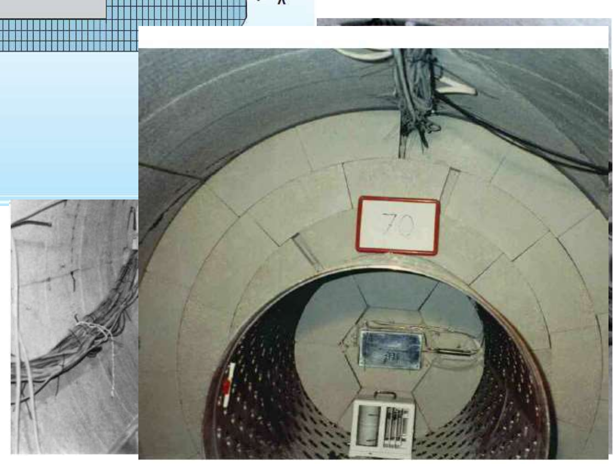

FEBEX IN SITU TEST: PREPARATION AND ASSEMBLY (1996-1997)

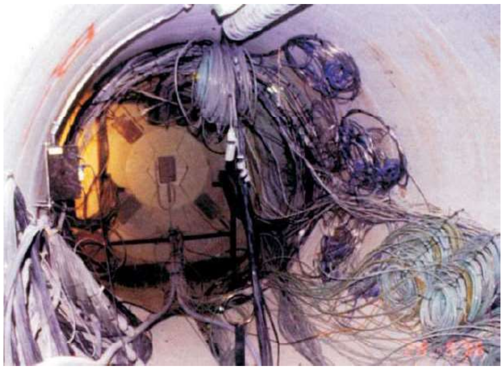

https://www.grimsel.com/images/stories/videos/febex.mp4

FEBEX IN SITU TEST: INITIAL EVOLUTION (5 YEARS)

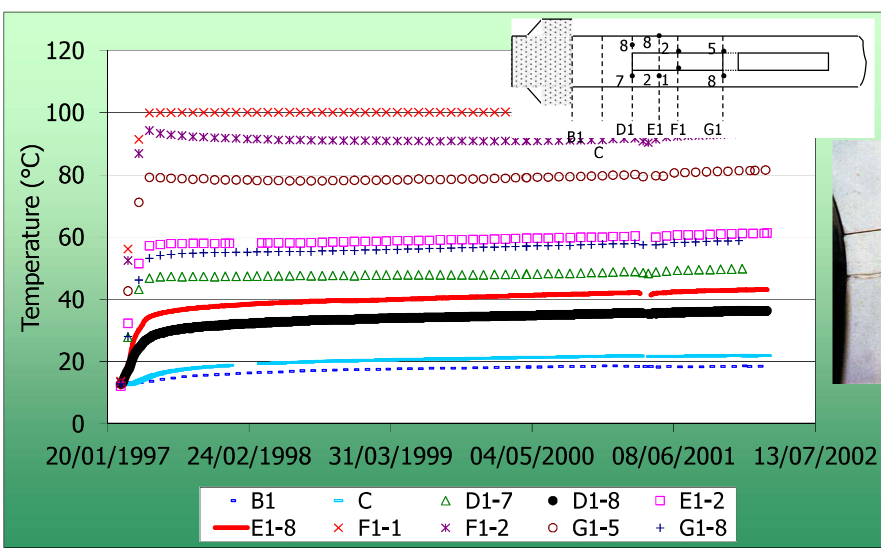

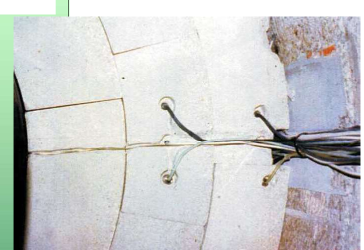

Bentonite section around heater 1

FEBEX IN SITU TEST: INITIAL EVOLUTION

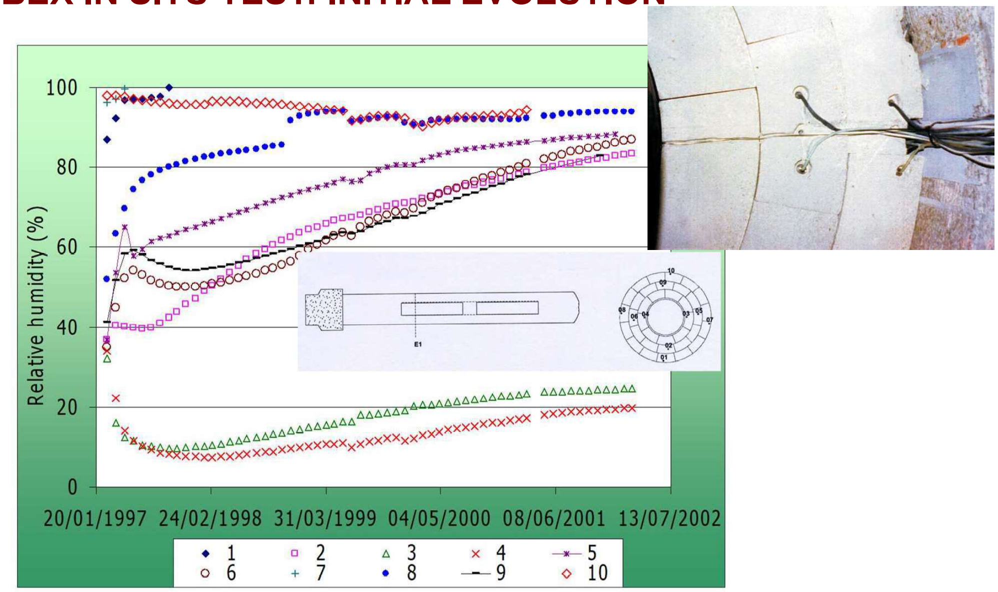

$$s = -10^{-6}\,\frac{R \times T}{V_w}\ln\left(\frac{HR}{100}\right)$$

Bentonite section around heater 1

TH coupling

How does temperature affect saturation?

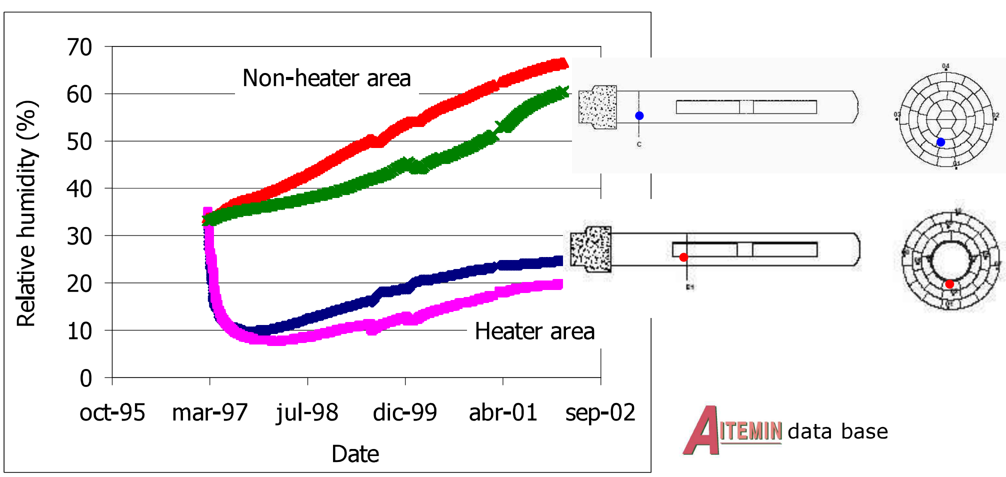

AITEMIN data base

Five years operation

FEBEX

THM coupling

Stress paths in FEBEX *in situ* test

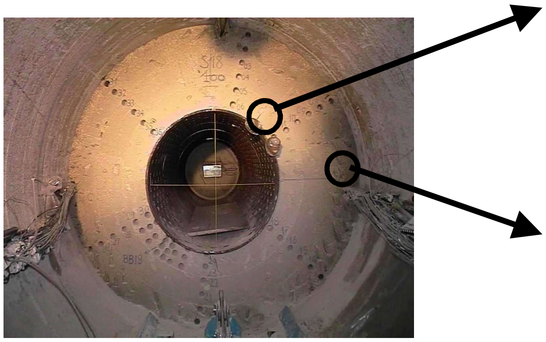

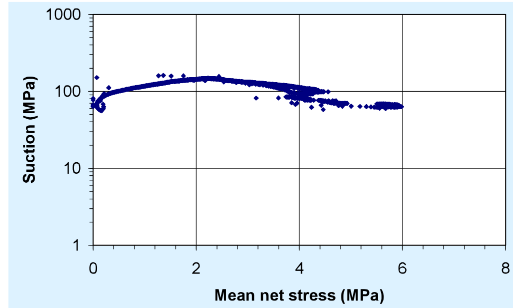

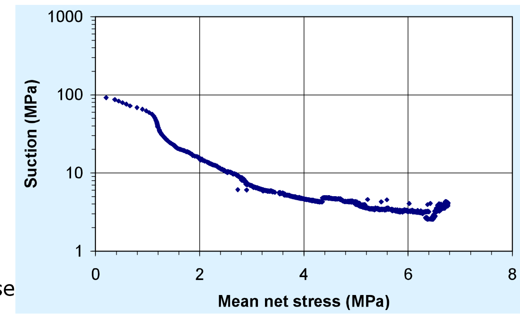

$$s = -10^{-6}\frac{R \times T}{V_w}\ln\left(\frac{HR}{100}\right)$$

AITEMIN data base

FEBEX

FEBEX IN SITU TEST: PARTIAL DISMANTLING (2002)

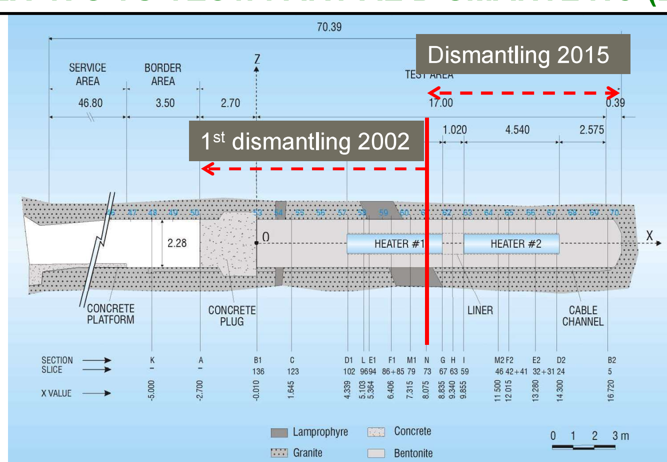

- After 5 years operation (heating + natural hydration) half of the experiment was dismantled
- Samples of bentonite and other materials were taken
- The void left by the back of heater 1 was replaced by a steel dummy
- The gallery was closed again with a concrete plug

AIMS OF PARTIAL DISMANTLING

Characterise the state of the barrier → Validate the sensors performance and the THM and THG models

Determine changes in bentonite properties → Check the performance and durability of the barrier

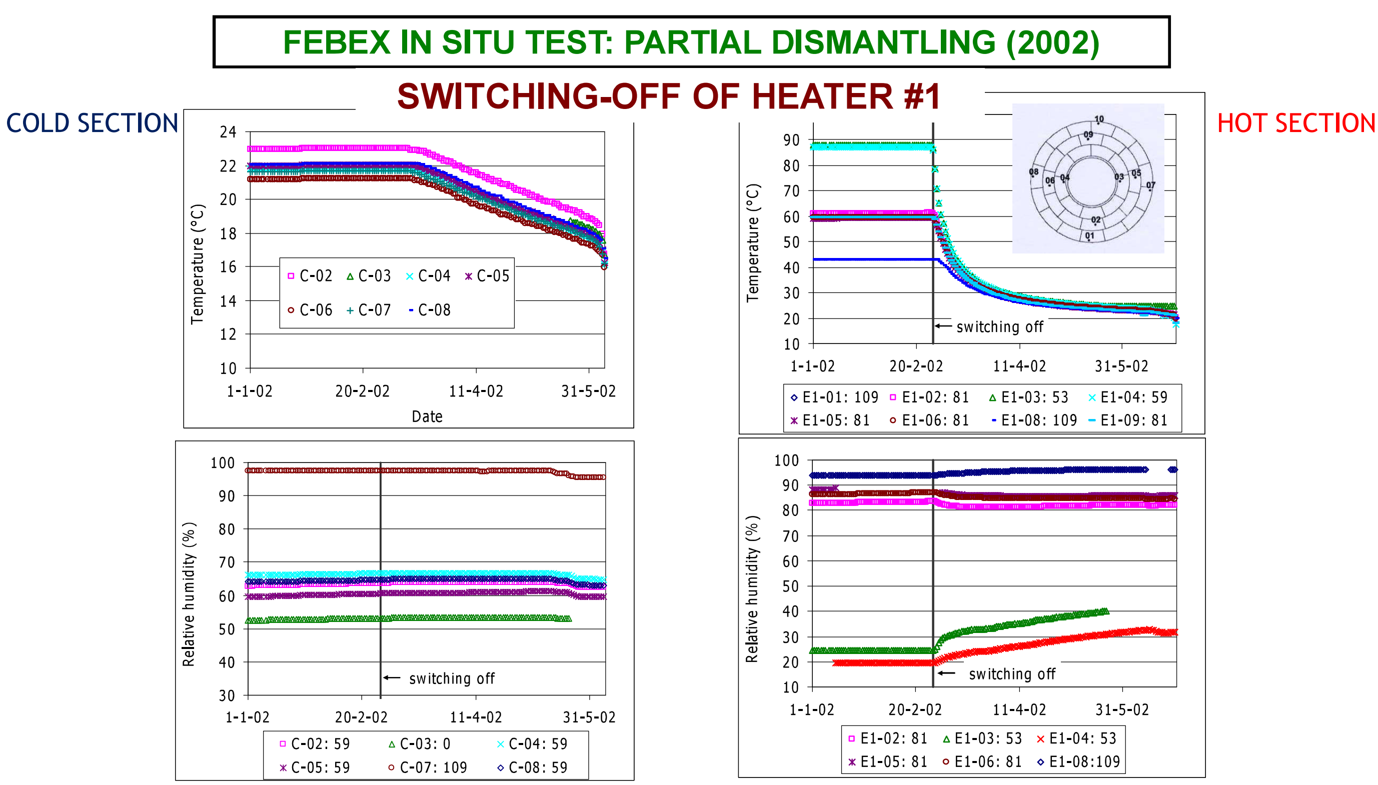

FEBEX IN SITU TEST: PARTIAL DISMANTLING (2002)

CONCRETE PLUG DEMOLITION

FIRST BENTONITE SLICES ARE REACHED

FEBEX IN SITU TEST: PARTIAL DISMANTLING (2002)

HEATER #1 EXTRACTION

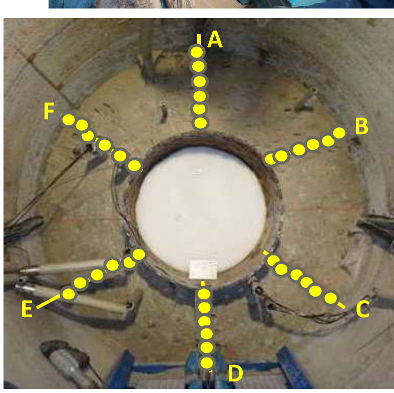

BENTONITE (AND OTHER MATERIALS) SAMPLING

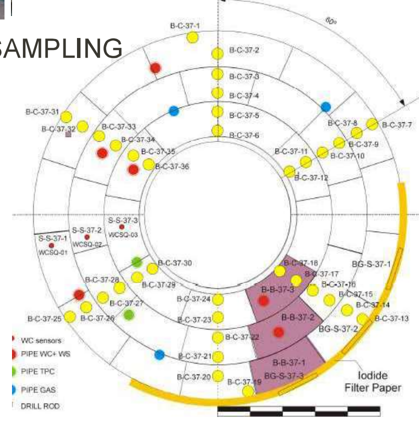

FEBEX IN SITU TEST: PARTIAL DISMANTLING (2002)

SAMPLING

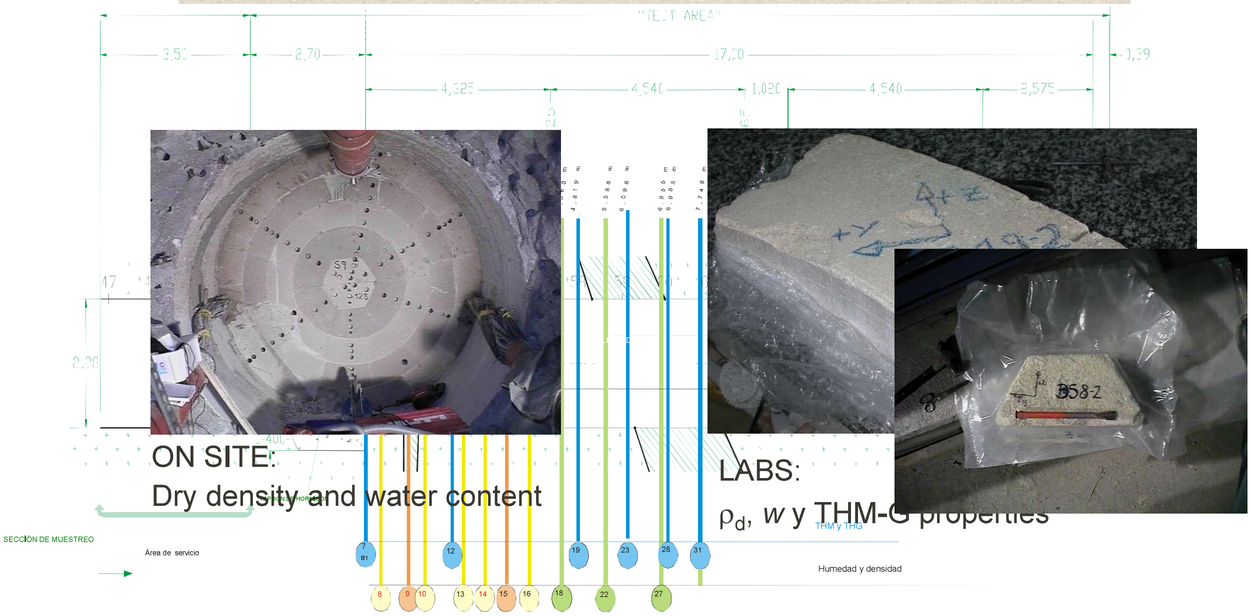

PARTIAL DISMANTLING: GAP SEALING

1997 | 2002

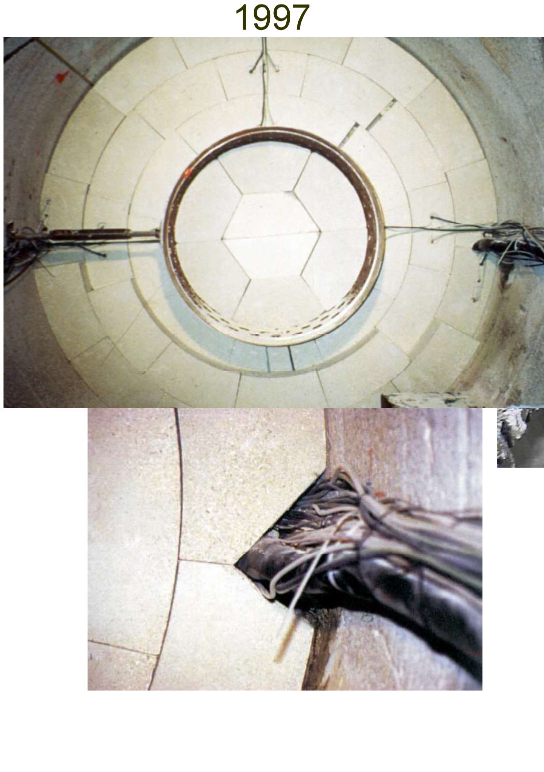

PARTIAL DISMANTLING: GAP SEALING

1997

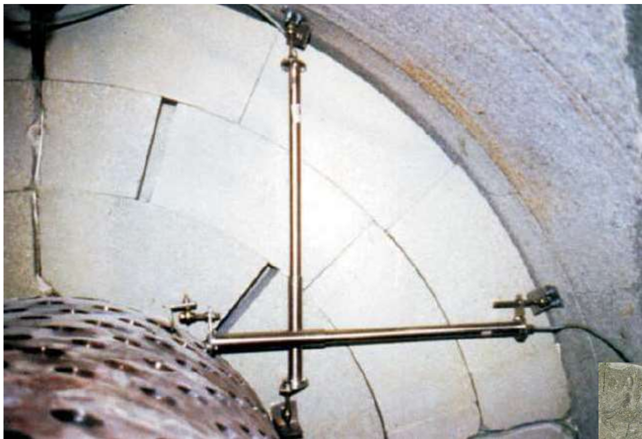

2002

HM coupling: changes in density

Filling of gaps: decrease of the density of bentonite

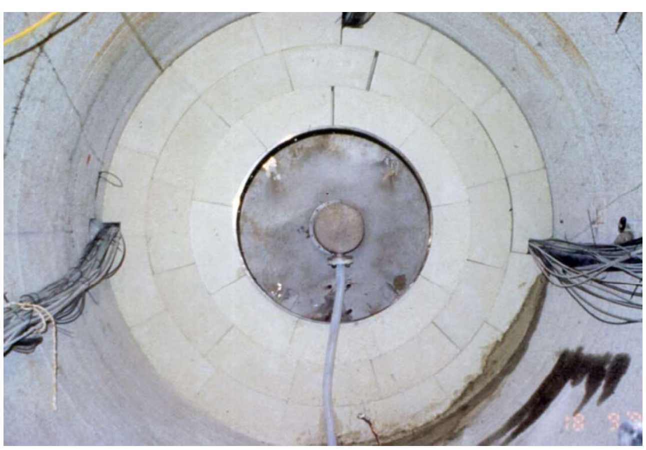

Initial block dry density: 1.70 g/cm^3

After 5 years: ρ_d=1.60 g/cm^3

FEBEX

Hydration: changes in water content

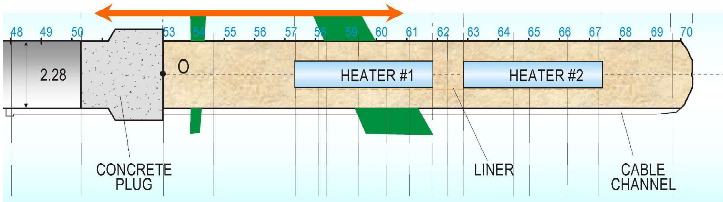

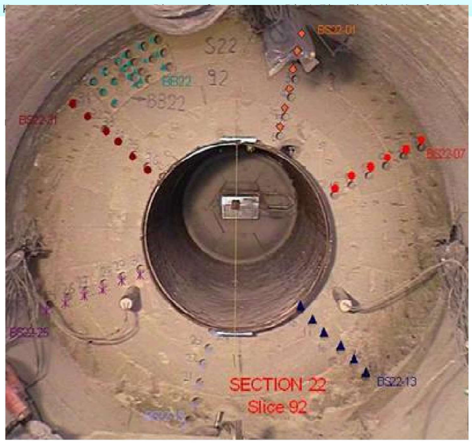

Partial dismantling after
5 years operation

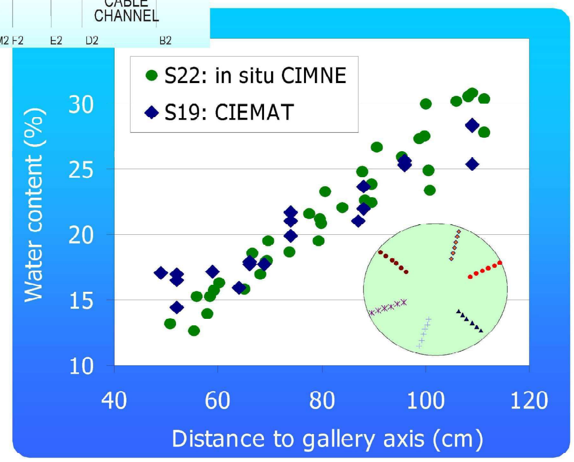

Villar *et al*. 2004

Hydration: changes in density

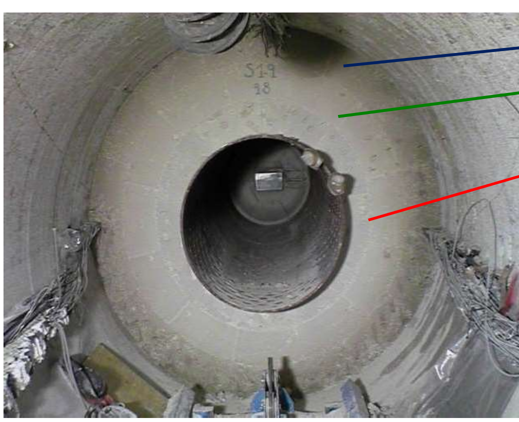

	ρ_d (g/cm^3)	w (%)	S_r (%)
External ring	1.51	27.6	95
Middle ring	1.59	21.8	85
Inner ring	1.65	16.1	67

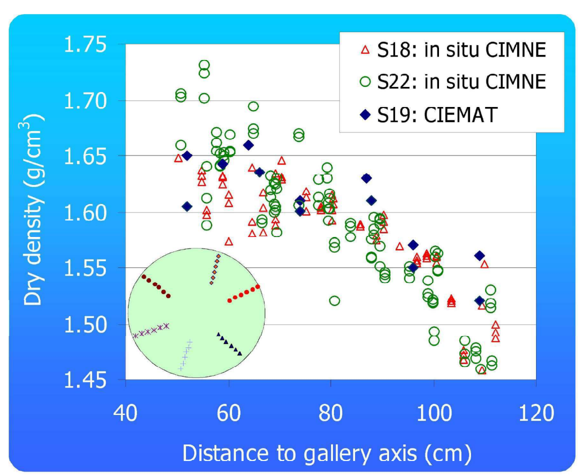

DENSITY AND WATER CONTENT AFTER 5 YEARS OPERATION AND 4 MONTHS COOLING

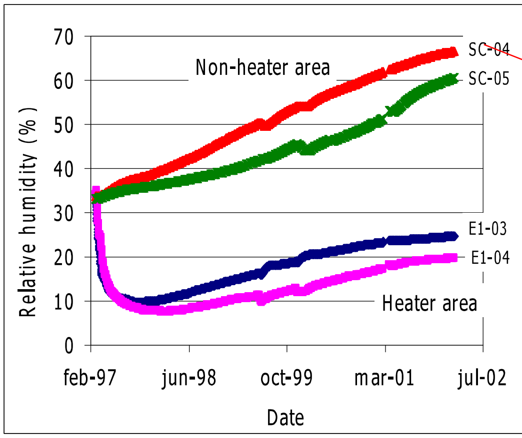

SENSORS PLACED AT 54 cm FROM GRANITE

$$s = -10^{-6}\frac{R \times T}{V_w}\ln\left(\frac{HR}{100}\right)$$

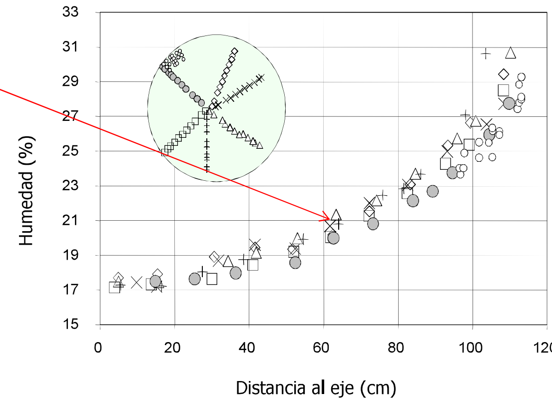

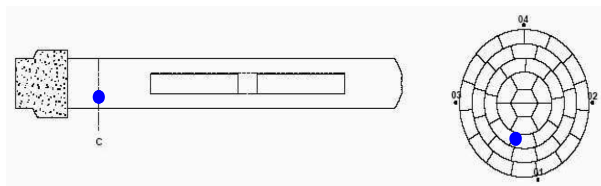

FEBEX IN SITU TEST: PARTIAL DISMANTLING

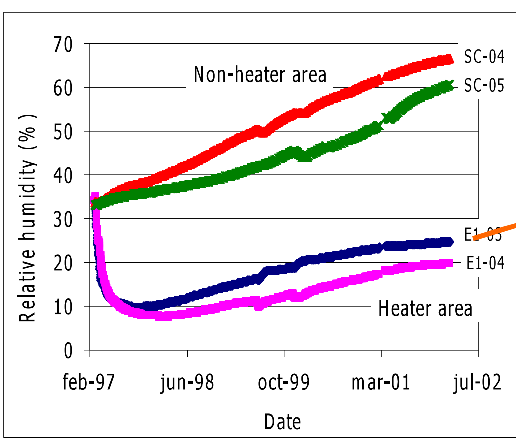

SENSORS PLACED AT 54 cm FROM GRANITE

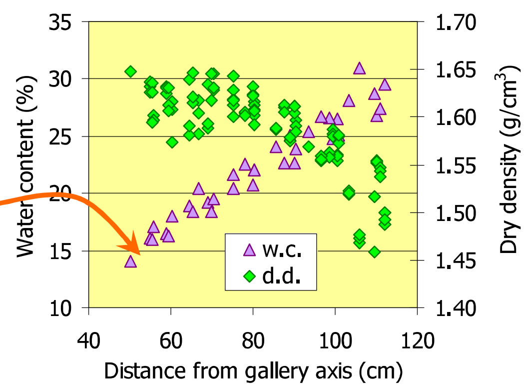

SECTION AROUND THE HEATER

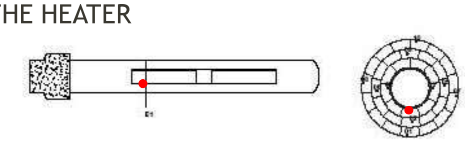

The relative humidity measured by the sensors can be converted into suction by Kelvin's law and related to water content via the water retention curves determined in the untreated bentonite at different dry densities

$$s = -10^{-6}\frac{R \times T}{V_w}\ln\left(\frac{HR}{100}\right)$$

FEBEX IN SITU TEST: OPERATION FROM 2002 TO 2015

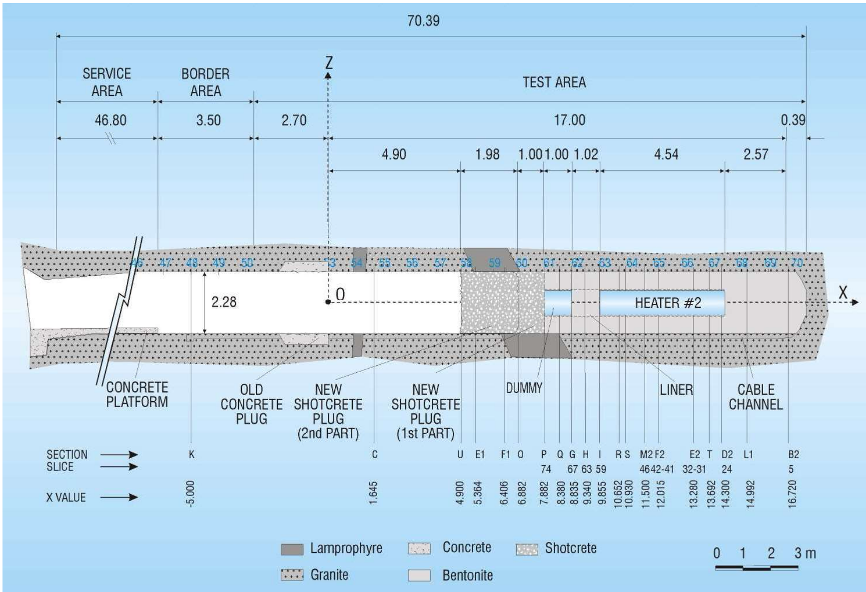

- The void left by the back of heater 1 was replaced by a steel dummy
- The gallery was closed again with a concrete plug and the experiment run for other 13 years
- Most sensors failed in this period

FEBEX IN SITU TEST: OPERATION FROM 2002 TO 2015 AND HEATER #2 SWITCHING OFF

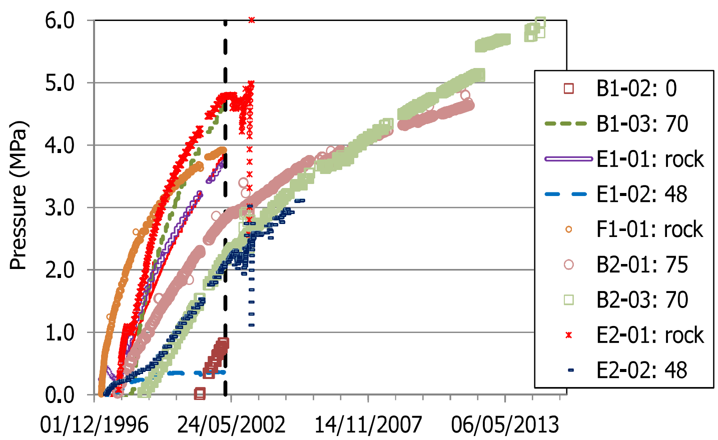

Total pressure evolution measured inside the bentonite from the beginning of operation. The distance of the sensor from the gallery axis is indicated in cm (rock: granite/bentonite contact), the dotted vertical line indicates the start of partial dismantling (Villar et al. 2020)

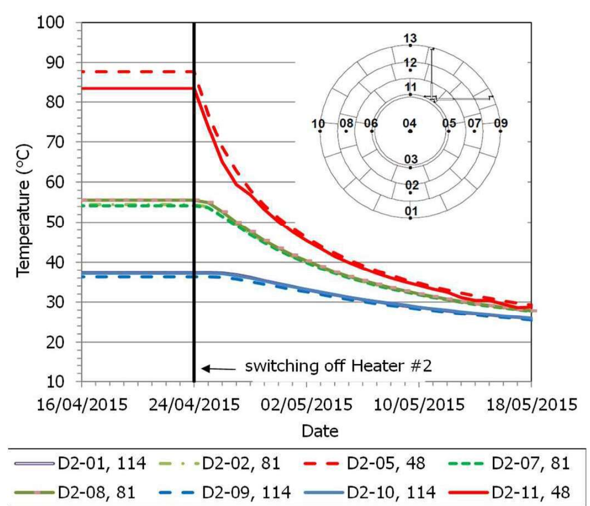

IN SITU FEBEX TEST: FINAL DISMANTLING (2015)

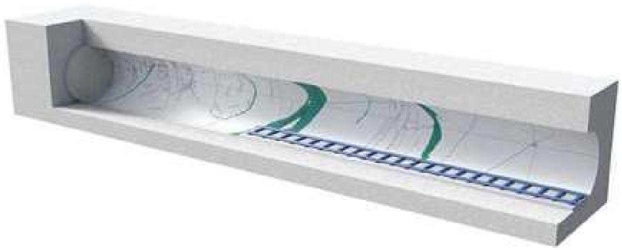

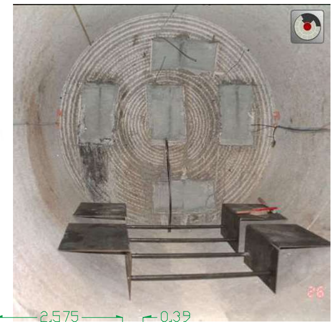

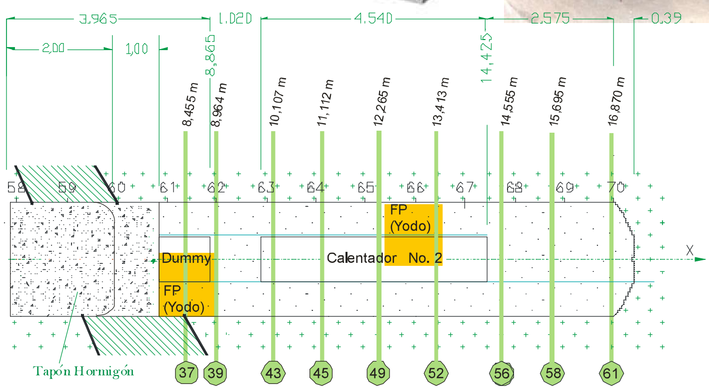

STATE OF THE BARRIER AFTER 18 YEARS OPERATION: VISUAL INSPECTION

The joints between blocks had dissapeared, as it was already observed in 2002

1997

2015

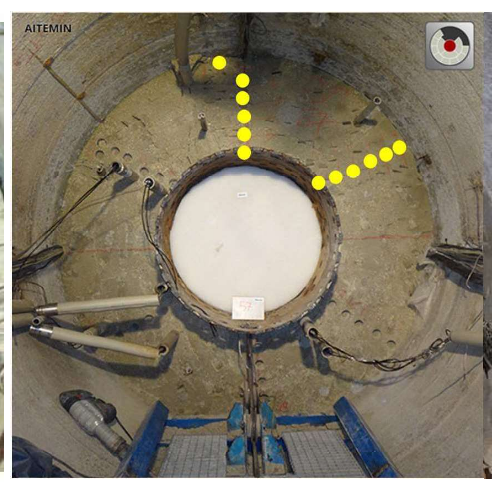

FINAL DISMANTLING: GAP SEALING

There were no gaps in the barrier, as it was already observed in 2002

1997

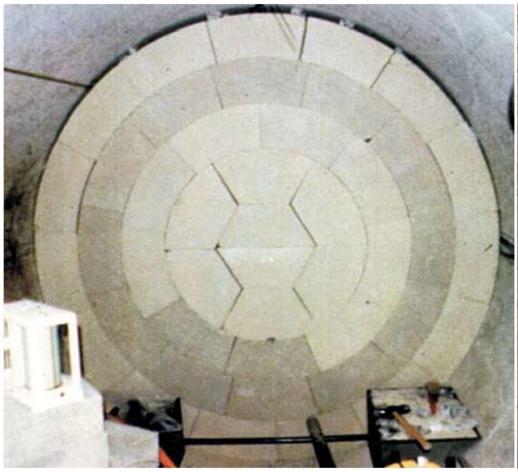

2015

STATE OF THE BARRIER AFTER 18 YEARS OPERATION: VISUAL INSPECTION

The contact between adjacent vertical sections and between granite and bentonite was tight

The bentonite intruded through the liner holes

STATE OF THE BARRIER AFTER 18 YEARS OPERATION: VISUAL INSPECTION

Sensor and other metallic elements: corrosion, stains

METHODOLOGY OF ONSITE ANALYSES

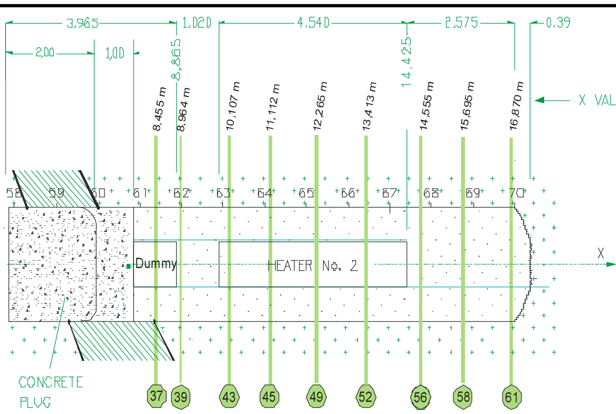

Sampling following a radial pattern

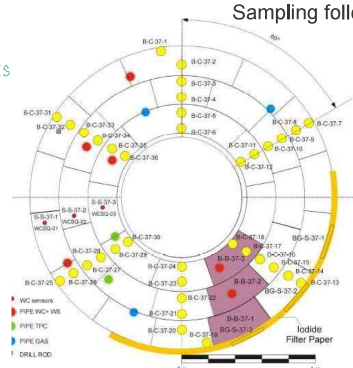

Drilling following a template

4-5 cm long core preserved before determination

Splitting the core in two, removing external parts, smoothing surfaces

Immersion of the samples in mercury to determine its volume befor drying in the oven

GOBIERNO DE ESPAÑA MINISTERIO DE ECONOMÍA Y COMPETITIVIDAD
Ciemat Centro de Investigaciones Energéticas, Medioambientales y Tecnológicas
Aitemin Centro Tecnológico

ONSITE MEASUREMENTS DURING DISMANTLING

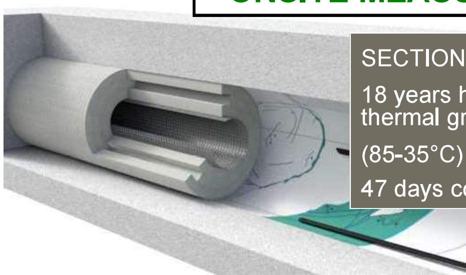

SECTION 43

18 years hydration under thermal gradient

(85-35°C)

47 days cooling

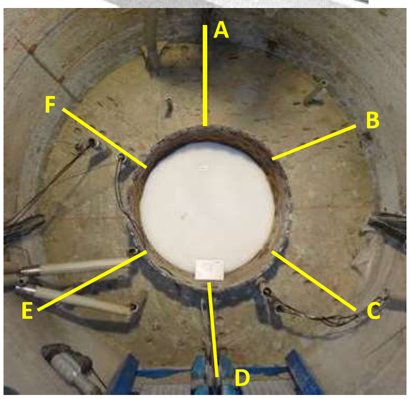

Average

w: 27.2%

ρ_d: 1.59 g/cm^3

S_r: 105%

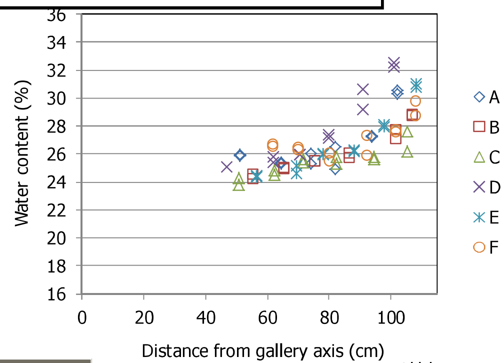

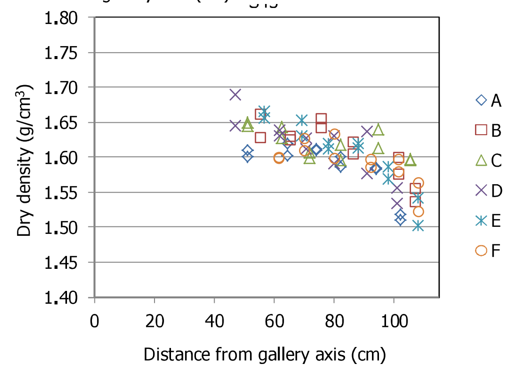

ONSITE MEASUREMENTS DURING DISMANTLING

SECTION 56

18 years hydration at T <36-88°C

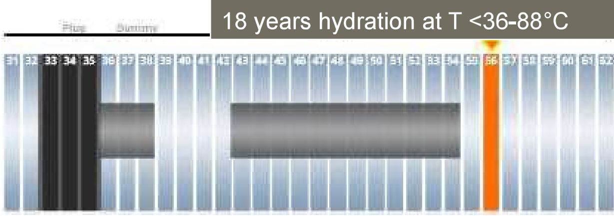

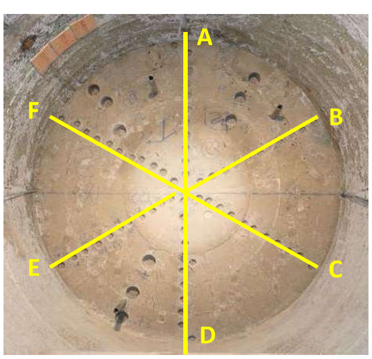

Average:

w: 26.0%

ρ_d: 1.57g/cm^3

S_r: 97%

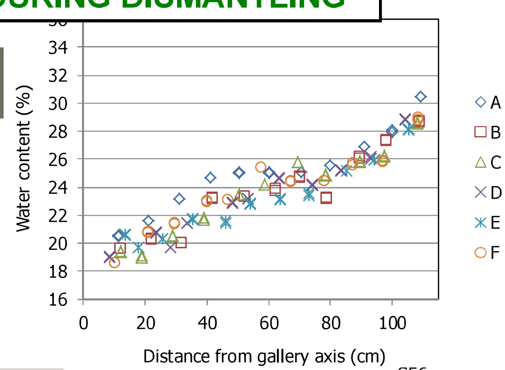

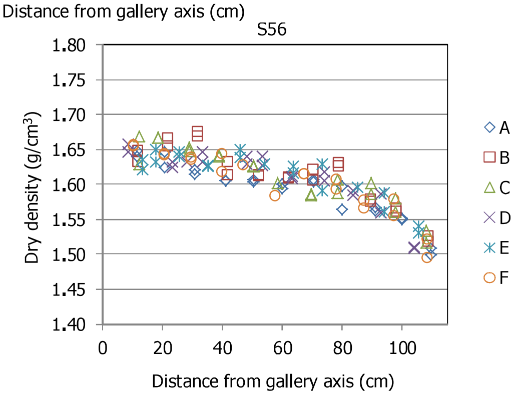

AXIAL SYMMETRY: COMPARISON “COOL/HOT” SECTIONS

WATER CONTENT

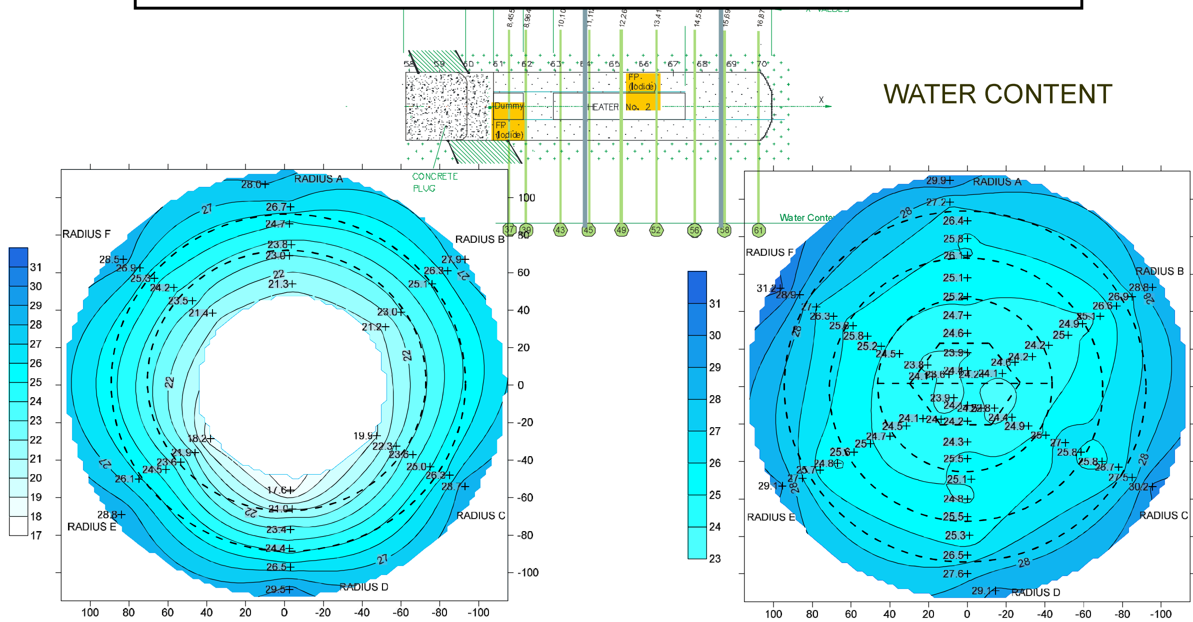

HOT SECTION (S45)

COOL SECTION (S58)

AXIAL SYMMETRY: COMPARISON “COOL/HOT” SECTIONS

DRY DENSITY

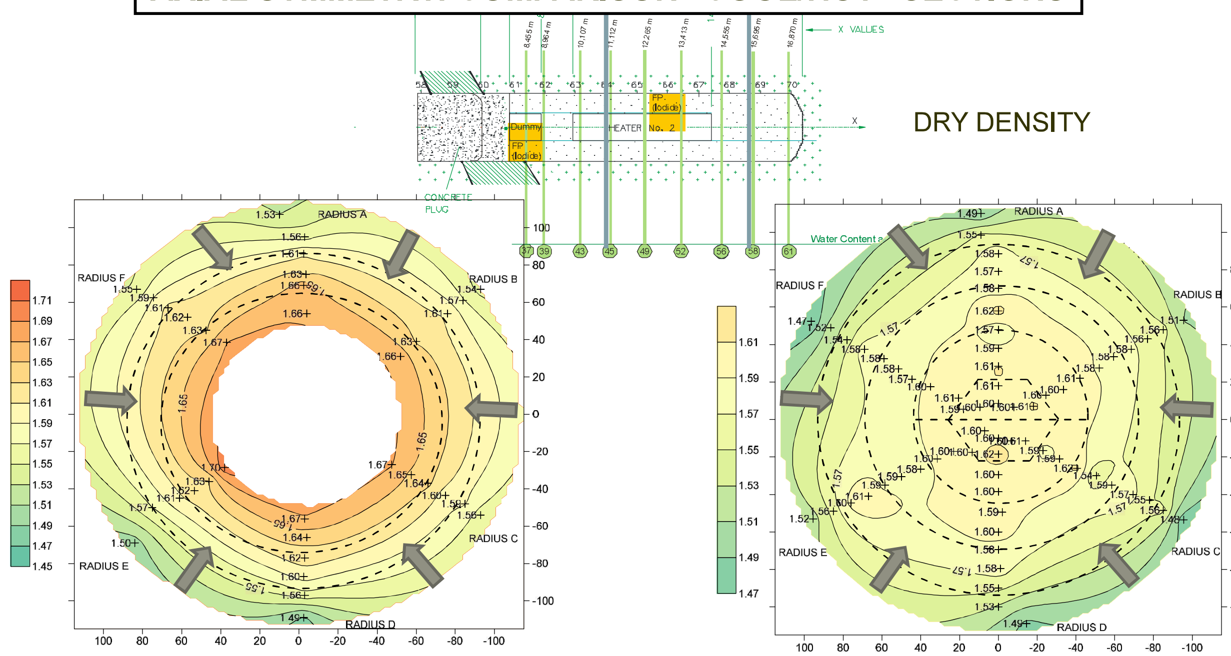

HOT SECTION (S45)

COOL SECTION (S58)

COMPARISON 5 – 18 YEARS OPERATION

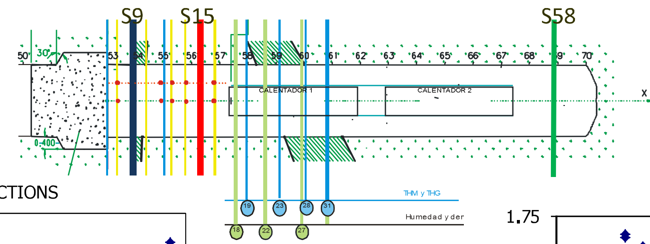

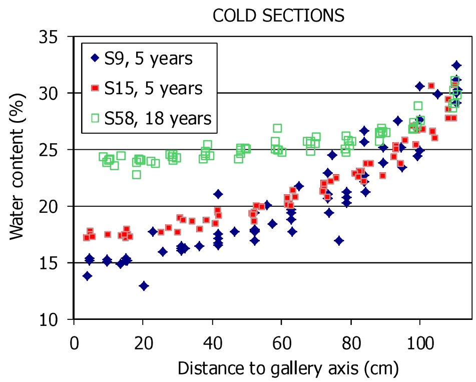

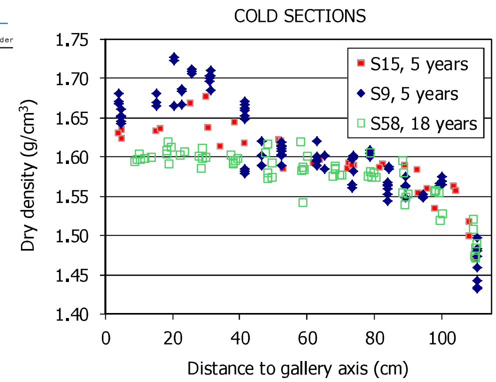

***w*, %** S9: 22.9%
S15: 22.8%
S58: 27.1%

S_r, % S9: 85%
S15: 86%
S58: 98%

ρ_d, g/cm³ S9: 1.58 g/cm³
S15: 1.58 g/cm³
S58: 1.55 g/cm³

COMPARISON 5 – 18 YEARS OPERATION

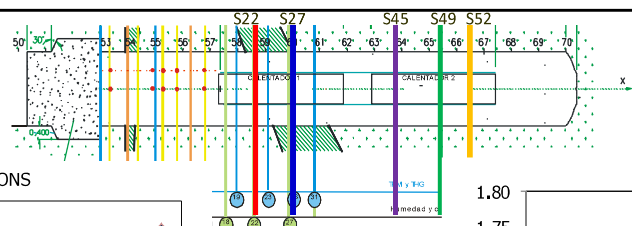

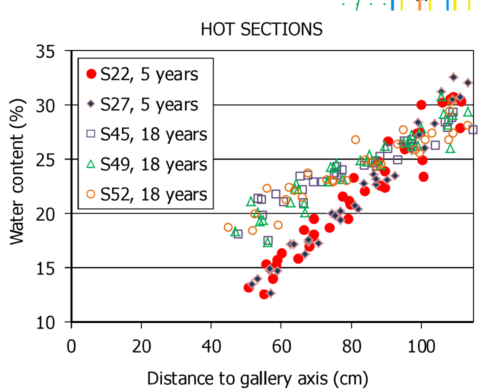

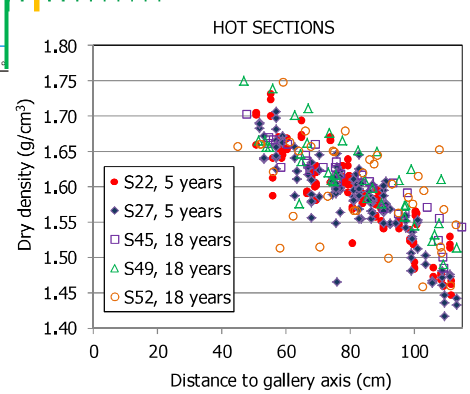

S22: 22.6% S45: 25.7%
S27: 22.6% S49: 25.9%
S52: 25.6%

S22: 85% S45: 98%
S27: 84% S49: 99%
S52: 98%

S22: 1.57 g/cm³ S45: 1.59 g/cm³
S27: 1.56 g/cm³ S49: 1.59 g/cm³
S52: 1.59 g/cm³

LONGITUDINAL DISTRIBUTION OF WATER CONTENT

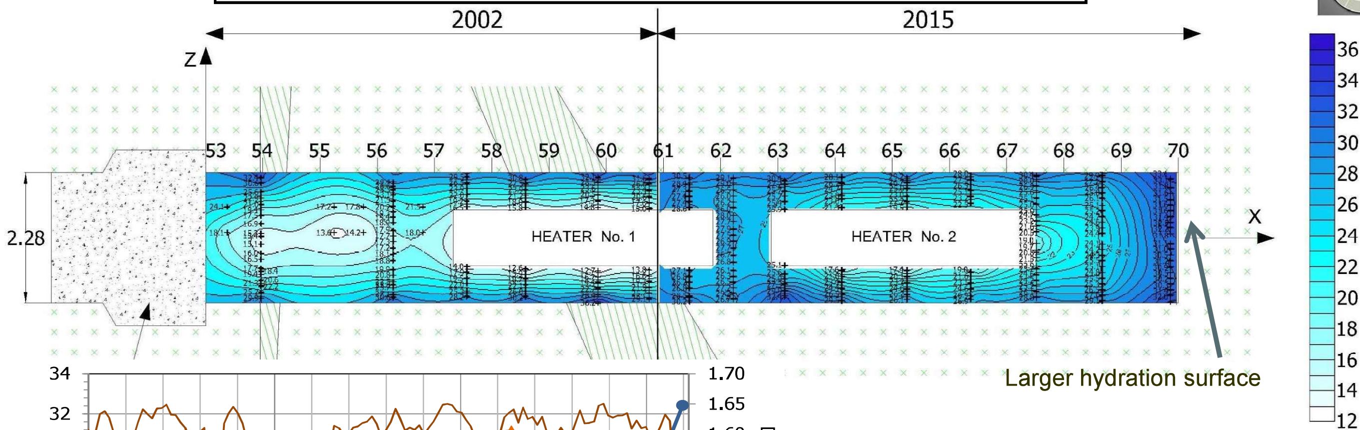

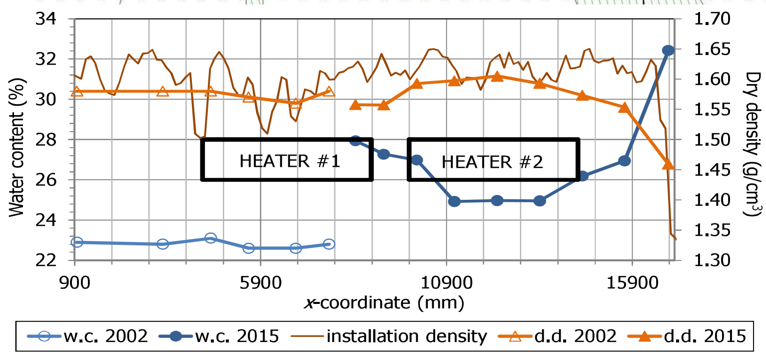

Dismantling date	*w* (%)	Installation ρ_d (g/cm^3)	ρ_d (g/cm^3)	S_r (%)
2002	22.9	1.59	1.58	87
2015	26.7	1.61	1.57	100

LONGITUDINAL DISTRIBUTION OF DRY DENSITY

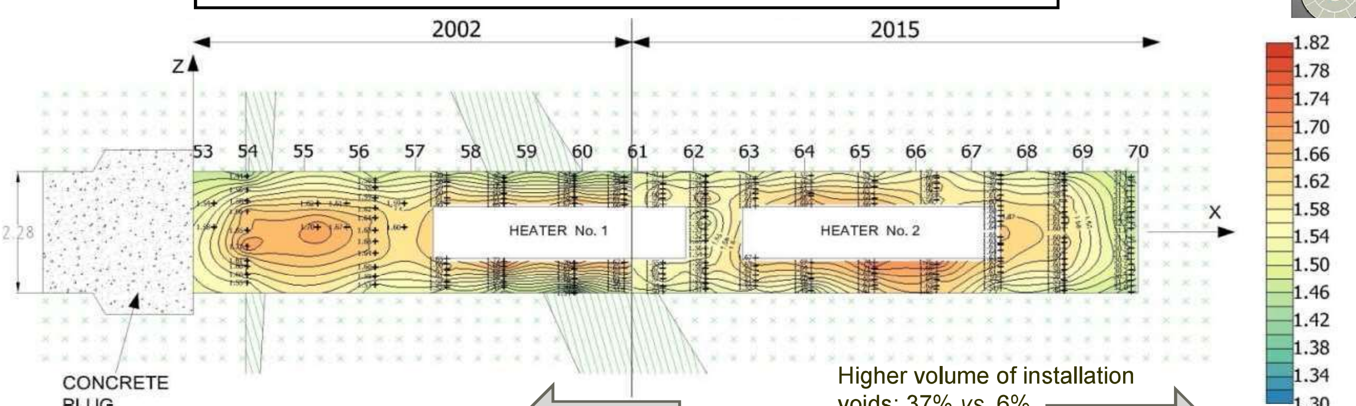

Higher volume of installation voids: 37% *vs.* 6%

FORWARDS

BACKWARDS

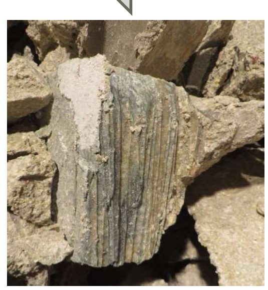

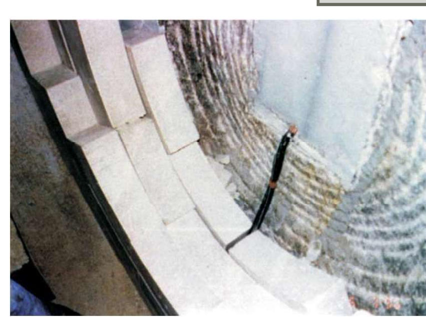

SAMPLING OF BLOCKS AND CORES FOR THM-G DETERMINATIONS IN LABS

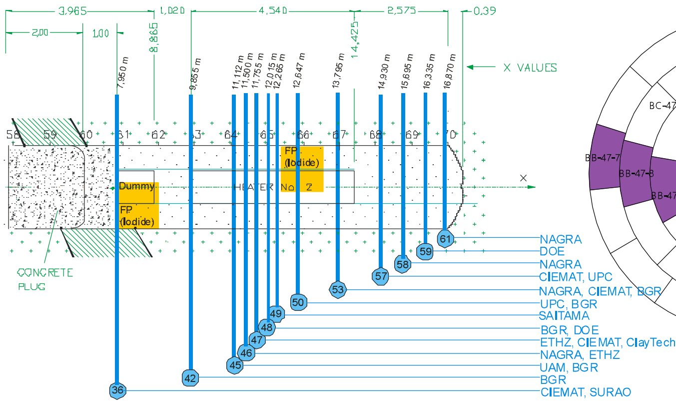

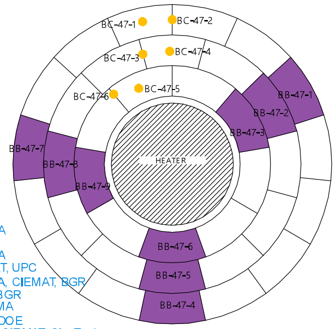

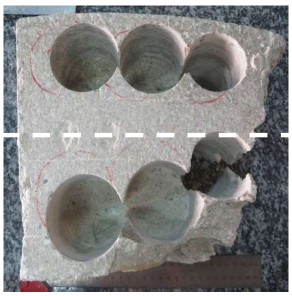

The hydro-mechanical properties of the FEBEX bentonite have been studied for many years. They depend mainly on the bentonite water content and dry density. Empirical correlations between permeability, swelling pressure, thermal conductivity, etc. and dry density and water content have been obtained over the years. In the labs these properties were determined in samples from the in situ test and compared with those of the untreated bentonites

THM PROPERTIES OF BARRIER SAMPLES AFTER OPERATION FOR 18 YEARS: THERMAL CONDUCTIVITY

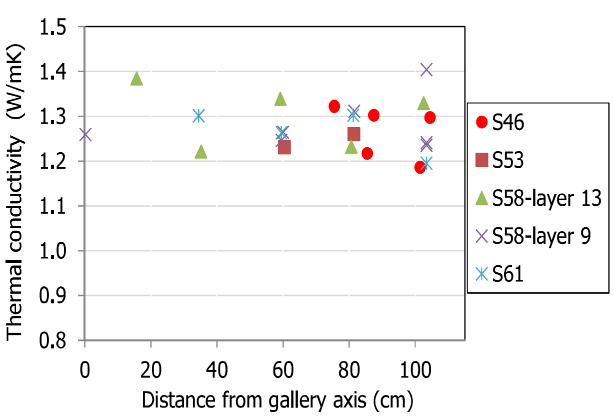

Thermal conductivity measured on site in different sampling sections

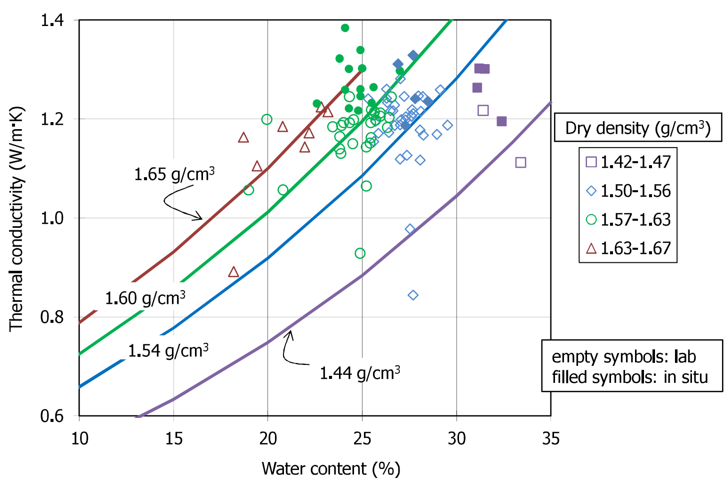

Comparison of values measured on site with empirical correlations obtained in untreated bentonite

THM PROPERTIES OF BARRIER SAMPLES AFTER OPERATION FOR 18 YEARS: WATER RETENTION AND HYDRAULIC CONDUCTIVITY

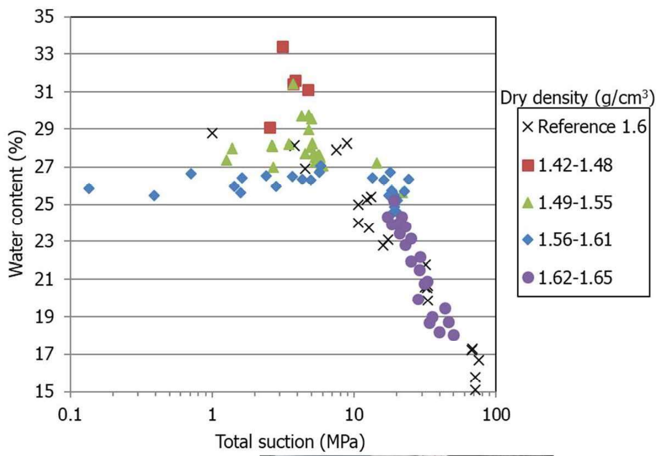

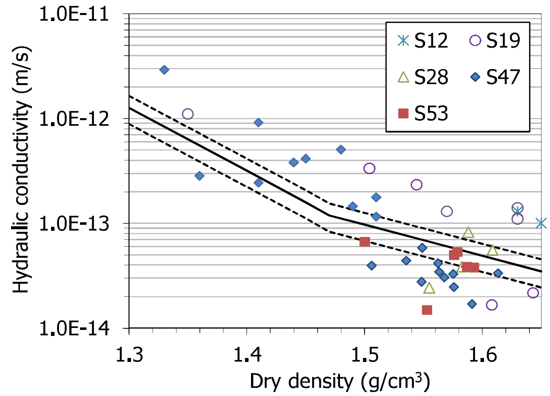

Measurement of suction in the lab with psychrometers

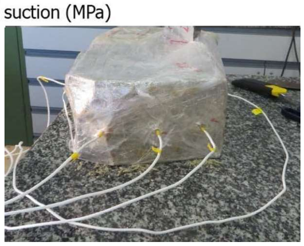

THM PROPERTIES OF BARRIER SAMPLES AFTER OPERATION FOR 18 YEARS: GAS PERMEABILITY: EFFECT OF JOINTS

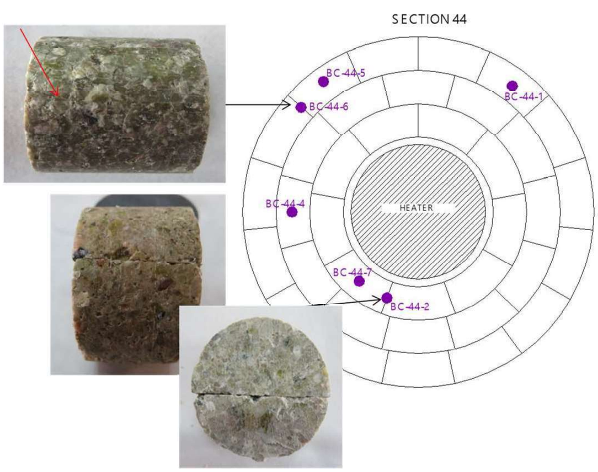

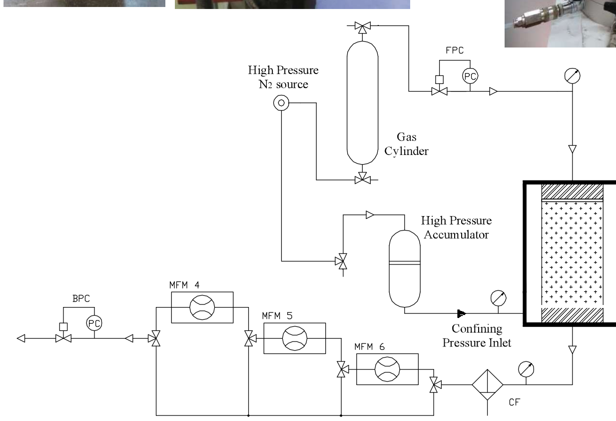

TRIMMING OF SAMPLES DRILLED FROM THE BLOCKS ON SITE (SOME IN THE MIDDLE OF BLOCKS AND OTHERS BETWEEN TWO BLOCKS) AND MEASUREMENT OF GAS PERMEABILITY

THM PROPERTIES OF BARRIER SAMPLES AFTER OPERATION FOR 18 YEARS: GAS PERMEABILITY: EFFECT OF JOINTS

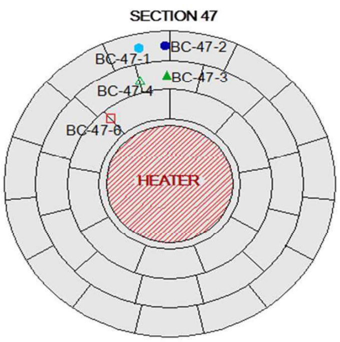

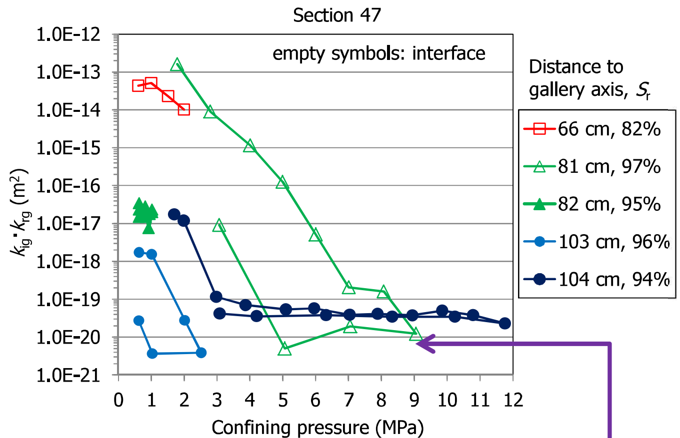

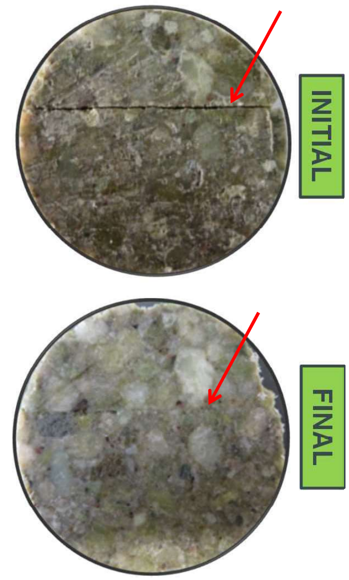

- ✓ Gas permeability decreases with confining pressure, particularly for P_{conf}<4 MPa (the dry density of the samples increased during the tests)
- ✓ Samples closer to the gallery axis (drier, lower S_r) have higher k_g
- ✓ The gas permeability of samples with interface is higher
- ✓ Samples with interface of the external ring (more saturated) behave as samples without interface

Irreversible closure of pathways during the test

THM PROPERTIES OF BARRIER SAMPLES AFTER OPERATION FOR 18 YEARS: GAS PERMEABILITY: EFFECT OF JOINTS

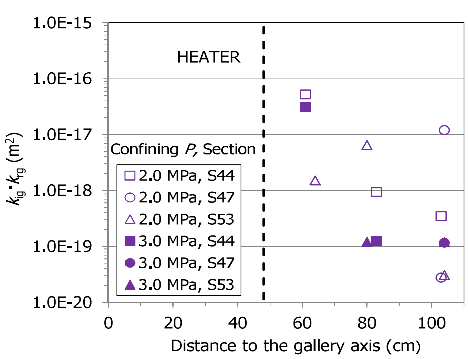

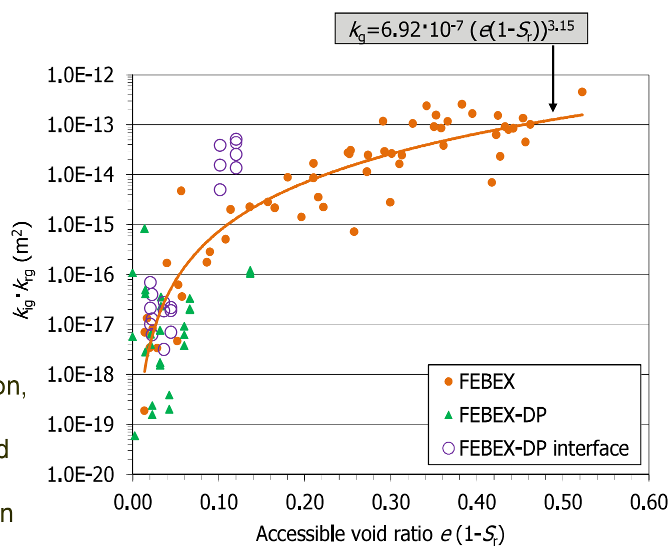

- ✓ Gas permeability decreases with the degree of saturation, and consequently is lower near the granite
- ✓ Effect of interfaces less noticeable in the more saturated samples
- ✓ Gas permeability of the FEBEX-DP samples depends on the accessible void ratio in the same way as was to be expected for the FEBEX reference bentonite

FEBEX/FEBEX-DP – Summary safety relevant aspects

- Low hydraulic conductivity	→	Properties not altered, diffusion dominated
- Chemical retention of RN	→	Sorption properties unlikely altered
- Sufficient density	→	Density gradients, mean 1.59 g/cm^3
- Sufficient swelling pressure	→	~6 MPa (for 1.6 g/cm^3); lab-scale confirmed in 1:1 exp.
- Mechanical support	→	Sufficient support
- Sufficient gas transport capacity	→	Not relevant
- Minimise microbial corrosion	→	No indication of MIC on canister, instruments
- Resistance to mineral transformation	→	No significant transformations detected
- Sufficient heat conduction	→	Confirmed

Kober et al. Davos Clay Conference 2017

CONCLUSIONS 1/2

✓In granite host rock with enough water availability, the bentonite expansive capacity is enough to fill all the voids , the initial dry density of the blocks (1.70 g/cm^3) decreasing to an average barrier density of 1.60 g/cm^3

✓After 18 years hydration the distribution of water content and dry density in vertical sections still showed axial symmetry, with higher water content and lower dry density in the external part of the barrier

✓The average water content and the humidity gradient was higher in hot sections, i.e. around the heater: heating delays hydration

✓Hence, the average water content and density values in vertical sections changed along the barrier

CONCLUSIONS 2/2

✓The state observed in some parts of the barrier seems to have been originated at the beginning of operation and has not been modified subsequently: some of the deformations occurred could be irreversible

✓The measurements taken upon dismantling do not reflect exactly those during operation, because 1) there was a cooling period and 2) the barrier experienced expansion when the concrete plug was demolished

✓**The importance of the water content and density changes in the barrier comes from the fact that the thermo-hydro-mechanical properties of bentonite (thermal conductivity, permeability, swelling capacity, water retention capacity) depend basically on these parameters**

Final remarks

- No irreversible modifications of THM properties of the buffer have been observed
- The influence of radiation on THM properties has not been tested
- Modelling is required to extrapolate to long-term behaviour

References

- Bárcena, I., Fuentes-Cantillana, J.L., García-Siñeriz, J.L. 2003. Dismantling of the heater 1 at the FEBEX "*in situ*" test. Description of operations. Publicación Técnica ENRESA 09/2003, Madrid, 134 pp.
- ENRESA 2006. FEBEX Full-scale Engineered Barriers Experiment, Updated Final Report 1994-2004. Publicación Técnica ENRESA 05-0/2006, Madrid, 590 pp.
- Fuentes-Cantillana, J.L.; García-Siñeriz, J.L. 1998. FEBEX. Final design and installation of the "in situ" test at Grimsel. Publicación Técnica ENRESA 12/98. Madrid, 184 pp.
- García-Siñeriz J.L.; Abós H.; Martínez V.; De la Rosa C. (AITEMIN) 2016. FEBEX-DP Dismantling of the heater 2 at the FEBEX "in situ" test. NAGRA Arbeitsbereicht NAB 16-011. Wettingen, 92 pp.
- Villar, M. V., Lloret, A. 2007. Dismantling of the first section of the FEBEX *in situ* test: THM laboratory tests on the bentonite blocks retrieved. Physics and Chemistry of the Earth, Parts A/B/C, 32(8-14), 716-729. DOI: 10.1016/j.pce.2006.03.009
- Villar, M.V.; García-Siñeriz, J.L.; Bárcena I. & Lloret, A. 2005. State of the bentonite barrier after five years operation of an in situ test simulating a high level radioactive waste repository. Engineering Geology 80(3-4): 175-198.
- Villar, M.V. (Ed.) 2006. FEBEX Project Final report. Post-mortem bentonite analysis. Publicación Técnica ENRESA 05-1/2006, Madrid, 183 pp.
- Villar, M.V., Iglesias, R.J., Abós, H., Martínez, V., de la Rosa, C., Manchón, M.A. 2016. FEBEX-DP onsite analyses report. NAB 16-012. 106 pp.
- Villar, M.V., Carbonell, B., Martín, P.L., Gutiérrez-Álvarez, C. 2021. The role of interfaces in the bentonite barrier of a nuclear waste repository on gas transport. Engineering Geology 286: 106087. https://doi.org/10.1016/j.enggeo.2021.106087
- Villar, M.V. 2017. FEBEX-DP Postmortem THM/THC Analysis Report. Technical Report NAB 16-017. 147 pp.
- Villar, M.V., Iglesias, R.J., García-Siñeriz, J.L. 2020. State of the in situ Febex test (GTS, Switzerland) after 18 years: A heterogeneous bentonite barrier after 18 years operation. Environmental Geotechnics 7(2): 147-159. https://doi.org/10.1680/jenge.17.00093
- Villar, M.V., Iglesias, R.J., García-Siñeriz, J.L., Lloret, A., Huertas, F. 2020. Physical evolution of a bentonite buffer during 18 years of heating and hydration. Engineering Geology 264: 105408. https://doi.org/10.1016/j.enggeo.2019.105408

The FEBEX project was financed by ENRESA and the EC Contracts FI4W-CT95-006 and FIKWCT-2000-00016

The FEBEX-DP Consortium (NAGRA, SKB, POSIVA, CIEMAT, KAERI) financed the dismantling operation and onsite determinations in 2015